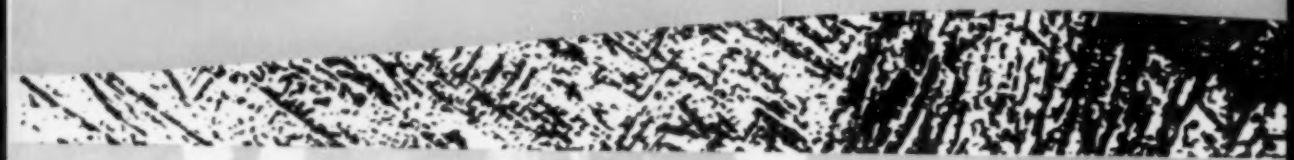

JOURNAL OF

METALS

IN 2 SECTIONS—SECTION 1

February 1955

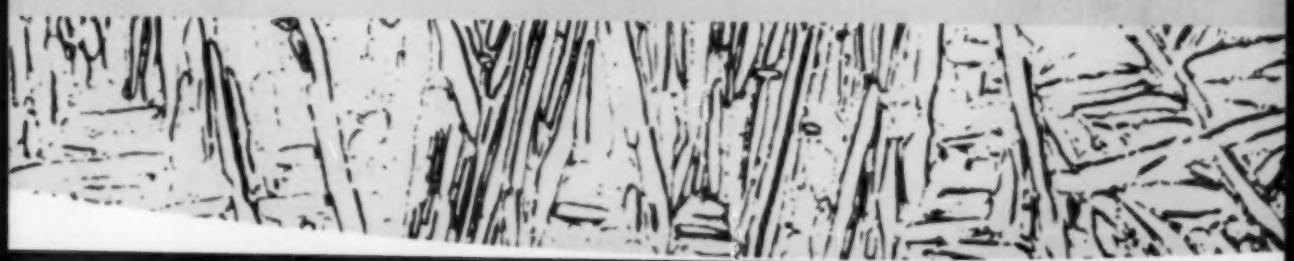

MAKE EVERY HEAT COUNT!

with RECARB-X. for the ladle

- **FAST CORRECTION FOR OFF-CARBON HEATS** — a convenient 50-pound bag of RECARB-X tossed into the ladle will give two points of carbon pick-up per 100-tons of steel.
- **REDUCED LADLE REACTION** — RECARB-X does not cause churning, boiling or other violent ladle reactions. It avoids oxidation of alloys and temperature losses by dissolving quickly and quietly.
- **IDEAL FOR QUALITY STEEL** — RECARB-X is consistently efficient at all carbon levels . . . effective in maintaining maximum rimming action on all high carbon rimmed heats . . . ideal for close carbon specifications.
- **HELPS THE MELTER** — RECARB-X added to the ladle will insure carbon specifications. RECARB-X gives the melter time to finish all heats to proper S, Mn, P, etc. specifications . . . and to tap at the best temperature.
- **SAFE** — no odor or flames to hurt workmen or damage equipment. Light 50-pound bag is easy to toss into the ladle.
- **ECONOMICAL** — RECARB-X is a profit-making investment. Keep your mill schedule. Put more heats into the soaking pit at exact carbon specifications. Make *every* heat count with RECARB-X.

Write for the RECARB-X bulletin today. Get the full facts and arrange a test . . . we will be happy to cooperate.

OUR 101st YEAR

190

THE UNITED STATES GRAPHITE COMPANY

DIVISION OF THE WICKES CORPORATION • SAGINAW, MICHIGAN

JOURNAL OF

METALS

Published to provide a continuing, authoritative, and up-to-date record of technological, engineering, and economic progress in all branches of the metals industry by the
Metals Branch
American Institute of Mining and Metallurgical Engineers, Inc.
29 West 39th Street, New York 18

ALVIN S. COHAN
Manager of Publications
Editor, JOURNAL OF METALS
EDWIN M. WEISS
Associate Editor

M. A. MATZKIN M. SNEDEKER
G. M. ZILL
Assistant Editors
GRACE PUGSLEY Production Manager
W. J. SEWING Asst. Prod. Mgr.

METALS BRANCH COUNCIL

R. R. McNaughton Chairman
E. O. Kirkendall Secretary
J. H. Scaff IMD Chairman
J. S. Marsh ISD Chairman
P. T. Stroup EMD Chairman
M. Cohen R. D. Parks
T. J. McLaughlin D. S. Eppelsheimer

EDITORIAL ADVISORY COMMITTEE

J. S. Smart, Jr. Chairman
W. A. Dean Evan Just
J. C. Kinnear, Jr. John Marsh
T. D. Jones M. Tenenbaum

TECHNICAL PUBLICATIONS COMMITTEES

Robert Aborn AIME Chairman
M. A. Jones ISD Chairman
S. J. Dickinson EMD Chairman
W. R. Hibbard, Jr. IMD Chairman
E. J. Kennedy, Jr. Secretary

WARREN V. SMITH
Eastern Advertising Manager
BOB WILSON
Western Advertising Manager
84 E. Randolph St., Chicago

The AIME Publishes:
Journal of Metals
Mining Engineering
Journal of Petroleum Technology

VOL. 7, NO. 2 FEBRUARY, 1955

COVER

Titanium technological progress has been considerable since commercial output began a few years ago. Contributing to this progress have been the meetings and discussions held by AIME. Harry Brocke gives his impression of the AIME Titanium Symposium on this month's cover.

NEWS

Industrial Notes	220	Trends	228
Coming Events	222	Drift of Things	230
Employment Service	224	Reporter	233
Books for Engineers	225	AIME News	269
Personals	277		

TECHNICAL FEATURES

Titanium Symposium Panel Discussion 234

Hydrogen Affects Critical Properties In Commercial Titanium H. D. Kessler, R. G. Sherman, J. F. Sullivan 242

General Physical Metallurgy of Titanium Reviewed R. I. Jaffee 247

TRANSACTIONS

Oxygen Solubility and Oxide Phases in the Fe-Cr-O System D. C. Hilty, W. D. Forgeng, R. L. Folkman 253

This issue of JOURNAL OF METALS is in two Sections:
Section 1—Magazine Section 2—Transactions Section

Published the first day of each month by the American Institute of Mining and Metallurgical Engineers, Inc., 29 West 39th Street, New York 18, N. Y. Telephone: PEnnsylvania 6-9220. Subscription $8 per year for non-AIME members in United States and North, South and Central America; $10, foreign; $6 for AIME members, or $4 additional in combination with a subscription to "Mining Engineering" or "Journal of Petroleum Technology." Single copies, 75 cents; single copies foreign, $1.00; special issues, $1.50 . . . The AIME is not responsible for any statement made or opinion expressed in its publications . . . Copyright 1955 by the American Institute of Mining and Metallurgical Engineers, Inc. . . . Registered cable address, AIME New York . . . Indexed in Engineering Index, Industrial Arts Index and Chemical Abstracts . . . Reentered as second-class matter Sept. 21, 1949, at the post office at New York, N. Y., under the Act of March 3, 1879. Additional entry established at Manchester, N. H.

"Rare Earths—Dollars and Sense"

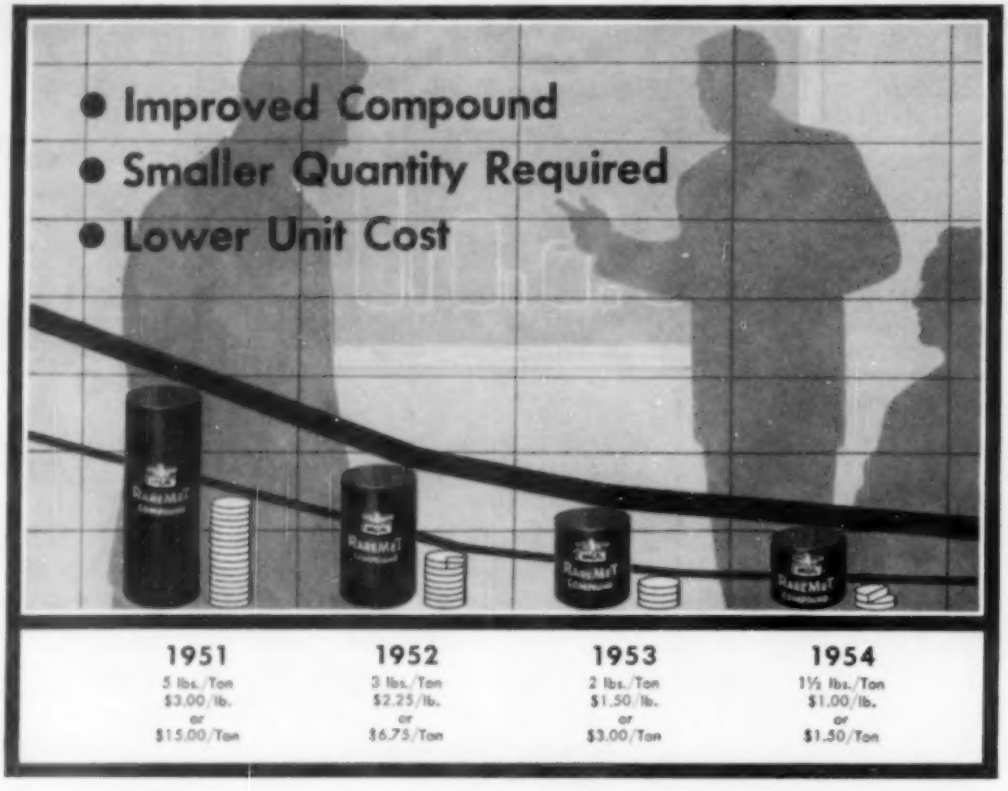

So rapid has been the advance in technical progress and use of rare earths (Trade Name: MCA RareMeT Compound) that in the brief span of four years, about one-fourth as much is needed to accomplish the desired results, at one-third the cost per pound. Now, the economics in favor of rare earths are ten times as great as they were four years ago.

In OPEN HEARTH STEELS, the improvement in addition practice is making rare earths more and more economical, actually cutting production costs. Excellent results with STAINLESS STEEL in hot workability and increased yield have been verified consistently.

Most steel producers, conscious of their customers' increasing demands for better quality, greater uniformity, and consistently good iron and steel are actively engaged in research employing rare earths. If the cost of iron and steel producing is at all interesting to you, or if customer rejections play any part in your operations, it will pay you to investigate the intelligent use of MCA RareMeT Compound. A letter addressed to any office will bring prompt and confidential response.

MCA

MOLYBDENUM

CORPORATION OF AMERICA

Grant Building Pittsburgh 19, Pa.

Offices: Pittsburgh, Chicago, Detroit, Los Angeles, New York, San Francisco
Sales Representatives: Edgar L. Fink, Detroit; Brumley-Donaldson Co., Los Angeles, San Francisco
Subsidiary: Cleveland-Tungsten, Inc., Cleveland Plants: Washington, Pa., York, Pa.

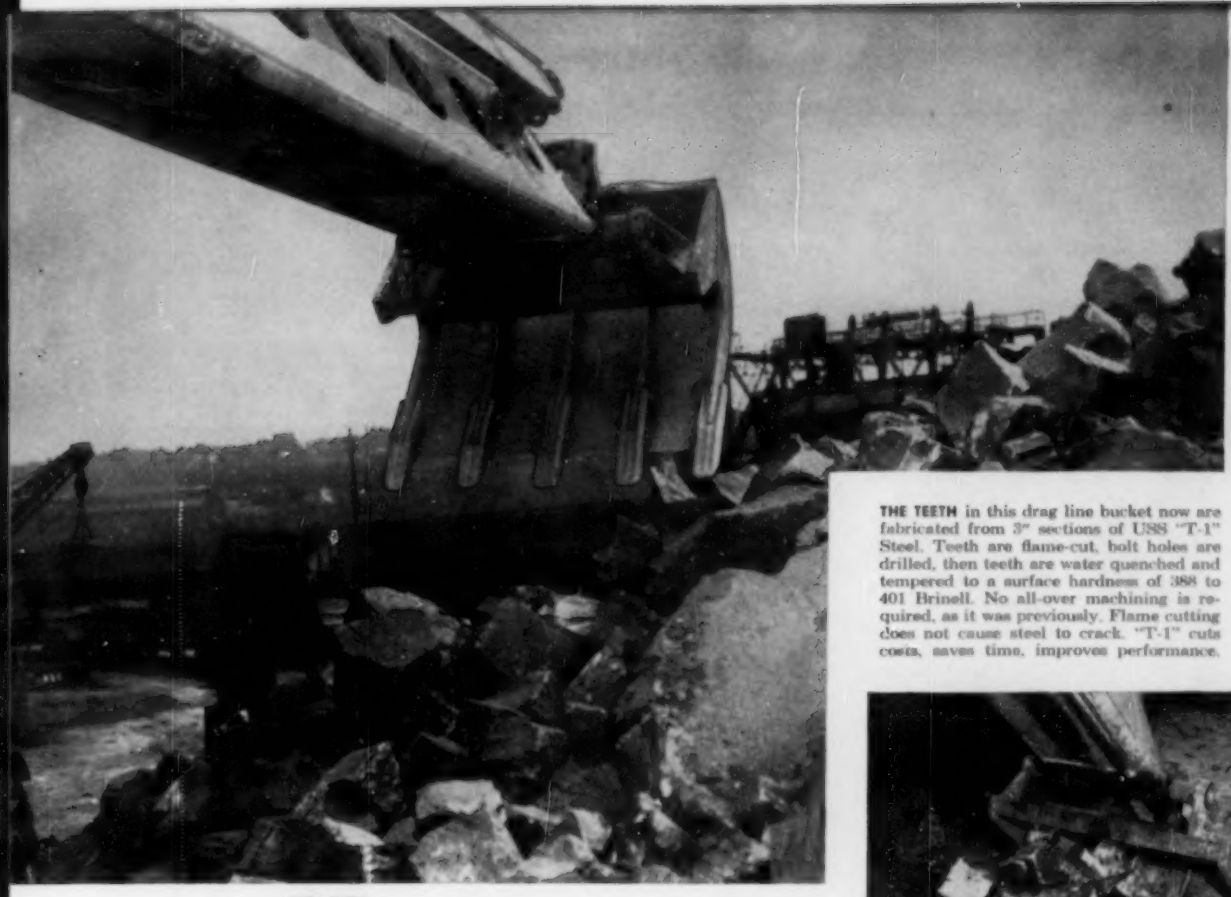

THE TEETH in this drag line bucket now are fabricated from 3" sections of USS "T-1" Steel. Teeth are flame-cut, bolt holes are drilled, then teeth are water quenched and tempered to a surface hardness of 388 to 401 Brinell. No all-over machining is required, as it was previously. Flame cutting does not cause steel to crack. "T-1" cuts costs, saves time, improves performance.

How USS "T-1" Steel in Drag Line Bucket Teeth increased service life ten times

This hefty drag line is used to break and load ferromanganese which is made by the Blast Furnace Department of U.S. Steel's Duquesne Works. Ferromanganese is extremely hard and dense, so the bucket teeth must have exceptional resistance to impact abuse and abrasion.

When we bought this machine, the manufacturer used the best steel then available for the job. But still the teeth broke easily – and lasted for only 4 to 8 hours of operation. Replacement down time was frequent and expensive.

Just as an experiment, we tried our new "T-1" Steel in this rugged application. It worked beautifully. Instead of 8 hours, we are getting *80 hours* of service from each set of teeth – ten times more. Down time and replacement costs are about *a tenth* of what they used to be. Naturally we'll continue to use "T-1" Steel in this job, in the entire bucket as well as the teeth.

USS "T-1" Steel can cut costs for you in a wide variety of applications. Write for detailed facts and figures.

USE "T-1" AT HIGH TEMPERATURES. New USS "T-1" Steel has good creep rupture strength up to 900° F. It is being used in heavy-duty parts that operate at high temperatures.

USE "T-1" AT LOW TEMPERATURES. This same steel is amazingly tough at sub-zero temperatures. In pressure vessels, it has survived impacts of 2,000,000 ft. lbs. at 38 degrees below zero F. In addition, it has good resistance to impact abrasion.

USE "T-1" TO CUT FABRICATING COSTS. You have a yield strength of 90,000 psi. in "T-1" yet you can weld or flame cut this steel without pre- or post-heating. Your welds will develop the *full* 90,000 psi. And you can fabricate parts either in the shop or the field—wherever it is more convenient and less costly. With "T-1" Steel you can save money or improve design—sometimes both—in bridges, pressure vessels, heavy-duty trucks, excavating machines, mine cars, high speed rotating machines, steel mill equipment, and stamping and forging presses.

UNITED STATES STEEL CORPORATION, PITTSBURGH • COLUMBIA-GENEVA STEEL DIVISION, SAN FRANCISCO
TENNESSEE COAL & IRON DIVISION, FAIRFIELD, ALA. • UNITED STATES STEEL SUPPLY DIVISION, WAREHOUSE DISTRIBUTORS, COAST-TO-COAST
UNITED STATES STEEL EXPORT COMPANY, NEW YORK

USS "T-1" CONSTRUCTIONAL ALLOY STEEL

USS

5-203

UNITED STATES STEEL

Industrial Notes

• *J. B. Arthur, president of the Mexico Refractories Co., announced purchase of the assets of the Niles Fire Brick Co., Niles, Ohio, valued at more than $3.5 million. Annual production capacity is more than 25 million silica and fire clay brick. Property included in the sale is in Ohio, Pennsylvania, and Kentucky. Mexico Refractories now owns and operates five plants, one in Mexico, Mo., and one each in Pennsylvania, Maryland, Canada, and Ohio.*

• **Forty-two sales engineers were recently added to the field sales force of Minneapolis-Honeywell Regulator Co.'s industrial div. in 23 branch offices. The appointment of the new sales engineers is in line with the firm's planned growth program to meet increased complexities of marketing in the automation field.**

• Year end statement by Benjamin J. Fairless pegs possible 1955 steel production for the entire industry at 95 million tons, the fourth highest tonnage of all time. The U. S. Steel Corp. board chairman also thinks this will be a good year for business in general. The nation's steel industry, incidentally, started 1955 with an annual capacity of 125,828,310 net tons of ingots and steel for castings, according to the American Iron & Steel Institute.

• Buehler Ltd. has placed on the market a new all-metal polishing desk for the metallographer in single, two, or three unit models. The polishing table is desk height and finished in gray hammertone. The top is black formica and the formica edge on the top and back prevent formation of water and dirt pockets often encountered when metal is used. Features are over-sized wash bowls of vitreous enameled iron and 12 in. swing spouts to supply water. Polishing heads are direct drive Buehler models 1500-F and 1505-2F. Literature is available from Buehler Ltd., 2120 Greenwood St., Evanston, Ill.

• *An executive of a leading manufacturer of electrical distribution equipment predicts an increase of 15 pct in the use of copper. J. B. Cottell, president of Continental Electric Equipment Co., says the general expansion and replacement of electrical equipment that will take place this year will be the reason for the sharp rise.*

• **Carnegie Institute of Technology has withdrawn the professional engineering degree because of small demand for the degree and the growing importance of professional engineer registration. Since 1916 the professional degree has been awarded to 133 graduates, but only four have been issued since 1946. Carnegie Tech noted that today "The candidates professional competence is passed on by a group of practicing professional engineers instead of an educational institution."**

• Free world nickel production during 1954 is estimated at 390 million lb, some 50 million lb higher than in the previous year. Canadian production is expected to reach 320 million lb, or 80 pct of the free world's total production, when the final figures are in. International Nickel Co., according to John F. Thompson, chairman of the board of directors, produced 275 million tons.

• Dow Chemical Co. renewed for three years its lease on the Government-owned magnesium plant at Velasco, Texas. While acting on its option to renew the lease the company withdrew its offer to buy the plant. The Dept. of Justice had expressed the opinion that the proposed sale would tend to maintain a situation inconsistent with the antitrust laws. The plant was built at an original cost of $26.5 million and was restored to production in 1950.

For maximum efficiency in the production of specimens in the metallurgical laboratory the Buehler cabinet type polishing table with companion storage cabinets represents the latest modern development of this type of equipment.

The convenience of this streamlined polishing equipment saves time and encourages the operator to produce the highest quality of polished sample.

Item No. 1511 is a two-unit polishing table with Formica top approximately 60" long x 27" deep by 30" high to table top. Two 12" swing spouts, drain, 8" diameter wash bowl, plumbing and wiring.

Recommended accessories to complete an efficient set up for maximum convenience are: No. 1512 storage cabinet with recessed light and No. 1513 supporting panel for installation above polishing desk. Or, No. 1514 floor model storage cabinet. Both these cabinets can be used together to advantage in most laboratories.

The Formica top and back on the table and cabinet is installed with a smooth Formica edge that eliminates all metal rims that may form pockets for water and dirt. Covers are held in place on the back by magnetic holders. The large 8" wash bowl is a new feature that enables the operator to use both hands in washing specimens.

All metal construction finished in hammer tone grey makes a very attractive appearance. Prompt delivery can be made on these new items.

The Buehler Line of Specimen Preparation Equipment Includes . . . Cut-Off Machines • Specimen Mount Presses • Power Grinders • Emery Paper Grinders • Hand Grinders • Belt Surfacers • Mechanical and Electro Polishers • Polishing Cloths • Polishing Abrasives

Buehler Ltd. METALLURGICAL APPARATUS
2120 Greenwood Avenue, Evanston, Illinois

AJAXOMATIC

AN AUTOMATIC POURING UNIT FOR THE PRODUCTION OF ALUMINUM DIE CASTINGS

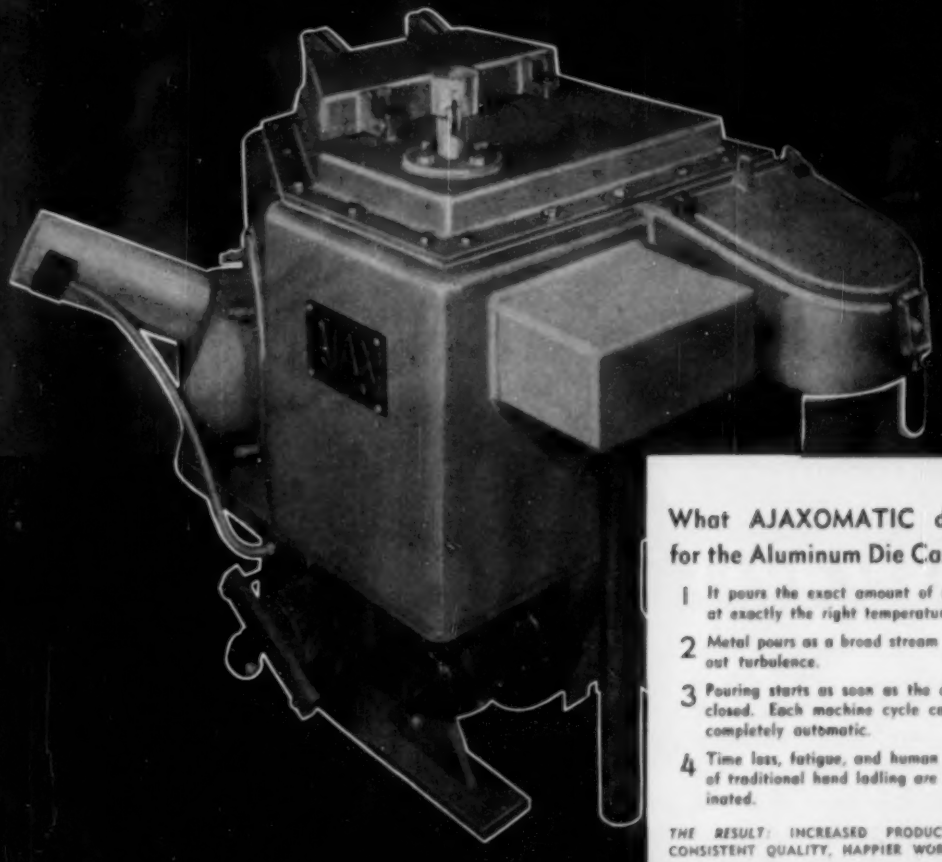

What AJAXOMATIC does for the Aluminum Die Caster

1. It pours the exact amount of metal at exactly the right temperature.
2. Metal pours as a broad stream without turbulence.
3. Pouring starts as soon as the die is closed. Each machine cycle can be completely automatic.
4. Time loss, fatigue, and human error of traditional hand ladling are eliminated.

THE RESULT: INCREASED PRODUCTION, CONSISTENT QUALITY, HAPPIER WORKERS.

AJAX ENGINEERING CORPORATION

TRENTON, N. J.

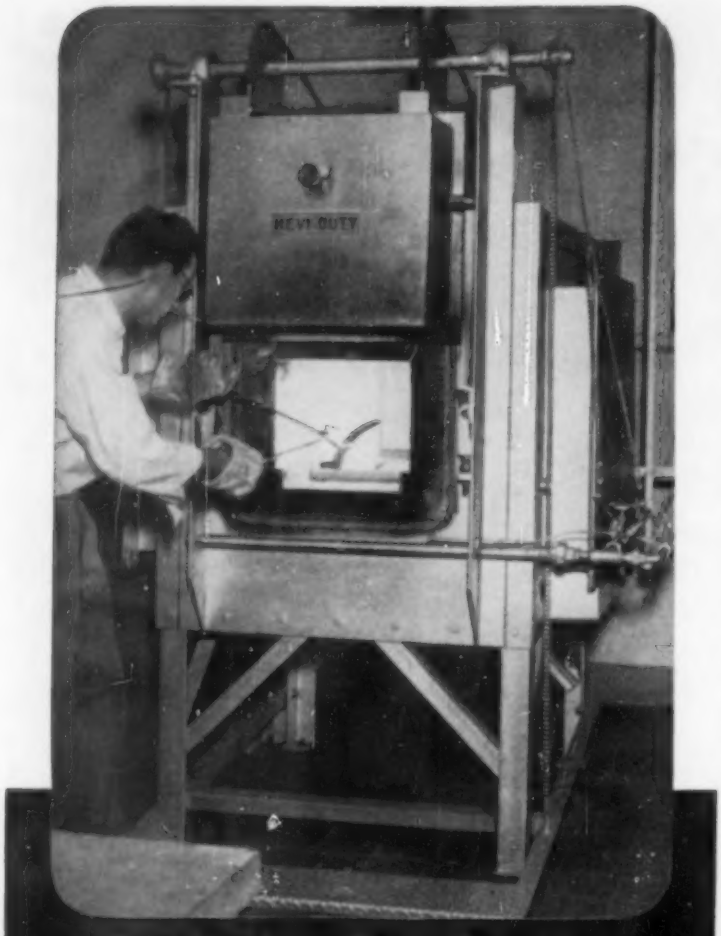

Production Heat Treating Techniques are Determined in

HEVI DUTY FURNACES

A large automotive and ordnance manufacturer uses Hevi Duty high temperature furnaces in its metallurgical laboratory for determining production heat treating cycles.

These furnaces provide the uniform heat needed in this important work. Temperatures are accurately controlled to 2600° F. For day in day out production or precision laboratory work rugged Hevi Duty furnaces will meet your requirements. Write for bulletin IND-741 today.

HEVI DUTY®

HEVI DUTY ELECTRIC COMPANY

MILWAUKEE 1, WISCONSIN

Heat Treating Furnaces... Electric Exclusively

Dry Type Transformers *Constant Current Regulators*

— Coming Events —

Mar. 1, AIME, Northern Ohio Section, NOHC, Pick-Ohio Hotel, Youngstown, Ohio.

Mar. 1-3, National Assn. of Corrosion Engineers, University of Tennessee Corrosion Conference, Knoxville, Tenn.

Mar. 9, AIME, Connecticut Local Section, Bridgeport, Conn.

Mar. 10, AIME, Cleveland Local Section, American Room, Manger Hotel, Cleveland.

Mar. 10-11, Porcelain Enamel Institute, Pacific Coast conference, Biltmore Hotel, Los Angeles, Calif.

Mar. 14-15, Steel Founders' Society of America, annual meeting, Drake Hotel, Chicago, Ill.

Mar. 15, Society for Applied Spectroscopy, Philadelphia Section, Philadelphia, Pa.

Mar. 16, AIME, Connecticut Local Section, annual meeting, Statler Hotel, Hartford, Conn.

Mar. 20-23, American Institute of Chemical Engineers, Kentucky Hotel, Louisville, Ky.

Mar. 28-Apr. 1, Western Metal Exposition, Western Metal Congress; Pan-Pacific Auditorium, Ambassador Hotel, Los Angeles, Calif.

Apr. 13, Material Handling Institute, spring meeting, Drake Hotel, Chicago, Ill.

Apr. 14, AIME, Cleveland Local Section, joint meeting with American Ceramic Society, NACA Laboratories, Cleveland Hopkins Airport.

Apr. 18-20, Third National Air Pollution Symposium, Pasadena, Calif.

Apr. 18-20, AIME, Blast Furnace, Coke Oven and Raw Materials and National Open Hearth Steel Conferences, Bellevue-Stratford Hotel, Philadelphia.

Apr. 19, Society for Applied Spectroscopy, Philadelphia Section, Princeton University, Princeton, N. J.

Apr. 19-21, Canadian Institute of Mining and Metallurgy, annual meeting, Royal York Hotel, Toronto.

Apr. 22-23, AIME, New England Regional Conference, Boston, Mass.

Apr. 28-30, AIME, Pacific Northwest Conference, Spokane, Wash.

May 1-4, American Institute of Chemical Engineers, Shamrock Hotel, Houston, Texas.

May 2-6, Electrochemical Society, Sheraton-Gibson Hotel, Cincinnati, Ohio.

May 6, American Assn. of Spectrographers, annual conference, Chicago.

May 14-22, Chemical Engineering & Equipment Exhibition, Frankfort am Main, Germany.

May 16-19, American Mining Congress, coal convention and exposition, Public Auditorium, Cleveland, Ohio.

May 18-20, Porcelain Enamel Institute, mid-year div. conference, Edgewater Beach Hotel, Chicago.

May 19, AIME, Utah Local Section and University of Utah Student Chapter, joint meeting.

May 30-June 1, Chemical Institute of Canada, annual conference, Quebec, Canada.

May 31, World Power Conference, International Executive Committee, Paris, France.

June 1-18, Joint Metallurgical Societies, European meeting.

June 20-24, American Society for Engineering Education, annual meeting, Pennsylvania State University, State College, Pa.

June 26-July 1, ASTM, annual meeting, Chalfonte-Haddon Hall, Atlantic City, N. J.

Improve ladle additions of chromium to steel with ELECTROMET Exothermic Ferrochrome

LOW CARBON PICKUP

ELECTROMET Exothermic Ferrochrome 8, which has a 12 to 1 chromium-to-carbon ratio, gives a carbon pickup of 0.08% for each per cent of chromium added. ELECTROMET's new Exothermic Ferrochrome 5, having a 20 to 1 chromium-to-carbon ratio, gives only about 0.05% carbon pickup for each per cent of chromium added.

HIGH CHROME RECOVERY

About 92% of the chromium is recovered regularly. This provides close control of chromium specifications in the finished steel with a minimum loss of alloy.

FAST SOLUBILITY

ELECTROMET exothermic ferrochrome generates the right amount of heat to melt the alloy quickly and prevent chilling the metal in the ladle.

Other advantages of ELECTROMET'S Exothermic Ferrochrome:

High ignition temperature (above 750 Deg. F.) gives maximum protection against fire hazard during storage.

For convenient, easy handling the alloy is packed in cans, or in strong, flameproof and moisture-proof bags. Cans or bags are shipped on pallets at customer option. Each pallet holds 60 cans or 80 bags.

No weighing is necessary since each can or bag holds exactly 25 lb. of contained chromium. Just count the cans or bags to obtain the weight desired.

FREE TECHNICAL ASSISTANCE . . . in the use of the material is furnished by ELECTROMET's experienced field representatives. Further information will be gladly furnished on request. Please contact one of the offices listed below.

The term "Electromet" is a registered trade-mark of Union Carbide and Carbon Corporation.

ELECTRO METALLURGICAL COMPANY

A Division of Union Carbide and Carbon Corporation

30 East 42nd Street UCC New York 17, N. Y.

OFFICES: Birmingham • Chicago • Cleveland • Detroit
Houston • Los Angeles • New York • Pittsburgh • San Francisco

In Canada: Electro Metallurgical Company, Division of Union Carbide Canada Limited, Welland, Ontario

Electromet

TRADE-MARK

Ferro-Alloys and Metals

— Personnel Service —

THE following employment items are made available to AIME members on a nonprofit basis by the Engineering Societies Personnel Service Inc., operating in cooperation with the Four Founder Societies. Local offices of the Personnel Service are at 8 W. 40th St., **New York 18**; 100 Farnsworth Ave., **Detroit**; 57 Post St., **San Francisco**; 84 E. Randolph St., **Chicago 1**. Applicants should address all mail to the proper key numbers in care of the New York office and include 6c in stamps for forwarding and returning application. The applicant agrees, if placed in a position by means of the Service, to pay the placement fee listed by the Service. AIME members may secure a weekly bulletin of positions available for $3.50 a quarter, $12 a year.

MEN AVAILABLE

Foundry Metallurgist, 39, married, three children. Experience includes electric steel castings, high tensile bronze, malleable gray iron, and magnesium castings. Published papers on melting practice, foundry molding materials, and quality control procedures. M-134.

POSITIONS OPEN

Metallurgist, experienced in metallurgical processing; thoroughly familiar with milling equipment such as ballmills, jigs, classifiers, flotation, etc. Salary open. Location, Texas. W-870.

Metallurgist, experienced in spot welding electronic tube material, nickel, molybdenum, stainless steel, etc., and refractory materials that are used in radio tubes. Smallest spot welding to medium size welding. Desire someone who can set up standards and various machines and to follow through on job. Prefer someone who has had welding and brazing experience. Location, Long Island, N. Y. W-862.

Assistant Division Metallurgist, metallurgical graduate, with three or four years experience in production metallurgy rather than metals research. Duties will include quality control and metallurgical and foundry developments. Salary open. Location, upper New York State. W-853(b)

Metallurgist, experienced in continuous casting to establish pilot plant and small production unit for copper alloys. Salary open with chance for investment in new company. Location, Pennsylvania. W-840.

Graduate Fellowships in physical metallurgy at eastern university. Salary to $2400 per academic year plus free tuition. Academic and experimental work leading to M.S. or Ph.D. degree. Possibility of summer employment. Positions available July or September 1955. W-839.

Industrial Engineer, under 40, preferably with experience in metallurgy, chemical or large milling operations. Salary open. Location, West. W-835(b).

Engineers. (a) Metallurgist or chemical engineer graduate, to assist melting dept. metallurgist in steel mill making high speed, tool, stainless, specialty steels, and high temperature alloys. (b) Metallurgical engineer, graduate, with several years' experience for process development in steel mill making high temperature alloys, high speed, tool, stainless and specialty steels. Duties would involve development of processing procedures for new alloys as well as the improvement of processes for established alloys under direction of process development metallurgist. (c) Metallurgist for laboratory work in steel mill, making high temperature alloys, high speed, tool, stainless and specialty steels, for examination of materials, writing of reports, conducting investigations of mill problems involving a large variety of alloys. Good opportunity for graduate with one to three years' experience. Reply giving education, experience, age, references, etc. Location, western Pennsylvania. W-800.

Metallurgist, graduate, with alloy steel experience in production or research laboratory. Must have ability to write reports. Salary, $5000 to $6000 a year. Location, Newark, N. J. area. W-795.

Engineer. (a) Junior metallurgist, under 30, will engage in research in the high temperature and wear resistant materials field. Salary, $4500 to $5400 a year. (b) Chief metallurgist or assistant director of research, 35 to 45, experienced in powder metallurgy and refractory metallurgy; in the fields of high temperature alloys, cermets, cemented carbides, and tool steels. Will take charge of a small group of young and progressive graduate metallurgists and chemical engineers. Salary, about $9000 a year. Location, Westchester County, N. Y. W-774.

General Foundry Foreman, 28 to 50. Must have had at least two years experience in supervising nonferrous foundry and be well versed in handling aluminum, brass, bronze, copper, lead, Monel, nickel, zinc, and related alloys. Metals poured in sand and aluminum; permanent molds. Aircraft quality castings are X-ray inspected. Automobile castings are polished and buffed to high finishes. Castings must be made in most economical manner by unskilled labor for competitive market. Must be able to plan and control production. Salary, $6000 to $7800 a year. Location, Ohio. C2472.

METALLURGICAL CHEMIST
ELECTRO CHEMIST
ANALYTICAL CHEMIST

Unusual opportunities for men with graduate training and experience qualifying them to do research on the chemistry and metallurgy of nickel and cobalt. The program includes the hydrometallurgical extraction and refining of these metals, and the development of related analytical methods.

Send full resume to:

Director, Research and Development Division
NICKEL PROCESSING CORPORATION
Subsidiary of National Lead Co.
4 Cherry St., Montclair, New Jersey

METALLURGISTS

Alloy Development—includes composition development for high temperature and magnetic alloys, phase diagrams, creep, precipitation hardening, vacuum melting and other techniques. Development experience in physical metallurgy or alloy systems, background in theoretical physical metallurgy and knowledge of solid state physics useful; M.S. or Ph.D. in Metallurgical Engineering. For application write to

Westinghouse Electric Corporation
Educational Department
East Pittsburgh, Pa.

ENGINEERING GRADUATES

Opportunity with small Midwestern steel plant. Recent metallurgical graduates preferred for steel plant observation work. Good starting salary and opportunity to work into supervision.

Box B-6M AIME
29 West 39th St., New York 18

RESEARCH PHYSICAL METALLURGISTS

Progressive company expanding research activities has several openings with excellent opportunities for advancement. Well equipped laboratory located in Pacific Northwest with attractive surroundings and pleasant climate. Liberal policy on publications.

Positions to be filled are:

(1) M.S. or Ph.D. interested in applications of X-Ray Diffraction to Metallurgical Problems.

(2) B.S. or M.S. to work with group studying phase diagrams and structures of light alloys.

(3) Experienced powder metallurgist preferably M.S. or Ph.D. to take charge of development of aluminum powder alloys and fabrication processes.

(4) Group leader with Ph.D. or equivalent experience for basic and applied research on aluminum alloy systems and fabrication. Positions also open in this field for B.S. or M.S. degrees.

Salaries depend upon experience and past record. Replies will be held in strict confidence. Send full details of experience and salary requirements to:

Department of Metallurgical Research
Kaiser Aluminum & Chemical Corp.
Spokane 69, Washington

Books for Engineers

ORDER YOUR BOOKS THROUGH AIME—Address Irene K. Sharp, Book Department. Ten pct discount given whenever possible.

Chemical Process Principles, Part I—Material and Energy Balances, second edition, by O. A. Hougen, K. M. Watson, and R. A. Ragatz. *John Wiley & Sons, Inc.*, $8.50, 504 pp., 1954—The significance of each industrially important principle of chemistry selected by the authors for discussion "is intensively developed and its applications and limits scrutinized," begins the preface of this book's precursor, *Industrial Chemical Calculations*. The current work continues to give intensive quantitative training in the practical applications of the principles of physical chemistry to the solution of complicated industrial problems and in methods of predicting missing physicochemical data from generalized principles.

Strength of Materials, second edition, by Joseph Marin and John A. Sauer. *Macmillan Co.* $6.75, 518 pp., 1954—This is a new edition of a beginning textbook and contains added chapters on creep and temperature properties of materials, and experimental methods of stress analysis. There are also new sections on vibrations of beams, stress concentration, and beam columns. Numerous changes have been made to bring material up to date, particularly in chapters on fatigue and impact properties, and theories of failure.

Mass Spectrometry, by A. J. B. Robertson. *John Wiley & Sons, Inc.* $2.00, 135 pp., 1954—This general introduction to the subject contains a brief historical review of the method, and concise chapters on the operation of mass spectrometers, on the ionization and dissociation of molecules induced by electron impact, and on the use of the technique in chemical analysis, free radical investigation, and measurement of isotopic abundance.

Physical Properties of Solid Materials, by C. Zwikker. *Interscience Publishers, Inc.* $8.75, 300 pp., 1954—The book is an attempt to summarize the entire field of solid state physics in a single volume. Coverage ranges from problems of mechanics and heat to electronic properties. Each topic is accompanied by a resume of the theoretical foundations presented and present knowledge is reviewed to the point where applications can be suggested. The MKS system is used throughout, and tables of conversion factors and other data are appended.

Metallurgy of the Non-Ferrous Metals, by W. H. Dennis. *Pitman Publishing Co.*, approx. $12.50, 647 pp., 1954—In creating this book, the author has collected, revised, and expanded the many articles on the subject which have appeared in various metallurgical and mining journals for the past 10 years. The text deals with the metals very roughly in order of their industrial production, giving first the source, secondly the operations concerned in the extraction from the mineral or minerals, the refining of the crude metal, and in the case of the major metals, their properties, alloys, and uses.

Physical Chemistry and Metal Extraction, by D. W. Hopkins. *Macmillan Co.*, $4.80, 232 pp., 1954—The book has been prepared for the use of extractive metallurgy students; research workers in the field of physical chemistry as applied to reactions between metallic compounds, metals, and slags; and technical personnel controlling or developing metal extraction processes. Theoretical basis is dealt with to the extent deemed necessary for an adequate understanding of the practical applications, along with special emphasis on development from fundamental definitions along simple mathematical lines. The application of this theory is then extended to roasting, reduction and oxidation, and slags. Detailed consideration is given to shaft furnace smelting and distillation.

Sonics, by Theodor F. Hueter and Richard H. Bolt. *John Wiley & Sons, Inc.*, $10.00, 456 pp., 1955—The unity of sonics is the keynote of the book. The authors draw upon material from physics, engineering, and electronics relating to the fundamental physics of vibration and sound, design principles of electro-acoustic and fluid-dynamic transfers, the choice of sonic variable for systems engineering, and special techniques for testing and processing. The information is given in a framework of basic physics, so that common features of seemingly unrelated techniques are made clear.

Report on the Elevated Temperature Properties of Selected Super-Strength Alloys. *American Society for Testing Materials*, $4.75, 208 pp., 1954—This is the third in a current series of reports prepared under the auspices of the Data and Publications Panel of the ASTM-ASME Joint Committee on the Effect of Temperature on the Properties of Metals. Primarily, the report is a graphic summary of the elevated-temperature strength data for 13 super-strength alloys. Included are 116 summary curves showing tensile strength; 0.2 pct offset yield strength; percent elongation and reduction of area; stresses for rupture in 100, 1000, 10,000, and 100,000 hr; and stresses for creep rates of 1 pct in 10,000 and 100,000 hr.

Directory of Welding and Fabricating Equipment, Section I: Metal Arc Welding Electrodes. *Louis Cassier Co. Ltd.*, approx. 52¢, 35 pp., 1954—This is the first time that a comprehensive guide to the entire range of electrodes now available in the United Kingdom has ever been published. The directory is divided into five parts, dealing with electrodes

(Continued on page 226)

A CAREER OPPORTUNITY
with **DU PONT**
For an Experienced
ENGINEERING MATERIALS ENGINEER

A unique career opportunity is now available in our Engineering Department to a graduate metallurgist or metallurgical engineer (advanced degree desirable) whose education included a minor in physical chemistry, engineering materials, or corrosion engineering. Experience should include evaluation, selection, specification, and use of materials of construction, both metallic and non-metallic, for process equipment. This should include both corrosion properties and fabrication procedures, including forming, welding, stress relieving, heat treating, and inspection.

The successful applicant will provide consulting service to operating plants and to the Engineering Department on problems in the above engineering materials fields. Problems in plant operations will include evaluation of performance of materials in process equipment to prevent product contamination and to reduce maintenance to a minimum. This provides an extremely wide field of application in a great variety of processes.

Please send complete résumé, including details of education and experience, to:
Mr. J. C. Costello, Jr., Engineering Dept., Personnel Section
E. I. du Pont de Nemours & Co., Inc.
Wilmington 98 Delaware

STRENGTH and RESISTANCE of METALS

By JOHN M. LESSELLS, Lessells and Associates, Inc. and M. I. T.

Fully describes the behavior of metals under stress. It provides the most up-to-date information on such conditions as: static tension or compression; creep at elevated temperatures; cyclically varying stresses, as in fatigue; suddenly applied loads, as in impact; high surface stresses, as in wear.

1954 450 pages Illus. $10.00

WELDING FOR ENGINEERS

By HARRY UDIN, M. I. T.; EDWARD R. FUNK, Goodyear Aircraft Company; and JOHN WULFF, M. I. T.

Treating welding engineering as a field in itself, this book presents a discussion of the fundamental principles and theory underlying the subject. It covers the joining of metals by brazing; gas, atomic hydrogen and resistance welding; stress concentration and relief; inspection and testing; and design of metallurgical aspects.

1954 430 pages Illus. $7.50

CHEMICAL PROCESS PRINCIPLES

Part I—Material and Energy Balances—2nd Edition

By OLAF A. HOUGEN, Univ. of Wisconsin; KENNETH M. WATSON, The Pure Oil Co.; and ROLAND A. RAGATZ, Univ. of Wisconsin.

Long recognized as the fundamental reference in its field, this work has been carefully revised to include the latest scientific advances. It offers sound, practical training in the application of physical and chemical principles to industrial problems, reflecting modern developments in chemical, metallurgical and petroleum processing.

1954 525 pages Illus. $8.50

Part II—Thermodynamics. 1947. 384 pages. $6.00

Part III—Kinetics. 1947. 303 pages. $5.25

SONICS

Techniques for the Use of Sound and Ultrasound in Engineering and Science

By THEODOR F. HUETER and RICHARD H. BOLT, both of M. I. T.

Offers a sound, useful, easy-to-read presentation of the principles and practices of this rapidly expanding field. Techniques and devices ranging from a few cycles to hundreds of megacycles per second are covered. Material is drawn from the fields of physics, engineering and electronics.

1955 456 pages Illus. $10.00

Mail for your ON-APPROVAL copies now

JOHN WILEY & SONS, Inc.
440 Fourth Ave., New York 16, N. Y.

Please send book(s) checked below for me to examine ON APPROVAL. Within ten days I will either return same and owe you nothing or will remit the price(s) indicated, plus postage.

- ☐ Strength and Resistance of Metals, $10.00
- ☐ Welding for Engineers, $7.50
- ☐ Chemical Process Principles, Vol. I, 2nd ed., $8.50
  - ☐ Vol. II, $6.00 ☐ Vol. III, $5.25
- ☐ Sonics, $10.00

Name _____

Address _____

City _____ Zone _____ State _____

☐ SAVE POSTAGE! Check here if you ENCLOSE payment, in which case we pay postage. Same return privilege applies, of course.

for arc welding mild steel, alloy steels, cast iron, nonferrous metals, and for hard facing. Electrodes are grouped under the name of the respective manufacturers, and the main details are given for each electrode, along with special features.

Bibliography on Unionization of Professional Engineers. *Engineering Societies Library.* $2.00, 8 pp., 1954—The bibliography has been prepared to aid in answering inquiries received at the library. The 100 references are to pamphlets and magazine articles from 1937 to 1954 which are in the Societies library.

The Chemistry of Portland Cement, second edition, by R. H. Bogue. *Reinhold Publishing Corp.* $16.50, 793 pp., 1955—The second edition of this volume brings the reader up to date in the most recent developments in cement chemistry and technology. Information covers such topics of current interest as single crystal X-ray techniques for studying the atomic structure of cement compounds, new uses of the electron microscope and electron diffraction apparatus in examining the morphology of materials, new applications of differential therma analysis and spectroscopic analysis, and the results of the latest crystal structure studies on both anydrous compounds and the hydrated materials in cement pastes.

Conserving Natural Resources, by Shirley W. Allen. *McGraw-Hill Book Co.* $5.50, 347 pp., 1955—The author covers the entire field of natural resources, including minerals, and discusses the nature of each group of resources and its significance to the individual and national economy. Practices leading to the depletion of natural resources and those which foster their fair distribution and conservation are analyzed. Throughout the book the interrelationships of the various resources and their management are pointed out, and both the techniques of conservation and the social and economic aspects of conservation are treated.

Minerals in World Industry, by Walter H. Voskuil. *McGraw-Hill Book Co.* $5.75, 324 pp., 1955—The book is concerned primarily with illustrating the part minerals play in economic productivity, and in the establishment and maintenance of a high standard of living. Most important is the emphasis upon the role of minerals in developing a distinctive American culture as illustrated by the exceptionally high standard of living enjoyed by an unusually large percentage of the population. The discussion begins with the study of iron. It goes on to consider fuels—coal, petroleum, natural gas, and alternative fuels. In subsequent chapters the author describes the distinctive use of each metal and mineral in the productive economy.

A Review of Productivity in the Wrought Non-Ferrous Metals Industry. *The British Productivity Council.* 21*s*, 26 pp., 1954—The report of the British productivity team that visited the U. S. is said to have been responsible for an increased interest in the whole question of productivity. The report on nonferrous metals covers the industry and its products, exports, trade associations, outlook, productivity, personal outlook, rationalization and standardization, education, work study, incentive schemes, and other aspects of the industry.

Superior
BLAST FURNACE
COPPER CASTINGS
Hot Blast Nozzles and Valve Seats
Blast Furnace Tuyeres. Licensed Manufacturers of all Leading Designs
Cooling Plates of all kinds including Heavy Nose Super Cooled Bosh Plates.
SMEETH-HARWOOD COMPANY
8324 Vincennes Ave., Chicago 20, Ill.
In Canada—The William Kennedy & Sons, Ltd., Owen Sound, Ontario
Blast Furnace Copper Castings—also Brass and Bronze Mill Castings

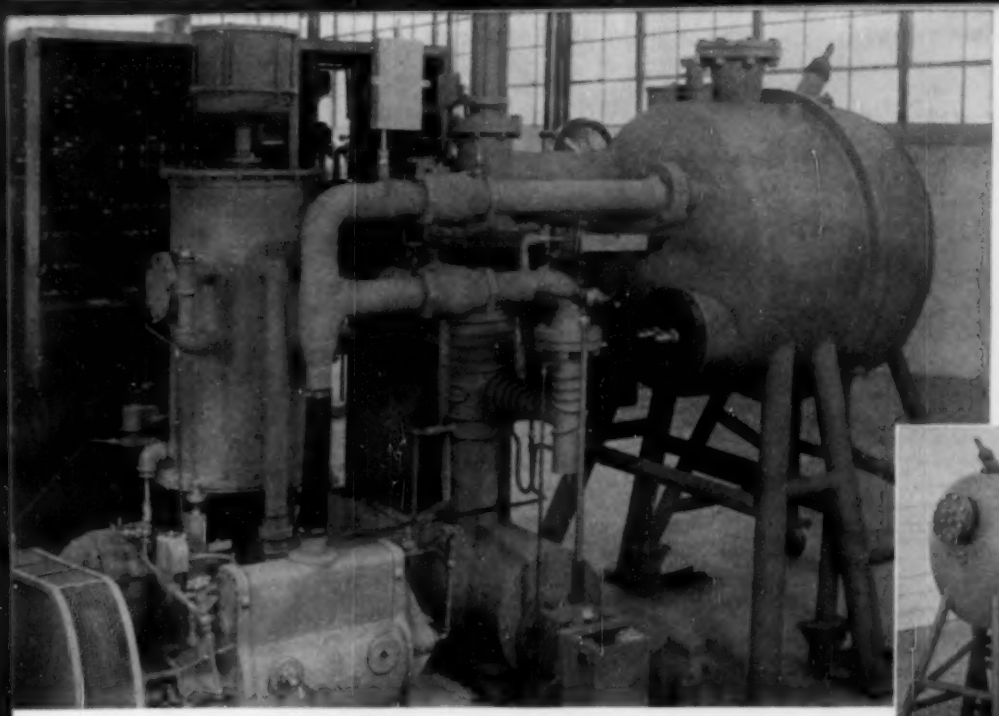

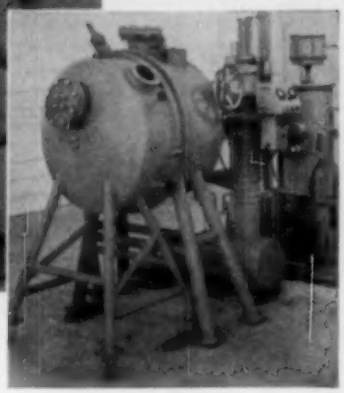

The stainless steel shell of the new CVC high vacuum laboratory furnace is 36" in diameter by 38" long. The shell has a bridge-breaker, a 1" sight tube over the crucible, a 6" window at eye-level for general observation. The whole unit is 6½-feet high and requires 90 sq. ft. of floor area. Inset shows working area.

CVC announces

a new high vacuum metallurgical research furnace

Every part of *CVC*'s new high vacuum laboratory furnace is designed for precise control and operating convenience. Here are the outstanding features—

1. Large vacuum pumping capacity is provided by *CVC*'s KS-600, *2-stage diffusion-ejector pump* which creates the low pressures (of the order of 10^{-4}mm Hg) required for a gas-free atmosphere, and provides ample capacity (up to 0.75mm Hg) for handling the pressure surges that occur during alloy additions and pouring.

2. You perform general observations, alloy additions, tilt pouring, optical and/or thermocouple temperature measurements, bridge-breaking, pressure readings, and high frequency control *all from one spot*.

3. A single semi-automatic, rotary sequence switch controls the pneumatically-operated valves, thus eliminating the need for manual operation.

4. You have a choice of five crucible sizes to accommodate melts of 5, 12, 17, 30 or 50 pounds.

5. Pre-pouring pressures range from 1 to 10 microns for a 50-pound melt of steel; correspondingly lower pressures are obtained when making smaller melts.

For detailed specifications on this new *CVC* laboratory vacuum furnace and for information on pilot or production type vacuum furnaces, write *Consolidated Vacuum Corporation, Rochester 3, N.Y.* (a subsidiary of Consolidated Engineering Corporation, Pasadena, California).

Typical performance of the new CVC high vacuum laboratory furnace with pumping system at normal heater input.

PRESSURE: Microns Hg	SPEED: Liters/Sec.	THROUGHPUT: Micron Liters/Sec.	THROUGHPUT: Micron Cu.Ft./Min.
.2	450	90	191
1.0	660	660	1,400
5.0	750	3,750	7,970
10.0	600	6,000	12,750
50.0	120	6,000	12,750
100.0	60	6,000	12,750

(Selective throughputs may be obtained by using the high, medium, and low heater switch mounted on the KS-600 pump.)

CVC

Consolidated Vacuum Corporation

ROCHESTER 3, N.Y.

Headquarters for High Vacuum

sales offices: NEW YORK, N. Y. • CHICAGO, ILL. • BOSTON, MASS. • SAN FRANCISCO, CALIF. • CAMDEN, N. J.

IT has become part of American tradition for big company representatives to descend on college campuses every June in an all-out attempt to grab engineering talent before the talent goes into the market place. There can be little doubt that the senior engineering student is aware of his importance—15 columns of engineering help wanted advertisements in the classified section of the New York Times every Sunday attest to the demand.

The engineer-to-be is usually given the full treatment. By the time the company representative is finished the prospect is certain that he is the last hope of industry; fame and fortune are his for the asking, and the nation has been stagnant, awaiting his particular genius to move it to the heights. Following graduation comes disillusionment.

The engineer may discover that his function is little understood by public, employer, or worse, by himself. There are several definitions for the engineer, according to George S. Odiorne, writing in a recent issue of *Harper's Magazine*. The society sees the engineer as someone who has accumulated technical knowledge above the workman stage. Salesmen and accountants could fit that definition too. The theoretical scientist pictures the engineer as a "watered-down physicist, chemist, or mathematician; a sort of hairy-chested scientist-gone-wrong." The engineer also has an idea of his own identity. Some still view themselves as Thorstein Veblen, the engineering-minded sociologist of the century's early years, pictured them—tough, neutral technicians—the best qualified to manage society. However, many pure scientists today view the engineer as someone to convert the products of the laboratory into practical applications and the best engineer is the one "most thoroughly steeped in science."

Some engineers, according to Mr. Odiorne, are half convinced of the validity of the idea, and thus seek to isolate themselves from the other end of the scale, where one finds the psychologists, sales managers, and public relations counselors. But the engineer also finds himself rejected by the pure scientist on one hand and often by the pure businessman as well. "He is by no means as lavishly paid as his scarcity might lead you to suppose, and even within industries of the highly technical nature his prestige may be far lower than that of the most junior executive," Mr. Odiorne states.

A *Fortune* article quoting the vice president of an electrical company supports Mr. Odiorne's stand; after pointing out that the ratio of engineers to non-engineers had risen.

"This results not from an increase in the proportion of engineering work but rather from the fact that engineers, as relatively cheap help, are now used for so many other activities than those for which they were trained. Anyhow, there is a general assumption that you can make more money being a manager. This has gone so far in my company that all engineers in supervisory positions are designated 'managers of engineering.'"

Mr. Odiorne traces much of the engineer's trouble to an overall failure to define "what an engineer is," other than to call him a graduate of an engineering college. He notes that "To their credit, many thoughtful engineers recognize" that a certain anxiety concerning the idea that the engineer is poised and self sufficient—balanced between two chasms into which he must never fall—underlies overt complaints about salary, job definition, and a higher place on the industrial scale. He feels that much of the job watering down (Mr. Odiorne calls it blending) has been brought about by engineering initiative. He favors this blending, but feels that management must also look to the best use of engineering talent.

◆◆◆◆◆◆

THE world's largest electric furnaces now going into operation at McLouth Steel Corp.'s Trenton, Mich. plant combine some new ideas with the latest in standard equipment. Because of the size of the furnaces many components had to be specially designed. However, where possible American Bridge engineers, builders of the furnaces, used standard equipment to keep costs in line. One place where this philosophy was exercised was in the selection of speed reducers to perform a variety of jobs. Seven Cone-Drive speed reducers are used.

Inside shell diam of the furnaces are 24½ ft and they will handle average heats of 180 tons. Combined weight of the furnace and heat is about 700 tons, requiring a double reduction Cone-Drive double-enveloping speed reducer with center distances of 10 and 21.837 in. to tilt the load. McLouth purchased two furnaces from American Bridge.

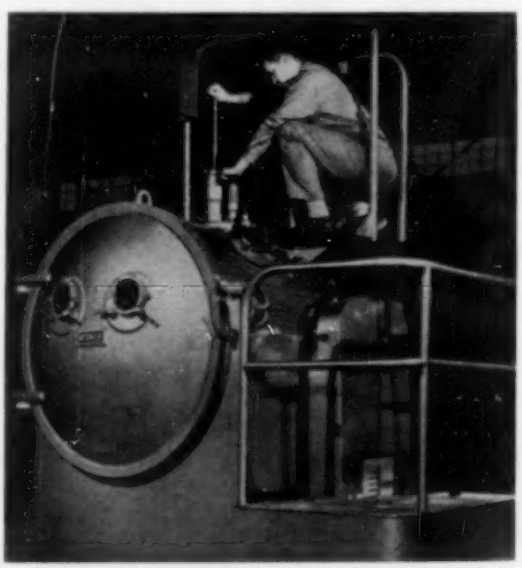

This is the 50 lb vacuum melting and casting furnace for moderate-scale production of high purity metals just introduced by F. J. Stokes Machine Co., Philadelphia, Pa.

BATTELLE MEMORIAL INSTITUTE has almost completed the first units of facilities for an expanded program of pilot plant and large scale research on a recently purchased 400-acre site at West Jefferson, just outside of Columbus, Ohio. Equipment will start moving into the buildings within a short time. According to Clyde Williams, Battelle's president and director, the new facilities will be employed primarily for large-scale studies in chemical engineering, metallurgy, and minerals processing.

The first results of the $300,000 construction program are two major buildings, totaling 13,000 sq ft, designed for large-scale experimental work. The provisions for water, natural gas, and electric power should take care of any forseeable pilot plant. The additional buildings envisioned will be constructed to fill specific needs as they arise.

Housed in the new laboratories will be extensive chemical engineering equipment, a 500 kva 3-phase transformer equipped with automatic controls and that can be used with a 1000 lb melting furnace or for continuous smelting studies. The men who will guide much of Battelle's expanded pilot plant research will be John W. Clegg, manager, dept. of chemical engineering; J. Harry Jackson, manager, dept. of metallurgy; and W. H. Browne, manager, dept. of mechanical engineering.

◆◆◆◆◆◆

ROBERT A. Lubker, manager of the metals research dept. at Armour Research Foundation of the Illinois Institute of Technology, Chicago, predicts that new alloys based on vanadium, chromium, rhenium, and silicon will appear on the industrial scene within a few years. Vanadium base alloys having a density of about six may provide a long-range answer to the problem of improved elevated temperature alloys for aircraft frames. Other alloys are being designed to give the necessary improvement in strength at elevated temperatures combined with relatively low density. Titanium alloys with a density of about 4.5 and a modulus of 16 million psi which will withstand a stress of about 50,000 psi at a temperature of 1000°F have been developed. Mr. Lubker added that improved alloy steels also warrant serious consideration for this application, depending upon the ultimate operating temperature of the aircraft.

Meanwhile, Alan V. Levy, supervisor of the materials and processing section of Marquardt Aircraft Co., told an audience at the Aircraft Research Seminar that power plants for guided missiles are producing temperatures that threaten to melt present high temperature metals. "These power plants include ramjet engines, afterburners for turbojects, and rockets." Mr. Levy feels that it is up to the materials engineer to find materials which will withstand service temperatures ranging from 1200° to 2400°F. The meeting was sponsored by the Southern California Section of the Society of Automotive Engineers. Mr. Levy pointed out that designers must look to molybdenum, ceramic coatings, or the cermets for the materials of the future.

"Operating a ramjet engine with hot spots at 2200° to 2300°F is working within 200° to 300°F of the melting temperatures of the best high temperature alloys," he said. "We will have to await new material developments and/or resort to cooling methods if advantage is to be taken of higher combustion temperatures to attain greater performance."

Right now, according to Mr. Levy, iron, nickel, and cobalt are the foundation of the high temperature alloy field. Attention is being directed to some extent toward alloys based on molybdenum, titanium, and possibly chromium.

One factor that has complicated the work of metallurgists is the Government's insistence on the use of a minimum of critical alloy content in the designs of power plants for piloted craft and missiles. The critical metals include nickel, cobalt, columbium, molybdenum, chromium, and tungsten.

Another report on high temperature alloy work eminates from North Carolina State College, School of Engineering. W. C. Bell, one of the top ceramic scientists in the nation has been directing a government project which introduced something new in compacting non-plastic powder and metals. Mr. Bell and his staff have introduced vibration as a means of compacting materials. Blended materials have withstood up to 3450°F temperatures and are now being studied further.

The huge new reduction cells developed by Reynolds Metals Co. consume some 4000 lb of alumina daily. Here alumina is fed into a cell from an overhead hopper carried by a crane. The cell has been installed at the Robert P. Patterson aluminum reduction plant at Arkadelphia, Ark.

Drift of Things

IN this issue, we are happy to present the proceedings of the Third Annual Titanium Symposium of the Institute of Metals Div. The symposium, under the Chairmanship of J. H. Jackson, Battelle Memorial Institute, was held during the IMD Fall Meeting in Chicago, November 2. The capacity crowd that attended proved that interest in titanium is definitely not lagging. Because of space limitations, it was necessary for us to defer for another month the publishing of two papers presented at the morning session of the symposium. These papers are: *Use of Titanium in Airframes*, by Gordon Fairbairn, and *Use of Titanium in Aircraft of the Future*, by N. E. Promisel. The afternoon session, a panel discussion and question period, is reported in its entirety. Chairmen for the morning session were W. L. Finlay and V. W. Whitmer; afternoon session chairmen were Walter Dean and L. D. Jaffe. We wish to extend our appreciation to all chairmen, authors, and panelists, for their cooperation in planning and preparing this report.

COULD the State Dept. have made a mistake in barring Soviet citizens from Brooklyn? Let us suppose that some Russian in search of amusement wanders across the Brooklyn Bridge and happens upon Ebbets Field. He plunks down a few rubles and enters into this particular area of summer madness. Our Russian friend suddenly feels at home. Them bums are playing Cincinnati. But he makes a mistake. With a daring that comes only from ignorance he cheers the Reds. This could be fatal. However, there are rational people in Brooklyn who never talk louder than five octaves above a boiler works. With one thing and another and the way arguments go in Flatbush, he is by now involved in international politics. And no one is a greater authority—on politics or anything else—than a Brooklynite, whose knowledge of baseball, hot dogs, and what will happen to those unspeakable Giants next year can be matched by no mortal.

Our Russian cannot withstand the onslaught of fact brought to bear. In no time he is a counterrevolutionary, an undying worshiper of Gil Hodges, and a hater of authority—umpires, dictators, or commissars. M. A. M.

CASE HISTORY: *Company Loyalty.* In "The Strange Case of the Round Manhole Covers," Thomas D. Jolly, vice president in charge of engineering and purchases for the Aluminum Co. of America, relates some of the success of the American Standards Assn., and details the spirit of cooperation by which its standards are developed and put to use. All is not standardized in the standards field, however, and we quote:

"Back in 1941 a half-dozen groups sponsored the standardization of manhole covers—the telephone group, the American Foundrymen's Association, the ASCE, the Gray Iron Foundrymen, and the Department of Commerce. Now a manhole cover is a simple piece of industrial equipment. It would seem obvious that if experts got together and worked out a national standard for manhole covers and frames, everyone would adopt it.

"Two years ago I heard a report by a man who had looked into this matter. He found that Annapolis had a manhole standard all its own. It is understandable, therefore that West Point should have its own standard . . . So did the Philadelphia Navy Yard, etc. . . . *One foundryman stated that he had to carry 134 patterns for manhole covers. He said he could reduce his price 30 percent if everyone would use the American Standard.*

"After I heard that report, I went back home and asked our boys if we had adopted the American Standard. They said yes, in every plant except New Kensington. I asked them, 'What's the matter with New Kensington—why can't they use the same thing everyone else uses?' So they brought me the drawing of the manhole covers used there.

"Now that's where I started in with the Aluminum Company years ago—in New Kensington. And I had forgotten all about this, but the drawings said: 'Designed by Jolly, Drawn by Jolly, Traced by Jolly.' Here you will recognize a little of that old company loyalty. The boys weren't going to let me down by using an American Standard over one designed by Jolly. I swear I didn't know then how to design a proper manhole frame and cover. I still don't know." R. A. B.

THE myth that metallurgists never acquire public acclaim or recognition outside of technical circles has been proven false. Men in the metal industries can take their place in the public eye along with men from other occupations. We, and we are sure countless others, were quite impressed when the National Junior Chamber of Commerce announcement of America's Ten Outstanding Young Men of 1954 contained the name of John Herbert Holloman, manager of the metallurgy dept., General Electric Research Laboratory. Dr. Holloman was honored for his leadership in metallurgy and metallurgical research, and for special service to his country in war and peace. The award was presented by the U. S. Junior Chamber of Commerce on January 22 in Louisville, Ky.

Candidates for the award are nominated through questionnaires sent to some 15,000 representatives of all fields of endeavor in 48 states. The age group for candidates is limited to young men, 21 to 35 years of age. To be considered, each nominee was required to have accomplished something of national importance. Two questions were asked: What outstanding contribution did the nominee make to his work or profession, and what outstanding contribution did the nominee make to the general welfare of the people?

To give an idea of the tremendous scope of the selections, the other Outstanding Young Men of 1954 were: Robert Kennedy, 29, chief of the Senate Subcommittee on Investigations; Maj. Charles Yeager, 31, Air Force test pilot; Terrence Brennan, 26, head football coach, Notre Dame University; Hamilton Richardson, 21, law student and Davis Cup tennis player; Dr. Wendell Phillips, 33, explorer; Dr. William Spencer, 32, director of Southwestern Poliomyelitis Respiratory Center; Frank Rose, 34, president of Transylvania College; Ernest Hollings, 32, Lt. Governor of South Carolina; and Arthur Kraft, 33, artist and sculpturer. This is indeed a distinguished group of young Americans.

A. S. Cohan

Titanium Metals Corp. of America

233 Broadway, N. Y., N. Y. Henderson, Nev.

first in Titanium

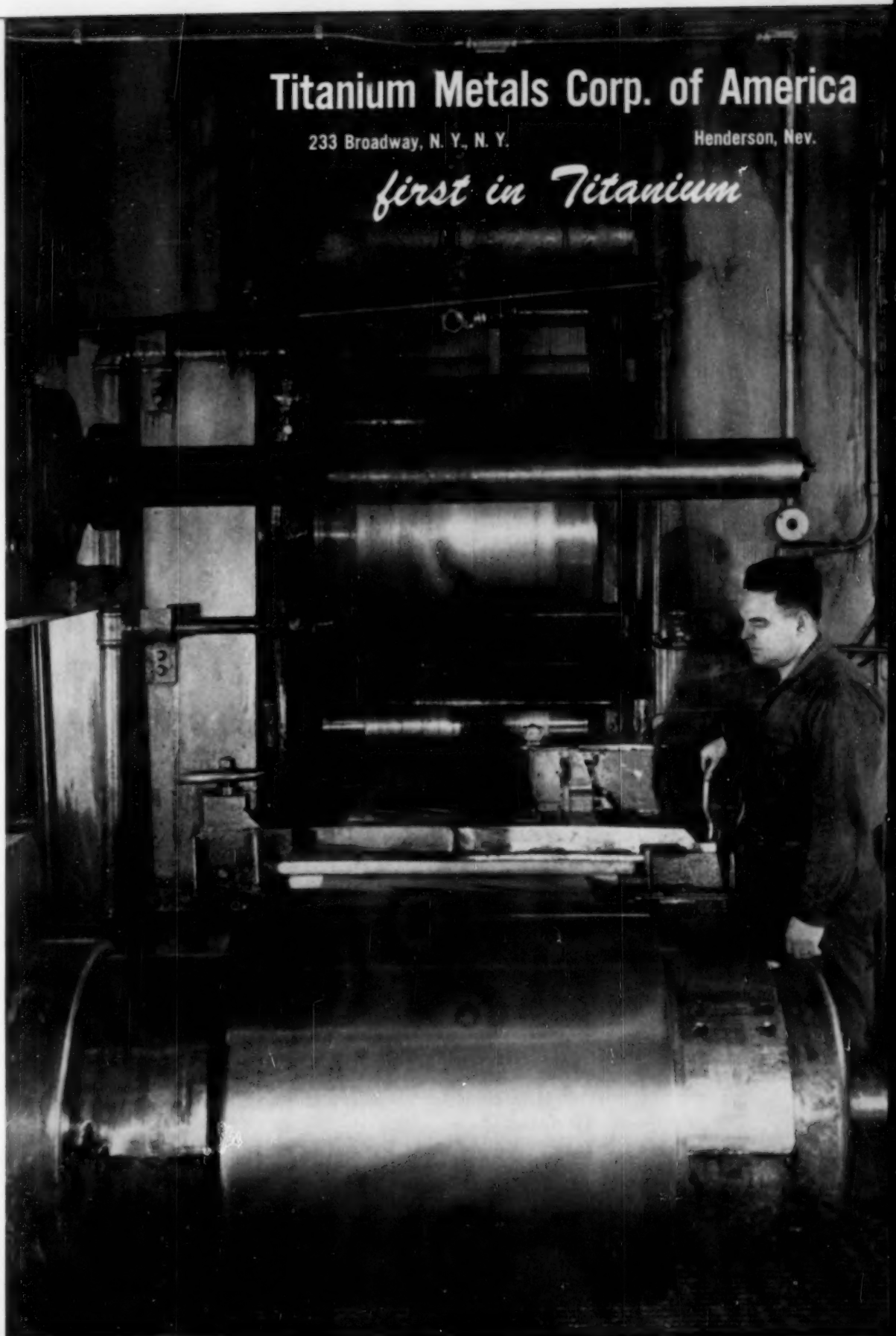

This Set of Dies, for forming attachment ends, has remarkable toughness imparted by nickel. As a result, these dies can withstand heavy-duty service for long periods in the field.

Drill Steel Showing Shank formed by an I-R Drill Steel Sharpener. The attachment end, also forged by the machine, is shown after threading.

Nickel Alloyed Steel Dies contribute to both efficiency and economy of Drill Steel Sharpeners like this Ingersol-Rand Model 54 . . . a type which often serves in remote parts of the world, where repair and replacement parts are sometimes difficult or impossible to obtain.

How Ingersoll-Rand extends life of Drill Steel Sharpener dies

Operated by compressed air, I-R Drill Steel Sharpeners not only form shanks and attachment ends on Jackrods, but are also used to turn out a variety of other small forgings needed in the field.

Accordingly, you can appreciate why all dies, formers, dollies and the like . . . supplied for this work . . . must have ample stamina for repeated use on the job.

And for this repeated use, Ingersoll-Rand produces these vital parts in a die steel containing from 1½ to 2% nickel.

The addition of nickel imparts toughness, along with ample strength and hardness. This combination of properties in a die enables the user to turn out uniform, accurate, true-to-shape forgings rapidly. For example, on one of the larger units, it is possible to forge as many as 50 shanks an hour.

This is one more example of the way nickel, either alone or in combination with other alloying elements, makes possible controlled improvement of specific properties. For the best set of properties to improve your products or equipment, look to alloys containing nickel. Send us details of your metal problem for our suggestions. Write us today.

INCO
TRADE MARK

THE INTERNATIONAL NICKEL COMPANY, INC. 67 WALL STREET NEW YORK 5, N. Y.

American Smelting & Refining Co. has completed preliminary negotiations with Cerro de Pasco Corp., Newmont Mining Corp., and Phelps Dodge Corp., for the financing of the Toquepala copper project in southern Peru. The Toquepala property, with the Quellaveco property of AS&R, and the Cuajone property owned by Cerro de Pasco and Newmont, also in southern Peru, will be transferred to a new group, Southern Peru Copper Corp. AS&R will own 57 3/4 pct of the capital stock, Cerro de Pasco, 16 pct; Newmont, 10 1/4 pct; and Phelps Dodge, 16 pct. Ore reserves in excess of 400 million tons have been proven for the Toquepala property with an average assay of slightly more than 1 pct copper.

Armco Steel Corp. has developed and is producing for commercial use a new type of aluminum coated steel. Known as Armco Aluminized Steel (Type 2), it is said to combine corrosion resisting and heat resisting qualities of aluminum with the strength of steel. As in Armco's aluminized steel, the new product is made by applying molten aluminum to cold rolled sheet steel by a patented continuous pretreatment and immersion process.

T. W. Lippert, manager of sales and technical service, Titanium Metals Corp. of America, states that many in the industry predict further declines in titanium sponge prices in 1955. Reasons for the drop are continuation of the industry's rapid production and development pace and exploitation of current pilot operations leading to the full recycling of scrap metal.

White Pine Copper Co., $80 million development in Michigan's upper peninsula, poured its first copper last month. The White Pine orebody contains about 309 million tons of 1.1 pct copper ore.

It has been reported that the Indian Government accepted in principle an offer by Russia to set up a 1 million ton per year steel plant. The acceptance makes India the first country outside of the Soviet orbit to receive substantial Russian assistance.

Production has been suspended at the former Stanley Steel Works, Bridgeport, Conn., pending conversion of the plant to the new $18 million electric steel mill under ownership of Northeastern Steel Corp. The newly formed Northeastern Steel plans to manufacture steel for aircraft and roller bearing industries.

Plans are in the making by American Brass Co. for a $25 million aluminum mill on the outskirts of Terre Haute, Ind. The Anaconda Copper Mining Co. subsidiary will break ground for the 500,000 sq ft mill as soon as engineers complete planning. In 1953 another subsidiary of Anaconda Copper, Anaconda Aluminum Co., started construction of an aluminum reduction plant for refined aluminum at Columbia Falls, Mont. This plant will supply requirements for the Terre Haute facility.

Titanium Symposium

A Panel Discussion Held During the AIME

Institute of Metals Div. Meeting, Chicago, Nov. 1 to 3, 1954

In 1950 the Institute of Metals Div. of the AIME appointed a Committee with the somewhat unglamorous name of Professional Consciousness Committee to recommend ways by which the IMD could better serve its members and the profession at large. This committee made several recommendations, among which was the suggestion that groups be organized in new and growing fields of metallurgical interest to develop programs for and to promote discussion among those working in these fields.

The first group formed was the Titanium Committee, under the leadership of Matthew A. Hunter. Those of you who were at the first symposium that this committee arranged in 1952 in Philadelphia, will readily recall that stirring session at which Dr. Hunter and others on the program unraveled the past and looked into the future of titanium. This symposium appeared in the February 1953 issue of JOURNAL OF METALS. The activities of this committee caught the interest of metallurgists everywhere and at the fall meeting in Cleveland in 1953 another successful meeting was held.

The present committee, under the chairmanship of Harry Jackson, Battelle Memorial Institute, has been responsible for the organization of this Third Annual Symposium on Titanium. This timely and diversified program is divided into two parts—the session this morning at which the technical review papers were presented, and the panel discussion this afternoon which is to operate on a less formal basis.

The panelists have been selected because they represent a variety of interests in titanium. There is a representative from an air frame consumer, one from a consumer of engine parts, one from a producer who is interested in peacetime applications of titanium and two other members who are also from producer organizations. The sixth member represents the military point of view. I hesitate to call them experts, or for that matter to refer to anyone as an expert in this rapidly expanding field—yet these men have developed enough background to qualify them to discuss this subject intelligently. I also know that there are many in the audience who are similarly qualified. I would guess, therefore, that among the panelists and among those in the audience we perhaps have represented most of the individuals who are active in this field.

While the panel will attempt to answer the questions you propose it is entirely possible that there are areas where answers are not available for lack of knowledge, for security reasons or because the information is considered confidential.

Walter A. Dean, Chairman

Chairman Dean: Now to get the discussion underway with a few brief introductions. Your Chairman is a graduate of the Cooper Institute of Technology, and of Rensselaer Polytechnic Institute. He is employed by Alcoa and after some 15 years in research and five years in plant activity is now the chief metallurgist of the Cleveland Works.

Your Co-chairman is Leonard Jaffe. In 1939 he graduated from MIT with an S.B. in metallurgy. He received his S.M. in 1940 and his S.D. in 1947. He was at Watertown Arsenal from 1940 to 1954 and was chief, metals research branch. He is now in charge of the materials section, jet propulsion laboratory, California Institute of Technology.

The first of the panelists is Frank H. Vandenburgh—a representative of a producer. Mr. Vandenburgh is a graduate of Antioch College with a degree in metallurgy, and continued his studies at the University of Michigan. He has been with the Revere Copper & Brass Co. and Battelle Memorial Institute. From 1940 to 1951, Mr. Vandenburgh was affiliated with the P. R. Mallory Co., Indianapolis, Ind., as a research metallurgist and as manager of the special metals div., at which time his early work on titanium was done.

His firm belief in the future of this metal helped organize the Mallory-Sharon Titanium Corp. in Niles, Ohio, of which he is vice president, general manager, and a member of the board of directors.

Frank H. Vandenburgh: We are primarily metallurgists and mill people. We are interested in taking the available raw materials, which today are titanium sponge and scrap, and converting them into useful structural materials.

I mention that today they are sponge and scrap. With the organized work that is going on in new methods of producing titanium, we are not sure what our raw materials will be a year, two years, or even five years from now but then we are attempting to be close enough to the picture so that we will be able to convert whatever raw materials are available into useful structural materials.

We recognize that because of the characteristics and nature of titanium, it is being used and will continue to be used by air frame and engine builders and other people in rather critical applications. This being true, then for the titanium industry to fulfill its part and for the military to have the best possible fighting equipment, we as producers must supply materials of espe-

cially high uniformity and quality. Our production and research efforts are dedicated and directed toward this end.

Quantity is very important but quality is more important. The quality of sponge—one of our raw materials today—is not yet all that is desired. The sponge producers, however, are improving quality and are working diligently towards a better starting raw material. Production of sheets, rods, bars, and forgings must be of more uniform and high quality as time goes on than the material that we have been supplying in the past. Alloys must be developed that are more stable and easier to handle. These are the phases of titanium that we are working on.

Titanium, as we have heard so many times, is a material that is very critical to the security of our nation. As such, I believe that in order to accomplish in a short time with titanium what has taken many, many years with other metals, the closest possible cooperation between producers, customers, research organizations, and the various government agencies is an absolute must.

Chairman Dean: Our next panel member, who will tell you briefly of some of his interests, is Luther A. Best—who is a representative of a consumer in the air frame field, Douglas Aircraft.

Mr. Best received an A.B. in physics from the University of California at Los Angeles in 1936. He has been with the Douglas Aircraft Co. since graduation, with the exception of two years spent as chief engineer of Walter O'Bannon Co., Tulsa, Okla.

Mr. Best is currently metallurgical engineer in the materials and process engineering dept. at Santa Monica and is in charge of the metals group assigned to manufacturing liaison and service problems. He is closely associated with the introduction of titanium into the structure of aircraft produced by this manufacturer and the attendant laboratory testing as well as the development of manufacturing techniques and procedures.

Luther A. Best: At the Santa Monica div. of Douglas Aircraft, we currently use titanium for skins, formed shapes, clips and firewalls in the aft portions of the nacelles.

Fabrication involves forming of shapes at room temperature on power brakes, hydropress, or progressive rolls, contouring of skins or shapes by stretching at room temperature and two hot forming operations, dimpling and joggling. The material is commercially pure titanium sheet purchased to a Douglas material specification.

The very earliest titanium received in 1949 was very difficult to bend over a radius of 3½ times the sheet thickness at room temperature, and formed parts occasionally cracked in normal installations. To minimize this rate of breakage and produce acceptable properties, all bending was performed at 600° to 800°F and extensive interstage annealing and post forming annealing was employed. All of the reasons for the difficulties were not known but some were obviously connected with poor surface conditions, inclusions, and oxygen and nitrogen pickup. At least one very brittle sheet which cracked during shop handling was found to contain distinct needles and a grain boundary network.

A decidedly improved material was available in 1952 when large scale use of commercially pure titanium was begun. Power brake bending was performed at room temperature and it was possible to form shapes on progressive rolls at room temperature. A radius of 3½ times the thickness was used for both operations.

With a thorough receiving inspection, which included formability and strength tests on each of thousands of sheets received, all forming operations were successful with negligible breakage.

At one time a general decrease of bend ductility was noted together with an increase in shop breakage. Microscopic examination of shop cracked material revealed the presence of dark needles which were subsequently identified as titanium hydrides. A marked heterogeneity was found. A sheet might bend successfully at one location and then shatter if a bend were attempted an inch from the original bend. Test strips cut from one end of a sheet formed satisfactorily yet parts formed from the balance of the sheet broke in forming. Similar heterogeneity was seen in the microstructure. One section might be heavily loaded with needles while another section an inch away might have only a trace. The predominant difficulty occurred in high strength sheets containing hydride needles.

Various tests have been used to pick out the brittle material. Among them has been the bend test, since it is readily conducted and closely simulates some of the more severe production forming. This test has consisted of power brake bending to progressively smaller male radii (1/32 in. increments) until failure occurs. Frequency curves show hydride bearing material to have considerably poorer bend ductility than normal material. Because of heterogeneity, however, the bend test may not disclose brittle material.

Brittle type failures which we have occasionally experienced in stretching of skins suggest an unusual sensitivity of some sheets to slight notches which are always present in production parts. We, therefore, have made some use of static notch tensile tests in which we chose specimen geometry, testing speed and temperature to simulate as closely as possible the most adverse loading combination to which a commercial air frame might be subjected.

We found that: A—At any ultimate strength level, hydride bearing material has a lower notch strength than normal material. B—Cold worked materials tend to have lower notch strength than as received material. C—Other factors than hydride needles and cold work affect notch strength.

The static notch test is time consuming and expensive and does not constitute a suitable test for receiving inspection.

Fatigue tests of the pull-pull type, axial loading, minimum stress equal to 1/3 the max, notched and unnotched, have been run and the presence of hydride needles has been found to decrease the fatigue strength in the longitudinal direction. Fatigue testing is also not a receiving inspection type of test.

Some thought has been given to control by chemistry. Analyses have been provided by the material producers for some of the sheets we have received, both hydride bearing and nonhydride bearing. The lowest hydrogen content showing needles was 0.027 pct and the highest hydrogen content showing absence of needles was 0.015 pct. However, we do not have facilities for hydrogen analysis and, since other factors enter in to produce brittleness, analysis is not yet the whole answer.

We have noted at various times that sheets which cracked in very brittle fashion during shop handling could easily be torn by hand once a short cut was made. This behavior prompted us to set up a controlled tear test in a universal testing machine. Normal material tears slowly and evenly and the curve of head travel vs load falls off gradually. If the material is brittle, it tears with an audible snap or series of snaps and the curve falls off sharply.

For control purposes we have established minimum loads at which the specimen tears through the scribe line or, if more convenient, the load on the curve midway between the load for initial start of tear and the load for dinal break. Both initial tear load and breaking loads are apparent as sharp breaks on the curve.

Chairman Dean: Our next panel speaker is Joseph B. Sutton, a representative of a sponge producer, who is very interested in potential civilian applications. Dr. Sutton graduated in 1933 from the University of West Virginia with a M.S. degree in chemical engineering. Two years later he received his Ph.D. in chemistry from the same university.

He is sales manager-specialty products in the pigments dept. of duPont. The pigments dept. manufac-

tures titanium metal and the specialty product section handles sale of the metal. Formerly as research supervisor in the chemical div. he was responsible for titanium metal research and development.

Joseph B. Sutton: There are two properties of ductile titanium which account for its importance as a material of construction. The first is its high strength-weight ratio at intermediate temperatures. Its density is only 56 pct that of steel and its alloys possess comparable strength. The second is its superior corrosion resistance to a host of severe environments which attack many of the more common materials of construction.

The high strength-weight ratio of titanium and its alloys accounts for the present major interest for application in high performance aircraft and aviation gas turbines. Although these uses to date have been predominantly military, application of titanium to commercial aircraft has not been overlooked. The new DC-7 Douglas embodies engine nacelles and firewalls constructed of unalloyed titanium sheet.

The corrosion resistance of titanium points to broad usage in industrial equipment at some time in the future. It is completely inert to all types of marine atmosphere. Excellent resistance is shown toward inorganic chlorides, chlorinated hydrocarbons, moist chlorine gas, nitric acid and many organic acids.

Published information on laboratory corrosion experiments is very extensive but little data has appeared in the press on resistance of titanium to attack under plant service conditions. However, numerous trial applications are under evaluation in the chemical, pharmaceutical and food processing industries. These include installation of specific pieces of titanium equipment in existing plant process lines as well as pilot units or prototype units constructed completely of titanium.

We have in duPont at the present time, applications where titanium is showing excellent service in: A—60 pct HNO_3 at 180° to 195°C; B—Brackish river water at room temperature; C—5 pct FeCl, at 70°C; and D—Dilute HCl at steam ejector temperatures.

Under (A) we have applications employing approximately the above conditions in both heating units and condensers. The brackish river water environment (B) is in a vacuum jet intercondenser where there is also a small concentration of HNO_3. The steam jet diffuser (D) operating in very dilute HCl has over two years exposure and shows no corrosion.

In summarizing, laboratory corrosion data on titanium metal is very extensive and many tests under plant service conditions are underway but results of few have been completed and reported. It will be surprising indeed, however, if titanium with the valuable properties shown to date does not develop into a very useful material of construction in many industries.

Admittedly, industrial applications of titanium at today's price are limited. However, manufacture of the metal in larger volumes will allow some reductions in price and expand the industrial fields of use.

Chairman Dean: The next panelist is Maj. Ralph J. Kotfila, a metallurgist representing the military interest. Major Kotfila graduated in February 1947, from Purdue University with a B.S. in metallurgical engineering. He attended Ohio State Graduate School for additional courses in metallurgy. He was a metallurgist for Western Electric Co., Lindberg Steel Treating Co., Electro-Motive div. of General Motors Corp., and plant metallurgist at the Shakeproof div., Illinois Tool Works.

Major Kotfila was recalled into service in September 1951. He assumed leadership in the titanium section, metals branch, material laboratory in June 1953, after the departure of Dr. H. K. Adenstedt. He has been responsible for planning the Air Force research program on titanium from that date. He has acted as Air Force advisor on titanium to the industry.

Maj. Ralph J. Kotfila: For the past two years my principal duty was directing the research effort on titanium metallurgy for the Air Force. Part of this research is being done internally in the materials laboratory but the greater bulk of it is contracted to private research organizations and universities. Certain monies have been allocated by the Dept. of the Air Force for just such a purpose.

It is essential that a balance be maintained in the research program; no particular phase of titanium technology should be exploited to the detriment of other phases. The overall research program is divided into the following categories, not listed in order of importance: A—Alloy development, B—Heat treatment, C—Physical metallurgy, D—Mechanical properties, E—Hot and cold working, and F—Fabrication.

The research that is planned is based first on the requirements of the Air Force. The design engineer and the metallurgist of the many primary Air Force contractors have submitted to the materials laboratory a list of requirements. A typical objective of one of these requirements is the development of a high strength weldable sheet alloy with excellent strength at elevated temperatures.

The interstitial problem of course fits into every category of the research program. During the very early years of commercial production of titanium, the interstitial elements oxygen, nitrogen, carbon, and hydrogen were present in sufficient amounts to reduce ductility to such an extent that formability, machineability, and weldability were definitely impaired. At that time sponge hardness, a measure of interstitial content, was high; added to this were interstitials picked up during melting and subsequent processing. The resultant product was in many instances of questionable quality. Since then, the sponge hardness has dropped to a point that in some cases interstitials are intentionally added to obtain the desired tensile strength. Melting and processing techniques have improved now that interstitial pickup is at a minimum. With the exception of hydrogen, it is my personal opinion that the interstitial problem is now of secondary importance. The low sponge hardness and the controls exercised by the producers during processing have brought this change. Any relaxation of these controls, as evidenced by the low ductility and high tensile strength of certain heats delivered to the consumers, may bring the interstitial problem into prominence again.

During the early production years, any failure or difficulty in processing was immediately attributed to interstitials. This was done in many instances without the benefit of analysis or laboratory investigation. At that time, the metallurgy of titanium was not fully understood. Even at the present time, the knowledge of physical metallurgy of this new metal is still in its infancy. The omission of analysis and laboratory investigations to properly determine the cause of premature failure and failures during fabrication may have overemphasized the importance of interstitials.

At the present time, about one fourth or more of the materials laboratory research is concentrated on the effects of interstitials. This may be of academic importance if progress in sponge manufacture and processing continues. The research effort may be redirected to other problems confronting the titanium consumer. However, the underlying cause of any problem cannot be determined without a laboratory investigation. Once the problem is recognized, if it is industrywide, the Air Force will sponsor such research necessary to solve the problem.

Chairman Dean: Our next speaker is Loring R. Frazier—a representative of a consumer organization interested in engines.

Mr. Frazier, after completing a General Electric Co. apprenticeship in machining and drafting in 1937, received a B.S. in metallurgical engineering from Purdue University in 1942. He was with the Wisconsin Steel Works before returning to General Electric in the Thomson laboratory at Lynn, Mass. Currently a member of the nonferrous and high temperature metals group, he has devoted years to developmental testing of titanium and to its physical metallurgy.

Loring R. Frazier: There are three subjects that we are currently investigating at our laboratories in connection with titanium. One line of exploration concerns heat treatment of titanium alloy forgings for ductility; another covers the effects of oxygen on the properties of commercial titanium alloys; the third looks into the mechanics of fatigue fracturing from fretting.

Micrographic studies show that as the quenching temperature is gradually increased, some of the alpha is lost by transformation to beta. It is our theory that the remaining alpha must contain a very high proportion of the oxygen and that quench hardening is a result of quenching beta with the original oxygen diffused through it. If there is enough alpha left in the structure, there is no quench hardening. If there is mostly beta, but a small amount of alpha, not enough alpha to contain all of the oxygen, quench hardening will occur.

Another aspect of heat treatment of titanium is developed from micro studies we have made which show that there is nearly always a phase around the boundaries of the beta phase. We have not been able to find any evidence that the grain boundary phase is alpha. While it may be similar to alpha in ordinary microexamination, there is no alpha response to polarized light. It is our theory that the phase which forms is an intermetallic between titanium and an impurity metal. An impurity which has received little attention is magnesium, nearly always present in small quantities in titanium produced by the Kroll process.

Going on to the subject of fretting in titanium, many of our vibration tests on titanium blades produced failures originating in fretted areas. The causes of such failures seemed to be the caking of the fretting products forming a high pressure between the grips and the blade, thereby crushing the titanium immediately under the cake, and forming a family of cracks. By sectioning several blade bases, we found evidence of the crushed condition of the metal. From the cracks, the fatigue or vibration failure progressed.

From evidence developed in these three fields of investigation, we feel that there is room for a great deal of thinking ahead in the physical metallurgy of titanium.

Chairman Dean: Our next and final panelist who will talk to you is Thomas W. Lippert, a representative of a producer. Mr. Lippert graduated from Carnegie Institute of Technology with a B.S. and M.S. in physics. He was editor-in-chief of Iron Age as well as a director of the Chilton Publishing Co., and in 1949 became manager of all publishing activities of the AIME in New York. In 1950 he was appointed general manager of Titanium Metals Corp. of America, a jointly owned subsidiary of National Lead Co. and the Allegheny Ludlum Steel Corp.

Thomas W. Lippert: It was just a year ago when the crucial role of hydrogen was first emphasized. During the ensuing 12 months there may have been some other subjects of conversation within the titanium fraternity, but you would have had to seek long and hard to find them.

Actually, with regard to hydrogen we are now dealing with past history, because we have for some months been working to a rigid hydrogen limitation. I just don't think there is a hydrogen problem today.

The cleanliness of titanium is par excellence, so much so that the other more common metals may well copy the titanium melting techniques to approximate equivalent cleanliness.

As far as the interstitial hardness, oxygen and nitrogen, their role is now well mapped out and their control is pretty well in hand. For the first time, I believe, physical metallurgists are now able to explore the true effects of metallic alloying elements and erect reliable alloy systems that we thought were only around the corner some four years ago. Of course, we must rightly expect some further troubles but today there is every indication that the industry has chopped a path through the worse underbrush of trial and error.

A year from now I do believe that we will be well into at least the initial commercial production of alloys that are truly and reliably heat treatable to very high tensile values. Then for the first time the titanium industry will compete with the heat-treated steels and the heat-treated aluminum alloys with complete advantage for titanium. Such alloys will in the conventional manner be formable at low strength levels and hardenable to high strength levels with quite reasonable ductility.

At this point the audience was requested to submit questions to the panelists on previously distributed cards.

Has the snap or tear test phenomenon been definitely laid to hydrogen content only or is it a combination of other interstitials with hydrogen?

L. A. Best: Perhaps it may be gathered from what I said earlier that we attribute all brittleness to hydrogen. Certainly that is not the case. It is hoped that the test will pick up brittleness no matter what it may be attributed to.

When will the price of titanium be competitive with, say, stainless steel?

J. B. Sutton: I doubt if the price of titanium will ever be competitive with stainless steel. I don't think that there is any doubt that the price will be lower than it is now and competitive with a lot of higher priced alloys but not competitive with stainless steel.

What lubricants have proven most successful for titanium extrusion?

T. W. Lippert: We use certain low melting point glasses and we use some combinations of rather conventional lubricants. We are constantly probing around the better combinations because we aren't completely happy with performance to date particularly as regards thin and complicated sections.

What method of hydrogen analysis is recommended for quality control checks on titanium sheet?

F. H. Vandenburgh: Wright Field has been doing extensive work in this field. We are, at the present time, using the vacuum fusion method and we feel it is quite reliable. Of course, whether or not it is the best, I don't know. I do know that samples have been sent around on a round robin and I hope that the Major has the answer.

Major Kotfila: Several methods have been proposed for the analysis of hydrogen. The method in most common use is a form of vacuum extraction, a method utilizing vacuum fusion apparatus. Laboratories using this method have obtained good correlation among themselves.

A round robin has been instituted to determine the correlation and accuracy of several proposed methods. One is the hydrogen equilibrium method developed by duPont. This round robin is in its initial phase but to date, of six laboratories participating in this phase, good agreement has been obtained. The bulk of the program remains to be done. Once the interlaboratory variance is determined, the variation in a sheet or heat will be determined.

How should the alpha and beta alloys be heated treated for maximum ductility, and what is the comparative ductility when slow cooled from the beta and when water quenched from beta and then overaged.

L. R. Frazier: I think that you can achieve good ductility with any or either method. I do not want to give a cook book method for annealing titanium because I know that you can always run into some forging that will not respond.

The very slow cooling from beta probably is as generalized a method as you can get but it is extremely slow cooling and it involves several days.

To what extent are the air frame manufacturers using titanium extrusions and forgings?

L. A. Best: At the Douglas Aircraft Santa Monica div., where I happen to be, we are not using any extrusions or forgings as yet. I believe that perhaps someone in the audience could tell a little bit more as to what North American is doing in this respect.

From the Floor*: We at North American are not using any extrusions at the present time. We have used a few forgings and the results to date have been something less than satisfactory. That is something that we anticipated and that is why we only used a few forgings.

Incidentally, we have gotten involved with the vacuum annealing of titanium forgings to restore ductility, and I can report that we have been able to restore good ductility to alloyed forgings by vacuum annealing. An example would be in one particular part of ours, where we increase the reduction of area from about 8 pct to 48 pct by vacuum annealing.

Major Kotfila: The use of titanium forgings in aircraft depends primarily upon the particular manufacturer's experience with his research and development stages. In some instances there have been cases where aircraft companies have been rather disappointed in the properties developed by forgings and thus dropped them at a very early stage.

However, today there is considerable interest to use titanium forgings extensively in aircraft. Up to now forgings and extrusions have been used primarily in the secondary structure of the aircraft. The aircraft laboratory is a little reluctant about releasing it for primary structures simply because of insufficient data. However, Convair is gathering such data for their aircraft. As soon as this information is checked a release will be given for use of forgings as primary structures.

This morning we were told that fasteners are being used or will be used to a larger extent in the near future. These fasteners probably will be made from extrusions.

Major Kotfila: Not necessarily will they be made from extrusions. Some people have used bar stock—ordinary bar stock which was subsequently heat treated.

What is the bar made from?

Major Kotfila: Forged bar. Some aircraft company has used extruded titanium bar and they are now running some tests on it to see the practicability of its applications. They have reported some unusually good results in extruded bar stock.

There was one question before about the lubricant for extrusions. I believe that molybdenum sulphide should be quite decent for a lubricant for these purposes.

Major Kotfila: I think that it has been tried and tried again by almost everybody who did any extrusion work. However, the results were not too good. I think that in extrusions the problem is to find the lubricant that will give us good die life. It is a combination of both die material and lubricant that holds back the wholesale exploitation of extrusions.

What is the feasibility of producing titanium castings commercially?

J. B. Sutton: I think that possibly this question is directed to the wrong person, since our company produces titanium in sponge form only. I don't believe titanium castings are being produced commercially at the present time but recent releases appearing in the papers and trade journals would indicate that considerable progress has been made in this direction.

Major Kotfila: The big thing holding back castings is suitable mold material. Once we have discovered a suitable mold material, then use of castings may progress at a faster pace. All supposedly suitable materials tried so far tend to contaminate the surfaces. Unless impact strength is not required and there is no objection to leaving a brittle surface exposed, the casting will have to be machined. If machining is required all over, the economies of using castings may be decreased.

L. Jaffe: I might say that in laboratory quantities castings have been produced satisfactorily in graphite molds without significant pickup of carbon. Now, of course, machining a graphite mold is hardly a production operation when you want a lot of castings, particularly since you cannot get many castings per mold. However, this is leading in the right direction and we do know of one material, carbon, which doesn't do too badly as a mold material.

What percentage of oxygen is permissible in different titanium products?

Major Kotfila: It all depends on what kind of alloy you have, and also what you want out of the particular material. If you want impact, naturally you want your interstitials, and especially oxygen, to be low. On the whole, let us put it this way—it is not strictly the oxygen content anyway which would give you a decrease in ductility. It is the total content of the interstitials that must be considered. The effects of interstitials are considered additive in many respects and consequently by just calling out the oxygen content, it would be telling you half the story.

Air Force specifications have set a maximum oxygen content at 0.20 pct for all alpha-beta type alloys. The limits for the other interstitials are 0.07 pct nitrogen, 0.20 pct carbon, and 125 ppm hydrogen.

What are the prospects of getting a homogeneous sheet using present or forseeable melting techniques?

F. H. Vandenburgh: I feel that they are very good. In fact, improvement along those lines in the last year has been very, very large. Our feeling is that by using consumable electrodes and double melting that we have gone a long way to producing a homogeneous ingot.

Now then, to process that ingot and to come out with a sheet that is homogeneous, depends a good deal upon how much care is used in processing and whether you have adequate controls and facilities to do the job.

I believe that the users of sheets will agree that the overall problem of homogeneity and uniformity is improving. I do not mean to say that the problem is whipped. I know that in our testing of sheets ready for shipment it would be very nice if, by checking each end, they were identical. Sometimes it is a question of which end to check.

What do you think of powder metallurgy as a method for making pure titanium and titanium alloy bodies—ingots and parts?

L. R. Frazier: In our own laboratory at Lynn we have explored the powder metallurgy parts. However, if there is anyone here from our Cincinnati laboratory then maybe they would comment on that. My own opinion is that they are very good for static parts but they will not lend themselves too well for dynamic rotating parts.

* Comments from the floor are necessarily anonymous because of the impossibility of checking the stenographic record with all participants. Only those comments made by the members of the Titanium Panel are individually identified.

Violent Reactions — Hardness — Elasticity

Are accidents or violent reactions with titanium attributed to any grade or have they been encountered only in the alloy grades?

Major Kotfila: Information reaching me is that they are prevalent in both alloy and other grades.

From the Floor: We had one of those so-called accidents. We had the commercially pure grade, which was not with the manganese addition. We got an explosion and we still don't know why but we suspect that a corrosion product was developed which was pressure sensitive. As yet we have no facts in relation to that.

However, the alloy titanium splattered and there was evidence of cratering on the alloy specimens and splattering on the commercially pure, although we did not observe any explosion or corrosion products due to the commercially pure itself.

What I am trying to say is that the alloy was affected and the pure was not. However, since then I understand that there was another explosion and in this case the pure material was used.

From the Floor: I would like to ask a question on this. The thought occurs to me as to the condition of the metal. Was it stressed or unstressed as tested? The reason I ask is because of the work recently published on stress corrosion of alloy titanium, and I believe that from our own experience in filter material, being about 50 pct density, it was tested at 160° for as much as 700 hr in 98 or 99 pct fuming white nitric acid. Evidently in the case of the stress materials there is some evidence of stress corrosion and maybe that has something to do with the actual chemical reaction here.

From the Floor: The specimens that we tested were not under stress. They had been prestressed to various percentages but, of course, this does not produce a residual tensile stress in the surface of the specimen—and so, if anything, it is a residual compressor stress and this should not lead to stress corrosion.

Major Kotfila: I would like to add that research is going on to definitely determine the cause of this action of titanium and we hope that within a year we will have the story for you.

From the Floor: I can offer the following information on some research work done at our company. We ran stress corrosion tests in red fuming nitric acid for a period of two years on titanium with no indications of any failure.

In addition, we are presently and have in the past conducted tests on stainless steel welded to titanium containers for these tests and after 1500 hr the tanks were inspected, with no evidence of stress corrosion or any other sort of attack. Those were unstressed, or, I should say, stress relieved welded containers made from TI-75-A.

What is the range of hardness of sponge now being produced by TMC at rate of 10 tons per day, and what is the average hardness before blending?

T. W. Lippert: They change so fast, and generally downward, that I haven't caught up with the last figures and, therefore, I hesitate to mention specific hardness levels. I can say that hardness ranges are quite adequate for any stockpiling purposes or for any of our own needs as regards the most advanced alloys.

We are under no pressure whatsoever as to hardness—that is, to make anything we want—or, in the case of stockpiling, to stockpile to government specifications. In fact, if anything, we might have an embarrassment of soft sponge. By soft I mean —140 Bhn or lower in that range.

Can alloying elements increase the modulus of elasticity of titanium?

L. Jaffe: Well, I rather doubt it. I don't think that there has been much success in that connection thus far other than perhaps an increase of 10 to 15 pct. It is possible that much would be obtained but I see very little hope for any major increase.

F. H. Vandenburgh: I agree with Dr. Jaffe. I don't believe that we have ever seen, with the various combinations that we have been checking, an increase of more than 2 or 3 million psi. I think that we could increase it a little bit but then I don't think that there is much hope in that field.

For other hexagonal metals, namely magnesium or zinc, there is markedly less yield strength in compression than in tension. Does titanium exhibit a similar difficulty?

From the Floor: That point has been tested with quite a few alloys and the compressive yield approximates the tensile yield in the case of quite a few titanium alloys. While I have this microphone in my hand I would like to go back to the previous point on modulus and ask if an increase to 10 to 15 pct is of interest to designers?

L. A. Best: Well, I would say that our design people would feel that something like that would be of value.

L. R. Frazier: We are frequently asked by our design people how they can increase the modulus to match that of steel but it has been my experience that only very high alloying with aluminum will markedly increase the modulus of titanium.

From the Floor: I feel, in self defense, that I would like to get on record and say that the strongest magnesium structural alloy is specified with the compressive strength used equivalent to the tensile yield strength.

From the Floor: I am referring to this modulus of elasticity from the design point of view. As far as I can remember we refer to the modulus being from 15.5 to 16.5. Our designer doesn't know which one is true.

L. Jaffe: I might make one comment here and the point does not only pertain to titanium but appears in other metals also. It is possibly a little more so in titanium. The modulus of elasticity is a function of the rate of loading so that the modulus that you measure at one rate of loading is not necessarily the same as that which someone else measures at a different rate of loading. Part of the difference may be the difference in equipment and technique. However, the little factor of the rate of loading also enters.

Major Kotfila: At a recent west coast meeting I talked the problem over with some designers and they have stated that 20 pct increase in modulus would be very beneficial and it would help titanium to be used in many more places. As a result of that conference we have instituted a research program to try to increase the modulus of the titanium. So far it is relatively new and no concrete results are available.

Do you contemplate the use of titanium alloys in the high strength heat treated conditions in the near future?

L. R. Frazier: We run into all kinds of troubles with machining and processing titanium at strength levels of about 140,000 to 160,000 psi tensile strength and I know of no plan to use them at higher strengths for any application in the immediate future.

Major Kotfila: There has been enough interest expressed by the aircraft industry in the use of high strength titanium alloys and I think that in the near future we will see titanium being used in the high strength levels on the order of 170,000 to 180,000 psi.

L. Jaffe: I did not mention one non-aircraft application that I know of at present, which is at least in the pilot plant stage, or perhaps we should call it limited

production—in which material is being used at a minimum of 150,000 psi yield strength, which means something like 170,000 psi tensile, heat treated.

From the Floor: I would like to comment that some of our present commercial alloys, those with fairly large amounts of stabilizing additions, are highly heat treatable. It is my opinion that for these alloys and some of the new alloys which will be developed in the next several years—the use of possible quench and age type heat treatments will be generally accepted for both bar and sheet applications and where we want strength on the order of from 170,000 to 200,000, chances are that we will heat treat the alloys, quench them to make them soft and then age them to make them hard after the machining operation. That would eliminate your problem.

What degree of vacuum is required in arc melting to reduce hydrogen to a safe level and if 150 ppm of hydrogen is considered a safe limit for mill products, what is a safe limit for sponge?

T. W. Lippert: We are quite indifferent to the amount of hydrogen in sponge, because in our vacuum melting hydrogen in the ingot is dropped to any level desired. In fact, it is very possible to actually eliminate some expensive steps in the sponge production cycle which possibly results in higher hydrogen in the sponge—but that's all a plus factor because it all comes out in melting at no cost.

Exactly what are the difficulties with rolling titanium aluminum alloys with high aluminum contents and if it is a question of high temperature strengths of these alloys, why are higher temperatures not used?

F. H. Vandenburgh: I wish that I could really answer that question. We are right in the middle of doing a lot of work on vanadium alloys with the aluminum content varying from possibly as low as 4 pct to as high as 8 pct. The hot hardness and strength of the titanium with aluminum additions goes up with the percentage of aluminum. In the laboratory and in the small mills it is very easy to roll at low temperatures. You have control over the heating time and how much hydrogen and oxygen or nitrogen may be absorbed from the atmosphere.

When you get into production mill equipment, trying to roll full size sheets down into thin sizes then it is a different problem, because the rolling temperature possibly has to be increased. Just what the effect the increased temperature has on the physical properties, that is something we are studying. Surely that is not the best way to keep hydrogen down. Also, I am sure that you will find that the surface condition of the sheet will vary markedly, depending upon the rolling temperature. It may be that to get a smooth surface on the sheet you will use one temperature and then there will be the temperature that we are forced to use—and we will just have to make the best of that.

I am sure that doesn't answer the question but then it does give you a few of the problems and possibly some of the other people who have been working with aluminum additional alloys and trying to make them into sheets would like to add their story.

What are the microscopic characteristics of titanium hydride, color, etching characteristics, hardness, etc.?

From the Floor: Well, it exists in three forms. It is present either as a grain boundary inclusion; as a plate, which in a microscopic section appears as a line or as a relatively new particle. It will develop brittle-like characteristics if it is slowly cooled to a temperature of approximately below 300°C. If it is quenched through this region then the hydride particles are very fine. The grain boundaries or grain boundary inclusion of hydrides are generally found at the slow cooling grades.

From the Floor: Under the microscope, when it is etched with any acids, it takes a gray color. When it is etched with a chrome etch, then it is a white color and I don't believe that it is harder than the matrix.

If we had beta in the texture, and we don't see any needles, do we still have fracture and is it still hydrogen?

L. Jaffe: Perhaps I can throw light on the question, if I interpret it correctly: "How do you distinguish between small quantities of beta and small quantities of hydride in the alpha matrix?"

There is a simple way, and that is to use polarized light. It does not matter what etch you use. It is better not to etch at all; look at the polished surface. The hydride shows very strong birefrigence under polarized light.

Major Kotfila: I would like to talk about it from the practical aspect of the thing. I think that you will observe its effect on mechanical properties long before you will see it in the microscope. By that I mean at the lower hydrogen contents. So far in the little work we have done, its effect on properties has been noticed before it has been observed under the microscope.

Do you have any information on the shear strength and Poisson's ratio of titanium and its alloys?

From the Floor: We have done a good deal of work on that and we find that it varies all over the lot—from 25 up to 32. We average around 28.

What is the panel's opinion as to the advisability of using titanium alloy forgings in the as-forged condition—that is, without machining or without etching off the outer layers of skin?

L. R. Frazier: We have made a number of thin titanium compressor blades and we feel quite confident that we could use them, not quite in the as-forged condition, but with a very thin layer of the surface removed by dry sandblasting. We have found in the bend test that the surface layer is low enough in ductility to initiate cracking unless we remove the contaminated layer to about 0.001 in. depth.

Major Kotfila: Of course, a lot will depend upon the size of the forging and where you want to use it. However, whenever possible, we always advocate machining off the surface because it has usually a hard and brittle layer. We definitely know that the original side or surface will give you a reduced fatigue life.

From the Floor: I think that last statement is an important one—namely that the original side, the brittle layer that we get under the scale is detrimental to fatigue life and it is inevitable that it is formed in forging and therefore should be removed. If you do not do it by machine then it can be done with nitric acid—with the acid content being high enough—25 pct for example. If you do that then there is no danger of accomplishing a hydrogen pickup. As to the high shear strength of titanium base materials, I don't know that there is any explanation now.

You mentioned that oxygen had not been seriously considered as a problem the last year. Does this also apply to alloy material in general?

T. W. Lippert: Possibly I don't understand your question. What you want to do is keep oxygen low. The matter of total oxygen is always of concern, and end requirement and entry of oxygen into the system other than by sponge would determine the level of sponge hardness tolerable. All that would be up to the producer, who balances his variables as he sees fit.

Major Kotfila: If you are speaking of beta alloys, the beta phase is more intolerable of oxygen. In the alpha-beta type of alloys the concept is that the alpha phase accounts for only the nitrogen and carbon. If you did not have an alpha phase to catch all of that then the

beta phase would become very brittle. You have to keep the oxygen down to quite low levels.

What are the limits of hydrogen that can be expected from the producers today?

J. B. Sutton: DuPont sponge, at the present time, runs below 25 ppm.

Major Kotfila: We have completed a survey of material out in the field and with the exception of one producer's material. With that exception, it was high in hydrogen. However, the hydrogen content is determined to a large extent by the form of the product.

Naturally, because of higher surface area to volume ratio the hydrogen content of sheet usually runs high. However, in bar stock it can run anywhere from about 20 to 300 ppm. The minimums observed have been as low as 30 ppm. Therefore, it can run over a wide range, depending upon the process controls.

Has Douglas Aircraft utilized vacuum process or any other process to reclaim sheet that exhibits hydrogen embrittlement?

L. A. Best: No, we have made no attempt to reclaim sheet that contains hydrogen embrittlement by vacuum annealing or other means.

L. Jaffe: We have observed no relationship between oxygen content and quench hardening ability. Increase in hardness as quenched is probably a function of stability of the beta and this in turn is a function of temperature. Quench hardness is also a function of quench rate.

What methods of melting sponge—other than arc melting—appear to have economic possibilities? Are there any such methods now being used commercially?

F. H. Vandenburgh: I don't know of any methods that are being used commercially other than arc melting methods, excepting the possibility of induction melting. In the laboratory we are working on two or three other methods and I am sure that other people are. I can only say that they are not being used commercially at the present time.

T. W. Lippert: Well, my personal opinion is that arc melting, particularly using large consumable electrodes, is such as efficient and precise melting technique that it would be most difficult to better by some other procedure.

Would you consider a 100 hr sustained loading room temperature stress rupture type of test a practical acceptance test for alpha-beta alloys to determine the extent or presence of hydrogen embrittlement? If not, what length of time?

L. A. Best: Again, I must say that this is a test with which I am not too familiar. We have not run a test of this nature in our laboratory.

From the Floor: We run some 20 hr tests and that was picked as a compromise between being able to let a test run overnight but not tying the equipment up for weeks, such as a 100 hr test would do.

We have found that most of the commercial alloys on the market passed both the 100 hr and the 20 hr test. The 100 hr was 95 pct and the other 110 pct of unnotched tensile.

From the Floor: In the rupture test, the selection of stress for a particular alloy is quite critical. If the stress is too low you may not run into the failure and if it is too high you may run into too much failure with fairly low hydrogen contents.

Chairman Dean: We are very reluctant to have to bring this discussion to a close. There are many questions which Dr. Jaffe has piled up before him and which I know that we are not going to get to. However, I am now going to ask Dr. Jaffe to summarize the highpoints of the discussion.

L. Jaffe: Well, one of the points that came out is that at present most of the use of titanium seems to be in the form of sheets but the tendency during the next year or two is going to be towards more and more forgings and eventually even castings and powder metallurgical products.

Scrap use was mentioned several times and apparently that is a problem on which the manufacturers are making progress.

On the properties, there was some interest in elastic modulus and a feeling that it should be worked on even though the improvements that can be expected are small. Similarly, high strength heat treatable material is coming into the picture and will be widely used in a year or so.

There was also much interest in the question of homogeneity and uniformity. There was a comment at the beginning that this was no longer a problem and there certainly seemed to be no doubt that there had been a lot of improvement but that there is still some trouble in this respect.

One possible field of application that apparently has not been gone into deeply is that of chemical products —where corrosion resistance rather than strength-weight ratio—is of prime importance.

In that connection there was one point well worth repeating—the question of titanium in nitric acid. Apparently some people have used it in one way or another and gotten away with it. Other people have had explosions.

Price was mentioned briefly and it might bear repeating that it doesn't look like titanium is going to be competitive pricewise with stainless steel.

There was also some argument on the question of impurities. Apparently we are not yet out of the woods on the interstitial elements. Possibly other impurity elements should also be considered. Magnesium was mentioned as one to be thought of further.

Oxygen apparently is getting under control although it seems there is still some question as to the role of oxygen, particularly when it comes to different forging or heat treating processes. Apparently if the oxygen were lower we would have less grief. I gather that good material is very low in oxygen. Also, I have a suspicion that not all of the material available is very good in that respect. Of course, it is much better than it was a few years ago.

Hydrogen seems to be the hottest question at the moment; and though discussion has been going on for some time, I presume that this question is one that could be argued for several more days if we had the time to devote to it. It looks as though there are a great many unsolved questions. There are various notched-tensile tests available and other methods but then these do not seem to solve the problem of just how much you can tolerate. I assume that this will be further discussed when we have another meeting at some future date.

Chairman Dean: Thank you, Dr. Jaffe. Gentlemen, the Titanium Committee under the leadership of Harry Jackson, has arranged and is responsible for this affair today and we hope that the information presented both this morning and this afternoon will be useful to all of you.

On behalf of the committee and the AIME, I would like to thank all of you for your participation and again to express our regrets in not having been able to answer all of the questions which you submitted. Also, our thanks to our panelists who have given of their time and knowledge.

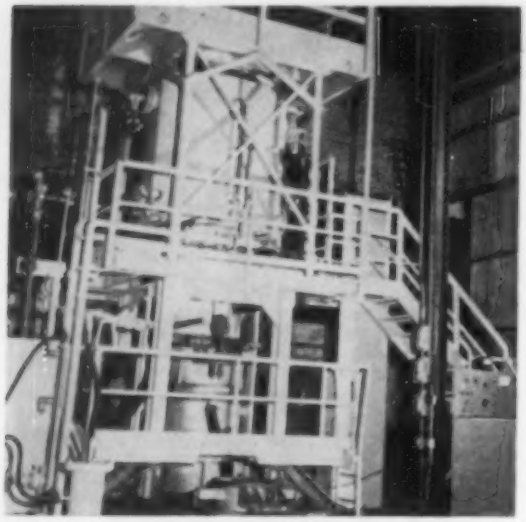

TMCA's 24 in. diam consumable electrode vacuum arc melting furnace has a capacity of 4000 lb. All ingots are double melted in vacuum to insure homogeneity.

Hydrogen Affects Critical Properties In Commercial Titanium

by H. D. Kessler, R. G. Sherman and J. F. Sullivan

HYDROGEN in titanium and titanium alloys has been the major headache of the titanium industry and aircraft frame and engine producers during the past year. Hydrogen embrittlement in commercially pure titanium sheet was detected during the forming of the complex aircraft parts; the high-hydrogen material failing in some cases with explosive violence during or soon after the forming operation. Hydrogen was also suspected to be the cause of cracking in alpha-beta alloy parts subjected to long time exposure to stresses within the design limits.

Hydrogen finds its way into titanium and titanium alloys during the preparation of sponge and ingots; from reducing atmospheres in furnaces used during forging, rolling and other hot forming operations; and from descaling baths and pickling solutions.

An understanding of the effect of hydrogen on titanium metal has been considerably aided by a knowledge of the phase relationships.[1-3] Fig. 1 shows the titanium-hydrogen equilibrium diagram and summarizes the work of McQuillan, who determined the high temperature portion of the system, and the work at Battelle, where the lower solubility curve of hydrogen in alpha titanium was determined. Because of the large decrease in solubility from about 8 atomic pct (0.18 wt pct) at 300°C (572°F) to 0.1 atomic pct (0.002 wt pct) at room temperature, even small amounts of hydrogen have a great effect on mechanical properties of titanium.

The following results are from the work at Battelle Memorial Institute:

A—The hydride phase precipitates from the alpha solid solution as plates at slow cooling rates and is a fine dispersion upon quenching as shown in Fig. 2.

B—The effect of hydrogen on mechanical properties of alpha-titanium including high purity iodide titanium, commercial titanium, and alpha alloys is to decrease the notch toughness without effecting tensile properties.

C—Variations in strain rate show no deleterious effect until higher hydrogen contents are reached.

D—The detrimental effects of hydrogen on notched toughness can be alleviated by vacuum annealing to remove hydrogen or by quenching through the precipitation range. The latter case gives a finely dispersed structure with enhanced toughness. Room temperature aging causes a subsequent decay in toughness and, therefore, heat treatment cannot be considered as a remedy for the detrimental effects of hydrogen.

E—The presence of iron as an impurity in commercial titanium stabilizes a small amount of retained beta phase to room temperature. Because hydrogen has a high solubility in beta, the room temperature solubility of hydrogen in commercial titanium is higher than in high purity titanium. This effect does not apparently eliminate the detrimental effects of hydrogen on notched toughness, perhaps because of embrittlement of the beta phase.

Considerable work has been done during the past year by the air frame manufacturers and the titanium producers to establish the maximum amount of hydrogen which can be tolerated in commercially pure titanium sheet. Various types of mechanical tests have been evaluated in an effort to obtain a fast procedure for determining the acceptability of titanium sheet. Bend tests, cupping tests, tensile tests (at various strain rates), notch tensile tests at low temperatures and other tests have been and are being investigated. The results to date point to the fact that a maximum of 0.015 pct hydrogen can be tolerated in commercial titanium sheet to be used in severely formed or critically stressed parts.

Fig. 3 shows the results of low temperature notch tensile tests as compared to low temperature standard tensile tests. The use of the low temperature notch tensile test to evaluate hydrogen in titanium was developed at the Douglas Aircraft Co. These

H. D. KESSLER and R. G. SHERMAN are Supervisor and Research Metallurgist, respectively, Metallurgical Div., Titanium Metals Corp. of America, Henderson, Nev. J. F. SULLIVAN is Metallurgist, Allegheny Ludlum Steel Corp., Watervliet, N. Y. This paper was presented at the AIME Institute of Metals Div. meeting, Chicago, Nov. 1 to 3, 1954.

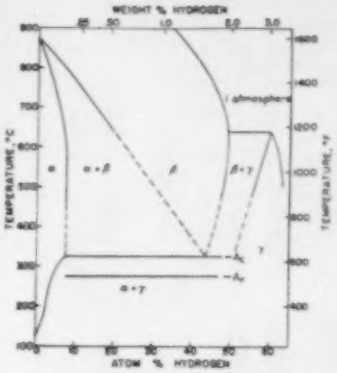

Fig. 1—Titanium-hydrogen equilibrium diagram summarizes the work of McQuillan[5,6,7,8] and Lenning et al.[4]

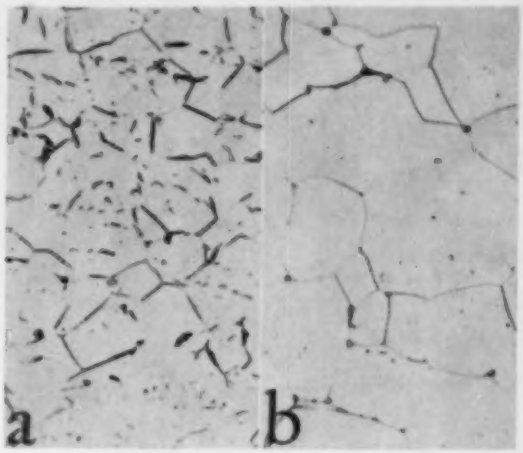

Fig. 2—Micrographs of commercially pure titanium at 750X are shown: a—prior to vacuum degassing and containing 0.046 pct hydrogen, and b—after vacuum degassing containing 0.005 pct hydrogen showing disappearance of hydride plates.

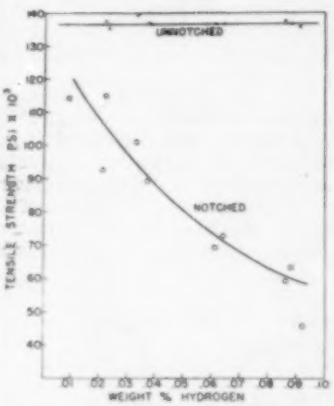

Fig. 3—Notched vs unnotched tensile test results at —65°F were run on hydrogenated commercially pure titanium, Ti-75A.

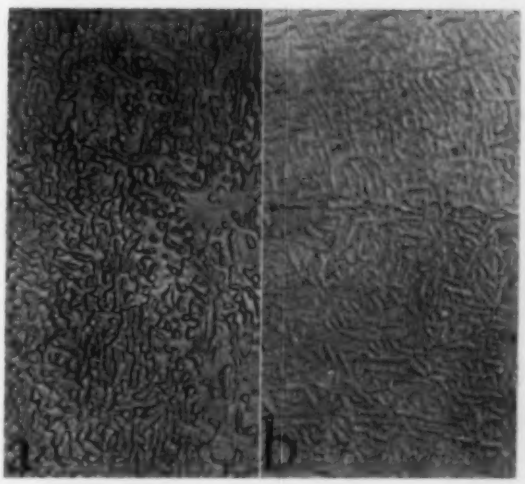

Fig. 4—Micrographs of Ti-150A at 750X show: a—0.030 pct hydrogen content, and b—0.012 pct hydrogen after vacuum degassing. No phase other than alpha and beta is present in these samples.

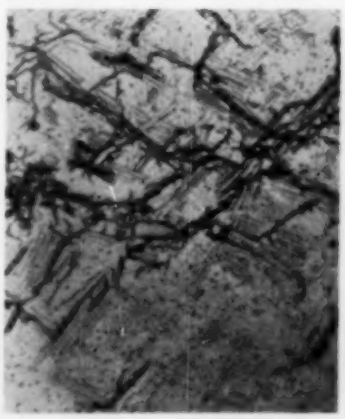

Fig. 5—Micrograph at 500X of alpha-beta alloy with 0.042 pct hydrogen shows network of dark etching phase.

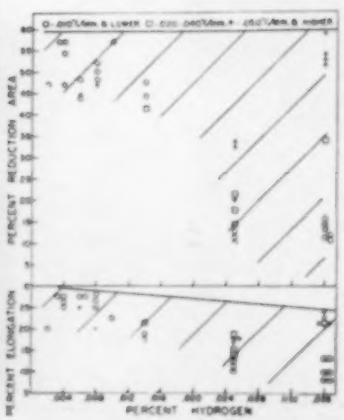

Fig. 6—Hydrogen content and strain rate effects are shown on the tensile ductility of Ti-140A.

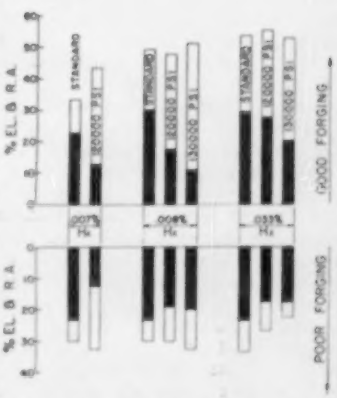

Fig. 7—Effect of hydrogen content and prior static loading for 5 hr are shown on the tensile ductility of Ti-140A.

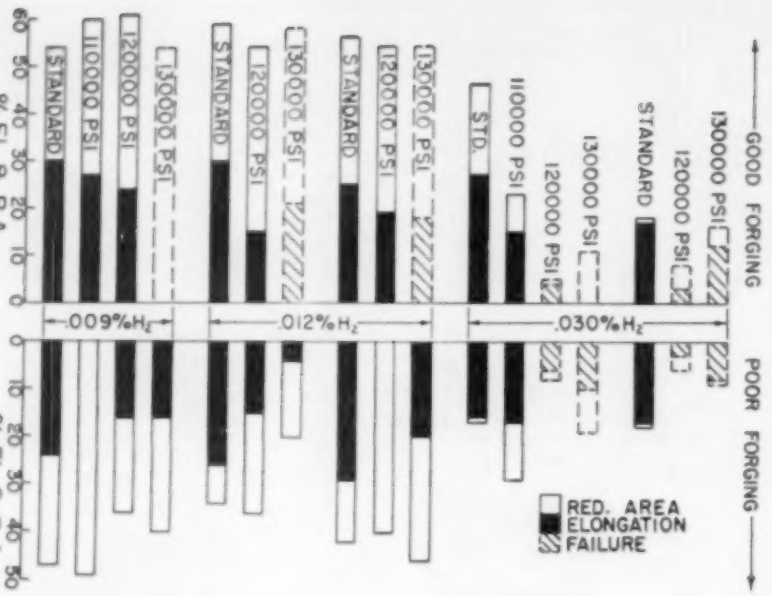

Fig. 8—Effect of hydrogen content and prior static loading for 5 hr at various stress levels is shown on the tensile ductility of Ti-150A.

results definitely substantiate the work at Battelle which indicated that hydrogen increased the notch sensitivity of titanium. Room temperature notch tensile tests also show a reduction in strength with increasing hydrogen content; however, the spread of values between standard and notch tensile tests is not as great as obtained at lower temperatures. Although the low temperature notch tensile test provides interesting information, it is a complex test and is probably no more useful than the bend, cupping or other tests which have been and are in the process of being developed. Actually, with the available knowledge on the effect of hydrogen on commercially pure titanium, these tests are no more than substitutes for hydrogen analyses. Where analytical facilities are available, it is recommended that the hydrogen extraction method[9] be used.

Alpha-Beta Alloys

The fact that the phase relationships of hydrogen in alpha-beta alloys have not been developed, and that intermediate phases involving hydrogen are not always present in the high hydrogen compositions as in the simple titanium hydrogen system, has rendered more difficult the understanding of the effect of hydrogen on the properties of alpha-beta alloys. The latter point is illustrated in Figs. 4 and 5. Fig. 4 compares the structures of high hydrogen and low hydrogen Ti-150A. It can be seen that despite the fact that the high hydrogen sample failed brittlely during the course of static load tests, no third phase is present. The high and low hydrogen structures appear similar. Fig. 5 is an example of a very high hydrogen alpha-beta alloy in which a third phase is present in the form of a dark etching crack-like appearing structure. When this sample was vacuum annealed, the dark etching phase disappeared. Whether this phase is a simple hydride precipitate or a complex eutectoid involving hydrides has not as yet been determined.

The following discussion summarizes the results of work carried out by the Titanium Metals Corp. in an effort to determine the upper safe limit of hydrogen content in the commercial alloys Ti-140A (2 pct Fe, 2 pct Cr, 2 pct Mo) and Ti-150A (2.7 pct Cr, 1.5 pct Cr). All tests on Ti-140A and Ti-150A were conducted on material which had been given the standard commercial annealing treatment of 24 hr at 1200°F. The results are largely a compilation of data obtained both in the Henderson Research

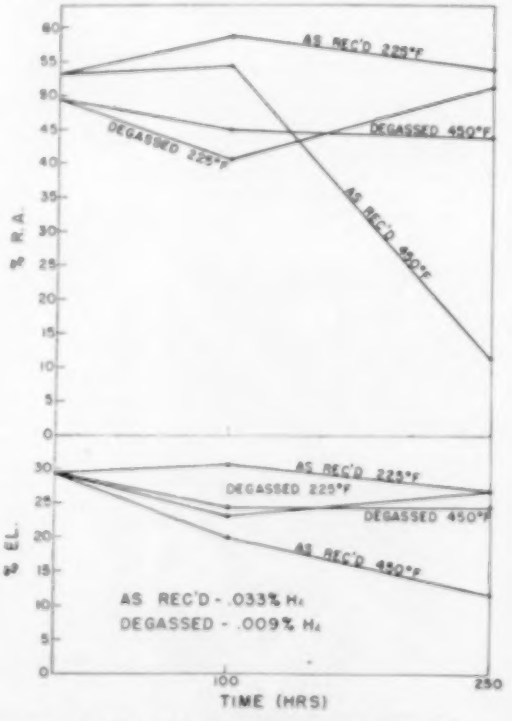

Fig. 9—Aging effect, at a static load of 50,000 psi at various temperatures, is shown on the room temperature tensile ductility of high and low hydrogen Ti-140A.

Laboratories of the TMCA and the Research Laboratories of Allegheny Ludlum Steel Corp.

The effect of hydrogen content and strain rate on the tensile ductility of Ti-140A is illustrated in Fig. 6. The results indicate that with increasing hydrogen content a considerable spread in tensile ductility values occurs. In general, the lower the speed of the test the lower the ductility obtained. These data would indicate the strain rate control becomes more important in the testing of high hydrogen than for low hydrogen material and that tests run at a rate of 0.050 in. per in. per min generally will not show the damaging effect of hydrogen. In general the tensile test is not a reproducibly accurate method of selecting material due to the large spread of ductilities at high hydrogen contents.

Figs. 7 and 8 illustrate the effect of hydrogen content and prior static loading on the tensile ductility of Ti-140A and Ti-150A. These data show that on static loading at or near the yield stress, there is little loss in ductility for Ti-140A at hydrogen contents to 0.033 pct. However, at the 0.03 pct level, considerable loss in ductility is shown by Ti-150A. The effect of forging practice is also illustrated in these figures. Good forging practice implies that at least 50 pct reduction in area was obtained during the last forging cycle after heating at 1600°F. Poor forging practice represents a reduction of 10 pct or less on the last forging cycle after heating at 1750°F. The data indicate that forging practice exerts a considerable influence on tensile ductility regardless of hydrogen content.

It was of interest to this investigation to determine if hydrogen would cause aging and embrittlement of Ti-140A and Ti-150A subjected to high

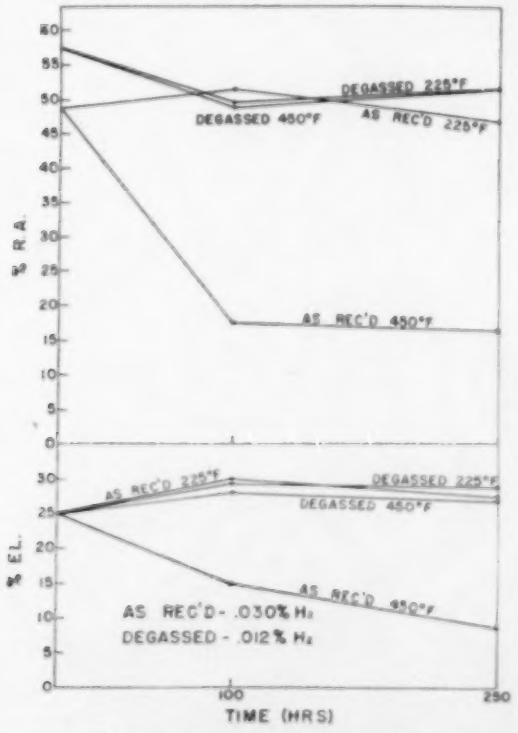

Fig. 10—Effect of aging at a static load of 50,000 psi at various temperatures is shown on the room temperature tensile ductility of high and low hydrogen Ti-150A.

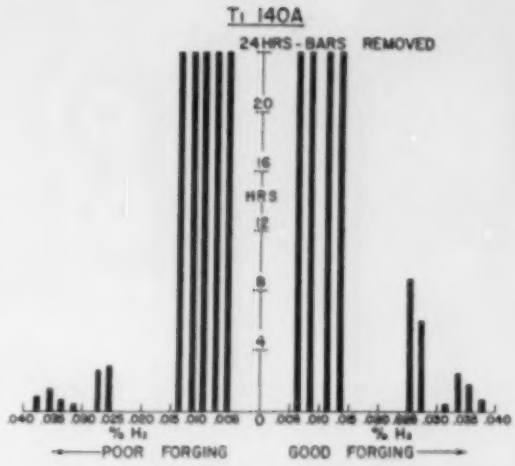

Fig. 11—Effect of hydrogen content on time to failure of notched test bars of Ti-140A statically loaded at 160,000 psi is shown.

stresses at temperatures of 450°F and below. Figs. 9 and 10 illustrate the results. The samples were aged at the temperatures indicated under load in stress-rupture units and were subsequently tensile tested at room temperature. The results for the two alloys are similar and show that little aging occurred at 225°F for either the low or high hydrogen materials. However, at 450°F considerable aging was evident for the as-received hydrogen stock. These results indicate that it is safe to use the two alloys at temperatures to 450°F and at stress levels to 50,000 psi if they are of low hydrogen content.

The aging reaction illustrated by the data in Figs. 9 and 10 should not be confused with the aging process that occurs at higher temperatures. The latter process is attributed to the precipitation of alpha from the unstable beta phase established during the prior annealing treatment.

A static loading test using standard 0.250 in. diam tensile specimens with 60° V-notch with a 0.178 in. root diam and a 0.005 in. notch radius, and stresses higher than the tensile strength determined with unnotched specimens seems to be the best method of detecting hydrogen sensitized alpha-beta alloy material. The general testing procedure was originally suggested by Pratt & Whitney Aircraft. The testing stress of 160,000 psi was selected on the basis of previously run step-loading tests which indicated that acceptable material would not fail in less than 5 hr at this stress level. Actually at this stress level low hydrogen Ti-140A, Ti-150A and Ti-155A have been tested for periods of more than 200 hours without failure. It should be noted that, whereas 160,000 psi is satisfactory for alloys having tensile strengths ranging from 130,000 to 150,000 psi, higher stress levels should be selected to give an acceptable factor of safety for materials having higher strengths. For alloys having strengths of the order of 120,000 psi or less, a lower stress level should be considered.

Figs. 11 and 12 show that with good forging practice alloys containing to 0.015 pct hydrogen invariably passed the test. Although Ti-140A successfully passed the test with even poor forging practice, some failures occurred in the poorly forged Ti-150A alloy at hydrogen contents below 0.015 pct. Based on these results a 0.015 pct hydrogen safe limit has been established for these alloys, with the assump-

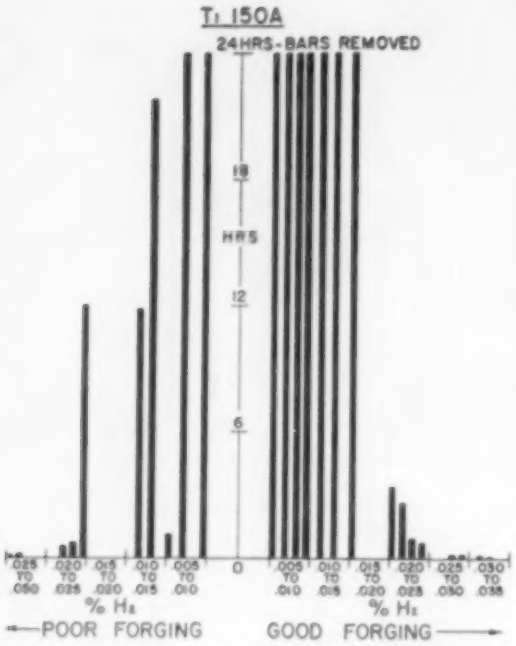

Fig. 12—Hydrogen content and its effect is shown on time to failure of notched test bars of Ti-150A statically loaded at 160,000 psi.

tion that good practice will be used in the hot working operations. These data are only examples of hundreds of tests which have been run on high and low hydrogen heats of the two alloys, and in no instances where the alloys met the required strength specification, did failures occur in material within the acceptable hydrogen range.

No data were given on Ti-155A (5 pct Al, 1.4 pct Fe, 1.4 pct Cr, 1.2 pct Mo) as most heats of this material were produced by the vacuum melting and were, therefore, of low hydrogen content. A few tests run on material which had hydrogen contents of the order of 0.025 pct, made prior to the use of the vacuum melting, indicated that even at this hydrogen level no time-fracture test failures occurred at 160,000 psi. However, one sample failed at 180,000 psi in 17 hr. Whether aluminum additions improved the hydrogen tolerance of titanium alloys or if this alloy simply passed the test because of its higher unnotched tensile strength level (155,000 to 170,000 psi) has not been ascertained. It is presumed, however, that if the stress level for the notch time-fracture test had been raised to perhaps 200,000 psi a definite separation could have been made between high and low hydrogen heats. This assumption is being checked.

Vacuum Degassing

All results point to the fact that hydrogen contents must be kept below the 0.015 pct limit for both commercially pure titanium and for the alloys Ti-140A and Ti-150A. Titanium alloys produced by vacuum melting with proper attention to mill practices including the use of oxidizing atmosphere furnaces for rolling and forging and safe descaling procedures will meet this requirement. To determine whether this high hydrogen material could be recovered, fundamental work[9] and large-scale vacuum degassing experiments[10] were conducted at TMCA on sheet and billet stock up to 8 in. in diam. The results of this work have indicated that hydrogen can be reduced below 0.010 pct in all such material by appropriate vacuum annealing treatment. Commercially pure titanium sheet which has been degassed shows anticipated improvement in properties, which are equivalent to those of the low hydrogen material presently being produced. Heavy bar stock which had been vacuum annealed at temperatures to 1700°F and subsequently upset in compressor wheels has shown very excellent combinations of strength and ductility and passed the 160,000 psi notch-rupture test.

Acknowledgments

The authors wish to thank their many associates at both the Titanium Metals Corp. and the Allegheny Ludlum Steel Corp. for their assistance in obtaining the data presented in this paper. They particularly acknowledge the encouragement and technical assistance given by S. A. Herres and thank R. P. Simmons for the permission to use unpublished data on the effect of hydrogen on notch tensile tests. The metallographic work by L. Dudas and the time-fracture tests performed by P. Methé are appreciated. The authors also wish to thank L. Schapiro and J. L. Waisman of the Douglas Aircraft Co. and R. H. Thielemann of Pratt & Whitney Aircraft for their interest and recommendations in connection with this work.

References

[1] R. I. Jaffee and I. E. Campbell: The Effect of Oxygen, Nitrogen and Hydrogen on Iodide Refined Titanium. *Trans.* AIME (1949) **185**, p. 646.

[2] C. M. Craighead, G. A. Lenning, and R. I. Jaffee: The Nature of the Line Markings in Titanium and Alpha Titanium Alloys. *Trans.* AIME (1952) **194**, p. 1317.

[3] F. C. Holden, H. R. Ogden, and R. I. Jaffee: Microstructure and Mechanical Properties of Iodide Titanium. *Trans.* AIME (1953) **5**, p. 238.

[4] G. A. Lenning, C. M. Craighead, and R. I. Jaffee: Constitution and Mechanical Properties of Titanium-Hydrogen Alloys. *Trans.* AIME (1954) **200**, p. 367.

[5] A. D. McQuillan: Titanium-Hydrogen System for Magnesium-Reduced Titanium. *Journal* Institute of Metals (1951) **79**, p. 379.

[6] A. D. McQuillan: Effect of Small Quantities of Hydrogen and Grain Size on the Alpha Beta Transformation of Titanium. *Nature* (1949) **164**, p. 537.

[7] A. D. McQuillan: Application of Hydrogen Equilibrium Pressure Measurements to the Investigation of Titanium Alloy Systems. *Journal* Institute of Metals (1951) **79**, p. 73.

[8] A. D. McQuillan: Experimental and Thermodynamic Investigation of the Hydrogen-Titanium System. *Proc.* Royal Society of London (1951) **A204**, p. 309.

[9] T. R. D. Gibb, Jr. and H. W. Kruschwitz, Jr.: The Titanium-Hydrogen System and Titanium Hydride I. Low Pressure Studies. *Journal* American Chemical Society (1950) **72**, p. 5365.

[10] C. F. P. Bevington, S. L. Martin, and D. H. Mathews: The Absorption of Gases By Titanium and Zirconium. *Proc.* XI International Congress on Pure and Applied Chemistry. p. 3.

[11] L. Kirschfeld and A. Sieverts: Titanium and Hydrogen. *Physikalische Chemie* (1929) **145**, Sec. A, p. 227.

[12] R. K. Young and D. W. Cleaves: Determination of Hydrogen in Titanium Metal by Hot Extraction. Report of Technical Dept., Titanium Metals Corp. of America, Henderson, Nev. (To be published).

[13] D. W. Cleaves and R. K. Young: (Paper to be published).

[14] H. D. Kessler: TMCA Hydrogen Extraction Experience. Unpublished TMCA report (September 1954).

General Physical Metallurgy of Titanium Reviewed

Serious physical metallurgy of titanium started about 1948. Viewed some six years later, there is no question but that the progress made has been tremendous. Because a short review cannot hope to summarize all of the excellent work accomplished, stress has been placed on the general principles of titanium physical metallurgy developed so far.

by Robert I. Jaffee

TITANIUM metallurgists have had to contend with a number of so-called gaseous contaminants in the starting material, these being oxygen, nitrogen, carbon, and hydrogen. In an attempt to improve mechanical properties, they have added a number of alloying additions. Those considered desirable enough to be put into commercial alloys are aluminum, tin, molybdenum, vanadium, manganese, chromium, and iron. It is possible that other commercially desirable alloying elements will emerge from alloy-development studies, but it must be conceded that the main alloying elements have been selected by now.

There are two major breakdowns in classifying the alloying elements. These are based on: A—whether or not the alloying elements are between the titanium atoms (interstitial) or replace titanium atoms (substitutional), and B—whether the alpha phase is entered preferentially (alpha stabilizing) or the beta phase is entered preferentially (beta stabilizing). The beta stabilizing elements generally are classified further, depending on whether or not there is a continuous series of solid solution between the alloying element and beta titanium (beta isomorphous), or the beta phase decomposes eutectoidally (beta eutectoid). The alloying elements fit into this classification, as shown in Fig. 1.

Oxygen, nitrogen, and carbon, the alpha stabilizing interstitials, have, respectively, increasing atom size and decreasing solubility in the alpha solid solution. These elements enter the so-called octahedral holes in the hexagonal close packed alpha lattice, which are the large holes between eight atoms in a close packed structure. The holes in the body-centered cubic structure are smaller than the close packed octahedral holes and do not fit the oxygen, nitrogen, and carbon atoms so well. Thus, the solubilities in beta are much smaller than in alpha. The alpha solubility of oxygen and nitrogen is very high (14.5 pct and about 9 pct, respectively), but the room temperature ductile range extends only to about 0.6 pct and 0.35 pct, and the hot workable range to about 1 pct and 0.5 pct. There is a range of interstitial content in alpha and alpha-beta alloys where enhanced properties are possible. However, because of some disadvantages, which are much more subtle than is popularly imagined, the interstitials currently have become synonymous with a bad word in titanium parlance.

Hydrogen is believed to dissociate and enter solid solution in titanium as protons. They are very small, and apparently enter the tetrahedral holes in the close packed alpha lattice to a limited extent (about 8 atomic pct max). The size fit of the protons in the interstitial holes in the body-centered cubic lattice is much better than in the tetrahedral holes in the hexagonal close-packed lattice. Consequently, the beta solubility of hydrogen is much higher (about 50 atomic pct). Hydrogen, therefore, is beta stabilizing. The tendency for hydrogen to form a hydride is still very strong. In alpha, the solubility decreased from a maximum of 8 atomic pct at 325°C to as low as 0.1 atomic pct at 125°C and below. The beta phase decomposes eutectoidally at 260°C on cooling, and the decomposition of beta to alpha and hydride cannot be suppressed (unless there is another beta stabilizer present).

Aluminum resembles oxygen and nitrogen in some respects. Like them, only part of the alpha-solubility range is ductile or hot workable, and, like them, it strongly elevates the transformation range. The chief differences are that a larger percentage of aluminum's alpha range is ductile, and the alpha + beta field is much more narrow. There is some thought that the limited alpha-ductile field with those elements is the result of a change in ionization, zone formation, or a shift to a less metallic bond.

There is some question as to whether tin can properly be called alpha stabilizing. Tin does not change the transformation temperatures much, and, at the limiting solubility of about 20 pct, the transformation temperature range is about the same as for pure titanium. Some workers believe that the soluble range terminates in a peritectoid reaction between alpha and beta, forming Ti_3Sn. This would make tin alpha stabilizing. Other workers have evidence for a beta-eutectoid reaction forming alpha and Ti_3Sn. In any event, it is apparent that tin has a high and substantially equal solubility in alpha and beta and little effect on the transformation

R. I. JAFFEE is Supervisor, Non-Ferrous Physical Metallurgy, Battelle Memorial Institute, Columbus, Ohio. This paper was presented at the AIME Institute of Metals Div. meeting, Chicago, Nov. 1 to 3, 1954.

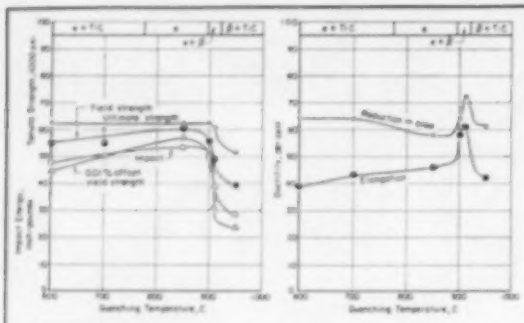

In the Ti-0.27C alloy, quenching from above 910°C, in the beta-plus-carbide field, will result in considerable softening.[1]

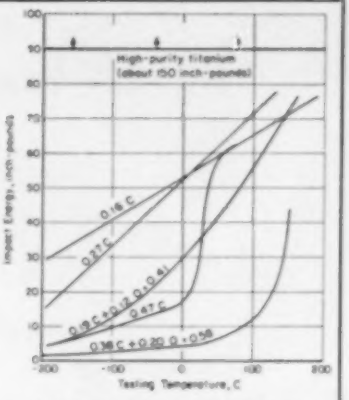

Effect of testing temperature on titanium containing various levels of interstitial elements in solid solution.[3] Alloys are in the 850°C annealed condition.

Comparison of substitutional and interstitial solutions with respect to strength, ductility, and toughness is shown.[4]

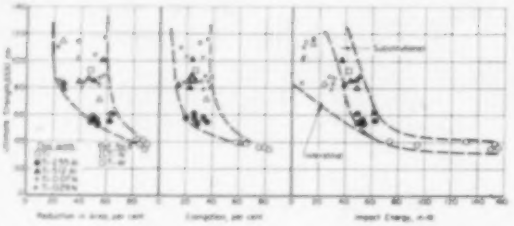

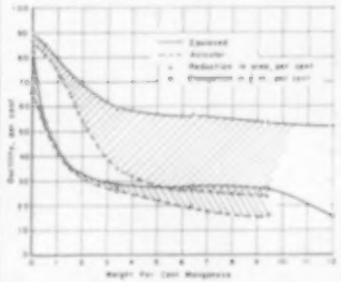

Tensile ductility for alpha-beta alloys in the equiaxed and acicular conditions are compared for Ti-Mn alloys.[5]

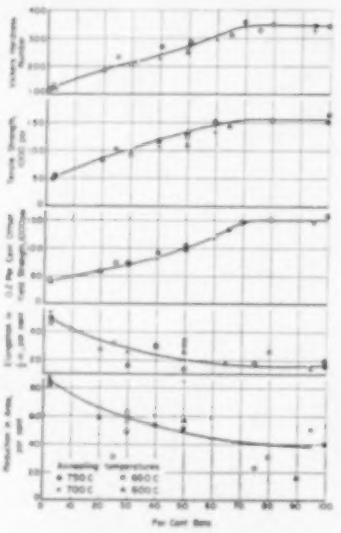

Tensile properties of Ti-Mn alloys annealed at given temperatures are correlated with retained beta content.

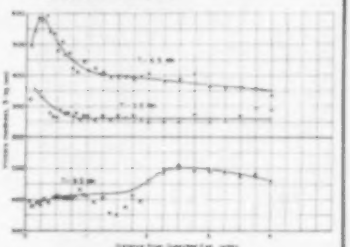

Hardenability curves are shown for Ti-Mn alloys (¾ in. diam bars, end quenched from 900°C).

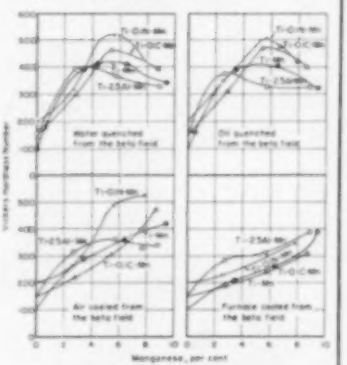
Water quenched from the beta field
Oil quenched from the beta field
Air cooled from the beta field
Furnace cooled from the beta field
Manganese, per cent

Effect of cooling rate is shown on the Vickers hardness of Ti-Mn alloys annealed in the beta field.[6]

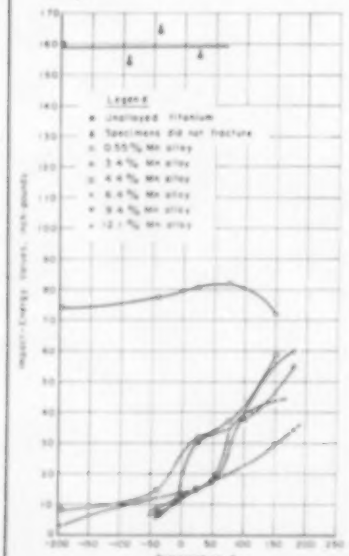

Effect of testing temperature on impact-energy values is shown for Ti-Mn alloys annealed 1 hr at 750°C and water quenched.[6]

Effect of quantity and composition of the beta phase are shown on the age hardening of Ti-Mn alloys at 400°C.[7]

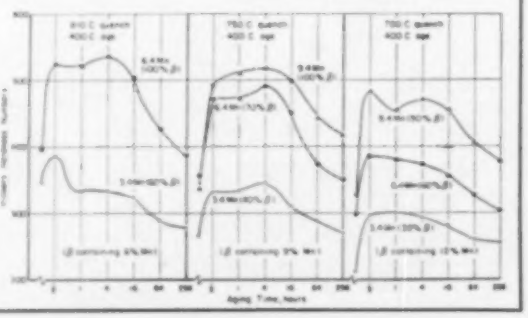

range. Also, the entire alpha range is ductile and workable. Perhaps, instead of either alpha or beta stabilizing, some new term should be invented to describe elements like tin, which have extensive solubility and appear to be equally at home in either alpha or beta titanium. They might be called neutral solutes.

Despite the much higher tin contents that can be worked, aluminum has a higher specific strengthening effect, and there is not much difference in the combinations of properties possible with the two. Aluminum and tin can be effectively used in conjunction with each other, because quite large amounts of tin can be added to a titanium-aluminum alloy without adversely affecting fabricability.

Of the beta-isomorphous beta-stabilizing elements, molybdenum and vanadium are of greatest interest because they are more strengthening than either columbium or tantalum. The beta phase, stabilized by molybdenum or vanadium, is not particularly strong, but is very ductile and easily stabilized. The amounts of these elements to retain beta after quenching (to bring M_s to room temperature) are 11 pct for molybdenum and 16 pct for vanadium.

Beta-Eutectoid Reactions

The beta-eutectoid reaction takes place more readily if it occurs at a lower alloy content or a higher eutectoid temperature. This is, of course, tantamount to saying that the diffusion process necessary to bring the beta phase of an alloy to the eutectoid composition occurs more easily if the composition difference is small and the temperature is high. The compositions and temperatures of the eutectoid reactions are given in Table I. The manganese beta eutectoid has the highest alloy content and the lowest temperature. It is so sluggish that it has never been observed. The eutectoid reaction had to be determined by extrapolation of the beta-phase-field boundaries. The chromium and iron eutectoids are sluggish, but may be observed at high alloy contents or when interstitial contamination is high, or under conditions of stress at elevated temperature. The eutectoid reactions in nickel and cobalt are more active, but probably not so active as the copper eutectoid, where beta is not seen at room temperature because martensite is formed if eutectoid products are not.

Thermal stability in beta-stabilized alloys is a major problem. There is some thought that the beta-isomorphous beta-stabilizing elements have an advantage because the product of beta instability is alpha phase, basically a ductile phase. The beta phase stabilized by beta-eutectoid elements ultimately can decompose to compound, which would be more brittle than alpha. So far as thermal stability is concerned, the very sluggish and the very active beta eutectoids would have the advantage. In the first case, the eutectoid would be too sluggish to proceed to compound. In the latter case, the eutectoid decomposition would occur before the alloy would be put into elevated-temperature service. Another expedient to avoid compound formation is to combine relatively active beta eutectoids so as to lower the beta-eutectoid temperature, and to increase the alloy content of the eutectoid if possible. Thus, iron plus chromium would have an advantage in thermal stability over iron or chromium alone.

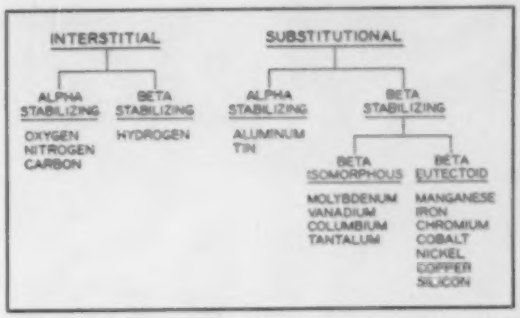

Fig. 1—Classification of titanium alloying elements demonstrates the two major divisions. The beta-eutectoid elements are listed in order of increasing activity of the eutectoid reaction.

The beta phases stabilized by the beta-eutectoid elements tend to be stronger but less ductile than the betas stabilized by the beta-isomorphous elements. Thus, for the strongest alpha-beta or beta alloys in the annealed condition, contents of manganese, iron, or chromium are desirable.

The Alloying Base

Titanium alloys, despite all their desirable qualities, can, under sometimes inexplicable sets of circumstances, exhibit weak and brittle characteristics. At such times, it is well to turn to the alloying base, pure titanium, for reassurance. It is really a remarkable material, which, except for strength, has ductility and toughness properties that are unsurpassed in structural materials. The strength level of 35,000 to 40,000 psi ultimate and 15,000 to 25,000 psi yield really is not bad; it compares favorably with all other pure metals. Pure titanium is notch tough at temperatures approaching absolute zero. It has a reduction in area, notched or unnotched, of 70 to 90 pct; it has 60 to 70 pct elongation (35 to 40 pct uniform), over 200 ft-lb Charpy at −196°C, is weld ductile, and can be cold rolled indefinitely without cracking. Pure titanium points up the task of alloy development—simply to increase the strength with minimum sacrifice in ductility and toughness. The task is formidable when one realizes that in many cases a fivefold increase in strength is desired.

There are minor decreases in strength properties as grain size increases, but it can be said that the mechanical properties of pure titanium are practically independent of grain size and shape or of heat treatment of any sort. Increased strain rate has a beneficial effect on pure titanium, increasing the flow stress and energy absorption without decreasing ductility.

Hydrogen contamination can reduce the excellent

Table I. Beta-Eutectoid Reactions Arranged in Order of Increasing Activity*

Element	Eutectoid Composition, Wt Pct	Eutectoid Temperature, °C	Alloy Content to Retain Beta After Quenching, Wt Pct
Manganese	20	550	6.5
Iron	15	600	4
Chromium	19	675	8
Cobalt[5]	9	685	7
Nickel	7	770	8
Copper	7	790	13[5]
Silicon	0.9	860	—

* Except where noted by a reference, data were taken from *Constitution of Titanium Alloy Systems*, by Hansen, McPherson, and Rostoker, WADC Technical Report 53-41, February 1953.

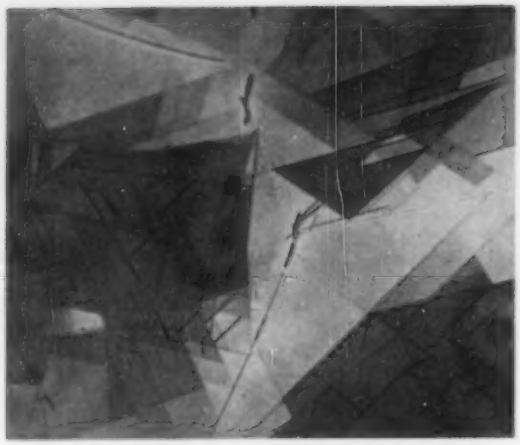

Fig. 2—Micrograph of an unstable beta alloy magnified 250X shows massive alpha rejected as plates and also rejected at the beta grain boundaries after low temperature aging.

ductility of pure titanium. Hydrogen, in conjunction with the presence of a notch and decreased temperature, can destroy the superb toughness of the metal. In unnotched slow-speed tension at room temperature, about 30 atomic pct hydrogen is required to make pure titanium brittle. In notched tensile-impact tests at room temperature, 2 atomic pct hydrogen results in brittleness, while at —40°C, only 1 atomic pct hydrogen is required. In notch-bend impact, serious reduction in toughness is found with 0.5 atomic pct (100 ppm). Hydrogen tolerance is strongly dependent on the conditions of testing.

Alpha-Stabilized Alloys

The tensile strength, ductility, and hardness of the alpha alloys, whether interstitially or substitutionally strengthened, are improved by fine grain size. Since transformation structures are basically large-grained alpha, beta transformation is somewhat detrimental to strength and ductility. The notch-bend impact properties of alpha alloys are relatively structure insensitive, but generally improve slightly with increasing grain size.

The lack of response of alpha alloys to beta-quenching heat treatment is the result of the absence of supersaturation in the quenched condition. The high-temperature equilibrium composition is the same as that below the transformation range. It is usually possible to find a set of conditions whereby alpha alloys may be softened rather than hardened by beta transformation. In Ti-C alloys, quenching from above 910°C, in the beta-plus-carbide field, will result in considerable softening. Alpha alloys generally can be softened somewhat if they are quenched from the alpha-plus-beta field at sufficiently high temperature so that the matrix is beta of lower alloy content. This is particularly true with respect to flow stress.

Alpha alloys generally are weld ductile, as might be expected since the as-welded condition is an extreme case of beta transformation. The only limitation on the ductility of welded alpha alloys appears to be the result of freezing segregation. The weld-ductile alloy contents for the interstitials are somewhat less than the ductile ranges of interstitials in wrought alloys. Ti-C alloys are particularly affected because of carbide-network formation.

The thermal stability of alpha alloys is excellent, since the alpha phase is the equilibrium phase at any presently conceivable service temperature.

In considering interstitial versus substitutional alpha solutes, it is not generally realized that so far as strength and ductility relationships are concerned, the interstitial solutes are as good and may be superior to substitutional solutes. When both substitutional and interstitial solutes are present, strengths higher than are possible with either may be obtained. The real reason for the disfavor in which interstitial solutes are held is increased notch sensitivity. This factor outweighs effects of increased strain rate. In fact, the data available indicate interstitial alpha alloys are more ductile at impact than at slow speed.

There are other indications of strain aging caused by the interstitials in alpha titanium. Both Ti-N and Ti-C alloys exhibit clear yield points when annealed in the alpha field. Ti-O alloys in the alpha-annealed condition, while not exhibiting an upper and lower yield point, have a sharp yield and a flat stress-strain relationship past the yield. Beta annealing eliminates the yield and changes the clear-alpha structure into one in which subgrain markings are evident.

The advantage of substitutional alpha solutes, like aluminum, is their notch insensitivity. For the same unnotched tensile properties, a Ti-N interstitial alloy may have a notch ductility about half that of a Ti-Al alloy. The question that needs deciding in any particular case is whether the improved tensile properties possible with combinations of substitutional and interstitial solutes are worth the worsened notch sensitivity.

Hydrogen embrittlement of alpha alloys reflects itself more in decreased notch toughness than in decreased tensile ductility. However, both properties are adversely affected, the embrittlement becoming greater at low temperature or increased strain rate. When hydrogen is present, the strain-aging effect noted previously is masked. Instead of ductility being better at impact speed, it becomes poorer.

The effect of temperature on notch-bend energy absorption of alpha alloys is very dependent upon the nature of the alpha solute. High-purity titanium or alpha titanium alloys with only a substitutional solute, such as aluminum, have energy absorptions which are relatively independent of testing temperature from room temperature to —196°C. When interstitial alpha solutes are present, notch-bend impact absorption values at the lower temperatures suffer.

Beta-Stabilized Alloys

Beta-stabilized alloys are being considered here as alloys with some untransformed beta phase present as a result of an intentional alloying addition. There is a gradual transition in alloy type and characteristics as the amount and alloy content of beta phase increases, traversing from alpha-matrix alpha-beta, to beta-matrix alpha-beta, to unstable (or metastable) beta, to practically stable beta, to stable beta. The alloy type may be modified somewhat through heat treatment, as in the case of alloys which are unstable betas after quenching from the beta field and which are alpha-beta alloys with a beta matrix if worked or annealed in the alpha-beta field. This is the case for the 8 pct Mn alloy, C-110M, for example. The practically stable beta alloys are those beta alloys which are so stable that they are safe to use in a service-temperature range, but which transform partially if they are heated be-

tween this service-temperature range and the beta-transus temperature. Truly stable beta alloys are those alloys which are so rich in beta-isomorphous alloy content that the alpha-plus-beta field is below room temperature. No known titanium-base alloy meets this requirement.

In alpha-beta alloys, the matrix shifts from alpha to beta at about 30 pct beta. At about 70 pct beta, strength values level off because of the dominating effect of the beta-phase matrix.

Generally, the beta phase in an alpha-beta alloy is considerably stronger than the alpha phase. This is especially true for alloys in which there is no intentional alpha-phase enrichment, as by aluminum or oxygen. The beta phase will be very ductile as well as strong if its interstitial content is kept low. The beta phase has a low tolerance for interstitials, and becomes easily embrittled at relatively low interstitial contents. The interstitials, oxygen and nitrogen, are strongly alpha stabilizing and, in an alpha-beta alloy, partition to the alpha phase, leaving the beta phase free of interstitials. One of the chief functions of the alpha phase in alpha-beta alloys is to absorb the interstitial content. It can be demonstrated that superior combinations of tensile strength and ductility are possible with controlled interstitial additions to alpha-beta alloys. However, the interstitials increase notch sensitivity, particularly at low temperature, and are in disfavor as intentional additions for this reason.

The partition of interstitials to the alpha phase which is so useful in alpha-beta alloys is of little advantage in unstable-beta alloys. Widmanstätten or grain-boundary alpha rejection from an all-beta alloy is embrittling because the interstitial content in the small amount of alpha present is so high that the alpha becomes essentially brittle internal plates and grain-boundary inclusions. Fig. 2 shows a striking structure, illustrating undesirable massive alpha rejection in an unstable-beta alloy containing 7.5 pct Mo and 7.5 pct Cr. The alloy had been cooled from 1000°C to slightly below the beta transus. Massive alpha had been rejected along the beta grain boundaries and as Widmanstätten plates. In this condition, the alloy was very notch brittle, although the all-beta structure was notch ductile. After low-temperature aging at 400°C, the areas bounded by the alpha plates aged to different degrees as a result of the redistribution of alloy content during massive alpha rejection.

The fine-grained equiaxed alpha-beta condition resulting from working and annealing in the alpha-beta field appears to be the optimum condition for alpha-beta alloys. The best ductility and toughness are generally found when the equiaxed alpha-beta condition is kept as fine as possible. Large losses in tensile ductility are found with transformed-beta structures. The loss in tensile ductility is seen to be chiefly for the reduction-in-area values. This suggests that the capacity for localized deformation is less in the acicular condition, and that the alpha plates act like internal notches. In notch-tensile tests, the reduction-in-area values for the equiaxed and acicular conditions are much closer.

Fig. 3 shows the effect of water quenching Ti-Mn alloys from the beta field. The hardness increases rapidly up to about 5 pct Mn, after which it drops sharply for the sheet and more gradually for the rod until, at about 9 pct, the two hardness curves coincide. Martensite structures are found in both cases up through 5 pct Mn; at 6.4 pct Mn, the structure is

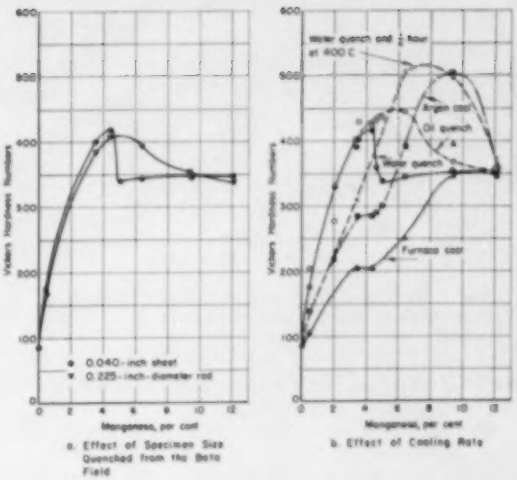

a. Effect of Specimen Size Quenched from the Beta Field

b. Effect of Cooling Rate

Fig. 3—Specimen size and cooling rate effects are shown on the hardness of beta-annealed Ti-Mn alloys.[5]

clear retained beta. The higher hardness caused by the slower cooling rate in the rod is the result of some sort of preprecipitation-hardening process. The beta, which is harder than it should be, has been variously termed beta prime, hard beta, or coherency-hardened beta. Decreasing the cooling rate, as shown on the right in Fig. 3, has the effect of shifting the curves to higher alloy content. Thus, the 9 pct Mn alloy, which had a soft retained-beta structure after water quenching, became hard and brittle after argon cooling (simulated air cooling). Jominy end-quench data[5] confirm these indications. In the martensite range up to 5 pct Mn, the hardness is greatest at the end of the bar. Above 6 pct Mn, there is a hardness peak at a depth which increases as the alloy content increases.

Alpha enrichment of alpha-beta alloys by substitutional or interstitial solutes has important effects on the formation of beta prime. The extent of coherency hardening (magnitude of the quench-hardening peak) is increased by the interstitials, while the addition of aluminum lowers the peak and shifts it to lower alloy content. This would indicate that interstitials increase and aluminum decreases the extent of beta decomposition during the quench. Thus, the addition of aluminum would appear to be beneficial in restricting formation of beta prime, while the presence of interstitials, decreased rates of cooling, or increased section size favor its formation.

Thermal Stability

The maintenance of thermal stability is of prime importance in alpha-beta alloys intended for elevated-temperature service. Thermal stability is considered here to be the ability of a material to remain unchanged in physical structure and mechanical properties after exposure to the intended service conditions of time, temperature, and stress. Heat treatments to attain thermal stability are generally to heat the alloy at 1100° to 1200°F for times ranging from a few hours to as long as 24 to 36 hr. Since most presently contemplated service temperatures are from 400° to 1000°F, and it is not possible to attain equilibrium below about 1100°F, perfect thermal stability is a goal that never can be attained. However, practical thermal stability can be attained

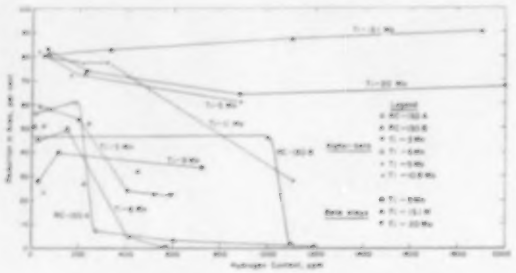

Fig. 4—Data on ductility in slow tension of a group of beta-stabilized titanium alloys containing hydrogen are shown.[7]

for long times at service temperatures for many of the alloys.

Although heating at 1100° to 1200°F may attain thermal stability, it will not necessarily restore ductility to a brittle alpha-beta alloy. To accomplish the task of restoring ductility, it is necessary to heat treat at temperatures in the so-called equilibrating range from 1200° to 1500°F or above. This is followed by reattainment of lower temperature equilibrium and stabilization of the alloy at 1100° to 1200°F. The equilibrated and stabilized alloy is in the softest and generally most ductile condition. Useful heat treatments have been developed which involve quenching from the equilibrating range followed by aging at 750° to 1000°F. The aging response depends primarily upon the amount of unstable-beta phase present. In a given alloy, this can be increased by raising the equilibration temperature. For a given equilibration temperature, the aging response can be increased by increasing the beta-stabilizing alloy content (e.g., the amount of beta). The aging of unstable-beta phase will reject alpha and enrich the beta sufficiently that practical thermal stability often can be achieved at a considerably higher strength level.

The hardening of beta-stabilized alloys as a result of cooling from the beta field is the basic cause of weld embrittlement in these alloys. Another contributing cause is freezing segregation. There are two possibilities for increased hardness resulting from beta transformation: martensite formation at the lower alloy content, and beta prime or fine alpha formation at higher alloy contents. There also are two alloy ranges where weld-ductile beta may be found. The first is low in alloy content, generally less than 3 pct beta-stabilizer content, where the hardening caused by martensite formation is not sufficient to make the quenched alloy brittle. The second is in the high-alloy range, if the formation of beta prime or fine alpha is restricted by sluggish beta transformation kinetics. This latter type of weld-ductile alloys is more difficult to achieve because of the variable cooling rates found in welding heavy sections or the complex heating cycles in multipass welds. The alpha-beta alloys which are brittle in the as-welded condition generally can be made ductile to a considerable extent by the equilibration and stabilizing heat treatments.

The beta phase in alpha-beta alloys is body-centered cubic and has the low-temperature-embrittlement characteristic of metals without close-packed crystal structures. Low-temperature embrittlement of beta phase depends upon the conditions of testing and the nature of the beta phase. Beta phase stabilized with molybdenum, for example, will be much more ductile at low temperature than that which is stabilized by manganese. As in all metals susceptible to ductile-brittle transition, the embrittlement temperature can be raised by the presence of notches. The low-temperature embrittlement is primarily the result of increased notch sensitivity, which increases with the amount of beta phase present.

Hydrogen Embrittlement

Hydrogen can embrittle alpha-beta alloys as well as alpha alloys, but the conditions under which embrittlement occurs are different from those of alpha alloys. For example, the decrease in notch-bend impact properties caused by hydrogen is small compared to the decrease in tensile ductility. In some cases, the embrittlement in tension occurs abruptly over a narrow range of hydrogen contents. In other cases, increased hydrogen content causes a progressive decrease in tensile ductility. It also is possible to hydrogen embrittle alpha-beta alloys in notch-rupture tests at room temperature. The susceptibility of titanium alloys to room-temperature creep at strength levels close to the yield point suggests that considerable strain is involved here too. Considerably higher hydrogen tolerances can be achieved in alpha-beta alloys through selection of alloy content and condition. Molybdenum beta-stabilized alloys have higher hydrogen tolerances than manganese and Fe-Cr alloys, for example. The addition of alpha-stabilizing aluminum to alpha-beta alloys also appears beneficial with respect to increasing hydrogen tolerance. The presence of alpha-beta interfaces seems to be part of the embrittlement process. Fig. 4 suggests intrinsically high hydrogen tolerances in the all-beta condition.

The mechanism through which hydrogen embrittles alpha-beta alloys under conditions of slow strain appears to be some sort of strain-aging reaction occurring at the alpha-beta interface. As the testing temperature decreases, less hydrogen appears to be required to cause embrittlement, although some data have been reported that ductility is restored at still lower temperatures, practically, the problem may be viewed in terms of the effect of hydrogen on a ductile-brittle transition in slow tension. Besides promoting brittleness in alpha-beta alloys at low temperatures by a strain-aging process, hydrogen apparently impairs thermal stability at elevated temperature. This is an additional reason for concern about hydrogen contamination in such alloys.

References

[1] F. L. Orrell, Jr. and M. G. Fontana: The Titanium-Cobalt System. *Trans.* ASM (1954) **47**.

[2] Unpublished data from Contract DA-33-019-ORD-1397.

[3] H. R. Ogden, R. I. Jaffee, and F. C. Holden: Structure and Properties of Ti-C Alloys. *Trans.* AIME (1955) **203**, p. 73.

[4] R. I. Jaffee, F. C. Holden, and H. R. Ogden: Mechanical Properties of Alpha Titanium as Affected by Structure and Composition. *Trans.* AIME (1954) **200**, p. 1282.

[5] F. C. Holden, H. R. Ogden, and R. I. Jaffee: Heat Treatment, Structure, and Mechanical Properties of Ti-Mn Alloys. *Trans.* AIME (1954) **200**, p. 169.

[6] H. R. Ogden, F. C. Holden, and R. I. Jaffee: Effect of Alpha Solutes on the Heat-Treatment Response of Ti-Mn Alloys. *Trans.* AIME (1955) **203**, p. 105.

[7] C. M. Craighead, G. A. Lenning, and R. I. Jaffee: Hydrogen Embrittlement of Beta-Stabilized Titanium Alloys. (submitted to AIME for publication).

Oxygen Solubility and Oxide Phases in the Fe-Cr-O System

by D. C. Hilty, W. D. Forgeng, and R. L. Folkman

The solubility of oxygen in molten Fe-Cr alloys has been determined at 1550°, 1600°, and 1650°C for alloys containing up to about 50 pct Cr and found to decrease as chromium increases to 6 pct and then to increase gradually. Phase relations in the Fe-Cr-O system at steelmaking temperatures have been evaluated and two previously unreported oxides have been identified.

OPERATIONS in the melting and refining of chromium steels are dependent to a major degree on the reactions of chromium and iron with oxygen and are primarily directed toward controlling and modifying these reactions to secure maximum advantage in the utilization of chromium. Although fairly effective practices have been developed empirically, understanding of the specific reactions is limited. Moreover, the ability of molten steel to dissolve oxygen that subsequently precipitates as oxide inclusions during solidification is well known, so that clarification of the effect of chromium on the nature and mechanism of formation of these inclusions is desirable.

Study of the problem indicated that increased knowledge of the fundamental Fe-Cr-O system is essential to further technical and economic improvement. Consequently, an investigation of the influence of chromium on the solubility of oxygen in molten iron and of phases and phase relations in the Fe-Cr-O system was undertaken at the Metals Research Laboratories of the Electro Metallurgical Co. as part of a general program on the effective utilization of chromium in chromium steel production.

Experimental Procedure

All of the experimental runs made during this investigation were carried out in the rotating crucible induction furnace which has been described in detail in a previous publication.[1] In review, the principle underlying this furnace is that rotational forces in the crucible cause the molten metal to assume a concave shape in such a manner that the slag is contained in the molten metal cup, thereby minimizing slag/crucible contact and subsequent reaction.

Practically all of the heats were melted in commercial-quality magnesia crucibles of the type usually furnished for laboratory induction furnaces. All of the runs were made under an argon atmosphere after the furnace chamber had been degassed. Bath temperatures were controlled by Pt—Pt-10 pct Rh thermocouples.

The basic furnace charge consisted of a premelted 12 to 15 lb electrolytic iron slug which had been cast to a shape convenient for fitting into the rotating furnace crucible. A typical analysis of the electrolytic iron slugs is given in Table I.

For certain runs, it was desirable to melt down charges containing high initial chromium contents. In these cases the chromium was added to the electrolytic iron during the premelting operations. Chromium was added to the rotating furnace bath in the form of electrolytic chromium of the analysis given in Table II.

In all of the constant temperature runs, the standard procedure was to melt down the electrolytic iron or alloy slug under vacuum, admit argon to slightly greater than atmospheric pressure, and adjust rotational speed to develop a well formed "cup" on the bath surface. The melt was then saturated with oxygen by an addition of ferric oxide and the temperature of the bath adjusted to within ±5°C of the desired level. At this point the heat was permitted to come to equilibrium prior to sampling or further addition. This time interval was varied from 15 min to 2 hr but generally was about 20 min. After sampling, the desired chromium addition was made and the bath again equilibrated prior to subsequent sampling. This cycle of addition and sampling continued for the duration of the run which lasted from 4 to 8 hr. At the end of this period, power was shut off and the bath allowed to solidify in the furnace.

Quenched metal samples were taken from the equilibrated melts by means of the "Taylor sampler" which has been described by Taylor and Chipman.[2] Before being submitted to chemical analysis, all samples were carefully examined for surface slag occlusions and cold shuts. Later in the study, each sample was radiographed and examined metallographically in cross-section to determine the presence of internal defects. On the basis of these examinations, sound and apparently clean specimens were selected from the Taylor samples for chemical analysis.

D. C. HILTY, Member AIME, and W. D. FORGENG are Technical Adviser and Chief Metallographer, Metals Research Laboratories, respectively, and R. L. FOLKMAN, Junior Member AIME, is Metallurgist, Technical Service and Development Laboratories, Electro Metallurgical Co., Niagara Falls, N. Y.

Discussion on this paper, TP 3959C, may be sent, 2 copies, to AIME by Apr. 1, 1955. Manuscript, Sept. 30, 1954. Chicago Meeting, February 1955.

The Transactions papers appearing in the Journal of Metals during 1955 will subsequently appear in AIME Transactions Volume 203, and may be permanently referenced to that volume.

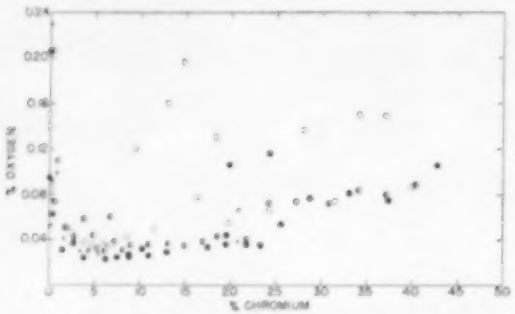

Fig. 1—Plot of isothermal data. Open circle is 1650°C; half-closed circle, 1600°C; closed circle, 1550°C; and X, 1600°C, chromite crucible.

Slag sampling proved quite difficult because of the low slag volume usually encountered and also because the slag was generally present as a dry frangible film on the surface of the liquid metal cup. Samples were obtained by lowering a clean cold steel rod (about ¼ in. diam) into the furnace through the sampling hole until it just touched the bath surface. Generally, a small amount of slag collected and adhered to the tip of the rod. The sample was then withdrawn and either cooled in the stream of incoming argon at the top of the furnace chamber or quenched in water.

Chromium analyses were made on chips machined from the complete cross-section of the Taylor samples. The standard analytical procedure of oxidation and potentiometric titration was used for chromium and gave results reproducible within ±0.01 pct Cr in the low chromium range and up to ±0.20 pct Cr in the high chromium range. Analyses for oxygen were made by the conventional vacuum fusion technique which gives results reproducible within ±0.001 pct O. After preparation of the metal samples as described previously, the vacuum fusion samples were electropolished in a 10 pct perchloric-acetic acid solution and deep etched in 50 pct HCl to eliminate all traces of rust or scale, washed with water, acetone, and ether, and then stored in a dessicator to await analysis.

Results of Constant Temperature Experiments

In efforts to determine the solubility of oxygen in molten Fe-Cr alloys at 1550°, 1600°, and 1650°C, series of isothermal runs were made at these temperatures. The results of these tests are shown in Fig. 1. Because of the excessive scatter of the data, no curves have been drawn. Moreover, the best attempts to evaluate and fit curves to the data resulted in an apparent solubility inversion demonstrated by the fact that the 1650°C isotherm tended to overlap the 1600°C isotherm in the lower chromium ranges. Since such an anomaly seemed quite unlikely in a system of this type, several tests were made to prove or disprove its existence. Because of the excessive scatter of the results, however, these tests were inconclusive.

Table I. Analysis of Electrolytic Iron Slugs

Element	Pct
Carbon	0.002
Manganese	0.0008
Phosphorus	0.0012
Sulphur	0.010
Silicon	<0.001
Aluminum (soluble)	0.0008
Aluminum (insoluble)	0.0005
Copper	Trace
Nickel	Trace

One of the isothermal runs was made at 1600°C in a chromite crucible. The choice of this crucible was based on the findings of Chen and Chipman[3] who considered that chromite is the stable solid phase in equilibrium with melts containing less than 5.5 pct Cr. As shown in Fig. 1, these data were not significantly different from those obtained in magnesia crucibles. For this reason and because of spalling difficulties encountered, the use of chromite crucibles was discontinued.

In a search for the cause of the inconsistencies in the data, consideration was given to the possibility of sample contamination which might have led to some of the apparently anomalous results. In this respect, several samples were reanalyzed for oxygen contents and Taylor samples examined metallographically in cross-section to determine the presence of gross contamination. In most instances, chemical reanalyses verified original results and metallographic examination of the Taylor samples revealed nothing but the normal dispersion of primary nonmetallic inclusions with no evidence of gross oxide contamination. However, when these data are compared with those obtained by Wentrup and Knapp,[4] Linchevskij and Samarin,[5] and Chen and Chipman, it is interesting to note that the solubility results of these authors are not only of the same order of magnitude, but also exhibit the same degree of scatter.

At this point in the investigation, efforts to rationalize the foregoing results were directed to an examination of all of the oxide phases encountered in these tests.

Oxide Phases

For purposes of calculation, it is commonly assumed that the oxide phases in equilibrium with molten Fe-Cr alloys are chromite ($FeO \cdot Cr_2O_3$) and Cr_2O_3. A review of the literature, however, indicates that some investigators have considered this assumption inadequate to explain their observations and strongly suspect that other oxides of chromium may be involved. Since $FeO \cdot Cr_2O_3$ and Cr_2O_3 are the most stable oxides of iron and chromium at low temperatures, direct observation of other possible phases has been difficult and their existence and specific identities have been largely a matter of speculation and inference.

In rationalizing his observations of the relation between carbon and chromium in molten iron under oxidizing conditions, Hilty[6] suggested CrO as the oxide phase involved on the basis that the equation

$$CrO_{(in\ slag)} + C_{(in\ metal)} = Cr_{(in\ metal)} + CO_{(gas)}$$

fit the observations quite well without complications regarding the thermodynamic activities of carbon and chromium in the relatively dilute solution. Subsequently, Dennis and Richardson[7] disagreed and presented calculations purporting to show that Hilty's results could be predicted from the activities of chromium and carbon and the assumption of Cr_2O_3 as the stable oxide.

Chen and Chipman summarized their observations with the statement that at 1595°C chromite was the stable phase in equilibrium with melts containing less than 5.5 pct Cr and at higher chromium concentrations in the metal Cr_2O_3 became the stable phase. Sims, Saller, and Boulger[8] reviewed Chen and Chipman's observations and attempted to explain their

oxygen solubility results by assuming a homogeneous metal phase containing CrO. They suggested that chromite and Cr_2O_3 inclusions observed to contain islands of metal could form by the precipitation and disproportionation of "dissolved" CrO. Zapffe[5] also discussed the possible formation of Cr_2O_3 by disproportionation of CrO. Linchevskij and Samarin[6] recognized only chromite and Cr_2O_3 as the solid phases in equilibrium with the metal, but postulated that at chromium concentrations above 16 pct in the metal CrO is formed as an entity dissolved in the metal, though not existing as a separate phase—a hypothesis that seems of doubtful tenability.

A fairly comprehensive investigation of nonmetallic phases in the Fe-Cr-O system was conducted by Wentrup and Knapp.[7] These authors demonstrated the presence of solid oxide phases other than the well known chromite and Cr_2O_3 inclusions and speculated as to their possible compositions. They concluded, however, that "chromium spinel-$FeO \cdot Cr_2O_3$" is stable even at high chromium contents in the metal and that "pure chromium oxides" are to be expected at chromium contents higher than 30 to 40 pct.

In the present investigation a detailed study of the composition, structure, and properties of the oxide inclusions was undertaken because it was considered that with sufficiently rapid cooling the primary inclusions are representative of the oxide phases in equilibrium with the metal at the time solidification begins. A comparison of the structure of the inclusions in rapidly cooled heats with those in heats cooled at a slower rate also was made to determine how the primary inclusions may be modified by subsequent reactions or transformations.

The characteristics of the inclusions were studied by microscopic examination of polished sections and also by microscopy and X-ray diffraction investigation of the inclusions isolated from the metallic matrix by electrolysis of the samples. Representative sections for metallographic examination were taken from the rapidly cooled Taylor samples and from the slowly cooled ingot at each chromium level. The color, shape, size, and distribution of the inclusions in the polished specimens were noted with ordinary illumination. Polarized light with crossed nicols was then employed to determine the true transmission color as well as the presence and degree of anisotropy of the inclusions.

The inclusions were isolated by electrolytic dissolution of the metal in a 10 pct aqueous solution of hydrochloric acid. The specimen was made the anode in a divided cell constructed from two 500 ml beakers joined by a short tube, 1 cm in diameter, at a point about 2 cm from the bottoms of the beakers.

Table II. Analysis of Electrolytic Chromium

Element	Pct
Manganese	0.039
Sulphur	0.046
Oxygen	0.56
Nitrogen	<0.001
Aluminum	0.002

The beaker forming the anolyte compartment was first filled to a point just below the junction tube with a layer of glycerine. The electrolyte then was carefully floated on the glycerine layer to avoid mixing. The purpose of the glycerine layer was twofold: first, it minimized attack on the inclusions after they were freed from the metal; and it provided a clear colorless collecting medium for subsequent handling when the electrolyte was siphoned off through the catholyte compartment. The cathode was a platinum strip. This divided cell arrangement prevented contamination of the extracted inclusions by electrodeposited metal that did not adhere to the cathode. The inclusions were freed from the glycerine layer by washing repeatedly with water. A portion of the residue was placed on a microscope slide and examined with a petrographic microscope. By this means the true shapes of the inclusions could be studied and their optical properties determined. Another portion of the residue was mounted in a small wedge-shaped holder and X-ray diffraction patterns were taken by the Debye-Sherrer method using unfiltered chromium radiation.

In order to provide further information on the nature of the oxide phases at the various chromium levels, X-ray diffraction patterns of the slag samples from each heat were taken. The slag samples always included some entrapped metal from the heats which was extracted from the crushed slags with a 10 pct solution of bromine in methanol.

In the following discussion of the results obtained by microscopic and X-ray examination, the alloys have been arbitrarily placed in the following categories: 1—low chromium, up to about 3 pct Cr; 2—medium chromium, 3 to about 9 pct Cr; 3—high chromium, 9 to about 25 pct Cr; and 4—very high chromium, over 25 pct Cr.

The inclusions in the low chromium alloys were the usual chromite type as illustrated in Fig. 2. In the rapidly cooled sample, Fig. 2a, the primary inclusions, though quite small, have fairly well defined crystalline outlines. The very small inclusions probably formed by eutectic reaction in spite of the rapid cooling rate. The primary inclusions in the slowly

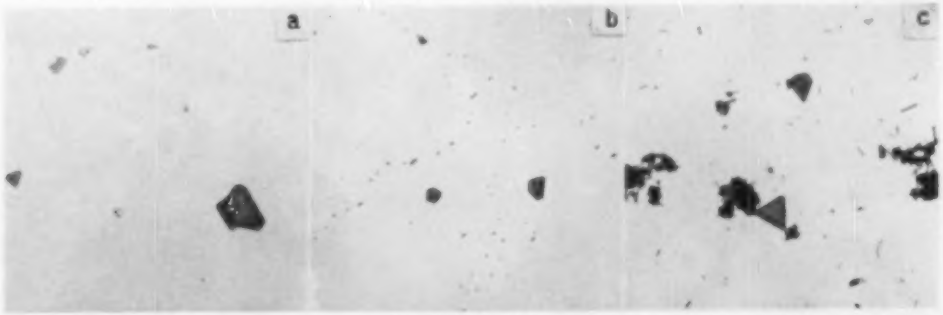

Fig. 2a—Low chromium heat. Chromite inclusions in Taylor sample. X2000.

Fig. 2b—Low chromium heat. Chromite inclusions in slowly cooled ingot. X250.

Fig. 2c—Low chromium heat. Inclusions extracted from slowly cooled ingot. X100.

cooled ingot are larger and have a better developed crystalline outline. The inclusions in Figs. 2a and 2b appear gray with ordinary reflected light and are isotropic and black with crossed nicols, although an occasional deep red internal reflection can be noted. In the micrograph of the inclusions extracted from the slowly cooled ingot, Fig. 2c, the true crystal shapes of the inclusions are quite apparent. These inclusions were red in color and, as expected from their cubic structure, were completely isotropic. An X-ray diffraction pattern of the residue in Fig. 2c showed a simple cubic structure of the spinel type, i.e., $FeO \cdot Cr_2O_3$.

The inclusions in the medium chromium alloys were similar to those shown in Fig. 3. In polished section with ordinary light, Figs. 3a and 3b, and even in the extracted residue, Fig. 3c, they appear identical with those from the low chromium heats. Their optical properties and X-ray patterns, however, are quite different from those of the chromite inclusions found in the low chromium heats. They show a moderate degree of double refraction with reflected polarized light and a cherry-red transmission color. As will be shown later, their X-ray structure is tetragonal with a variable axial ratio and appears to have resulted from a distortion of the cubic spinel structure.

In the high chromium heats, Fig. 4, the primary inclusions are markedly different from either the chromite inclusions of the low chromium alloys or from the distorted spinels of the medium chromium heats. Fig. 4a shows primary crystals both singly and agglomerated into a pseudospherical shape in the rapidly cooled Taylor sample. With ordinary

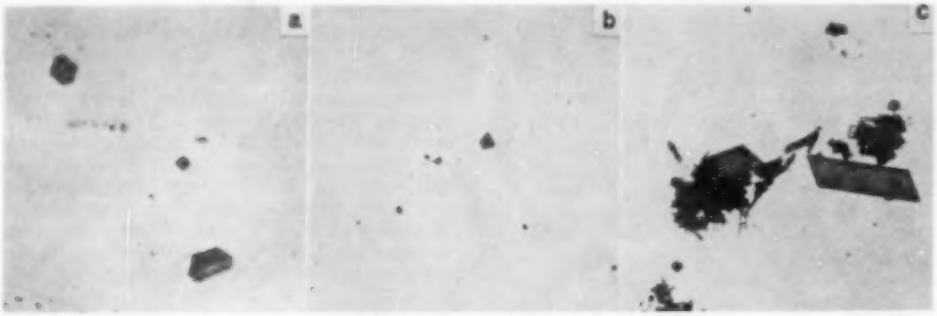

Fig. 3a—Medium chromium heat. Distorted spinel inclusions in Taylor sample. X2000.

Fig. 3b—Medium chromium heat. Distorted spinel inclusions in slowly cooled ingot. X250.

Fig. 3c—Medium chromium heat. Inclusions extracted from slowly cooled ingot. X100.

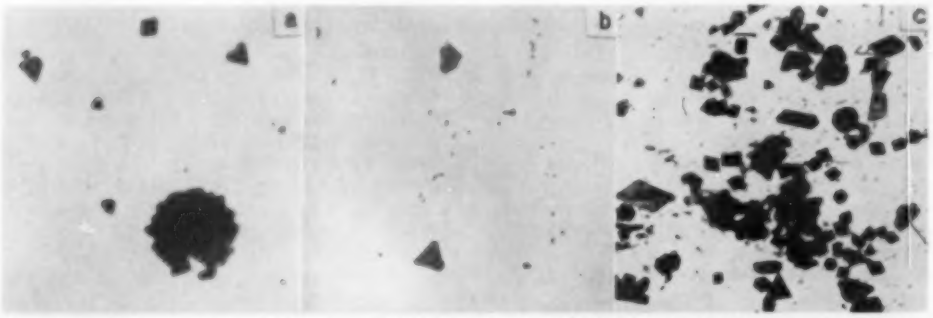

Fig. 4a—High chromium heat. Cr_2O_3 inclusions in Taylor sample. X2000.

Fig. 4b—High chromium heat. Cr_2O_3 and chromite inclusions in slowly cooled ingot. X250.

Fig. 4c—High chromium heat. Inclusions extracted from slowly cooled ingot. X100.

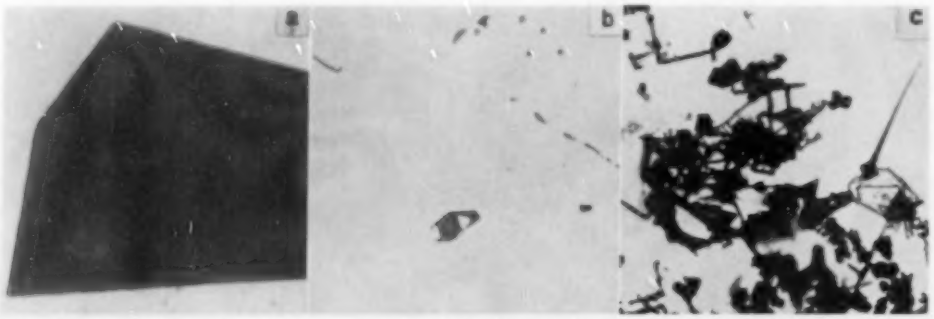

Fig. 5a—Very high chromium heat. Striated Cr_2O_3 inclusion in slowly cooled ingot. X2000.

Fig. 5b—Very high chromium heat. Cr_2O_3 inclusions in slowly cooled ingot. X250.

Fig. 5c—Very high chromium heat. Inclusions extracted from slowly cooled ingot. X100.

light, faint striations may be seen on the surface of some of the larger inclusions, and with crossed nicols the inclusions are very strongly doubly refractive and show prominent banding. In the slowly cooled ingot Fig. 4b, the inclusions are similar but a few small chromite inclusions also can be noted. As will be discussed later, the latter probably resulted from eutectic transformation. A study of the inclusions extracted from the slowly cooled ingot of a high chromium heat, Fig. 4c, reveals a tendency for the inclusions to have elongated shapes. The inclusions vary in color from red to yellow, are strongly anisotropic, and usually show prominent striations or twin markings. The X-ray pattern of these inclusions indicates a tetragonal structure with an almost constant axial ratio, c/a, of 0.88. It will be shown subsequently that a chemical analysis of this phase approximates that of the compound Cr_3O_4 with a small amount of iron substituting for chromium.

At very high chromium contents and even in chromium itself, the Cr_2O_3 phase appears to be the only primary inclusion. Its typical forms in a very high chromium heat are illustrated in Fig. 5. Fig. 5a illustrates a large well developed crystal with noticeable striations at high magnification. Fig. 5b, at lower magnification, shows a primary Cr_2O_3 inclusion with some binary eutectic Cr_3O_4 inclusions as well. The extracted residue from this heat, Fig. 5c, consists of well shaped primary forms and the dendritic branching eutectic.

An outstanding characteristic of the Cr_2O_3 phase is its tendency to disproportionate upon slow cooling or reheating. The reaction apparently proceeds as follows:

$$3\ Cr_2O_3 \rightarrow Cr + 4\ Cr_3O_4$$

This behavior is illustrated in Fig. 6. Fig. 6a shows a typical Cr_2O_3 inclusion in a slowly cooled very high chromium heat. This inclusion was orange-red and highly doubly refractive when viewed with crossed nicols. The inclusion in Fig. 6b is of similar shape but with more irregular outlines and containing small droplets of metal. The ingot in which it occurred was cooled very slowly. With crossed nicols, this inclusion was a vivid green and highly doubly refractive. Both the disproportionated and undisproportionated types of inclusions were present in close proximity in very slowly cooled specimens of high chromium alloys, although the Cr_2O_3 type always predominated. Fig. 6c illustrates the change that takes place when an ingot with a very high chromium content containing only the Cr_2O_3 type inclusions shown in Fig. 6a is reheated to 1400°C for a short time. The inclusions are transformed from the straight-sided angular type of Fig. 6a to the irregularly shaped duplex Cr_3O_4-metal aggregate of Fig. 6c. The extracted inclusions from the reheated ingot are shown in Fig. 6d. Comparison of their shapes with those of inclusions from the as-cast ingot, Fig. 5c, shows a loss of angularity and general coalescence.

Disproportionation of Cr_2O_3 inclusions also takes place in chromium metal itself. Fig. 7a shows a field of Cr_2O_3 inclusions in as-cast chromium metal. These inclusions appeared reddish-orange and anisotropic when examined under polarized light. The duplex oxide-metal inclusion in Fig. 7b occurred in the same specimen. With polarized light the inclusion was green and anisotropic.

The striking difference in appearance that oxide inclusions extracted from Fe-Cr alloys exhibit is shown in the color micrographs of Fig. 8. Fig. 8a is a group of inclusions extracted from a high chromium heat. The large striated, rhomb-shaped, reddish-yellow inclusion is typical of Cr_2O_3. The small dark inclusions are isotropic chromite and the green irregular inclusion is Cr_3O_4. The change in color of the inclusions when the very high chromium ingot was reheated as described previously is illustrated in Figs. 8b and 8c. The inclusions from the as-cast ingot consist mainly of the red and yellow Cr_2O_3 type, Fig. 8b, while those from the heat-treated ingot are entirely the green Cr_3O_4 type, Fig. 8c.

The microscopic studies of the Fe-Cr alloys indicated four oxide phases that could be recognized and differentiated one from the other by their optical

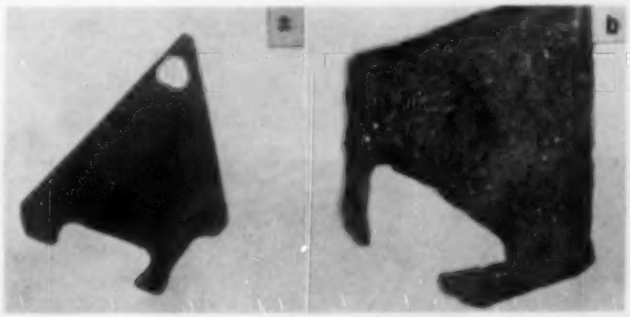

Fig. 6a—Very high chromium heat. Cr_2O_3 inclusion retained in a slowly cooled ingot. X2000.

Fig. 6b—Very high chromium heat. Cr_3O_4-metal aggregate resulting from disproportionation of Cr_2O_3 during ingot solidification. X2000.

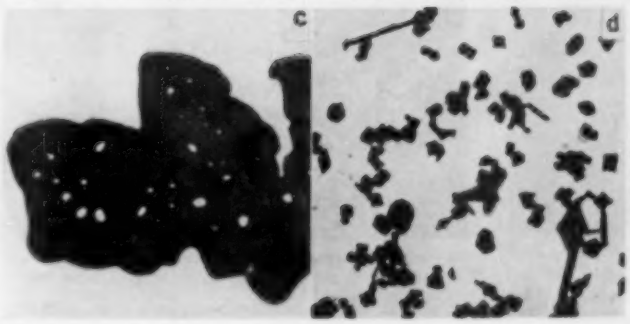

Fig. 6c—Very high chromium heat. Cr_3O_4-metal aggregate resulting from disproportionation of Cr_2O_3 inclusion by reheating ingot to 1400°C. X2000.

Fig. 6d—Very high chromium heat. Inclusions extracted from ingot that was reheated to 1400°C. X100.

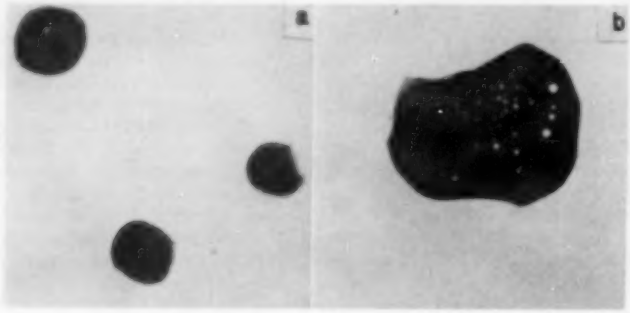

Fig. 7a—As-cast chromium metal. Cr_2O_3 inclusions. X2000.

Fig. 7b—As-cast chromium metal. Cr_2O_3-metal aggregate resulting from disproportionation of Cr_2O_3 inclusion during cooling.

properties. X-ray diffraction patterns of residues extracted from alloys in the various chromium ranges verified the presence of four distinctly different crystalline individuals. These have been tentatively designated as follows:

1—Chromite: a solid solution of Fe_2O_3 in $FeO \cdot Cr_2O_3$, cubic spinel type with an a_o varying with the Fe_2O_3 content of the inclusions from 8.23 to 8.30Å.

2—Distorted spinel: probably intermediate in composition between Cr_2O_3 and $FeO \cdot Cr_2O_3$, a deformed spinel arrangement which can be indexed as a face-centered-tetragonal crystal with the a_o varying from 8.39 to 8.48Å and the axial ratio, c/a, varying from 0.98 to 0.95 as a function of both cooling rate and composition.

3—Cr_2O_3: This compound can also be indexed as face-centered-tetragonal. With a limited amount of iron substituting for some of the chromium, its a_o is 8.64 and its axial ratio, c/a, is 0.88. In the absence of iron, its a_o is 8.72 and its axial ratio, c/a, is 0.86.

4—Cr_2O_3: a solid solution of Fe_2O_3 in rhombohedral Cr_2O_3. The parameters of this phase are very nearly those of the pure oxide, i.e., $a_o = 5.38$, $\alpha = 59°50'$.

The interplanar spacings and relative intensities of the diffraction lines for chromite, distorted spinels with axial ratios of 0.97 and 0.95, Cr_2O_3 with an axial ratio of 0.88, and Cr_2O_3 are listed in Table III.

The relationship among the diffraction patterns of chromite, distorted spinels, and Cr_2O_3 is shown diagrammatically in Fig. 9. It may be noted that, while the reflections from the octahedral planes (111), (222), and (333) of the chromite are relatively unchanged in progressing through the distorted spinels to Cr_2O_3, reflections from other planes are split and change position gradually through the distorted spinel range and then shift position abruptly in going from distorted spinel to Cr_2O_3.

The results of X-ray diffraction studies of inclusions extracted from alloys of various chromium contents slowly cooled in ingot form and as-quenched in a Taylor sampler from 1650°, 1600°, and 1550°C are summarized in Table IV.

The inclusions extracted from one of the high chromium heats containing approximately 42 pct Cr were found by X-ray diffraction to consist almost entirely of the tetragonal Cr_2O_3 phase. In view of the relative absence of other phases, it was felt that a chemical analysis of this residue would give a reliable indication of the composition. The following results were obtained: 63.0 pct Cr, 29.3 pct O (vacuum fusion), 7.25 pct Fe, and a total of 99.55 pct.

Using a weighted average atomic weight for chromium and iron, the phase may be represented adequately by the formula, Cr_2O_3, with limited substitution of iron for chromium. Generally, it has been observed that the chromium to iron ratio for inclusions from alloys in the 40 to 50 pct Cr range is about 9 to 1.

A portion of the residue from the same high chromium ingot was utilized to provide additional information on the thermal stability and the kinetics of the disproportionation reaction of the Cr_2O_3 phase. Small samples of the residue were wrapped in platinum foil and heated in platinum crucibles under an argon atmosphere at different temperatures and for varying lengths of time. X-ray diffraction patterns were taken of the heat-treated residues with the results listed in Table V.

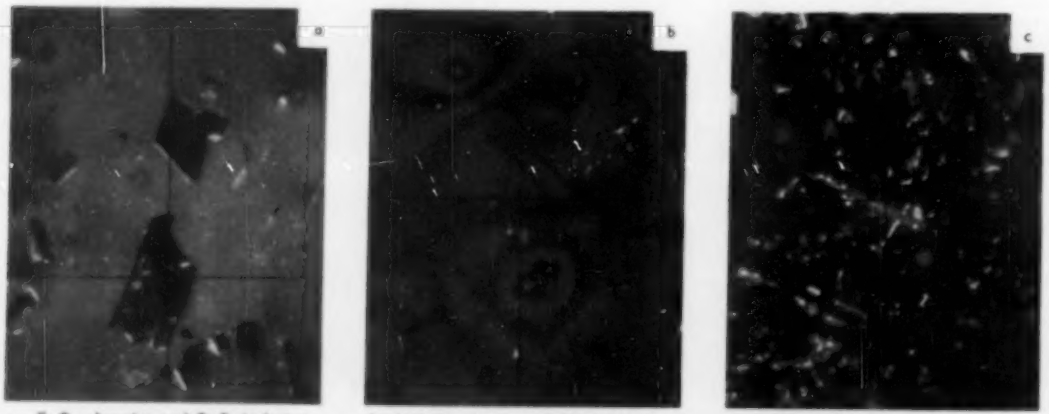

a—Cr_2O_3, chromite, and Cr_2O_3 inclusions from a high chromium ingot.

b—Inclusions from a very high chromium ingot in as-cast condition.

c—Inclusions from same ingot as b after reheating ingot to 1400°C.

Fig. 8—Color micrographs of extracted inclusions; crossed nicols. X250.

Table III. Interplanar Spacings and Relative Intensities of Oxide Phases

Chromite			Distorted Spinel, c/a = 0.97			Distorted Spinel, c/a = 0.95			Cr_2O_3, c/a = 0.88			Cr_2O_3		
d, A	I	(hkl)	d, A	I	(hkl)	d, A	I	(hkl)	d, A	I	(hkl)	d, A	I	hkl, Hexagonal
4.80	3	111	4.82	4	111	4.85	5	111	4.78	4	111	3.6	4	102
2.93	6	220	2.98	4	220	2.99	6	220	3.05	3	220	2.64	10	104
2.50	10	113	2.92	6	202	2.91	8	202	2.86	4	202	2.48	6	110
2.40	1	222	2.52	10	131	2.53	10	131	2.56	10	131	2.17	3	113
2.075	8	400	2.43	5	113	2.44	9	113	2.39	3	222	1.80	3	204
1.695	1	224	2.40	4	222	2.40	2	222	2.34	1	113	1.662	8	116
1.595	9	333 115	2.10	4	400	2.12	7	400	2.16	6	400	1.436	3	124
1.466	10	440	2.03	3	004	2.02	3	004	1.90	2	004	1.422	5	300
1.401	3	135	1.71	2	242	1.72	5	242	1.725	3	242	—	—	—
1.315	1	260	1.68	1	224	1.67	1	224	1.655	9	151	—	—	—
1.268	3	335	1.62	5	151	1.63	7	151	1.590	2	333	—	—	—
—	—	—	1.60	5	333	1.60	4	333	1.535	6	440	—	—	—
—	—	—	1.58	2	115	1.55	6	115	1.432	8	404	—	—	—
—	—	—	1.483	4	440	1.491	8	440	1.348	1	602	—	—	—
—	—	—	1.460	6	404	1.455	10	404	1.287	3	262	—	—	—
—	—	—	1.325	1	260	1.340	1	260	1.280	5	353	—	—	—
—	—	—	1.274	3	353	1.278	7	353	1.217	1	335 206	—	—	—
—	—	—	1.265	1	335	1.254	2	335	—	—	—	—	—	—

It is apparent that upon reheating the Cr_2O_3 phase, disproportionation to Cr_2O_3 and metal (α) occurs even at fairly low temperature, the rate increasing with temperature. The metal was a body-centered-cubic chromium-rich solid solution.

Efforts to reverse the disproportionation reaction at temperatures up to the melting point of the metal proved unsuccessful. Thus, the reaction appears to be irreversible in that the Cr_2O_3 phase forms and is stable above the melting point of the metal and may be retained only in a metastable state at lower temperatures.

Attempts were made to produce massive crystals of the Cr_2O_3 phase for further investigation of the properties of the compound. While no success was achieved in forming such crystals, varying quantities of the Cr_2O_3 phase in mixtures with the other oxides of iron and chromium were synthesized by several methods. Fusion of low carbon ferrochromium in an oxidizing oxy-acetylene flame produced appreciable quantities of Cr_2O_3. Smaller amounts of this phase were formed when 8 to 1 mixtures of Cr_2O_3 and Fe_2O_3 were melted in neutral or reducing oxy-acetylene flames. Similar experiments using an oxidizing flame failed to produce Cr_2O_3. These results suggest that Cr_2O_3 is stable at high temperatures and under conditions of low oxygen pressure.

While the nature of the distorted spinel phase was not studied as extensively as that of the Cr_2O_3 phase, conclusive evidence was obtained that it also disproportionates in a manner similar to that of Cr_2O_3, but with different products. This phenomenon was initially observed when a slag sample, predominantly distorted spinel ($c/a = 0.95$) according to X-ray diffraction, was heated to 1400°C in argon. The resulting constituents were chromite and metal. The disproportionation was confirmed in an ingot section from a medium chromium heat in which the distorted spinel inclusions in the as-cast metal were completely transformed to chromite containing small amounts of Cr_2O_3 and droplets of metal after the specimen had been reheated to 1400°C for 3 hr. The change in appearance of the inclusions closely paralleled that observed for Cr_2O_3 inclusions in very high chromium heats previously illustrated in Fig. 6.

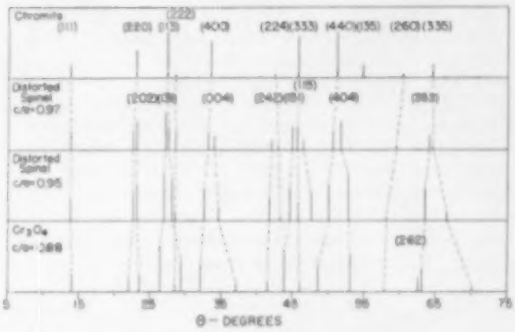

Fig. 9—Comparison of diffraction patterns.

Only limited chemical analyses of the distorted spinel phase were made, and these were not sufficient to establish its complete composition. An oxygen determination by vacuum fusion on a small relatively pure sample of distorted spinel inclusions extracted from an ingot of medium chromium content, however, indicated an oxygen content not greatly different from that of chromite. On the basis of the observations, it is considered that the distorted spinel phase may be a combination of $FeO \cdot Cr_2O_3$ with Cr_2O_3. It has a variable composition range and disproportionates at temperatures below the melting point of the metal into $FeO \cdot Cr_2O_3$ and metastable Cr_2O_3 which is subject to further disproportionation into Cr_2O_3 and metal.

In general, X-ray diffraction examination of the previously mentioned slag samples confirmed the results of the inclusion examination with regard to existence, regions of stability, and disproportionating characteristics of the various oxide phases. In the high chromium regions, however, the ratio of Cr_2O_3 to the other constituents was somewhat higher than

Table IV. X-Ray Diffraction Results

		Low Chromium	Medium Chromium	High Chromium	Very High Chromium
Quenched samples	1650°	Chromite	Distorted spinel	Cr_2O_3	Cr_2O_3
	1600°	Chromite	Distorted spinel	Cr_2O_3	Cr_2O_3
	1550°	Chromite	Distorted spinel	Cr_2O_3	Cr_2O_3
Ingot samples		Chromite	Distorted spinel	Cr_2O_3	Cr_2O_3
			Cr_2O_3 Chromite Cr_2O_3	Cr_2O_3 Chromite	Cr_2O_3 Chromite

Table V. Phases Present after Heat Treatment of Cr_2O_3

Temperature, °C	Time, Min	Phases	
		Major	Minor
500	15	Cr_2O_3	—
700	60	Cr_2O_3	Cr_2O_3, α
700	180	Cr_2O_3	α
800	15	Cr_2O_3	Cr_2O_3, α
900	5	Cr_2O_3	α
900	15	Cr_2O_3	α

would be expected from the inclusion studies. This observation is considered to be a further demonstration that Cr_2O_3 is the stable phase in equilibrium with the liquid metal and at low oxygen pressures. Since the conditions under which the slag samples were cooled were considerably more oxidizing than when the slags were in contact with the bath, the Cr_2O_3 in the slag samples is believed to have resulted both from oxidation of the lower oxides and from disproportionation of Cr_2O_3.

Experimental Constant Chromium Runs

During attempts to clarify the inconsistencies in the constant temperature runs, a constant chromium (0.65 pct Cr) content heat was made in which the heat was equilibrated at temperatures ranging from 1550° to 1650°C in 25° gradations. In this heat, the previous practice of melting the electrolytic iron slug under vacuum, adjusting rotation, admitting argon, and saturating with Fe_2O_3 was followed. The nominal chromium charge was added as electrolytic chromium and the bath equilibrated at the desired temperature. After equilibrium was presumably attained and sampling performed, the temperature was adjusted to the next desired level and held constant for 20 min to 1 hr prior to sampling. This procedure was repeated for all the desired temperature levels. At the end of the run, the remaining melt was allowed to solidify in the crucible under argon.

Table VI. Results of Constant Composition, Varying Temperature Heats Made in Magnesia Crucibles

Run No.	Nominal Chromium Content, Pct	Sample No.	Temperature, °C	Analytical Results		Pct O Adjusted to Nominal Chromium Content
				Pct Cr	Pct O	
CC-1	0.06	1	1647	0.07	0.200	0.215
CC-1		2	1600	0.06	0.170	0.170
CC-1		3	1605	0.06	0.180	0.180
CC-1		4	1549	0.04	0.148	0.123
CC-1		5	1631	0.05	0.210	0.192
CC-2		1	1653	0.06	0.210	0.210
CC-2		3	1556	0.04	0.150	0.122
CC-3	0.65	1	1649	0.79	0.065	0.070
CC-3		2	1633	0.74	0.059	0.062
CC-3		3	1600	0.64	0.051	0.051
CC-3		4	1601	0.64	0.053	0.053
CC-3		5	1573	0.59	0.039	0.037
CC-3		6	1558	0.59	0.039	0.037
CC-3		7	1584	0.57	0.043	0.040
CC-3		8	1623	0.67	0.055	0.055
CC-3		9	1654	0.64	0.067	0.067
CC-4	1.65	2	1604	1.76	0.031	0.031
CC-4		3	1555	1.68	0.023	0.023
CC-4		4	1657	1.44	0.050	0.048
CC-5	3.50	2	1597	3.68	0.032	*
CC-5		3	1554	3.68	0.024	
CC-5		4	1600	3.39	0.033	
CC-5		5	1644	3.38	0.042	
CC-5		6	1698	3.39	0.064	
CC-6	—	2	1576	3.44	0.025	*
CC-6		3	1626	3.35	0.035	
CC-6		4	1678	3.23	0.047	
CC-7	5.35	2	1600	5.38	0.025	*
CC-7		3	1554	5.33	0.018	
CC-7		4	1599	5.33	0.025	
CC-8	8.0	1	1674	8.14	0.042	*
CC-8		2	1629	8.08	0.032	
CC-8		3	1565	7.99	0.021	
CC-9	9.0	2	1608	9.05	0.028	*
CC-9		3	1551	9.05	0.018	
CC-9		4	1600	9.05	0.028	
CC-9		5	1652	8.96	0.039	
CC-10	24.7	1	1651	24.76	0.062	*
CC-10		2	1597	24.58	0.047	
CC-10		3	1548	24.64	0.036	
CC-11	37.0	1	1649	37.08	0.088	*
CC-11		3	1594	36.96	0.067	
CC-11		4	1548	37.10	0.053	

* Oxygen content not adjusted. Variation in chromium content insignificant.

Data obtained from this run did not substantiate the questionable solubility inversion noted in the earlier tests. Moreover, it was found that when the logarithms of the oxygen contents observed were plotted against the reciprocals of the absolute temperatures, straight lines with little scatter of the data were obtained. Therefore, this procedure was repeated for another complete series of runs covering the entire chromium and temperature range previously studied. Runs were made at the following chromium levels: 0.06, 0.65, 1.65, 3.5, 5.35, 8.0, 9.0, 25, and 37 pct.

The variation in chromium content in any one run was small in most instances. However, for the sake of accuracy in evaluating the results, it was believed desirable to correct oxygen contents to the average chromium content within a run in those cases where variation appeared significant. The corrections were estimated from the constant temperature data on the assumption that within limited ranges of chromium content, the slope of the curve on a pct O-pct Cr plot gave a close approximation of the incremental effect of chromium on oxygen concentration. At the lower chromium concentrations, this correction, though small, was important but its relative significance decreased with increasing chromium contents. Because of the proportionally greater constancy of chromium concentrations above 3.5 pct Cr, the correction proved negligible and was ignored. The analytical results for these runs are given in Table VI.

During evaluation of the results from the constant chromium runs, an observation appearing to be of special significance with regard to the scatter of the isothermal data was made. In four of the runs, the oxygen content observed in the first sample taken from the heat was excessively high, differing so greatly from the general oxygen level of the other samples from that heat that it seemed to bear no relation to them, although it was within the scatter of the previous isothermal data. In two of the runs, a sample taken later in the heat gave a similar result.

As in the case of the isothermal experiments, no explanation of these discrepancies was immediately apparent. Repeated oxygen analyses merely confirmed the initial results, while metallographic and radiographic inspection of the samples failed to reveal evidence of sample contamination by foreign enclosures such as entrapped slag or coarse inclusions. Upon thorough review of the logs of the runs however, a definite pattern, clearly relating these anomalous oxygen results to the melting practice, emerged. Without exception, the four runs, in which the first sample taken gave an irregular result for oxygen, were characterized by the fact that following the addition of the required chromium and ferric oxide to the heat after meltdown there was no substantial change in the temperature of the molten bath until after the first sample was taken. On the other hand, in all of the other runs there was a considerable change in bath temperature, either up or down, between the chromium addition and the first sample. Furthermore, in the two cases where sam-

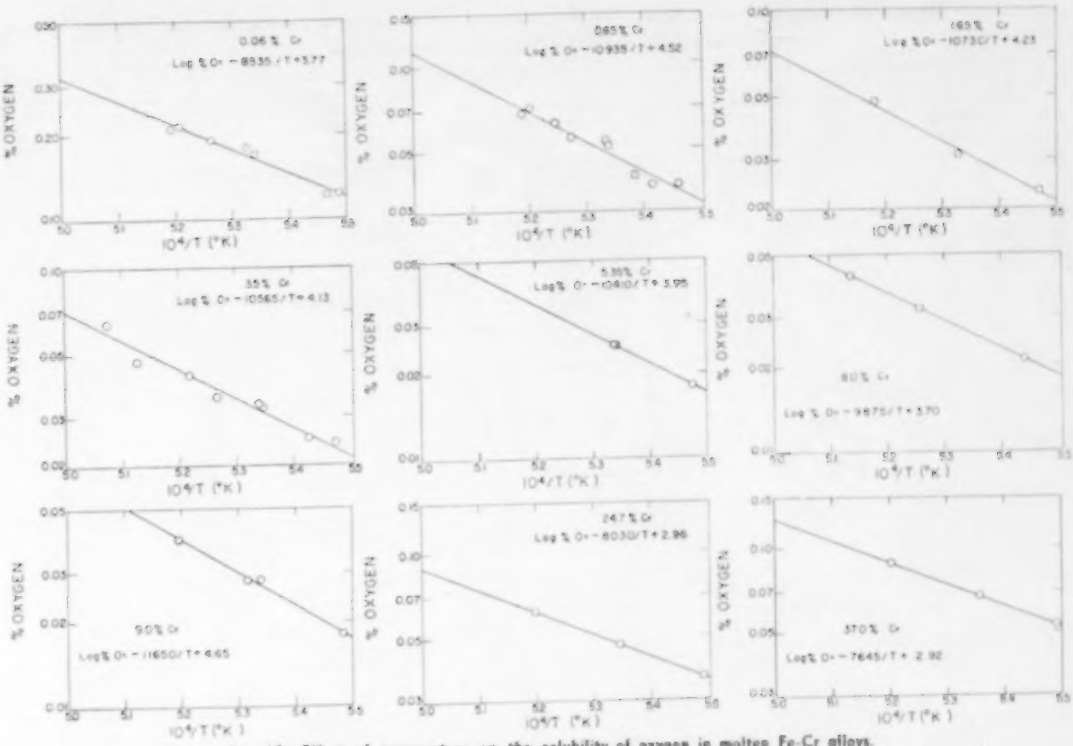

Fig. 10—Effect of temperature on the solubility of oxygen in molten Fe-Cr alloys.

ples taken late in the runs also gave excessively high results for oxygen, both of these samplings were preceded by a small addition of ferric oxide (on the order of 0.02 pct O) 1 to 2 hr before sampling, at the temperature level of the sample, and with no intervening temperature change.

It was concluded, therefore, that the additions induced in the melts an extra-equilibrium condition, analogous to supersaturation, that persisted until the temperature of the bath was changed significantly. Consequently, the results from the samples in question were eliminated from further consideration and are not listed in Table VI.

Although the specific mechanism of this extra-equilibrium effect is not known, the effect itself offers a reasonable explanation of the inconsistency of the original isothermal results. Since the nature of the isothermal runs required additions to the bath between successive samples while the temperature was maintained relatively constant, it is now evident that many of the results must have been influenced by the persistent extra-equilibrium effect. The specific mechanism of the effect, however, and its rather obvious practical implications with regard to the manufacture of chromium steels must be established by further investigation.

Oxygen Solubility

The adjusted oxygen contents of the constant chromium runs listed in Table VI were plotted on a semilogarithmic scale against the reciprocals of the absolute temperatures to give the family of curves shown in Fig. 10. It is apparent that at each chromium level the data are fitted excellently by a straight line from which the deviations of individual points are almost negligibly small.

By interpolation from Fig. 10, it is now possible to construct isotherms for the solubility of oxygen in molten Fe-Cr alloys. When such construction is attempted, however, it becomes immediately evident that the points interpolated from Fig. 10 for a plot of oxygen content vs chromium content at constant temperature cannot be connected by a continuous smooth curve. That is, the isotherms are indicated to contain inflections. Inflections in an oxygen solubility curve of this type are, of course, indicative of changes in the oxide phase in equilibrium with the metal, and in view of the occurrence of the different oxide phases described in the earlier section, such inflections in the curves might be expected in this system.

Although strongly indicating discontinuities in the oxygen solubility curves, the observations listed in Table VI and the curves of Fig. 10 are, of themselves, insufficient to establish the location of the inflections in more than a general way. Therefore, in order to define the limits of the oxide phase regions and thereby locate the inflection points with greater precision, inclusions in the Taylor samples and ingots from the constant chromium runs and in ingots from the isothermal runs were studied critically. These observations are reported in detail in Table VII and are summarized graphically in Fig. 11. On the basis of Table VII and Fig. 11, it appears that the boundary between the distorted spinel and Cr_2O_3 phases can be located with reasonable certainty at a metal composition approximating 9 pct Cr.

Inclusions extracted from the Taylor samples taken from the 9 pct Cr run at approximately 1550°, 1600°, and 1650°C and from the 8 pct Cr run at 1565°C gave extremely diffuse X-ray diffraction patterns that were not specifically identifiable. These results suggest that these samples were very close to the phase boundary, so that effective crystallization of either phase did not occur during the extremely

Table VII. Results of Inclusion Examination

Run	Sample	Temperature, °C	Chromium Content, Pct	Microscopic Observations	X-Ray Diffraction Patterns	Identity of Inclusions (by Microscopy and X-rays)
CC-1	1	1647	0.07	A few small idiomorphic inclusions, deep red to opaque; isotropic. Many small round inclusions both random and in network; gray and opaque.	No X-rays taken	Chromite and wüstite, the chromite being primary.
	2	1605	0.06	Similar to Sample 1, except inclusions very small in size.	No X-rays taken	Chromite and wüstite
	3	1569	0.04	All inclusions extremely small.	No X-rays taken	Too small for positive identification. Probably chromite and wüstite.
	Ingot	—	0.05	Small rod-shaped crystals and small round inclusions containing idiomorphic crystals. All gray, opaque, and isotropic.	FeO-Cr_2O_3, strong	Chromite and chromite-wüstite eutectic.
CC-3	1	1649	0.79	Small idiomorphic crystals, deep red to opaque; isotropic.	No X-rays taken	Chromite
	3	1600	0.64	A few small idiomorphic crystals, deep red to opaque; isotropic. Many extremely small, poorly developed crystals in eutectic distribution; isotropic.	No X-rays taken	Chromite
	6	1558	0.59	All extremely small, poorly developed crystals in eutectic distribution; isotropic.	No X-rays taken	Probably chromite
	Ingot	—	0.64	Large idiomorphic crystals, deep red to opaque; isotropic. Many small crystals in eutectic distribution; mainly opaque.	FeO-Cr_2O_3, very strong	Chromite
CC-4	2	1604	1.76	A few small idiomorphic crystals, red and isotropic. Many extremely small, poorly developed crystals in eutectic distribution; reddish and isotropic.	FeO-Cr_2O_3, strong	Chromite
	3	1555	1.68	Many small, poorly developed, irregular crystals in eutectic arrangement; reddish and isotropic.	FeO-Cr_2O_3, moderately strong	Chromite
	4	1657	1.44	Mostly small, idiomorphic crystals, deep red and isotropic.	FeO-Cr_2O_3, strong	Chromite
	Ingot	—	1.44	Many idiomorphic crystals; few small inclusions in eutectic pattern. All opaque to red, isotropic.	FeO-Cr_2O_3, very strong	Chromite
CC-5	2	1597	3.68	Mostly extremely small, poorly developed, elongated crystals in eutectic arrangement. Quite transparent, red and weakly anisotropic.	Distorted spinel, strong	Distorted spinel
	3	1554	3.60	Similar to Sample 2 above.	Distorted spinel, moderately strong	Distorted spinel
	4	1600	3.39	A few deep red, moderately anisotropic idiomorphic crystals. Many very small, poorly developed crystals in eutectic arrangement, red and weakly anisotropic.	Distorted spinel, strong	Distorted spinel
	5	1644	3.38	Mostly small, idiomorphic crystals, cherry red and weakly anisotropic.	Distorted spinel, strong	Distorted spinel
	Ingot	—	3.5	Many medium-sized idiomorphic crystals. All deep red to cherry red and weakly anisotropic.	Distorted spinel, exceptionally strong and well developed pattern.	Distorted spinel
CC-7	2	1600	5.38	A few idiomorphic crystals, red and weakly anisotropic. Many very small, poorly developed inclusions in eutectic arrangement, various shades of red and weakly anisotropic.	Distorted spinel, fairly strong	Distorted spinel
	3	1554	5.33	Extremely small, rod-shaped inclusions in eutectic arrangement. All weakly anisotropic and ranging from rather light to deep red.	Distorted spinel, weak pattern	Distorted spinel
	4	1589	5.33	Similar to Sample 2 above.	Distorted spinel, strong. Chromite, weak	Distorted spinel. (Chromite probably resulted from disproportionation of distorted spinel.)
	Ingot	—	5.12	A few medium-size idiomorphic crystals, opaque to red and weakly anisotropic. A few small inclusions in eutectic network red and yellow, both anisotropic but the yellow very strongly so.	Distorted spinel, strong and a trace of Cr_2O_3.	Distorted spinel with minor amounts of Cr_2O_3 in eutectic.
CC-8	1	1674	8.14	Mostly small idiomorphic crystals, but a few very small, poorly developed crystals in eutectic arrangement. All red to orange-red and weakly anisotropic.	Distorted spinel, weak and diffuse pattern. Not well developed.	Distorted spinel
	2	1629	8.08	Entirely similar to Sample 1 above.	Distorted spinel, diffuse pattern not well developed.	Distorted spinel

rapid solidification of the samples. Microscopic examination of the few small primary inclusions in the 1600° and 1650°C samples containing 9 pct Cr, however, indicated that those in the 1600°C sample were probably Cr_2O_3, while those in the 1650°C sample were distorted spinel. The inclusions in the 1550°C sample of the 9 pct Cr heat were extremely small and poorly defined, but appeared to have the optical

Table VII. Results of Inclusion Examination—*Continued*

Run	Sample	Temperature, °C	Chromium Content, Pct	Microscopic Observations	X-Ray Diffraction Patterns	Identity of Inclusions (by Microscopy and X-rays)
	3	1565	7.99	Inclusions too small to be resolved at highest magnification used (X2000).	Very diffuse pattern in chromite, distorted spinel, Cr_2O_3 series; unidentifiable.	Not identified
	Ingot	—	7.99	Not many inclusions. All appeared as small irregularly shaped crystals in a network. This sample appeared entirely eutectic in character. Inclusions mostly red and yellow crystals, the red weakly anisotropic and the yellow strongly so. Some small, green, strongly anisotropic and a few red or opaque isotropic particles also present.	Very diffuse pattern not specifically identifiable.	Distorted spinel and Cr_2O_3 with minor amounts of Cr_3O_8 and chromite.
CC-9	2	1608	9.00	A few small idiomorphic crystals, reddish yellow and strongly anisotropic. Many extremely small, irregularly shaped inclusions, yellow and yellowish-red, strongly anisotropic.	Very diffuse pattern belonging to chromite-Cr_2O_3 series, but not specifically identifiable.	Cr_2O_3
	3	1551	9.05	All extremely small, elongated, poorly developed crystals in a eutectic pattern; reddish-yellow and strongly anisotropic.	Very diffuse pattern belonging to chromite-Cr_2O_3 series, but not specifically identifiable.	Cr_2O_3
	4	1600	9.03	Similar to Sample 2 above.	Very diffuse pattern belonging to chromite-Cr_2O_3 series, but not specifically identifiable.	Cr_2O_3
	5	1652	8.96	Numerous very small idiomorphic crystals, cherry to light red and weakly to moderately anisotropic.	Very diffuse pattern, some indication of distorted spinel, but not specifically identifiable.	Distorted spinel
C-6	Ingot	—	9.07	A few idiomorphic crystals yellowish-red and strongly anisotropic. Some pseudospherical inclusions with ragged edges, orange to green and anisotropic. Very small opaque, red, and yellow particles in eutectic arrangement, the red weakly anisotropic and the yellow strongly so.	Rather diffuse patterns but showing Cr_2O_3 weak; Cr_3O_8 weak; distorted spinel, trace; and FeO-Cr_2O_3, trace.	Cr_2O_3 with minor amounts of Cr_3O_8, distorted spinel, and chromite.
C-7	Ingot	—	19.86	Idiomorphic and irregular crystals, red, yellow with a few green. All strongly anisotropic.	Cr_2O_3, moderate; Cr_3O_8, weak; and FeO-Cr_2O_3, weak and diffuse.	Cr_2O_3 with minor amounts of Cr_3O_8 and chromite.
C-1	Ingot	—	21.75	Idiomorphic and small, branching-type crystals, reddish yellow and strongly anisotropic. A few small opaque inclusions. A few green, anisotropic crystals.	Cr_2O_3, moderate; and chromite, weak.	Cr_2O_3 with minor amounts of chromite and Cr_3O_8.
C-5	Ingot	—	21.81	Same as Run C-1 above.	Cr_2O_3, moderate; and chromite, weak.	Cr_2O_3 with minor amounts of chromite and Cr_3O_8.
CC-10	1	1651	24.76	Small, idiomorphic, orange-red crystals, strongly anisotropic.	Cr_2O_3, strong.	Cr_2O_3
CC-11	1	1649	37.08	Numerous small idiomorphic crystals. Many extremely small, round, angular, and elongated inclusions in eutectic-like patterns. All reddish-yellow and strongly anisotropic.	Cr_2O_3, strong.	Cr_2O_3
	3	1594	38.90	Mostly extremely small, poorly developed inclusions. An occasional small idiomorph. A few small round inclusions with ragged edges. All red and yellow and strongly anisotropic.	Diffuse pattern indicating Cr_2O_3.	Cr_2O_3
	4	1548	37.10	Similar to Sample 3 above.	Cr_2O_3, weak	Cr_2O_3
C-10	Ingot	—	42.20	A few large idiomorphic crystals, red to yellow and strongly anisotropic.	Cr_2O_3, very strong and well developed.	Cr_2O_3
C-8	Ingot	—	42.41	Red, with occasional yellow, idiomorphic and dendritic crystals. Strongly anisotropic.	Cr_2O_3, strong; and chromite, very weak and diffuse.	Cr_2O_3 with trace of chromite.
C-2	Ingot	—	46.48	Red, yellow, and green idiomorphic and dendritic crystals with red and yellow predominating. All strongly anisotropic. The green inclusions contained minute particles of metal and had ragged edges.	Cr_2O_3, strong and Cr_3O_8, moderate.	Cr_2O_3 with minor amounts of Cr_3O_8.

properties associated with Cr_2O_3. Those in the sample taken from the 8 pct Cr run at 1565°C were insufficiently developed for identification. The Taylor samples taken from the 8 pct Cr run at 1629° and 1674°C contained primary inclusions that were identified both microscopically and by X-rays as distorted spinel, although the diffraction pattern in the case of the 1629°C sample was again somewhat

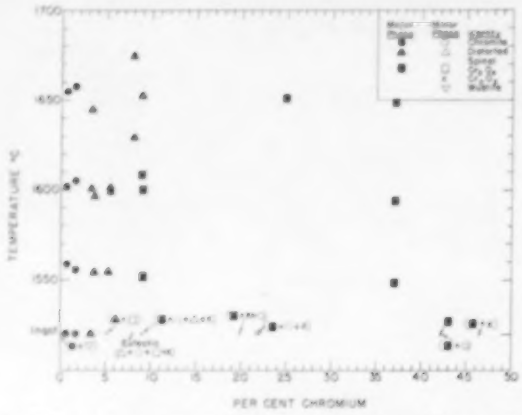

Fig. 11—Inclusions precipitated in Taylor samples and ingots of Fe-Cr alloys.

diffuse. In addition, most of the inclusions in an ingot containing 7.99 pct Cr appeared to be in a characteristic eutectic distribution, gave a very diffuse X-ray diffraction pattern, and were identified microscopically as probably distorted spinel and Cr_2O_3 with lesser amounts of Cr_2O_3 and chromite. On the other hand, Cr_2O_3 was definitely identified as a major constituent of the inclusions in an ingot containing 9.07 pct Cr.

It is considered, therefore, that the boundary separating the distorted spinel and Cr_2O_3 regions lies at chromium contents in the liquid metal slightly higher than 9 pct at 1650°C, and slightly lower than 9 pct, possibly around 8 pct, at temperatures approaching the solidification point of the metal. This conclusion implies that, at temperatures above 1550°C at least, metal containing 8 pct Cr is in equilibrium with the distorted spinel phase, while at temperatures from the freezing point up to approximately 1650°C, metal containing 9 pct Cr is in equilibrium with the Cr_2O_3 phase. In this connection, the different slopes of the 8 and 9 pct Cr curves in Fig. 10 are notable.

The boundary separating the $FeO \cdot Cr_2O_3$ phase from the distorted spinel phase, however, is located with somewhat less certainty. From Table VII and Fig. 11 it may be concluded only that the boundary must fall within the rather broad range of from 1.75 to 3.3 pct Cr. Fortunately, however, this range can be narrowed considerably on the basis of X-ray diffraction results on a few slag samples taken from some of the early isothermal runs. These observations are recorded in Table VIII. They suggest that the boundary lies above 2.7 pct Cr at 1600°C, below 2.7 pct Cr at 1650°C, and at less than 2.4 pct Cr at 1780°C. In addition, the distorted spinel inclusions in the ingot containing 3.39 pct Cr from run CC-5, Table VII, were thoroughly developed, but no chromite inclusions were observed in this ingot—a good indication that this composition is well within the distorted spinel field even at temperatures approaching the solidification range of the metal. It appears, therefore, that in the temperature range from 1550° to 1650°C the boundary between chromite and distorted spinel falls between 2.5 and 3 pct Cr in the metal and slopes toward lower chromium contents at high temperatures.

With the foregoing considerations regarding locations of the oxide phase boundaries in mind, oxygen solubility isotherms for 1550°, 1600°, and 1650°C were constructed by plotting on a logarithmic scale chromium and oxygen contents interpolated from Fig. 10, and fitting to the points within individual phase regions the best smooth curves that would both pass through the interpolated points and, without distortion, intersect as required. This construction is illustrated by Fig. 12. It is evident that the resulting curves are in complete agreement with the data and are remarkably consistent with each other at the different temperatures.

In Fig. 13 the oxygen solubility curves derived from the constant chromium runs as shown in Fig. 12 are compared with the original isothermal results. It will be observed that the lower limits of the scatter bands of the isothermal data are fitted quite well by the curves with none of the points falling significantly below the lines. Consequently, this comparison appears to offer further confirmation of the curves.

As far as the solubility of oxygen in molten Fe-Cr alloys is concerned, then, the results of the present investigation can be summarized as shown in Fig. 14. With increasing chromium content, the oxygen solubility decreases, reaching 0.017, 0.025, and 0.034 pct at 6 pct Cr and 1550°, 1600°, and 1650°C, respectively. With further increase in chromium concentration, the oxygen solubility rises although for practical purposes it may be considered to be substantially constant within the range of 6 to 10 pct Cr. In metal containing 40 pct Cr, it appears to be on the order of 0.057, 0.073, and 0.095 pct at 1550°, 1600°, and 1650°C, respectively. The minimum in oxygen solubility is notable. It implies that in low chromium alloys chromium is a deoxidizer for iron, while in high chromium alloys iron is a deoxidizer for chromium, and it may have special significance in regard to the deoxidation and inclusion problem in high chromium steels and alloys. With reference to low alloy steel, chromium in concentrations up to 1.5 pct appears to be practically identical to manganese in deoxidizing power.

The Fe-Cr-O Liquidus Surface

On the basis of observations made during the present investigation and the published diagrams for the Fe-O and the Fe-Cr binary systems,[9] a qualitative liquidus surface diagram for the metal and oxide portion of the Fe-Cr-O system has been deduced as shown in Fig. 15. The melting point of chromium has not been established with certainty, but the recent work of Bloom and coworkers[10, 11] indicates that it is slightly over 1900°C, and possibly as high as 1930°C. The melting point of Cr_2O_3 is reported by Bunting[12] to be 2275°C. The melting points of the oxides, $FeO \cdot Cr_2O_3$, distorted spinel, and Cr_2O, are unknown; but from observations of the slags formed during the oxidizing period of chromium steel heats, they are presumed to be relatively

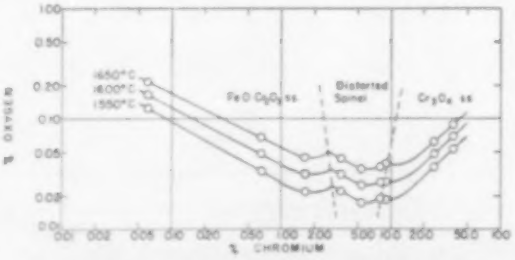

Fig. 12—Oxygen solubility curves interpolated from Fig. 10.

Table VIII. Constituents in Slag Samples from Low Chromium Heats

Run No.	Slag Sample No.	Temperature, °C	Pct Cr in Metal	Constituents Identified by X-Rays
C-6	2	1648	1.78	$FeO \cdot Cr_2O_3$ solid solution
	3	1655	2.50	Distorted spinel
C-9	4	1598	2.66	$FeO \cdot Cr_2O_3$ solid solution
	5	1595	3.49	Distorted spinel + Trace $Fe \cdot Cr_2O_3$ solid solution
C-11	3	1607	1.82	$FeO \cdot Cr_2O_3$ solid solution
	4	1596	3.97	Distorted spinel + Trace $Fe \cdot Cr_2O_3$ solid solution
C-12	1	~1780	2.37	Distorted spinel

high, that is, in excess of 1800°C. Melting points in the Fe-O system are, of course, well established and range from 1539°C for iron to 1371°C for the iron-wüstite eutectic. Observations made during melting electrolytic chromium in air in a magnesia crucible have indicated that a liquid slag forms on the metal, thereby demonstrating the presence of a liquid miscibility gap between molten chromium and chromium oxide. Further evidence of such a miscibility gap is illustrated by Fig. 16. Fig. 16 is a micrograph of the inclusions in a small ingot of high purity chromium saturated with oxygen that was melted under argon in a tungsten arc furnace. The inclusions were identified as primarily Cr_2O, and some Cr_2O_3 which presumably resulted from the disproportionation of Cr_2O, during cooling. It is evident that many of these inclusions were formed by precipitation of an immiscible liquid phase during solidification of the metal. It would be expected, then, that this miscibility gap extends into the system from the Cr-O side and joins the Fe-O miscibility gap, thus forming a continuous region of liquid immiscibility between the metal and oxide phases.

The appearance of the inclusions in Fig. 16 also demonstrates the occurrence of a metal-oxide eutectic situated between the miscibility gap and Cr_2O_3. Figs. 4 and 5, however, show that primary crystals of Cr_2O, are precipitated from liquid metal in the high chromium range. Consequently, in at least part of this region the metal-oxide eutectic must lie between the miscibility gap and the Fe-Cr side of the diagram. Therefore, the $Cr\text{-}Cr_2O$, eutectic progresses into the diagram, intersects the miscibility gap at a constant temperature tie line, and continues on the metal side of the miscibility gap toward lower chromium contents as indicated in the diagram. The specific location of this intersection of the metal-oxide eutectic with the miscibility gap is not known, but it is probably relatively close to the Cr-O side of the system.

It is not clear whether Cr_2O, and Cr_2O_3 form a peritectic or eutectic system. Because of the disproportionating character of Cr_2O, and by analogy with the Fe-O system, however, it has been assumed that Cr_2O, melts incongruently and forms by a peritectic reaction between Cr_2O_3 and the liquid. Similarly, it is not clear whether $FeO \cdot Cr_2O_3$ and distorted spinel are eutectic or peritectic with each other. It has been assumed that distorted spinel forms peritectiely from $FeO \cdot Cr_2O_3$ and the liquid on the basis of the similarity of the crystal structures of these two phases and the apparent disproportionating nature of distorted spinel. Consequently, the portion of the diagram enclosing these four phases is highly speculative.

The Cr_2O_3-Cr_2O, peritectic extends into the diagram from the Cr-O side and is immediately joined by a distorted spinel-Cr_2O, eutectic at a ternary peritectic point to form the boundary between distorted spinel and Cr_2O, phases. From the results of the inclusion studies, this boundary is believed to be binary eutectic in nature. It intersects the miscibility gap along a tie line and continues on the metal side of the miscibility gap to join the metal-oxide eutectics between metal and Cr_2O, and between metal and distorted spinel at a ternary eutectic composed of metal, Cr_2O,, and distorted spinel. The location of this ternary eutectic point is considered to be reasonably well established at approximately 8 pct Cr and on the order of 0.015 pct O. The observations listed in Table VII show that an ingot containing approximately 5 pct Cr exhibited primary distorted spinel inclusions with a small amount of Cr_2O, inclusions as

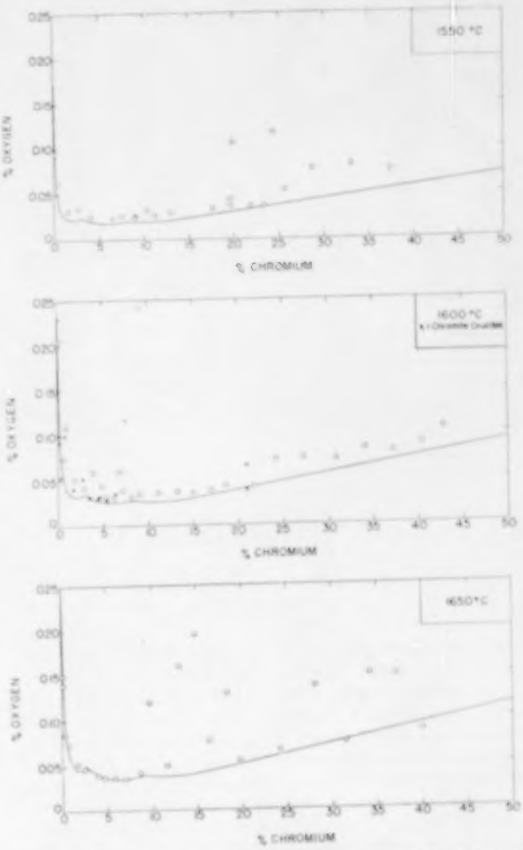

Fig. 13—Comparison of derived solubility curves with isothermal results.

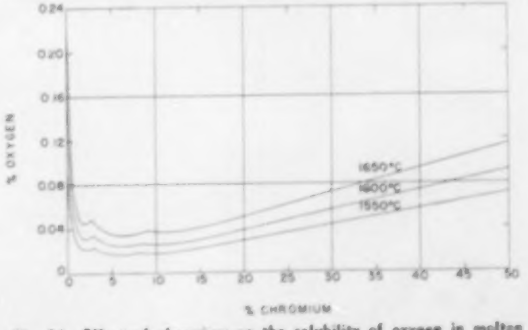

Fig. 14—Effect of chromium on the solubility of oxygen in molten Fe-Cr alloys.

Fig. 15—Qualitative diagram of the liquidus of the Fe-Cr-O system.

a secondary phase, while an ingot of 9 pct Cr content contained primary Cr_2O_3 inclusions. The inclusions in an 8 pct Cr ingot were practically all the result of freezing of a metal-oxide eutectic as illustrated in Fig. 17. Petrographic examination of a residue extracted from this ingot indicated that the inclusions were distorted spinel, Cr_2O_3, Cr_3O_4, and chromite ($FeO \cdot Cr_2O_3$), the latter two constituents presumably occurring as the result of disproportionation of the others. The temperature of this eutectic is inferred to be on the order of 1500°C. In any case, it cannot lie above the temperature of the minimum point in the Fe-Cr system which is approximately 1505°C at 22 pct Cr.

The chromite-distorted spinel peritectic also intersects the miscibility gap and continues on the metal side, joining the metal-chromite eutectic to form a metal-distorted spinel eutectic that eventually reaches the ternary eutectic point at 8 pct Cr. On the basis of the discussion in the previous section regarding the location of the $FeO \cdot Cr_2O_3$-distorted spinel phase boundary on the metal side, it appears that the ternary peritectic point may be situated quite close to 3 pct Cr.

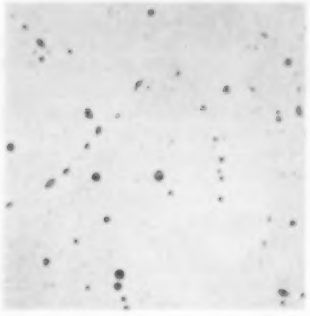

Fig. 16—Inclusions in ingot of oxygen-saturated high purity chromium. X250.

Fig. 17—Inclusions in ingot of 8 pct Cr alloy. X250.

The metal-chromite eutectic that occurs in the corner of the system, as shown earlier by Fig. 2, is believed to move downward in temperature on either side of a join between Fe and $FeO \cdot Cr_2O_3$. As already described, at higher chromium contents it must join with the $FeO \cdot Cr_2O_3$-distorted spinel peritectic. On the other hand, the inclusions in an ingot containing 0.05 pct Cr were identified as chromite and wüstite, an observation strongly indicating that on the low chromium side the metal-chromite eutectic joins with a wüstite-chromite eutectic at an invariant point. These inclusions are illustrated in Fig. 18 from which it is apparent that they consisted of primary crystals and a substantial number of inclusions precipitated as an immiscible liquid phase during solidification of the ingot. Consequently, the metal-chromite eutectic must intersect the miscibility gap at very low chromium concentration and continue on the other side to a ternary eutectic of metal, wüstite, and Fe_3O_4-rich chromite.

Although qualitative in nature, this diagram fits the observations quite well. Within its limitations it is considered a useful guide to the interpretation of phase relations and of the progress of solidification in the Fe-Cr-O system.

Isothermal Fe-Cr-O Diagram

An isothermal diagram of the system at 1600°C was derived on a fairly quantitative basis and is shown in Fig. 19. During the early stages of this investigation, a charge of Armco iron was melted in air in a chromite crucible and held for a considerable period of time at approximately 1600°C. Chemical analysis of a Taylor sample taken from this melt at the end of the holding period indicated a chromium

content of 0.024 pct. This observation established the L_1 corner of the L_1—L_2—S triangle of Fig. 19. In their study of oxidation of Fe-Cr alloys at 1600°C, Wentrup and Knapp observed a marked difference in the chromium to iron ratio in slags formed from metal containing 0.02 and 0.03 pct Cr. At 0.02 pct Cr in the metal, they reported a liquid slag having a chromium to iron ratio of approximately 1 to 10. The L_2 or liquid oxide corner of the triangle, therefore, is placed at a chromium to iron ratio just slightly higher than 1 to 10, and an oxygen content slightly less than that in FeO. At 0.03 pct Cr in the metal, Wentrup and Knapp reported a mushy slag with a chromium to iron ratio of about 1 to 5. Consequently, the S or chromite corner of the three-phase triangle is considered to lie at a chromium to iron ratio just a little higher than 1 to 5, and at an oxygen content slightly below the Fe_3O_4-$FeO \cdot Cr_2O_3$ join. (In connection with the chromite phase, it is important to note that Fe_3O_4 and $FeO \cdot Cr_2O_3$ are isomorphous spinels and are presumed to form a continuous series of solid solutions.)

The L_1 or liquid metal corners of the $L_1 - D - S$ and the $L_1 - D - T$ triangles were established by the oxygen solubility curves. In the absence of evidence to the contrary, the S corner of the $L_1 - D - S$ triangle was located at the $FeO \cdot Cr_2O_3$ composition as the end member in the chromite solid solution series. Since the X-ray diffraction observations indicated that the distorted spinel field covered a range of compositions, the D corners of the two triangles were located at opposite ends of that field. The position and extent of the D field itself is based upon the following considerations: 1—Vacuum fusion analysis of distorted spinel inclusions extracted from an ingot in the 3 to 9 pct Cr range indicated an oxygen content of 28.5 pct. 2—In the manufacture of chromium steels by the conventional arc furnace techniques, it has been observed that after the oxidation period the slags on heats containing from 3 to 9 pct Cr have chromium to iron ratios ranging from approximately 2.5 to 1 to 3 to 1. The extent of the T or Cr_2O_3 field and the position of the T corner of the L_1—D—T triangle were estimated mainly from the results of chemical analyses of inclusions extracted from melts containing more than 9 pct Cr, as described in a previous section. These analyses indicated that the Cr_2O_3 phase contained about 29.3 pct O and up to about 8 pct Fe although, in view of the relative constancy of the lattice parameter of Cr_2O_3, it is doubted that the iron content greatly exceeds 8 pct.

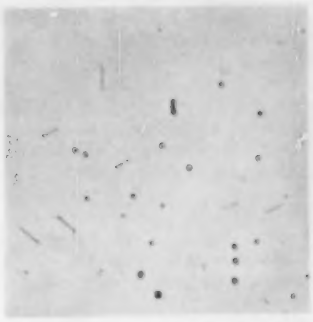

Fig. 18—Inclusions in ingot of 0.06 pct Cr alloy. X250.

The L_1 and α corners of the L_1—α—T triangle are estimated from extrapolation of the 1600°C oxygen solubility curve and the Fe-Cr diagram. The T corner of this invariant region is arbitrarily located on the boundary of the T field at less than 8 pct Fe because, as discussed earlier, chemical analysis of the Cr_2O_3 inclusions extracted from an ingot containing 42 pct Cr indicated an iron content of approximately 7 pct in the inclusions. Since the T corner of the L_1—α—T triangle denotes oxide in equilibrium with liquid metal containing considerably more than 42 pct Cr, the iron content of this oxide must be less than the iron content of the oxide in equilibrium with the lower chromium metal.

The high oxygen side of this diagram is, of course, completely unknown and has been left open. On the basis of phase rule considerations, however, the phase regions that probably occur have been indicated.

While this diagram has been constructed specifi-

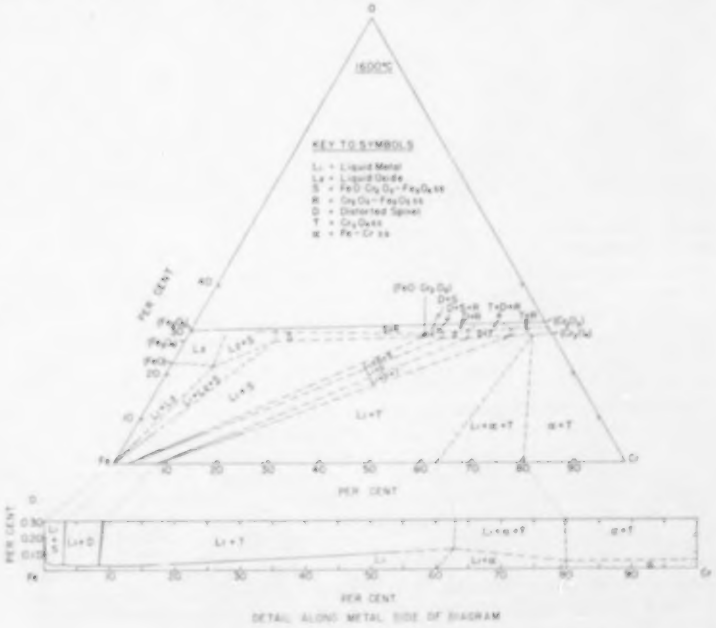

Fig. 19—Isothermal section of Fe-Cr-O system at 1600°C.

cally for the temperature of 1600°C, it is apparent that with very slight modification it can apply over quite a range of temperatures above the melting point of iron. At 1650°C, for example, the L_1-L_2-S triangle will move slightly toward higher chromium concentrations; the L_1 corners of the L_1-D-S and the L_1-D-T triangles will shift very slightly toward lower and higher chromium concentrations respectively; the $L_1-\alpha-T$ triangle also will move toward higher chromium concentration by a small amount predictable from the diagram of the Fe-Cr system. Since no assumptions with regard to the various eutectics or peritectics among the oxide phases were involved in its derivation, this diagram is much less speculative than the liquidus surface diagram in Fig. 15. Some uncertainty regarding the specific locations of the invariant points along the oxide phase boundaries is evident; but it is felt that these discrepancies are of small magnitude and relatively unimportant for practical purposes, so that the diagram is considered to be an adequate representation of phase relations between molten metal and solid oxides in the Fe-Cr-O system. Within the temperature range of interest in the melting of chromium steels, the diagram demonstrates that metal of very low (on the order of 0.02 pct) chromium content is in equilibrium with a liquid slag of variable composition very rich in iron oxide; metal containing up to 2.5 to 3 pct Cr is in equilibrium with a solid chromite phase ranging from a composition rich in Fe_3O_4 to $FeO \cdot Cr_2O_3$; metal of intermediate chromium content in the approximate range of 3 to 9 pct is in equilibrium with an oxide phase varying in composition within a small range intermediate between $FeO \cdot Cr_2O_3$ and Cr_2O_3; and metal containing more than about 9 pct Cr is in equilibrium with a solid oxide approximating the composition Cr_2O_3 in which a small amount of iron may substitute for chromium. The diagram further indicates that in contradiction to the conventional assumptions Cr_3O_4 does not occur as a phase in equilibrium with the liquid metal.

Summary

The effect of chromium on the solubility of oxygen in molten Fe-Cr alloys containing up to approximately 50 pct Cr has been determined in the temperature range 1550° to 1650°C. With increasing chromium concentration, the oxygen solubility is lowered, reaching minima of about 0.017, 0.025, and 0.034 pct O at 6 pct Cr and temperatures of 1550°, 1600°, and 1650°C. With further increase in chromium content, the oxygen solubility rises and, in metal containing 40 pct Cr, attains levels of 0.057, 0.073, and 0.095 pct O at temperatures of 1550°, 1600°, and 1650°C, respectively. During evaluation of the oxygen solubility data, it was found that additions of chromium or oxide to the molten bath without a subsequent change in bath temperature led to anomalous results.

Two previously unreported oxides with unique optical properties were recognized and subsequently identified as primary phases in the Fe-Cr-O system. One, having the composition Cr_2O_3 with up to about 8 pct Fe substituting for chromium, was indexed as a tetragonal crystal with an axial ratio of 0.86 in the absence of iron and 0.88 when saturated with iron. The other, designated "distorted spinel," appears to be intermediate in composition between $FeO \cdot Cr_2O_3$ and Cr_2O_3. It has also been indexed as tetragonal, but with an axial ratio varying from 0.95 to 0.98. Both of these phases are stable only at high temperatures and at temperatures below the freezing point of the metal may be disproportionated, distorted spinel yielding $FeO \cdot Cr_2O_3$ and Cr_2O_3, and Cr_2O_3 yielding Cr_3O_4 and chromium-rich metal.

Relations among the oxide phases and molten Fe-Cr alloys were established and have been represented in ternary diagrams. At usual steelmaking temperatures metal containing on the order of 0.02 pct Cr is in equilibrium with a liquid oxide rich in FeO, and metal containing from about 0.02 to 3 pct Cr is in equilibrium with solid oxides in the chromite-magnetite solid solution series. At higher chromium concentrations in the liquid metal, the tetragonal oxides, distorted spinel and Cr_2O_3, appear successively as the equilibrium phases, the former being associated with metal in the 3 to 9 pct Cr range and the latter with alloys over 9 pct Cr up to chromium itself. A ternary eutectic involving metal, Cr_2O_3, and distorted spinel is located in the vicinity of 8 pct Cr and 0.015 pct O and freezes at a temperature of approximately 1500°C.

Acknowledgments

The authors wish to thank John Chipman, Professor of Metallurgy, Massachusetts Institute of Technology, for his many valuable suggestions and criticisms; and they gratefully acknowledge the generous cooperation and assistance of their associates on the staff of the Metals Research Laboratories, Electro Metallurgical Co., particularly J. J. Darby, E. F. Johnston, K. H. Dawdy, Gloria Faulring, H. L. Hamner, and L. A. De'Aeth.

References

[1] D. C. Hilty and W. Crafts: The Solubility of Oxygen in Liquid Iron Containing Aluminum. *Trans.* AIME (1950) **188**, p. 414; JOURNAL OF METALS (February 1950).

[2] C. R. Taylor and J. Chipman: Equilibria of Liquid Iron and Simple Basic and Acid Slags in a Rotating Induction Furnace. *Trans.* AIME (1943) **154**, pp. 228-245.

[3] H. M. Chen and J. Chipman: The Chromium-Oxygen Equilibrium in Liquid Iron. *Trans.* ASM (1947) **38**, p. 70.

[4] H. Wentrup and B. Knapp: Reactions of Iron Chromium Alloys with Oxygen. *Tech. Mitteillungen* Krupp (1941) **4**, No. 11, pp. 237-256.

[5] B. V. Linchevskij and A. M. Samarin: Solubility of Oxygen in Iron-Chromium and Iron-Chromium-Nickel Alloys. *Izvestiya Akademii Nauk SSSR Otdel Tekhn. Nauk* (1953) No. 5, pp. 691-704.

[6] D. C. Hilty: Relation Between Chromium and Carbon in the Refining of Chromium Steel. *Proc. Electric Furnace Steel Conference* AIME (1948); *Trans.* AIME (1949) **185**, p. 91; JOURNAL OF METALS (February 1949).

[7] W. E. Denis and F. D. Richardson: The Equilibrium Controlling the Decarburization of Iron-Chromium-Carbon Melts. *Journal* Iron and Steel Institute (1953) **175**, p. 264.

[8] C. E. Sims, H. A. Saller, and F. W. Boulger: Relative Deoxidizing Powers of Some Deoxidizers for Steel. *Trans.* AIME (1949) **185**, p. 814; JOURNAL OF METALS (November 1949).

[9] C. A. Zapffe: Dissociation Reactions Within Inclusions. *Journal* Iron and Steel Institute, London (1946) No. II, pp. 155-161.

[10] *Metals Handbook.* (1948) Cleveland. ASM

[11] D. S. Bloom, J. W. Putnam, and N. J. Grant: Melting Point and Transformation of Pure Chromium. *Trans.* AIME (1952) **194**, p. 626; JOURNAL OF METALS (June 1952).

[12] D. S. Bloom and N. J. Grant: Chromium-Nickel Phase Diagram. *Trans.* AIME (1951) **191**, p. 1009; JOURNAL OF METALS (November 1951).

[13] E. N. Bunting: Phase Equilibria in the System Cr_2O_3-Al_2O_3. *Journal of Research* National Bureau of Standards (1931) **4**, No. 6, p. 948.

AIME OFFICERS:
President—Leo F. Reinartz
Vice-Presidents—T. B. Counselman, L. E. Elkins, Harold Decker, O. B. J. Fraser, A. B. Kinzel, J. B. Morrow
President-Elect—H. DeWitt Smith
Treasurer—G. F. Moulton
AIME STAFF:
Secretary—E. H. Robie
Administrative Ass't. Sec'y.—Ernest Kirkendall
Ass't. Secretaries—J. B. Alford, H. N. Appleton, E. J. Kennedy, Jr., R. E. O'Brien
Ass't. Treasurer—P. J. Apol

aime NEWS

Reinartz Scholarship Award Created By National Open Hearth Committee to Honor President of AIME

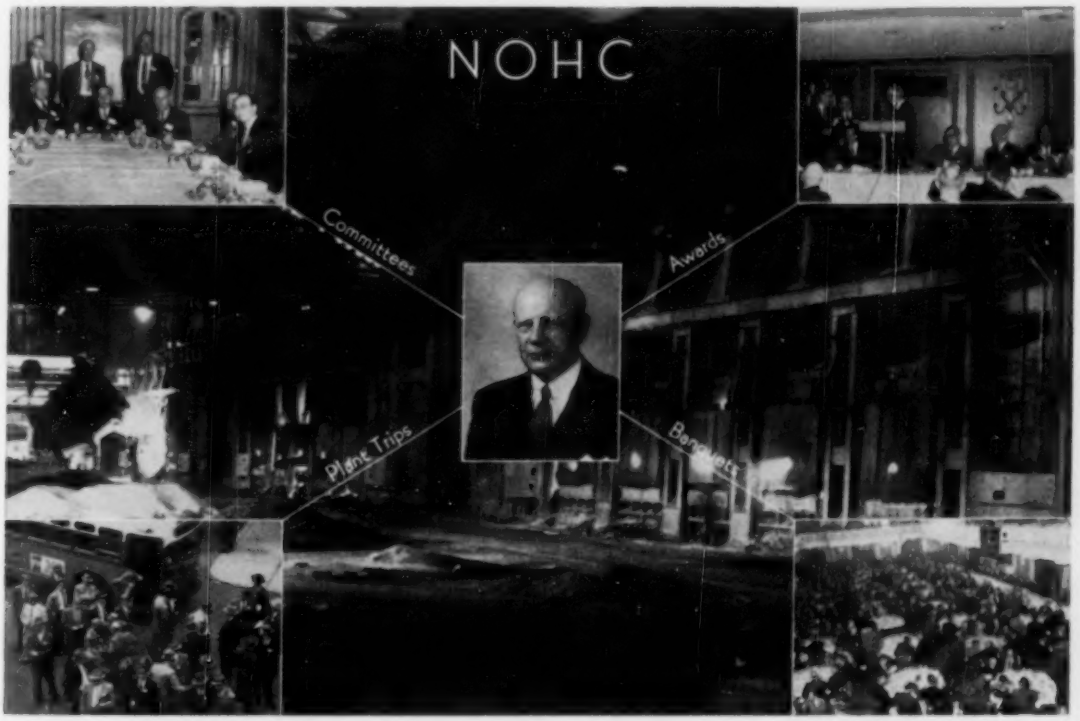

At the NOHC Executive Board meeting held Nov. 6, 1954 in Columbus, Ohio a fund of $15,000 was appropriated to finance an annual scholarship at Carnegie Institute of Technology. H. G. Grim, Chairman of the Scholarship Committee, said that funds for the scholarship were provided by the NOHC to honor Leo Reinartz, vice president of Armco Steel Corp., for his outstanding work during the early years of the open hearth committee.

The scholarship award will be used to attract promising young men to the field of metallurgical engineering. "It was Leo's choice," Mr. Grim stated, "that his Alma Mater, Carnegie Tech, be the school to have the benefit of this award."

In 1950 Frank T. Sisco wrote a *Footnote to the History of the National Open Hearth Committee* in the Proceedings that ably describes Leo Reinartz's contribution to the organization. Mr. Sisco wrote in part: "In November 1927, when Leo Reinartz assumed the chairmanship, the NOHC had been in existence for two years and had held five rather flacid semi-annual meetings with an average attendance of 40. Secrecy and an attitude of 'get all you can but give nothing' on the part of most of the registrants, accompanied by considerable suspicion of the motives of the others present, with no cooperation or at most a lukewarm attitude by most of the steel companies, and a tendency to exaggerate and make extravagant claims in discussing furnace practice, were plainly apparent at these first meetings.

"Beginning almost at once and continuing for years, Chairman Reinartz urged frankness, honesty, and industry-wide cooperation and hammered away to secure recognition of the now universally accepted principle that the contribution of any one individual is far exceeded by the benefits he and his company receive from an open discussion by others confronted with the same problem."

The Leo F. Reinartz AIME NOHC Scholarship Award is a lasting expression of the esteem in which Leo Reinartz's many friends hold him for his dedicated service to the profession and to the industry.

H. DeWITT SMITH

PRESIDENT, AIME, 1955

H. DeWITT SMITH sits behind his desk at 14 Wall St., New York, and talks easily and knowledgeably of many things. The sun streams through the window at his back and plays strange light patterns on the map of Africa on the wall to his left. The conversation ranges from Alaskan mining camps to Mexico, to South Africa, to England, Bolivia, and Chile. Through all the years of his association with mining, his chief interest has been copper. The winning of that metal has brought Mr. Smith into contact with some pretty rugged living. Today he is still active in South African copper mining. He retired as a vice president of Newmont Mining Co. in September 1954, but is still a member of the board, chairman of O'okiep Copper Co. Ltd. and consulting engineer for O'okiep and Tsumeb.

From the time he joined Newmont, Mr. Smith participated in many large copper property merger transactions, including Rhodesian Congo Border Concession Ltd.—Bwana M'Kuba; Phelps Dodge—Calumet & Arizona; and the Phelps Dodge purchase of United Verde. It is with the development of Newmont's South African ventures that Mr. Smith is most closely identified.

As the conversation moves from one mining topic to another, Mr. Smith ties the minerals industry history of the last 50 years into a unified whole. As the story unfolds he pauses for a moment and then ponders that "The romance seems to have gone out of mining for a lot of people." Mr. Smith doesn't agree.

"If there is no longer romance in the minerals industry it is only because no one wants to find it there."

Born Sept. 30, 1888 in Plantsville, Conn., H. DeWitt Smith received his E. M. from Yale's Sheffield School in 1910. His travels started early in his career. As one of the last junior engineers trained by Joshua Edward Spurr, he saw most of the western part of the U. S. and much of Mexico.

Mexico produced several bits of excitement. Mr. Smith was working at the Santa Eulalia mine in 1910 when Mexico erupted in revolution. The rebels swept toward the mine, capturing the town. Federal troops promptly recaptured it. Two years later, while he was working at Sierra Mojada the railroad to Torreon was cut. Mr. Smith got out of the way by pumping a handcar to Chihuahua City.

Speaking of that period of his career, Mr. Smith recalls that "I decided that a geologist must have a basic understanding of mine operations. So when the chance came along to go to Kennecott's Alaskan copper mine as foreman, I took it." The mine crew was one of the best he has ever seen, composed of hardbitten, experienced prospectors, and husky Scandinavians and Russians—a combination of skill and strength, he noted. "They were strong men, not afraid to work." The Alaskan operation proved to be the basis for Kennecott's tremendous growth in the copper business. Before leaving Alaska, Mr. Smith rose to become successively mine superintendent, and assistant manager. He then went to United Verde in Jerome, Ariz., first as mine superintendent and then as general superintendent.

In 1924 Mr. Smith put aside the rough clothes of a mining man and went into the industrial department of the New York Trust Co. "One of the remarkable things about the department at that time, was that the personnel consisted largely of mining engineers." Mr. Smith performed such diverse duties as operating a silk ribbon business and a milking machine company before he left the bank to return to mining and United Verde. Finally, in 1930 he joined Newmont. Since then, there has been only one break in the relationship. Mr. Smith was executive vice president of the Metals Reserve Co., Reconstruction Finance Corp. subsidiary. He was in charge of all domestic metals procurement activities, from 1941 to 1944.

While with Metals Reserve he established a reputation for quickly cutting away red tape and superfluous negotiations on contracts. One representative of a large company walked into the Metals Reserve offices expecting hours of wrangling over vague details. Fifteen minutes later he and his lawyer were walking out the door, the executive recalls, with a signed contract. The soundness of the contracts arranged by Metals Reserve was proven after the end of the war when not one of its agreements had to be renegotiated. An escape clause in each pact elaborated on the exact procedure to be followed for its termination or at the end of hostilities.

In 1939, the British liner Athenia was torpedoed off the Hebrides, with Mr. and Mrs. Smith and one of their daughters aboard. As the passengers were loaded into the lifeboats the family was separated and not until days later did they know of each other's safety. Mr. Smith remembers that he had to bail for dear life to help keep the lifeboat he was in afloat. Eventually, all survivors were picked up and the Smith family was reunited.

Mr. Smith joined the Institute in 1911 and has been active in its affairs for many years, holding office as Chairman of the Nominating Committee in 1939, as a Director, Chairman of the Seeley W. Mudd Memorial Fund Committee, and Vice Chairman of the 75th Anniversary Committee. One of his prime objectives as 1955 President of the AIME will be to strengthen the grass roots movement among the sections that was started during previous presidencies.

Mr. Smith is vitally concerned with the problem of attracting young men to the mining industry, and has been instrumental in the O'okiep program which brings young men to the U. S. from South Africa each year. The South Africans study in U. S. schools for three years under the plan. Many of his training ideas evolved from the United Verde mining training program that operated in the years following World War I. Mr. Smith feels that the training methods used were some of the best ever practiced in the domestic mining industry. Mining engineers who came under the United Verde influence at that time have moved on to positions of leadership throughout the industry.

Mr. Smith believes that the best way to start in the mining business is as a mucker, miner, or timberman. Another way to attract the kind of men the mining industry needs is the payment of adequate wages. In the final analysis it's up to management to provide the climate that will make mining attractive.

Mr. Smith married Ellen Dawson Burke of Plainfield, N. J. in 1916. They have three children, C. DeWitt Smith, Mrs. Alfred Sanford, II, and Mrs. J. Clifton Rodes. C. DeWitt Smith is with St. Joseph Lead Co., carrying on the family tradition of making one's own way.

If there is one thing in the world that will distract Mr. Smith from mining and the romance of copper, it's surfcasting. Nantucket beaches, early in the morning or just before sundown, are his favorite spots. His biggest catches have been a 9½ lb bluefish and a 23½ lb striped bass, both hooked and landed off Nantucket.

Raymond Award Procedure Changed

Instead of appointing a separate committee to select the recipient of the Rossiter W. Raymond Award, as has been the procedure in the past, the AIME Technical Publications Committee will hereafter select the winner. The award is made annually to the Institute member under 33 who individually has contributed the best paper in the period under review. The TP Committee passes on papers for the Alfred Noble Prize, for which the authors must be under 31. The new procedure avoids the duplication of effort when the recipients of the two awards must be respectively selected by two different committees.

Plan to Publish AIME Directory

Following careful study and review of various proposals and suggestions for publishing a directory or directories of AIME members, the following plan has been approved:

Names, positions, and addresses of all AIME members as carried on the master file cards of the Institute on Feb. 1, 1955 will be used. Both an alphabetical and geographical listing will be typed and printed by offset. The geographical listing will, as in the last Directory, indicate which members are available for consulting work, and will also indicate the field of their primary and subsidiary professional interests. It is planned that the Directory may be available not later than June. A supplement to the Directory, similar to that published in the last four years, containing a list of the officers, Branches, Divisions, Local Sections, Student Chapters, committee personnel, and the Bylaws of the Institute will also be published, possibly as part of the Directory.

Following the procedure now adopted by the ASCE, ASME, AIEE, and AIChE, the Directory will be mailed only to those members in good standing who request it. A coupon will be published in the March issues of the Institute's journals, offering the Directory. This coupon, when filled out and returned, will serve as the address label for mailing the Directory. Members should request copies of the Directory by filling out this coupon.

The Petroleum Branch of the Institute will follow the practice established last year of printing a separate directory of Petroleum Branch members as a bound-in supplement to the June issue of the JOURNAL OF PETROLEUM TECHNOLOGY. However, the all-Institute Directory will be available, on return of the coupon, to all members of the Petroleum Branch who may wish to have the complete Directory.

EJC to Sponsor Nuclear Congress

Engineers Joint Council is sponsoring a Nuclear Congress to be held in Cleveland Dec. 12 to 16, 1955. All phases of nuclear science and engineering will be covered except restricted matter principally of a military nature. It is planned to make the meeting a worthy successor to, and expansion upon, the meeting so successfully conducted by the American Institute of Chemical Engineers at Ann Arbor last year. Most of the constituent societies of EJC will take part, as will many others, notably the newly formed American Nuclear Society. Well over 1000 are expected to attend.

At present the Institute of Metals Div. of the AIME is the only Division of the AIME to have a committee on this subject—the Nuclear Metallurgy Committee. This Committee expects to have several sessions at the Congress, and it is probable that several other Divisions of the Institute will set up committees to arrange for papers on other phases of the nuclear energy program that come within their respective fields.

Report on Local Section Finances

A special task committee on Local Section Finances (T. B. Counselman, Chairman, with A. B. Kinzel, Gail F. Moulton, M. B. Penn, H. DeWitt Smith, and Clark Wilson) reported at the December 15 meeting of the AIME Executive and Finance Committees. The Committee recommended that the Council of Section Delegates be reduced in number to between 20 and 30, inasmuch as the larger Council was unwieldy and it had been a considerable drain on the Institute treasury to pay the expenses of delegates from 60-odd Local Sections to the Annual Meeting. Instead, it was proposed to allow two delegates from each of the ten AIME Directoral districts, with additional delegates from the seven outlying Local Sections not embraced in any of the Directoral districts. A rotational plan would be devised for selecting the delegates from the various Local Sections in the respective districts. The Committee recommended further that in 1956 the rebate to the Local Sections be increased from 50¢ to $1 provided the budget could be balanced if such a rebate were paid. A bottom limit of $100 per Section would, however, be established. (In 1955, travel expenses of delegates from each Local Section have been authorized, so the rebate would not be increased until 1956). The Committee felt that the rebate to Local Sections of half the initiation fees paid by new members in their respective territories should be continued, and should be expanded to include half the initiation fees paid by Junior Members who advance to a higher grade. If an employer were willing to pay a delegate's expenses, the Committee felt that he should not accept expenses from the Institute.

The Committee's recommendations have been referred to the Council of Section Delegates for consideration.

Pittsburgh Sections Hold Meetings

The Ninth Annual Off-the-Record meeting of the Pittsburgh Sections of the American Institute of Mining and Metallurgical Engineers and the National Open Hearth Committee was held at Hotel William Penn on Friday, Oct. 29, 1954. Total registrations were 725, a new record.

The meeting consisted of a total of nine technical sessions sponsored by the Open Hearth Committee, the Coal, Institute of Metals, and Petroleum Divisions of AIME, the Engineering Society of Pennsylvania, and a session on Fuels by the AIME-ASME Joint Fuels Conference.

Heading the list of honored guests at the Banquet attended by 360 guests was President L. F. Reinartz who was introduced by L. A. Lambing, Chairman of the National Open Hearth Committee; also present were: W. S. Major, Vice Chairman, Fuels Div. ASME; Joseph Clark, Assistant Secretary, ASME; E. J. Kennedy, Assistant Secretary, AIME; Ernest Kirkendall, Administration Assistant Secretary, AIME. Toastmaster was E. H. Hollingsworth, Chairman of Pittsburgh Section AIME.

The Annual F. L. Toy Award was presented by J. O. Dague, Bethlehem Steel Co., Lackawanna, N. Y. by S. J. Dougherty, Chairman, Pittsburgh Section NOHC. The Student Prize Paper Award was presented to L. D. Kirkbride of Carnegie Tech by D. W. Pettigrew, Award Chairman. Dinner speaker was R. G. Fithian, of the Bell Telephone Co. who gave an interesting talk on *"The Transistor—The Mighty Midget."*

Apr. 15, 1955 is the deadline for papers that are to be presented at the Institute of Metals Div. Fall Meeting in Philadelphia, Oct. 17 to 19, 1955. Papers received by this deadline but requiring revision may not be processed in time to permit scheduling for this meeting.

Electric Furnace Steel Conference Sets New Attendance Record in Pittsburgh

Pittsburgh, the golden triangle city, was host to the 882 electric furnace steel conferees on Dec. 1 to 3, 1954. The Twelfth Annual Conference held at the William Penn Hotel topped all previous attendance records.

Wednesday featured plant trips to the ingot producing shop of U. S. Steel's Duquesne Works and to the steel casting shop of McConway & Torley Corp. Formal technical sessions began on Thursday with a welcome from C. F. Staley, Chairman of the Conference, and from F. O. Lemmon, Chairman of the Executive Committee.

The first technical session covered the new developments in vacuum melting with W. M. Farnsworth, Republic Steel Corp., and R. J. Wilcox, Michigan Steel Castings Co., as Associate Chairmen. The simultaneous afternoon sessions were on Refractory and Masonry and a Metallurgical Session on Melting. D. L. Clark, Simonds Saw & Steel Co., and L. W. Cashdollar, Pittsburgh Metallurgical Co., were Associate Chairmen for the former session and C. G. Mickelson, American Steel Foundries, and V. E. Zang, Unitcast Corp., for the latter session.

Simultaneous technical sessions were again held on Friday. A meeting on Quality was chairmened by G. G. Zipf, Babcock & Wilcox Co., and R. B. Shaw, Allegheny Ludlum Steel Corp.; and a session on Operations in Foundry Melting had C. B. Williams, Massillon Steel Castings Co., and C. W. Vokac, Whiting Corp., as Associate Chairmen. Friday afternoon was reserved for informal discussion groups. The Ingot Bull Session was lead by G. Derge, Carnegie Institute of Technology, and T. V. Wainwright, Bethlehem Steel Co., and the Castings Bull Session by Charles Locke, West Michigan Steel Foundry Co., and J. B. Caine, consultant.

D. R. Loughrey, Jones & Laughlin Steel Corp., was the toastmaster for the Annual Banquet Thursday evening. The banquet speaker was Pressly H. McCance, president, Duquesne Light Co. Mr. McCance spoke on *Power and Steel* and stressed the cooperative relationship which exists between electric furnace operators and power companies. Pointing out the greater efficiency of electric heating, Mr. McCance said, "It is little wonder that electric heating is so rapidly becoming of greater and greater importance in steelmaking."

Awards were presented to F. O. Lemmon and R. K. Kulp for their outstanding service to AIME and the Electric Furnace Steel Conference.

One of the 70-ton electric furnaces at Duquesne Works, U. S. Steel Corp., seen by members on plant trip during the Electric Furnace Steel Conference in Pittsburgh.

Columbia Section And Students Meet

The student members of the AIME of the University of Moscow met with those of the State College of Washington in Pullman the night of Dec. 7, 1954, to be introduced to the Columbia Section Student Chapter Counsellor, J. "Barney" Haffner, President of the Bunker Hill & Sullivan Mining Co.

In addition to the students, the deans of the schools as well as members of the faculties of minerals industries were present. Also present were the Chairman of the Columbia Section, Lynn Kinney; the Chairman for 1955, Norm Sather; A. Bethune, Chairman of the Pacific Northwest Regional Conference for 1955; and F. R. Morral, Secretary-Treasurer of the Columbia Section. An informal round-table discussion was held by the group discussing topics such as advantages of AIME membership and what industry expects from the graduate engineer. Mr. Haffner pointed out in particular the importance of the "King's" English.

One of the problems confronting the student chapters is getting speakers. A roster of speakers available in this area will be prepared. After the meeting with the students the faculty and the officers of the Columbia Section discussed plans for student participation at the regional conference Apr. 28 to 30, 1955, at which faculties and students of the State College of Washington, Universities of Idaho, Washington, Utah, Reno, Montana, and British Columbia will be invited.

The meeting, attended by a total of 40 persons, was encouraging to the officers of the Columbia Section and the faculty. The chairmen of the student chapters—H. A. Crisp of Washington State College and Townsend of the University of Idaho, Associated Miners, plan to work out more joint meetings at which engineers from the area will discuss their experiences.

It might be added that Mr. Kinney drove 205 miles to attend the meeting! Both Mr. Sather and Mr. Bethune drove 120 miles through snowstorms to reach Pullman, and Messrs. Haffner and Morral came about 80 miles to be present!

W. V. Smith Joins AIME Staff

Beginning the first of the year, Warren V. Smith took over the job held by Frederick A. Stanley the last two years as Eastern Advertising Manager for MINING ENGINEERING and the JOURNAL OF METALS. Mr. Stanley had resigned to join the staff of the Penton Publishing Co.

Mr. Smith has recently been in charge of advertising and sales promotion for the Star-Kimble Motor Div. of the Miehle Printing Press & Mfg. Co. at Bloomfield, N. J. He has a degree of Bachelor of Business Administration from Upsala College, and has done graduate work at Seton Hall University and Rutgers. He is a member of the U. S. Naval Reserve. Mr. Smith, who is 28 years old, lives in East Orange, N. J. with his wife and two sons.

Local Sections Approved by AIME

Three new Local Sections of the AIME, all comprising essentially Petroleum Branch members, were finally approved at the December 15 meeting of the Executive Committee of the Institute. One, the Illinois Basin Petroleum Section, supercedes the former Illinois Basin Chapter of the Petroleum Branch and includes all Petroleum Branch members in the territory of the St. Louis Section of the AIME. This embraces the entire state of Iowa; all of Missouri except Barton, Jasper, Newton, McDonald, Dade, Lawrence, Barry, Greene, Christian, and Stone Counties; all of Illinois south of and including Rock Island, Mercer, Warren, Fulton, Mason, Logan, Dewitt, Piatt, Champaign, and Vermilion Counties; the following Counties in Indiana: Virgo, Clay, Sullivan, Knox, Daviess, Pike, Gibson, Warrick, Vanderburg, and Posey; Kentucky west of and including Carroll, Henry, Franklin, Anderson, Washington, Marion, Casey, Russell, and Clinton Counties; and Tennessee west of and including Robertson, Davidson, Williamson, Marshall, and Giles Counties.

The second new Section is the Venezuela Petroleum Section, to embrace the entire Republic of Venezuela. A Local Section there was organized in 1947 but had to be abandoned shortly after because of a conflict with the laws of the country which forbid local sections of foreign societies at that time.

Formal recognition of the New York Petroleum Section was given following release of the Petroleum Branch members in the area of the New York Section. It is an overlaying Section, with the same territory as the New York Section.

The following sections have also been established by action of the AIME Board.

Panhandle, consisting largely of Petroleum Branch members in the Panhandle area of Texas. Counties embraced in the new Section's area were listed on page 49 of the JOURNAL OF PETROLEUM TECHNOLOGY for July 1954.

Hugoton, consisting of an area in Texas, Oklahoma, Colorado, and Kansas as specified in the July issue of JPT. The new Section was formerly organized as the Tri-State Gas and Oil Assn.

Niagara Frontier, a Section in an area not previously included in the territory of any Local Section—western New York State. The following counties are included; Cayuga, Tompkins, Chemung, Seneca, Wayne, Monroe, Ontario, Yates, Schuyler, Steuben, Livingston, Allegheny, Wyoming, Cattaraugus, Chatauqua, Genessee, Orleans, Niagara, and Erie. Headquarters will be in Buffalo or Niagara Falls. The organizing committee consisted of D. Swan, Chairman; Walter Crafts, D. C. Hilty, I. S. Servi, and H. R. Spedden.

The Section recently elected officers. Chairman is D. Swan, Electro Metallurgical Co., Niagara Falls, N. Y.; Vice-Chairman, R. Cameron, Colorado Fuel & Iron Co., Tonawanda, N.Y.; Secretary, E. L. McCandless, Linde Air Products Co., Tonawanda, N. Y.; and Treasurer, C. W. Hart, Republic Steel Corp., Buffalo, N. Y. Directors for the Section are: G. L. Cox, International Nickel Co., Rochester, N. Y.; W. L. Harbrecht, Electro Metallurgical Co., Niagara Falls, N. Y.; W. Stephens, Carborundum Metals Co., Akron, N. Y.; G. Mitchie, Electro Refractories Co., Buffalo, N. Y.; and D. L. Clark, Simonds Saw & Steel Co., Lockport, N. Y.

Form Student Chapter

A second Student Chapter of the AIME has been established at West Virginia University, for students interested in the field of the Petroleum Branch. The only other school boasting of two Student Chapters is Pennsylvania State University.

S. J. Cort First Recipient of Fairless Award

STEWART J. CORT

Stewart J. Cort, vice president of the Bethlehem Steel Co., has been selected as the first recipient of the newly established Fairless Award of the AIME. The award, consisting of a plaque, will be made at the Annual Banquet in Chicago, Feb. 16, 1955. It is to recognize distinguished achievement in iron and steel production and metallurgy. The citation reads, "For his leadership in iron and steel manufacturing which has made his company an outstanding producer in the industry."

This annual award has been made possible by a fund given by the U. S. Steel Corp. to provide an achievement award in the iron and steel field comparable to the Douglas medal in the nonferrous metallurgy field.

ANNUAL MEETING

Research in Progress

The Research in Progress session has been one of the most consistent attractions at recent annual meetings. This is the place where the research man gets an opportunity to present his work during its most critical period.

The list includes: Studies of Spiral Growth During Vapor Deposition of Cadmium; Reactions in Mercuric Iodide; A Possible Technique for Measurement of Solute Adsorption at Grain Boundaries; Rate of Propagation of Cleavage and Brittle Fracture; Grain Boundary Migration in Aluminum Bi-Crystals; Polygonization in a Bent Single Crystal of Silicon Iron; Dislocations in Plastic Bending of Germanium Single Crystals; Subgrain and Electrical Resistivity Studies of Molybdenum Single Crystals; The Application of Zone Melting to High Melting Point Metals.

Evidence for Solidification to Body-Centered Cubic Phase in 70.8 Pct Iron, 29.2 Pct Nickel Alloy; Metallographic Identification and Crystal Symmetry of Titanium Hydride; Electron Effects in Titanium Alloys; Preferred Orientation in Magnesium Alloy Extrusions; Hardening Mechanism in Mg-Li Base Alloys; Production of Ductile Iron-Aluminum Base Alloys; and High Nitrogen Cast Austenitic Steels. This group of papers will be given at 2 pm in the Waldorf Ballroom at the Conrad Hilton in Chicago.

Three other papers to be presented at other sessions are: Summary of the Hot Pressing of Aluminum Powder; Iron-Boron-Carbon System; and Bainite Reaction in a Plain Carbon, Hypoeutectoid Steel.

Nuclear Metallurgy

Another session, to be presented for the first time in the history of the Annual Meeting, is the one on Nuclear Metallurgy. Papers to be offered include: Deformation Texture and Recrystallization Texture of Rolled Uranium Sheet; Preparation of Alpha Uranium Single Crystals; Deformation Mechanisms of Alpha Uranium Single Crystals; An Electrolytic Process for Refining Commercial Uranium; and Melting of High Purity Uranium.

AIME Annual Meeting Program, Feb. 12 to 17, 1955

Conrad Hilton Hotel, Chicago

Names of Divisions and Subdivisions are coded as follows: MIED—Mineral Industry Education Div. MED—Mineral Economics Div. M—Mining Subdiv. G—Geology Subdiv. Geophys.—Geophysics Subdiv. NM—(nonmetallics) Industrial Minerals Div. Coal—Coal Div. MBD—Minerals Beneficiation Div. EMD—Extractive Metallurgy Div. IMD—Institute of Metals Div. ISD—Iron & Steel Div. Petroleum Branch—Named as such. SEG—Society of Economic Geologists.

SATURDAY, FEBRUARY 12

10 am
Council of Section Delegates
5:30 pm
National Membership Steering Committee

SUNDAY, FEBRUARY 13

9 am
Mining Branch Council
10 am
National Membership Committee
11 am
Inter Branch Council
12:30 pm
National Membership Committee Luncheon
2 pm
Board of Directors
2:30 pm
MIED—Teaching of Recent Developments in Mineral Engineering
5:30 pm
MIED—Cocktails
6 pm
MIED—Buffet Supper
7 pm
MIED—Teaching of Recent Developments in Mineral Engineering
IMD Publication Committee
8:30 pm
IMD Program Committee

MONDAY, FEBRUARY 14

8 am
Registration
9:45 am
Petroleum Branch Executive Committee
9:30 am
ISD—Statistical Methods
9:45 am
MIED—Engineering Enrollments
M—Small Mines Problems
G—Exploration
G—Uranium
Geophys—General
NM—Ceramics
Coal—Preparation-Flotation
IMD—Nuclear Metallurgy
IMD—Constitution
10 am
Metals Branch Council
MBD Business Meeting
MIED Executive Committee
12 noon
Welcoming Luncheon
J. D. Rettaliata
President, Illinois Institute of Technology
2:30 pm
MGGD Executive Committee
M—Open Pit Mining
G, Geophys—Exploration
G, SEG—Exploration Studies
NM—Mineral Aggregates
Coal—Preparation
MBD—Analytical Techniques
MBD—Materials Handling
ISD, EMD—Thermochemistry of Slags
EMD—Aluminum
IMD—Nuclear Metallurgy
IMD—Recrystallization
Petroleum—World Developments During 1954
3 pm
JOURNAL OF METALS Editorial Advisory Board
4 pm
Metals Branch Research Publications Fund Committee
4:30 pm
IMD Membership Committee
6:30 pm
Cocktail Party
8 pm
Dinner-Smoker

TUESDAY, FEBRUARY 15

7:30 am
EMD Executive Committee Breakfast
IMD Titanium Committee Breakfast
8 am
MBD Scotch Breakfast
9 am
MED Business Meeting—Economics
M—Block Caving, Underground Problems
G—Mineral Resources
NM—Rare Minerals
NM—Cement, Lime, Gypsum
Coal—Utilization, Carbonization
ISD—New Processes in Industry
IMD—Deformation I
Petroleum—Technical Session
9:30 am
MBD—Concentration
EMD, MBD—Hydrometallurgy; Solution, Precipitation
10 am
Mining Branch Council
10:45 am
ISD Business Meeting
11 am
Howe Memorial Lecture
J. S. Marsh
12:15 pm
MGGD Luncheon
ISD Physical Chemistry of Steelmaking Luncheon
IMD Executive Committee Luncheon
Coal Luncheon
2 pm
MED—Economics
NM—Fillers, Fibers, Pigments
Coal—Steam, Air Pollution
MBD—Concentration
ISD—Mechanical Working
EMD—Physical Chemistry
EMD, MBD—Hydrometallurgy; Solution, Precipitation
IMD—Deformation II
Petroleum—Technical Session
2:30 pm
MGGD Jackling Lecture
E. D. Gardner
3:45 pm
MGGD—General Session
4 pm
Annual AIME Business Meeting
Coal Executive Committee
5 pm
Board of Directors, Executive Session
6 pm
Metals, Mining, Petroleum Branches Cocktail Parties
7 pm
Metals, Mining, Petroleum Branches Annual Dinners
9 pm
Informal Dance

WEDNESDAY, FEBRUARY 16

7:30 am
ISD Executive Committee Breakfast Meeting
EMD Committee Chairmen Breakfast
9 am
MED—Economics
M—Research
G, Geophys—Iron Ore Exploration
NM—Industrial Waters
Coal—Underground Mining
MBD—Symposium: Mill Design
MBD—Concentration
ISD—Sulphur and Oxygen
ISD—Blast Furnaces and Refractories
EMD—Symposium: Refractories for Processing Liquid Metals, Slags
IMD—Transformation I
NOHC—Basic Furnaces, Refractories
9:30 am
Petroleum—Technical Session
10:45 am
IMD Annual Business Meeting
11 am
IMD Lecture
Clarence Zener
12:15 pm
NM Luncheon
EMD Stag Luncheon and Business Meeting
2 pm
MED—Economics
MIED, MGGD—Engineering Talent
M—Drilling Problems
Geophys—Technique
G, Geophys—Iron Ore Exploration
NM—Industrial Waters
NM—Chemical Raw Materials
Coal—Underground Mining
MBD—Symposium: Planning Ore Beneficiation Plant
MBD—Concentration
ISD—Structure, Segregation, Rimming Steel Ingots
EMD—Symposium: Refractories for Processing Liquid Metals, Slags
IMD—Transformation II
NOHC—Rimming Ingots, Steelmaking Developments
3 pm
AIME Nominating Committee
4 pm
NM Executive Committee
7 pm
Annual Banquet
President's Reception

THURSDAY, FEBRUARY 17

9 am
M—Stratified Mining
G—Features
NM—Sands, Abrasives
Coal, SEG—Geology
MBD—Crushing, Grinding
MBD—Solids-Fluids Separation
ISD—High Temperature Kinetics
ISD—Steelmaking
EMD—Pyrometallurgy, Hydrometallurgy of Zinc, Lead
EMD—Titanium
IMD—Diffusion, Powder Metallurgy
IMD—Research in Progress
12:15 pm
MBD Annual Luncheon
EMD Physical Chemistry Luncheon
IMD Powder Metallurgy Luncheon
2 pm
Geophys—Radioactivity
NM—Sands, Abrasives
Coal, SEG—Symposium: Differential Thermal Analysis
ISD—High Temperature Thermodynamics
EMD—Titanium-Zirconium
IMD—Symposium: Powder Metallurgy
IMD—Oxidation, Melting
2:30 pm
MBD—Clean-up Session

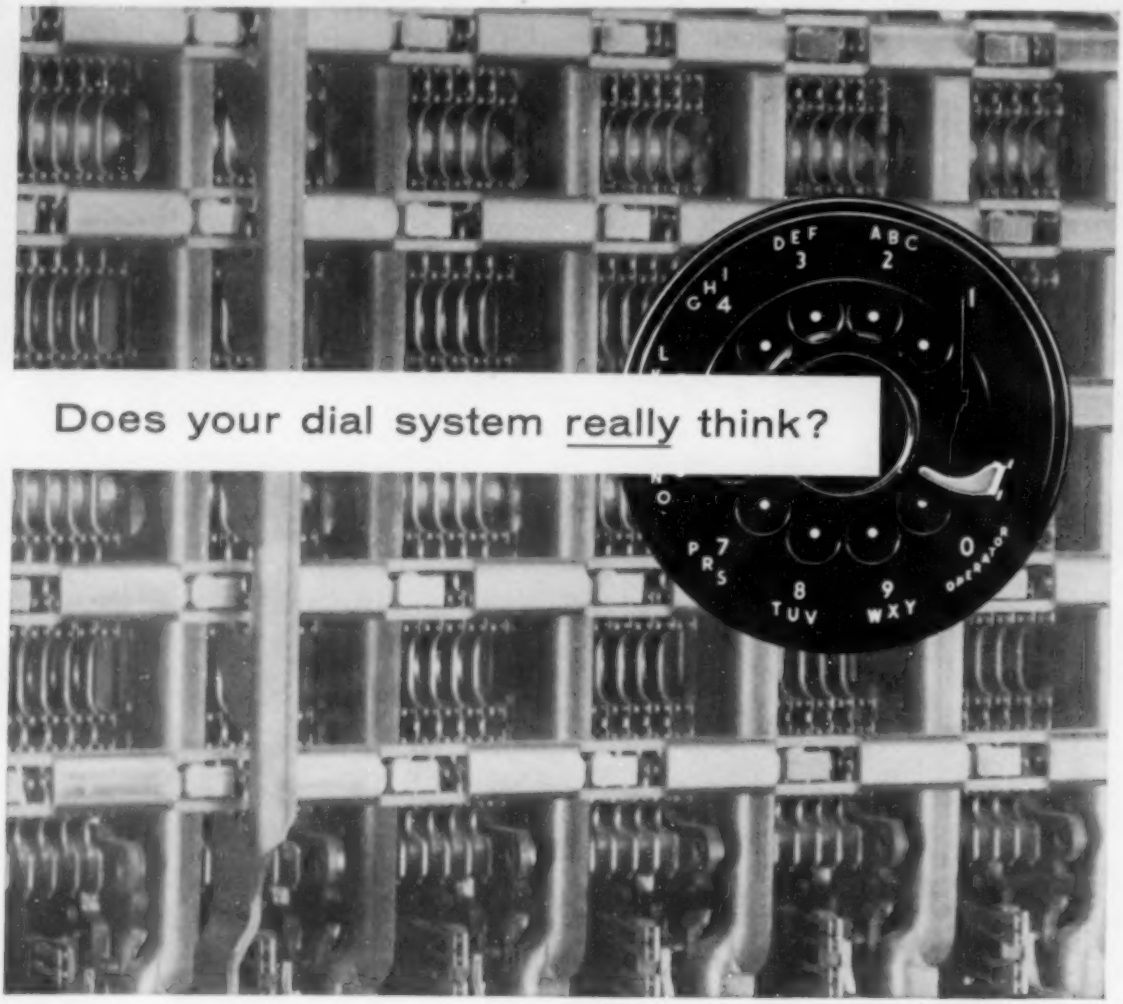

Does your dial system really think?

Part of the control equipment of a modern dial system—dial telephony's equivalent of a brain. It goes into action the instant you dial a call, selecting the telephone you want to reach and directing the switches that set up the connection . . . just as the brain directs the muscular actions of the body.

This question can't be answered until we learn more about the nature of thought. But dial telephone systems *do* simulate many of the processes of the human brain. For example, when a number is dialed, Bell's newest switching system—

COUNTS the dial pulses

REMEMBERS them

DECIDES ON the best route to a nearby town or across the nation

TESTS to see if the route is clear

SELECTS an alternate if the first route is busy

REPORTS difficulties in circuits, if any

Today's automatic switching reflects the creative thinking of many scientists and engineers at Bell Telephone Laboratories. Each year your dial telephone is able to do more for you. And this is but one phase of the continuing effort to keep your Bell telephone service the world's best.

BELL TELEPHONE LABORATORIES

IMPROVING TELEPHONE SERVICE FOR AMERICA PROVIDES CAREERS FOR CREATIVE MEN IN SCIENTIFIC AND TECHNICAL FIELDS

Personals

L. W. DAVIS

Leroy W. Davis has been appointed technical superintendent at the aluminum forging plant, Kaiser Aluminum & Chemical Corp., Erie, Pa. Mr. Davis had been technical superintendent of the Kaiser aluminum plant at Halethorpe, Md. He has had many years of experience in the aluminum forging and casting industries.

R. Maddin, visiting lecturer in metallurgy at the University of Birmingham for 1954, has returned to his post as associate professor at the Johns Hopkins University.

R. W. Dickson, U. S. Steel Corp., has been promoted from division superintendent, west mills, Gary Steel Works, to assistant general superintendent, Youngstown District Works.

Howard F. Davis, Jr., is now metallurgical engineer for the Quebec Metallurgical Industries Ltd., Ottawa, Ont., Canada. Mr. Davis had been associated with the Buckeye Steel Castings Co., Columbus, Ohio.

Howard W. Leavenworth, Jr., has joined the laboratory of the Pratt & Whitney Aircraft Co., Waterbury, Conn.

William P. Achbach is now principal metallurgical engineer for the Battelle Memorial Institute, Columbus, Ohio. Mr. Achbach had been an experimental metallurgist with the Aero-Allison Div., General Motors Corp., Dayton, Ohio.

B. Egeberg has retired from the International Silver Co., Meriden, Conn., and is now conducting a private consulting business in Meriden, Conn.

Frederick F. Franklin has been appointed district manager of the Cleveland office of Vanadium Corp. of America. Mr. Franklin was formerly assistant district manager.

Theodore B. Counselman is no longer associated with the Dorr Co., Stamford, Conn. He has become an associate member of Behre Dolbear & Co., New York, N. Y. Mr. Counselman is a vice president and director of AIME.

Robert Raisig is production manager for the Apex Smelting Co., Long Beach, Calif. He had been assistant production manager at the Chicago office.

F. WEIR

Frank Weir has been appointed assistant general sales manager for the Harbison-Walker Refractories Co., Pittsburgh, Pa. He had been Pittsburgh district sales manager since 1949. Mr. Weir has been associated with Harbison-Walker since 1923.

F. A. KAUFMAN

Fred A. Kaufman was appointed vice president in charge of sales and manufacturing, McKay Co., Pittsburgh, Pa. Prior to his present appointment he had been general sales manager of all McKay products.

W. S. MOUNCE

William S. Mounce has joined the International Nickel Co., development and research div., as a member of the constructional alloy steel section. Mr. Mounce has been with Inco since 1945.

John H. Hollomon, manager of the metallurgy dept., General Electric Research Laboratory, Schenectady, N. Y., has been announced by the National Junior Chamber of Commerce as one of America's 10 outstanding young men of 1954.

W. P. Ruemmler has resigned as production superintendent, National Lead Co., Fredericktown, Mo., to accept the position of plant engineer for the Pacific Smelting Co., Torrance, Calif.

Norman C. Michels has been appointed to the newly established position of assistant vice president in charge of engineering for the U. S. Steel Corp.'s Tennessee Coal & Iron Div., Fairfield, Ala. Mr. Michels had been located at Pittsburgh, where he was chief engineer, project development, U. S. Steel Corp., engineering div.

Richard S. Mateer is now assistant professor, dept. of metallurgical engineering, University of Pittsburgh, Pa. He had been associated with the Kaiser Aluminum & Chemical Corp., Spokane, Wash.

Joseph H. Bach, formerly section head, atomic energy div., Sylvania Electric Products Inc., Bayside, N. Y., is now assistant to manager, fuel elements, Westinghouse Atomic Power Div., Bettis Field, Pittsburgh.

Boris Lubienski, mill superintendent for the Empresa Minera San Jose, Oruro, Bolivia, is now metallurgist for the New York & Honduras Rosario Mining Co., San Juancito, Honduras.

F. M. Hamilton, who had been supervisor of agglomeration research at Jones & Laughlin Steel Corp., ore research div. laboratory, Negaunee, Mich., has been appointed to a similar capacity at J&L's Star Lake, N. Y., ore div. Mr. Hamilton has been with J&L for 20 years.

Frank H. Riddle, vice president, Champion Spark Plug Co., has been named the 1955 recipient of the Albert Victor Bleininger Award. The award is conferred by the American Ceramic Society, Pittsburgh Section, for distinguished achievement in the field of ceramics.

J. W. Duncan, U. S. Steel Corp., is superintendent, blast furnaces, Gary Steel Works, Gary, Ind. He had been technical assistant, blast furnaces, Pittsburgh, Pa.

William T. Reynolds has joined the Aluminum Co. of America, process metallurgy div., research laboratories, New Kensington, Pa. Mr. Reynolds has been a research assistant in the metals research laboratory, Carnegie Institute of Technology, Pittsburgh, Pa.

Oliver A. Gottschalk, formerly assistant controller of the Carborundum Co., Niagara Falls, N. Y., has been appointed assistant to the president.

A. P. GAGNEBIN

Albert P. Gagnebin has been appointed assistant manager of the nickel sales dept., International Nickel Co., and **Edward B. Bitzer** was named assistant manager of the nickel alloys dept. **Keith D. Millis** is in charge of the ductile iron section of the development and research div., succeeding Mr. Gagnebin. Mr. Gagnebin is co-inventor of the company's *Ductile Iron.* He joined Inco at the research laboratory in Bayonne, N. J. in 1932. Mr. Bitzer has been associated with the company since 1931, and had been located in Pittsburgh, Cleveland, and Chicago until 1935 when he was transferred to New York. Mr. Millis was a member of the research laboratory when he joined the firm in 1939. He is also a co-inventor of *Ductile Iron.*

W. M. Kelley has been elected president of Reserve Mining Co., jointly owned by Republic Mining Co. and Armco Steel Corp. Mr. Kelley, who was vice president in charge of operations, Republic Mining Co., still will be available to Republic in a consulting capacity.

Samuel S. Douglas, Joy Mfg. Co., Pittsburgh, has been made a special representative to the iron and steel industry. Mr. Douglas has been a member of the Joy organization as a representative in the Pittsburgh district since 1948.

Fritz V. Lenel, professor of metallurgical engineering at Rensselaer Polytechnic Institute, has been authorized by the U.S. Metals Refining Co., Carteret, N. J., to open a program of research on porous metal sheets.

James A. Wilson has been appointed plant manager of the Kaiser Aluminum & Chemical Corp., Baton Rouge, La., alumina plant. Mr. Wilson had been manager of the chemical phosphate dept., International Minerals & Chemical Corp., Bartow, Fla.

R. J. Studders, magnet development engineer, Carboloy Dept., General Electric Co., has been appointed manager of magnetic products engineering.

Charles N. Kimball, president of the Midwest Research Institute, Kansas City, Mo., has been elected to the board of governors of the Scientific Research Society of America.

John C. Neemes, Jr., International Nickel Co., Inc., has been elected chairman of the mining and metallurgy committee of the Alumni Assn., Institute of Technology, University of Minnesota.

Harry O. Zimmerman was appointed manager of Inland Steel Co., coal properties, Wheelwright, Ky. Mr. Zimmerman was formerly assistant to the manager.

Joseph K. Balkwill recently joined the staff of Electro Metallurgical Co., metals research laboratories, as a senior research assistant in the engineering research group.

John J. Murray and **Richard Doughton, Jr.,** have been appointed development engineers in the product development div., Jones & Laughlin Steel Corp., Pittsburgh.

Thomas A. Ratkowski has been appointed division manager for engineering and development, American Manganese Steel Div., American Brake Shoe Co., New York. He will be located at Chicago Heights, Ill.

Niels C. Beck, program development engineer, has been promoted to assistant manager of program development, Armour Research Foundation, Illinois Institute of Technology, Chicago, Ill.

Michel E. Puyans has been elected vice president, finance and **William O. Ashe** was elected treasurer, Great Lakes Carbon Corp., New York.

Joseph Daniels, professor emeritus of mining engineering and metallurgy, University of Washington, was recently named to the Washington State College educational mission to Pakistan. He will establish a dept. of mineral engineering at the Punjab University College of Engineering and Technology in Lahore.

Roger J. Wighton has been appointed a sales engineer in the chemical div., Kaiser Aluminum & Chemcial Sales, Inc., Pittsburgh.

William R. Clough and **Arthur L. Gear** have joined the staff of the Electro Metallurgical Co.'s metal research laboratories, Niagara Falls, N. Y.

Archie K. Beard was appointed manager of the metal processing div. and eastern divisional manager of the new chem-mill div., Turco Products, Inc., Los Angeles, Calif.

H. W. Seyler, general superintendent of Clairton Works, has been appointed assistant vice president, coal chemical operations, U. S. Steel Corp., New York. Mr. Seyler has been general superintendent of Clairton Works for 11 years.

Frank M. Cashin, manager of the chemicals div., has been appointed a vice president of Kaiser Aluminum & Chemical Corp., Oakland, Calif.

S. Sydney Minault was named general manager of the equipment div., National Research Corp., Cambridge, Mass.

Philip F. Thayer was appointed vice president and general manager of the metals div., General Metals Corp., San Francisco, Calif.

C. P. Lavelle has been appointed division manager of the Hygrade metal finishing div., U. S. Hoffman Machinery Corp., New York, N. Y. Mr. Lavelle was formerly plant engineer for the Sikorsky Helicopter div., United Aircraft Corp., Bridgeport, Conn.

H. W. North was recently appointed chief engineer of the newly established process equipment dept., engineering works div., Dravo Corp. Mr. North will be located at Neville Island, Pittsburgh, Pa.

Andrew H. Bowman has been promoted to assistant secretary of the Wheeling Steel Corp. and subsidiary companies. In 1917, Mr. Bowman joined the general offices of Whitaker-Glessner Co., predecessor to Wheeling Steel.

Frederic L. Moffet has been appointed chief metallurgist of the Park Works, Crucible Steel Co. of America, Pittsburgh. Mr. Moffet

joined Crucible in 1934 as a metallurgist.

Joseph W. Kennedy, Jr., was recently named vice president in charge of the Ohio seamless tube plant at Shelby, Ohio of the Copperweld Steel Co. **Reid Pittenger** was named manager of industrial relations and **Raymond E. Dewey** has been made manager of operations.

Ralph C. Froehlich is head of the new Phoenix office of the Micro Switch div., Minneapolis-Honeywell Regulator Co. **Donald S. Schultz** is being transferred from Philadelphia to take charge of the Charlotte office and **Richard J. Petersen** is in charge of the Denver area.

Howard N. Farmer, Jr., has joined the development and research div., International Nickel Co., Inc., as a member of the west coast technical field section, Los Angeles, Calif.

Hilary A. Humble has been named product sales manager for various magnesium products, Dow Chemical Co., Midland, Mich. Mr. Humble had been product sales manager for cathodic protection activities, magnesium dept.

G. E. Brock, acting staff engineer, rolling mills, Jones & Laughlin Steel Corp., has been named resident engineer at J&L's Aliquippa Works.

Dewey O. Olson was appointed mill works manager of the Follansbee plant, Follansbee, W. Va. Mr. Olson has been general superintendent of the Michigan steel div., Great Lakes Steel Corp., for 16 years.

Norman N. Breyer, formerly chief of the armor section, Detroit Arsenal, has joined the Continental Foundry & Machine Co., East Chicago, Ind., as metallurgist for the armor div.

James Boyd has been appointed vice president, exploration, Kennecott Copper Corp., New York. He succeeds **Anton Gray** who recently resigned due to ill health. Mr. Boyd had served as manager of the corporation's exploration dept. since 1951, when he joined the organization. Prior to that he had been director of the U. S. Bureau of Mines.

Obituaries

An appreciation of

Malcolm Black

By R. L. Healy

Malcolm Black, mill superintendent of Wright-Hargreaves Mines Ltd., died suddenly at his home in Kirkland Lake, Ont., on Nov. 7, 1954 at the age of 69 years.

He was born in Carluke, Scotland, on Apr. 26, 1885 and was educated in the technical schools of that country.

He came to Cobalt about 1906 and prospected in Cobalt and Larder Lake areas of northeastern Ontario and in northern Manitoba.

Early work in mines and mines of Cobalt was followed by metallurgical and milling experience at the old Vipond mine in Porcupine and at the Hollinger mill in Timmins for about eight years. During World War I he was at the Moose Mountain iron mine. He was in charge of milling at the Argonaut mine east of Kirkland Lake between 1923 and 1926 which was followed by two years with the Associated Goldfields mill near Larder Lake. He joined Wright-Hargreaves Mines Ltd. in August 1928 of which milling plant he was in charge until the time of his death. It was between 1932 and 1933 that the mill capacity was doubled to 1250 tons per day.

Mr. Black had an ever-inquisitive mind toward improving the metallurgy and efficiency of his cyanide milling plant and was recognized by his fellow metallurgists and millmen in the gold mining camps of Canada and the U. S. as a keen student of his work. In that regard, he contributed of his experience in the following papers:

Sampling Methods at the Mill of Wright-Hargreaves Mines, Trans., CIM, Vol. 38, 1935. *Milling and Metallurgy at the Wright-Hargreaves Mines, Limited*, Trans., CIM, Vol. 38, 1935. *Wright-Hargreaves Improves its Milling Practice*, Engineering & Mining Journal, March, April, and May, 1939. *Recent Improvements in Milling Practice at Wright-Hargreaves*, Trans., CIM, Vol. LI, 1948.

He was a member of the Canadian Institute of Mining and Metallurgy, the AIME (1940), and the Assn. of Professional Engineers of Ontario.

He was constructively interested in people and was especially active among boys. His work with the camera was well recognized, many of his pictures having been shown in the salons of Canada and the U. S. His adeptness with the movie camera has been recorded in the filming of the mining, milling, and surface operations of the Wright-Hargreaves mine and more recently in his colored films of holidays spent in the Maritime Provinces and in Scotland and England.

Mr. Black was a member of the United Church. He was a member of the Masonic lodge in Kirkland Lake which order he joined in 1907; he was also a charter and life member of the Timmins lodge.

He is survived by his wife, the former Ascelia Baxter of Cobalt, and by two sons and one daughter, Andrew a metallurgical engineer of Cobalt, Keith of Ottawa, and Margaret (Mrs. G. M. Douglas) of Chatham, Ont.

An Appreciation of

Alfred Hollis Geisler

By W. R. Hibbard

Alfred Hollis Geisler, research associate in the metallurgy dept., General Electric Research Laboratory, died at Schenectady, Dec. 7, 1954, after a brief illness. He was 38 years old.

Dr. Geisler was born in Pittsburgh, Pa., where he attended the public schools and Carnegie Institute of Technology, receiving a B.S. degree in 1938 and a D.Sc. in 1942. Before joining the General Electric

A. H. GEISLER

laboratory in 1946, he was a senior research metallurgist at the Alcoa Research Laboratories, New Kensington, Pa.

His work as a physical metallurgist was widely recognized in the fields of alloy transformations, X-ray and neutron diffraction, metallography and electron microscopy. He authored more than 35 technical papers, one of which won an AIME Mathewson Award as the outstanding IMD paper in 1943. Significant contributions were made by him to the science of precipitation hardening, transformation of martensite, permanent magnet alloys, crystallography, and pole figures. He served on the IMD Technical Publications Committee.

In addition to the AIME, he was a member and committee worker in the ASM and the American Crystallographic Assn. He was a member of Sigma Xi. In Schenectady he was affiliated with Union Presbyterian Church and was active in Cub Scout work.

Surviving are his wife, the former Martha Donald of Pittsburgh, and two sons, Donald R., 11, and Alfred H., Jr., 9.

Raymond F. Bacon (Member 1914) died on Oct. 14, 1954. Dr. Bacon had been a consulting chemical engineer in New York City. He was born in Indiana and attended DePauw University, and the University of Chicago. During his career he was an instructor at various universities and was also associated with Mellon Institute.

Harold James Walker (Member 1950), formerly associated with Re-

public Steel Corp., Warren, Ohio died on Aug. 7, 1954. Mr. Walker was a native Pennsylvanian. He joined the Youngstown Sheet & Tube Co. in 1924. In 1929 he became associated with the Republic Steel Corp., as a melter. In 1939 he was promoted to open hearth superintendent and in 1947 was named general superintendent of steel production at Warren, Ohio.

Necrology

Date Elected	Name	Date of Death
1946	Peter M. Anderson	Nov. 5, 1954
1952	J. R. Crenshaw	Unknown
1942	Michael Dwyer	Dec. 1953
1915	L. B. Eames	Dec. 3, 1953
1918	Alfred H. Geisler	Dec. 7, 1954
1945	Ray G. Gibson	Oct. 16, 1954
1923	Silas L. Gillan	Nov. 9, 1954
1947	Francis G. Hoffman	Nov. 24, 1954
1918	William Wallace Inglis	Jan. 19, 1953
1937	C. H. McNaughton	Unknown
1914	Royden C. Philpott	Feb. 7, 1954
1929	Erwin Sohn	Unknown
1946	E. J. Tompkins	Aug. 25, 1954
1921	Jay Tuttle	Nov. 3, 1954
1945	Lawrence Vander Leck	Unknown
1921	Alexander Walker	Aug. 3, 1954
1944	Everett Wilcox	Nov. 2, 1954
1953	John E. Wilcox	Unknown

Proposed for Membership

— Metals Branch AIME —

Total AIME membership on Dec. 31, 1954 was 21,816; in addition 2179 Student Associates were enrolled.

ADMISSIONS COMMITTEE

O. B. J. Fraser, Chairman; R. B. Caples, Vice-Chairman; F. A. Ayer, A. C. Brinker, R. H. Dickson, Max Gensamer, Ivan A. Given, Fred W. Hanson, T. D. Jones, Sidney Rolle, J. H. Scaff, John T. Sherman, F. T. Sisco, Frank T. Weems, R. L. Ziegfeld.

The Institute desires to extend its privileges to every person to whom it can be of service, but does not desire as members persons who are unqualified. Institute members are urged to review this list as soon as possible and immediately to inform the Secretary's office if names of people are found who are known to be unqualified for AIME membership.

In the following list C/S means change of status; R, reinstatement; M, Member; J, Junior Member; A, Associate Member; S, Student Associate.

California
Long Beach—Raisig, Robert (M) (C/S—A-M)
Los Angeles—Frederick, Stewart F. (J) (R-J)

Connecticut
Orange—Connors, Henry E. (M)

Delaware
Wilmington—Symonds, John (J)

Idaho
Kellogg—Bird, Robert L., (J)
Triumph—Jorgensen, M. A. (M) (R. C/S—J-M)

Illinois
Calumet City—Dexter, Eli W. (M)
Chicago—Mohr, Joseph S., Jr. (A)
Collinsville—Fornero, John M. (A)
Elmhurst—Richey, James T. (M)

Indiana
Long Beach, Michigan City—Leahy, Frank W. (A)
Michigan City—McBride, Robert J. (A)

Kentucky
Louisville—Meyer, John K. (M)

Maryland
Baltimore—Muth, Frank A. (M)
Baltimore—Slocum, John C. (M)
Baltimore—Treppe, Vincent J. (A)
Catonsville—Funke, Richard H., Jr. (M)

Massachusetts
Belmont—Orowan, Egon (M)
Cambridge—Kichino, Niwa (M)
Wilbraham—Safford, Alden (M)

Michigan
Birmingham—Nimeth, Anthony J. (A)
Birmingham—Reilly, William J. (M)
Grosse Pointe—Gottfredson, Lawrence, Jr. (A)
Palmyra—Hart, Robert A. (M)
Plymouth—King, James (A)

Missouri
St. Louis—Bollwerk, George P., Jr. (J)

New Jersey
Summit—Hittinger, William C. (M)

New York
Albany—DeVries, Ralph P. (M)
Grand Island—Saunders, Earle R. (M)
Lewiston—Hamby, Durward E. (M) (C/S—J-M)
Londonville—Reynolds, Edward E. (M) (C/S—A-M)
New York—Kee, Herbert L. (J) (R. C/S—S-J)
Niagara Falls—Lamont, John L. (M)
Niagara Falls—Martin, Roy C. (M) (C/S—J-M)
Troy—Nelson, Edward C. (M) (C/S—A-M)
Utica—Zleman, John G. (M)
White Plains—Cohan, Alvin S. (M) (C/S—J-M)
White Plains—Ydstie, Birger L. (M) (C/S—A-M)

North Carolina
Raleigh—Austin, William W., Jr. (R. M)

Ohio
Canton—Hearn, William L. (A)
Chagrin Falls—Farrow, Cecil (A)
Cleveland—Miller, Richard G. (M)
Cleveland Heights—Miller, William R. (M)
Columbus—Berger, Lewis W. (J)
Middletown—Bergmann, William W. (M)
Middletown—Sigi, Robert L. (J)
Poland—Ott, Kenneth W. (M)
Salem—Sabol, Frank P. (M)
South Euclid—Wyatt, James L. (M) (C/S—J-M)
Trenton—Nitterhouse, Frank W. (M)
Warren—Anderson, Harry L. (M) (C/S—A-M)
Youngstown—Phillips, James E. (M)

Oklahoma
Henryetta—McCutcheon, Frank G. (M)

Pennsylvania
Beaver Falls—Marshall, Frank I. (A)
Bethlehem—Lehman, Albert L. (M)
Birdsboro—Heck, George W., Jr. (M)
Bridgeville—Zook, James R. (A)
Butler—Ford, Thomas B. (A)
Butler—Schiebel, Ralph J. (M)
Carnegie—Green, John J. (A) (R. C/S—S-A)
Johnstown—Rhine, Bryant A. (A)
Johnstown—Swank, E. Ferguson (A)
Lebanon—Templeton, Harold C. (A)
Library—Vogt, Edward G. (M)
McKeesport—Hunter, Harry B. (M) (C/S—A-M)
New Kensington—Farmer, Max C. (M)
North Braddock—Paviovic, Dusan (M) (C/S—A-M)
Philadelphia—Janney, John B. (A)
Pittsburgh—Baisley, John H. (A)
Pittsburgh—Dally, Robert W. (A)
Pittsburgh—Freeman, Hyman (M)
Pittsburgh—Handf, Edward A. (A)
Pittsburgh—Harman, Eugene S. (M)
Pittsburgh—Hastings, Philip J. (A)
Pittsburgh—Hill, Omar K. (A)
Pittsburgh—Morgan, Willard L. (A)
Pittsburgh—Oxnard, Robert T. (A)
Pittsburgh—Wolfe, Richard A. (J)
Tarentum—Bryan, Ralph J. (J)
Willow Grove—Barkley, William J., Jr. (M)

Tennessee
Knoxville—Collins, Douglass S. (A)

Washington
Snohomish—Miller, Ralph E. (A)
Spokane—Fetzer, Maurice C. (M) (R. C/S—J-M)
Vancouver—Howard, Elmer E. (M)

British Guiana
Kwakwani, Rio Berbice—McDonald, Romie T. (M)

Canada
Ottawa, Ont.—Faurechou, Donald K. (A)
Ottawa, Ont.—Gertsman, Sol L. (A)
Pte. Claire, Que.—Tibbits, John W. (A)
Toronto, Ont.—Fincham, Christopher J. B. (J)
Vancouver, B. C.—Halpern, Jack (M)

Korea
Seoul—MacCallum, Robert L., Jr. (J) (R. C/S—S-J)

Mexico
Coahuila—Regalado', Fernando R. (J)
Monterrey—Elizondo, Gilberto G. (M)

Sweden
Sandviken—Angel, Tryggve G. (M) (C/S—J-M)

Switzerland
Neuhausen am Rheinfall—Bloch, Ernst A. (M)

Advertisers' Index

Air Reduction Co., Inc. *G. M. Basford*	*
Ajax Electrothermic Corp. *Thomas R. Sunheim Adv.*	*
Ajax Engineering Corp. *Eldridge, Inc.*	221
Aluminum Co. of America *Fuller & Smith & Ross Inc.*	*
American Bridge Div., U. S. Steel Corp. *Batten, Barton, Durstine & Osborn, Inc.*	*
Bailey Co., Wm. M. *Walker & Downing*	*
Basic Refractories Inc. *The Griswold-Eshleman Co.*	*
Bell Telephone Labs. *N. W. Ayer & Son, Inc.*	276
Buehler Ltd. *Kreicker & Meloan, Inc.*	220
Carondelet Foundry Co. *Whitehead & Sprague, Inc.*	*
Consolidated Vacuum Corp. *Charles L. Rumrill & Co., Inc.*	227
Electro Met. Div., Union Carbide & Carbon Corp. *J. M. Mathes, Inc.*	223
Ferro Engineering Co. *C. A. Reece Ind. Publicity*	*
General Electric Co., X-Ray Dept. *Klau, Van Pietersom-Dunlap Assoc.*	*
Great Lakes Carbon Corp. *Davis, Parsons & Strohmeier, Inc.*	*
Harbison-Walker Refractories Co. *Walker & Downing*	*
Hevi Duty Electric Co. *Camm, Costigan, Inc.*	222
International Nickel Co. *Marschalk & Pratt Co.*	232
Minneapolis-Honeywell Regulator Co. *Atkin-Kynett Co., The*	*
Molybdenum Corp. of America *Smith, Taylor & Jenkins, Inc.*	218
Morgan Construction Co. *Davis Press, Inc., The*	Third Cover
National Carbon Div., Union Carbide & Carbon Corp. *William Esty Co., Inc.*	Fourth Cover
Pittsburgh Lectromelt Furnace Corp. *Fuller & Smith & Ross Inc.*	*
Ramtite Co., The *Marsteller, Gebhardt and Reed Inc.*	*
Smeeth-Harwood Co. *Allbright Associates Adv.*	226
Stokes Machine Co., F. J. *John Mather Lupton Co., Inc.*	*
Swindell-Dressler Corp. *Walker & Downing*	*
Titanium Alloy Mfg. Div., National Lead Co. *Comstock & Co.*	*
Titanium Metals Corp. of America	231
United States Graphite Co., The *Price, Tanner & Willox, Inc.*	Second Cover
U. S. Steel Corp. Columbia-Geneva Steel Div. Tennessee Coal & Iron Div. U. S. Steel Supply Div. U. S. Steel Export Co. *Batten, Barton, Durstine & Osborn, Inc.*	219
Wyman-Gordon Co. *John W. Odlin Co., Inc.*	*

* Previous issue.

A Straight Shot of 925 FEET

At the NEW
FAIRLESS WORKS
of the United States Steel Corporation

A MORGAN
Horizontal-Vertical Continuous Rolling Mill reduces billets to merchant bar sections "straightaway" for 925 feet from furnace to cooling bed

MORGAN CONSTRUCTION COMPANY
WORCESTER, MASSACHUSETTS RM-51

Rolling Mills · Morgoil Bearings · Wire Mills
Regenerative Furnace Control · Ejectors · Gas Producers

English Representative
International Construction Co., 56 Kingsway, London, W. C. 2, England

NATIONAL PITCH-RESERVOIR NIPPLES*

TRADE-MARK

THE NEW PITCH-RESERVOIR NIPPLE, an exclusive "National" product, is another major contribution by National Carbon Company to more efficient electric furnace operation. You can now be sure that tight joints will stay tight under normal load and service conditions.

"NATIONAL" PITCH-RESERVOIR NIPPLES, designated Type PR-F, are now available for electrode diameters from 14" to 24". Thoroughly proved in service, they are identical in strength, size, shape, tolerances, composition and quality to our standard, tapered, graphite nipples. Talk it over soon with your National Carbon Company electrode representative.

***PATENTS PENDING**
EXCLUSIVE DESIGN

HERE'S HOW IT WORKS:

Reservoirs near each end of the nipple contain pitch. As the electrode column becomes hot in service, the pitch flows from the reservoirs into the threaded sections of the joint and cokes out, cementing and locking the threads of the nipple and sockets together.

FOR ELECTRODES AND ELECTRODE SERVICE...
Rely on NATIONAL CARBON COMPANY!

The term "National" is a registered trade-mark of Union Carbide and Carbon Corporation

NATIONAL CARBON COMPANY
A Division of Union Carbide and Carbon Corporation
30 East 42nd Street, New York 17, N. Y.

Sales Offices: Atlanta, Chicago, Dallas, Kansas City, Los Angeles, New York, Pittsburgh, San Francisco. *In Canada:* Union Carbide Canada Limited, Toronto

Journal of METALS

FEBRUARY 1955

VOL. 7, NO. 2, IN TWO SECTIONS—SECTION TWO

TRANSACTIONS SECTION

Embrittlement of Molybdenum by Neutron Radiation	C. A. Bruch, W. E. McHugh, R. W. Hockenbury	281
Solid Solubility of Calcium in Magnesium	E. C. Burke	285
A Study of the Room Temperature Fatigue Properties of Molybdenum	W. L. Bruckart, W. S. Hyler	287
Allotropic Transformation at High Temperatures—A Discussion	A. G. Metcalfe (Reply by J. O. McCaldin, P. Duwez)	290
Molybdenum Deposition on Titanium	S. Taur, A. Styka, G. Fischer	291
Continuous Multistage Separation by Zone-Melting	W. G. Pfann	297
An Evaluation of Dissociated Ammonia and Hydrogen Atmospheres for Sintering Stainless Steel	H. S. Kalish, E. N. Mazza	304
Relation of Strength, Composition, and Grain Size of Sintered WC-Co Alloys	J. Gurland, P. Bardzil	311
Microstructures of Pyrophoric Alloys	R. D. Reiswig, D. J. Mack	315
A Study of the Microstructure of Titanium Carbide	H. Blumenthal, R. Silverman	317
High Temperature Vacuum Etching on Pure Titanium	W. D. Bennett	322
Influence of Heat Treatment on the Ductile-Brittle Transition Temperature of Semikilled Steel Plate	R. H. Frazier, F. W. Boulger, C. H. Lorig	323
Isoembrittlement in Chromium and Molybdenum Alloy Steels During Tempering	G. Bhat, J. F. Libsch	330
Oxidation of Cobalt Metal	R. E. Carter, F. D. Richardson (With an Addendum by C. Wagner)	336
Ductility of Vacuum Heat-Treated Molybdenum Wires	W. E. Few, G. K. Manning	343
Vanadium-Zirconium Alloy System	J. T. Williams	345
Gallium-Antimony System	I. G. Greenfield, R. L. Smith	351
Effect of Boron on the Relative Interfacial Tension of Gamma Iron	A. M. Adair, J. W. Spretnak, R. Speiser	353

Table of Contents Continued

Magnesium-Rich Corner of the Magnesium-Lithium-Aluminum System — J. A. Rowland, Jr., C. E. Armantrout, D. F. Walsh — 355

Magnetic Properties of Manganese-Germanium Alloys — R. J. Quigg, G. P. Conard, J. F. Libsch — 359

Structure and Magnetic Properties of Some Transition Metal Nitrides — G. W. Wiener, J. A. Berger — 360

Preliminary Investigation of the System Ti-Mg — J. W. Fredrickson — 368

Recrystallization Characteristics of Superpurity Base Al-Mg Alloys Containing 0 to 5 Pct Mg — E. C. W. Perryman — 369

Some Aspects of the Crystallization and Recrystallization of Vapor-Deposited Vitreous Selenium — N. E. Brown, F. L. VerSnyder — 379

On the Relationship of Texture Changes of Cold-Rolled Face-Centered-Cubic Metals During Recrystallization — Y. C. Liu, W. R. Hibbard, Jr. — 381

Effect of Zinc Content on the Rolling Texture and Annealing Texture of Alpha Brass — A. Merlini, P. A. Beck — 385

Crystal Structure and Some Properties of the Compound Zr_2Al — J. H. Keeler, J. H. Mallery — 394

Preferred Orientations in Beta-Annealed Zirconium — J. H. Keeler, A. H. Geisler — 395

Cold-Rolled Textures of Silicon-Iron Crystals — P. K. Koh, C. G. Dunn — 401

Cellular Structure in High Purity Zinc — R. P. Steijn — 406

Formation of Cold-Worked Regions in Fatigued Metal — R. Webeler — 408

Crystal Structure of Neodymium Metal — F. H. Ellinger — 411

Temper Brittleness of Some Fe-Ni-Cr Alloys — L. D. Jaffe — 412

Decomposition of Beta Titanium — F. K. Bloom, E. L. Norman, Jr., A. R. Troiano — 413

Sigma Phase in the Molybdenum-Ruthenium System — D. S. Bloom — 420

A Calorimetric Investigation of the Energy Relations in Alloys of Composition Cu_3Au — L. R. Rubin, J. S. Lt. Leach, M. B. Bever — 420

Metallographic Techniques for Cu-Au Alloys — R. Rickett, W. D. Robertson — 424

Copyrighted by American Institute of Mining and Metallurgical Engineers, Inc.
Printed in U.S.A.

Embrittlement of Molybdenum by Neutron Radiation

by C. A. Bruch, W. E. McHugh, and R. W. Hockenbury

Commercially pure molybdenum specimens were irradiated in the Materials Testing Reactor for an estimated exposure of 1.9 to 5.9x10^{20} thermal nvt. Prior to irradiation, the material was ductile in the tension test; whereas after irradiation, it was brittle. The results of tension tests conducted at various temperatures revealed that the transition temperature for this material had been increased from −30° to +70°C as a result of the radiation exposure. From metallographic studies, it is concluded that the embrittlement is due to submicroscopic changes which raise the flow stress-temperature curve of the material.

PRIOR to ten years ago, the bombardment of metals with high speed heavy particles such as protons, deuterons, α particles, and neutrons was primarily of academic interest. These particles existed in extremely small numbers in a few laboratories and only under very special conditions. With the introduction of the nuclear power reactors, these particles are now available in enormous quantities and it has become important from a practical standpoint to learn how well metals withstand severe reactor radiations. The principal radiations of concern in reactors are neutrons and γ rays, since the heavier charged particles exist only in limited regions of reactors. Seitz,[1] in a theoretical approach, has shown that all of these high energy particles, except γ rays, have enough energy to knock atoms from lattice sites and that these knocked-on atoms have enough energy to cause additional displacements of neighboring atoms. The result of this process would be a lattice containing many imperfections in the form of interstitial atoms and vacancies. Hence, it would be expected that the properties of metals can be changed by reactor radiations, and such has been found to be the case.

Only a limited amount of data have been published in the open literature,[2-5] and these data have been for relatively low integrated-neutron-flux exposures. In general, one effect of reactor radiations on the mechanical properties of metals has been to increase strength and decrease ductility.

It is now possible to irradiate specimens in the Materials Testing reactor at much higher fluxes and to higher integrated exposures than previously possible.[6] The data which are being presented here describe the effects of a relatively high exposure on some mechanical properties of molybdenum.

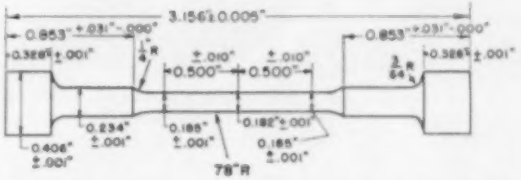

Fig. 1—Tensile specimens were prepared according to the specifications shown in the figure.

Experimental Procedures

Material: The molybdenum used in this investigation was obtained from the Climax Molybdenum Co. The two heats from which the material originated were melted under a vacuum of 5 to 30 microns and cast in 7 in. diam water-cooled copper molds. One ingot contained 0.061 pct C and the other 0.066 pct. Both ingots were hot worked by extrusion and rolling into $\frac{5}{8}$ in. diam rods, after which they were annealed and straightened.

The rods were subsequently heated to 1100°C in a hydrogen atmosphere and swaged to ½ in. diam rods at the Research Laboratory of the General Electric Co. The resulting material had an average hardness of 264 VPN, or 99.2 R_B, and had an average of 5000 grains per sq ml in the transverse section.

Test Specimens: Substandard-size tensile specimens were prepared according to the specifications shown in Fig. 1. These specimens were used also for hardness measurements.

The metallographic specimens were small disks which were polished, etched, and photographed at X1000 prior to irradiation. The field studied was

C. A. BRUCH, W. E. McHUGH, and R. W. HOCKENBURY are associated with Knolls Atomic Power Laboratory,* General Electric Co., Schenectady.

Discussion of this paper, TP 3940E, may be sent, 2 copies, to AIME by Apr. 1, 1955. Manuscript, Sept. 10, 1954. Chicago Meeting, February 1955.

* Knolls Atomic Power Laboratory is operated by General Electric Co. for the United States Atomic Energy Commission under Contract No. W-31-109 Eng. 52.

The Transactions papers appearing in the Journal of Metals during 1955 will subsequently appear in AIME Transactions Volume 203, and may be permanently referenced to that volume.

a—Molybdenum etched, prior to irradiation.

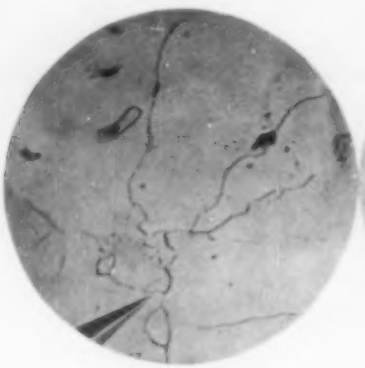

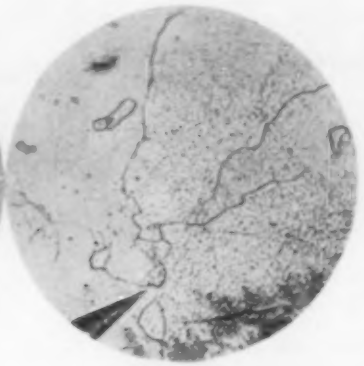

b—Same as *a*, after irradiation without additional polishing or etching.

c—Same as *b*, except etched 30 sec.

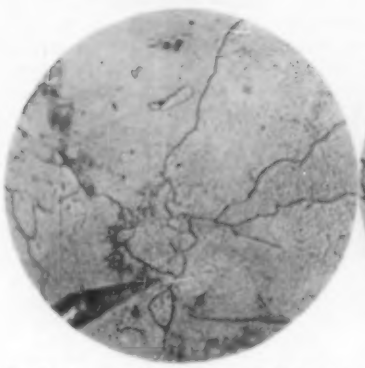

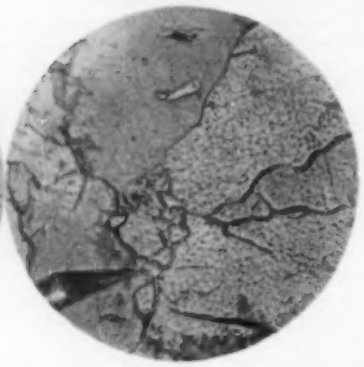

d—Same as *c*, except etched an additional 60 sec.

Fig. 2—Micrographs of the same field for various conditions. Etched with 1 part 10 pct NaOH in water and 1 part 10 pct $K_3Fe(CN)_6$ in water. X1000. Area reduced approximately 35 pct for reproduction.

identified by means of a Knoop hardness indentation.

Irradiation: 12 tensile specimens and 6 metallographic specimens were enclosed in two aluminum capsules, each approximately 24 in. long. These were irradiated in active lattice position L-41 of the Materials Testing reactor for 22 days. The estimated exposure for these specimens varied from 1.9×10^{20} to 5.9×10^{20} thermal nvt, due to variations in the flux about the reactor horizontal center plane. The temperature of the specimens during the exposure was approximately 90°C.

Test Equipment: A motorized Rockwell hardness tester, model 3QR modified for remote operation, was used for hardness testing.

A special remotely operable metallograph, described elsewhere,[5] was used for metallographic examinations of the irradiated specimens. A conventional metallograph was used for the specimens in the unirradiated condition.

Tensile tests were performed on two testing machines, one a standard hydraulic machine and the other a screw-loaded horizontal machine built for remote operation. The rate of cross-head motion during each test was held constant, with exceptions noted, at 0.010 in. per min corresponding to an initial strain rate of 1.3×10^{-4} sec^{-1}. Testing at other than room temperature was done with the specimen immersed in a liquid bath during the test. Acetone cooled by dry ice was used for low temperatures and water heated by immersion heaters was used for the higher temperatures. For the room temperature tests, the screw-loading machine was used, as well as a remotely operable extensometer built at this laboratory. The extensometer has two active linear differential transformers. The signal from one activates a recorder which magnifies the extension of the gage length of the specimen (approximately 0.75 in.) 10 times; the signal from the other activates a recorder which magnifies the extension either 100 or 1000 times. Since the recorders were of load-elongation type, two load-extension diagrams were recorded autographically and simultaneously. Strain gages were not used in the tests of specimens immersed in liquid baths.

All tensile test values, such as yield strength, percentage of reduction in area, and so forth, were obtained by conventional methods.

Table I. Hardness Test Results

Material Condition	Rc* Average Value	Rc* Minimum, Maximum	BHN	Ra* Average Value	Ra* Minimum, Maximum	BHN
Unirradiated	23.8	19.7 to 24.9	242	62.0	59.9 to 63.0	243
Irradiated	28.5	24.2 to 31.7	275	64.9	62.8 to 66.5	280
Change	+ 5.0	+ 2.0 to + 7.7	+ 33	+ 2.9	+ 0.5 to + 4.4	+ 37

* Each number in the table represents the average of test results for 12 specimens. At least three Rockwell hardness measurements of each kind were made per specimen.

Experimental Results

Metallographic Examination: In Fig. 2 are micrographs originally magnified X1000 of the same field for the following conditions: 2a, etched prior to irradiation; 2b, same as *a* after irradiation without additional polishing or etching; 2c, same as *b* except etched 30 sec; and 2d, same as *c*, except etched

an additional 60 sec. The etchant consisted of 1 part of 10 pct NaOH in water and 1 part of 10 pct $K_4Fe(CN)_6$ in water.

Neither the micrographs nor the microscopic examination revealed any visible change in the microstructure as a result of the irradiation. In Fig. 2, the microstructure of 2b looks different from 2a in that the grain interiors are speckled. Part of this difference is due to differences in the illumination characteristics of the two metallographs used and part is due to surface contamination accumulated during the irradiation. As the specimen was progressively overetched, 2c and d, the interior of the grains became more deeply pitted and the grain boundaries more deeply etched, giving the double boundary effects characteristic of overetched surfaces. However, there was no evidence of grain-boundary migration, new grain boundaries, or new phases.

Hardness Testing: The results of the Rc hardness tests taken on the flat ends of the tensile specimens are summarized in Table I. This table also gives BHN, as converted from the Rockwell hardness measurements.

As a result of the irradiation, the molybdenum hardened by approximately 35 BHN. No correlation was found between the hardness increase and the position of the specimen with respect to the reactor horizontal center plane. In other words, the amount of hardening was independent of the integrated thermal flux in the range studied.

Tensile Testing: 12 specimens were tested at various temperatures. Five specimens were unirradiated, five were irradiated, and two were unirradiated but "aged" for thirty days at 90°C to simulate the thermal history of the irradiated specimens. Complete load-elongation curves were obtained for the tests which were conducted at room temperature, whereas only a limited amount of data was obtained for each of the other six specimens tested in liquid baths.

In Fig. 3 are load-elongation curves for two irradiated and two unirradiated specimens which were tested at room temperature. These curves show that, prior to irradiation, the material had a sharp yield point and considerable ductility as measured by elongation. After irradiation, the material was completely brittle, and each specimen fractured in two places. Multiple fracture of brittle materials also has been observed elsewhere.[5]

In Fig. 4 are load-elongation curves for the two specimens which were "aged" at 90°C for 30 days; for comparison, the curves for the two unirradiated specimens are also included. It can be seen that the

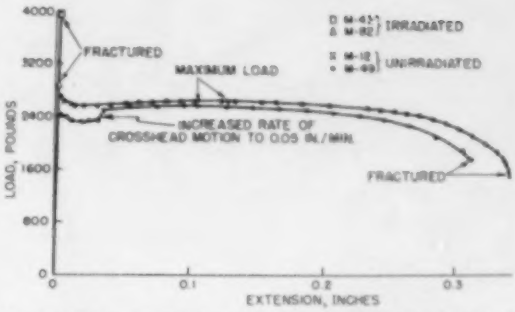

Fig. 3—Load vs elongation at room temperature for irradiated and unirradiated molybdenum.

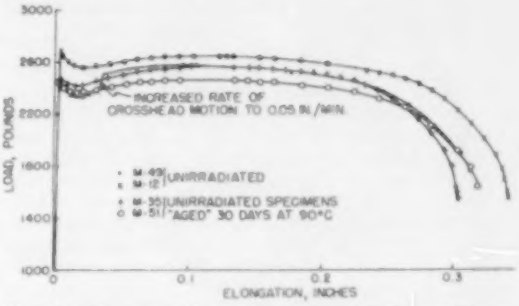

Fig. 4—Load vs elongation at room temperature for molybdenum, "aged" at 90°C for 30 days, and unirradiated molybdenum.

90°C heating had very little effect, if any, on the tensile properties of the material. The results indicate that the "aging" may have slightly reduced the tensile strength and elongation, but these differences are not considered significant.

The data obtained from all of the tensile tests have been summarized in Table II, in which the following results are considered significant:

1—The unirradiated material was ductile in tests conducted at room temperature and at −20°C as evidenced by the relatively high values of percentage of reduction in area and elongation; whereas at −40° and −60°C, the material was completely brittle.

2—The unirradiated material "aged" at 90°C had essentially the same tensile properties at room temperature as the unaged specimens.

3—The irradiated material was completely brittle in tests conducted at room temperature and at +60°C. At +80° and +100°C, the irradiated material was ductile.

Table II. Data from All Tensile Tests

Specimen Designation	Condition	Integrated Thermal-Neutron-Flux	Test Temperature, °C	Upper Yield Point, Psi x 10^3	Tensile* Strength, Psi x 10^3	Fracture Stress, Psi x 10^3	Pct Elongation	Pct Reduction in Area
M-12	Unirradiated	—	+23	102.5	100.8	214.0	48.7	72.4
M-49	Unirradiated	—	+23	93.8	98.8	193.0	41.7	65.0
M-44	Unirradiated	—	−20	128.5	130.0	243.0	32.8	63.8
M-58	Unirradiated	—	−40	—	123.0	123.0	0	0
M-36	Unirradiated	—	−60	—	142.0	142.0	0	0
M-35	"Aged"†	—	+24.6	94.4	97.7	192.6	40.8	67.4
M-51	"Aged"†	—	+24.6	94.0	94.2	181.6	43.5	68.2
M-43	Irradiated	5.1×10^{20}	+21.8	151.7	151.7	149.0	0	0.08
M-82	Irradiated	5.1×10^{20}	+22.4	—	109.7	109.7	0	0
M-31	Irradiated	5.55×10^{20}	+60	—	148.5	148.5	0	0
M-37	Irradiated	5.88×10^{20}	+80.5	143.5	143.5	180.0	14.7	60.7
M-64	Irradiated	5.8×10^{20}	+100	111.5	111.5	134.0	10	59.7

* Maximum load divided by original area.
† Unirradiated specimen heated for 30 days at 90°C.

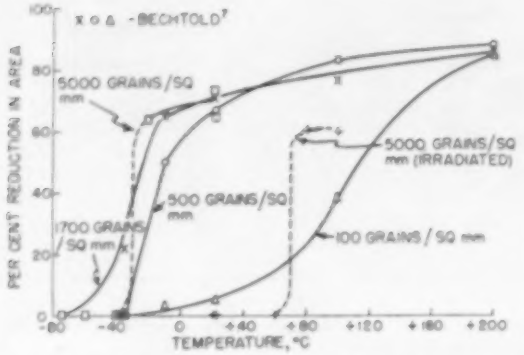

Fig. 5—Effect of temperature, grain size, and neutron radiation on the percentage of reduction in area of molybdenum tensile specimens.

In Fig. 5 are graphs of percentage of reduction in area vs temperature for both the unirradiated and irradiated specimens. Included in this figure are data reported by Bechtold[7] for arc-cast molybdenum. For purposes here, the transition temperature will be defined as the inflection point of the curves, which occurs in all cases at approximately 40 pct reduction in area. Irradiation has changed the transition temperature from approximately −30° to approximately +70°C, an increase of about 100°C. The transition temperature for the irradiated material is the same as for unirradiated material having approximately 200 grains per sq ml.

Discussion

The commercially pure molybdenum used in this investigation was a normal material and comparable to that used by other investigators. For example, in Fig. 6 are graphs of both the yield strength at room temperature and the transition temperature vs the reciprocal of the average grain diameter, using data reported by Bechtold[7] and those data obtained in this investigation. Curves have been drawn through the points and the agreement is good. The material used in this investigation behaves in the manner which would be predicted from the data of Bechtold.

The irradiation hardening was moderate, and as such, did not indicate the significant changes which had occurred in the room temperature tensile properties. Tabor[8] has shown that there is a direct correlation between indentation hardness and yield stress; hence, an increase in hardness implies an increase in yield stress, a shift in the flow stress-temperature curve, and a possible shift in the transition temperature. However, in order to determine the effect of some variable on the transition temperature, it is necessary to use a destructive test such as the tension or notched-bar impact.

The results of the tensile tests show clearly that irradiation has embrittled molybdenum in that the transition temperature increased from approximately −30° to +70°C. It has been pointed out already that this corresponds to a transition temperature for unirradiated molybdenum having approximately 200 grains per sq ml. Since the material had approximately 5000 grains per sq ml prior to radiation and since metallographic examinations have shown that there were no microscopically visible changes in the structure, it must be concluded that the radiation embrittlement was caused by submicroscopic changes.

The gross effect of radiation has been to change the relative position of the flow curve with respect to the fracture curve. To illustrate this point, in Fig. 7 are plotted yield stresses and fracture stresses vs temperature for irradiated molybdenum as well as unirradiated material having various grain sizes. Some of the data were obtained from Bechtold's results.[7] Two curves have been drawn for each condition of the metal, and these have been separated by a vertical line which represents the highest temperature at which the reduction in area of the test specimen was zero. The curve to the right of the vertical line is the yield stress or flow stress-temperature curve, that to the left is the fracture curve. The best average flow stress-temperature curves consistent with the limited amount of data were drawn through the yield-stress points. Average fracture curves were drawn through the fracture-stress points, and these were drawn horizontally because of the very limited amount of data. All points agree fairly well with the curves as drawn except the one for the irradiated specimen which had a fracture stress of 109,700 psi at room temperature. This specimen showed a nonlinear behavior in the early part of the tension test. The reason for the behavior is not understood, although it may have been due to specimen misalignment or slippage of the strain gage. The data presented in Fig. 7 show that both the flow-stress and fracture-stress curves for unirradiated molybdenum are raised with decreasing grain size and that the effect is quite pronounced. They also show that the flow stress-temperature curve is appreciably raised by irradiation, and the indication is that the fracture stress-temperature is also raised, but to a lesser degree.

The mechanism by which neutron irradiation causes a shift in these curves is not fully understood. It is generally agreed that three types of defects are produced in the metal lattice by neutron bombardment: lattice vacancies, interstitial atoms, and foreign atoms created by transmutation. The latter effect is believed to be entirely negligible in this experiment because the calculated concentration of impurity atoms is of the order of 0.01 pct. Since little is known about the effects of lattice vacancies, the most that can be said with certainty is that the effect of neutron irradiation has been to produce lattice defects which impede slip, or in other words, which increase the critical resolved stress required for slip.

It has been observed for some other materials that

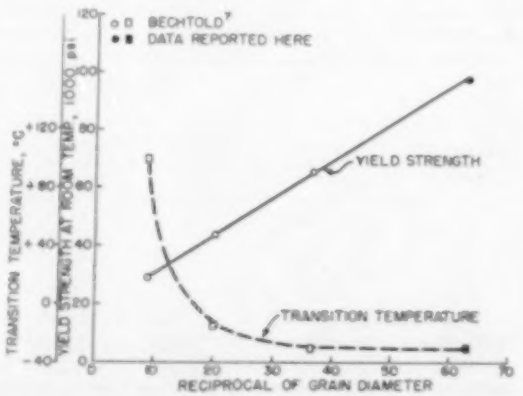

Fig. 6—Yield strength at room temperature and transition temperature as a function of the reciprocal of the average grain diameter.

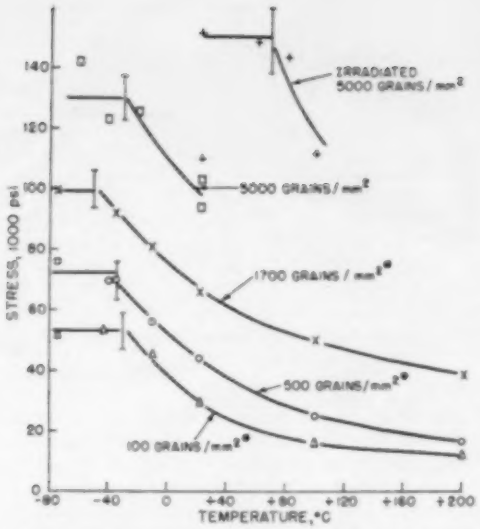

Fig. 7—Yield and fracture stress as a function of grain size, neutron radiation, and temperature. Fracture-stress curves are to the left of vertical lines and flow-stress curves are to the right. (*Bechtold.[7])

the irradiation hardening and increase in yield strength is less for specimens irradiated at higher temperatures. This effect is assumed to arise because lattice vacancies and interstitials either agglomerate or annihilate each other at higher rates, due to increased mobility at the elevated temperatures. Consequently, it should be possible to irradiate a given metal at a temperature at which the annealing rate equals the defect-production rate and at which there is no radiation hardening. For molybdenum this should mean that the radiation embrittlement decreases as the temperature of the material during the irradiation is increased. Some results obtained for molybdenum, which was irradiated in a reactor other than the Materials Testing reactor, indicate that the temperature at which there would be no embrittlement will probably be quite high. These results showed that molybdenum, irradiated at 400°C for an estimated 3×10^{20} thermal nvt (3×10^{19} fast nvt), increased in hardness from 169 to 216 BHN (as converted from Rb values), an increase of 47 BHN. This hardness increase was somewhat greater than that for the material reported here, although the final hardness was less than the hardness of the unirradiated material used in this investigation. The reason for the greater hardening of the material irradiated at 400°C is believed to be due to the fact that the material was of lower original hardness. It has been generally observed that, for a given metal, the lower the original hardness, the greater will be the radiation hardening. Because of the rough correlations between hardness, yield strength, and transition temperature, these results indicate that the rate of defect production in molybdenum at 400°C exceeds the annealing rate and that the material is embrittled even at this temperature.

Acknowledgments

The authors are indebted to the personnel of the Radioactive Materials Laboratory for help received in performing tests, as well as to J. W. Czarkowski for preparation of metallographic specimens. The authors also wish to thank J. R. Low, Jr., A. N. Holden, and C. E. Lacy for helpful discussions of this work. In addition, appreciation is extended to members of the Materials Testing Research staff of the Phillips Petroleum Co. for their cooperation in scheduling the irradiations and handling the specimens.

Discussion of this paper, if any, will appear in JOURNAL OF METALS, November 1955, and in AIME Metals Branch *Transactions*, Vol. **203**, 1955.

References

[1] F. Seitz: On the Disordering of Solids by Action of Fast Massive Particles. *Discussions* Faraday Society (1949) No. 5, p. 271.

[2] S. Siegel: Radiation Damage as a Metallurgical Research Technique. *Trans.* ASM (1953) **45A**, p. 312.

[3] F. W. Kunz and A. N. Holden: The Effect of Short Time, Moderate Flux Neutron Irradiation on the Mechanical Properties of Some Metals. To be published in *Acta Metallurgica*.

[4] J. R. Hoffman: The Materials Testing Reactor. *Nucleonics* (1954) **12**, No. 4, p. 21.

[5] New Instrument Aids Atomic Research. *Chemical Engineering News* (1951) **29**, p. 5062.

[6] J. Miklowitz: Elastic Waves Created During Tensile Fracture—The Phenomenon of Second Fracture. *Journal of Applied Mechanics* (1953) **20**, No. 1, p. 122.

[7] J. H. Bechtold: Recrystallization Applied to Control of the Mechanical Properties of Molybdenum. *Trans.* ASM (1954) **46**, p. 1449.

[8] D. Tabor: The Hardness and Strength of Metals. *Journal* Institute of Metals (1951) **79**, p. 1.

Technical Note

Solid Solubility of Calcium in Magnesium

by Edmund C. Burke

IN view of rather widespread use of calcium as an alloying addition to magnesium alloys, it is rather surprising to find that, although the general features of the Mg-Ca equilibrium diagram are known with a fair degree of certainty,[1,2] considerable ambiguity concerning the solid solubility of calcium in magnesium exists. By using the disappearing phase technique in a metallographic study, Haughton[1] found that 0.6 pct Ca was soluble at 300°C and 1.8 pct was soluble at 516°C, the eutectic temperature

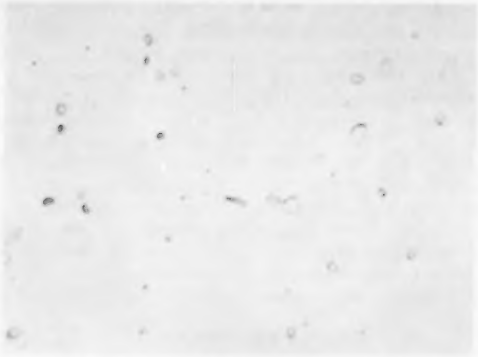

Fig. 1—Mg + 1.25 pct Ca. Heat treated 100 hr at 508°C. Etched in 1 pct nital. X500. Area reduced approximately 25 pct for reproduction.

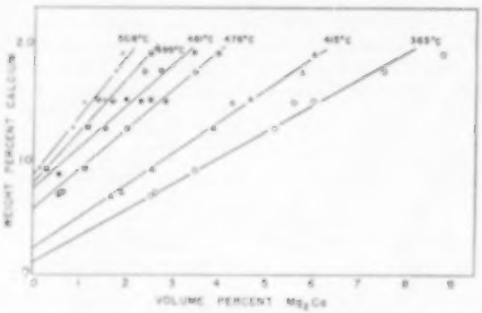

Fig. 2—The relationship between the volume percent of Mg_2Ca observed in the microstructure vs the weight percent of calcium after heat treating at indicated temperatures.

between Mg and Mg_2Ca. Vosskühler[3] used a similar technique and found that 0.18 pct Ca was soluble at 300°C and 0.78 pct was soluble at 516°C.

Because the peripheral zone on each of the heat-treated metallographic specimens was impoverished in Mg_2Ca, Vosskühler[3] believed that this had introduced some error in his determination and thought that Haughton's results were more reliable. However, Haughton reported that he had encountered experimental difficulties with the chemical analyses and was forced to exclude several cooling curves from his equilibrium diagram study because of erratic calcium determinations.

For this study, experimental melts of 125 g with various additions of high purity Ca were prepared with sublimed Mg to produce alloys varying from 0.68 to 1.90 pct Ca, as determined by the best present day methods of chemical analysis. The impurity content in the alloys was: Al, <0.0001 pct; Cu, 0.0001 pct; Fe, 0.0010 pct; Mn, 0.0011 pct; Ni, <0.0002 pct; Pb, 0.0005 pct; Si, <0.001 pct; Sn, <0.001 pct; and Zn, <0.02 pct. The alloys were melted in a graphite crucible and poured at 705°C to produce small rods, ¾ in. in diameter by 1 in. long, from which metallographic specimens were obtained. The specimens were heat treated for 100 hr in two different ways: 1—exposed to an atmosphere of air + 0.7 pct SO_2 and 2—wrapped in molybdenum foil and sealed in glass under a partial helium atmosphere. The specimens heat treated under the first condition had a greater peripheral zone of Mg_2Ca depletion than those obtained by the second method. However, the excellent agreement between the results from quantitative metallography for both heat-treating procedures showed that the small amount of surface depletion had an insignificant effect on the solubility determination.

E. C. BURKE, Member AIME, is associated with the Metallurgical Laboratories, The Dow Chemical Co., Midland, Mich.
TN 238E. Manuscript, Aug. 20, 1954.

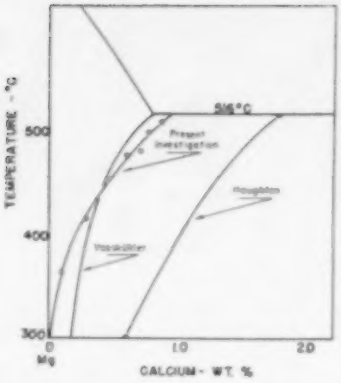

Fig. 3—The magnesium terminal side of the Mg-Ca equilibrium diagram.

Since calcium produces an insignificant change in the lattice parameters of magnesium,[4] a Hurlbut counter[5] was used to measure the volume percent of Mg_2Ca. Fig. 1 is representative of the general shape and distribution of the Mg_2Ca constituent after a heat treatment of 100 hr at 508°C.

The relationship between the volume percent of Mg_2Ca observed in the microstructure vs the weight percent of calcium after heat treating at selected temperatures is shown in Fig. 2. The intersection of the extrapolation of each line (obtained from a least-squares solution) with the weight-percent axis represents the solid solubility of calcium in magnesium at the indicated temperature. Although the volume percent is actually a parabolic function of the weight percent, the straight-line relationship introduces no serious error at these low calcium additions, since the difference in density between the solid solution and the Mg_2Ca is not marked.

The variation in the solid solubility of calcium in magnesium obtained in the present investigation as compared to previous determinations is shown in Fig. 3. The relatively close agreement between these results and those of Vosskühler suggests that Haughton's solid-solubility determination is too high.

References

[1] J. L. Haughton: *Journal* Institute of Metals (1937) **61**, p. 241.

[2] H. Vosskühler: *Ztsch. Metallkunde* (1937) **29**, p. 137.

[3] *The Technology of Magnesium and Its Alloys.* (1940) Ed. by Adolf Beck. London. F. A. Hughes and Co. Ltd.

[4] R. S. Busk: *Trans.* AIME (1950) **188**, p. 1460; JOURNAL OF METALS (December 1950).

[5] R. T. Howard and M. Cohen: *Trans.* AIME (1947) **172**, p. 413; METALS TECHNOLOGY (August 1947).

A Study of the Room Temperature Fatigue Properties of Molybdenum

by W. L. Bruckart and W. S. Hyler

The powder metallurgy and arc-cast types of wrought molybdenum stock were studied in rotating beam fatigue. Endurance ratios of unnotched specimens after 5×10^7 cycles were found to be 0.74 and 0.81, respectively. Fatigue notch factors (K_f) of 1.36 and 2.05, respectively, were obtained on V-notched specimens having a theoretical stress-concentration factor $K_t = 3.1$.

MOLYBDENUM and its alloys are rapidly gaining importance as engineering materials of construction for high temperature applications. As a wrought material, molybdenum and its alloys are outstanding above 1800°F. It is necessary, however, with molybdenum to provide elevated temperature oxidation protection. This is currently being studied by a number of investigators. Thus far, there have been no published data on the fatigue behavior of molybdenum either at room temperature or at elevated temperature. The knowledge of fatigue behavior, particularly notched fatigue behavior, becomes increasingly important as the engineering importance of a material increases, especially from the design standpoint.

The work described here was directed toward determination of the notched and unnotched rotating beam fatigue characteristics of molybdenum at room temperature. Also, it was desired to learn whether any difference exists between wrought molybdenum of the powder metallurgy and the arc-cast types.

Fabrication History of Bar Stock

For this work, bar stock was procured from Climax Molybdenum Co. (arc-cast type) and from Westinghouse Electric Corp. (powder metallurgy type). The processing histories of these materials are listed in Table I. The first lot of arc-cast molybdenum was deoxidized by aluminum additions. The second lot was deoxidized by carbon.* Both lots of the powder metallurgy product were deoxidized by the hydrogen used as a sintering atmosphere.

While both types of molybdenum were given similar reductions, the fabrication temperatures used on the powder metallurgy molybdenum were about 100°C lower than those used on the arc-cast material. Apparently, this difference does not affect the resulting room temperature tensile and fatigue properties.

* For convenience, these are designated arc-cast *A* and arc-cast *C*.

W. L. BRUCKART, Member AIME, and W. S. HYLER are Assistant Chief, Nonferrous Physical Metallurgy Div., and Assistant Chief, Applied Mechanics Div., respectively, Battelle Memorial Institute, Columbus, Ohio.

Discussion of this paper, TP 3941E, may be sent, 2 copies, to AIME by Apr. 1, 1955. Manuscript, Sept. 13, 1954. Chicago Meeting, February 1955.

Microstructure

A microscopic examination of these materials, as received, revealed the powder metallurgy molybdenum to be free of inclusions and to be finely fibered. On the other hand, the arc-cast *C* molybdenum possessed numerous carbide inclusions, and the arc-cast *A* appeared to have coarse grained fibers. These are shown in Fig. 1. Owing to the large apparent difference in fineness of fiber between the arc-cast *A* and the powder product and arc-cast *C*, a check was made of the recrystallized grain sizes to determine whether these differences persisted.

A series of recrystallization anneals revealed mixed grain sizes in both the arc-cast *A* and the powder product. Variations in grain diameter of as much as 50 times were found after full recrystallization at 1200°C for 30 min. There was no distinction between the two. Arc-cast *C* was not checked.

Room Temperature Mechanical Properties

Prior to subjecting the materials to fatigue tests, room temperature mechanical properties were determined. These data, together with the tensile strength of the notched bars, are listed in Table II.

There were no significant differences in the tensile strengths of the two types of molybdenum. However, the powder metallurgy material was generally more ductile and yielded at a somewhat lower stress than the arc-cast material.

Tensile strengths of the notched specimens indicated a slightly greater notch strengthening effect in the arc-cast *C* than in the powder product, lot 2.

Room Temperature Fatigue Properties

Sample Preparation: Specimens were prepared for use in R. R. Moore rotating beam fatigue machines. These specimens had a continuous radius test section with a minimum diameter of 0.260 in. The specimens were prepared by grinding to shape and polishing to produce a smooth unworked surface. Polishing consisted of rotating a disk in the continuous radius section on which were attached, successively, emery belts of 240, 400, and 600 grit. The specimens were slowly rotated during the operation. The belt speed was high, and rotation was such that polishing scratches were longitudinal.

Unnotched Fatigue Properties: Unnotched fatigue data were obtained from a number of specimens of each of the four lots of molybdenum. The results of the tests are presented in Fig. 2. From this figure,

Table I. Processing History of Molybdenum Used in Room Temperature Fatigue Tests

Source of Stock	Consolidation	Fabrication		
		Procedure	Reduction in Area, Pct	Carbon Content, Pct
Arc-cast A*	Arc cast in argon to 2½ in. diam turned to 2⅛ in., deoxidized with aluminum	Breakdown by forging to 2 3/16 in. octagon, turned to clean up, and finish rolled to ½ in. round at 1025° to 1200°C	97	0.006
Arc-cast C†	Same, but deoxidized with carbon	Same	97	0.04
Powder metallurgy,‡ Lots 1 and 2	Pressed from powder and sintered in hydrogen as a 2¼ in. sq bar	Rolled to ⅝ in. round, beginning at 1100°C and using reheats at successively lower temperatures to 950°C	94	0.02

* This lot was used in the tests of unnotched bars only, *A* stands for aluminum deoxidized.
† This lot was used in tests of both unnotched and notched bars, *C* stands for carbon deoxidized.
‡ Two lots were received. Each had this history.

Table II. Room Temperature Mechanical Properties of Molybdenum Used in Fatigue Tests*

Source of Stock	Specimen No.	Offset Yield Strengths, Psi			Ultimate Tensile Strength, Psi	Elongation in 1 In., Pct		Reduction in Area, Pct	Modulus (from Tensile Curves), 10^6 Psi	VHN, 10 Kg Load
		0.01 Pct	0.1 Pct	0.2 Pct		Uniform	Total			
Tensile Data from Standard Specimens										
Arc-cast *A*	1A	65,000	87,600	94,100	109,000	8	28	48.5	42.9	270
Arc-cast *C*	856A	53,500	84,700	91,100	97,100	6	20	40.0	53.2	277
	856B	47,000	79,600	89,000	96,500	6	36	28.0	—	—
Powder metallurgy, Lot 1	2A	52,700	74,500	79,900	97,000	15	86	70.0	49.8	293
	4A	52,300	73,700	79,300	97,000	17	60	68.5	50.5	—
Powder metallurgy, Lot 2	871A	66,900	82,800	87,400	101,900	15	46	39.2	—	—
Tensile Data from Notched Fatigue Bars										
Arc-cast *C*	856N-12	—	—	—	126,400	—	—	—	—	—
	856N-13	—	—	—	148,800	—	—	—	—	—
Powder metallurgy, Lot 2	871N-9	—	—	—	111,800	—	—	—	—	—
	871N-14	—	—	—	122,600	—	—	—	—	—
	871N-15	—	—	—	112,300	—	—	—	—	—

* 3/16 in. diam tensile specimens.

a—Powder metallurgy molybdenum. b—Arc-cast *A* molybdenum. c—Arc-cast *C* molybdenum.

Fig. 1—Longitudinal sections of molybdenum bar stock as received. X100. Area reduced approximately 20 pct for reproduction.

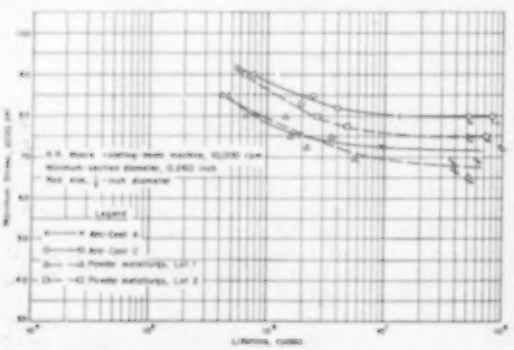

Fig. 2—Rotating beam fatigue-test results on unnotched molybdenum specimens.

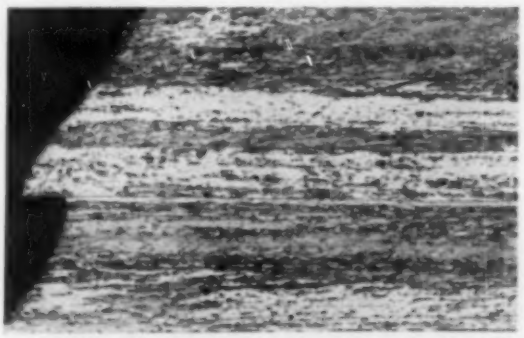

Fig. 3—Micrograph through fatigue fracture of arc-cast *A* molybdenum specimen. X100. Area reduced approximately 20 pct for reproduction.

it can be seen that the fatigue limit of arc-cast molybdenum ranged from 72,000 to 80,000 psi at 5×10^7 cycles and that of powder metallurgy molybdenum ranged from 68,000 to 75,000 psi. These data suggest that the differences in fatigue limits between the two types of molybdenum may be less than the variation between lots of either type of molybdenum. The data suggest also that the arc-cast molybdenum has slightly better fatigue behavior than does the powder metallurgy molybdenum.

The endurance ratios† of the arc-cast *A* and *C* molybdenum were 0.66 and 0.81, respectively, and 0.70 and 0.74 for the powder metallurgy, lots 1 and 2, respectively. It is significant from these data that molybdenum possesses an unusually high endurance ratio in comparison to other metals.

† Endurance ratio is defined as the fatigue limit divided by the ultimate strength.

The fractures observed in the two types of materials were of considerable interest. The arc-cast specimens had a fracture surface typical of most materials, Fig. 3. A description of the fatigue failure of the powder metallurgy material is most adequately described as "woody" in appearance. Longitudinal splits were common. A typical example of such a failed specimen is shown in Fig. 4. A micrograph of the failed section is shown in Fig. 5 where the longitudinal splits appear to be along grain boundaries. These distinctive fractures were observed also in the notched specimens, as discussed later.

Notched Fatigue Properties: The critical test section of the specimen used in the notch fatigue study is illustrated in Fig. 6. The fatigue-test data are given in Figs. 7 and 8. The results of the fatigue tests on arc-cast *C* and powder metallurgy lot 2 are compared in Table III.

Table III. Comparison of Results of Fatigue Tests

Source	Fatigue Limit at 5×10^7 Cycles, Psi			
	Unnotched	Notched	Unnotched Endurance Ratio	K_f*
Arc-cast C	80,000	38,000	0.81	2.05
Powder-metallurgy Lot 2	75,000	55,000	0.74	1.36

* K_f = fatigue notch factor = $\frac{\text{fatigue limit, unnotched}}{\text{fatigue limit, notched}}$.

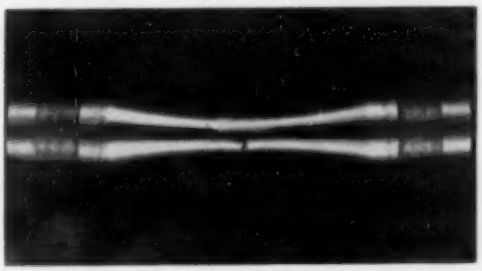

Fig. 4—Typical rotating beam fatigue fracture on powder metallurgy specimen. X1. Area reduced approximately 20 pct for reproduction.

Fig. 5—Micrograph through fatigue fracture of powder metallurgy molybdenum specimen. X100. Area reduced approximately 20 pct for reproduction.

Discussion

The failures of powder metallurgy molybdenum were reproducibly different in appearance than those of arc cast, both in static tension and in rotating bending fatigue. Thus, the "woody" appearing failures of unnotched fatigue specimens of powder metallurgy molybdenum were observed also in notched

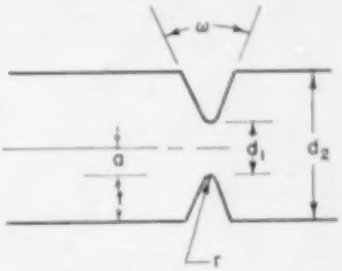

Fig. 6—Details of notched fatigue specimens. $K_t = 3.1$ = theoretical stress concentration, "Neuber's Nomograph." $d_1 = 0.260$ in., $d_2 = 0.400$ in., $\omega = 45°$, and $r = 0.008$ in.

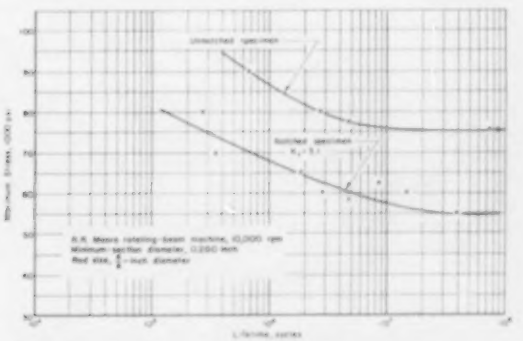

Fig. 7—Rotating beam fatigue-test results on notched and unnotched powder metallurgy lot 2 molybdenum specimens.

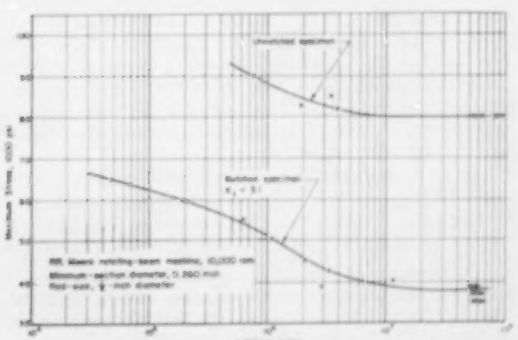

Fig. 8—Rotating beam fatigue-test results on notched and unnotched arc-cast *C* molybdenum specimens.

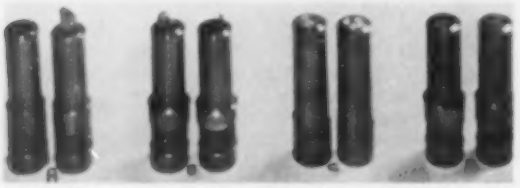

Fig. 9—Typical notch-tensile failures of arc-cast and powder metallurgy molybdenum specimens. A is powder metallurgy molybdenum, static failure; B, powder metallurgy molybdenum, fatigue failure; C, arc-cast molybdenum, static failure; and D, arc-cast molybdenum, fatigue failure.

specimens tested in fatigue and in static tension. Typical failures of notched specimens of the two types of fabrication are shown in Fig. 9. Regardless of the differences in appearance of the failures, the two types of molybdenum behaved in a nearly similar manner both in static tension tests and in fatigue.

This study has revealed that molybdenum has unusually good unnotched and notched fatigue behavior. The endurance ratios in the range 0.65 to 0.81 for the two types of molybdenum compare favorably with the endurance ratios of steel (0.4 to 0.6) and aluminum (0.2 to 0.4). Fatigue notch factors of $K_f = 2.05$ and 1.36 for the arc-cast and powder metallurgy materials, respectively, appear low for the notch severity studied, $K_t = 3.1$. This is particularly the case for powder metallurgy molybdenum.

In both types of molybdenum, the applied stress was in the direction of the fibrous structure (working direction). This may be an influencing factor on the observed fatigue behavior. Some additional fatigue studies of specimens from recrystallized material or of specimens from worked material at orientations other than the working direction would provide helpful information to better categorize the fatigue behavior of these products.

Acknowledgments

The authors wish to express their appreciation to J. B. Johnson, E. J. Hassell, and the United States Air Force for permission to publish these results of work done at Battelle Memorial Institute under Contract No. AF 33(038)-12641.

Discussion of this paper, if any, will appear in JOURNAL OF METALS, November 1955, and in AIME Metals Branch *Transactions*, Vol. **203**, 1955.

Technical Note

Allotropic Transformation at High Temperatures—A Discussion

by Arthur G. Metcalfe

(Reply by James O. McCaldin and Pol Duwez[1])

THE failure to detect any change in the thermal properties of cobalt at the Curie point would appear to indicate that the apparatus may have a limited sensitivity. The Curie temperature has been determined by direct methods to be 1121±3°C[2] and 1131°C.[3] The specific heat has been determined many times[4-7] and weighted values are given in Table I.

The allotropic transformations in iron and titanium, used by the authors to test the experiment method, involved a volume change of the order of 3 pct on going from the close-packed to the body-centered-cubic lattice. These energy changes are likely to be much larger than those involved in a diffusionless transformation from a hexagonal to a cubic-close-packed lattice. However, it has been pointed out that thermal observations are unreliable in the detection of phase changes when these are near a Curie point.[8]

James O. McCaldin and Pol Duwez *(authors' reply)*—The sensitivity of the present technique is limited to first-order transformations, so that gradual changes in specific heat, e.g., in the vicinity of Curie points, are not detected. Furthermore, the existence of first-order transformations with latent heats much smaller than those occurring in the known allotropic transformations of iron and titanium is, we agree, still pending.

Table I. Weighted Values for Cobalt

Temperature, °C	500	600	700	800	900	1000	1100	1200	1300	1400
True specific heat	0.126	0.136	0.147	0.159	0.172	0.187	0.204	0.166	0.167	0.168

A. G. METCALFE is Research Metallurgist, Armour Research Foundation of Illinois Institute of Technology, Chicago, J. O. MCCALDIN, Student Associate AIME, and P. DUWEZ, Member AIME, are Graduate Student and Professor of Metallurgical Engineering, respectively, California Institute of Technology, Pasadena, Calif.

TN 246E. Manuscript, Aug. 18, 1954.

References

[1] J. O. McCaldin and P. Duwez: Allotropic Transformations at High Temperatures. *Trans.* AIME (1954) **200**, p. 619; JOURNAL OF METALS (May 1954).

[2] H. P. Myers and W. Sucksmith: *Proceedings* Royal Society (1951) **207A**, p. 427.

[3] A. J. P. Meyers and P. Taglang: *Comptes Rendus* (1950) **231**, p. 612.

[4] S. Umino: *Science Reports* Tohoku Imperial University (1927) I, **16**, p. 593.

[5] F. Wust, A. Meuthen, and R. Durrer: *Forsch. Ver. Deut. Ing.* (1918) p. 204.

[6] F. M. Jaeger, E. Rosenbohm, and A. J. Zuithoff: *Recueil des Travaux Chimique* (1940) **59**, p. 831.

[7] L. D. Armstrong and H. Grayson-Smith: *Canadian Journal of Research* (1950) **28A**, p. 51.

[8] A. C. Metcalfe: *Proceedings* World Metallurgical Congress, Detroit (October 1951); *Trans.* ASM (1952) pp. 717-731.

Molybdenum Deposition on Titanium

by Sam Tour, Andre Styka, and George Fischer

Described herein are the results obtained during research work involving coating titanium alloys with molybdenum by vapor-deposition methods. Results show that the method can be used successfully to deposit hard adherent wear-resistant coating of metallic molybdenum on titanium or titanium alloys without changing the microstructure of the titanium base.

PRODUCTION and use of titanium and its alloys have increased tremendously in the past few years. The physical, mechanical, and chemical properties of this engineering metal have caused considerable enthusiasm among metallurgists and engineers. However, as with all materials, there are some drawbacks. For example, titanium is susceptible to seizing and galling on wearing surfaces.

In order to produce a good wear-resistant surface, many investigations have been conducted evaluating oxidizing, carburizing, nitriding, carbonitriding, siliconizing, and chromizing of titanium. All of these processes require high temperatures for rather extensive periods of time. It has been possible to produce hard surfaces on titanium and its alloys by a number of these processes at the expense of a deterioration of the physical properties of the base material. A practical solution to the problem of providing titanium and titanium alloy parts with a satisfactory wear-resistant nongalling surface must be one that does not involve excessive temperatures for long periods of time.

Sam Tour & Co. Inc. has completed a research and development contract for the United States Army Ordnance Corps on vapor deposition of molybdenum on titanium and titanium alloys. On the basis of results obtained from the research program, titanium alloys can be coated successfully with molybdenum to provide a hard wear-resistant surface without harm to their base mechanical properties. The remainder of this article is a description of the techniques used to apply the coating and the results obtained from wear tests on molybdenum-coated titanium.

Theory

Basically, the technique used was the application of molybdenum by a vapor-deposition method, thermal decomposition of molybdenum hexacarbonyl [$Mo(CO)_6$] with hydrogen as the carrier gas. The selection of this method was based chiefly on the following considerations: 1—low plating temperature which would minimize excessive grain growth, 2—low decomposition temperature of the carbonyl, 3—possibilities of controlling the hardness of the plate by adjusting the carbon content using the plating temperature and pressure as the primary variables, 4—use of high vacuum, thereby avoiding unnecessary oxidation and other complex reactions with the atmosphere. Free energy data[1] show the strong tendency for titanium to combine with O_2, N_2, or carbon from normal temperatures to temperatures above its melting point. To maintain the titanium in a film free condition, the use of as high a vacuum as possible is indicated. The literature[2] indicates that the reaction product of hydrogen with titanium is unstable in vacuum at around 400°C. 5—Although it is indicated from the thermodynamic standpoint that there is little possibility of removing carbon from either titanium or molybdenum, the work of Lander and Germer[3] indicates that the use of a suitable H_2/CO ratio is somewhat effective in minimizing carbon deposition. 6—Availability of molybdenum carbonyl. In the simplest form, the conditions of equilibrium[4] in chemical reactions involving decomposition of carbonyl are as follows:

$$Mo(CO)_6 \rightleftarrows Mo + 6CO$$

$$2CO \rightleftarrows C + CO_2$$

The plating rate is proportional to the rate of evolution of CO from the decomposed carbonyl, i.e., it is proportional to the pressure of the gaseous decomposition products. Carbon released from CO gas is the significant constituent for the variability of the physical properties of the product. High carbon deposition is favored by increasing pressure. Limitations are imposed in the selection of plating temperature and pressure. Excessive temperature re-

S. TOUR, Member AIME, A. STYKA, and G. FISCHER, Junior Member AIME, are associated with Sam Tour & Co. Inc., New York.

Discussion of this paper, TP 3947E, may be sent, 2 copies, to AIME by Apr. 1, 1955. Manuscript, July 2, 1954. Chicago Meeting, February 1955.

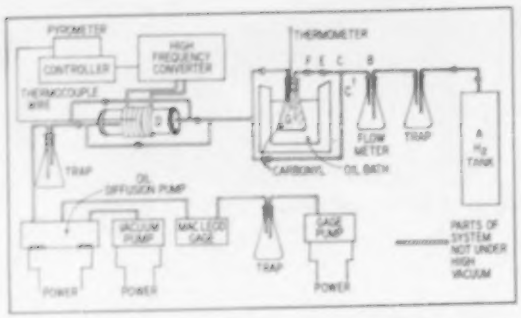

Fig. 1—The major parts of the plating setup—atmosphere generator, chamber with heating coil, vacuum pumps, and temperature controls—are shown in this schematic diagram of the vapor deposition unit.

quires reduced permissible CO pressure which tends towards a low plating rate and premature decomposition of the carbonyl.

The primary function of H_2 is to serve as a carrier of carbonyl vapor and to increase its flow. Theoretically, low CO/H_2 ratio means complete removal of carbon, but in practice, it has been found[5] that the selection of suitable CO/H_2 ratio is limited again from the view point of plating rate and early decomposition of carbonyl.

Apparatus

A description of the apparatus and materials used follows and a schematic diagram is included in Fig. 1. The hydrogen used was of a technical grade from tanks obtained from Linde Co. Molybdenum carbonyl was obtained from Climax Molybdenum Co.

Hydrogen from the tank *A* was regulated by two microvalves and a trap and flow meter *B* where the rate of flow was observed and regulated. For some experiments, when a humid atmosphere was desired, a humidifier was put into the line after the flow meter. From the junction, *C*, the line was divided. One branch, *C'*, led directly to the plating chamber, *D*, and the other branch led through two microvalves, *E* and *F*, into the carbonyl bottle, *G*, and then into the plating chamber, *D*. Both branches were provided with clamps and microvalves to aid in regulating the hydrogen flow.

The carbonyl bottle was immersed in a thermostatically controlled oil bath in order to regulate the partial pressure of molybdenum carbonyl. The carbonyl bottle was provided with a thermometer located at the gas outlet. Difficulties were encountered with the crystallization of molybdenum carbonyl in the colder portion of the line between the carbonyl bottle and the plating chamber. These difficulties were overcome by heating the line between the carbonyl bottle and the plating furnace with a nichrome resistance wire wound around the tubing.

The gas lines and four valves around the plating chamber permitted reversing the direction of the gas flow within the chamber.

Gases from the chamber passed through the trap, the two-stage oil diffusion pump, and to the mechanical pump. The purpose of the trap was to absorb undecomposed molybdenum carbonyl passing from the plating chamber.

The plating chamber or furnace was a quartz tube 8 in. long with 1 3/16 in. OD. The specimens were heated by high frequency induction. An induction coil (¼ in. copper tube, 1½ in. ID) was adjusted around the middle of the tube. Asbestos paper and an auxiliary resistance wire heating element located between the tube and the coil were used for stabilization of the temperature.

For temperatures up to 1300°F, an Ecco 1 kva converter was used as the source of high frequency current. For higher temperatures, a 10 kva unit was used. Iron-constantan thermocouples were used with the lower, and chromel-alumel thermocouples were used for the higher temperatures. The temperature of the specimens was controlled and recorded by a pyrometer controller. The thermocouple wires were sealed in a ⅛ in. diam quartz tube. The ends of the quartz tube were water cooled to prevent overheating of the rubber stoppers.

During early experiments, the specimens were held in the center with respect to the induction coil and supported by inserting the thermocouple tube inside a hole in the specimen.

A few modifications were tried before the temperature of a thin sheet sample could be held accurately and the sharpness of temperature oscillations decreased. Finally, the method adopted was simply to lay the thin specimen on a titanium block and attach it to the block by a wire of a high melting point material. The titanium block was 1½ to 3 in. long with a ½x½ in. cross-section. A hole was drilled in the block to receive the thermocouple.

During early runs, the thermocouple quartz tube was located in a hole drilled in the center of the sample. Temperature control was difficult. Temperature oscillations were as high as 40°F. Modifications tried included heavy asbestos insulation, additional resistance heating elements, and the use of ceramic and porcelain sleeves between the sample and the wall of the quartz tube. It was found that, when the hole in the sample was very close to the edge, the oscillations decreased down to approximately ±3°F. This procedure was adopted.

During decomposition, hydrogen was passed through the carbonyl bottle. The hydrogen and the carbonyl vapor mixture, as a plating atmosphere, entered the plating chamber. In most cases, the carbonyl bottle was kept at room temperature to decrease the CO partial pressure and CO/H_2 ratio. In order to further decrease the CO/H_2 ratio, amounts of H_2 were bypassed around the carbonyl container as shown in Fig. 1.

By regulating the microvalves, it was possible to control the carbonyl concentration from zero up to almost the amount present at the saturation point at the temperature of the thermostat.

During the course of experiments, the oil in the oil diffusion pump was changed and the mercury in the MacLeod gage was purified as necessary in order to be able to obtain a vacuum of the order of 1×10^{-4} mm Hg in the system.

Table I. Materials Used in Plating Runs

Alloy	Form	Composition, Pct
Ti-75A	½x1 in. bar stock HR, annealed and pickled.	99.5 Ti
Ti-150A	½x1 in. bar stock HR, annealed and pickled.	2.7 Cr
RC-130A	½ in. sq stock ½x1 in. bar stock HR, annealed.	7 Mn
RC-130B	½x1 in. bar stock	4 Al, 4 Mn
RC-55	Annealed sheet (0.030 in. thick).	99.5 Ti

Procedure For Vapor Plating

The vapor plating procedure consisted of the following steps: 1—preparing and mounting the samples, 2—closing and tightening the system, 3—evacuating the system, 4—vapor plating, and 5—finishing operations.

Rectangular samples were mounted directly on the quartz thermocouple tube. Titanium sheet samples were attached to titanium blocks mounted on the tube. The titanium samples were centered in the deposition chamber before plating.

Necessary connections were greased with high vacuum silicone grease, valves were closed, rubber stoppers were inserted into the quartz tube, and the whole system was tightened.

Mechanical and oil diffusion pumps were turned on. Evacuation was for about 1 hr prior to the deposition in order to remove moisture from the system. After evacuating, the whole system was flushed thoroughly with hydrogen for about 15 min.

Immediately before the application of high frequency induction heating, the line to the plating chamber was closed to prevent deposition during the temperature rise. When the desired temperature was reached, the line, and then the microvalves at the carbonyl bottle were opened slowly while the pressure was checked constantly.

To finish the deposition, the hydrogen valve and the line to the plating chamber were closed, the high frequency induction heat turned off, and the temperature allowed to drop. After about ½ hr, when the temperature of the sample was below 200°F, the vacuum was broken and the samples removed.

The most advantageous ratio of CO/H_2 appears to be between 5/1 and 1/1. Runs were made with CO/H_2 ratios ranging from 7/1 to 1/2 or less. Different CO/H_2 ratios in the foregoing range had little effect on adherence and galling characteristics of the coating. Adherent and wear-resisting coatings were deposited at CO/H_2 ratio equal to 7/1 and down to 1/2 or less.

Hydrogen is necessary as a carrier gas as it increases the flow of the carbonyl vapor from the vapor generating unit into the plating chamber. When the hydrogen flow is decreased below a certain value, *the flow effect*, which is always present to some extent during plating, becomes appreciable. The term *flow effect* signifies a phenomenon characteristic of vapor deposition which consists of building up the heaviest deposit at the surface facing the gas inlet and a gradual decrease with the distance from the inlet toward the outlet where the deposits are at a minimum. Increasing the hydrogen flow makes it necessary to decrease the carbon monoxide pressure in order to keep the total pressure below the critical value. That, however, decreases the speed of deposition. Carbon monoxide pressures can be regulated either by keeping the molybdenum carbonyl container at a lower temperature or by sending some hydrogen through a bypass around the molybdenum carbonyl container shown in Fig. 1.

These two effects of the speed of deposition and the flow effect set the CO/H_2 ratio between 5/1 to 1/2. These values were found to be true for samples approximately 2 in. long; the effect will be more pronounced on longer samples. The flow effect is more pronounced at the higher temperature of deposition. Among other modifications which were tried to overcome this difficulty was the use of a porous alundum sleeve. Some improvement was achieved with it. The greatest improvement was obtained in the uniformity of the deposition by reversing the flow of the plating atmosphere. By using this technique, a uniform coating on longer samples can be obtained.

Table II. Test Conditions for Plating Runs

Run	Material	Temperature, °F	Pressure, Mm Hg	Approximate CO/H_2	Time, Hr
1	RC-130A	884	0.55	10/1	3
2	RC-130B	884	0.20	3/1	1½
3	RC-130A	1050 to 884	0.23	3/1	5½
4	Ti-150A	950	0.21	3/1	3
5	Ti-75A	980	0.18	4/1	3
6	RC-130A	1030	0.21	3/1	2
7	Ti-75A	1080	0.20	3/1	2
8	RC-130B	1180	0.32	3/1	4½
9	RC-130B	1180	0.18	4/1	2
10	Ti-75A	1400	0.20	3/1	2
11	Ti-150A	1200 to 1300	0.20	3/1	1½
12	RC-55	850	0.11	5/1	5/12
13	RC-55	1030	0.32	5/1	3¼
14	RC-55	1030	0.28	3/1	3
15	RC-55	880	0.12	4/1	2
16	RC-55	1030	0.08	3/1	3
17	RC-55	1030	0.09	3/1	4
18*	RC-55	1090	0.08	3/1	3
19*	RC-55	1080	0.03	5/1	3
20*	RC-55	1020	0.07	5/1	3
21	Nickel	1030	0.10	4/1	1/3
22	RC-55	1380	0.05	—	1/3
23	RC-55	1380	0.05	5/1	1
24	RC-55 & Steel	1020	0.02	6/1	1
25	RC-55 & Steel	1380	0.04	5/1	2
26	RC-55	1700	0.06	5/1	2
27	RC-55	1600	0.04	5/1	2
28*	RC-55	1600	0.04	5/1	2
29*	RC-55	1700	0.15	5/1	¾
30	RC-55	1700	0.50	7/1	½
31	RC-55	1700	1.20	9/1	7/12
32	RC-55	1700 to 1100	0.05	5/1	2
33	RC-55	1700 to 1000	0.05	5/1	4
34*	RC-55	1700 to 1060	0.07	5/1	2½
35	RC-55	1700 to 1000	0.05	5/1	3
36	RC-55	1700 to 1000 to 1700	0.07	5/1	½
37	RC-130A	1700	0.06	5/1	2
38	RC-130B	1700	0.03	5/1	2
39	RC-130A	1700 to 1000	0.04	5/1	¾
40	RC-130B	1700 to 1080	0.04	5/1	½

* Flow Reversed was used.

Materials

The materials used are given in Table I. Runs 1 to 11 in Table II were made with ½ in. cube specimens. Runs 12 to 36 were made with ½x0.050x3 in. and shorter specimens of titanium RC-55 sheet. Runs 37 to 40 were made with ½x½x1½ in. specimens of RC-130A and RC-130B. One to three surfaces of the specimens were polished to a metallographic finish and degreased in boiling carbon tetrachloride immediately before the plating runs.

Plating

Tables II and III give the data of the plating runs made. The first 12 runs were made at temperature intervals of about 50°, 100°, and 200°F with occasional duplications. The pressure during run 1 was kept high (0.55 mm Hg) in an effort to find the upper limit of pressure for deposition and the resulting speed. The temperature of the oil bath for the carbonyl container was kept at 37°C (99°F). The CO/H_2 ratio was estimated to be approximately 10/1. The coating was thick (0.008 in.) and hard (surface hardness between 1400 and 1500 DPH), but had very poor adherence. Run 2 was made with the carbonyl container kept at room temperature. The lower total and CO pressures greatly improved the adherence of the coating, but decreased the rate of deposition. CO/H_2 ratio was between 3/1 and 5/1.

On the basis of the first 12 runs, the temperature of 980° to 1180°F was established as being the best from the standpoint of appearance of the coating. The coatings were adherent and had good appearance but failed on deformation of the specimen. The

Table III. Test Results of Titanium Plating Samples

Run	Thickness, In.*	Surface Hardness, DPH*	Bend Test**	Wear Test	Appearance†
1	0.008	1450	—	No	Very poor
2	0.0003	N.D.	—	No	Poor
3	N.D.	N.D.	—	No	Poor
4	N.D.	N.D.	—	No	Fair
5	0.0008	N.D.	—	No	Good
6	N.D.	N.D.	—	No	Good
7	N.D.	N.D.	—	No	Very poor
8	N.D.	1047	—	No	Good
9	N.D.	N.D.	—	No	Good
10	N.D.	N.D.	—	No	Fair
11	N.D.	N.D.	—	No	Very poor
12	N.D.	N.D.	Poor	No	Good
13	0.004	N.D.	Poor	No	Poor
14	N.D.	N.D.	Poor	No	Fair
15	N.D.	N.D.	Poor	No	Very good
16	N.D.	N.D.	Poor	No	Very good
17	N.D.	N.D.	Poor	No	Very good
18	N.D.	700	Poor	No	Very good
19	N.D.	N.D.	Poor	No	Very good
20	N.D.	1426	Poor	No	Very good
21	N.D.	N.D.	—	No	—
22	N.D.	N.D.	—	No	Coloration
23	N.D.	N.D.	—	No	—
24	0.0001	N.D.	Poor	No	Very good
25	N.D.	N.D.	Poor	Yes	Very good
26	0.002	808	Very good	No	Very good
27	0.001	N.D.	Poor	Yes	Very good
28	0.001	N.D.	Poor	No	Very good
29	0.001	N.D.	Very good	Yes	Very good
30	N.D.	N.D.	Very good	Yes	Very good
31	0.001	893	Very good	No	Poor
32	N.D.	N.D.	Good	No	Very good
33	0.0003	N.D.	Good	No	Very good
34	0.0002	639	Good	Yes	Very good
35	0.0002	N.D.	Good	No	Very good
36	N.D.	N.D.	Good	Yes	Very good
37	N.D.	N.D.	—	Yes	Very good
38	N.D.	N.D.	—	Yes	Very good
39	N.D.	N.D.	—	Yes	Very good
40	N.D.	N.D.	—	Yes	Very good

* N.D. stands for not determined.

** Poor is when a coating on the 0.80 in. thick sample could stand only a few degrees bending. Good is when a coat could stand stronger bending up to about 30° over a bending radius of ⅛ in., but would eventually peel off. Very good is when the base metal can be deformed until it cracks without peeling of the coating. Values not shown were for block samples, since no bend tests were performed on the bars.

† Very poor and poor is when a coating peeled off during the deposition run. Very good is when a coating, as deposited, looked entirely sound.

first 11 runs were made with ½ in. cubes of 75A, 130A, 130B, and 150A titanium and titanium alloys. The surface microhardness of all these coatings were above 1000 DPH.

X-ray diffraction photographs were taken of the coatings from runs 3, 7, 11, 16, and 29. It was found that the amount of molybdenum carbides present in the molybdenum coatings depended mostly upon the total pressure of the deposition.

Runs 12 to 36 were made with 0.050 in. thick sheet samples of titanium RC-55. These samples, when coated, were subjected to bending in order to test the adherence and ductility of the coating.

Runs 13 to 20 were made at the optimum temperature obtained, which was approximately 1020°F. Only when the total pressure was lower than 0.12 mm Hg (run 15) was a coating of good appearance obtained. On bending, however, the coating failed. Run 20 produced a coating whose surface microhardness was found to be equal to 1426 DPH.

From runs 16 through 40, the total pressure was kept below 0.1 mm Hg. Runs 16 to 25 were at temperatures below the critical temperature of titanium. A few runs were made to overcome the flow effect. A great improvement was achieved by reversing the flow of plating atmosphere during the runs.

Run 21 was made to determine if the molybdenum would deposit on nickel. An adherent coating was not obtained.

The literature on vapor plating of molybdenum contains a statement that the ductility of the coatings is improved by humidity in the plating atmosphere. Runs 22 and 23 were made under such conditions. In run 22, the titanium became discolored when heated in humid hydrogen. In run 23, when using humid plating atmosphere, the coating was not adherent. It is evident that the moisture reacts with the titanium surface to interpose a layer of titanium oxide.

It was claimed by J. J. Lander and L. H. Germer[7] that ductile molybdenum coatings were obtained on steel. In runs 24 and 25, samples of low carbon steel strip were included with the RC-55 titanium for plating. In both cases the low carbon steel samples became coated with molybdenum. In run 24, the coating on the steel was approximately 0.0001 in. thick while in run 25 it was approximately 0.0003, in. thick. In both cases, the coating was sufficiently adherent and ductile as to withstand a 90° bending of the steel strip without failure.

The molybdenum coatings produced on the titanium during runs 24 and 25 failed in bending. The results indicated that the thin molybdenum coating itself is ductile and that the adherence of the coating depends primarily on the bonding of the coating to the base metal. This thought led to an attempt to improve the bonding by using higher temperatures of deposition in order to initiate diffusion.

The positive results obtained on steel might have been further utilized in experimenting thin iron electroplates on titanium followed by molybdenum deposition from carbonyl. This was not done.

Run 26, at 1700°F, produced the first successful results in obtaining adherent and ductile coatings on titanium. No peeling was observed when the coating was subjected to free bending to 180°. The surface microhardness of the coating was 808 DPH. That diffusion of the molybdenum into the titanium had taken place is evident in Fig. 2.

In run 26, upon removing the titanium from the furnace, it was observed that the titanium sheet

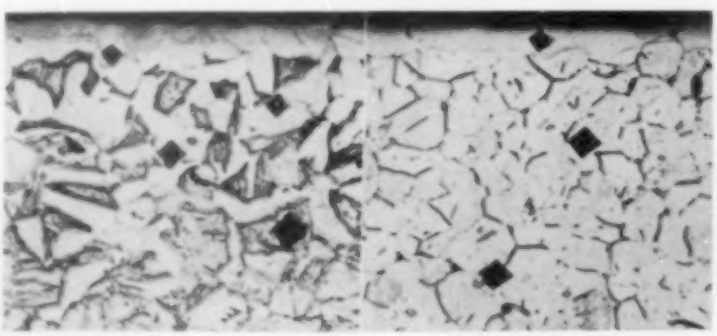

Fig. 2—RC-55 in run 26 shows the diffusion of molybdenum into the titanium which took place during the plating process. X250. Area reduced approximately 25 pct for reproduction.

Fig. 3—RC-55 in run 27 demonstrates good adherence between molybdenum and titanium although the sample gave a poor bend test. X250. Area reduced approximately 25 pct for reproduction.

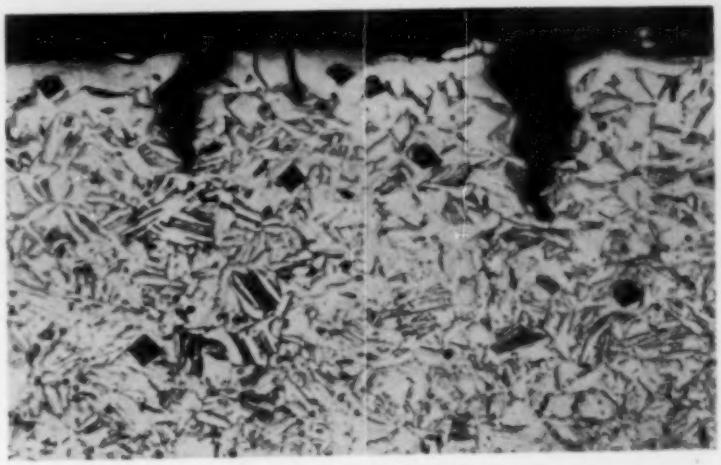

Fig. 4—RC-55 in run 29 shows coating so adherent that base metal could be deformed until it cracked without peeling of the coating. X250. Area reduced approximately 25 pct for reproduction.

Fig. 5—RC-55 in run 31 shows cracking of base metal without peeling of coating although coating had cracks as deposited. X250. Area reduced approximately 25 pct for reproduction.

sample adhered to the titanium block to such an extent that it had to be pried and hammered to separate it from the block.

In runs 27 and 28, a lower temperature of 1600°F was tried, but it did not produce a coating which would withstand bending more than a few degrees although the adherence was very good, as shown in Fig. 3.

At 1700°F, a sound coating was formed at a much faster rate than at lower temperatures. At the higher temperature, higher pressures can be used successfully. The deposition rate has been found to be approximately 0.001 in. per hr at 1700°F and 0.50 mm Hg, 0.0005 in. per hr at 1600°F and 0.10 mm Hg, and 0.0001 in. per hr at 1000°F and 0.10 mm Hg.

A total pressure of 0.15 mm Hg, run 29, and 0.50 mm Hg, run 30, at 1700°F produced perfect coatings. Higher pressure, however, of 1.20 mm Hg, run 31, produced a coating which had cracks as deposited. The coatings were so adherent that the base metal could be deformed until it cracked without peeling of the coatings, as shown in Figs. 4 and 5, respectively.

It was observed that adherence of coatings decreased as temperatures during deposition were increased from approximately 1380° to approximately 1600°F. At 1700°F, however, when the diffusion took place, the adherence was very good.

It was thought that a flash coating at 1700°F followed by a longer period of coating at a lower temperature might retain the good adherence of the high temperature coatings and, simultaneously, avoid the severe grain coarsening that is created by the 1700°F temperature.

Runs 32, 33, 34, and 35 were made accordingly. Deposition was started at 1700°F and maintained for only about 3 min and the temperature allowed to fall to 1100° or 1000°F and plating allowed to continue for about ½ hr or longer.

This procedure has produced good adherent and wear-resistant coatings; the microstructure of the titanium-base metal was not affected by the short high temperature flash. The coatings were ductile enough to take a strong bend without apparent failure. This procedure has been termed the *duplex method*.

The thickness of the molybdenum coatings produced by the duplex method was about 0.0001 in. or more. It was believed that in measuring the microhardness, the diamond pyramid indenter penetrated the thin molybdenum coating. Therefore, the measured hardness may be lower than the true hardness of the coating. This approximate surface microhardness was found to be 639 DPH (100 g).

In addition to the aforementioned 40 runs, five runs were made which are not described in this report. Of these five runs, two were preliminary trial tests and three were unsuccessful tests. The latter three test failures were due to leaks developed in the vacuum system, a burned thermocouple, and a sample which slid off during the deposition.

A second flash of the high temperature, at the end of the run, developed no increase of ductility and adherence of the coating (run 36).

Runs 37 to 40 inclusive were made to prepare molybdenum-coated samples of titanium alloys RC-130A and RC-130B for qualitative wear-testing as described later in this report.

Wear Tests

A shaper was modified to accommodate a ½ in. diam steel ball upon which a variable load could be imposed by a lever-arm dead weight method. Pivot blocks were made of wood and steel with a lever arm for weight loading. The hardened steel ball was held rigidly in a modified tool holder and allowed to rub against the titanium specimens under the desired force. The general arrangement was similar to that described in the *Interim Technical Report on Chemical Surface Treatment of Titanium*.[4]

The hardness of the steel ball was checked and found to be Rc 65. When lubricating oil was used, it was SAE 10. When SAE 10 oil was not used, the samples and the hardened steel ball were cleaned with acetone or carbon tetrachloride immediately before tests to remove any traces of grease.

Qualitative wear tests were made to determine the galling characteristics of molybdenum-coated titanium and titanium alloys. Tests were made also on untreated titanium.

It was found that either with or without lubrication, one to two strokes produced appreciable wear and galling on untreated RC-55 titanium as shown in Fig. 6. Pieces of titanium metal were torn out of the sample and accumulated at the ends of the stroke. The force applied against the sample during testing was approximately 23 lb, resulting in a pressure in the order of 50,000 lb per sq in. at the end of the second stroke as calculated from the width of the wear mark.

Table IV. Wear Test Results of Plating Samples

Material	Sample from Coating Run	Load Applied, Lb	No. of Strokes	Lubricant	Results
RC-55	24	23	12,000	Oil	Slight burnishing.
RC-55	25	100	Few	Oil	Ti base yielded in compression.
RC-55	25	100	100 to 200	Oil	Mo coating flaked.
RC-55	25	100	12,000	Oil	No seizing or galling.
RC-55	Untreated	—	Few	Oil + Mo particles from 2.	Surface worn.
RC-55	27	100	100,000	Oil	Coating did not fail. Grooving and burnishing developed.
RC-55	25	23	40	None	Scoring
RC-55	25	23	100	None	Galling
RC-55	27	23	100	None	Seizure began.
RC-55	27	23	1,000	None	Galling
RC-55	29, 30	23	360 to 700	None	Scoring
RC-55	29, 30	23	630 to 810	None	Seizure
RC-55	29, 30	23	900 to 1,320	None	Galling
RC-130A	37	23	25	None	Polishing marks.
RC-130A	37	23	100	None	Seizure
RC-130B	38	23	25	None	Polishing marks.
RC-130B	38	23	25	None	Seizure
RC-130A	37	23	30,000	Oil	Polished track.
RC-130B	38	23	30,000	Oil	No scoring, seizure, or galling.
RC-130A	39	23	30,000	Oil	Polished track.
RC-130B	40	23	30,000	Oil	No scoring, seizure, or galling.

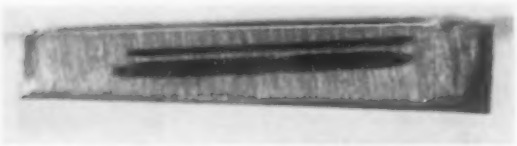

Fig. 6—Two wear strokes on untreated RC-55 resulted in the narrow band of wear. The wider band is the result of 64 strokes.

Tests on titanium and titanium alloys coated with molybdenum, by any of the three methods developed, have shown that, when lubricating oil was used, the coating withstood thousands of strokes. The only result was a polished mark.

For comparison, several samples of RC-55 titanium were simply heated to 1400°F in the plating chamber in a high vacuum, but no molybdenum was deposited on the samples. These samples, when subjected to qualitative wear tests with application of lubricating oil, failed instantaneously like those which were untreated.

The wear test results are shown in Table IV.

Conclusions

1—Temperature and pressure are the most important factors in obtaining a sound deposit.

2—Adherent molybdenum coatings on titanium and titanium-base alloys can be obtained by any of three techniques.

3—At temperatures of 900° to 1380°F and total pressures up to 0.1 mm Hg, hard coatings (up to 1000 DPH) can be obtained on RC-55, Ti-75A, RC-130A, RC-130B, and Ti-150A at a rate of approximately 0.0001 in. per hr. The coatings, however, are rather brittle and will stand only a few degrees of bending. The titanium microstructure undergoes little change.

4—At temperatures of 1700°F and above and total pressures up to 0.5 mm Hg, ductile and somewhat softer coatings (hardness up to 800 DPH) can be obtained on titanium alloys RC-55, RC-130A, and RC-130B at a rate of approximately 0.001 in. per hr. The microstructure of the titanium is changed by grain growth. At about 1700°F, some diffusion of molybdenum into the titanium base is obtained.

5—A duplex method of deposition at different temperatures starting at 1700°F for approximately 3 min and continuing while the temperature is dropped to 1000°F and maintained at 1000°F for about 20 min gives a coating that is adherent, hard, and ductile. The structure of the titanium base is unaffected by the short exposure to high temperature. The thickness of the coating is approximately 0.0001 in. Such coatings have been deposited on RC-55, RC-130A, and RC-130B.

6—It was impossible to obtain molybdenum coating on titanium by pyrolytic decomposition of molybdenum carbonyl at 1600°F or below, which would stand bending more than a few degrees.

7—The higher the temperature and/or the greater CO/H, ratio, the greater is the flow effect during vapor deposition. By reversing the flow of the plating atmosphere, the uniformity of the deposit can be improved.

8—X-ray diffraction examinations of the molybdenum coatings indicate the presence of molybdenum and molybdenum carbide. The relative amounts are dependent upon the plating conditions.

9—Qualitative wear tests show remarkable wear resistance of the molybdenum-deposited coatings on titanium. The improvement over untreated titanium is especially pronounced when lubrication is used.

10—A good wear-resistant coating of molybdenum can be applied to annealed titanium or titanium alloys in 1 or 2 hr without harm to the structure or mechanical properties of the titanium.

11—The process is possibly of commercial application.

Discussion of this paper, if any, will appear in JOURNAL OF METALS, November 1955, and in AIME Metals Branch *Transactions*, Vol. **203**, 1955.

References

[1] Project Rand, United States Air Force. Battelle Memorial Institute. R-108 (July 1948), R-137 (Mar. 1949).

[2] E. A. Gulbransen and K. F. Andrew: Kinetics of the Reactions of Zirconium with O_2, N_2, and H_2. *Trans.* AIME (1949) **185**, p. 515; JOURNAL OF METALS (August 1949).

[3] J. J. Lander and L. H. Germer: Plating Molybdenum, Tungsten, and Chromium by Thermal Decomposition of their Carbonyls. *Trans.* AIME (1948) **175**, p. 648; METALS TECHNOLOGY (September 1947).

[4] H. A. Pray, P. D. Miller, and R. L. Gibbs: *Interim Technical Report on Chemical Surface Treatment of Titanium.* (Jan. 31, 1952). Columbus. Battelle Memorial Institute.

Continuous Multistage Separation by Zone-Melting

by W. G. Pfann

A simple method of obtaining multistage batch separations by crystallization was described recently. Known as zone-refining, it comprises passing short molten zones through a long solid charge. This technique can now be used on a continuous basis by means of the *zone-void method* described in this paper. Feed enters, at an intermediate point, a column down which molten zones travel, and waste and product leave at the ends. Materials move in the column through the agency of voids, which are introduced at the ends and travel toward the feed inlet. The voids and molten zones are moved by external heaters in a simple manner, and the principle of reflux is utilized.

A NEW method of obtaining multistage separations by crystallization was described recently.[1] Named *zone-refining*, the method comprises slowly passing a series of molten zones through a long solid charge. Solute becomes concentrated at one or the other end of the charge, depending on whether it raises or lowers the freezing point of the solvent. The separation increases with the number, P, of zone-passes, approaching a limit as P approaches infinity. Zone-refining has been highly effective in purifying germanium and other substances,[2,3] and new applications are steadily increasing.

Zone-refining is a batch method and as such it has certain limitations inherent in batch operation. If it could be made continuous, its scope and utility would be greatly broadened.

This end has been achieved by the *zone-void method* described in this paper. In the zone-void method feed is introduced continuously at an intermediate point in a column down which molten zones travel, while impure waste and purified product leave at the ends. Both the flows of feed, waste and product, and also the travels of the zones, are actuated by external moving heaters in a simple manner; and the system utilizes the principle of reflux. The method provides, in the field of crystallization, the counterpart of the continuous fractionation column in the field of distillation. The following will be discussed: apparatus and mode of operation, fundamental nature of the separation, design theory, and practical considerations.

The method will be described in terms of a binary solute-solvent system in which the solute is an impurity to be removed and the solvent is the desired product. The distribution coefficient, k, defined as the ratio of solute concentration in the solid freezing out of a molten zone to that in the liquid in the zone, is assumed to be constant and less than one. The process is equally effective for k's greater than one and for ternary or higher order systems.

Method and Apparatus

The essential features of a continuous zone-refining process are represented in highly generalized form in Fig. 1. A series of molten zones, produced by moving heaters, travels slowly down the column or charge (to the left in Fig. 1). If there were no flows of feed, waste, or product, the process would simply be batch zone-refining, the action of the molten zones being to sweep solute *down* the column, solvent up the column. For the process to be continuous, with stripping and enriching sections in the column, feed must enter, and waste and product must leave, as indicated. The zone-void process accomplishes both objectives, namely, the indicated movements of zones and the indicated flows of material. Zones are moved by moving heaters, just as in batch zone-refining. Materials are made to flow by creating voids at the waste and product exits and causing these voids to move to the feed inlet. Since there must be a net flow of material from the feed inlet to each of the outlets, the indicated movements of voids are in the desired directions, because movement of a void in a given direction corresponds to flow of material in an opposite direction.

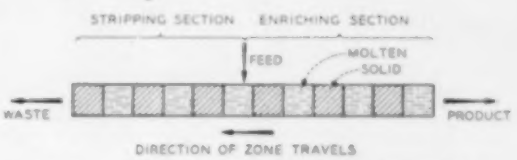

Fig. 1—Continuous zone-refining apparatus (generalized).

In order to produce the desired movements of voids, the column is folded into two vertical sections having the feed inlet in common at their upper ends. Voids are displaced upward by the liquids in the molten zones and their travel is actuated by the motions of the zones. Voids travel with the zones in the enriching section and move continuously. Voids travel opposite to the zones in the stripping section and move intermittently. Creation and travel of voids will now be examined in detail.

The *enriching section* of a column in operation, with its void generator, is shown in Fig. 2. The column section is a vertical tube around which a series of closely fitting, regularly spaced heaters travel slowly upward. Each heater produces a molten region, the temperatures of the heaters and the cooling between heaters being controlled so as to maintain the molten zones approximately constant in size. A void is normally present atop the molten zone in each heater. As the heater rises, it continuously melts solid above it, which drips through the void into the molten zone and continuously freezes out solid below it, of concentration k times that of the liquid in the zone. When a molten zone and void reach the feed inlet, which is kept molten, the void is displaced by an equal volume of feed liquid.

Generation of voids of controlled size in the enriching section is shown in Fig. 3. The void generator is a tube of small cross-section, provided with lateral heat-conducting fins which sense the position of the heater. Liquid can escape only when the entire outlet tube is within the heater. If any part of the outlet tube is outside the heater, liquid cannot escape,

W. G. PFANN, Member AIME, is associated with Bell Telephone Laboratories Inc., Murray Hill, N. J.

Discussion of this paper, TP 3986E, may be sent, 2 copies, to AIME by Apr. 1, 1955. Manuscript, July 19, 1954. Chicago Meeting, February 1955.

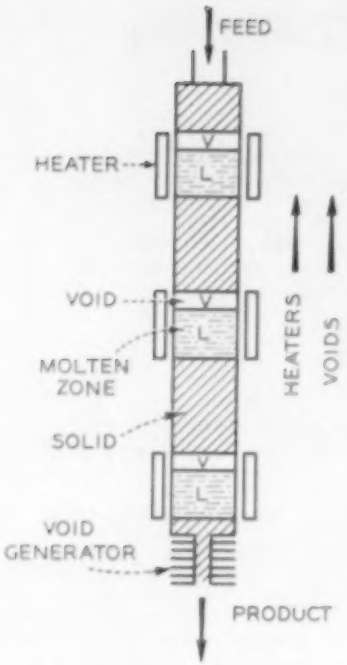

Fig. 2—Enriching section of zone-void refiner.

since the walls of the tube, being cool, freeze the liquid and thereby block the tube. In *b*, Fig. 3, the maximum volume of liquid which can escape is shown; and its escape has created a void of volume V. In *c* and *d* the void is seen moving "down" the column atop the moving molten zone.

In connection with Fig. 3, it can be visualized that if the outlet were simply a small hole, not a tube, then all of the liquid inside a heater would escape and a series of voids, without molten zones, would travel through the enriching section. This would merely achieve flow of matter from inlet to outlet, but would not accomplish "reflux action" (see a subsequent section) by the molten zones. However, by means of the outlet tube, liquid is prevented from escaping once the bottom of the heater rises above the lower end of the outlet tube. Thus a molten zone of length l and a void of length h-l is produced by a heater of length h, where l is the length of the outlet tube, each time a heater travels past the end of the column. (The volume of the outlet tube is assumed negligible.)

Many other designs of void generator are feasible. A vent tube may be provided to assist the flow of liquid through the exit tube. Another type is simply a valve at the end of the column, whose opening and closure are regulated by the position of the heater. The primary consideration is that a controlled volume of liquid be ejected each time a heater passes the end of the column.

In the *stripping section* voids are created much as in the enriching section, even though the heaters move downward. (As may be seen from Fig. 3b, a void of length h-l will be produced when the heater is in the indicated position, for either travel direction.) Motion of the voids is intermittent, as shown in Fig. 4 which shows the creation of two voids, beginning with a column free of voids. In *a* a void, V_1, has just formed. In *b* the molten zone above V_1 eats into the intervening solid, while the void remains stationary. In *c* the bridge of solid has melted through, the void has bubbled up through the zone, and the zone has fallen one void length, the lower portion of it freezing. In *d*, void V_1 has been left behind by the zone and solidification of zone L_1 by normal freezing[1] has been in progress. In *e*, V_1 has risen through L_2 and void V_2 has formed. It may be noted that the zone length is h in the stripping section and l in the enriching section. Better control of heater temperature and cooling conditions is required in the former because at times there are two solid zones for each heater.

Thus, in both the stripping and enriching sections, material flows through the column continuously, despite the fact that both column sections are at all times blocked by plugs of solid material. The moving voids make these material movements possible.

A complete zone-void refiner comprising rectifying and stripping sections is shown in Fig. 5. The heaters move with reciprocating motion, travelling forward slowly and backward rapidly a distance equal to the heater interval, d. This type of motion has the effect of causing the zones to move continuously in the desired direction (down the column), permits freedom in design of the apparatus, and has other merits described elsewhere.[4]

Theory

In this section, the basic nature of the zone-void process will be considered and some comparisons with other separation methods will be made. Equations useful for the design of zone-void apparatus will be given. While these involve a number of simplifying assumptions and hence must be regarded as approximate, they serve to show how various parameters affect the separation, and they provide a basis for more exact treatments.

Steady State at Total Reflux: By "total reflux" the author means here that no flows of feed waste or product occur as the molten zones move down the column. It has been shown[1] that under such circumstances a steady state is reached after a large (theoretically, an infinite) number of passes of molten zones down the column. The solute concentration C as a function of the distance x from the end of the column at which zones begin their travel is given approximately by

$$C = Ae^{kx} \qquad [1]$$

where

$$k = Bl/(e^{Bl} - 1) \qquad [2]$$

and

$$A/C_o = BL/(e^{BL} - 1) \qquad [3]$$

and where l denotes zone length; L, column length; and C_o is the mean solute concentration. The constant A is the concentration at $x = 0$ and hence the ratio A/C_o may be taken as a separation ratio.

It is found, by solving Eq. 3 for a wide range of

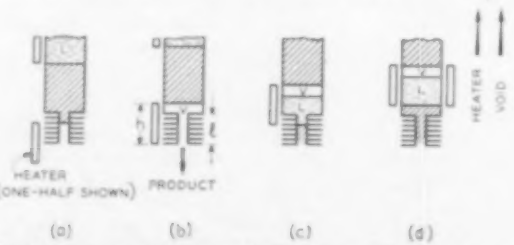

Fig. 3—Creation and travel of void in enriching section of zone-void refiner.

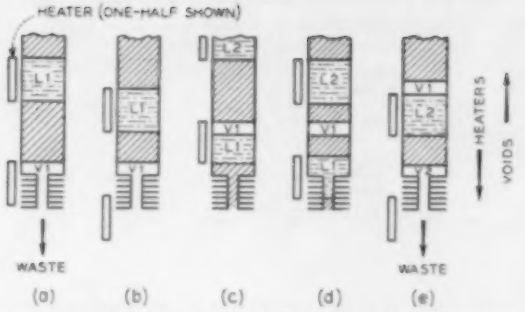

Fig. 4—Creation and travel of voids in stripping section of zone-void refiner.

values of k, l, and L, that A/C_o can be represented empirically as follows

$$A/C_o = k^{fN} \qquad [4]$$

where $N = L/l$ is the number of zone lengths in the column and f is a fairly constant factor given in Table I. Eq. 4 tells that fN is the number of theoretical stages (factors of k in A/C_o) in a zone-void refiner at total reflux and that this number is roughly proportional to the number of zone lengths in the column. Under conditions of partial reflux, the number of theoretical stages will be less than fN, in general.

Steady State at Partial Reflux: **Nature of the Flows**—The flows of matter in a continuous multistage separation process involving reflux may be separated for purposes of discussion into two parts: the flows which comprise the reflux aspects of the process, and the flows of feed, waste, and product which give the process its continuous nature. In many processes, such as distillation, these flows are readily distinguishable as actual quantities of matter moving up and down the column.

In distillation a countercurrent flow exists between rising vapor and falling liquid, and calculations of column performance involve these flows in the form of the reflux ratio, which, by one definition, is the ratio of liquid downflow to distillate removed.[4,5]

In zone-void refining the effects of countercurrent flow between liquid and solid phases are achieved by the molten zones. While the liquid in the zones does not flow in quite the same sense as the liquid in a still, the effect on solute distribution of passing a molten zone down* a column is much the same as if the same volume of liquid actually flowed down the column, equilibrating itself with the solid as it traveled. Thus the volume flow of molten regions down the column may be considered as analogous to the liquid downflow in distillation.

* In the system under consideration, solute travels with the zones, down the column, leaving as waste; solvent travels opposite the zones, up the column, leaving as product.

Since, in the operation of the refiner, one void is created each time a molten zone enters or leaves a column section, the ratio $l/(h-l)$ of molten volume to void volume is analogous to a reflux ratio. This concept is brought out here to indicate the nature of the zone-void process. Direct use of a reflux ratio as such is not made in the equations which follow.

A unique aspect of molten-zone, or "zonal," reflux is the degree of contact between the countercurrent phases. In distillation the approach to complete equilibration is limited by the degree of contact, that is, the interfacial area between liquid and vapor. In zonal reflux, contact is perfect in that the solid phase is completely dissolved in the liquid phase throughout the cross-section of the zone. The perfect contact afforded by zonal reflux greatly simplifies column construction in that packing media or bubble-cap plates are unnecessary.

Table I. Values of f in Eq. 4

N =	2	10	50	250
k = 0.01	1.1	1.3	1.4	—
0.1	1.1	1.4	1.5	—
0.5	1.1	1.4	1.7	—
0.9	1.0	1.2	1.6	1.9
0.99	1.0	1.1	1.2	1.6

As in distillation, diffusion in the liquid phase limits the approach to perfect equilibration. It is affected by the rate of motion and degree of stirring in the zones. By moving the zone slowly, or by stirring the liquid, the equilibrium value of k, which gives the greatest separation, can be approached. Effective k's, which obtain at higher rates can be determined by simple experiment or from published data or theory.*

* For example, k as a function of growth rate is given by McFee[6] for solutes in NaCl; Slichter and Kolb,[7] for solutes in germanium. Theory for k under various growth conditions is given by Burton, Slichter, and Prim[8] and Wagner.[9]

The flow rates of feed, waste, and product, designated F, W, and P, respectively, are determined by the volume flow rates of voids, as has been indicated. They are related by the overall material balance

$$F = W + P. \qquad [5]$$

If the flows of waste and product are properly coordinated, the feed tank will remain at the feed concentration, C_f.** The ratio P/W will depend on C_f and C_o, the concentrations of solute in product

** While this condition is not a necessary one for operation of the refiner, it shall be assumed in the following.

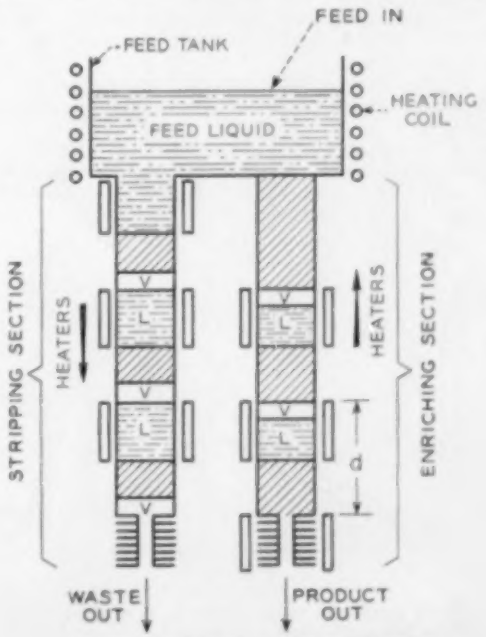

Fig. 5—Complete zone-void refiner (schematic).

and waste, as follows: Let

$$C_p = \alpha C_f \quad [6]$$

$$C_w = \beta C_f. \quad [7]$$

From Eqs. 5, 6, and 7 and a solute balance, the following is obtained

$$P/W = (\beta-1)/(1-\alpha). \quad [8]$$

For example, if $\beta = 3.5$ and $\alpha = 0.01$, the ratio P/W is 2.52. This ratio can be achieved in various ways, e.g., by different cross-sections in the two sections of the column, by different void-lengths, heater spacings, or travel rates.

Next, operation of the refiner in the steady state will be described and equations for the steady states in the enriching and stripping sections will be given. These together with Eq. 8 provide an outline of design theory required to construct a zone-void refiner for a given problem of separation. (Constructional details and heat balances will not be considered here.) The writer is greatly indebted to H. Reiss for the mathematical conception and solution of these steady-state equations, as well as for much valuable insight as to their interpretation.

The enriching and stripping sections meet at the feed inlet or tank and have in common at this point the feed concentration, C_f. Feed entering the column divides into two portions, one of which travels through each section. The action of the enriching section is to remove *solute* from that portion of the feed which travels through it and to transfer this solute to the feed tank. The action of the stripping section is to remove *solvent* from that portion of the feed which travels through it and to transfer this solvent to the feed tank.

Equations for Enriching Section—When a molten zone travels through the enriching section, from product exit to feed inlet, the following events, which can be visualized with the aid of Fig. 6, occur:

1—A void is formed by draining out length h-l of material at the product exit.

2—The void travels through the section, causing a shift in the solute distribution a distance h-l toward the exit.

3—The zone, in its travel through the section, removes solute therefrom and transports it toward the feed tank.

4—The zone arrives at the feed tank and its contents mix with the feed liquid. Solute is transferred to the feed tank because the concentration in the zone is greater than C_f.

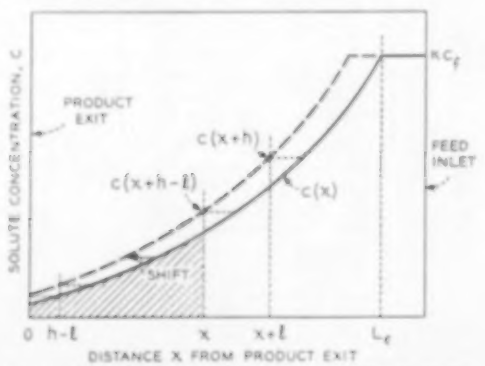

Fig. 6—Steady-state solute distribution in enriching section (full). Shift in the distribution caused by passage of void is shown by dashed curve.

Table II. Limits of the Purification Ratio, $\alpha = C_p/C_f$, for Enriching Section

Value of k	Range of α		Range of ψ	Range of ω	Sign of B_0
	$L=0$	$L=\infty$			
$k<l/h$	$\frac{\omega\psi}{1+\omega}$	0	0 to $-\infty$	-1 to 0	$(+)$
$l/h<k<1$	$\frac{\omega\psi}{1+\omega}$	ψ	0 to k	<-1	$(-)$
$k>1$	$\frac{\omega\psi}{1+\omega}$	ψ	k to $+\infty$	>0	$(-)$

If the steady state has been reached, the sequence of steps 1 to 4 leaves the solute distribution in the column section unaltered. It can be shown from a solution of the steady-state equations (see Appendix) that the section length L_e required for a separation ratio α in the enriching section is given by

$$L_e = \frac{1}{(0.434)B_0} \log \omega \left[\frac{\psi}{\alpha} - 1 \right] \quad [9]$$

where B_0, ω, and ψ are constants depending on h, l, and k and are given by

$$e^{B_0 h} = 1 + B_0 l/k \quad [10]$$

$$\omega = \frac{k}{(1-k)B_0 l} [1 - e^{B_0(h-l)}] \quad [11]$$

$$\psi = (hk-l)/(h-l). \quad [12]$$

The length L_e of the column section in Eq. 9 is defined as the distance from the exit end to the point at which the solute concentration in the solid is kC_f. In practice this length will usually be about one heater length less than the actual section length.

These equations place certain restrictions on the values of α which can be attained in a section of finite length. These are summarized in Table II, with other pertinent information. The restrictions involve the relationship of the parameters h, l, and k, where the heater length h is equal to the sum of the zone length l and the void length h-l. For $k < 1$, if $k<l/h$, then there is no theoretical limit on α, an α of zero being in principle attainable in a section of infinite length. For $l/h < k < 1$, there will be a minimum α which is greater than zero, even for an infinite section length. For $k > 1$, values of α greater than k are desired and are attainable, but as in column 2, Table II, they are limited by the value of ψ.

Because the equations are least accurate near $L_e = 0$, the value of α at $L = 0$, $\omega\psi/(1+\omega)$ in Table II is not particularly meaningful. The actual value of α for $L = 0$ is presumably between 1 and k.

Illustrative Calculation—Given $h = 1$, $l = 0.8$, $k = 0.5$, and desiring $\alpha = C_p/C_f = 0.01$, find the required section length, L_e. From Eq. 10

$$e^{B_0} = 1 + B_0 \frac{(0.8)}{(0.5)}$$

$$B_0 = 0.87.$$

From Eq. 11

$$\omega = \frac{0.5}{(0.5)(0.87)(0.8)} [1 - e^{0.87(1-0.8)}] = -0.27.$$

From Eq. 12

$$\psi = \frac{(1)(0.5) - 0.8}{1 - 0.8} = -1.5.$$

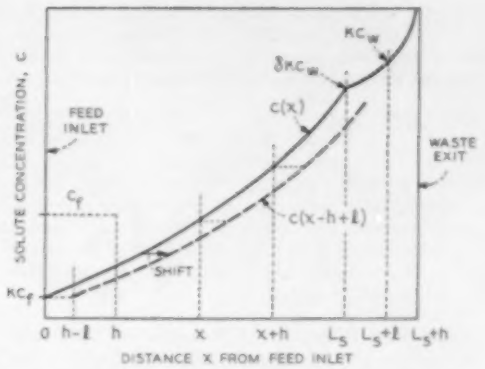

Fig. 7—Steady-state solute distribution in stripping section (full), showing shift caused by passage of void (dashed).

From Eq. 9

$$L_s = \frac{1}{(0.434)(0.87)} \log \left[(-0.27)\left(\frac{-1.5}{0.01}\right) - 1 \right] = 4.2.$$

Equations for Stripping Section—The following events, which can be visualized with the aid of Fig. 7, occur when a molten zone moves through the stripping section from the feed inlet to the waste exit:

1—At the start of its travel, adjacent the feed inlet, the heater forms a molten zone whose contents mix with the feed and thereby assume concentration C_f. As a result, solute is introduced into the stripping section, and solvent to the feed tank, because C_f is greater than the mean concentration which is replaced.

2—The molten zone travels through the section, the first-to-freeze concentration being kC_f.

3—When the leading edge of the heater reaches the end of the section, further travel causes solidification of the zone by normal freezing, as can be seen from Figs. 4 and 7.

4—When the leading edge of the heater reaches the lower end of the exit tube of the void generator, the remaining liquid runs out, as waste. This liquid is concentrated in solute, due both to the zone-refining action in the section and to the normal freezing action at the end of the section.

5—The void which is formed in step 4 travels with discontinuous motion through the stripping section to the feed tank and thereby shifts the solute distribution one void length toward the waste exit. Its travel requires the cooperation of succeeding molten zones and depends on the length and spacing of the heaters.

Table III. Limits of β for Stripping Section

Value of k	Range of β		Sign of γ	Sign of B_0
	$L_s=0$	$L_s=\infty$		
$k<1$	k/δ	$\frac{h(1-k)}{(h-l)}$	(+) If $\beta<\frac{h(1-k)}{(h-l)}$	(+)
	k/δ	$\frac{h(1-k)}{(h-l)}$	(−) If $\beta>\frac{h(1-k)}{(h-l)}$*	(+)
$1<k<h/l$	k/δ	0†	(−)	(+)
$k>h/l$	k/δ	$(k-\gamma)/\delta$	(+)	(−)

* Note 1: If $\beta>h(1-k)/(h-l)$, then β at $L_s=\infty$ will be less than k/δ, and hence a normal freezing section only, is indicated. For $k<1$, k/δ is always >1.

† Note 2: $\beta=0$ occurs at $L_s=1-k/\delta$, suggesting that a perfect separation can be approached at finite L_s for $1<k<h/l$.

6—In its travel the molten zone encounters a number of voids. Each encounter advances the zone one void length, $(h-l)$. One encounter occurs for each heater ahead of the heater at the feed tank, because each such heater in effect produces one void which eventually must pass the heater in question. These advances shorten the effective length of the section for refining.

As in the enriching section, a steady state is reached. It can be shown (see Appendix) that the section length L_s required to produce a separation β is given by

$$L_s = \frac{1}{(0.434)B_s} \log \left[\left(\frac{\beta\delta - k}{\gamma} \right) + 1 \right] \quad [13]$$

where B_s, δ, and γ are constants depending on h, l, k, and β are given by

$$e^{B_s l} = 1 + B_s \frac{h}{k} \quad [14]$$

$$\delta = k \left(\frac{h-l}{h} \right)^{1-k} \quad [15]$$

$$\gamma = \frac{B_s[(h-l)\beta - h(1-k)]}{(1 + B_s h - e^{B_s l})}. \quad [16]$$

The length L_s of the column section in Eq. 13 is defined by

$$L_s = L'_s - h - n_s(h-l) \quad [17]$$

where L'_s is the actual section length and n_s is the number of void encounters.

The quantity δ represents the contribution of normal freezing action to the solute-concentrating action of the stripping section. Its value is the ratio of the concentration of the solid at the start of normal freezing to that of the liquid waste, C_w. Under certain conditions normal freezing will represent the major contribution to the concentrating action in the stripping section. In such cases, it may be desirable therefore to have a short stripping section, in which normal freezing constitutes the entire action.

The restrictions which the equations place on the attainable values of β are indicated in Table III with other pertinent information.

In the stripping section, $\beta > 1$ is desired for $k < 1$ and $\beta < 1$ is desired for $k > 1$. The value of β at $L_s = 0$ in Table III is felt to be exact, as it can be shown that β will have this same value, k/δ, for a normal freezing section only, of length h. Table III shows that a limit on β exists, except for the case $1 < k < h/l$. For this case the equations suggest that a β of zero is attainable at a total section length, L'_s, which is less than $2h$. While a tendency undoubtedly exists for this remarkable condition to be approached, the equations are not sufficiently accurate in this range of L_s for the expectation that it will be attained completely.

Illustrative Calculation—Given $h = 1$, $l = 0.9$, $k = 0.5$, $\beta = C_w/C_f = 3.5$, find L_s. From Eq. 14

$$e^{0.9B_s} = 1 + (B_s)\frac{(1)}{(0.5)}$$

$$B_s = 1.40.$$

From Eq. 15

$$\delta = (0.5)\left(\frac{0.1}{1}\right)^{0.5} = 0.158.$$

From Eq. 16

$$\gamma = \frac{(0.1)(3.5) - 1(0.5)}{(1 + 1.40 - e^{1.26})} \cdot (1.40) = 0.127.$$

From Eq. 13

$$L_r = \frac{1}{(0.434)(1.40)} \log \left[\left(\frac{(3.5)(0.158) - 0.5}{0.127} \right) + 1 \right]$$

$$= +0.26.$$

From Eq. 17

$$L'_r = L_r + h = 1.26.$$

(The section length is too short to have more than one heater. Hence n_r is zero.)

General Considerations

The significant parameters of a zone-void refiner are the zone length l, the heater length h, and the heater interval d. A general design objective is to have all of these as small as possible for the following reasons: Reducing h and d reduces the holdup (amount of material in the refiner) and the startup time (time to reach the steady state). Reducing h increases the number of stages in a column of given length. Reducing d increases the yield of product per unit of time. The value of l is dictated primarily by the separation equations and how small a value of $(h\text{-}l)$ is practical.

In this connection in scaling up a refiner to handle large volumes of material, every effort should be made to keep l as small as possible while increasing the cross-sectional area of the zones to a desired value. Values of l of the order of inches or less with areas of the order of square feet appear quite feasible.

A mechanically simple zone-void refiner could be constructed with but one heater in each section or even with one heater in all. It could produce separation equivalent to that of a multiheater refiner, but the yield per unit time would be less.

While a refiner with an enriching and a stripping section has been discussed, it will be evident that a refiner with only one section, in which the feed inlet would be close to either exit, can be constructed from these principles. The design illustrated is merely exemplary and many variations of the zone-void technique are possible, including, for example, columns of helical form.

In common with batch zone-refining, the zone-void process is particularly applicable to crystallization from the melt and to systems in which bulk solids can be readily frozen with a smooth liquid-solid interface and without entrapment of liquid. With respect to crystallization from solvents, the zone-void process has a distinct advantage in that fresh solvent can be continuously introduced and removed. For systems having a tendency to freeze out fine crystals, either process can still be used to advantage even though the situation is somewhat less ideal.

It is recognized that the assumption that k is constant, upon which the equations are based, is not applicable to all solute-solvent systems. It is felt to be reasonable for low concentrations of solute but it obviously cannot hold for wide ranges of concentration, as in binary systems of complete solubility. In such cases it may be more fruitful to use a parameter such as the separation factor α, used in distillation, defined by

$$\alpha = \frac{y(1\text{-}x)}{x(1\text{-}y)}$$

where x and y are mol fractions of a component in liquid and vapor; as such a parameter may vary less with composition than k does.

The approach to the steady state will be slower the closer k is to unity. This problem has been treated by Reiss[10] who finds that for k's of about 0.5 or more several hundred passes may be needed to sensibly approach the steady state.* This fact emphasizes the value of a continuous zone-refining method, for once the steady state is reached all material which is processed receives the maximum separation; and the time required to pass a quantity of feed through the refiner is relatively short compared to the time to attain the steady state.

* The statement in ref. 1 that ". . . at least 14 passes are required to approach the ultimate distribution [in batch zone-refining] . . ." is valid for k's of about 0.1 but is a serious understatement for k's closer to unity.

Appendix: Derivation of Steady-State Equations (after H. Reiss)

Enriching Section: Let $C(x)$, Fig. 6, be the solute distribution in the steady state. Pass a molten zone of length l and a void of length $(h\text{-}l)$ through the section from the product exit to the feed inlet. The effect of the void is to shift $C(x)$ to the left a distance $(h\text{-}l)$, as shown, raising the solute concentration at all points. The molten zone sweeps this extra solute out, returning the $C(x)$ curve to its original position. The abscissae of certain points on the shifted curve in Fig. 6, are shown in terms of their corresponding abscissae on the $C(x)$ curve.

Consider a molten zone at position x. The amount of solute in it is

$$C(x) \cdot \frac{l}{k}.$$

This amount is the difference between the amount under the shifted curve from 0 to $x + l$ and the amount under the $C(x)$ curve from 0 to x. Therefore the following may be written

$$C(x)\frac{l}{k} = \int_{h-l}^{x+h} C(x)dx - \int_{0}^{x} C(x)dx. \quad [18]$$

The solution of Eq. 18 is

$$C = A_u + A_h e^{Bx}. \quad [19]$$

If the boundary condition $C(L) = kC_f = A_u + A_h e^{BL}$ is assumed, the constants A_u, A_h, and B, can be evaluated.

Substituting Eq. 19 in 18 and equating the e^{Bx} terms, the following is obtained

$$e^{Bh} = 1 + B \cdot \frac{l}{k}. \quad [10]$$

Equating the constant terms, and utilizing the boundary condition, gives

$$A_u = \frac{kC_f}{e^{BL} + \omega} \quad [20]$$

$$A_h = \frac{\omega kC_f}{e^{BL} + \omega} \quad [21]$$

where

$$\omega = \frac{k}{(1\text{-}k)Bl}\left[1\text{-}e^{B(n-l)}\right]. \quad [11]$$

The product concentration C_p is

$$C_p = \int_{0}^{n-l} \frac{(A_u + A_h e^{Bx})dx}{(h\text{-}l)} =$$

$$A_u + \frac{A_h}{B(h\text{-}l)}\left[e^{B(n-l)} - 1\right]. \quad [22]$$

From Eqs. 20, 21, and 22, it is straightforward to show that

$$e^{B_s L_s} = \omega \left(\frac{\psi}{\alpha} - 1 \right) \qquad [23]$$

$$L_s = \frac{1}{0.434 B_s} \log \omega \left(\frac{\psi}{\alpha} - 1 \right) \qquad [9]$$

where

$$\psi = \frac{hk\text{-}l}{h\text{-}l} \qquad [12]$$

and

$$\alpha = C_p / C_f. \qquad [6]$$

Stripping Section: Let $C(x)$, Fig. 7, be the solute distribution in the steady state. The curve has two portions, a zone-refining portion and a normal-freezing portion, which are joined at $x = L_s$. The effect of forming a void at the waste exit and causing this void to travel to the feed inlet is to shift $C(x)$ to the right a distance $(h\text{-}l)$, as indicated by the dashed curve. When the molten zone begins its travel, adjacent the feed inlet, it contains molten feed of concentration C_f, as indicated by the dashed rectangle. Hence the first solid to freeze has concentration kC_f. The liquid waste of concentration C_w which is ejected at the end of the cycle corresponds to the portion of the normal-freezing distribution beyond $x = L_s + l$.

By reasoning similar to that for the enriching section, it can be shown that the integral equation for the steady state, valid up to $x = L_s$, is

$$C(x) \cdot \frac{h}{k} = hC_f + \int_0^{x-h} C(x - h + l)\, dx - \int_0^x C(x)\, dx. \qquad [24]$$

Eq. 24 transforms to

$$C(x) = \frac{k}{h} \left[hC_f + \int_l^{x-l} C(x)\, dx - \int_0^x C(x)\, dx. \right. \qquad [25]$$

The solution of Eq. 25 is

$$C = A_u + A_v e^{B_v x}. \qquad [26]$$

Substituting Eq. 26 in 25 and equating the e^{Bx} terms, the following is obtained

$$e^{B_v l} = 1 + B_v \cdot \frac{h}{k}. \qquad [14]$$

Equating the constant terms, and using Eq. 14, gives

$$kC_f = A_u + A_v. \qquad [27]$$

which is already known to be a boundary condition at $x = 0$. Another relation between A_u and A_v can be gotten from a solute balance over a cycle. Equating solute entering to solute leaving, the following is had

$$hC_f = \int_0^h C(x)\, dx + (h\text{-}l)\beta C_f \qquad [28]$$

where $\beta = C_w / C_f$. From Eqs. 27 and 28 are obtained

$$A_v = \gamma \cdot C_f \qquad [29]$$

$$A_u = (k\text{-}\gamma) C_f \qquad [30]$$

where

$$\gamma = \frac{(h\text{-}l)\,\beta - h\,(1\text{-}k)}{(1 + B_v h - e^{B_v l})} \cdot B_v. \qquad [16]$$

To obtain a relation between L_s and β, it is assumed that Eq. 26 is valid up to $x = L_s$ (see Fig. 7) and the normal freezing equation is valid from $x = L_s$ to $x = L_s + h$. Then βC_f is the concentration in the liquid at $x = L_s + l$ which is ejected as waste. Hence β can be related, through the normal freezing equation, to the concentration in the solid at $x = L_s$ by a factor δ as follows

$$C(L_s) = A_u + A_v e^{B_v L_s} \qquad [31]$$

$$C_w = \beta C_f = \frac{C(L_s)}{k} \left(1 - \frac{l}{h} \right)^{k-1}$$

$$C(L_s) = \beta \delta C_f \qquad [32]$$

where

$$\delta = k \left(\frac{h\text{-}l}{h} \right)^{1-k}. \qquad [15]$$

From Eqs. 29 through 32 are obtained

$$e^{B_v L_s} = \left[\frac{\beta\delta\text{-}k}{\gamma} + 1 \right]$$

or

$$L_s = \frac{1}{0.434\, B_v} \log \left[\frac{\beta\delta\text{-}k}{\gamma} + 1 \right]. \qquad [13]$$

Acknowledgments

The writer is pleased to express his appreciation to H. Reiss for the conception and derivation of the steady-state equations and for many stimulating discussions which have helped to provide a valuable mathematical framework for the study of this new technique. He is indebted also to E. E. Schumacher and J. H. Scaff for advice and encouragement and to L. S. Darken for valuable comments on the manuscript.

Discussion of this paper, if any, will appear in JOURNAL OF METALS, November 1955, and in AIME Metals Branch *Transactions*, Vol. **203**, 1955.

References

[1] W. G. Pfann: Principles of Zone-Melting. *Trans.* AIME (1952) **194**, p. 747; JOURNAL OF METALS (July 1952).

[2] W. G. Pfann and K. M. Olsen: Purification and Prevention of Segregation in Single Crystals of Germanium: *Physical Review* (1953) **89**, p. 322.

[3] M. Tanenbaum, A. J. Goss, and W. G. Pfann: Purification of Antimony and Tin by a New Method of Zone Refining. *Trans.* AIME (1954) **200**, p. 762; JOURNAL OF METALS (June 1954).

[4] M. Benedict: Multistage Separation Processes. *Trans.* American Institute of Chemical Engineers (1947) **43**, p. 41.

[5] Badger and McCabe: *Elements of Chemical Engineering.* (1936) 2nd Ed., chap. 9. New York. McGraw-Hill Book Co.

[6] R. H. McFee: Foreign Ion Rejection in the Growth of NaCl Crystals from the Melt. *Journal of Chemical Physics* (1947) **15**, p. 856.

[7] W. P. Slichter and E. D. Kolb: *Physical Review* (1953) **90**, p. 987.

[8] J. A. Burton, R. C. Prim, and W. P. Slichter: *Journal of Chemical Physics* (1953) **21**, pp. 1987, 1991.

[9] C. Wagner: Theoretical Analysis of Diffusion of Solutes During the Solidification of Alloys. *Trans.* AIME (1954) **200**, p. 154; JOURNAL OF METALS (February 1954).

[10] H. Reiss: Mathematical Methods for Zone-Melting Processes. *Trans.* AIME (1954) **200**, p. 1053; JOURNAL OF METALS (September 1954).

An Evaluation of Dissociated Ammonia and Hydrogen Atmospheres for Sintering Stainless Steel

by Herbert S. Kalish and Edmund N. Mazza

The effect of sintering types 302, 302B, and 430 stainless steel powder compacts in hydrogen and dissociated ammonia was investigated. It was found that sintering in dissociated ammonia resulted in as much as 0.5 wt pct increase in the nitrogen content of stainless steel even though the dissociation of the gas was complete. Sintering in hydrogen, on the other hand, reduced the nitrogen content of the stainless steel to less than 0.01 wt pct. In the case of the 302-type stainless steel, the low nitrogen content resulted in a material that was largely ferritic, whereas the high nitrogen content rendered the material fully austenitic. Sintering in dissociated ammonia resulted in lower density, generally lower tensile strength, less ductility, and higher hardness than sintering under equivalent conditions in hydrogen. The reduction of oxides on both stainless steel and iron particles was found to be effected by hydrogen partial pressure in the sintering atmosphere. Compacting pressure was found also to effect oxide reduction during sintering.

DISSOCIATED ammonia often is used as a substitute[1-3] for hydrogen in sintering and in annealing, since economic advantages sometimes can be obtained by such a substitution. In addition, anhydrous ammonia contains very little impurity. Thus, dissociated ammonia gas is very dry whereas tank hydrogen often must be freed of oxygen and water vapor prior to use in many applications.

The sintering of stainless steel powder compacts as well as bright annealing is well recognized as requiring a hydrogen atmosphere and for the foregoing reasons dissociated ammonia is frequently substituted. It has generally been overlooked, however, that the nitrogen in dissociated ammonia might have an important effect on the sintering process and on the properties of stainless steel compacts.

Considered an inert gas in many applications, nitrogen, on the other hand, is very reactive with certain metals. Dissociated ammonia could not be used for hydriding zirconium or titanium. Nitrogen reacts with columbium, tantalum, chromium, uranium, thorium, and many other active metals. Iron and iron-base alloys are, for the most part, inert in nitrogen but there are many borderline cases. It has been reported that stainless steel stabilized with columbium or titanium should not be sintered in dissociated ammonia.[3] Molybdenum has been reported as reacting with dissociated ammonia to a minor extent.[1] Although most of the reactions with iron-base alloys are attributed to the action of undissociated ammonia and the action of nascent nitrogen, Uhlig[4] showed how readily pure molecular nitrogen reacts with and diffuses into 18-8 stainless steel at 1150°C. He also pointed out how readily nitrogen diffuses out of 18-8 stainless steel when heated in pure dry hydrogen, and these thorough investigations on the subject show that commercial stainless steels are nitrogen-bearing, since they are melted in air.

The effects of nitrogen in stainless steel, particularly the 18-8 Cr-Ni type, previously have received considerable attention.[5] In 1926, it was pointed out

H. S. KALISH and E. N. MAZZA, Members AIME, are Section Head and Senior Engineer, respectively, Atomic Energy Div., Sylvania Electric Products Inc., Bayside, N. Y.

Discussion of this paper, TP 3972E, may be sent, 2 copies, to AIME by Apr. 1, 1955. Manuscript, Mar. 23, 1954. Chicago Meeting, February 1955.

that chromium alloys may contain a considerable amount of nitrogen.[6] The many observations and investigations indicated that nitrogen stabilized austenite and even could be used to replace nickel[7] in the formation of austenite. As a consequence the nitrogen also caused a change in magnetic and electrical properties and increased the yield strength.

Improvements in deep drawing properties have been reported[7] when nitrogen was added to stainless steels; and many other effects, some beneficial and some detrimental, also have been observed. The addition of nitrogen to stainless steel may improve or decrease the corrosion resistance depending upon the medium, but the subject still seems rather controversial.[6, 8]

Based on this information, different properties should be expected for stainless steel sintered or even annealed in hydrogen or dissociated ammonia. Indeed, the hydrogen treatment should remove nitrogen, whereas dissociated ammonia might impart quite different properties by the addition of nitrogen. In this investigation, the effect of nitrogen as contained in dissociated ammonia on stainless steel during the sintering process was studied. The properties of ferrous parts sintered in hydrogen and dissociated ammonia are evaluated.

Materials

The stainless steel powder of primary interest was an 18-8 type classified as 302B and obtained from Vanadium-Alloys Steel Corp. There is considerable information in the literature[9-11] about this powder. It is a high silicon content material made by atomization in water. The silicon tends to make the material form more irregularly shaped particles and this results in better compaction. The chemical analysis of the powder used is shown in Table I.

The particle shape of this powder is primarily spherical with protuberances, but about one-quarter of the particles are irregular. The as-received material is basically −100 mesh with a particle size distribution as shown in Table II. The apparent density of the powder is 2.99 g per cu cm; the pycnometer density, 7.65 g per cu cm; and the compression ratio, 2.15 to 1 at 50 tsi.

For comparative purposes 302-type stainless steel powder low in silicon content and a 430-type stainless steel were used. The chemical analysis of these powders is shown in Table I. The particle shape and size distribution is essentially the same as that for the type 302B powder shown in Table II.

The type 302 and 302B powders are somewhat magnetic due either to cold work or to a lack of nitrogen or both. The 430 stainless steel powder is, of course, completely ferritic and strongly magnetic.

The iron powder used in this investigation was Swedish sponge iron powder type MH-100 manufactured by Hoganäs Co.

Experimental Procedure

Samples were compacted in all cases without the use of lubricant. Two types of samples were compacted. One was the standard powder metallurgy tensile bar 1 in. gage length, with a rectangular cross-section of 0.250x0.200 in. in the gage length at 50 tsi. The thickness of sample varied with compacting, since a fixed weighed charge of 25 g of powder was used for each compact. These compacts after sintering were used for tensile strength and transverse rupture strength measurements.

The other type was pressed in a cylindrical double action die 0.788 in. in diameter to a nominal thickness of 0.200 in. These compacts were used for as-pressed and sintered density measurements, chemical analysis, and corrosion tests.

The samples were sintered at temperatures from 1200° to 1300°C for ½ to 1 hr in a fused silica 3 in. diam tube globar-heated furnace. Where gas mixtures were used, the mixture was made prior to the purification train, which enabled the most efficient purification of the gases. The gas passed through a Deoxo unit (palladium catalyst), Lectrodryer (activated alumina), and a dry-ice-acetone cold trap. This insured a dew point of −68°C. Since dissociated ammonia is very low in oxygen and consequently very dry, the purification train was bypassed for these runs.

The furnace tube was kept well closed at both ends during operation, flame curtains were avoided, and thorough purging of the tube was used before the charge was stoked into the furnace and after it had emerged to the cooling chamber.

Analysis for nitrogen, hydrogen, and oxygen in the powders and sintered compacts was by vacuum fusion.

Sintering Prealloyed Stainless Steel

Early in investigatory work on sintering of stainless steel, it was found essential to have a reducing atmosphere and, since a carburizing atmosphere would be prohibitive, pure hydrogen was a basic choice.[9, 10-14] The powders as-manufactured contain oxide film which must be reduced during sintering or by prior hydrogen reduction. Pickling was deemed impractical in experiments made by Vanadium-Alloys Steel Corp.[10]

The oxide films are in no way detrimental, and prior reduction is not considered practical. During sintering, an adequately dry hydrogen atmosphere is needed to maintain oxide-free parts, and such an atmosphere will readily reduce the oxides present. The dryness of the atmosphere is indeed a variable unless maintained below a specific level, and this led to the use of a cold trap.

With the methods described, it was possible to produce sintered parts which were extremely bright and appeared to be free of oxide film. In addition, it

Table I. Chemical Analysis of Several Stainless Steel Powders

Type	C	Si	Mn	S	P	Cr	Ni
302, normal silicon	0.10	0.94	0.40	0.007	0.023	17.51	7.98
302B, high silicon	0.11	2.47	0.92	0.001	0.023	18.42	8.49
430, high silicon	0.08	2.18	0.20	0.006	0.015	16.20	—

Table II. Particle Size Distribution, Apparent Density, and Compression Ratio of Type 302B Stainless Steel Powder

Mesh Fraction	Wt Pct
+100	4.7
−100 +120	10.2
−120 +140	11.5
−140 +170	12.6
−170 +200	13.7
−200 +230	3.0
−230 +270	11.3
−270 +325	9.6
−325	23.4
Total	100.0

Apparent density, 2.99 g per cu cm. Compression ratio (as-received powder): 30 tsi, 1.91 to 1; 50 tsi, 2.15 to 1; and 70 tsi, 2.26 to 1.

a—Sintered in dry hydrogen.

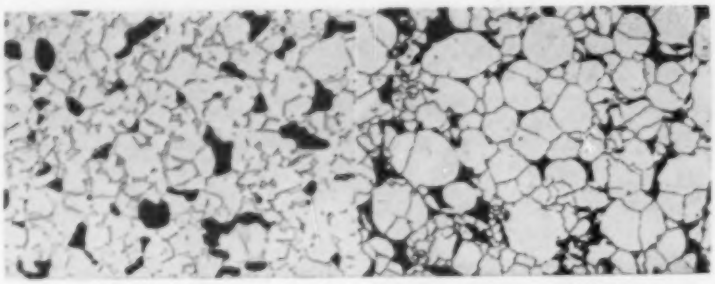

b—Sintered in dissociated ammonia.

Fig. 1—Microstructure of type 302B (high silicon) stainless steel compacts sintered ½ hr at 1210°C in dry hydrogen and dissociated ammonia. X250. Area reduced approximately 45 pct for reproduction.

is quite likely that the reduction of the oxide films during sintering increases the rate of sintering by presenting an active surface layer of metal for bonding between particles.

Effects of Sintering Atmosphere on the Properties

Preliminary experiments were made using a pure hydrogen atmosphere compared to a mixture by volume of 3 parts of hydrogen and 1 part of nitrogen. A large series of samples were sintered in each atmosphere at 1210°C for ½ hr. The results were very revealing.

The samples sintered in hydrogen had a brighter appearance and showed significantly greater shrinkage than those sintered in the synthetic dissociated ammonia atmosphere. In addition, after sintering in hydrogen the compacts were magnetic, as was the powder from which the compacts were made, but the $3H_2 + N_2$ mixture rendered the compacts nonmagnetic after sintering.

The microstructure as shown in Fig. 1 and the nitrogen analysis of Table III revealed exactly what had occurred. Sintering in hydrogen had reduced the nitrogen content appreciably, whereas about 0.3 pct of nitrogen was picked up by the stainless steel when sintering was carried out in a $3H_2 + 1N_2$ mixture. The low nitrogen content of the hydrogen sintered compact caused a large amount of ferrite to form. Fig. 1a reveals about 25 pct ferrite, as shown by the dark etched grains after utilizing the stained ferrite etchant as outlined in ASTM designation E3-39T.[7] The high nitrogen content of the compact sintered in a H-N gas mixture, on the other hand, stabilized the austenite. The microstructure of such a compact is shown in Fig. 1b. The stabilization of the austenite might, in itself, be beneficial as indicated by other investigators,[8] but the retardation of the sintering process and the actual effect of this on the properties of sintered stainless steel could be most important.

Table III. Nitrogen Analysis of Type 302B (High Silicon) Stainless Steel Compacts Pressed at 50 Tsi and Sintered ½ Hr at 1210°C in Dry Hydrogen and a Dry Gas Mixture of 3 Parts Hydrogen and 1 Part Nitrogen

Sample	Nitrogen Content, Wt Pct
As compacted	0.076
H_2 sintered	0.008
$3H_2 + N_2$ sintered	0.346

A complete series of samples was then sintered for ½ hr at 1210°C in hydrogen and in actual dissociated ammonia. The results of this investigation are shown in Table IV. In all cases the density of hydrogen-sintered samples was better than that of samples sintered in dissociated ammonia. With the coarser particle sizes, the tensile and transverse-rupture strengths were superior with hydrogen sintering, but with finer particle size, the strength of the stainless steel sintered in dissociated ammonia was greater. Ductility, as indicated by the elongation, was appreciably higher for compacts sintered in hydrogen than for those sintered in dissociated ammonia and the hardness data agree with these results.

Sintering at higher temperatures and for longer times, as shown in Table V, resulted in a considerable improvement in the properties regardless of

Table IV. Effect of Sintering Type 302B (High Silicon) Stainless Steel in Hydrogen and in Dissociated Ammonia for ½ Hr at 1210°C

Powder Fraction	Compacting Pressure, Tsi	Sintering Atmosphere	Density, G per Cu Cm		Ultimate Tensile Strength, Psi	Transverse-Rupture Strength, Psi	Elongation, Pct	Hardness, Rr
			Compacted	Sintered				
−100 mesh	30	Hydrogen	5.71	5.71	—	—	—	—
−100 mesh	50	Hydrogen	6.47	6.51	24,400	78,600	6.6	69
−100 mesh	70	Hydrogen	6.63	6.69	33,600	76,300	10.1	83
−100 mesh	30	Dissociated NH_3	5.71	5.67	—	—	—	—
−100 mesh	50	Dissociated NH_3	6.39	6.39	20,000	57,500	0.4	78
−100 mesh	70	Dissociated NH_3	6.71	6.68	27,600	70,300	0.7	89
−230 + 270	30	Hydrogen	5.57	5.63	17,800	47,300	5.8	35
−230 + 270	50	Hydrogen	6.33	6.39	30,500	76,800	10.0	71
−230 + 270	70	Hydrogen	6.60	6.66	38,900	90,800	12.6	81
−230 + 270	30	Dissociated NH_3	5.57	5.56	11,600	39,500	1.0	49
−230 + 270	50	Dissociated NH_3	6.33	6.34	25,700	63,500	1.4	80
−230 + 270	70	Dissociated NH_3	6.60	6.58	33,200	80,800	1.8	87
−325	30	Hydrogen	5.67	5.84	19,800	50,600	9.3	47
−325	50	Hydrogen	6.37	6.51	33,500	79,200	13.1	70
−325	70	Hydrogen	6.63	6.72	37,300	91,300	17.0	81
−325	30	Dissociated NH_3	5.67	5.66	15,200	33,400	1.8	64
−325	50	Dissociated NH_3	6.33	6.37	39,800	82,100	3.9	84
−325	70	Dissociated NH_3	6.63	6.63	50,400	103,500	4.8	90

Table V. Effect of Sintering Type 302B (High Silicon) Stainless Steel in Hydrogen and in Dissociated Ammonia for 1 Hr at 1275°C

Powder Fraction	Compacting Pressure, Tsi	Sintering Atmosphere	Sintered Density, G per Cu Cm	Ultimate Tensile Strength, Psi	Transverse-Rupture Strength, Psi	Elongation, Pct	Hardness, Rr
−100 mesh	70	Hydrogen	7.01	87,000	137,800	20.9	90
−100 mesh	70	Dissociated NH_3	6.96	45,500	107,500	3.9	91
−230 + 270	50	Hydrogen	6.31	24,500	83,700	5.9	67
−230 + 270	50	Hydrogen	6.70	45,650	113,750	16.3	94
−230 + 270	50	Dissociated NH_3	6.23	19,700	62,800	0.7	92
−230 + 270	50	Dissociated NH_3	6.57	32,600	98,200	4.3	91
−325	30	Hydrogen	6.70	19,400	85,800	7.4	70
−325	50	Hydrogen	6.89	42,900	115,800	13.9	91
−325	70	Hydrogen	7.06	56,400	141,300	22.7	96
−325	30	Dissociated NH_3	6.43	14,600	68,800	3.0	70
−325	50	Dissociated NH_3	6.70	32,600	110,000	9.0	85
−325	70	Dissociated NH_3	6.96	62,800	140,000	11.5	93

condition, but identical trends prevailed. Sintering in dissociated ammonia resulted in poor density, poor ductility, and, except for the −325 mesh powder, in decreased tensile strength. Improved tensile strength is to be expected as ductility decreases and hardness increases, but only where sufficient densification occurs does this effect result in a strength higher than is obtained after sintering in hydrogen.

The vacuum-fusion gas analysis for stainless steel sintered in actual dissociated ammonia is shown in Table VI in comparison to samples sintered in hydrogen. Oxide reducton is retarded by sintering in dissociated ammonia and very significant amounts of nitrogen are picked up. A comparison of this data with Table III, where a synthetic mixture of dry hydrogen and nitrogen was used, clearly indicates that nitrogen pickup is not a function of undissociated ammonia. The nitrogen content for samples sintered ½ hr at 1210°C is almost identical in both cases, viz., 0.348 in the synthetic H-N mixture and 0.388 in dissociated ammonia. To verify that the presence of hydrogen was unnecessary and that the stainless steel can absorb nitrogen in large amounts from molecular nitrogen, 302B stainless steel compacts were sintered in pure dry nitrogen. These results are shown in Table VI for the purpose of comparison with the hydrogen and dissociated ammonia data. The results show clearly the large amount of nitrogen which was picked up—almost identical to that found after sintering in dissociated ammonia. No oxide reduction took place in the nitrogen atmosphere, however, and this resulted in a compact which had no bond between particles, and hence the sintered compact was essentially in the as-pressed condition. The only change in the compact which had been effected by sintering in nitrogen was the large increase in nitrogen content and a conversion of the powder from a mixed ferrite and austenite to a fully austenitic structure.

Since the nitrogen which is absorbed from dissociated ammonia manifests itself in stabilizing the austenite in the type 302B stainless steel, it must be primarily in solid solution although the precipitation of nitrides (CrN and Cr_2N) is also probable. In addition, the nitrogen seems to prevent grain boundary movement and retards the sintering process. This prevention of grain boundary movement verifies earlier work in which it has been reported that nitrogen is a grain refiner in wrought stainless steel.[4] Table VI reveals that the nitrogen content is a maximum for samples sintered at 1200°C in dissociated ammonia with decreasing content for higher temperatures. Apparently the limit of nitrogen solubility is obtained in these compacts during sintering, and this is about a maximum at sintering temperatures.

Table VI. Vacuum-Fusion Gas Analysis for Type 302B (High Silicon) Stainless Steel Compacts Pressed at 50 Tsi and Sintered as Indicated in Dry Hydrogen or Dissociated Ammonia

Sintering			Gas Content, Wt Pct		
Temperature, °C	Time, Hr	Atmosphere	Hydrogen	Oxygen	Nitrogen
Green Compact			0.0008	0.088	0.005
1200	½	Dry hydrogen	0.0008	0.017	0.007
1200	½	Dissociated ammonia	0.0005	0.036	0.474
1200	½	Dry nitrogen	0.0023	0.083	0.530
1210	½	Dry hydrogen	0.0017	0.007	0.008
1210	½	Dissociated ammonia	0.0003	0.034	0.388
1300	1	Dissociated ammonia	0.0001	0.016	0.309

The fact that the nitrogen content, and hence solubility, decreases markedly from 1200°C as temperature is increased, is verified by the nitrogen analysis data shown in Tables III and IV, both of which represent additional independent data used to investigate the nitrogen absorption effect.

The hydrogen content seems to be unchanged by sintering, differences noted probably being insignificant. The differences in oxygen content are, however, quite significant and show that less oxide reduction is obtained in the dissociated ammonia atmosphere than in the pure hydrogen atmosphere. This oxide reduction effect is either a function of the nitrogen being absorbed in the stainless steel or the reduced partial pressure of the hydrogen in the gas mixture.

In addition to interest in determining the source of the decreased oxide reduction, it is important to determine if reduced hydrogen partial pressure caused by the nitrogen dilution has any effect on the sintering of the stainless steel and also to determine the

Table VII. Vacuum-Fusion Gas Analysis and Hardness for Iron Compacts Sintered in Hydrogen, 75 Vol Pct H-25 Pct N, and 75 Vol Pct H-25 Pct Argon Gas Mixtures for ½ Hr at 1200°C. All Gases Were Dried to a Dew Point of −68°C

Sintering Atmosphere	Compacting Pressure, Tsi	Gas Content, Wt Pct			Hardness, Rr
		Hydrogen	Oxygen	Nitrogen	
Hydrogen	30	0.0015	0.082	0.003	39
Hydrogen	70	0.0013	0.139	0.004	71
3 hydrogen + argon	30	0.0008	0.106	0.002	28
3 hydrogen + argon	70	0.0013	0.188	0.003	73
3 hydrogen + nitrogen	30	0.0006	0.104	0.010	48
3 hydrogen + nitrogen	70	0.0024	0.188	0.004	77

Table VIII. Properties of Sintered Type 302 and 302B Stainless Steel and Cast Type 302 as Affected by Nitrogen Content. Sintered Material Made from —325 Mesh Powder Compacted at 70 Tsi and Sintered at 1275°C

	302 Cast, Uhlig[4]		302 Sintered for 1 Hr		302 Sintered for 4 Hr	302B Sintered for 1 Hr		302B Sintered for 4 Hr
	In Hydrogen (1)	In Nitrogen (2)	In Hydrogen (3)	In Dissociated Ammonia (4)	In Dissociated Ammonia (5)	In Hydrogen (6)	In Dissociated Ammonia (7)	In Dissociated Ammonia (8)
Structure	Partially Ferritic	Austenitic	Partially Ferritic	Austenitic	Austenitic	Partially Ferritic	Austenitic	Austenitic
Nitrogen analysis, pct	0.001	0.24	—	0.427	0.413	—	0.321	0.333
Density, g per cu cm	7.78	7.90	6.93	6.59	6.83	7.33	6.63	6.70
Ultimate tensile strength, psi	117,000	104,500	62,000	54,400	68,467	93,387	69,400	73,533
Elongation, pct*	65	59	15	6	11	37	13	14
BHN	240	148	100	117	138	188	123	139

* Cast: 2 in. gage length. Sintered: 1 in. gage length.

effects of nitrogen on other ferrous alloys. For this purpose an abbreviated investigation using iron compacts was undertaken, the results of which showed quite clearly that sintering of iron is not retarded by the use of a N-H or hydrogen-argon mixture. However, the samples sintered in a nitrogen-bearing atmosphere were, as indicated in Table VII, somewhat higher in hardness.

Vacuum-fusion gas analysis as shown in Table VII revealed some extremely interesting effects. The oxygen content of iron samples sintered in a pure hydrogen atmosphere is lower than samples sintered in a 75 vol pct H mixture containing either nitrogen or argon. In addition, the oxygen content is considerably lower in samples compacted at 30 than at 70 tsi. In the denser compacts, i.e., those compacted at higher pressure, less contact of the hydrogen can occur with the oxide surfaces and effect reduction. Furthermore, as the pores become closed by sintering, water vapor formed by the reduction of the oxides cannot escape and this would tend to retard reduction.

Of most importance, however, is the effect of reduced partial pressure of hydrogen on the reduction of the oxides in the iron powder. This is an important result indicating that sintering atmospheres can have some very subtle effects on the ultimate product. Of course, the implications of greater oxide reduction with lower compacting pressure cannot be ignored, which may help to explain the relatively larger amount of densification which often occurs with compacts pressed at lower pressures. In these iron compacts, however, virtually no densification occurred during sintering. Even so, the effects are of considerable significance.

The effect of nitrogen, however, is not nearly as obvious from the analysis. The nitrogen content of 0.010 encountered in the 30 tsi compact sintered in the H-N mixture is the highest of any of the iron samples. This seems to indicate that some increase in nitrogen content can occur in sintering in a dissociated ammonia atmosphere even where the degree of dissociation is complete. The nitrogen increase accounts nicely for the slightly higher hardness of these compacts and is, indeed, the only plausible explanation.

Table IX. Vacuum-Fusion Gas Analysis of Various Basic Types of Stainless Steel Sintered in a Mixture of 3 Parts of Hydrogen and 1 Part of Nitrogen by Volume. Sintered for ½ Hr at 1200°C in Gas Dried to a Dew Point of —68°C

Stainless Steel Type	Gas Content Wt Pct		
	Hydrogen	Oxygen	Nitrogen
302 (normal silicon)	0.003	0.072	0.567
302B (high silicon)	0.002	0.047	0.513
430 (high silicon)	0.002	0.061	0.347

The effect of sintering in a mixed atmosphere containing a true inert gas and the effects of different compacting pressures on the oxide reduction was so pronounced in iron that it was important to see how these effects manifested themselves in type 302B stainless steel. A series of samples was compacted at 30 and 70 tsi and sintered ½ hr at 1200°C in hydrogen and in mixed atmospheres. The effects were very similar to those found in iron. Oxide reduction was far less in stainless steel compacts sintered in the atmospheres containing 1 part argon, helium, or nitrogen to 3 parts of hydrogen than in a pure hydrogen atmosphere. Thus, reduced partial pressure of hydrogen appreciably lowers the reducing potential of the gas. The effect of compacting pressure on the oxygen content after sintering was even more pronounced for the 302B stainless steel than for iron and the effcts were greatest where the most densification during sintering occurred. Thus, as the compact becomes less porous during sintering, oxide reduction is impeded just as it is by less initial porosity because of higher compacting pressure.

Although these oxide reduction effects could be very significant in some metals, they seemed to have no effect on the properties of 302B stainless steel. Compacts sintered in hydrogen diluted with argon or helium showed the same shrinkage, same sintered density, and identical hardness as compacts sintered in a pure hydrogen atmosphere. Nitrogen dilution has a very significant effect on the properties, as indicated previously. Thus, the effects of nitrogen in dissociated ammonia can be isolated. Dilution of the hydrogen gas is responsible for less oxide reduction but the nitrogen diffusing into the stainless steel is responsible for all the property changes, i.e., the nitrogen causes the densification to be retarded, results in lower ductility, higher hardness, and generally lower tensile strength in the sintered compacts.

To gain a better understanding of the effect of increased porosity due to the presence of nitrogen during sintering as opposed to the intrinsic property effects caused by the nitrogen in the stainless steel, a comparison was made with Uhlig's[4] data, as shown in Table VIII.

First, it must be realized that more nitrogen is

dissolved during sintering than during melting because of the large surface area of the metal exposed to the gas. In addition, sintering temperatures coincide with the upper portion of the γ loop and the nitrogen solubility in austenite is much greater than in ferrite. On this basis, then, in comparing the data of this investigation with Uhlig's, the lower nitrogen content of the latter must be kept in mind.

Also of importance is the fact that no attempt was made to obtain the densest possible sintered material for this investigation so the densities are considerably lower than that obtained in the cast material. The true density of austenite is considerably greater than ferrite, indicating that the austenitic sintered product has even more porosity than indicated simply by the difference in density.

The key to the comparison, however, lies in the hardness and tensile strength. Uhlig shows lower hardness and tensile strength for the fully austenitic nitrogen-bearing stainless steel than for the nitrogen-free partially ferritic stainless steel, whereas this investigation shows higher hardness and higher tensile strength (where densities are anywhere near the same) for the former. Sintering in the presence of nitrogen so retards the sintering process that much greater porosity results. Even so, in the case of 302, the hardness was higher for the fully austenitic product. When a longer sintering time is used, the hardness and the tensile strength becomes considerably higher than the hydrogen sintered compact, even though there is still considerable porosity.

Assuming the validity of Uhlig's data, it seems logical to conclude, then, that the higher tensile strength and hardness observed for the sintered austenitic stainless steel over the sintered ferritic stainless steel is due to the excess amount of nitrogen dissolved at the sintering temperature. Upon cooling, this must precipitate out as nitrides (CrN or Cr_2N), making the austenitic product harder. These precipitates, if present, are too small to resolve metallographically and X-ray diffraction studies were considered beyond the scope of this investigation.

It is interesting to note the dramatic effect of silicon for obtaining optimum sintered properties in this material, as shown in Table VIII for the 302B stainless steel. This data is for some of the newest

Fig. 2—Corrosion of sintered stainless steel disks after 10 days in distilled boiling water. Sample 371 compacted at 70 tsi and sintered in dissociated ammonia. Samples 332 and 372 compacted at 30 and 70 tsi, respectively, sintered in hydrogen.

Table X. Effect of Sintering Atmosphere on the Corrosion Resistance of Type 302B Stainless Steel Compacts in Distilled 100°C Water. Compacts Pressed and Sintered as Indicated

Compacting Pressure, Tsi	Sintering Atmosphere	Sintered Density, G per Cu Cm	Corrosion Rate in Weight Gain Mgm per Sq Cm at the Following Times			
			48 Hr	141 Hr	188 Hr	235 Hr
30	Hydrogen	5.84	0.062	0.073	0.105	0.115
70	Hydrogen	6.78	—	0.056	0.088	0.120
70	Dissociated ammonia	6.63	0.217	0.401	1.075	0.467

powder available of this type and indicates that very good density, tensile strength, and elongation can be attained if hydrogen sintering is used. Where nitrogen is present in the sintering atmosphere, however, there is very little benefit from the silicon. Although the silicon was added to the powder to obtain more irregular-shaped particles and aid in compacting, it has a far greater effect during sintering. Due to the immense difference in densities shown between columns 6 and 8, Table VIII, there remains a superiority of tensile strength and a higher hardness for the hydrogen sintered product. Considerable other data show clearly, however, that if the density of the nitrogen-bearing product had reached anywhere near the levels of the nitrogen-free compact, higher hardness and tensile strength would result because of the precipitation hardening phenomena postulated previously.

The results of this investigation, then, are consistent with the findings of Uhlig[4] and others.[5-7] Two new effects are described here. One is the factual retardation of the densification of stainless steel powder metallurgy compacts sintered in the presence of nitrogen which considerably affects the gross properties of the material. The second is the postulated precipitation of nitrides from the compacts sintered in the presence of nitrogen which accounts for the hardening effects observed intrinsically in the stainless steel.

The reaction of molecular nitrogen with stainless steel during sintering and its manifestation on the properties of sintered compacts is, from the foregoing data, quite well established. The composition effects are of considerable importance and an effort was made to determine some of the factors involved. It was shown that very little nitrogen is picked up by iron compacts during sintering in dissociated ammonia. To ascertain the effects of silicon and nickel, compacts made from three basic types of stainless steel were sintered in a $3H_2 + N_2$ atmosphere. The vacuum-fusion gas analysis for these compacts after sintering is shown in Table IX. Clearly nitrogen pickup is not a function of silicon content, since both the high and normal silicon-content 302 stainless steels show equivalent nitrogen analysis after sintering.

Nitrogen content seems to be very much influenced by nickel content, since, as shown in Table IX, a far lower nitrogen content is obtained in the type 430 stainless steel which is nickel-free. The nitrogen absorption apparently is influenced by the solubility of nitrogen in austenite.

It is the influence of the nickel content on the quantity of austenite present at the sintering temperature which determines the extent of the nitrogen solubility. Ferritic stainless steels of the 430 type are, however, as shown, definitely susceptible to nitrogen

pickup during sintering in dissociated ammonia because of the presence of austenite, and dependent upon the amount of austenite present, at the sintering temperature.

Pure nickel, Fe-Ni alloys, and the like were not investigated, but it is expected that these would be far less prone to nitrogen pickup than the chromium-bearing stainless steels. Basically, then chromium seems to be the necessary element in this nitrogen reaction phenomenon, but nickel increases the effects markedly.

It has been reported[7] that the nitriding of stainless steels results in a loss of corrosion resistance. Cursory corrosion tests on sintered compacts were conducted in boiling water in a reflex condensor. The data as shown in Table X indicate that the stainless steel sintered in dissociated ammonia corrodes at a significantly greater rate than that sintered in hydrogen, even if the density of the hydrogen sintered sample is considerably lower. After only 188 hr in boiling water, the material sintered in dissociated ammonia has reached the point of rapid deterioration. These corrosion tested samples are shown in Fig. 2.

Conclusions

1—Chromium and Cr-Ni stainless steels pick up nitrogen from dissociated ammonia sintering atmospheres even though dissociation is complete.

2—Molecular nitrogen reacts with both chromium and Cr-Ni stainless steels, at sintering temperatures.

3—Nitrogen in the sintering atmospheres as a major constituent results in retarding of the sintering process for both chromium and Cr-Ni stainless steels.

4—Nitrogen pickup in 18-8 stainless steel during sintering has the following effects on the gross properties of the sintered compact: 1—decreased density, 2—decreased ductility, 3—decreased water corrosion resistance, 4—increased hardness (although the trend may be reversed by very low densities often obtained in sintering in the presence of nitrogen), and 5—generally decreased tensile strength (unless high densities are obtained, in which case the trend is reversed).

5—Nitrogen pickup in 18-8 stainless steel during sintering has the following effects on the intrinsic properties of sintered stainless steel: 1—decreased water corrosion resistance, 2—increased hardness, and 3—increased tensile strength.

6—The properties of stainless steel sintered in the presence of nitrogen are influenced by the following factors: 1—retardation of the sintering process, i.e., densification is slowed down, 2—stabilization of the austenite by nitrogen, and 3—precipitation of nitrides (CrN or Cr_2N) resulting in precipitation hardening.

7—The presence of a diluent of a semi-inert gas such as nitrogen or a completely inert gas such as argon in the hydrogen sintering atmosphere decreases the reduction of the oxides present on stainless steel and iron particles. The reduced partial pressure of hydrogen, as such, does not, however, seem to effect the densification or the properties of the sintered compact.

8—The pressed density of a compact has an important bearing on the amount of oxide reduction which can take place during sintering. The denser the compact for a given particle size, i.e., the higher the compacting pressure used, the less the oxide reduction which will occur during sintering in a reducing atmosphere. These effects were studied in iron and stainless steel compacts only, but probably occur in other metal powders compacts having oxidized surfaces. Similar effects are to be expected as a function of particle size although this would be complicated by the greater amount of surface oxide present in finer particles and the lower pressed density for the finer particle compacts. These factors would tend to operate in opposite directions.

Nitrogen plays an important role in sintering atmospheres and cannot be considered inert to stainless steel. These results may have an important bearing on the effect of bright annealing stainless steel parts in dissociated ammonia and, in accordance with the earlier work of Uhlig and others, bear further surveillance.

Acknowledgments

The authors wish to take this opportunity to thank C. C. Gregg for vacuum-fusion gas analyses and G. E. Taborsky for experimental work in the early phases of this investigation. We are also indebted to R. F. Doran for initially suggesting that this matter be investigated, and to L. W. Kates for several valuable suggestions in the interpretation of the data.

Discussion of this paper, if any, will appear in JOURNAL OF METALS, November 1955, and in AIME Metals Branch *Transactions*, Vol. **203**, 1955.

References

[1] H. M. Webber and A. G. Hotchkiss: *Furnace Atmospheres for Sintering.* Spring Meeting, Powder Metallurgy Assoc. (June 13, 1946).

[2] A. G. Hotchkiss and H. M. Webber: *Protective Atmospheres.* (1953) New York. John Wiley & Sons Inc.

[3] C. V. Small: Effective Use of Dissociated Ammonia. *Metals and Alloys* (1945) **22**, p. 727.

[4] H. H. Uhlig: The Role of Nitrogen in 18-8 Stainless Steel. *Trans.* ASM (1942) **30**, p. 947.

[5] R. Scherer, G. Riedrick, H. H. Kessner, and C. M. Cosman: Nitrogen in chrome-nickel Steels. *Iron Age* (1945) **155**, No. 13, p. 56.

[6] F. Adcock: *Journal* Iron & Steel Institute (1926) **114**, p. 117.

[7] R. Scherer: *Chem. Fabrik* (1940) **13**, p. 373.

[8] *Metals Handbook.* (1948) Cleveland. ASM.

[9] A. H. Grobe and G. A. Roberts: Mechanical Properties of Stainless Steel Powder. *Trans.* AIME (1951) **191**, p. 125; JOURNAL OF METALS (February 1951).

[10] A. H. Grobe and R. Hoffman: Stainless Steel Powder for Mechanical Parts. *Production Engineering* (1951) **22**, No. 12, pp. 168-172.

[11] A. H. Grobe and G. A. Roberts: Technology of Prealloyed Stainless Steel Powders—Properties, Production, Uses. *Bulletin No. 3* Vanadium-Alloys Steel Corp. (1952).

[12] J. D. Dale: Stainless Steel Powder. *Proceedings* Metal Powder Assoc. (1947) **III**, p. 4.

[13] G. Stern: A New Type of Stainless Steel Powder. *Proceedings* Metal Powder Assoc. (1950) **IV**, p. 49.

[14] P. Duwez and H. E. Martens: *Preparation and Physical Properties of Porous Iron.* (Aug. 29, 1947) Pasadena. Jet Propulsion Laboratory.

[15] A. H. Grobe: Mechanical Properties of Spherical and Irregular 18-8 Stainless Steel Powder as Manufactured and After Pickling. *Metallurgical Dept. Report* Vanadium-Alloys Steel Corp. (Mar. 14, 1947).

[16] A. H. Grobe: Spherical and Irregular Stainless Steel Powder, Type 430. *Metallurgical Dept. Report* Vanadium-Alloys Steel Corp. (Jan. 10, 1951).

[17] Tentative Methods of Preparation of Metallographic Specimens. *ASTM Designation E3-39T* Amer. Soc. for Testing Materials (1939) Etching Reagent No. 15, Table V, Group II, p. 17.

Relation of Strength, Composition, and Grain Size of Sintered WC-Co Alloys

by J. Gurland and P. Bardzil

An experimental study of the variation of transverse-rupture strength with composition and grain size has shown that the strength reaches a maximum for values of the mean free path between carbide particles of 0.3 to 0.6 microns. The fracture originates in and proceeds through the carbide grains mainly. Impact strength and hardness also were recorded.

MOST of the physical properties of sintered carbides vary linearly with composition. The transverse-rupture strength, however, shows a unique behavior. As the amount of binder metal is varied from 6 to 25 pct by weight, the strength at first increases; then, between 15 and 20 pct Co, it reaches a maximum of nearly 400,000 psi, and finally decreases with further additions of binder metal. This behavior of the transverse-rupture strength has been reported, among others, by Engle[1] and Sandford and Trent.[2] The significance of these observations has not been discussed in the literature. That it may be of more than specific importance is indicated by the very similar variation of strength with composition encountered in other systems sintered in the presence of a liquid phase, such as TiC-Ni[3] and Fe-Cu.[4]

Experimental Details

All compacts were prepared and sintered according to normal industrial practice. The average diameter of WC grains and the mean free path between grains were measured on metallographically prepared samples by a method of linear and planar analysis[5] using the relations

$$d = \frac{4}{\pi} \frac{N_L}{N_A} \qquad [1]$$

$$P = \frac{1-f}{N_L} \qquad [2]$$

where d is the average diameter of dispersed grains; N_L is the number of noncontiguous grains intersected on a metallographic plane by a line of unit length; N_A is the number of noncontiguous grains per unit area; P is the mean free path between grains of dispersed phase; and f is the volume fraction of dispersed phase.

Approximately 1000 grains were counted on each sample. For each composition d^3 was plotted against P, the resulting straight lines serving as a check on the measurements. The distribution curves of the WC powders of different average diameters were homologous, and no attempt was made to influence the grain size by blending powders, adjusting the sintering conditions, or otherwise altering the particle size distribution.

J. GURLAND, Junior Member AIME, and P. BARDZIL are associated with Firth Sterling Inc., Pittsburgh.

Discussion of this paper, TP 3943E, may be sent, 2 copies, to AIME by Apr. 1, 1955. Manuscript, Aug. 6, 1954. Chicago Meeting, February 1955.

Densities were measured by differential weighings in air and water. The degree of densification did not vary consistently with either composition or grain size. The density is influenced by slight amounts of impurities, specifically by 0.1 to 0.2 pct Fe which enters the powders during ball milling. As an illustration of the experimental variations, a number of measured densities are listed in Table I. They are expressed in percentage of theoretical density, as calculated from the published X-ray densities of WC and Co.[6]

For the purpose of determining the transverse-rupture strength, rectangular test specimens (3/16x 3/8x3/4 in.) were broken by loading at the center of a 9/16 in. span. The average strength of five or more samples is reported for each composition and grain size. The compacts were ground on two parallel surfaces only. The load was applied at an average rate of 6,800 psi per sec. Since the elongation after fracture of the alloys is very small, it was assumed that the compacts deform elastically to failure and the fracture stress was calculated by the conventional beam formula. The data for one alloy are presented in Table II as an example of the results and scattering ranges encountered. The precision of the test, as measured by the average difference between duplicates, is of the order of 15,000 psi. The results are strictly comparable only to compacts prepared and tested in the manner described and of similar chemical composition and grain size characteristics.

Unnotched Charpy specimens were used for impact testing. Each point represents the average of 3 to 20 samples, the larger number being used in an attempt to determine the influence of grain size. Considerable scatter was encountered, the range from lowest to highest value often amounting to 30 pct of the impact strength. The hardness is reported as a RA reading, using a 60 kg load with diamond brale indenter. Compositions are given in weight percent.

Table I. Measured Densities of Sintered WC-Co Alloys

6 Pct Co		16 Pct Co		25 Pct Co	
WC Grain Size, Microns	Density, Pct	WC Grain Size, Microns	Density, Pct	WC Grain Size, Microns	Density, Pct
1.7	97.8	1.8	99.6	1.9	99.5
3.9	99.1	2.6	99.3	2.2	99.7
4.4	99.4	2.8	99.4	2.4	99.5
4.6	99.3	3.7	99.5	3.0	99.5
4.9	98.8	5.1	99.4	3.3	99.4
5.1	99.1	15.9	96.8	4.6	99.3
5.4	99.7	—	—	17.4	99.6

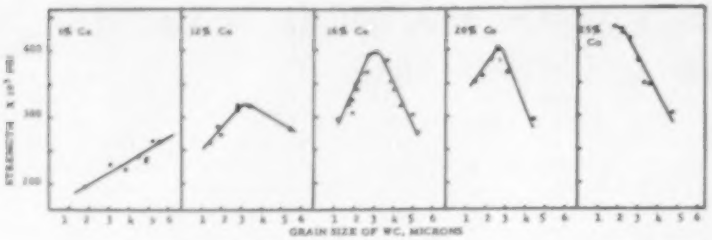

Fig. 1—Variation of transverse-rupture strength with grain size of WC.

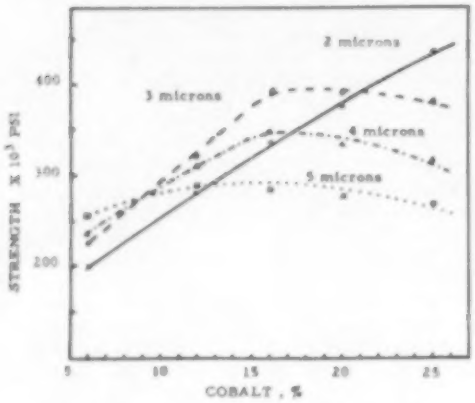

Fig. 2—Variation of transverse-rupture strength with composition.

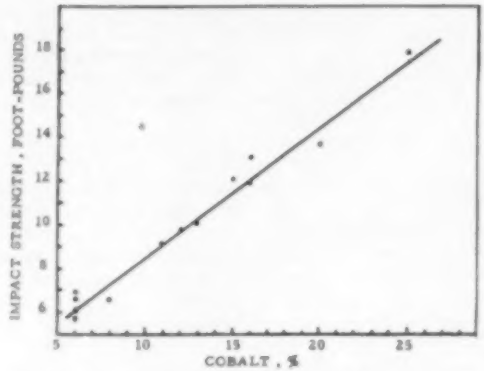

Fig. 4—Impact strength of WC-Co alloys of compacts having a WC grain size from 1.4 to 3.1 microns.

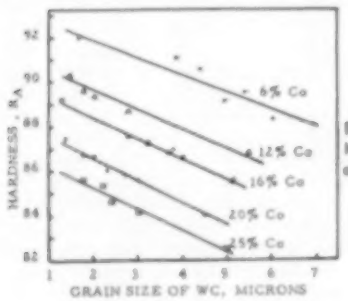

Fig. 3 — Rockwell hardness of WC-Co alloys.

Experimental Results

Physical Properties: Strength and hardness vary with composition and grain size as shown in Figs. 1 to 4. The transverse-rupture strength goes through a maximum with grain size at constant composition, Fig. 1, and with composition for a given grain size, Fig. 2. As the level of the maximum strength is raised by higher binder contents, it is also shifted towards a smaller grain size. The hardness is reduced by increased amounts of binder and by larger grain sizes of WC, Fig. 3.

Composition has a decided influence on the impact strength; the higher the percentage of cobalt, the greater is the resistance to impact. The data of Fig. 4 apply to compacts having a WC grain size from 1.4 to 3.1 microns. The effect of grain size in this range was obscured by the dispersion of the experimental data and therefore could not be ascertained.

Since the structure of these alloys is usually thought to consist of carbide grains more or less surrounded by the binder phase, it may be assumed that the thickness of the layers of cobalt metal between the dispersed particles of the hard phase is an important variable. A plot of the transverse-rupture strength vs the mean free path through the binder phase is presented in Fig. 5. Although the highest strengths of each composition do not occur at exactly the same interparticle distance, they do fall within a narrow range (0.3 to 0.6 microns) of the mean free path. The variation of hardness with the mean free path is shown in Fig. 6 on semi-logarithmic coordinates. Within a rather broad scatter band, the hardness decreases linearly with the logarithm of the mean free path between WC particles. In general, the points from samples of high binder content are at the lower edge of the band and those from low cobalt samples are at the upper edge, so that the width of the band is determined by the compositions.

Fracture Path: On a microscopic scale, a fracture may run through the WC grains, the carbide to carbide grain boundaries, the carbide-binder interface, and the binder phase. By examining the fracture path after breaking the samples by transverse rupture, it was found that the fracture occurs preferentially within the carbide grains and at the carbide to carbide grain boundaries. Table III summarizes the results of such an examination, during which the path of the fracture at or near approximately 2000 grains was analyzed. The alloys were selected to be on either side of the strength maximum. Two types of fractures were measured: well developed continuous fractures and noncontinuous cracks. The latter were presumably located in areas where the stress was insufficient to produce a complete fracture. The two types are shown in Figs. 7 and 8. A separate analysis of the two types would reveal, it was hoped, the relative resistance to fracture of the constituents.

Table III shows that the fracture tends to avoid the cobalt and seems to originate in the carbide phase. The principal difference between alloys of high and low binder contents is found in the relative proportion of failures at the carbide to carbide grain

boundaries. These are much more numerous in low binder alloys. The volume fractions of binder metal in the two alloys of Table III are respectively 10 and 37 pct.

The microstructure of compacts broken by impact reveals a great number of cracks in the WC grains as shown in Fig. 9. These cracks were undoubtedly produced by the shattering blow of the impact test.

A number of samples were subjected to transverse bending in the fixture shown in Fig. 10. This permitted microscopic observation of the bottom surface while the load was applied. Low binder alloys (6 pct Co) broke without any evidence of preliminary cracking. On high binder alloys (20 pct Co), the following sequence was observed: 1—The polishing and grinding marks became accentuated as stress was first applied. 2—Small cracks appeared in isolated grains as shown in Fig. 11. 3—On continued loading, more of the carbide grains showed these cracks; a number of such grains usually being aligned parallel to a polishing direction. The binder metal shows evidence of being disturbed in the vicinity of the damaged carbide grains as shown in Fig. 12. Under certain conditions, the micro cracks can be introduced in the structure by severe grinding and polishing; however, sufficient care was taken so that the samples were free of such effects before stressing. 4—At times, long shallow grooves were formed as shown in Fig. 13, and these followed the fractured grains discussed previously. 5—Eventually the sample fractured in a direction perpendicular to the applied stress and parallel to the majority of the micro cracks and grooves.

Table II. Transverse-Rupture Strength of an Alloy of 84 Pct WC-16 Pct Co

WC Grain Size, Microns	No. of Samples Tested	Transverse-Rupture Strength (10^3 Psi)		
		Average	Range	
			High	Low
1.8	8	319	341	289
2.6	7	368	404	341
2.8	6	386	434	375
3.7	5	389	404	380
5.1	6	303	330	280
15.9	8	185	194	179

This evidence shows that the carbide grains are damaged during the grinding and polishing operations and that micro cracks are formed on the application of stress. The damaged grains eventually fracture and cause the failure of the compact.

Discussion of Results

The experimental data indicate that the strength of WC-Co alloys is a function of the amount of binder phase and of the thickness of the binder film. The strength is limited by the susceptibility to frac-

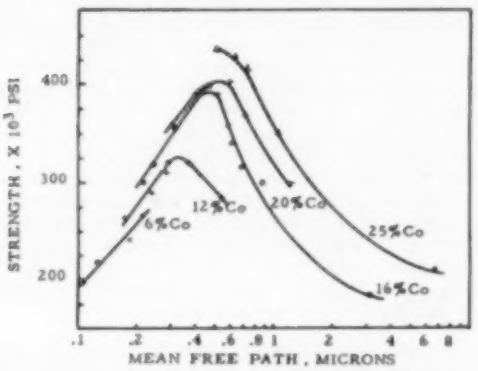

Fig. 5—Plot of the transverse-rupture strength as a function of mean free path.

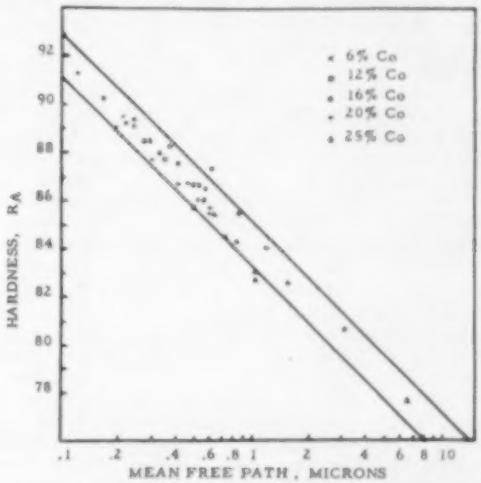

Fig. 6—Rockwell hardness as a function of the mean free path.

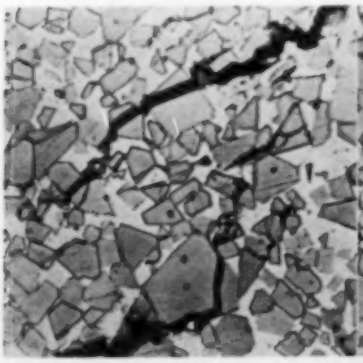

Fig. 7—Fractures in sintered WC-Co alloy; 80 pct WC, 20 pct Co. X1500. Area reduced approximately 30 pct for reproduction.

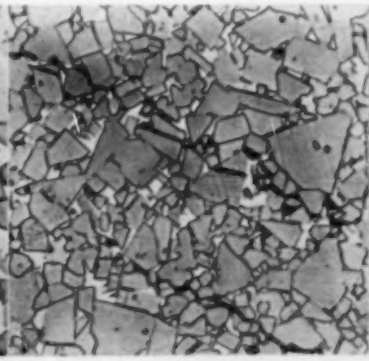

Fig. 8—Cracks in sintered WC-Co alloy; 94 pct WC, 6 pct Co. X1500. Area reduced approximately 30 pct for reproduction.

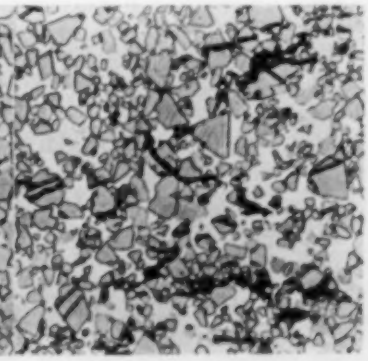

Fig. 9—Cracks in WC grains caused by impact loading; 75 pct WC, 25 pct Co. X1500. Area reduced approximately 30 pct for reproduction.

Fig. 10 — Transverse bending fixture. Sample is in position above the lens of microscope; load is applied through steel ball.

ture of the carbide grains. A number of the factors, determining the interaction between carbide and binder, are considered subsequently.

In common with the more familiar dispersion-hardened metals, the strength of sintered WC-Co alloys is based on the effect of a hard constituent embedded in a softer matrix. A general survey of the properties of a number of such alloys by Unckel[9] resulted in the conclusion that there is an exponential relation between the hardness or tensile strength and the spacing of the hard particles. Reference should also be made to the more detailed work on yield strength and mean free path of steels[7] and Al-Cu alloys[8] and to the correlation of fracture stress and pearlite spacing of carbon steels.[6] The strength of these metals increases as the interparticle distance is reduced.

In the case of sintered carbides, the hard constituent forms the major part of the volume. The state of stress of the binder, during deformation, is probably very similar to that found generally in thin films attached to another material of very different modulus of elasticity. It has been reported that the rupture strength of such films is inversely proportional to their thickness.[10-12] Orowan[13] has suggested that the thin films are under "plastic constraint" and it is believed that this condition causes the strengthening and embrittling effects observed, for instance, in brazing and adhesive materials. Similarly, triaxial stresses are introduced into the binder of sintered carbides by the mechanical restraint exerted by the carbide particles upon the thin films of cobalt.

But even in the absence of deformation, lattice strains of considerable magnitude have been found in the binder[14] as well as in the carbide.[15] These have been attributed to residual stresses arising from the unequal coefficients of thermal expansion of the constituents. It has been suggested previously[16] that complex micro stresses from both sources are responsible for the high strength and lack of ductility of WC-Co alloys.

From such considerations, it would be expected that the resistance to deformation of the binder increases as the mean free path between carbide particles is decreased. In the range of composition under study, failure of the metal is initiated, not by rupture of the binder, but through the propagation of cracks which originated within the tungsten carbide grains. Even at much lower concentrations of carbide inclusions in steel[17] and in molybdenum,[18] micro cracks within carbide grains have been observed to precede fracture.

The variation of the transverse-rupture strength with composition can be regarded as the result of two competing factors as the percentage of cobalt is lowered: 1—the more severe *plastic constraint* on the binder results, at first, in an increase of strength and loss of ductility; but 2—the strength of the composite alloy eventually falls off because the relative amount of binder decreases and that of the more brittle carbide increases.

To account for the decrease of strength of low cobalt alloys with smaller tungsten carbide grain size at constant composition, it is necessary to consider the observed increase of fracture incidence at the carbide to carbide grain boundaries. With smaller carbide grains, as well as with less binder, there is an increasing area of carbide to carbide contact, i.e., an incomplete surrounding of carbide grains by the cobalt matrix. It is not known whether the grain boundaries in themselves are weak or whether their failure is due to stress concentrations caused by the uneven distribution of the binder phase. It had been noted previously[15] that the fracture path in sintered carbides tends to be transcrystalline if the grains are large and intercrystalline if the grains of WC are small.

The impact strength is a function, mainly, of the amount of the brittle phase present in the alloy. It continues to increase with the percentage of cobalt throughout the range of composition studied here. The effect of grain size is relatively small.

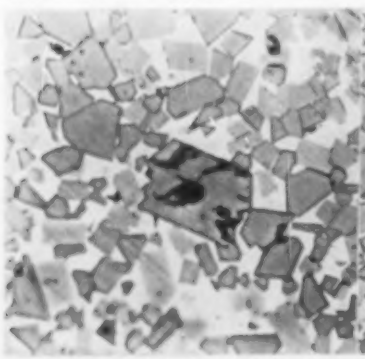

Fig. 11—Incipient cracks in WC grain. X1500. Area reduced approximately 30 pct for reproduction.

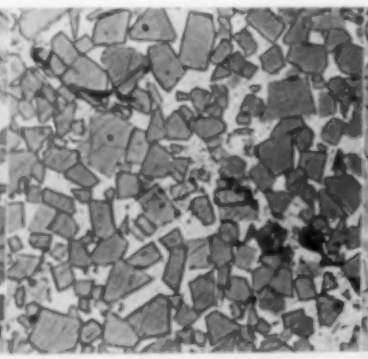

Fig. 12—Incipient cracks in WC grains. X1500. Area reduced approximately 30 pct for reproduction.

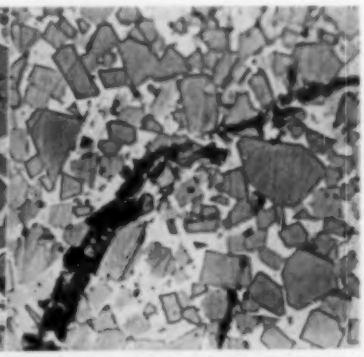

Fig. 13—Groove formed during stressing of WC-Co alloy. X1500. Area reduced approximately 30 pct for reproduction.

Table III. Percentage of Fracture Path Through Microstructural Features

Nature of Failure	Alloy, Pct Co	WC Grains	Carbide-Carbide Grain Boundary	Carbide-Binder Interface	Binder
Intermittent Cracks	6	57	41	—	—
	35	75	20	2	—
Continuous Fracture	6	58	39	3	0.2
	25	32	24	20	4

Conclusions

The results of this paper can be summarized as follows: 1—The hardness of sintered WC-Co alloys varies with the interparticle distance according to an exponential relation. 2—The impact strength increases with the binder content. 3—It has been shown that the transverse-rupture strength reaches a maximum for values of the mean free path between 0.3 to 0.6 microns. The mean free path is determined by the composition and grain size of the alloy. 4—The transverse-rupture strength increases as the film of binder metal becomes thinner, but eventually the strength is reduced by increased amounts of the brittle phase and incomplete dispersion of the carbide grains.

Discussion of this paper, if any, will appear in JOURNAL OF METALS, November 1955, and in AIME Metals Branch *Transactions*, Vol. **203**, 1955.

References

[1] E. W. Engle: Cemented Carbides. *Powder Metallurgy*. (1942) Ed. by J. Wulff. p. 436. Cleveland. ASM.

[2] E. J. Sandford and E. M. Trent: The Physical Metallurgy of Sintered Carbides. Symposium on Powder Metallurgy. *Special Report No. 38*. The Iron and Steel Institute (1947) p. 84.

[3] J. W. Graham: Sintered Titanium Carbides. *The Iron Age* (1953) p. 148.

[4] L. Northcott and C. J. Leadbeater: Sintered Iron-Copper Compacts. *Special Report No. 38*. The Iron and Steel Institute (1947) p. 142.

[5] R. L. Fullman: Measurement of Particle Sizes in Opaque Bodies. *Trans.* AIME (1953) **197**, p. 447; JOURNAL OF METALS (March 1953).

[6] H. Unckel: The Relation of Structure and Mechanical Properties in Two-Phase Alloys. *Metall* (1951) **5**, p. 146.

[7] M. Gensamer, E. B. Pearsall, W. S. Pellini, and J. R. Low, Jr.: Tensile Properties of Steel. *Trans.* ASM (1942) **30**, p. 983.

[8] R. B. Shaw, L. A. Sheppard, C. D. Starr, and J. E. Dorn: The Effect of Dispersions on the Tensile Properties of Aluminum-Copper Alloys. *Trans.* ASM (1953) **45**, p. 249.

[9] M. Gensamer, E. B. Pearsall, and G. V. Smith: The Mechanical Properties of the Isothermal Decomposition Products of Austenite. *Trans.* ASM (1940) **28**, p. 380.

[10] E. Orowan: Fracture and Strength of Solids. *Report on Progress in Physics* (1948-1949) **12**, p. 185.

[11] *Adhesion and Adhesives*. (1951) Ed. by DeBruyne, p. 78. New York. Elsevir Press.

[12] J. W. Beams, W. E. Walker, and H. S. Morton: Mechanical Properties of Thin Films of Silver. *Physical Review* (1952) **87**, Ser. 2, p. 524.

[13] E. Orowan: Fundamentals of Brittle Behavior in Metals Fatigue and Fracture of Metals. (1952) Ed. by W. Murray, p. 139. Cambridge. Massachusetts Institute of Technology.

[14] C. Ritzau: Contribution to the Magnetic Analysis of Hard Metals. *Stahl und Eisen* (1940) **60**, p. 891.

[15] H. Pfau and W. Rix: On the Lattice Structure and Strength of WC Grains in Hard Metals. *Ztsch. für Metallkunde* (1952) **43**, p. 440.

[16] J. Gurland and J. T. Norton: Role of the Binder Phase in Cemented Tungsten Carbide-Cobalt Alloys. *Trans.* AIME (1952) **194**, p. 1051; JOURNAL OF METALS (October 1951).

[17] W. H. Bruckner: The Micro-Mechanism of Fracture in the Tension-Impact Test. *Welding Journal* (1950) **29**, Part 2, p. 467.

[18] C. H. Lorig: A Metallurgist Looks at Fracture. *Trans.* ASM (1952) **44**, p. 31.

Technical Note

Microstructures of Pyrophoric Alloys

by R. D. Reiswig and David J. Mack

THE use of pyrophoric alloys in ignition devices dates back more than fifty years to a German patent granted to Carl Auer von Welsbach in 1903.[1] This patent named a composition essentially the same as that used in most present-day cigarette lighter "flints:" 70 pct mischmetal, 30 pct Fe, referred to here as "Auer alloy." Among the few current exceptions to this composition are those "flints" based on titanium or zirconium.

The rare-earth metals of which mischmetal is composed are so similar chemically and physically remarkable similarity in their alloying behaviors would be expected. Comparison of the binary phase diagrams[2] of these elements with nonrare-earth metals shows that this is true to a striking degree, so much so, in fact, that it appears that a mixture of these elements may be treated as a single component of alloys without fear of serious error. In considering alloys containing mischmetal, therefore, the mixture of rare-earth elements will be referred to merely as "cerium," the predominant element in mischmetal.

In polishing cerium alloys for metallographic examination, it was soon discovered that aqueous polishing media were highly corrosive. Free cerium in the alloys acts similarly to calcium (though not quite so rapidly) in evolving bubbles of hydrogen at the metal-water interface; thus, special metallographic techniques are required. The simplest polishing technique found to be satisfactory consisted of slow hand grinding on dry emery papers through

R. D. REISWIG, Student Associate AIME, and D. J. MACK, Member AIME, are Graduate Student and Associate Professor of Metallurgical Engineering, respectively, Dept. of Mining and Metallurgy, University of Wisconsin, Madison, Wisc.

TN 252E. Manuscript, Mar. 19, 1954.

This paper is based on a portion of thesis by R. D. Reiswig submitted, in partial fulfillment of the requirements for the degree of Master of Science, to the University of Wisconsin.

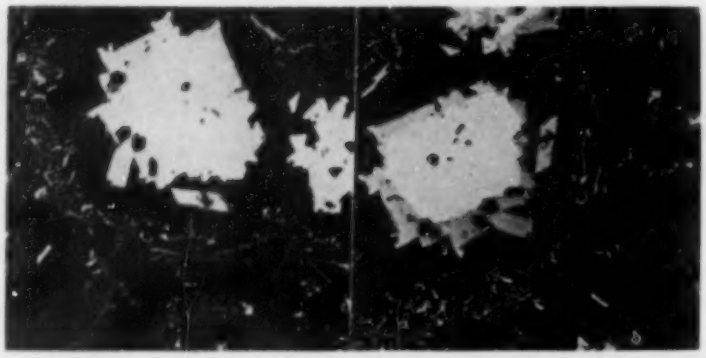

Fig. 1—Commercial Ce-Fe lighter flint containing about 70 pct Ce and 30 pct Fe. Primary dendrites of Ce_2Fe_7 with peritectic wall of $CeFe_2$ in eutectic matrix composed of "Chinese-script" $CeFe_2$ and free cerium. No etch. X150.

Fig. 2—Same composition as in Fig. 1. Allowed to "air etch" for one week to show $CeFe_2$ peritectic wall on Ce_2Fe_7 primary dendrites. X150.

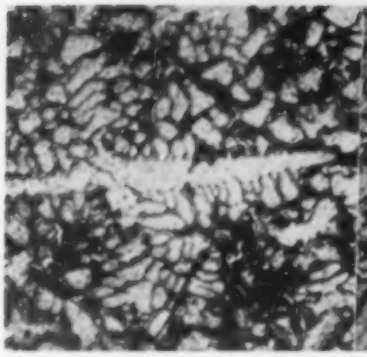

Fig. 3—Ce-10 pct Mg alloy showing CeMg primary dendrites in matrix of cerium with minor amount of unidentified impurity phase at dendrite boundaries. No etch. X150.

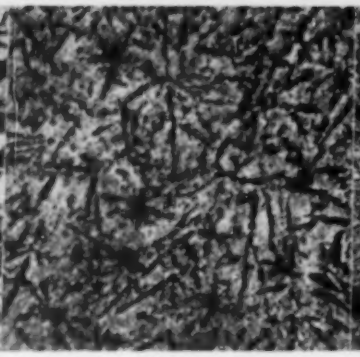

Fig. 4—Ce-11 pct Mg-10 pct Bi alloy showing primary dendrites of (probably) Ce_3Bi in matrix of CeMg with occasional dark patches of residual free cerium. No etch. X150.

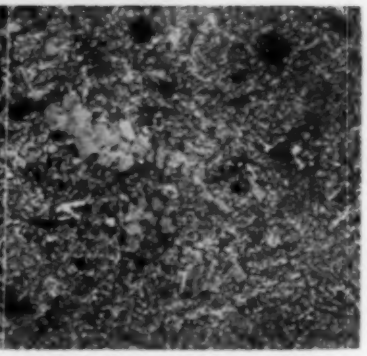

Fig. 5—Ce-6.6 pct Mg-10.7 pct Sb alloy showing large particles of dove-gray Ce_3Sb dispersed in matrix of CeMg with occasional patches of residual free cerium. No etch. X150.

3/0, followed by a final grind on 4/0 paper covered with a solution of paraffin in kerosene and a final polish on a soft-cloth wheel charged with a paste made from magnesium oxide and kerosene. No etching was necessary, since the cerium-rich areas in the microstructure darkened within a few seconds after rinsing off the polishing mixture with petroleum ether. Further exposure of the polished sections to the atmosphere (even in a dessicator) resulted in more extensive etching, sometimes serving to delineate special features of the microstructures, such as showing up peritectic walls and differentiating between the various intermetallic compounds present.

Fig. 1 shows the microstructure of a commercial Ce-Fe lighter flint immediately after polishing. Fig. 2 shows the same area after "air etching" for one week in a dessicator to show the peritectic wall of $CeFe_2$ surrounding the primary dendrites of Ce_2Fe_7.

Fig. 3 shows a Ce-10 pct Mg alloy. Increasing the magnesium content to 14.3 pct resulted in the virtual elimination of the residual free cerium visible in Fig. 3.

A Ce-11 pct Mg-10 pct Bi alloy is shown in Fig. 4. Here again, the presence of free cerium has been nearly completely avoided, thus largely eliminating the tendency to corrode in normal ambient atmospheres.

It appears that the ideal microstructure of a pyrophoric alloy for use in ignition devices consists of an intrinsically pyrophoric matrix in which are dispersed harder, more brittle particles arranged so as to divide the matrix into regions of a certain optimum size. These dispersed particles facilitate the tearing loose of particles of the matrix by the abrading mechanism and increase the probability of ignition of the freed particles by increasing the gross hardness of the surface against which they are rubbed by the abrading mechanism to attain their ignition temperature by friction.

Pure cerium is intrinsically pyrophoric, but is relatively soft. The dispersion of Ce-Fe intermetallic compounds in cerium performs the service outlined in the preceding paragraph. If sufficient magnesium could be added to a Ce-Fe alloy to convert all the free cerium to the intermetallic compound CeMg, the tendency of the matrix to corrode in air could be reduced materially. Unfortunately, this is not easily realizable in practice because the presence of iron in Ce-Mg alloys raises the liquidus temperature to the point where the vapor pressure of the dissolved magnesium approaches atmospheric pressure. This is not the case, however, if antimony is added to form the intermetallic compound Ce_3Sb dispersed in a matrix of CeMg. Such an alloy is shown in Fig. 5. Flints made from this alloy appear to have superior corrosion resistance in humid atmospheres, lower wear rates in ignition devices, and better flame-kindling efficiencies than flints prepared from Auer alloy.

Acknowledgment

The authors wish to thank the Parker Pen Co., who sponsored the fellowship grant under which this work was carried out.

[1] C. A. von Welsbach: Dent. Reich Patent 837017.
[2] M. Hansen: *Aufbau der Zweistofflegierungen*. (1936) Berlin, Springer.

A Study of the Microstructure of Titanium Carbide

by Herman Blumenthal and Ronald Silverman

It was found that despite the similarity of chemical analyses of different titanium carbides used as base materials for cermets, the physical properties, especially transverse-rupture strengths, of test bars were different. Hence this metallographic study attempts to link physical properties to microstructures. It is shown that microstructure, grain shape, and grain growth are functions of three interrelated factors: 1—powder production procedure, 2—surface conditioning of the particles, and 3—impurities either contained in the original powder or acquired during ball milling. An explanation is offered for the "coring effect," long observed, but heretofore of unknown origin. The explanation is based on assumption of an oxide film and on chemical analyses which substantiate these findings.

TITANIUM carbide has become in recent years a material of great interest in the high temperature field. Consequently, many manufacturers in the United States and Europe are producing titanium carbide for cermet applications as well as for additions to the well known tungsten carbide tools.

All present commercial processes of titanium carbide production utilize the chemical reaction of titanium dioxide and carbon to form as nearly as possible stoichiometric TiC. This reaction is carried out in three ways: 1—in a menstruum of molten metal,[1] 2—in the solid state, either in a protective atmosphere[2] or in vacuum;[3] or 3—in an arc-melting operation.[4, 5]

In spite of the fact that the pure carbides obtained in these operations are almost identical chemically, the physical properties vary considerably when they are combined with a binder (Ni, Co) to form cermets. This fact led the authors to examine metallographically nickel-bonded titanium carbide in order to find the possible reasons for this behavior.

Materials and Methods

Five different titanium carbides were used in this investigation. They are identified in Table I.

The first four materials were used in the as-received condition. Material *E*, received in lumps, was crushed to −100 mesh and carried through a flotation process in order to bring its graphite content in line with the other products. A Galagher flotation cell was used with pine oil as frothing agent. The chemical analyses of the investigated materials are given in Table II. The binder used was carbonyl nickel of 9 to 14 microns particle size, supplied by A. D. Mackay.

The materials were ball milled at a ball to charge ratio of 6:1 using procedures described under "Experiments and Results." All particle sizes mentioned are averages determined with a Fisher Sub-Sieve Sizer. Test bars (1x0.40x0.16 in.) were prepared by 1—hot pressing to 85 to 95 pct of theoretical density at pressures between 1 and 1½ tsi and temperatures from 1600° to 1800°C, 2—cold presssing after 3 pct camphor had been added, or 3—wet pressing, both 2 and 3 at pressures between 5 and 10 tsi. All pressed bars were sintered in a vacuum of 10^{-5} to 10^{-4} mm Hg for 2 hr at 1350°C. Transverse-rupture strengths were determined by breaking on a Baldwin Universal Testing Machine over a 9/16 in. span. Densities were measured by water displacement.

H. BLUMENTHAL and R. SILVERMAN are associated with American Electro Metal Corp., Yonkers, N.Y.

Discussion of this paper, TP 3938E, may be sent, 2 copies, to AIME by Apr. 1, 1955. Manuscript, Sept. 14, 1954. Chicago Meeting, February 1955.

Table I. Investigated Materials

Material	Supplier	Production Procedure
A	Kennametal Inc.	Menstruum process
B	Metallwerk Plansee, Austria	Solid-state reaction in a protective atmosphere
C	Metro Cutanit, England	Solid-state reaction in vacuum
D	Titanium Alloy Mfg. Co.	Arc melting, pure product
E	Morton Co.	Arc melting, technical product

The preparation of the specimens for micrographs was done according to Silverman and Doshna Luscz.[6] All magnifications are at X1000. A sodium picrate electrolytic etch was used.

Experiments and Results

The influence of ball-milling procedure, ball-milling medium, pressing procedure, and sintering procedure on the microstructure of 80/20 – TiC/Ni were investigated.

Ball Milling of Materials A, B, and C in a Steel Mill: Figs. 1 and 2 show microstructures of hot-pressed and vacuum-sintered test bars of materials *A* and *B* after the respective materials had been ball milled to 2.1 microns particle size in a steel mill and mixed with 20 pct Ni binder. Material *A* (Fig. 1) shows considerable grain growth. Also evident is a tendency of the carbide grains to coalesce. The density is 98 pct and the low transverse-rupture strength of 111,000 psi is probably caused by many large grains and an unfavorable packing factor. Almost all grains show a slight indication of "coring."

Material *B* (Fig. 2), although showing grain growth, still has many small particles and a better distribution of binder and carbide due to the relative absence of the coalescing tendency. "Coring" can be observed in almost all grains. The high transverse-rupture strength of 179,000 psi and the density of 100 pct are believed to be due to the many small grains completely surrounded by the binder phase.

There is also a preference to form spherical grains with material *A*, while most grains of material *B* preserve their angular shapes. Material *C*, of which no picture is given, stays between *A* and *B* in every respect. Rounding of some grains can be observed as well as coring, but the latter to a lesser degree than with material *B*. Its densification is good and the transverse-rupture strength obtained is 142,000 psi.

Ball Milling of Materials A, B, C, and E in a WC Mill: When the TiC powders were ball milled to 2 microns particle size in a WC mill, then ball-mill mixed with 20 pct Ni binder, hot pressed, and vacuum

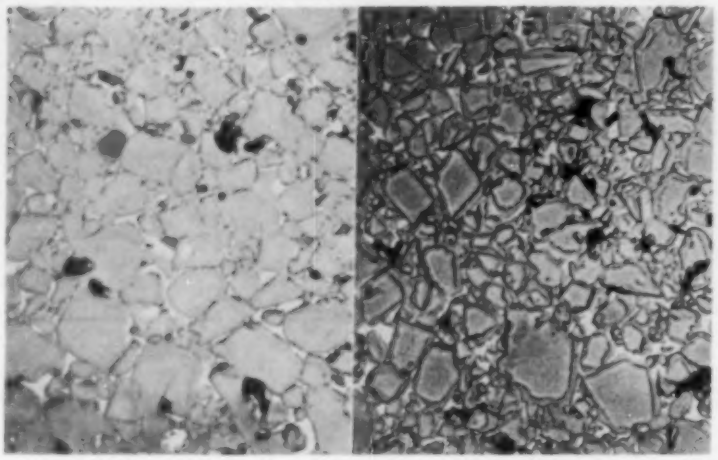

Fig. 1—Material *A* ball milled in steel mill, ball-mill mixed with binder, hot pressed, and vacuum sintered. X1000. Area reduced approximately 25 pct for reproduction.

Fig. 2—Material *B*, ball milled in steel mill, ball-mill mixed with binder, hot pressed, and vacuum sintered. X1000. Area reduced approximately 25 pct for reproduction.

sintered, grain growth was much less than when ball milling was done in a steel mill. In the tungsten carbide mill, the powders picked up 3 to 4 pct WC. Figs. 3, 4, and 5 represent this group. Figs. 3 and 4 look somewhat similar. Coring of grains is a little more pronounced in material *C* (Fig. 4) than in *A* (Fig. 3) and both have a continuous carbide skeleton. There are fine dark particles visible in Fig. 3 which are not present in Fig. 4. X-ray diffraction analysis of material *A* (Fig. 3) revealed the presence of a small amount of unidentified impurities and a trace of free WC. With structures of Figs. 3 and 4 nearly alike, transverse-rupture strengths are identical (see Table III). Material *B* (no micrograph given) shows a tendency for particles to sinter together and a very pronounced coring. Its transverse-rupture strength is higher than for materials *A* and *C*, 176,000 as compared with 153,000 psi. Spherical particles are formed preferably with material *C* (Fig. 4), less with material *B*, and indicated in material *A* only by a rounding of edges. Material *E* (Fig. 5) looks entirely different from the others, since there is no rounding of particles and hardly any coring. Its heterogeneous appearance is due to its high impurity content (mostly iron oxide). Its density is less than 90 pct, and as a consequence, the transverse-rupture strength is very low (69,000 psi).

Addition of Tungsten Carbide to Material A: Compared to the foregoing, Fig. 6 shows material *A* ball milled to 2 microns in a steel mill, ball-mill mixed with 3 pct WC and 20 pct Ni, hot pressed, and vacuum sintered. The addition of WC makes the chemical composition of this material very similar to that shown in Fig. 3. Its microstructure, however, is completely different. It shows pronounced grain growth, angular particles, and the presence of fine particles in the binder phase. X-ray diffraction analysis also revealed here the presence of a small amount of free WC. Despite these differences in the microstructures (compare Figs. 3 and 6), the densities obtained as well as the transverse-rupture strengths were practically identical.

Simultaneous Ball Milling to Size and Mixing with the Binder: When ball milling to 2 microns particle size and mixing is done simultaneously in a WC mill, the microstructures obtained are very similar to those described under "Ball Milling of Materials *A*, *B*, *C*, and *E* in a WC Mill." There might be a little more grain growth, but there is a better distribution of grain size and binder. The microstructure of material *D* is very similar to that of material *A*. Coring is very pronounced, especially with material *B*, which is shown in Fig. 7. This figure should be compared with Fig. 2 which shows the same material ball milled in a steel mill. The similarity is obvious, but the smaller grain size and the better grain size and binder distribution of the bar pictured in Fig. 7 resulted in a higher transverse-rupture strength (see Table III).

The effect of ball milling to size and mixing with the binder in one or two operations expresses itself not only in the microstructure but also in the physical properties obtained. Table III compares average particle sizes after ball milling, final densities, and transverse-rupture strengths, and shows the superiority of the simultaneous sizing and mixing operation.

Influence of Ball-Milling Medium on Material A: Material *A* was ball milled to an average particle size of about 2 microns and mixed simultaneously with the binder in acetone, carbon tetrachloride, alcohol, and hexane. After vacuum drying the powders, hot pressing, and vacuum sintering, elongated grains had been formed. Fig. 8 shows the microstructure obtained after ball milling in carbon tetrachloride. With the other liquids unidirectional grain growth is not as excessive as with carbon tetrachloride, hexane shows the least, and acetone and ethyl alcohol are in between in this order. In the presence of a large number of elongated grains, dense packing could not be obtained. Transverse-rupture strengths therefore decreased as the number of elongated grains increased. The final density of a bar after ball milling the powder in hexane was 97

Table II. Chemical Composition of Commercial Titanium Carbides

Material	*A*	*B*	*C*	*D*	*E**
Ti	79.7	78.0	78.0	78.1	78.0
$C_{comb.}$	19.4	19.0	19.0	19.1	18.8
C_{free}	0.21	0.73	0.54	0.20	0.45
O_2	0.16	0.09	0.16	0.57	1.93
N_2	0.15	0.07	0.07	0.48	0.88
Fe	0.06	0.12	0.11	0.22	1.54
Mo		0.19†			
W		0.12†			
Total	99.62	100.23	99.48	99.04	99.58
$C_{comb.}/(Ti + C_{comb.})$	19.6	19.4	19.4	19.5	17.7

* Flotation purified.
† Spectrographic analyses.

pct and the transverse-rupture strength 144,000 psi, while the bar pictured in Fig. 8 had a density of 91 pct and a transverse-rupture strength of 90,000 psi. The weird picture presented after ball milling in carbon tetrachloride (Fig. 8) should be compared with the picture of the same material after ball milling in air (Fig. 3).

Ball Milling in Carbon Tetrachloride to a Small Particle Size: All materials were ball milled in carbon tetrachloride for 144 hr in order to obtain an average particle size of one micron, vacuum dried, hot pressed, and vacuum sintered. Material *A* still shows the tendency to form elongated grains but, since the grains are much smaller than in the previous case, dense packing may be obtained (Fig. 9). The grains also show a very high degree of coring. The density obtained is almost 100 pct and the transverse-rupture strength 161,000 psi. Wet pressing or cold pressing of this material after drying resulted in similar microstructures, but the grains show less unidirectional growth and less coring. Densities obtained were just as good and transverse-rupture strengths after wet pressing were 170,000 psi and 139,000 psi after cold pressing.

The other four materials presented the same microstructure as material *A* (Fig. 9) and densities were high. As far as transverse-rupture strengths are concerned, only material *E* was below 150,000 psi.

Influence of Sintering Procedure on Material B: Material *B* was ball milled to 2 microns and mixed simultaneously with nickel. Vacuum sintering was done at temperatures ranging from the standard 1350° to a maximum of 1520°C, varying the sintering time from 4 hr at the lower temperatures to 5 min at 1520°C. The microstructures obtained are completely identical. Fig. 10 shows a typical picture. A bar sintered for 4 hr at temperatures up to 1420°C does not show more grain growth than a bar held at 1520°C for five min. There is a continuous carbide skeleton formation which is not further advanced after 4 hr than after 5 min. There is no evidence of coring, although material *B*, when hot pressed, shows this phenomenon to an especially high degree. With microstructures and final densities practically identical, transverse-rupture strengths are also similar, namely between 127,000 and 140,000 psi. The presence of 1 pct Fe in one of the experiments did not change microstructure or physical properties.

Discussion

Coring: The appearance of cored particles observed especially in the microstructures of material *B* and

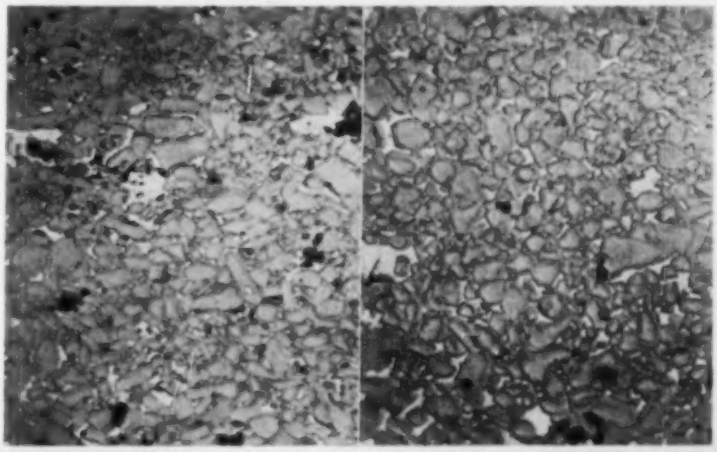

Fig. 3—Material *A*, ball milled in WC mill, ball-mill mixed with binder, hot pressed, and vacuum sintered. X1000. Area reduced approximately 25 pct for reproduction.

Fig. 4—Material *C*, ball milled in WC mill, ball-mill mixed with binder, hot pressed, and vacuum sintered. X1000. Area reduced approximately 25 pct for reproduction.

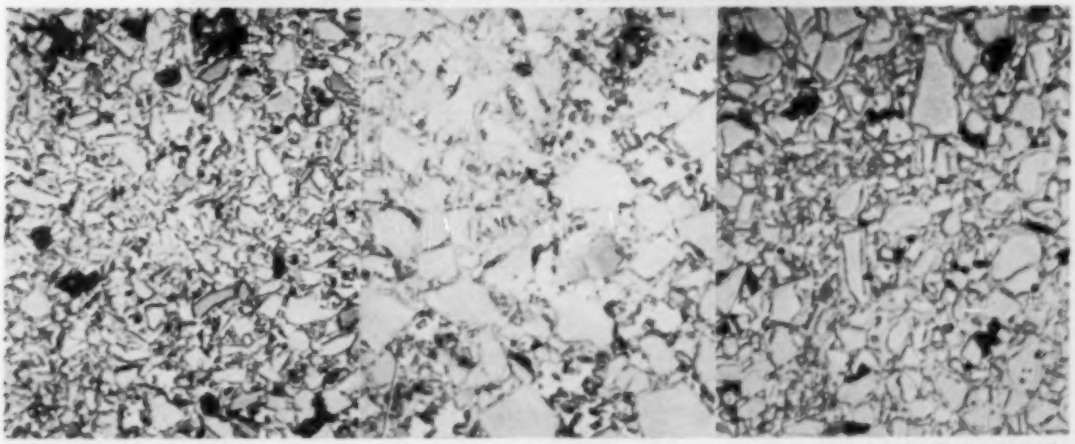

Fig. 5—Material *E*, ball milled in WC mill, ball-mill mixed with binder, hot pressed, and vacuum sintered. X1000. Area reduced approximately 25 pct for reproduction.

Fig. 6—Material *A*, ball milled in steel mill, ball-mill mixed with 3 pct WC and binder, hot pressed, and vacuum sintered. X1000. Area reduced approximately 25 pct for reproduction.

Fig. 7—Material *B*, ball milled and mixed with binder in WC mill, hot pressed, and vacuum sintered. X1000. Area reduced approximately 25 pct for reproduction.

less frequently with the other materials, unless they were ball milled in CCl_4 for 144 hr, was reported before in Ni-Cr bonded TiC.[7] X-ray diffraction patterns and electron microscope studies of cored materials did not reveal anything which could be used as a possible explanation for this phenomenon. The following thoughts are offered only as a possibility and should be considered as such: During ball milling all powders pick up oxygen, at least part of which is present as a film of TiO_2 around the individual particles. This could be shown by leaching a ball-milled powder with dilute hydrochloric acid. The powder lost oxygen in this operation, as proven by chemical analysis, and the spent acid contained titanium. The ratio of oxygen to titanium removed by leaching was constant and corresponded to the formula TiO_2. During hot pressing and vacuum sintering, the powder may lose some of this oxygen or retain it all, as numerous analyses have shown. The oxygen still present may be in the form of an oxide film or be in solid solution as TiO in TiC. It is believed that at least part of the oxygen is present as a film in cases where coring occurs. TiC dissolved in the nickel binder may be precipitated on this film and protect it from being reduced by free carbon present in the binder phase. The presence of the oxide as a layer now acts as a boundary between the original grain and the precipitated TiC. These three regions give the appearance of what is called a "cored grain." Growth of the original grain can now occur only by diffusion of TiC through the oxide layer.

Grain Growth: Three mechanisms have been proposed as an explanation for grain growth.[8] They are: 1—coalescence of adjacent grains, 2—solution in the binder phase during heating and reprecipitation during cooling, and 3—transfer of carbide from smaller to larger grains by diffusion through the liquid binder.

Only the first of these mechanisms can take place in the absence of a binder. In the presence of a binder, it is impossible to state which one of these mechanisms is effective. Most probably all three take part at the same time to various degrees. It seems, however, that in materials *A* and *D* coalescence of adjacent grains provides the major source for large particles, and it is believed that the reason for this can be found in their production procedures. Material *A* is produced in a bath of molten metal, resulting in fairly large and well formed single crystals of TiC. These crystals are broken up by grinding and ball milling, and the small fragments obtained have much higher surface energy than the same size particles of materials *B* and *C*. The latter two can be produced in small particle sizes, if so desired, by taking TiO_2 of small particle size as a starting material and reacting it in the solid state with carbon. The influence of the particle size of the starting material on the particle size of the product is well known and described in the literature on WC materials. *D* and *E* are produced by arc melting and it can be assumed that in this process large crystals will form on solidification of the molten mass.

WC picked up during ball milling seems to prevent excessive grain growth (compare Figs. 1 and 3). There is, instead, a tendency towards spheroidization of grains and formation of grains of uniform sizes. Fig. 4 is a good example of this. Spheroidization of grains is an indication of solution and precipitation of TiC from the binder phase and is well known in TiC-containing cutting tool materials. Addition of WC and ball milling in a steel mill has not the same effect as ball milling in a WC mill (see Fig. 6). The iron picked up from the steel mill (very probably in the form of oxide) has a similar effect as the impurities present in material *E* (Fig. 5).

The strictly angular grains of Figs. 5 and 6 might also be due to the high oxygen content of these materials (probably in solid solution), which amounts to 1.46 and 0.58 pct, respectively. It has been reported for WC that powders of high oxygen content sinter with greater difficulty.[9] The same might be true for TiC.

The third mechanism of grain growth, a diffusion of TiC not only through the binder phase but also through an oxide layer surrounding the original grains, is believed to be effective especially in those cases where "coring" occurs. This phenomenon is highly pronounced with material *B* (see Figs. 2 and 7), clearly visible also in material *C* (see Fig. 4),

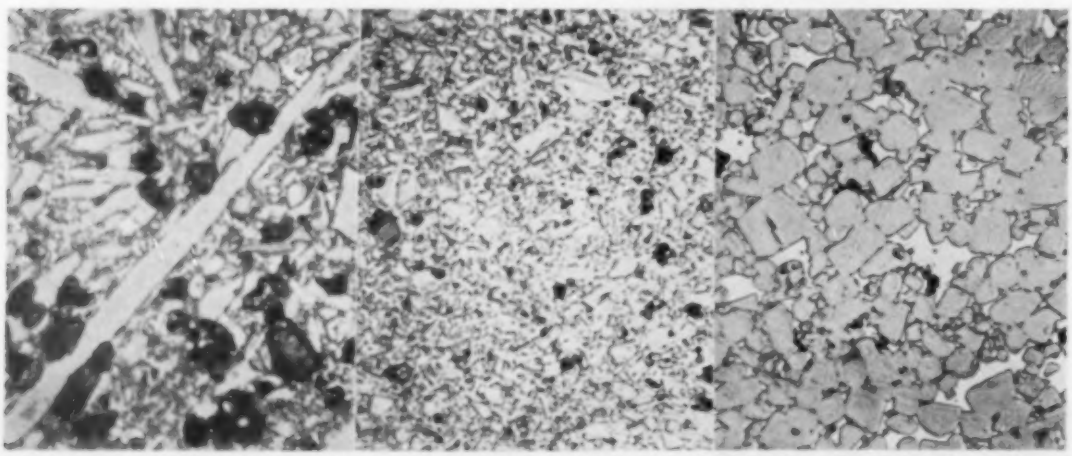

Fig. 8—Material *A*, ball milled and mixed with binder in WC mill in CCl_4 to 2.2 microns, hot pressed, and vacuum sintered. X1000. Area reduced approximately 25 pct for reproduction.

Fig. 9—Material *A*, ball milled and mixed with binder in WC mill in CCl_4 to 1.8 microns, hot pressed, and vacuum sintered. X1000. Area reduced approximately 25 pct for reproduction.

Fig. 10—Material *B*, ball milled and mixed with binder in WC mill, cold pressed, and vacuum sintered. X1000. Area reduced approximately 25 pct for reproduction.

Table III. Physical Properties of Different Materials as a Function of Ball-Milling Procedure

Material	A				B				C				D		E	
Ball-Milling Procedure*	1	2	3	4	1	2	3	4	1	2	3	4	3	4	2	4
Ball-milling time, hr	96	96	96	144	48	96	72	144	48	96	72	144	144	144	96	144
Average particle size, microns	2.1	1.9	1.7	1.0	2.1	2.0	2.2	1.1	2.3	2.3	2.4	1.3	1.8	1.3	1.9	1.3
Density, g per cc	5.28	5.48	5.44	5.46	5.39	5.48	5.41	5.33	5.21	5.40	5.39	5.28	5.43	5.44	4.80	5.43
Transverse-rupture strength, 1000 psi†	111	153	161	161	179	176	186	174	142	152	166	154	158	204	69	112
Fig.	1	3	—	9	2	—	7	—	—	4	—	—	—	—	5	—

* Ball-milling procedures: 1—Ball milled and mixed in steel mill in two operations, 2—Ball milled and mixed in WC mill in two operations, 3—Ball milled and mixed in WC mill in one operation, and 4—Ball milled and mixed in WC mill in CCl_4 in one operation.
† All results are maximum values of six specimens tested.

and occurs in other materials to a considerable degree only if ball milling for a long time has raised the oxygen content (Fig. 9). Vacuum sintering of cold-pressed bars prevents coring even of material *B* (see Fig. 10). Particle growth occurs in this case mainly by sintering together of adjacent grains and, as the rounding of particles indicates, by solution and reprecipitation.

Ball-Milling Medium: The use of a liquid ball-milling medium enhances grain growth and causes segregation (see Fig. 8). The latter can be counteracted by ball milling to a small enough particle size (see Fig. 9). As it is inconceivable that the elongated grains of Fig. 8 could have formed during ball milling, they must have formed during hot pressing and vacuum sintering. Nevertheless, it is believed that the reason for their formation lies in the ball-milling medium. Certain ball-milling media give the particles a surface conditioning which enhances grain growth in one direction. This is especially pronounced with carbon tetrachloride. Nevertheless, good densities and high transverse-rupture strengths are obtainable using it, if ball milling is done for a long time in order to get small enough particle sizes. By vacuum sintering of hot-pressed bars, grains grow and form more elongated shapes than by sintering of wet or cold-pressed bars; but due to the original small particle size, they are still small enough to allow dense packing. Coring is still prevalent with grains of the hot-pressed and vacuum-sintered specimen. Fig. 9 resembles closely Figs. 2 and 7 which are considered to have a very desirable microstructure. The presence of coring was linked previously to an oxide film. Powder used for these experiments had an oxygen content of 1.7 pct after ball milling. Hot pressing reduced this amount to 0.53 pct and the following vacuum sintering to 0.35 pct. Wet-pressed or cold-pressed and vacuum-sintered bars showed an oxygen content of 0.2 to 0.17 pct, respectively. The high vacuum seems to destroy the oxide film before sintering occurs. The transverse-rupture strength of cold-pressed and vacuum-sintered bars is inferior to those wet or hot pressed. This might have its cause in the nonuniform distribution of fairly large pores.

Sintering Time: The fact that cold-pressed bars, vacuum sintered for times ranging from 5 min to 4 hr, have completely identical microstructures, makes it appear as if grain growth takes place only in the initial stage of the sintering process. The reason for this is unknown. The presence of 4 pct WC after ball milling here again might prevent excessive grain growth. Coring, which is especially characteristic of material *B*, does not occur, probably due to the lack of an oxide film. The powders as ball milled had an oxygen content of about 0.6 pct and after sintering of only 0.1 pct. The high vacuum seems to have destroyed this film before sintering, as mentioned previously. The nonuniform binder distribution, the presence of large lakes, and the absence of coring are the reasons for the inferior transverse-rupture strength of this material, although the densities are satisfactory.

Conclusions

Correlating the micrographs and the transverse-rupture strengths of the discussed materials, it must be concluded that the following microstructure is the most desirable in order to obtain the highest transverse-rupture strength: highly cored angular-shaped particles surrounded completely by the binder phase which has almost the character of a film. No binder lakes should be present. A certain amount of grain growth is tolerable as long as there are enough small and medium-sized grains present to insure dense packing.

It is quite conceivable that changes in ball-milling or sintering conditions can produce this "ideal structure" for materials which do not show it under the conditions they were treated in this investigation. The great differences between material *A* (see Fig. 1) and material *B* (see Fig. 2) and the similarity of the latter product with the one shown in Fig. 7 might have its cause in the small amounts of tungsten (and probably molybdenum) present in the as-received material *B*.

It appears that ball-mill mixing and sizing in one operation leads to thoroughly nickel-coated particles in contrast to a poorer nickel to carbide distribution for the separate operations. The thin film, surrounding each particle more uniformly, insures a better preparation of this powder for sintering. The superior transverse-rupture strength of the thus prepared materials, especially material *B*, might be attributed to a better "packing factor." Obviously, a more favorable fine to coarse grain ratio results in better packing and takes better advantage of more nickel-coated surfaces contributing towards a more complete bonding during sintering.

In this connection, reference is made to two articles which deal with a theory of "stronger bonding through thinner films." It is possible that these thoughts could be applied to the previous discussion.

Acknowledgment

The authors wish to acknowledge the assistance of Mrs. Patricia Doshna Luscz who prepared the micrographs and Mr. Frank Hodi who did some of the experimental work. This investigation was sponsored by the United States Air Force, Wright

Air Development Center. Permission of this agency to publish the paper is gratefully acknowledged.

Discussion of this paper, if any, will appear in JOURNAL OF METALS, November 1955, and in AIME Metals Branch *Transactions*, Vol. **203**, 1955.

References

[1] P. M. McKenna: United States Patent 2,515,463 (1948).

[2] P. Schwarzkopf and R. Kieffer: *Refractory Hard Metals*. (1953) p. 78. New York. The MacMillan Co.

[3] L. D. Brownlee, G. A. Geach, and T. Raine: *Research Report* Iron and Steel Institute, London (1941) No. 38, p. 73.

[4] H. Moissan: *Comptes Rendus* (1897) **125**, p. 839.

[5] P. Schwarzkopf and R. Kieffer: *Refractory Hard Metals*. (1953) p. 49. New York. The MacMillan Co.

[6] R. Silverman and P. Doshna Luscz: *Powder Metallurgy Bulletin* 7 (1954) p. 25.

[7] P. Schwarzkopf and R. Kieffer: *Refractory Hard Metals*. (1953) p. 399. New York. The MacMillan Co.

[8] J. Gurland: *Trans.* AIME (1954) **200**, p. 287; JOURNAL OF METALS (February 1954).

[9] E. J. Sandford: *Alloy Metals Review* (1949) **7**, p. 2.

[10] J. T. Norton: *Powder Metallurgy Bulletin 6* (1951) p. 75.

[11] J. Gurland and J. T. Norton: *Trans.* AIME (1952) **194**, p. 1051; JOURNAL OF METALS (October 1951).

Technical Note

High Temperature Vacuum Etching on Pure Titanium

by W. D. Bennett

AN interesting effect has been observed in the vacuum etching of titanium in the high temperature β phase. Using a high vacuum annealing furnace, operating at less than 2×10^{-4} mm with a tubular titanium liner, it has been found possible to etch polished metallographic specimens at different temperatures between room temperature and 1000°C without contamination or increase in hardness.[1] Heat etching of titanium has been reported by other workers,[2] but the following example is of interest as an experiment under high vacuum in the absence of any contamination.

Two polished specimens of iodide-processed titanium are placed at different positions along the axis of the furnace corresponding to temperatures of 900° and 800°C above and below the α-β transus. The specimens are then raised to these temperatures and annealed simultaneously for 3 hr under the same high vacuum conditions. After cooling and withdrawing the specimens, their surfaces are photographed without further treatment. Figs. 1 and 2 show the results for the 800° and 900°C specimens, respectively. Fig. 1, corresponding to a vacuum etch in the α region, shows a typical equiaxed structure with what appears to be a slight shift of grain boundaries. Fig. 2, corresponding to a vacuum etch in the β region, shows an equiaxed type of structure with the growth of striations in certain grains. The striations are only superficial, as a light polish and chemical etch restores the clean equiaxed structure. The vacuum etch, occurring as it does above the α-β transus, records the state of the metal in the β phase by means of the surface relief produced by the selective evaporation of metal from different grains; the metal itself reverts to the equiaxed α on cooling.

The nature of the "β etch" (Fig. 2) suggests that, in transforming from the close-packed-hexagonal α to the body-centered-cubic β, lenticular-shaped laminae are formed parallel to common planes of the two structures. This would explain why some grains appear to be unaffected by the etch. The technique has interesting possibilities in the investigation of the mechanics of high temperature transformation.

W. D. BENNETT is Physical Metallurgist, Physical Metallurgy Div., Mines Branch, Dept. of Mines and Technical Surveys, Ottawa, Ont., Canada.

TN 248E. Manuscript, July 14, 1954.

Acknowledgment

This note is published by permission of the Deputy Minister, Dept. of Mines and Technical Surveys, Ottawa, Ont., Canada.

[1] W. D. Bennett: Vacuum Heat-Treatment. *Metal Industry* (1954) **84**, No. 13.

[2] F. C. Holden, H. R. Ogden, and R. I. Jaffee: Microstructures and Mechanical Properties of Iodide Titanium. *Trans.* AIME (1953) **197**, p. 238; JOURNAL OF METALS (February 1953).

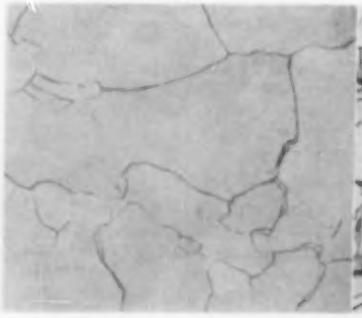

Fig. 1—Titanium vacuum etched at 800°C (α etched). X100. Area reduced approximately 35 pct for reproduction.

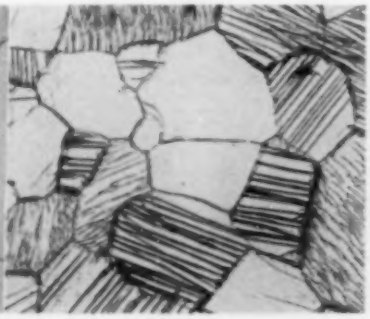

Fig. 2—Titanium vacuum etched at 900° C (β etched). X100. Area reduced approximately 35 pct for reproduction.

Influence of Heat Treatment on the Ductile-Brittle Transition Temperature of Semikilled Steel Plate

by R. H. Frazier, F. W. Boulger, and C. H. Lorig

This investigation establishes the effect of ferrite grain size resulting from various heat treatments on the transition temperature of a semikilled steel plate. Different austenitizing temperatures and various cooling rates were used. The ductile-brittle transition temperatures were determined by the Navy tear test and the keyhole Charpy test.

THE data presented in this paper deal with quality characteristics of ship-plate material which were investigated in a research project sponsored at Battelle by the Bureau of Ships, Dept. of the Navy. Specifically, the object of this investigation was to establish the effect of ferritic grain size (resulting from various heat treatments) on the so-called transition temperature of ship-plate steel.

Transition temperature is not a fixed property of steel. It is derived from a series of static or dynamic tests made at various temperatures and is qualified by specifying the type of test employed as well as the testing criteria. Because in earlier investigations of ship-plate quality[1, 2] the so-called Navy tear test and standard notched-bar tests (keyhole Charpy) proved to be useful in interpreting instances of brittle behavior of ship plate in service, these tests were used in the investigation reported in this paper. By definition,[1] in the Navy tear tests the highest temperature at which one or more of four specimens breaks with a brittle fracture (that is, when less than 50 pct of the fracture area has a dull fibrous texture) is termed "transition" temperature. In the Charpy tests, the 12 ft-lb level of energy absorption was used as a criterion indicating the "transition" temperature, although other levels of energy absorption were also used for comparison.

Earlier work[2] on ship-plate steels indicated that the temperature at which ship plate is finished has a very significant effect on its notched-bar properties. Plates rolled in the laboratory, where the finishing temperature can be carefully controlled, showed a 16°F decrease in tear test transition temperature when the finishing temperature was lowered 200°F (from X° to Y°F). The same plates showed a drop of 10°F in the keyhole Charpy transition temperature from the same decrease in finishing temperature. Commercially finished plates[4] exhibit a similar trend.

When the ferrite grain size of the hot-rolled laboratory plates was determined, a close relationship was found between the ferrite grain size and the notched-bar transition temperature.[5, 6] The indicated relationship between grain size and transition temperature was in agreement with the findings on low carbon steels of Hodge, Manning, and Reichhold[7] despite the differences in composition of the steels.

The cooling rate after rolling varies from one steel plant to another. This variation changes the microstructure[2] and appears very likely to affect the notched-bar properties of the steel plates. In the investigation summarized in the present paper, heat treatments simulating finishing practices in the hot rolling of ship plate were used in order to vary the ferritic grain size. It is believed that the indicated relationship between grain size and transition temperatures of the ship-plate material will prove useful in estimating the effect of rolling temperature and of cooling rates from rolling temperatures on the notched-bar properties of semikilled steel plate.

Material

The semikilled steel plate used in this investigation was a ¾ in. hot-rolled plate from an open hearth heat. Other plates from this heat have been used on many other studies performed for the Ship Structure Committee,[1, 6, 8] and the heat has been identified as project steel "A". The chemical composition of the plate[2] was 0.25 pct C, 0.49 pct Mn, 0.011 pct P, 0.045 pct S, 0.04 pct Si, and 0.004 pct N.

R. F. FRAZIER, F. W. BOULGER, Members AIME, are Assistant Chief and Chief, respectively, Div. of Ferrous Metallurgy, and C. H. LORIG, Member AIME, is Technical Director, Battelle Memorial Institute, Columbus, Ohio.

Discussion of this paper, TP 3952E, may be sent, 2 copies, to AIME by Apr. 1, 1955. Manuscript, May 17, 1954. Chicago Meeting, February 1955.

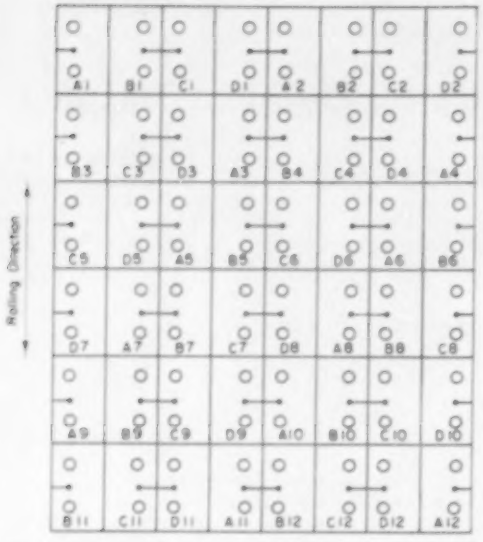
Rolling Direction
A1 B1 C1 D1 A2 B2 C2 D2
B3 C3 D3 A3 B4 C4 D4 A4
C5 D5 A5 B5 C6 D6 A6 B6
D7 A7 B7 C7 D8 A8 B8 C8
A9 B9 C9 D9 A10 B10 C10 D10
B11 C11 D11 A11 B12 C12 D12 A12

Fig. 1—Location of tear test specimens from as-rolled project steel "A."

its tensile strength[1] was 58,650 psi, and its elongation was 33.4 pct in 8 in.

The Navy tear test properties of the as-rolled plate were determined at Battelle using 48 specimens divided into four groups as shown by the diagram in Fig. 1. Each group was tested as an individual steel. Four tear test specimens from each group were broken at +70°, +80°, and +90°F. The results of these tests are summarized in Table I. When tested at +90°F, all 16 specimens had fractured surfaces exhibiting more than 50 pct ductile type of failure. At +70°F, 15 of the 16 specimens showed a brittle fracture as defined earlier. This corresponds to a very sudden transition in fracture texture, much sharper than is characteristic of most steels. Based on the definition of transition temperature as the highest temperature at which one or more specimens out of four are brittle, the transition temperatures of the four groups shown in Table I are 80°, 70°, 80°, and 80°F, respectively. Kahn[1] reported the transition temperature of this steel as 70°F.

The keyhole Charpy transition curve for this steel in the hot-rolled condition is shown in Fig. 2. The properties in two directions were determined by specimens notched normal to the plate surface. The Charpy values of the transverse specimen are generally lower than the values in the longitudinal direction. At the 12 ft-lb level, used as a criterion in this investigation, the respective transition temperatures of longitudinal and transverse specimens were 10° and 34°F. The 12 ft-lb level was chosen because frequency distribution plots made by Vanderbeck[2] indicated that such a criterion is more informative than other levels of energy absorption in the keyhole Charpy tests.

Table I. Summary of Tear Test Results from As-Rolled Project Steel "A"

Group No.	Testing Temperature, °F	Maximum Load, Lb	Energy, Ft-Lb		Average Pct Shear in Fracture	Number of Brittle Specimens
			To Start Fracture	To Propagate Fracture		
A	70	37,100	740	200	21	4
A	80	36,425	735	350	45	2
A	90	37,125	740	610	79	0
B	70	36,990	735	85	13	4
B	80	36,240	680	610	76	0
B	90	36,810	710	610	82	0
C	70	37,625	780	310	37	3
C	80	38,790	780	300	38	3
C	90	36,550	720	670	81	0
D	70	36,710	705	180	13	4
D	80	37,040	710	285	40	3
D	90	37,423	720	710	84	0
All	70	37,105	750	175	23	15
All	80	36,615	710	385	50	8
All	90	36,980	720	650	82	0

Heat Treatment

The heat treating was performed in a large electric furnace which had sufficient heating capacity to heat treat at least six 6x12½ in. sections of ¾ in. plate. The six plates were placed in a hot furnace on edge and separated by small sections of refractory brick splits. Since the two outer plates might have different heating and cooling rates, these plates were not used in the test program. One of the center plates contained a thermocouple for determining the heating and cooling rates that would be typical of the three remaining test plates. A typical heating curve is shown in Fig. 3. Five austenitizing temperatures ranging from 1500° to 1900°F were used in this study. After the plates had been in the furnace for 1½ hr, they were withdrawn and cooled at four different rates.

With the exception of the 1500°F furnace temperature, the 1½ hr heating time was sufficient for all the plates to reach furnace temperature. At a 1500°F furnace temperature, the thermocouple showed a temperature of only 1480°F when 90 min had elapsed. The austenitic grain size resulting from

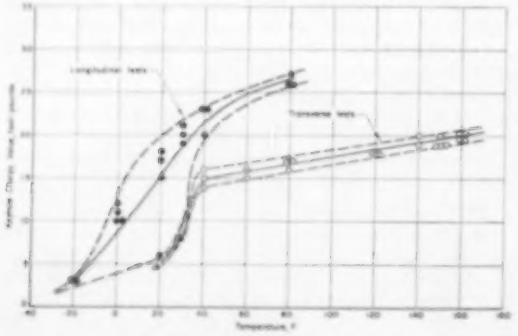

Fig. 2—Keyhole Charpy transition curves for longitudinal and transverse specimens from as-rolled project steel "A."

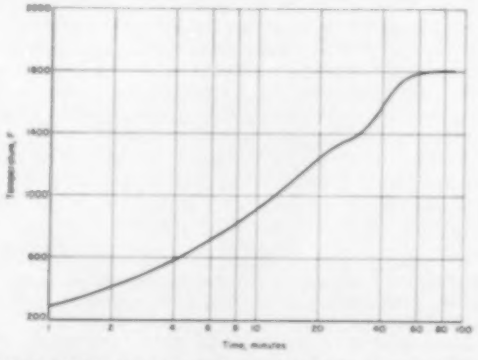

Fig. 3—Heating rate for center of ¾ in. plate. Furnace temperature was 1800°F.

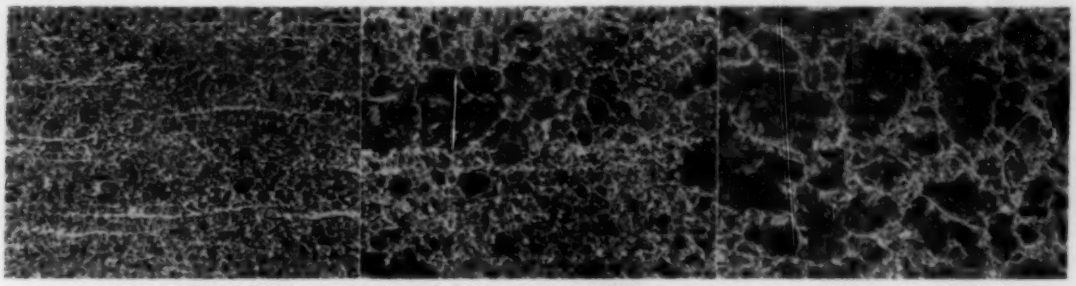

a—Austenitized at 1500°F. b—Austenitized at 1600°F. c—Austenitized at 1700°F.

Fig. 4—Microstructure after water quenching from various austenitizing temperatures after heating 1½ hr. Picral etch. X100. Area reduced approximately 45 pct for reproduction.

the 90 min treatments is shown by the micrographs in Fig. 4. Since the plates treated at 1500°F for 1½ hr did not reach furnace temperature, another group of plates was heat treated at 1500°F for 8 hr. The austenitic grain size, after such a treatment, was very similar to the one shown for the 1600°F treatment in Fig. 4. This was a mixture of large and small grains.

The austenitic grain-coarsening temperature of this steel is about 1600°F. Both coarse and fine grains were found in the plate heated 1½ hr at this temperature. Heating for 8 hr at 1600°F produced uniformly coarse austenite grains.

The four methods of cooling used to give different cooling rates and thus produce different ferrite grain sizes varied from air-blast cooling to furnace cooling. The air-blast cooling was done by placing the plates, still separated by the refractory brick splits, in front of a large electric fan, thus cooling the plates in circulating air. Still-air cooling, done in a similar way but without the fan, produced a somewhat slower cooling rate. The third method consisted of burying the plates in vermiculite. This produced a faster cooling rate than that resulting from furnace cooling. The last and slowest cooling rate was produced by furnace cooling. Typical cooling curves are shown in Fig. 5.

Microstructure

The ferrite grain sizes of the heat-treated steels were determined by counting the number of ferrite grains in a 4 sq in. area of a micrograph taken at 100 diam, dividing by four. The counts of longitudinal and transverse direction were in good agreement, as shown in Table II. In addition to changing the ferrite grain size, the heat treatments change the pearlite distribution and spacing. The pearlite distribution was measured by counting the patches of pearlite in the same areas used for the ferrite grain-size counts. This count was also divided by four to give pearlite areas per square inch at 100 diam, as shown in Table III. Pearlite spacing was not determined quantitatively, but microscopic examination of the specimens indicated a variation in spacing with the different cooling rates. The spacing was wider for slower cooling rates.

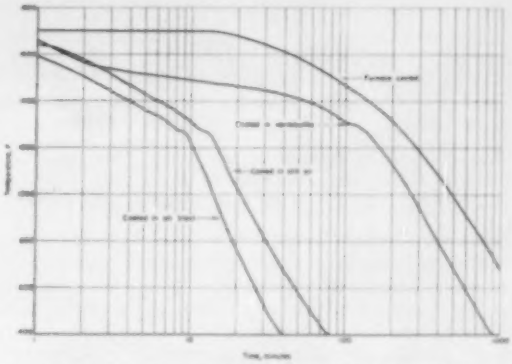

Fig. 5—Cooling curves of plate austenitized at 1700°F.

Table II. Ferrite Grain Sizes of Specimens of Project Steel "A" Plate Heated at Various Temperatures and Cooled at Various Rates to Room Temperature

Austenitizing Temperature, °F	Type of Cooling	Ferrite Grain Size, Grains per Sq In. at X100		
		Longitudinal	Transverse	Average
	Furnace Time: 1½ Hr			
1500	Air blast	90	96	93
1500	Still air	139	108	123
1500	Vermiculite	82	82	82
1500	Furnace	82	98	90
1600	Air blast	126	131	128
1600	Still air	98	100	99
1600	Vermiculite	57	45	51
1600	Furnace	56	62	59
1700	Air blast	114	139	126
1700	Still air	87	84	85
1700	Vermiculite	45	36	42
1700	Furnace	28	37	31
1800	Air blast	60	64	62
1800	Still air	51	46	48
1800	Vermiculite	21	23	22
1800	Furnace	18	20	19
1900	Air blast	52	61	56
1900	Still air	45	47	46
1900	Vermiculite	26	22	24
1900	Furnace	18	21	19
	Furnace Time: 8 Hr			
1500	Air blast	100	86	95
1500	Still air	86	77	81
1500	Vermiculite	64	64	64
1500	Furnace	41	44	42

The variations in ferrite grain size and pearlite distribution are shown by the micrographs in Fig. 6. These are longitudinal sections austenitized at 1700°F for 1½ hr. The space between the lamellae in the pearlite increased with slower cooling rates. The size of the ferrite grains increased with decreases in cooling rate. These samples were etched to show the ferrite grain boundaries and pearlite distribution but do not show the lamellae of the pearlite plainly.

The effects of austenitizing temperature and various cooling rates on ferrite grain size and pearlite distribution are shown in Figs. 7 and 8, respectively. The number of pearlitic areas increases as the number of ferrite grains increase, as shown in Tables II and III. Of course, many other changes in microstructure occur when steels are cooled from various temperatures and at various rates. One of the most noticeable changes is in the distance between bands of pearlite; the slower the cooling rate, the wider the bands. This change is accompanied by a variation in the size of the pearlite areas; therefore, one

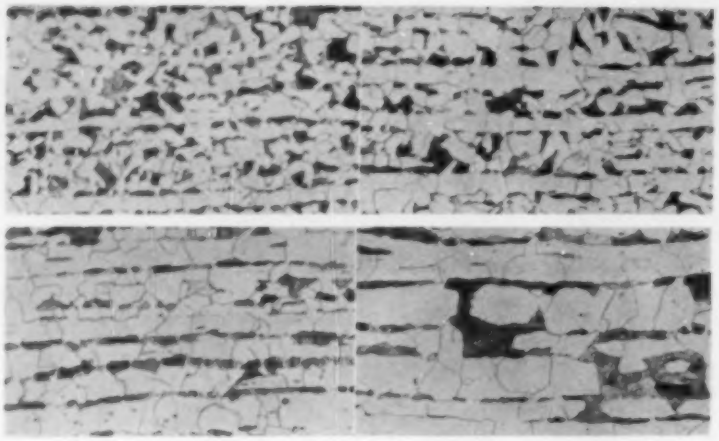

a—Cooled in air blast.

b—Cooled in still air.

c—Cooled in vermiculite.

d—Furnace cooled.

Fig. 6—Microstructure of ¾ in. plates cooled by various methods from an austenitizing temperature of 1700°F. Nital etch. X180. Area reduced approximately 30 pct for reproduction.

characteristic is related to the other. For the purpose of this study, the ferrite grain size and the number of pearlitic areas were used as parameters.

Influence of Heat Treatment on Tear Test Properties

Sufficient material was heat treated to prepare 12 tear test specimens representing each condition. In a few cases, unfortunately, some of the specimens were lost in their preparation. The remaining ones were broken at various temperatures to determine transition temperatures.

As stated earlier, the transition temperature is defined as the highest temperature where 25 pct or more of the specimens are brittle.[1] This is the method recommended by Kahn[1] and was used because of the limited number of specimens from the heat-treated plates available for this study. Additional work in progress at Battelle suggests that there are some advantages in defining tear test transition temperatures on the basis of 50 pct probability of cleavage fracture.

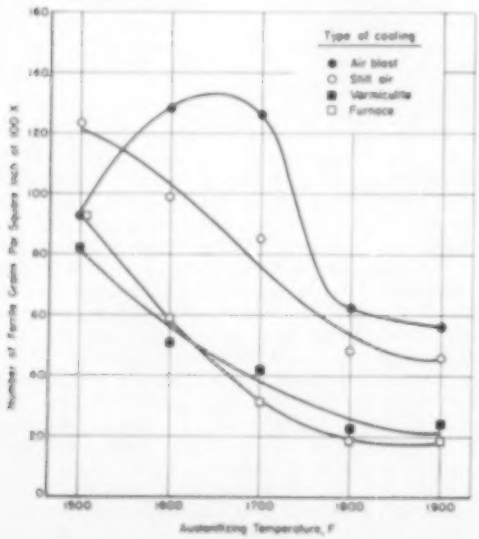

Fig. 7—Effect of austenitizing temperature and cooling rate on ferrite grain size.

A summary of the transition temperatures for the plates heated 1½ hr is shown in Table IV. For the plates heated 8 hr at 1500°F, the transition temperatures are listed in Table V. Fig. 9 shows the influence of austenitizing temperature on the tear test transition temperature of the heat-treated steel.

When the ferrite grain size of the steels is considered, the steels with the coarser, i.e., smaller number of, grains tend to have the higher transition temperatures, as shown in Fig. 10. According to results shown in Fig. 10, the transition temperature decreases 10°F for an increase of 12 grains per 0.01 in. sq area. This effect was the same for all cooling rates.

Heat treatment also affected the maximum load necessary to break the test specimen, the energy absorbed by the specimen before maximum load, and the energy absorbed after the maximum load was reached. Table VI is a summary of these properties. The maximum load was decreased by an increase in austenitizing temperature and slower cooling rates. Since this load is a crude measurement of the ultimate strength and ductility, it is difficult to decide which property was affected most by the heat treatment. A general tendency exists for the amount of energy required to initiate and propagate the fracture to decrease with an increase in austenitizing temperature and a slower cooling rate. These properties are dependent on the maximum load, so therefore should follow the same pattern as maximum load.

Influence on Keyhole Charpy Properties

Four keyhole Charpy specimens representing each heat treatment were broken at each 10°F tempera-

Table III. Pearlite Distribution in Specimens of Project Steel "A" Plate After Heat Treatment

Austenitizing Temperature, °F	Number of Pearlite Areas per Sq In. at X100			
	Cooled in Air Blast	Cooled in Still Air	Cooled in Vermiculite	Furnace Cooled
	Furnace Time: 1½ Hr			
1500	80	64	28	26
1600	48	41	21	25
1700	49	41	18	12
1800	29	25	8	9
1900	27	24	11	8
	Furnace Time: 8 Hr			
1500	48	41	29	18

Table IV. Summary of Tear Test Transition Temperatures of Project Steel "A" Plates Heat Treated in Various Ways

Type of Cooling	Tear Test Transition Temperature, °F* Austenitizing Temperature, °F				
	1500	1600	1700	1800	1900
Air blast	100†	50	80	100	110
Still air	90†	50	80	110	110
Vermiculite	110†	60†	130	130	140
Furnace	70	100	120	130	140

* The tear test transition temperature is defined as being the highest temperature where one or more of four specimens breaks with less than 50 pct of the fracture area exhibiting a dull or fibrous texture.

† Transition temperatures are based on limited data. Only one to three ductile specimens were tested at temperatures 10° higher than the transition temperature reported. These temperatures will not be used in the study.

ture interval throughout the transition range. The specimens were parallel to the direction of rolling and were notched perpendicular to the plate surface. As shown in Fig. 2, the Charpy value at room temperature is well above 25 ft-lb for the as-rolled plate in the longitudinal direction. However, many of the heat treatments reduced the values to approximately 20 ft-lb, far above the transition temperature; therefore, a 12 ft-lb transition value was used. Table VII is a summary of the transition temperatures for the 10, 12, 15, and 20 ft-lb criteria. The Charpy value at 80°F also is shown for comparison.

The effect of austenitizing temperature on the 12 ft-lb transition temperature is shown in Fig. 11. Lowering the temperature from 1900° to 1800°F had no significant effect. The major change in transition temperature, with austenitizing temperature, occurred between 1800° and 1600°F. In most cases, the longer austenitizing time at 1500°F gave a lower transition temperature. The effect of cooling rate appeared to be far more important than austenitizing temperature. As shown in Fig. 5, the major difference in cooling rate was between the plates

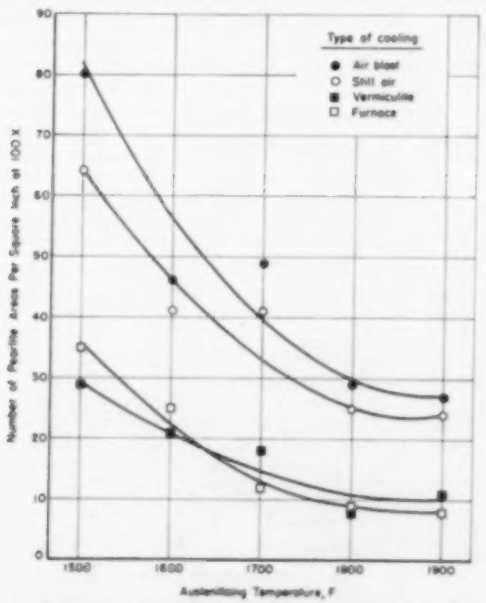

Fig. 8—Effect of austenitizing temperature and cooling rate on distribution of pearlitic areas.

Table V. Summary of Tear Test Transition Temperatures of Project Steel "A" Plates Austenitized at 1500°F for 8 Hr

Type of Cooling	Tear Test Transition* Temperature, °F
Air blast	70
Still air	80
Vermiculite	110
Furnace	100

* The tear test transition temperature is defined as being the highest temperature where one or more of four specimens breaks with less than 50 pct of the fractured area exhibiting a dull or fibrous texture.

cooled in still air and those cooled in vermiculite. This is shown also in Fig. 11 where the major difference in transition temperature was between the plates cooled in air and those cooled in vermiculite.

The relationships between ferrite grain size and Charpy transition temperature are shown in Fig. 12. For plates cooled at equal rates, the transition temperature decreased regularly with grain size. As in the previous discussion, the plates can be considered representative of two significantly different cooling rates. Steels that were cooled fairly rapidly, in still air or by an air blast, showed the same influence of grain size. The Charpy transition temperature decreased about 30°F for an increase of one ASTM number. This value agrees with data reported by previous investigators.[6,7]

The plates cooled slowly in vermiculite or in the furnace behaved approximately alike. The effect of ferrite grain size on the Charpy transition temperature of these steels is less pronounced than for the other groups. The transition temperature decreased only 13°F for each ASTM number in the case of the materials cooled fairly slowly from the austenitizing temperature.

For ferrite grain sizes approximating ASTM No. 6½, the Charpy transition temperature is about 30°F higher for the plates cooled at the slower rate.

The four points shown on the two dashed lines are for the plates heated to 1500°F for 1½ hr. They do not fit the curves for the remainder of the plates. For the same ferrite grain size, the transition temperature was higher than that for plate austenitized 8 hr at the same temperature.

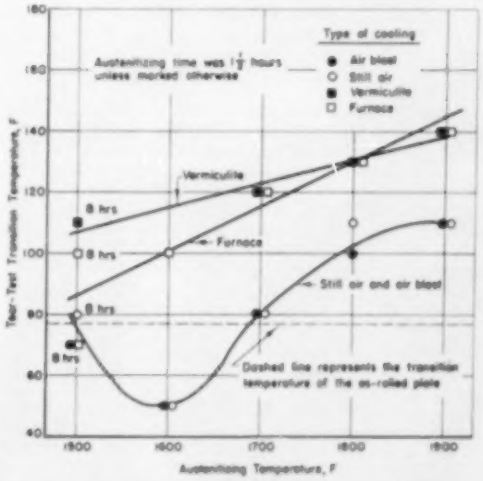

Fig. 9—Effect of austenitizing temperature and cooling rate on tear test transition temperature of project steel "A."

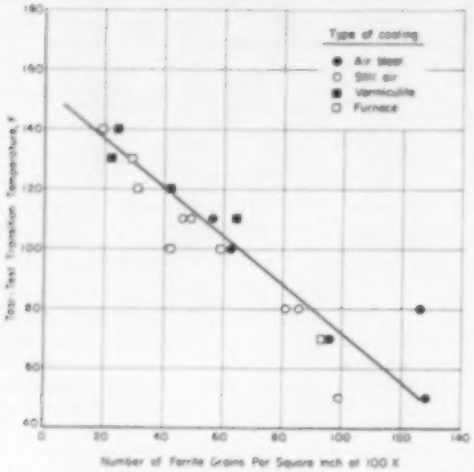

Fig. 10—Effect of ferrite grain size on tear test transition temperature.

Correlation Between Tear Test and Keyhole Charpy Transition Temperatures

It seems natural to expect a correlation between transition temperatures established by different kinds of notched-bar tests. At least, several investigators have suggested formulas for estimating Charpy transition temperatures from data obtained with other notches or at other energy levels. Conversions of this kind can be misleading. Earlier experiments on this project showed that a particular change in nitrogen or manganese content does not have the same effect on the transition temperature in Charpy tests as it does in tear tests. That is, the difference between the two transition temperatures is influenced by chemical composition. The present study shows that the relationship between the transition temperatures of a particular steel is influenced also by microstructure. This conclusion is illustrated by Fig. 13.

Fig. 13 is a correlation chart for transition temperatures determined in the tear test with those set by the 12 ft-lb Charpy level. It shows that specimens cooled relatively rapidly fit a trend line differ-

Table VI. Tear Test Properties of Project Steel "A" After Heat Treatment

Austenitizing Temperature, °F	Type of Cooling	Maximum Load, Lb	Energy to Initiate Fracture, Ft-Lb*	Energy to Propagate Fracture, Ft-Lb*
1500	Air blast	37,480	580†	630†
1500	Still air	36,610	720†	630†
1500	Vermiculite	33,480	730†	700†
1500	Furnace	33,580	690	530
1600	Air blast	37,290	810	650
1600	Still air	36,350	745	550
1600	Vermiculite	32,990	770†	510†
1600	Furnace	31,472	630	560
1700	Air blast	36,025	780	660
1700	Still air	35,235	700	580
1700	Vermiculite	31,390	580	490
1700	Furnace	31,430	600	500
1800	Air blast	35,670	730	645
1800	Still air	31,180	725	660
1800	Vermiculite	31,350	600	490
1800	Furnace	30,580	590	485
1900	Air blast	35,640	690	645
1900	Still air	34,900	770	640
1900	Vermiculite	30,410	540	480
1900	Furnace	29,960	535	470

* Average of the results from the four ductile specimens broken 10°F above the transition temperature.
† Average, based on limited number of tests.

Table VII. Summary of Keyhole Charpy Properties of Project Steel "A" Plates After Various Heat Treatments

Austenitizing Temperature, °F	Type of Cooling	Charpy Value at 80°F	Transition Temperature, °F: 10 Ft-Lb Level	12 Ft-Lb Level	15 Ft-Lb Level	20 Ft-Lb Level
	As-Rolled	26.3	4	10	19	34
	Furnace Time: 1½ Hr					
1500	Air blast	22.8	33	37	43	54
1500	Still air	23.0	24	29	35	51
1500	Vermiculite	13.8	65	71	79	93
1500	Furnace	16.3	63	69	79	95
1600	Air blast	26.5	3	7	12	22
1600	Still air	27.0	2	6	13	29
1600	Vermiculite	16.5	58	64	72	92
1600	Furnace	12.8	69	75	84	102
1700	Air blast	28.5	2	8	15	28
1700	Still air	23.0	19	25	33	47
1700	Vermiculite	15.3	69	76	86	105
1700	Furnace	8.8	77	83	92	108
1800	Air blast	30.0	34	42	54	75
1800	Still air	30.5	39	43	48	72
1800	Vermiculite	7.8	85	88	97	117
1800	Furnace	8.6	87	93	103	122
1900	Air blast	34.5	35	40	48	60
1900	Still air	34.5	33	35	39	55
1900	Vermiculite	9.3	68	87	95	113
1900	Furnace	8.5	87	95	105	126
	Furnace Time: 8 Hr					
1500	Air blast	26.0	10	15	21	32
1500	Still air	26.0	8	12	19	34
1500	Vermiculite	19.8	53	57	65	82
1500	Furnace	11.8	67	74	84	99

ent from that for the plates cooled quite slowly from the same austenitizing temperatures. The graph indicates that changing the rate of cooling can cause a variation of about 35°F in Charpy transition temperature between plates of this steel having the same transition temperature in tear tests. Similarly, two plates having 12 ft-lb Charpy values at the same temperature could perform quite differently in the tear test.

As discussed previously, slow cooling increased the size of the pearlite patches and the spacing of the pearlite bands. Variations in cooling rate had no effect on transition temperatures of tear-test specimens having the same ferrite grain size. This was not true for Charpy specimens. If the slight differences in slopes of the trend lines are neglected, Fig. 13 shows that slow cooling consistently raised the Charpy transition temperature. Therefore, the data show that the Charpy test is more sensitive than the tear test to variations in microstructure other than grain size. The results of these experiments emphasize the dangers of predicting transi-

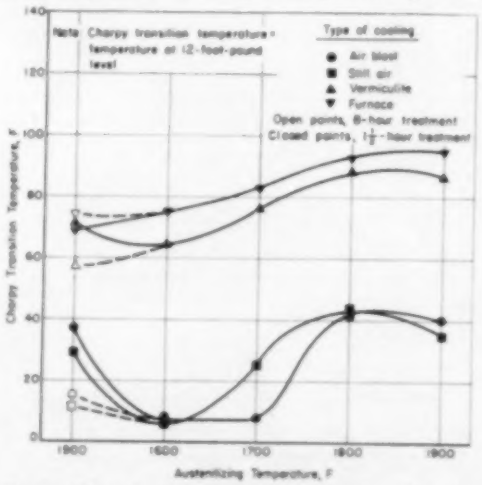

Fig. 11—Effect of austenitizing temperature and cooling rate on Charpy transition temperature of steels cooled by various methods.

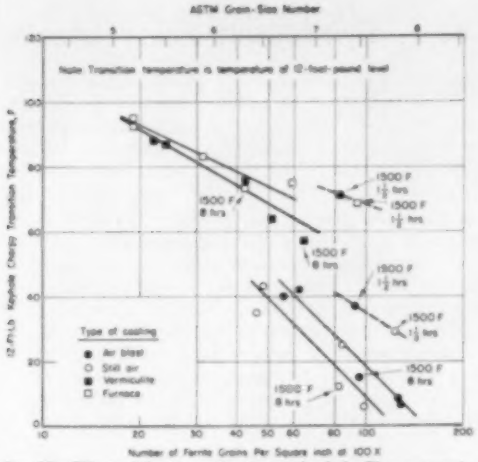

Fig. 12—Effect of ferrite grain size on keyhole Charpy transition temperature of project steel "A" cooled at different rates. The variation in grain size was obtained by using different austenitizing temperatures and cooling rates.

tion temperatures for one type of test from transition temperatures determined in other types of notched-bar tests.

Summary

The results of this work may be summarized as follows:

1—The average ferrite grain size was found to be dependent on the cooling rate as well as on the austenitizing temperature.

2—The number of pearlite areas was also found to be dependent on both the cooling rate and austenitizing temperature.

3—The tear test transition temperature of this steel was found to depend only on the ferrite grain size resulting from various heat treatment. An increase of 12 ferrite grains per square inch of image at X100 corresponds to a decrease of 1°F in transition temperature. This change is the same for all cooling rates. The maximum load and the energy required to start or to propagate fracture decreased by increasing the austenitizing temperature and by decreasing the cooling rate.

4—The keyhole Charpy transition temperature was dependent not only upon the ferrite grain size, but also upon other changes in microstructure caused by differences in cooling rate. The ferrite grain size has the greatest effect on transition temperature on steels cooled rapidly from the austenitic condition. For air-cooled steels, the change is approximately 30°F for each ASTM grain size number.

The number of pearlitic patches was related to the number of ferrite grains; therefore, the Charpy transition temperature was also dependent on the number of pearlitic patches. Other variables in the pearlitic structure were not determined quantitatively.

5—Data obtained in this study illustrate the difficulty of estimating accurately transition temperatures for one type of notched-bar test from data obtained on another kind of specimen. The transition temperatures measured in tear tests and in Charpy tests, on this semikilled steel, were not affected equally by changing the cooling rate from the austenitizing temperature.

Acknowledgment

The opinions expressed herein are those of the authors. They do not necessarily represent those of the Ship Structure Committee, the Bureau of Ships, the Dept. of the Navy, or the Advisory Committees of the National Academy of Sciences, National Research Council.

Discussion of this paper, if any, will appear in JOURNAL OF METALS, November 1955, and in AIME Metals Branch *Transactions*, Vol. **203**, 1955.

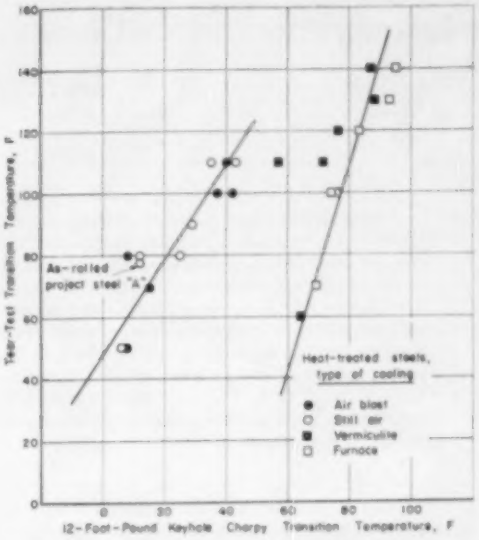

Fig. 13—Comparison between tear test transition temperatures and 12 ft-lb keyhole Charpy transition temperatures of a heat-treated ship plate steel.

References

[1] N. A. Kahn and E. A. Imbembo: A Method of Evaluating Transition From Shear to Cleavage Failure in Ship Plate and Its Correlation With Large Scale Plate Tests. *The Welding Journal* (1948) **27**, No. 4, Research Supplement, pp. 169s-182s.

[2] R. W. Vanderbeck: Evaluating Carbon Plate Steels by the Keyhole Charpy Impact Test. *The Welding Journal* (1951) **30**, No. 1, Research Supplement, pp. 59s-64s.

[3] H. M. Banta, R. H. Frazier, and C. H. Lorig: Some Metallurgical Aspects of Ship Steel Quality. *The Welding Journal* (1951) **30**, No. 2, Research Supplement, pp. 79s-90s.

[4] S. Epstein: Notch Resistance of Carbon-Steel Ship Plate. *Reprint* Philadelphia Regional Meeting, AISI (1951).

[5] J. E. Campbell, R. H. Frazier, and H. O. McIntire: Ferrite-Grain-Size Measurements for Ship Plate Steel. *The Welding Journal* (1952) **31**, No. 2, Research Supplement, pp. 78s-94s.

[6] F. W. Boulger and R. H. Frazier: Some Metallurgical Aspects of Low Temperature Behavior of Metals. Presented, Conference on Materials and Design for Low-Temperature Service, sponsored by the Scientific Council, Engineer Research and Development Laboratories, Fort Belvoir, Va. (May 1952).

[7] J. M. Hodge, R. D. Manning, and H. M. Reichhold: The Effect of Ferrite Grain Size on Notch Toughness. *Trans.* AIME (1949) **185**, pp. 233-240; JOURNAL OF METALS (March 1949).

[8] A. Boodberg, H. E. Davis, E. R. Parker, and G. E. Troxwell: Causes of Cleavage Fracture in Ship Plate—Tests of Wide Notched Plates. *The Welding Journal* (1948) **27**, No. 4, Research Supplement, pp. 186s-199s.

[9] E. P. Klier, F. C. Wagner, and M. Gensamer: The Correlation of Laboratory Tests With Full-Scale Ship Plate Fracture Tests. *The Welding Journal* (1948) **27**, No. 2, Research Supplement, pp. 71s-96s.

Isoembrittlement in Chromium and Molybdenum Alloy Steels During Tempering

by Gopalkrishna Bhat and Joseph F. Libsch

Isoembrittlement curves depicting the influence of time and temperature in the range 800° to 1260°F (425° to 680°C) on the development of embrittlement in a commercial chromium alloy steel and a commercial molybdenum alloy steel are presented. Two distinct regions of embrittlement occur in the chromium alloy steel: 1—at 800° to 1000°F (425° to 540°C) and 2—in the region just below the lower critical temperature. Embrittlement is most pronounced at 800° to 1000°F, decreasing very rapidly with increasing temperature above this region, only to increase again as the lower critical temperature is approached. The data suggest two distinct modes of embrittlement with possible superposition of the two modes at extended embrittling times in the temperature range 1100° to 1150°F (590° to 620°C). While the molybdenum alloy steel shows little susceptibility to embrittlement at 800° to 1000°F (425° to 540°C), considerable embrittlement may occur just below the lower critical temperature.

THE subject of temper embrittlement in alloy steels has received considerable attention in the last few years. Points of view on the mechanism of embrittlement differ, however, resulting in part from the incompleteness of the data developed and in part from the speculation regarding the susceptibility of plain carbon steel to temper embrittlement.

Libsch, Powers, and Bhat[1] carried out short-time embrittling treatments on an AISI 1050 steel and demonstrated that hardened plain carbon steels are quite susceptible to embrittlement when tempered in the range from 850°F (455°C) to the lower critical temperature. The isoembrittlement diagram,[1] representing the embrittling characteristics of this steel, is reproduced in Fig. 1. It is evident from the shape of the curves shown that embrittlement in plain carbon steel increases progressively with both temperature and time in the embrittling range.

A comparison of the isoembrittlement diagram for AISI 1050 steel with that presented by Jaffe and Buffum[2] for an SAE 3140 steel shows that up to 930°F (500°C) the isoembrittlement characteristics of the plain carbon steel are similar to those of SAE 3140 steel, although the embrittlement is much more severe in the latter steel. Above 930°F (500°C), the rate of embrittlement in the plain carbon steel increases continuously with increasing temperature; whereas, in the SAE 3140 steel, the embrittlement rapidly decreases.

The influence of alloying elements upon embrittlement during tempering thus appears to cause a decrease in embrittlement above the region of maximum embrittlement, i.e., 850° to 1000°F. The question naturally arises as to what effect individual alloying elements have upon the embrittling characteristics of the plain carbon steel.

Current knowledge on the influence of alloying elements on temper brittleness may be found in the review papers of Hollomon[3] and Woodfine.[4] Hollomon,[3] from the results of other investigators, has shown that, in general, the amount of embrittlement increases with increasing alloy content (except for molybdenum and possibly tungsten and columbium). Jaffe and Buffum,[2] by a comparison of the embrittlement in a plain carbon steel with that of a SAE 3140 steel postulated that the presence of alloying elements in moderate amounts tends to retard the development of temper brittleness.

It is difficult to determine what effect chromium has upon temper brittleness, since most of the information available has been based on the combined effect of other elements with chromium, particularly nickel and manganese. However, Wilten,[5] and recently Jolivet and Vidal,[7] Vidal,[8] and Woodfine[4] have reported that chromium steels are temper brittle, that the embrittlement is reversible with a maximum rate of embrittlement at approximately 975°F (525°C),[8] and that the susceptibility increases with increasing amounts of chromium.[7] Taber, Thorlin, and Wallace[10] have found a large embrittling effect with increasing chromium content in a medium C-Mn-Ni steel. But Hultgren and Chang,[11] from their experiments conducted on synthetically prepared ternary Fe-C-Cr alloys, could not conclude that these alloys are susceptible to temper embrittlement. However, on addition of manganese or phosphorus, these Fe-C-Cr alloys became susceptible, from which fact they concluded that the embrittlement developed in chromium-bearing Fe-C alloys is due chiefly to the presence of these elements.

Considerable data are available to show that molybdenum decreases the susceptibility of steel to temper embrittlement. However, its effectiveness in preventing or decreasing embrittlement appears limited to its presence in small amounts. Vidal[8] has shown that a plain 2 pct Mo steel was susceptible. Hultgren and Chang[11] also have shown that molybdenum additions in excess of 2 pct to synthetically prepared Ni-Cr steels did not prevent embrittlement. Jolivet and Vidal[7] and Lea and Arnold[12] found that molybdenum reduced temper brittleness. Lea and Arnold further stated that molybdenum decreased the rate of embrittlement rather than the total amount of embrittlement, whereas Preece and Carter[13] have shown that the presence of molybdenum greatly reduces the equilibrium extent of the change at a given temperature but does not appear to influence the rate of embrittlement. There appears to be very little information as to how molybdenum by itself affects the temper brittleness susceptibility of a plain carbon steel.

G. BHAT is Graduate Student and Research Associate, Lehigh University, and J. F. LIBSCH, Member AIME, is Professor of Metallurgy, Lehigh University, Bethlehem, and Consulting Metallurgist, Lepel High Frequency Laboratories Inc., New York.

Discussion of this paper, TP 3957E, may be sent, 2 copies, to AIME by Apr. 1, 1955. Manuscript, Aug. 2, 1954. Chicago Meeting, February 1955.

It is evident from the literature that several aspects of the brittleness occurring during tempering of steel, particularly the influence of the common alloying elements on the nature of the embrittling reaction, need clarification. It further appears that isoembrittlement diagrams based upon the newer concept of an unembrittled state[1] and extension of the embrittlement studies to higher temperatures and shorter times may be helpful in understanding the true behavior of the alloying elements.

It is the object of this investigation, therefore, to study the kinetics of the embrittling reaction in a chromium (AISI 5140) and a molybdenum (AISI 4047) steel and to construct isoembrittlement diagrams for comparison with the isoembrittlement diagram for the plain carbon steel.

Experimental Details

Material: The steel stock received for this investigation was in the form of ⅝ in. hot-rolled rounds. Both steels were prepared in the basic open hearth furnace and were aluminum-killed heats. The chemical analyses of the steels are given in Table I. The lower critical temperatures were determined by metallographic analysis of specimens, induction tempered at 20°F intervals. The details of the austenitizing treatment and results on the two heats studied are recorded in Table II.

Preliminary Treatment: All hardened specimens were first tempered by induction heating at 1260°F (680°) for 5 sec. This treatment was designed to minimize the hardness differential in isothermally embrittled specimens. Since it also provided the minimum transition temperature observed in each steel (Tables III and IV), it was considered to represent the essentially unembrittled state and used as a basis for comparison for all subsequent embrittling treatments. Actual treatment was accomplished with a high frequency converter operating at a frequency of approximately 300,000 cycles per second. In order to insure uniform heating of the specimen, a coil that provided a relatively loose coupling was used. Specimens were heated at a rate of approximately 200°F (110°C) per second, maintained at temperature for 5 sec, and quenched immediately upon completion of the heating cycle by means of a spray quench arrangement surrounding the load coil. Temperature control was achieved by percussion welding the individual wires of a chromel-alumel thermocouple to the specimen at its midpoint and connecting them to a high speed recorder controller. This preliminary tempering treatment provided a uniformly tempered martensitic structure and the tempered hardness for both steels is recorded in Table II.

Table I. Chemical Composition of the Steels Used in this Investigation

	Carbon	Manganese	Sulphur	Phosphorus	Silicon	Nickel	Chromium	Molybdenum
AISI 5140	0.45	0.77	0.013	0.015	0.35	—	0.72	—
AISI 4047	0.48	0.83	0.015	0.019	0.26	0.14	0.13	0.25

Table II. Details of Hardening and Preliminary Tempering Treatment

	Hardening Treatment, °F, Oil Quench	Grain Size, ASTM No.	Hardness, Rc	Tempering Temperature, °F, 5 Sec Induction	Tempered Hardness, Rc
AISI 5140	1540, 1 hr	7	60	1260	38.5
AISI 4047	1500, ½ hr	7	59	1260	38.5

Isothermal Embrittling Treatment: Subsequent to the preliminary heat treatment, specimens were divided into a number of series and embrittled in the range from 800°F (425°C) to the vicinity of the lower critical temperature for the steel in question, for periods varying from 5 sec to 100 hr, as indicated in Tables III and IV, respectively, for AISI 5140 and 4047 steel. All specimens were water quenched from the embrittling temperature.

Testing Procedure: The embrittled specimens were machined into standard *V*-notched Charpy specimens. Impact tests were conducted over a range of temperatures to develop the transition from ductile to brittle-type failure. Testing temperatures higher than room temperature were obtained by immersing the specimens in hot water, while the low temperatures were secured by dry ice-alcohol or alcohol-liquid nitrogen mixtures. The specimens were held at the required testing temperatures for not less than 5 min to attain equilibrium. They were then transferred to the anvil of a 264 ft-lb impact ma-

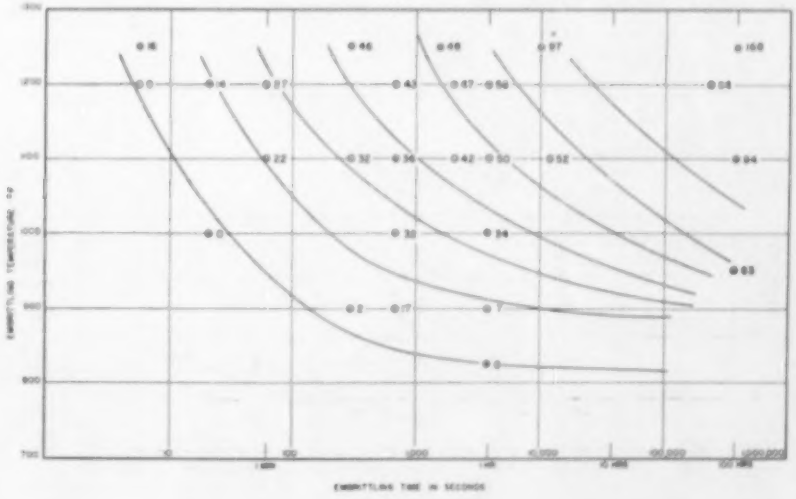

Fig. 1—Isoembrittlement curves for AISI 1050 steel. Figures beside points represent the increase in transition temperatures (°F) from the unembrittled condition. Data of Libsch, Powers, and Bhat.[1]

Table III. Heat Treatment, Transition Temperatures, and Hardness Values for Specimens of AISI 5140 Steel Isothermally Embrittled

Series No.	Embrittlement Temperature, °F	Time	Hardness, Rc	Transition Temperature, °F a*	b**	c†
1	1260	5 sec	38.5	−38	−80	−80
2	1260	5 min	31.5 to 32.5	−20	−74	−64
3	1260	1 hr	26.5 to 27	−24	−76	−62
4	1260	5 hr	21 to 22	0	−46	−46
5	1260	24 hr	15.5 to 16.5	22	−26	−6
6	1260	100 hr	10	74	4	0
7	1200	1 hr	29.5	−24	−70	−56
8	1200	5 hr	22.5 to 23.5	−8	−54	−24
9	1200	24 hr	20.5	14	−40	−16
10	1100	5 min	35.5 to 36.5	8	−34	−27
11	1100	1 hr	33 to 33.5	12	−28	−40
12	1100	5 hr	30 to 30.5	−6	−46	−34
13	1100	24 hr	25 to 26	−10	−44	−32
14	1100	100 hr	21.5	8	−40	−18
15	1000	1 min	38	−12	−46	−46
16	1000	5 min	35.5 to 37	4	−44	—
17	1000	1 hr	35 to 36.5	50	4	−40
18	1000	5 hr	34.5	70	14	0
19	1000	24 hr	29.5 to 30.5	58	10	18
20	1000	100 hr	29 to 29.5	30	−12	0
21	900	5 min	37 to 38.5	−15	−72	—
22	900	1 hr	37.5 to 38	+20	−32	−38
23	900	5 hr	37 to 38	85	12	−4
24	900	100 hr	34.5	170	94	74
25	800	1 hr	38	−16	−66	—
26	800	24 hr	37 to 38	−2	−32	−38
27	800	100 hr	36 to 37	56	18	0

* a: lowest temperature at which fracture is 100 pct fibrous.
** b: temperature at 50 pct fibrous fracture.
† c: temperature at ½ maximum impact energy level where the fracture observed is still 100 pct fibrous.

Table IV. Heat Treatment, Transition Temperatures, and Hardness for Specimens of AISI 4047 Steel Isothermally Embrittled

Series No.	Embrittlement Temperature, °F	Time	Hardness, Rc	Transition Temperature, °F a*	b**	c†
1	1360	5 sec	38.5	−94	−122	−122
2	1360	5 min	28 to 29	−62	−92	−82
3	1360	1 hr	26.5 to 27.5	−34	−78	−54
4	1360	10 hr	21	−10	−60	−44
5	1360	100 hr	13.5 to 14.5	48	−10	—
6	1200	5 sec	36	−98	−124	−130
7	1200	5 min	32	−70	−106	−96
8	1200	30 min	31.5 to 32	−70	−102	−100
9	1200	1 hr	29 to 30.5	−50	−80	−72
10	1200	5 hr	27 to 28	−40	−84	−60
11	1200	100 hr	20	14	−30	−14
12	1100	1 min	33.5	−80	−106	−83
13	1100	1 hr	32	−60	−104	−100
14	1100	3 hr	31.5	−60	−92	−84
15	1100	10 hr	28.5	−58	−78	−68
16	1100	100 hr	21.5 to 22.5	−16	−56	−44
17	1000	1 min	36 to 37	−78	−106	−114
18	1000	5 min	36.5	−70	−92	—
19	1000	1 hr	36	−66	−98	−90
20	1000	5 hr	35	−78	−100	−94
21	1000	10 hr	33.5 to 33.5	−62	−102	−96
22	1000	100 hr	33.0	−50	−88	−80
23	950	10 hr	35.0	−66	−100	−110
24	950	50 hr	34.5	−72	−110	−110
25	900	1 min	38.5	−86	−104	−110
26	900	1 hr	36.5	−72	−100	−84
27	900	10 hr	34.5 to 35.5	−60	−102	−92
28	900	28 hr	34.5 to 35	−60	−100	−98
29	900	100 hr	33.5 to 33	−70	−110	−110
30	800	1 hr	37.5 to 38.5	−80	−112	−108
31	800	12 hr	34.5 to 35.5	−74	−108	−104
32	800	100 hr	34 to 35	−70	−104	−88

* a: lowest temperature at which fracture is 100 pct fibrous.
** b: temperature at 50 pct fibrous fracture.
† c: temperature at ½ maximum impact energy level where the fracture observed is still 100 pct fibrous.

chine, having a striking velocity of 16.5 ft per sec, and broken immediately.

From the data of the impact test, curves representing the transition from ductile to brittle-type failure were plotted for each of the series. The percentage of fibrous fracture was obtained by actual measurements on each of the broken specimens.

Results: Included in Tables III and IV are the transition temperatures and Rockwell hardness values obtained for each of the embrittling treatments. Typical plots of energy absorbed in breaking and percentage of fibrous fracture vs testing temperature are presented in Fig. 2. Three separate criteria were considered to represent transition temperature. These criteria included 1—the lowest testing temperature at which the fracture observed was 100 pct fibrous, 2—the temperature where the fracture observed was 50 pct fibrous, and 3—the temperature at one-half of the maximum impact energy level obtained for completely fibrous fractures. The transition temperatures based on the foregoing three criteria were read from the transition curves developed for all embrittling treatments and are assembled in Tables III and IV. The actual transition curves developed for all the embrittled series have been presented in unpublished reports.[15,16]

While the absolute values of the transition temperature vary with the criteria used in determination, the trend appears generally consistent with all criteria. In plotting the isoembrittlement diagram, however, the transition temperature criterion used was based on the lowest testing temperature at which fracture was still 100 pct fibrous. This was done to effect a direct comparison of the results of this work with previously published work on an SAE 3140 steel.[2]

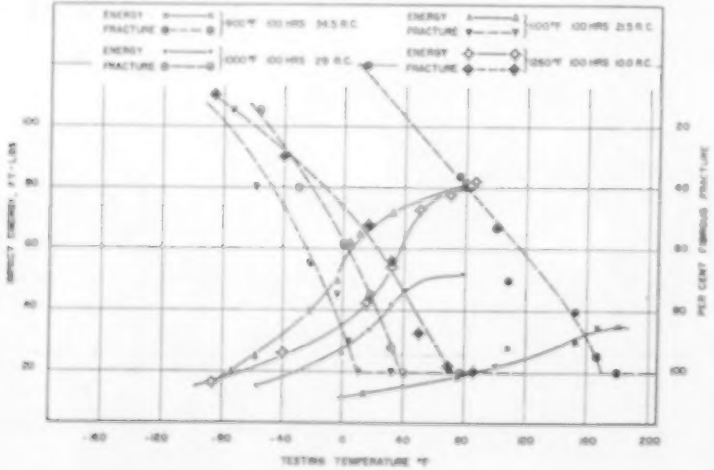

Fig. 2—Typical Charpy impact energy and fracture appearance vs testing temperature curves for AISI 5140 steel.

decreases with time. Higher temperature, i.e., sary, to consider the total embrittlement during

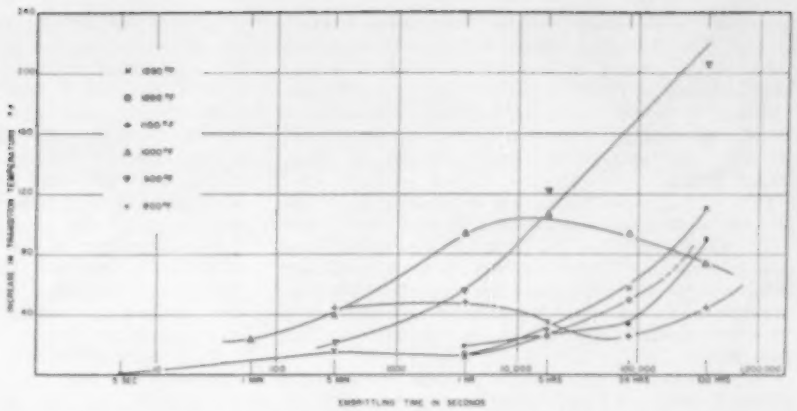

Fig. 3—Increase in transition temperature vs embrittling time for various embrittling temperatures, AISI 5140 steel.

In Fig. 3 the difference in transition temperature between an unembrittled series and the embrittled series for the AISI 5140 steel is plotted as a function of the embrittling time for each of the embrittling temperatures used. Fig. 4 represents a similar plot for the AISI 4047 steel. Using the information from Figs. 3 and 4, the isothermal embrittlement characteristics of the AISI 5140 and 4047 steel are presented in Figs. 5 and 6, respectively. The curves given represent equal degrees of embrittlement developed by various combinations of tempering temperature and time. Since the transition temperature determined for the specimens considered unembrittled was used as a basis in constructing Figs. 5 and 6, it is apparent that the curves given also represent the increase in transition temperature caused by various embrittling temperatures and times. The actual increase in transition temperature represented by each curve is shown in the boxes at the top of the figures.

Discussion of Results

Effect of Chromium: A study of the isoembrittlement diagram presented for the AISI 5140 steel (Fig. 5) leads to the following observations:

1—The embrittlement characteristics of the chromium alloy steel are markedly different from those observed in the plain carbon steel.

2—In the chromium steel, two distinct regions of severe embrittlement occur: one associated with embrittling temperatures in the region 800° to 1000°F (425° to 540°C), and the other with temperatures just below the lower critical.

3—Embrittlement decreases very rapidly as the temperature is increased above the region 800° to 1000°F (425° to 540°C). This behavior is similar to that observed by Jaffe and Buffum[4] in an SAE 3140 steel. The extent of embrittlement at 900°F (480°C) is particularly severe. Embrittlement at 1000°F (540°C) may develop in a matter of a minute.

4—The embrittlement occurring below the lower critical temperature is similar in nature to that observed in a plain carbon steel (Fig. 1). The embrittling reaction progresses with increase of both time and temperature. However, the rate, as well as the extent of embrittlement, appears to be slightly retarded in this region by the addition of chromium.

5—At extended times the course of embrittlement at 1100°F (590°C) appears to be influenced by the superposition of the two modes of embrittlement occurring just below the critical temperature and in the temperature range 800° to 1000°F (425° to 540°C).

A study of the increase in transition temperature with embrittling time at constant embrittling temperatures of 1000° (540°) and 1100°F (590°C) is also enlightening (Fig. 3). While the embrittlement occurring at 1000°F (540°C) is initially rapid, it

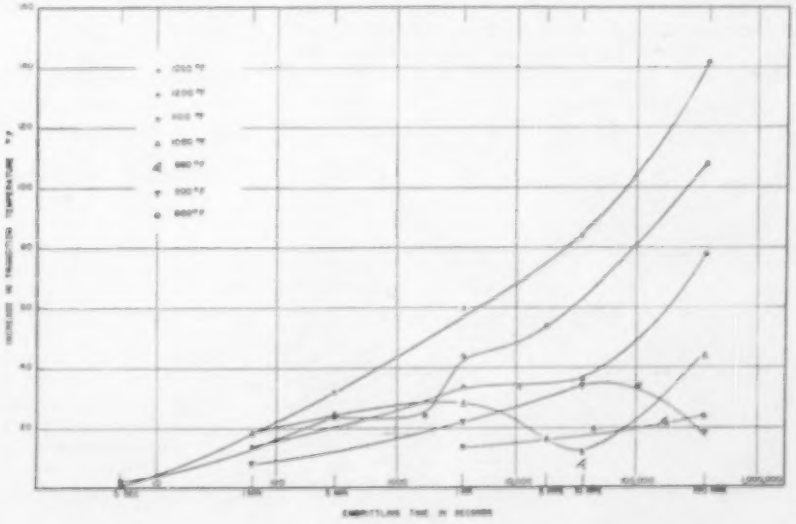

Fig. 4—Increase in transition temperature vs embrittling time for various embrittling temperatures, AISI 4047 steel.

decreases with time. Higher temperature, i.e., 1100°F (590°C), has a similar but more pronounced effect in decreasing embrittlement at short times. Longer times at 1100°F (590°C), however, initiate a change in behavior, i.e., an increase in embrittlement, presumably as the result of the superposition of the high temperature embrittlement at these longer times.

Effect of Molybdenum: An examination of the isoembrittlement diagram for the AISI 4047 steel (Fig. 6) shows that, in general, the embrittling characteristics of the molybdenum alloy steel are similar to those for the plain carbon steel. The embrittlement in this steel increases rather uniformly with temperature and time up to the lower critical temperature.

Molybdenum in the amount present causes little embrittlement in the temperature range 800° to 1000°F (425° to 540°C). However, molybdenum only slightly retards the development of embrittlement shown by the plain carbon steel just below the lower critical temperature.

A study of Fig. 4, representing the increase in transition temperature with embrittling time at constant embrittling temperatures, illustrates a behavior not at once clear in the isoembrittlement diagram. Each of the curves representing embrittlement at 900° (480°), 1000° (540°), 1100° (590°), and 1200°F (650°C) indicates irregular behavior, i.e., a decrease in embrittlement with time (900°F), followed by an increase in embrittlement at longer times (1000°, 1100°, and 1200°F). The increase in embrittlement occurs at shorter times as the embrittling temperature is raised. This behavior is represented on the isoembrittlement diagram by the data included in the dashed lines. Although the magnitude of the change in embrittlement is smaller in the molybdenum alloy steel, it again appears that two embrittling mechanisms superimpose.

General Discussion

A consideration of the results presented in this paper for the AISI 5140 and 4047 steels, as well as the embrittling characteristics for an AISI 3140 steel,[9] a 1050 steel,[1] and a high manganese steel with and without boron[10] indicates that two distinct regions of embrittlement may occur during tempering: 1—in the region of 800° to 1000°F (425° to 540°C) and 2—in the region just below the lower critical temperature. Since at long embrittling times the two regions of maximum embrittlement may superimpose, it appears desirable, as well as necessary, to consider the total embrittlement during tempering in the range 800° to 1260°F (425° to 680°C) and not to isolate the specific embrittlement at 800° to 1000°F (425° to 540°C) as a separate phenomenon designated as temper brittleness. In this connection, it appears that two different mechanisms of embrittlement may occur during tempering between 800° and 1260°F (425° to 680°C). An attempt to identify these mechanisms is now underway.

A comparison of the embrittling characteristics of the chromium and molybdenum alloy steels with the plain carbon steel shows that alloying elements may have a pronounced influence on the course of embrittlement during tempering from 800° to 1260°F (425° to 680°C). Thus, chromium increases markedly the rate and extent of embrittlement at 900°F (480°C). Results for a Ni-Cr alloy steel by Jaffe and Buffum,[9] as well as the results of Powers and Carlson for a manganese and Mn-B steel,[10] show similar behavior. The severe embrittlement caused by the presence of the alloying elements (except molybdenum) at 900°F (480°C) decreases rapidly with an increase of temperature to 1100° to 1150°F (590° to 620°C). As the lower critical temperature is approached, however, embrittlement proceeds in the alloy steels in a manner similar to that for a plain carbon steel. Apparently the alloying elements, chromium and molybdenum, have a retarding influence on the embrittlement just below the lower critical temperature.

The irregular influence of temperature upon the embrittling characteristics in alloy steels points out a distinct danger in attempting to determine the specific influence of each alloying element from tests at a single embrittling temperature. This appears especially significant when the very rapid decrease which may take place in embrittlement with increasing temperature is recognized.

The data presented also continue to leave doubt concerning the validity of securing an essentially unembrittled state for comparison with embrittled specimens by heating just below the lower critical temperature and quenching prior to isothermal embrittling treatments. It appears quite possible that this method may not only fail to attain an unembrittled state, but further, that the high temperature tempering treatment may influence the subsequent development of embrittlement at 900° to 1000°F (480° to 540°C).

It is interesting to note from the data on AISI 5140 steel that an attempt to relate the hardness and

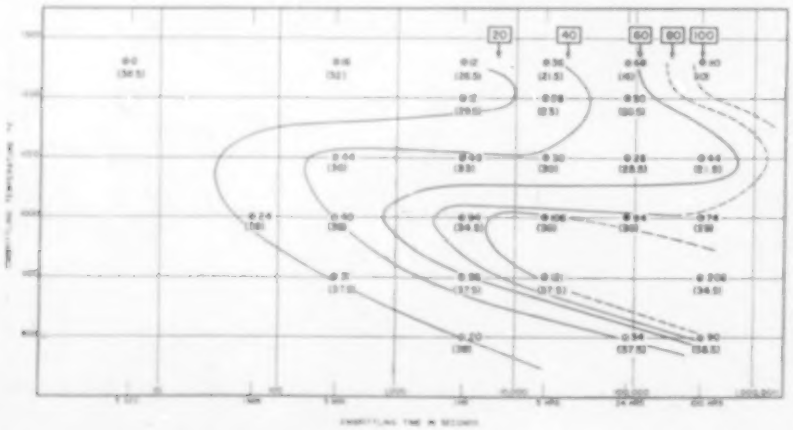

Fig. 5—Isoembrittlement curves for AISI 5140 steel. Figures beside points represent increase in transition temperatures (°F) based on transition temperatures of specimens tempered at 1260°F for 5 sec. Figures in parentheses are the average hardness of the specimens in that series.

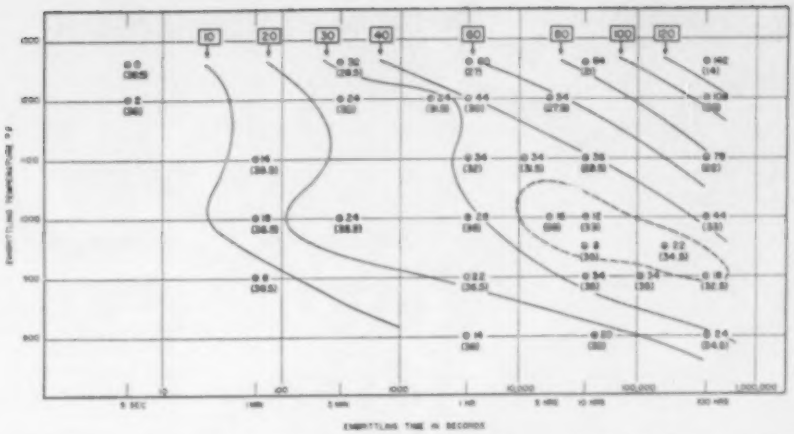

Fig. 6—Isoembrittlement curves for AISI 4047 steel. Figures beside points represent increase in transition temperature (°F) based on transition temperatures of specimens tempered at 1260°F for 5 sec. Figures in parentheses are the average hardness of the specimens in that series.

transition temperature at long times leads to results opposite from those proposed by Woodfine[9] in an analysis of the data presented earlier for the plain carbon steel. It appears, therefore, that the transition temperature is related to a basic variable causing embrittlement which may or may not be related to hardness.

Summary

1—Isoembrittlement diagrams for an AISI 5140 and 4047 steel are presented.

2—The diagram for the molybdenum alloy steel resembles that of the plain carbon steel, while that for the chromium alloy steel is strikingly different.

3—A study of these diagrams shows that the presence of alloying elements may define two distinct regions of embrittlement, one at 800° to 1000°F (425° to 540°C) and another in the temperature range just below the lower critical.

4—Chromium appears to cause a pronounced increase in the rate and extent of embrittlement at 800° to 1000°F (425° to 540°C). Molybdenum has little influence in this range.

5—The embrittlement caused by chromium at 900°F (480°C) decreases very rapidly with a small increase in temperature.

6—Both molybdenum and chromium appear to retard the development of embrittlement just below the lower critical temperature when compared to a plain carbon steel.

7—At extended embrittling times, the embrittlement occurring at temperatures of 1100° to 1150°F (590° to 620°C) may be influenced by the superposition of the high and low temperature modes of embrittlement. Experimental work attempting to determine the influence of alloying elements should, therefore, consider embrittlement over the entire tempering range.

Acknowledgments

The authors wish to acknowledge the financial support provided by the Ordnance Dept., United States Army, and Watertown Arsenal to conduct the experimental work reported. Special thanks are extended to Dr. L. D. Jaffe for his critical review. The authors also wish to express their appreciation to the Lepel High Frequency Laboratories Inc. for the use of the induction heating equipment necessary for the work and to the Bethlehem Steel Co., particularly Mr. John Horvath, for supplying the steel and aiding in the preparation of specimens.

Discussion of this paper, if any, will appear in JOURNAL OF METALS, November 1955, and in AIME Metals Branch *Transactions*, Vol. **203**, 1955.

References

[1] J. F. Libsch, A. E. Powers, and G. Bhat: Temper Embrittlement of Plain Carbon Steels. *Trans.* ASM (1952) **44**, p. 1058.

[2] L. D. Jaffe and D. C. Buffum: Isothermal Temper Embrittlement. *Trans.* ASM (1950) **42**, p. 604.

[3] J. H. Hollomon: Temper Brittleness. *Trans.* ASM (1946) **36**, p. 473-540.

[4] B. C. Woodfine: Temper Brittleness: A Critical Review of the Literature. *Journal* Iron and Steel Institute (1953) **173**, Part 3, p. 229.

[5] L. D. Jaffe and D. C. Buffum: Temper Brittleness of Plain Carbon Steels. *Trans.* AIME (1949) **185**, p. 513; JOURNAL OF METALS (August 1949).

[6] H. M. Wilten: Correlation of Failures from Embrittlement of 4 to 6 Per Cent Chromium Steel with the Notched Bar Impact Test. *Trans.* ASM (1935) **23**, pp. 915-967.

[7] H. Jolivet and G. Vidal: Value of the Resilience Test for the Study of Temper Brittleness. *Revue de Metallurgie* (1944) **41**, pp. 378-388, 403-408.

[8] G. Vidal: Temper Brittleness of Chromium, Molybdenum and Tungsten Steels. *Revue de Metallurgie* (1945) **42**, pp. 149-155.

[9] B. C. Woodfine: Some Aspects of Temper Brittleness. *Journal* Iron and Steel Institute (1953) **173**, Part 3, p. 240.

[10] A. P. Taber: J. F. Thorlin, and J. F. Wallace: Influence of Composition on Temper Brittleness in Alloy Steels. *Trans.* ASM (1950) **42**, pp. 1033-1055.

[11] R. Hultgren and J. C. Chang: Effect of Chemical Composition on Susceptibility of Steels to Temper Brittleness. *Preprint No. 26*, ASM (1953).

[12] R. Hultgren and J. C. Chang: Investigation on the Temper Brittleness of Steels—Effect of Chemical Composition. *Final Report*, University of California, Berkley, Calif.

[13] F. C. Lea and R. N. Arnold: The Embrittlement of Alloy Steels. *Proceedings* Institute of Mechanical Engineers, London (1935) **131**, pp. 539-602.

[14] A. Preece and R. D. Carter: Temper Brittleness in High Purity Iron-Base Alloys. *Journal* Iron and Steel Institute (1953) **173**, Part 4, pp. 387-398.

[15] U. G. Bhat and J. F. Libsch: Isothermal Embrittlement of AISI 5140 Steel. Third Partial Report on Temper Brittleness in Steel. *Report No. 801/6-17* (November 1953) Lehigh Institute of Research, Bethlehem.

[16] U. G. Bhat and J. F. Libsch: Isothermal Embrittlement of AISI 4047 Steel. Second Partial Report on Temper Brittleness in Steel. *Report No. 801/6-12* (August 1953) Lehigh Institute of Research, Bethlehem.

[17] A. E. Powers and R. G. Carlson: The Effect of Boron on Notch Toughness and Temper Embrittlement. *Preprint No. 21* ASM (1953).

Oxidation of Cobalt Metal

by R. E. Carter and F. D. Richardson
(With an Addendum by C. Wagner)

By means of inert markers of radio-platinum, it has been shown that cobalt metal oxidizes by outward diffusion of cobalt atoms through the oxide. Oxidation rates have been measured at various temperatures and oxygen pressures and have been found to agree with the rates calculated from the Wagner equation and the authors' values for the diffusion coefficient of cobalt in the oxide. The distribution of radio-cobalt in growing oxide layers has been accurately measured and found to be different from that predicted from the Wagner oxidation theory. Attempts have been made to measure the change of lattice parameter of the oxide with composition.

SEVERAL investigators have shown that cobalt metal oxidizes according to the parabolic law,[1-3] but no detailed study has been made of the oxidation mechanism. Cobaltous oxide has a metal-deficient lattice, but the defect concentration which is dependent on the oxygen pressure is only approximately known.[1] From the similarities in the structures of "CoO" and "FeO" and the rate laws governing the oxidation of cobalt and iron, Gulbransen[2] has suggested that cobalt, like iron,[3] oxidizes by diffusion of cobaltous ions through the oxide layer. To substantiate this hypothesis, he has attempted to measure the oxidation rate of cobalt as a function of the oxygen pressure but has been able to report only that the rate depends on a "small" power of the pressure. On the other hand, Preece,[4] Valensi,[5] and Arkharov[6] all have suggested from indirect evidence that oxygen diffuses through the CoO to the metal-oxide interface.

The present authors, in a previous paper,[4] have shown that the rate of diffusion of cobalt in cobaltous oxide is dependent on the oxygen pressure. In that investigation, they also found that cobaltous oxide disks made by complete oxidation of cobalt metal were porous at their centers (Fig. 5L, ref. 4). Both these facts strongly suggest that oxidation of the metal proceeds via outward diffusion of cations. In order to establish the mechanism unequivocally, oxidation experiments were made with inert radioactive platinum markers, and the dependence of oxidation rate on oxygen pressure was measured. In addition, an attempt was made to determine the form of the cation vacancy gradient, which the marker experiment showed must exist across a growing oxide layer. This was done by depositing radioactive Co^{60} on the surface of a cobalt disk and then measuring the tracer distribution across the oxide layer produced by partial oxidation of the metal. Finally, an X-ray examination was made in an attempt to find the expected change of lattice parameter of CoO with oxygen pressure.

R. E. CARTER, Junior Member AIME, formerly Graduate Student, Nuffield Research Group in Extraction Metallurgy, Royal School of Mines, London, England, is associated with Mines Branch, Dept. of Mines and Technical Surveys, Ottawa, Ont., Canada. F. D. RICHARDSON, Member AIME, is Director of the Nuffield Research Group in Extraction Metallurgy, Royal School of Mines, London, England, and C. WAGNER, Member AIME, is Visiting Professor, Dept. of Metallurgy, Massachusetts Institute of Technology, Cambridge, Mass.

Discussion of this paper, TP 3942E, may be sent, 2 copies, to AIME by Apr. 1, 1955. Manuscript, June 7, 1954. Chicago Meeting, February 1955.

Experimental

The apparatus and materials used were substantially the same as those previously described by the authors.[4]

Marker Studies: The use of inert markers to follow oxidation reactions was first attempted by Pfeil[7] in 1929, and radioactive markers have recently been used by Davies et al.[8] In the investigation reported here, the markers were applied as an $(NH_4)_2PtCl_6$ slurry in several thin streaks across both faces of four disks of cobalt metal 1 mm thick and 14 mm in diameter. The disks were then oxidized almost to completion at 1200°C in pure oxygen. After oxidation, they were mounted and sectioned and autoradiographs were taken to locate the markers.

Oxidation Rate: The oxidation rate of cobalt was measured at 1148°C at oxygen pressures ranging from 0.0055 to 1.0 atm and at 1000°, 1148°, and 1350°C under 1 atm of oxygen. The rate was deter-

Table I. Oxidation Rate (Parabolic) Constant of Cobalt Metal

No.	Temperature, °C	Oxygen Pressure, Atm	Oxidation Time, Hr	Gas Flow at Standard Temperature and Pressure Ml per Min	Attack Constant G θ; Cm^{-4} $Sec^{-1/2}$ x 10^{5}
C-5	1148	1.0	6.2	450	3.05
C-6	1148	0.18	24.4	460	2.24
C-3	1148	0.0065	23.3	610	1.48
C-2	1000	1.0	31.0	450	1.56
C-25	1350	1.0	2.83	300	8.85

mined by weighing cobalt disks before and after oxidation and by measuring the thicknesses of the oxide layers on sectioned disks with a microscope.

Tracer Distribution in Growing Oxide: Four disks of cobalt metal, 1 mm thick, were coated on one side each with very thin layers of Co^{m} which was deposited by evaporation. The disks then were oxidized in pure oxygen at 1150°C. Afterwards they were mounted in "lucite" and the concentration distribution of the tracer in the oxide determined by grinding off thin parallel sections from the active faces. The grinding was continued to within 0.005 cm of the metal-oxide interface at which point the oxide layer began to break up. The total thickness of oxide was measured with a calibrated microscope after the disks had been sectioned and polished normal to the oxide film. The tracer distribution was found both by counting the activity in each thin section and by counting the residual β activity after removing each section.

X-Ray Studies: X-Ray photographs were taken of cobaltous oxide prepared at 1150°C under oxygen pressures of 1.0, 0.006, and 0.00136 atm and quenched as in the previously described composition studies.[4] To obtain the greatest possible lattice change, one specimen, an oxide made under 0.005 atm of oxygen, was compacted with cobalt filings and heated under "oxygen-free" nitrogen for 64 hr at 1150°C.

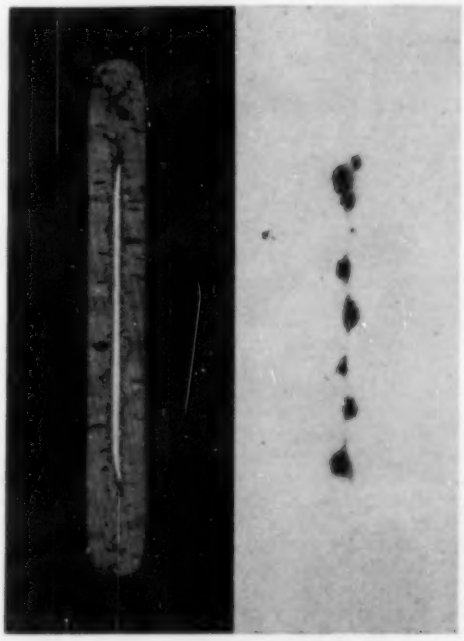

a b

Fig. 1—Comparison of a sectioned oxidation specimen (a) and its autoradiograph (b) showing the Pt^{197} markers concentrated along the metal-oxide interfaces. X6.0.

The Debye-Scherrer photographs were taken on a 19 cm camera of the Bradley-Jay type with CoKα radiation, $K\alpha_{av}$ = 1.79015Å, $K\alpha_1$ = 1.78890Å, and $K\alpha_2$ = 1.79278Å. Each photograph was taken with the same camera under exactly the same conditions, the temperature of the camera being measured during the exposure. The photographs were not as sharp as might be expected for a simple cubic structure, but doublets could be measured above a Bragg angle of 44°. Because of line width, the lines in the back-reflection region could not be measured with an accuracy better than ±0.005 cm. This uncertainty, which was larger than any other, determined the accuracy of the results. The usual Nelson and Riley extrapolation was made on the ten lines above a Bragg angle of 42°.

Results and Discussion

Marker Studies: One of the four sectioned disks and its autoradiograph are shown side by side in Fig. 1. It is clear that the radio-platinum markers are situated at the metal-oxide interface. This proves conclusively that cation diffusion is the principal, if not the only, mechanism operating during the oxidation of cobalt.

Since platinum and cobalt form a complete range of solid solution, the platinum may be considered not to be a truly inert marker. Because the rate of diffusion of platinum into cobalt metal would, however, be expected to be much slower than the rate of oxidation of cobalt metal, particularly during the initial stages of oxidation, there appears to be little chance for alloying to have occurred. The possibility of alloying is further reduced by the tendency of the $(NH_4)_2PtCl_6$ to form small balls of metal during decomposition rather than to form a thin continuous film. That alloying is not significant is indicated by an examination of Fig. 1 where the radioactive areas are separated by the thin streak of residual cobalt metal, the edges of the active areas next to the metal being flat and parallel to the plane of the cobalt.

Oxidation Rate: Since a number of investigators have shown that cobalt oxidizes by the parabolic law, the oxidation rates shown in Table I are reported in terms of the parabolic attack constant K_p, defined by the equation

$$\frac{W}{A} = K_p t^{1/2} \qquad [1]$$

where W is the grams of oxygen added, A is the area, and t is the oxidation time. The constants given are the mean of the values obtained both by weighing the disks and measuring the thicknesses of the oxide layers. Agreement from disk to disk and method to method was better than ±15 pct.

The oxidation rate at 1 atm of oxygen was well within the limits of the rates found by Chauvenet,[8] Johns and Baldwin,[10] and Dunn[9] (Fig. 2). The results of both Johns and Baldwin and of Dunn were obtained in air; they were corrected to 1 atm of oxygen on the assumption of an average oxygen pressure exponential of 0.30.

The oxidation rate at 1148°C is shown as a function of oxygen pressure in Fig. 3. The rate was proportional to the 0.29 power of the oxygen pressure, which is in close agreement with value of 0.30 for the diffusion rate, and thus consistent with the finding that the oxidation of cobalt occurs by diffusion of the cobalt ions through the oxide as demanded by Wagner's[11] theory of metal oxidation.

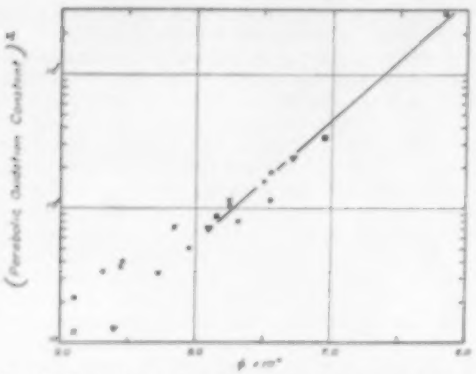

Fig. 2—The oxidation rate of cobalt metal at an oxygen pressure of 1 atm as a function of the absolute temperature. X represents data of Dunn and Welkins;[2] closed circle, Chauvenet;[3] inverted triangle, Johns and Baldwin;[10] and closed square, this investigation. The constant plotted is expressed in (mgm of oxygen per sq cm)^2 per hr.

Since the diffusion coefficient of cobalt in CoO has been measured as a function of oxygen pressure,[4] it is possible to test Wagner's equations[11] by calculating the oxidation rate of cobalt metal and comparing it with the experimentally determined rate.

On the assumption that oxidation of cobalt occurs only by cation diffusion across the oxide film to the gas-oxide interface, Wagner's rate equation may be expressed in the form

$$K_r = |Z_v| c_v \int_{a'_v}^{a''_v} \frac{Z_i}{Z_v} D \, d\ln a_v \qquad [2]$$

where K_r is the rational rate constant, the number of chemical equivalents of oxide formed per second per square centimeter when the oxide layer is 1 cm thick; Z_i, Z_v are the average valency of cobalt and oxygen in the cobaltous oxide; c_v is gram-atoms of oxygen per cubic centimeter of oxide; D is the self-diffusion coefficient of cobalt in CoO; and a_v the activity (or pressure) of oxygen in equilibrium with cobaltous oxide at various points across the layer.

The primed and double-primed quantities refer to the inner and outer surfaces of the growing CoO layer, respectively.

The derivation of this equation involves no assumption about the form of the vacancy concentration gradient across the growing oxide. It demands only that the vacancy concentrations at each interface are constant during growth and that the self-diffusion coefficient at a fixed temperature is proportional to a constant power of the oxygen pressure, i.e., it is independent of changes in the proportion of associated vacancies which may occur as the concentration of vacancies increases. That the diffusion coefficient of CoO is proportional to a constant power of the oxygen pressure has already been shown by the authors to be approximately true.[4]

Table II. Comparison of Measured and Calculated Rate Constants (P_{O_2} = 1 Atm)

No.	Temperature, °C	Calculated Rate Constant Equivalent, O_2 Cm^{-1} Sec^{-1} x 10^6	Calculated Attack Constants, G O_2 Cm^{-2} Sec$^{-1/2}$ x 10^6	Experimental Attack Constants, G O_2 Cm^{-2} Sec$^{-1/2}$ x 10^6	Difference Between Calculated and Experimental, Pct
C-0	1000	1.29	1.60	1.50	6
C-5	1148	5.15	3.35	3.05	10
C-25	1350	31.25	8.26	8.85	7

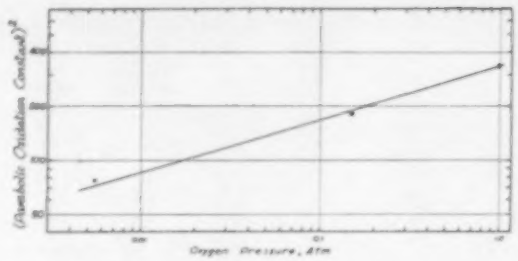

Fig. 3—The parabolic oxidation constant of cobalt as a function of oxygen pressure. The constant plotted is expressed in (mgm of oxygen per sq cm)^2 per hr.

For the oxidation of cobalt the terms of Eq. 2 have the following values:

$Z_v = 2, Z_i = Z_v \times \frac{O}{Co}$ ratio = 2 (within 1 pct), a_v = the oxygen pressure at all points in the oxide, and c_v = 0.086 gram-atoms of oxygen per cubic centimeter of oxide calculated from a lattice density of 6.45 g per cu cm from a lattice parameter of 4.2603A.

Eq. 2 therefore reduces to

$$K_r = 0.396 \int_{a'_v}^{a''_v} D \, d \log Po_2 \qquad [3]$$

where the oxygen pressure over the growing oxide is one integration limit and the dissociation pressure of the CoO to free cobalt metal[10] the other. Eq. 3 was integrated graphically by means of D vs log Po_2 plots calculated from an extrapolation of Fig. 7 of the authors' previous paper.[4] This integration is not sensitive either to the accuracy of the extrapolation or to the dissociation pressure of CoO, because D falls rapidly to relatively small values as the oxygen pressure is decreased.

The parabolic rate constant K_p defined by Eq. 1 and the above rational rate constant K_r are related by the equation

$$K_p^2 = \frac{2 M p f K_r}{z} \qquad [4]$$

where M is the weight of one gram-atom of oxygen = 16, f is the weight fraction of oxygen in the growing oxide layer = 0.2135, p is the density of the oxide layer 6.45 g per cu cm, and z is the valency of the oxygen = 2.

Therefore

$$K_p = 4.68 K_r^{1/2}. \qquad [5]$$

The calculated oxidation rate constants at an oxygen pressure of 1 atm are compared with the experimental constants in Table II. Agreement between the calculated and experimental constants is within the experimental errors of both the diffusion and oxidation measurements. A simpler equation relating the oxidation rate constant and the diffusion coefficient is due to Mott and Gurney.[12] On the assumption that oxidation occurs only by diffusion of cations via a vacancy mechanism through the oxide layer and the vacancy gradient through the oxide is linear, it can be shown that for *divalent* cations

$$K = 3 D_v (f_s - f_\infty) \qquad [6]$$

where K is the parabolic rate constant defined by the equation $dx/dt = K/x$, D_v is the diffusion co-

efficient of vacancies, and f_s, f_m is the defect fraction at the gas-oxide and metal-oxide interfaces, respectively. The diffusion coefficient of the cations (D) at the surface of the oxide is related to the vacancy diffusion coefficient by

$$D = D_v f_v \qquad [7]$$

If the vacancy concentration at the metal-oxide interface is small compared to that at the gas oxide interface, i.e., $(f_s - f_m) = f_s$, Eq. 6 reduces to

$$K = 3\,D. \qquad [8]$$

In Table III the experimental parabolic attack constants are compared with the experimental diffusion coefficients at an oxygen pressure of 1 atm.

The poor agreement of the experimental K/D ratio with the theoretical ratio of 3 suggests that the assumptions underlying Eq. 6 are incorrect. The most obvious weakness (from which the Wagner theory does not suffer) is the assumption of a linear vacancy gradient across the oxide layer.

Distribution of Radio-Cobalt across a Growing Oxide Layer: The inadequacy of the Mott and Gurney relationship between the diffusion coefficient and the parabolic oxidation constant strongly suggests that the vacancy gradient across a growing CoO layer may not be linear as is usually supposed. A knowledge of the gradient is, however, important to any theory of metal oxidation. To date this problem has been the subject of only three investigations.

Bardeen, Brattain, and Shockley[14] have developed the following expression (Eq. 9) giving the distribution, in a growing oxide layer with univalent cations, of a tracer, which was present initially as an infinitely thin layer on the surface of the metal to be oxidized:

$$c_{(x,t)} = \frac{A}{t^{1/2}} \left(\frac{x}{X}\right)^2 e^{-\frac{\alpha^2}{x}} \qquad [9]$$

where A is a constant, $c_{(x,t)}$ is the concentration of tracer in the growing oxide layer, t is the oxidation time, and X is the thickness of the oxide layer at time t.

The assumptions in their treatment were that 1—Oxidation and diffusion occur only by motion of cations into vacant lattice sites. 2—The concentration of vacant sites varies linearly between the limiting concentrations n_m and n_s at the oxide-metal and oxide-gas interfaces, respectively. No account was taken of the possible association of vacant cation sites and defect electrons or of any change of association with concentration.

Bardeen et al. tested Eq. 9 by one experiment. They plated a thin layer of Cu^{64} on one face of a copper block which was oxidized in air at 1000°C for 18 min and at 500°C for 3 min. Four successive layers of oxide were then removed by etching with nitric acid, the thickness of each layer being determined by reweighing the specimen. Each layer removed was analysed for Cu^{64} by precipitation of the copper as copper sulphide which was then spread on a filter paper and wrapped around a Geiger tube. They found that the fraction of Cu^{64} in each layer agreed closely with the fractional area under equivalent sections of their predicted concentration-distance curve.*

* Sample 1 in their Table III runs from Z = 0.87 to 1.00, not 0.77 to 1.00 as printed. Sample 2 correspondingly from 0.50 to 0.87.

This problem has also been examined by Moore and Selikson.[15] These investigators plated Cu^{64} on copper blanks, which they then partially oxidized to Cu_2O. After oxidation, they etched off thin layers of Cu_2O from the active faces and analyzed each section. The resulting log concentration vs x^2 plot was a straight line. Such a straight-line plot, if it is assumed that diffusion in Cu_2O occurs via a vacancy mechanism, suggests that no vacancy gradient exists across a growing Cu_2O film, and this appears to be unreasonable from present knowledge of metal oxidation. Earlier, Castellan and Moore[16] had measured the diffusion rate of copper in Cu_2O, using a similar technique. The diffusion coefficients which they calculated from their results varied only slightly from layer to layer and generally decreased as the metal surface was approached. None of their six disks gave a linear log c vs x^2 plot, though five gave curves which are slightly concave downward.

Table III. Comparison of Self-Diffusion Coefficients for CoO and Parabolic Oxidation Rate Constants of Cobalt Metal in 1 Atm O_2

No.	Temperature, °C	Experimental D, $Cm^2\ Sec^{-1}$ x 10^9	Experimental K, $Cm^2\ Sec^{-1}$ x 10^9	K/D
C-2	1000	2.55	6.4	2.50
C-9	1148	9.5	24.6	2.59
C-25	1350	51	193	3.78

In view of the differences between these results and because the grinding technique used here was considered to be more accurate than the previously used etching techniques, the distribution of Co^{60} in growing layers of CoO was studied. Four experiments were made and the results are shown in Fig. 4. Although agreement between duplicate experiments was good, a stationary distribution was not reached even after 15.53 hr, when approximately 75 pct of the metal had been oxidized. Furthermore, the deviation from the distribution forecast by the Wagner equation increased with the length of the oxidation period. Throughout this work, there could have been no significant evaporation of the Co^{60}, since activity was never detected in either the exit gases or on the inside of the furnace tube at the end of the investigation.

The distribution of tracer in one of the 15.53 hr specimens is also shown as curve A in Fig. 5. The other curves show the distributions, which can be calculated for the same quantity of Co^{60}, on the basis

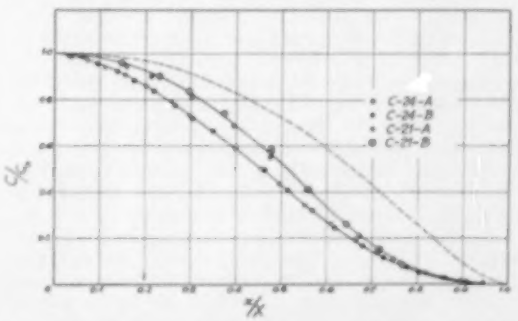

Fig. 4—Distributions of Co^{60} (initially a very thin layer on the cobalt blank) obtained in four specimens oxidized at 1150°C at 1 atm O_2, compared with that calculated from Eq. 25 in Wagner's Addendum. Specimen C-24-A oxide 0.0658 cm thick; C-24-B, 0.0675 cm; both after 15.53 hr; C-21-A, 0.0300 cm; C-21-B, 0.0306 cm after 4.00 hr. Broken line represents Wagner equation. Concentration of tracer is C_0 at gas-oxide interface and thickness of oxide is X.

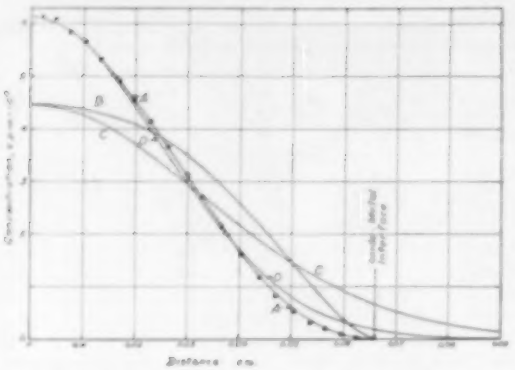

Fig. 5—The distribution of Co^{60} across the layer of cobalt oxide growing from the cobalt metal in oxygen at 1 atm pressure at 1150°C. Curve *A* is experimental specimen C-24-A; curve *B*, from Eq. 25 in Wagner's Addendum; curve *C*, Eq. 2, ref. 4, *Dt*, 5.6×10^{-4} sq cm; curve *D*, Eq. 2, ref. 4, $Dt = 3.04 \times 10^{-4}$ sq cm.

of various assumptions. Curve *B* was calculated directly from the equation for the tracer distribution in a growing oxide with divalent cations, as developed by Dr. C. Wagner in the Addendum to this paper. Curve *C* was calculated from Eq. 2 of the authors' previous paper[4] (diffusion of an infinitely thin source into a semi-infinite cylinder) by assuming that all of the oxide was in equilibrium with 1 atm of oxygen at 1150°C (i.e., all the oxide had the same composition as at the gas-oxide interface) and the diffusion coefficient had the correspondingly constant value of 1.0×10^{-6} sq cm sec^{-1}. For curve *D*, again calculated from Eq. 2 ref. 4, the diffusion coefficient was taken as constant and equal to 0.54×10^{-6} sq cm sec^{-1}, this value being chosen, as it makes the surface concentration equal to that found experimentally (curve *A*).

In Fig. 6 the same data are represented on a semi-log plot, which has the advantages of reducing the distributions with constant diffusion coefficients to straight lines and of expanding the curves near the metal-oxide interface.

An examination of Figs. 5 and 6 reveal that: 1—The tracer diffused into the growing oxide much more slowly than simple theory demands. 2—The tracer diffuses much more slowly than into a uniform oxide in equilibrium with the oxygen pressure obtaining at the gas-oxide interface. 3—The tracer distribution in the growing oxide agrees closely with that given by a constant diffusion coefficient for approximately two-thirds of the oxide thickness, and then falls towards zero at the oxide-metal interface. 4—Near the gas-oxide interface, the slope of the experimental log concentration vs x^2 plot is about twice that for the distribution calculated by the Wagner equation and about twice that for an oxide in equilibrium with the gas phase.

These results suggest that, contrary to the development of Wagner (see Addendum), the diffusion coefficient across the growing layer does not vary linearly with distance. A very short distance from the gas-oxide interface, the diffusion coefficient appears to be about half that for an oxide in equilibrium with the oxidizing atmosphere. The coefficient then remains constant for about two-thirds of the way across the oxide layer; and near the metal oxide interface, it falls towards the value in equilibrium with the metal, although this indeed may never be reached. The conclusion that, for most of the way across the oxide layer the diffusion coefficient is approximately constant, is in general agreement with the results obtained with copper oxide by Moore and Selikson[18] and Castellan and Moore.[19]

The vacancy concentration would be expected to be directly proportional to the diffusion coefficient. It thus seems that the concentration of vacancies at, or immediately beneath, the gas-oxide interface is always substantially less than the equilibrium value. This is a condition which could arise if, for example, the rate of adding oxygen atoms to the oxide at the gas-oxide interface were slow compared with the rate of diffusion of cobalt atoms in the body of the oxide. This, however, is not a satisfactory explanation, because the Wagner equation for oxidation (Eq. 3) given previously gives the correct rate when the integration of Eq. 3 is carried between the two *equilibrium* limits for Po_2. The rate constants, which can be calculated if the higher Po_2 limit is reduced to the value theoretically in equilibrium with oxide having a diffusion coefficient of 0.54×10^{-6} sq cm sec^{-1} (corresponding to curve *D* and Po_2 10^{-1}), are only about half those found experimentally. The authors are unable to explain why the Wagner equation should hold for the oxidation rate but not for the distribution of tracer in the growing layer.

Measurements of Lattice Parameter: The results are shown in Table IV, and they all lie within ±0.0005Å (the expected experimental error) of the average. The oxygen pressure had no effect on the measured parameters in specimens quenched to below red heat in 15 sec. Since, as the authors have already shown,[4] the O:Co ratio changes from about 1.002 to 1.008 at 1150°C when the oxygen pressure is increased from 0.005 to 1.0 atm, a change in lattice parameter is to be expected. By analogy with FeO, this should be about 0.0026Å.

It appears almost certain that the reason why no change could be detected in the quenched specimens is that the excess oxygen was precipitated as Co_3O_4 on cooling. As Fig. 7 shows, a second phase, which may well be Co_3O_4, appears in quenched specimens of CoO produced at relatively high oxygen pressures.

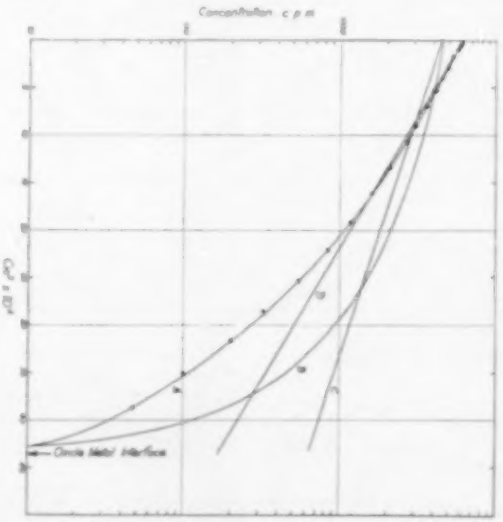

Fig. 6—Log concentration vs (distance)^2 plot of the curves shown in Fig. 5.

Fig. 7—Cobaltous oxide after prolonged heating at 1250°C in air and quenching. X450. Area reduced approximately 20 pct for reproduction.

This precipitation and subsequent straining of the lattice may also explain the slightly diffuse X-ray diffraction patterns obtained. The decomposition of CoO appears to be faster than FeO, and measurement of the change in lattice parameter therefore requires a high temperature X-ray camera.

In support of this hypothesis, the CoO in contact with cobalt metal was always single phased. The concentration of the second phase, which first appeared in the oxide film approximately one-quarter of the distance from the metal to the gas interfaces, increased as the gas-oxide interface was approached.

The lattice parameters listed in Table IV are slightly higher than those reported in the older literature, but they are in excellent agreement with the value of 4.2596Å recently reported by Cooper[11] for CoO prepared by decomposing cobaltous carbonate under "oxygen-free" nitrogen at 500°C.

The foregoing results in no way support the findings of Arkharov and Graevskei.[7] These investigators report lattice parameters from 4.2548 to 4.2508Å at the air and metal interfaces, respectively, of a CoO layer formed on a thick cobalt blank in 4 hr at 1175°C and then cooled in still air. The large difference of 0.005 to 0.01Å between their lattice parameters and those found during this investigation is at least ten times the expected error. In addition, their results suggest a vacancy gradient from the metal to the gas interface, thus indicating oxygen diffusion during oxidation in complete disagreement with the findings of this work. The criticism can be made, however, that Arkharov and Graevskei, using a back-reflection technique, measured only one line compared to the 13 lines measured during this investigation. In addition, their film to specimen distance was only half that used here.

Table IV. Lattice Parameter of Cobaltous Oxide Prepared at 1150°C

Specimen No.	Oxygen Pressure During Oxidation, Atm	Subsequent Treatment	Lattice Parameter,* A
C-4	0.0055	1150°C, P_{O_2} = 1.0, 18 hr	4.2601
C-4-A	0.0055	1150°C, compacted with cobalt filings, N_2, 64 hr	4.2598
5	0.00136	none	4.2604
5	0.00136	none	4.2601
6	1.00	none	4.2604
6	1.00	none	4.2604
7	1.00	none	4.2606
7	1.00	none	4.2606
8	0.006	none	4.2602

* Average = 4.2603 ± 0.0005Å.

Conclusions

The oxidation of cobalt metal occurs almost entirely, if not completely, by cation diffusion across the growing oxide film.

At 1148°C, the oxidation rate of cobalt metal is proportional to the 0.29 power of the oxygen pressure.

Close agreement between the measured and calculated oxidation rates of cobalt has shown that Wagner's oxidation equation holds for cobalt metal.

Measurements of the distribution of radio-cobalt in a growing layer of cobaltous oxide disagree with the distribution which can be calculated from the Wagner theory of oxidation. This therefore appears to be inadequate in certain respects.

From the distribution measurements, it appears that the concentration of vacancies varies in a complex manner across a growing oxide layer.

The lattice parameter of *quenched* cobaltous oxide (4.2603Å) does not change with oxygen pressure obtaining at the high temperatures at which it is prepared because of rapid precipitation of the excess oxygen, probably as Co_3O_4, during cooling.

Addendum

by C. Wagner

The distribution of a radioactive tracer in a growing oxide layer on cobalt may be derived by modifying the equation derived by Bardeen, Brattain, and Shockley[12] for an oxide with univalent cations on the assumption of ideal behavior of cation vacancies and electron holes. This latter restriction, however, may easily be avoided by using more general equations. For prevalent electronic conduction, the transport rate of metal ions per unit cross-section is given by[13]

$$\frac{\dot{n}_i}{A} = -D_i^* \, c_i \frac{d \ln a_{Me}}{dx} \qquad [1]$$

where D_i^* is the (local) self-diffusion coefficient of the metal ions, c_i their concentration in mol per cu cm, a_{Me} the local activity of the metal Me, and x the distance from the metal-oxide interface. The equation involves the assumption that migration takes place only via vacant or interstitial sites and that cations on regular lattice sites do not exchange their positions.

It can be assumed that the self-diffusion coefficient as a function of a_{Me} is given by the empirical or theoretical relation

$$D_i^* = D_i^{*(m)} a_{Me}^{-m} \qquad [2]$$

where m is a constant, the activity of pure metal a_{Me} prevailing at the metal-oxide interface is taken as unity, and $D_i^{*(m)}$ is the self-diffusion coefficient for $a_{Me} = 1$. Carter and Richardson[4] have indeed shown that for CoO the diffusion coefficient is proportional to $(P_{O_2})^{1/6}$ and hence virtually proportional to $(a_{Co})^{-0.5}$.

Substitution of Eq. 2 in Eq. 1, and integration, gives

$$\int_0^x \frac{\dot{n}_i}{A} dx = -\int_1^{a_{Me}} \frac{D_i^{*(m)} c_i}{a_{Me}^{-m-1}} da_{Me}. \qquad [3]$$

Since $\dot{n}_i/A$ and c_i are essentially constant if deviations from the ideal stoichiometric ratio are small, Eq. 3 becomes

$$\frac{\dot{n}_i}{A} x = \frac{D_i^{*(m)} c_i}{m} \left[a_{Me}^{-m} - 1 \right] \qquad [4]$$

whence

$$a_{x=0} = 1 + \frac{\dot{n}_i\, m}{A\, D_i^{*(0)}\, c_i}\, x \cdot \qquad [5]$$

Substitution of Eq. 5 in Eq. 2 yields

$$D_i^*(x) = D_i^{*(0)} \left[1 + \frac{\dot{n}_i\, m}{A\, c_i\, D_i^{*(0)}}\, x \right] \cdot \qquad [6]$$

Hence, if Eqs. 1 and 2 hold and electronic conduction prevails, the self-diffusion coefficient D_i^* of the metal ions is a linear function of distance x regardless of other more special assumptions.

If

$$z = x/X \qquad [7]$$

where X is the thickness of the oxide layer at a given time, Eq. 6 may be rewritten as

$$D_i^* = D_i^{*(x)} [\alpha' + z(1-\alpha')] \qquad [8]$$

where $D_i^{*(x)}$ is the self-diffusion coefficient in the oxide layer next to the outer surface ($x = X$) and

$$\alpha' = D_i^{*(0)}/D_i^{*(x)}. \qquad [9]$$

Letting $x = X$ in Eq. 4, dividing through by X, and using Eq. 2, the following is obtained

$$\frac{\dot{n}_i}{A} = \frac{c_i}{mX} \left[D_i^{*(x)} - D_i^{*(0)} \right] \cdot \qquad [10]$$

According to Bardeen, Brattain, and Shockley,[11] the drift velocity of V of the metal ions with respect to the anion sublattice is equal to the increase in thickness of the oxide layer per unit time. From Eq. 10 it follows that

$$V = \frac{dX}{dt} = \frac{1}{c_i}\frac{\dot{n}_i}{A} = \frac{1}{mX}\left[D_i^{*(x)} - D_i^{*(0)} \right] \qquad [11]$$

$$= \frac{1}{mX} D_i^{*(x)} (1-\alpha').$$

Upon integration of Eq. 11 with respect to time t, it follows that

$$\tfrac{1}{2}X^2 = \frac{1}{m} D_i^{*(x)} (1-\alpha')t \qquad [12]$$

whence

$$\frac{D_i^{*(x)}}{X^2} = \frac{m}{2(1-\alpha')t} \cdot \qquad [13]$$

The rate of change of the concentration c of radioactive tracer with time t is, according to Bardeen, Brattain, and Shockley, Eq. 15.

$$\left(\frac{\partial c}{\partial t}\right)_x = -\frac{\partial}{\partial x}\left[-D_i^* \frac{\partial c}{\partial x} + Vc \right] \cdot \qquad [14]$$

Substitution of Eqs. 7, 8, and 11 in Eq. 14 yields

$$\left(\frac{\partial c}{\partial t}\right)_z = \frac{D_i^{*(x)}}{X^2}$$

$$\frac{\partial}{\partial z}\left\{ [\alpha' + (1-\alpha')z] \frac{\partial c}{\partial z} - \frac{1-\alpha'}{m} c \right\} \qquad [15]$$

According to Eq. 18 of the paper by Bardeen, Brattain, and Shockley, the author lets

$$c = \frac{g(z)}{\sqrt{t}} \qquad [16]$$

whereupon, in view of Eqs. 7 and 12

$$\left(\frac{\partial c}{\partial t}\right)_z = -\tfrac{1}{2} g t^{-3/2} - \tfrac{1}{2} z \frac{dg}{dz} t^{-3/2} \qquad [17]$$

which is Eq. 23 of the paper by Bardeen, Brattain, and Shockley. Substitution of Eqs. 17 and 13 in Eq. 15 gives

$$\frac{m}{2(1-\alpha')} \frac{d}{dz}\left\{ [\alpha' + (1-\alpha')z] \frac{dg}{dz} - \frac{1-\alpha'}{m} g \right\}$$

$$+ \tfrac{1}{2}\left(g + z \frac{dg}{dz} \right) = 0 \cdot \qquad [18]$$

Dividing through by $\frac{1}{2}m/(1-\alpha')$, Eq. 18 may be rewritten as

$$\frac{d}{dz}\left\{ [\alpha' + (1-\alpha')z] \frac{dg}{dz} + \frac{(1-\alpha')}{m}(z-1)g \right\}$$

$$= 0 \qquad [19]$$

which is equivalent to Eq. 27 of Bardeen, Brattain, and Shockley.

Assuming that no radioactive tracer leaves the oxide layer and using the boundary conditions formulated by Bardeen, Brattain, and Shockley, integration of Eq. 19 yields

$$g = A \left\{ [\alpha' + (1-\alpha')z]^{\frac{1}{1-\alpha'}} e^{-z} \right\}^{1/m} \cdot \qquad [20]$$

Hence

$$g \cong A (z\, e^{-z})^{1/m} \qquad [21]$$

if $\alpha' << 1$.

For convenience, the following may be substituted

$$A = A' e^{1/m} \qquad [22]$$

whereupon Eq. 21 becomes

$$g \cong A' [z\, e^{(1-z)}]^{1/m}. \qquad [23]$$

In Eq. 23, the expression in brackets is unity for $z = 1$, i.e., at the outer surface of the oxide layer. This normalization makes it easy to compare the calculated distribution function with experimental values.

The equilibrium determining the concentration of cation vacancies in cobalt oxide may be formulated as

$$Co + \square\,(Co^{\cdot\cdot}) + 2Co^{\cdot\cdot\cdot} = 3Co^{\cdot\cdot}. \qquad [24]$$

If the laws of ideal solutions applied, the concentration of cation vacancies and likewise the self-diffusion coefficient of cobalt would be inversely proportional to the third root of the activity of cobalt, i.e., $m = 1/3$.

Actually, the laws of ideal solutions do not hold. According to the experimental results obtained by Carter and Richardson,[7] the self-diffusion coefficient of cobalt is proportional to the 0.3 power of the partial pressure of oxygen molecules, and, therefore, inversely proportional to the 0.6 power of the activity of cobalt. Thus, the empirical value of m in Eq. 2 is 0.6, whereupon Eq. 23 becomes

$$g = A' [z\, e^{(1-z)}]^{1.67}. \qquad [25]$$

Acknowledgments

The authors wish to thank C. B. Alcock for advice and help throughout this work and Dr. C. Wagner for valuable criticisms and for the Addendum. One of the authors is indebted to the National Research Council of Canada for an Overseas Scholarship.

Discussion of this paper, if any, will appear in JOURNAL OF METALS, November 1955, and in AIME Metals Branch *Transactions*, Vol. **203**, 1955.

References

[1] G. Valensi: *J. Metallurgical Italiana* (1950) **3**, p. 77; *Mettaux et Corrosion* (1950) **15**, p. 283.

[2] J. Dunn and F. Weikins: Review of the Oxidation and Scaling of Heated Metals. II. *The Oxidation of Non-Ferrous Metals.* (1936) p. 67. London. H. M. Stationery Office.

[3] E. A. Gulbransen and K. Andrew: *Journal* Electrochemical Society (1951) **98**, p. 241.

[4] R. E. Carter and F. D. Richardson: *Trans.* AIME (1954) **200**, p. 1244; JOURNAL OF METALS (November 1954).

[5] M. Davies, M. Simnad, and C. Birchenall: *Trans.* AIME (1951) **191**, p. 889; JOURNAL OF METALS (October 1951).

[6] A. Preece and G. Lucus: *Journal* Institute of Metals (1952) **81**, p. 219.

[7] V. Arkharov and K. Graevsksi: *Journal of Tech. Phys.* Moscow (1944) **14**, p. 132.

[8] L. B. Pfeil: *Journal* Iron and Steel Institute (1929) **119**, p. 501.

[9] G. Chauvenet: Thesis, University of Caen (1942).

[10] C. Johns and W. Baldwin: *Trans.* AIME (1949) **185**, p. 720; JOURNAL OF METALS (October 1949).

[11] C. Wagner: Diffusion and High Temperature Oxidation of Metals. *Atom Movements.* (1951) p. 153. Cleveland. ASM. *Ztsch. für Physik. Chem.* (1933) **B21**, p. 25.

[12] E. Shibata and J. Mori: *Ztsch. für Physik. Chem.* (1929) **A142**, p. 151.

[13] N. F. Mott and R. W. Gurney: *Electronic Processes in Crystals.* (1948) p. 257. Oxford. Clarendon Press.

[14] J. Bardeen, W. N. Brattain, and W. Shockley: *Journal of Chemical Physics* (1946) **14**, p. 714.

[15] W. J. Moore and B. Selikson: *Journal of Chemical Physics* (1951) **19**, p. 1539.

[16] G. W. Castellan and W. J. Moore: *Journal of Chemical Physics* (1949) **17**, p. 41.

[17] G. Cooper: Ph.D. Thesis, Royal College of Science, Imperial College of Science and Technology, Univ. of London (1951).

Technical Note

Ductility of Vacuum Heat-Treated Molybdenum Wires

by W. E. Few and G. K. Manning

WORK on the effect of vacuum heat treatment of 0.040 in. diam sintered and wrought molybdenum wires has been sponsored by the Office of Naval Research at Battelle for the past several years. An electrical resistance furnace[1] capable of maintaining a vacuum of less than 0.1 micron of mercury at temperatures as high as 4000°F was used for heat treating the wires. Early in the work, it was found that the introduction of a few microns pressure of oxygen into the furnace resulted in a rapid increase in the oxygen content of the wire specimens and the appearance of a discrete oxide phase. Subsequent elimination of the oxygen atmosphere caused the disappearance of the oxide phase. This was used to determine the solid solubility of oxygen in molybdenum over the temperature range of 2000° to 3000°F.[2] It was observed that, with the disappearance of the oxide phase, the wires regained some ductility. Single-phased wires possessed from 5 to as much as 40 pct elongation in 2 in.

Later, attention became centered on determining the cause of this wide range in ductility. Wires containing less than 0.002 pct C, less than 0.0007 pct O, less than 0.0005 pct N, and less than 0.00003 pct H exhibited the erratic ductility noted above. These percentages represent approximately the limit of accuracy of presently available methods of analysis and thus it became apparent that chemical analysis would be of little help in the study.

W. E. FEW and G. K. MANNING, Member AIME, are associated with Battelle Memorial Institute, Columbus, Ohio.

TN 260E. Manuscript, Nov. 30, 1954.

Table I. Effect of Heating Rate and Time at 3800°F on Tensile Properties of Molybdenum Wire

Experiment No.	Heating Time, Min	Time at 3800°F, Hr	Pct Elongation in 2 In.	Pct Reduction in Area	Tensile Strength, 1000 Psi
196	3	1/12	14 to 37	25 to 62	67 to 76
156	3	1/6	36 to 44	62 to 70	60 to 61
196	3	1/4	42 to 49	65 to 73	79 to 81
165	3	1	39 to 49	49 to 76	75 to 78
185	45	1/12	5 to 23	5 to 26	67 to 73
172	45	1	8 to 10	7 to 16	63 to 70
176	45	3	10 to 43	10 to 66	66 to 74
201	45	6	26 to 39	35 to 67	71 to 75
203	45	8	30 to 44	48 to 67	72 to 76
203A*	*	*	29 to 35	40 to 62	78 to 80

* Several wires from experiment No. 203 were reheated to 3800°F in 45 min and held at temperature ¼ hr. These are designated as experiment No. 203A. Note that recovery of ductility was permanent.

A number of possible explanations for the wide range in ductility were suggested during the course of the work. It was first suspected that variations in the grain size of the recrystallized wire specimens might be responsible. Wire from several lots of material was available. One of these lots tended to develop very large grains when recrystallized, the others all developed an ASTM grain size of 3 to 4 when heated above 2700°F. No correlation between grain size and ductility could be found. It was thought that back diffusion of oil from the diffusion pump might cause contamination of the wire, principally with carbon, but when wires were treated without cooling the cold trap in the pumping system,

Table II. The Reversibility of the Heating Rate Effect

Experiment No.	1st Treatment* Heating Time, Min	2nd Treatment* Heating Time, Min	3rd Treatment* Heating Time, Min	Pct Elongation in 2 in.	Pct Reduction in Area	Tensile Strength, 1000 Psi
166A	15	—	—	5 to 15	5 to 19	56 to 71
166B	15	3	—	41 to 45	51 to 68	77
166C	15	2	15	1 to 12	6 to 12	46 to 69
167	2	—	—	42 to 60	60 to 69	43 to 72
167A	2	45	—	2 to 13	3 to 15	24 to 49
168	45	—	—	9 to 26	20 to 30	42 to 47
168A	45	3	—	23 to 39	30 to 39	51 to 72
169	90	—	—	9 to 15	12 to 20	62 to 67
169B	90	3	—	34 to 42	40 to 72	72 to 74
170	180	—	—	9 to 13	11 to 17	65 to 69
170B	180	3	—	39 to 47	41 to 61	71 to 72

* All specimens held at 3800°F 1 hr each time heated.

thus permitting greater than usual back diffusion of pumping oil, it was found that the erratic ductility still persisted.* Other wires were treated in the presence of a few microns of hydrogen and nitrogen without appreciable effect. The presence of a few microns of oxygen pressure in the furnace, of course, caused the wires to become glass brittle, but oxygen pressure in the furnace did not seem to be a complete explanation, since wires treated at the same time showed the full range of ductility. It was hypothesized also that there might be a sharp transition temperature for tensile tests and that this, by chance, was located at about room temperature. Wires were tested over a temperature range of 34° to 180°F. A sharp transition temperature was not observed and small chance variations in testing temperature did not seem to explain the variation in ductility.

* Failure to cool the diffusion pump trap did cause the formation of a thin carbide network in the wire, but even with this network some wire exhibited as much as 35 pct elongation in 2 in.

It was found, eventually, that heating rate had a pronounced influence on the ductility of the wire specimens. In the early experiments most of the samples were heated to 3800°F in about 15 min. It later developed that this approximated a sort of critical rate that frequently led to erratic results. Samples heated more rapidly were ductile; samples heated less rapidly were much less ductile unless held at 3800°F for several hours. Table I illustrates some of the data obtained. It is obvious that two factors influenced the elongation of the wire specimens, heating rate, and time at 3800°F. Specimens held at 3800°F for 6 hr or more exhibited more than 25 pct elongation in 2 in. even though the initial heating rate had been slow. Presumably solid-state purification had occurred. Once the wires had been so "purified," they remained ductile even though slowly reheated. The effect was permanent and nonreversible.

However, if the specimens were held at 3800°F for only 1 hr, then the ductility appeared to be dependent on the heating rate employed for the last treatment. The effect was reversible. This is illustrated in Table II.

Table III shows the effect of changing the heating rate during a single treatment. It appears that low ductility results from slowly heating the wire through the temperature range of about 3000° to 3300°F. This suggests a solubility inversion of the controlling impurity,† i.e., the existence of an eutectic temperature between 3000° and 3300°F. However, the presence of an eutectic temperature does not explain why a slowly heated "embrittled" wire should be made ductile by a rapid reheat and so cannot be the basis of a complete hypothesis. A few tests were made in which the cooling cycle of the specimens was interrupted. These results are shown in Table IV. Interruption of the cooling for even extended times did not affect the ductility, but additional information should be obtained particularly on slowly heated specimens.

† It is suspected that oxygen may be the controlling impurity simply because it is known that, percent for percent, oxygen has a more powerful effect on ductility than the other elements, carbon, N_2, and H_2, which can be removed from the wire at 3800°F.

Table III. Effect of Rapidly Heating to Intermediate Temperature, Then Slowly Heating to 3800°F

Experiment No.	Intermediate* Temperature, °F	Pct Elongation in 2 in.	Pct Reduction in Area	Tensile Strength, 1000 Psi
172	None	5 to 10	7 to 16	63 to 70
190	2500	4 to 13	5 to 14	53 to 73
191	3000	9 to 26	9 to 27	70 to 76
188	3250	10 to 20	17 to 28	74 to 78
195	3450	36 to 43	45 to 68	79 to 81
165	3800	36 to 49	49 to 76	75 to 78

* Heated to intermediate temperature in 2 min, then heated to 3800°F at a rate equivalent to the 45 min heat-up cycle. Held at 3800°F 1 hr.

Table IV. Effect of Interrupting the Cooling of Wires Heated to 3800°F

Experiment No.	Temperature of Interruption, °F	Time Cooling Delayed, Hr	Pct Elongation in 2 In.	Pct Reduction in Area	Tensile Strength, 1000 Psi
225*	3000	6	36 to 42	57 to 71	80 to 81
214*	3100	1	36 to 42	36 to 76	77 to 81
215*	3100	5	39 to 44	71 to 76	77 to 81
222*	3450	3	40 to 44	65 to 73	78 to 80
223*	3450	7	39 to 46	57 to 74	78 to 80
255**	3100	1	7 to 18	6 to 11	57 to 70

* Heated to 3800°F in 2 min; held at 3800°F for ½ hr.
** Heated to 3800°F in 45 min; held at 3800°F for ½ hr.

However, it has been suggested that, during slow heating, the vapor pressure or dissociation pressure of some "trace" compound may be sufficient to rupture the metal. However, there is as yet no actual experimental evidence that, under the test conditions, a compound is formed with the vapor pressure or dissociation pressure sufficient to rupture the metal. It has been suggested also that a liquid phase may form above about 3200°F and that during slow heating it migrates readily to the grain boundaries. But again this does not appear to be a complete explanation because it is not consistent with the "reversibility" that has been observed.

No general hypothesis which explains the various behaviors illustrated by the data can be offered at present. The information is presented here largely in the hope that it may prompt others to bring forth additional information which will help in reaching a satisfactory explanation.

Acknowledgment

Work performed under Contract No. N9-onr-82100, Task Order No. N9-onr-82101, Project NR 039-003.

[1] W. E. Few and G. K. Manning: A 4000°F Furnace. *Metal Progress* (1951) pp. 364-365.

[2] W. E. Few and G. K. Manning: Solubility of Carbon and Oxygen in Molybdenum. *Trans.* AIME (1952) 194, pp. 271-274; JOURNAL OF METALS (March 1952).

Vanadium-Zirconium Alloy System

by J. T. Williams

The equilibria in the V-Zr alloy system were investigated by solidus temperature determinations, thermal analysis, dilatometry, electrical resistance measurements, microscopic examination, and X-ray diffraction analysis. There is a eutectic reaction at 1230°C between a compound, V_2Zr, and a solid solution containing 10 pct V in β zirconium. V_2Zr decomposes at 1300°C into liquid and a solid solution containing about 10 pct Zr in vanadium. The eutectic composition is probably about 30 pct V. A eutectoid reaction between V_2Zr and α zirconium takes place at 777°C at a very high rate. The eutectoid composition is 5 wt pct V. The limit of solubility of zirconium in vanadium was estimated to be 5 pct at 600°C. No attempt was made to determine the liquidus for the system.

THE recent availability of large quantities of high purity zirconium has stimulated the study of zirconium binary systems. The equilibrium diagram for the V-Zr system has received little attention, however. Wallbaum[1] appears to have made the first report concerning the equilibria in these alloys. He reported the existence of a compound, V_2Zr, having the $MgZn_2$ ($C14$) type of structure with $a_o = 5.277$ kX and $c_o = 8.647$ kX. Anderson, Hayes, Roberson, and Kroll[2] made a survey of some potentially useful zirconium binary alloys and found that zirconium probably dissolves a small amount of vanadium. They reported the probable existence of a compound between the two elements and suggested that the zirconium-rich solid solution undergoes a eutectic reaction with this compound. Pfeil,[3] in a critical review of the existing information, estimated that the solubility of vanadium in zirconium is less than 4.7 pct and probably less than 1.8 pct. Rostoker and Yamamoto[4] proposed a partial diagram for the V-Zr system in a survey paper on vanadium binary alloys. Their diagram indicates the compound, V_2Zr, a eutectic reaction at 1360°C, a peritectic reaction at 1740°C, and a limit of solubility of zirconium in vanadium of about 3 pct. They obtained no information on the equilibria in the zirconium-rich alloys.

In view of the potential utility of the V-Zr alloys and the incomplete knowledge concerning the equilibria in the system, an attempt was made to establish the constitutional diagram.

Preparation of the Alloys

Raw Materials: The vanadium for making up these alloys came from the Electro Metallurgical Corp. Zirconium came from two sources. In the beginning of the investigation, sponge zirconium from the Bureau of Mines was used in making some of the alloys. Later, iodide metal made at the Westinghouse Atomic Power Development Laboratories became available. This material was used in the preparation of all the dilatometric and resistance specimens and about two-thirds of the solidus temperature specimens.

J. T. WILLIAMS is associated with Dept. of Chemistry and Institute for Atomic Research, Iowa State College, Ames, Iowa.

Discussion of this paper, TP 3897E, may be sent, 2 copies, to AIME by Apr. 1, 1955. Manuscript, July 15, 1954. Chicago Meeting, February 1955.

Table I. Typical Analysis of Vanadium from the Electro Metallurgical Corp.

Element	Amount Present, Wt Pct
Carbon	0.19
Hydrogen	0.0014
Nitrogen	0.095
Oxygen	0.036
Other	0.10

A typical manufacturer's analysis of the vanadium is shown in Table I. No other analysis of the vanadium was made. The metal contained a dispersed second phase and did not have a sharp melting point.

Typical results of spectrographic analysis of the Westinghouse zirconium are shown in Table II. These data indicate a very high purity. The Bureau of Mines sponge metal was probably less pure but had good ductility.

Melting: All of the alloys used in the investigation were made by melting pieces of vanadium and zirconium together in a dc electric arc furnace similar to those of Geach and Summers-Smith,[5] Craighead, Simmons, and Eastwood,[6] and others. Melting was done in an atmosphere of helium scavenged of residual air by the preliminary melting of a separate charge of zirconium. Each ingot was turned over and melted at least three more times before removal from the furnace to aid in the attainment of homogeneity.

Alloys prepared for use in the investigation are listed with the results of solidus determinations in Table III with the exception of the following compositions upon which no solidus determinations were made: 0.29, 0.54, 4.57, and 5.55 pct V.

Analysis: The weight of each ingot made from iodide zirconium was within 0.1 g of the total weight of the initial charge, about 90 g. Since each component of each charge was weighed to the nearest 20 mg for amounts less than 10 g and to the nearest 0.1 g otherwise, the gross composition of an ingot could be calculated accurately. Chemical analysis for the vanadium content of several alloys agreed

Table II. Typical Analysis of Iodide Zirconium

Element	Amount Present, Wt Pct
Aluminum	<0.003
Calcium	<0.001
Chromium	<0.003
Copper	0.005
Hafnium	<0.05
Iron	<0.02
Magnesium	<0.001
Nickel	0.002
Silicon	<0.014
Titanium	<0.002

well with the calculated composition. The result of chemical analysis has been used to specify composition when available; calculated compositions were considered to be reliable enough in other cases.

Fabrication: Pieces of alloys amenable to fabrication were placed in steel jackets, the jackets were welded shut, and the assemblies were either swaged or rolled at about 850°C. The jackets were then stripped off the alloys. Rods ⅛ in. in diameter could be cold swaged to wires. Alloys containing from 10 to 90 pct V could not be fabricated satisfactorily.

Qualitative spectrographic analysis of nine wires prepared in this way showed no contamination by copper, tungsten, or iron. It was assumed that fabrication of the alloys introduced no significant amounts of impurities.

Apparatus and Procedure

Solidus Temperature Determinations: The method of Pirani and Alterthum[7] was used for determining the temperature of the solidus for a given composition. Specimens were cut from the ingots and heated in an apparatus similar to that described by Wilhelm, Carlson, and Lunt[8] by passing a large electric current (about 1000 amp) through them. Fig. 1 shows a cross-sectional view of the furnace, and Fig. 2 shows the shape of specimens and method of mounting them. The cylindrical furnace shell, *C*, and electrodes, *E*, are water cooled. Clamps, *H*, between which the specimen is held, are cooled by conduction to the electrodes. A double-walled, water-cooled steel door bearing a rubber gasket which fits the edge of the furnace shell closes one end of the furnace. The other end is connected to a high speed vacuum system which maintains the furnace pressure at or below 10^{-4} mm Hg.

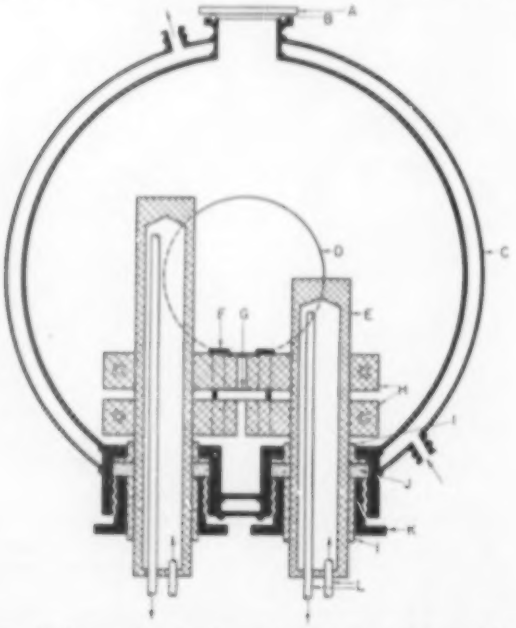

Fig. 1—Cross-section of melting point furnace. *A* is pyrex sight glass; *B*, rubber "O" ring; *C*, double-walled water-cooled steel furnace shell; *D*, lead to vacuum system; *E*, copper cylindrical electrodes; *F*, steel bolt, screwed into lower of clamps *H*; *G*, specimen; *H*, copper clamps; *I*, linen-base bakelite insulating rings; *J*, rubber gasket; *K*, steel compression nut; and *L*, copper tubing for water cooling of electrodes.

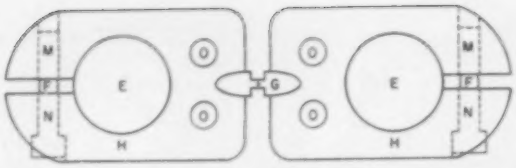

Fig. 2—Clamps and method of mounting specimen in melting point furnace. *E* is electrode; *F*, ⅜ in. Allen screw; *G*, specimen; *H*, lower specimen clamp; *M*, hole drilled and tapped for ⅜ in. Allen screw; *N*, hole drilled and recessed for ⅜ in. Allen screw; and *O*, hole drilled and tapped for ½ in. bolt.

The depth-to-diameter ratio of the holes drilled in these samples was four or greater. Measurements of the melting point of zirconium had shown no significant variation with the ratio down to values this low. It was assumed that four was a large enough figure to ensure a good approximation to black-body conditions.

Specimen temperatures were increased from 2° to 5° every 15 min in the neighborhood of the solidus. To check the effect of the heating rate, the specimens listed in Table IV were heated for 40 hr at about 1290°C before the determination was made. The heating was done with the specimens resting on a tantalum boat in a mullite tube evacuated to 5×10^{-5} mm Hg. The solidus temperatures for specially treated specimens were the same as those for speci-

Table III. Solidus Temperatures of V-Zr Alloys

Composition, Wt Pct V	Solidus Temperature, °C
0	1860
1.03	1770
2*	1705†
3.00	1670
3.80	1575
5.28	1505
6*	1465
6.8*	1430
7.08	1405
10*	1235
15*	1230
20*	1240†
30*	1225†
40*	1235†
45.50	1235
49.06	1255†
51.08	1290
53.08	1295
54.10	1275
57.00	1235†
60*	1280
65*	1290
68.32	1325†
70*	1305
77.16	1300†
85*	1500
88.05	1580†
94.33	1675†
90*	1640
96.54	1685
98*	1775†
98.78	1805†
100	1860

* Calculated composition.
† Only results on alloys made from Bureau of Mines zirconium available.

Table IV. Solidus Temperatures of Some Specially Homogenized V-Zr Alloys

Composition, Wt Pct V	Solidus Temperature, °C
53.02	1305
75*	1290 to 1310
83*	1330

* Calculated composition.

mens of the same compositions run in the ordinary way.

Pyrometer readings were corrected for absorption in the furnace sight glass either by calculations based upon Wien's law and the percentage of transmission of the glass or by sighting the pyrometer through the glass at a standard lamp, the current through which was varied to produce the brightness match. In the latter case, corrected solidus temperatures were derived from the calibration curve of lamp current vs temperature. The two methods gave results that agreed to within ±10°C.

Dilatometry: An apparatus designed by Dooley and Atkins[7] was used to measure changes in length in rods cut from ingots. The sensitive element in this dilatometer is a linear differential transformer, the core of which is mechanically linked to the specimen by a fused silica rod. Change of length of specimen is plotted against temperature automatically on a Minneapolis-Honeywell "Function Plotter" by putting the amplified rectified output of the transformer into the chart drive circuit and the output of a thermocouple in contact with the specimen into the pen drive circuit of the instrument. A pressure of about 10^{-4} mm Hg can be maintained in the specimen enclosure.

Electrical Resistance Measurements: A potentiometric method was used to measure the electrical resistance of wires from these alloys. A diagram of the electrical circuit is shown in Fig. 3. Each of the pieces of tantalum rod, *T*, was fastened to the specimen, *X*, by inserting one end of the specimen into a hole drilled into one end of the rod and swaging the assembly. Two chromel wires and one alumel wire were welded together at one end and inserted into a hole in the other end of one of the rods, *T*. The tantalum was then squeezed tightly against the bead. Two other chromel wires were fastened in a hole in the other rod in similar fashion. The alumel wire, *N*, and the chromel wire, *P'*, formed a thermocouple for measurement of the specimen temperature. Chromel wires *P* and *P'* were the leads to the potentiometer on which the voltage drop across the specimen was measured and chromel wires *C* and *C'* conducted the current to and from the specimen.

Specimens were heated in a fused silica tube at a pressure of 10^{-4} mm Hg or less. Lead wires *N*, *P*, *P'*, *C*, and *C'* were brought out of an extension of the silica furnace tube through wax seals. Measurements were made only after the specimen had been at a given temperature for 1 hr or longer, except that waiting periods at 900°C or above were shorter to minimize possible reaction between the silica and the wire. The current through the specimen was adjusted to 50.00 ma before each measurement by changing the resistances R_1 and R_2 in the battery circuit until the potential drop across the 0.1 ohm standard resistance, R_s, was 5.000 mv.

Quenching Method: Specimens to be quenched were sealed in evacuated, fused silica capsules. The capsules were heated for the desired length of time at the chosen temperature, and the specimens were quenched by crushing the capsule in a mixture of dry ice and trichloroethylene. Heating times were 25 hr at 1150°C, 46 hr at 1100°C, 89 hr at 1000°C, 385 hr at 800°C, and 455 hr at 600°C.

Pieces of ingots which could not be fabricated were given a preliminary heating before sealing into capsules. Those containing 50 pct V or less were heated for 30 hr at about 1220°C on a tantalum boat in a mullite tube at a pressure below 10^{-4} mm Hg; the others were heated for 40 hr at about 1290°C in the same way.

X-ray Diffraction Methods: Pieces of alloys containing from 30 to 70 pct V were readily crushed to powder in a Plattner mortar. A fine silica fiber coated with a hydrocarbon grease was rolled in the powder to produce the specimen proper. This was exposed to copper radiation filtered by nickel foil in an 11.459 cm Debye-Scherrer-type camera with Straumanis film mounting.

Results and Discussion

The Equilibrium Diagram: The information gained from this investigation is summarized by the equilibrium diagram for the V-Zr system shown in Fig. 4. The results of solidus temperature determinations have been plotted on the diagram. Dilatometry and measurement of electrical resistance changes were relied upon to establish the eutectoid horizontal and the lower boundary of the β region. The results of electrical resistance measurements have been plotted in Fig. 4. Microscopic examination of quenched alloys fixed the composition of the intermetallic compound and X-ray diffraction analysis of alloy powders showed no evidence of a transformation.

The Solidus: The complete solidus is composed of two steeply sloping portions that descend, respectively, to a eutectic and a peritectic horizontal in the central portion of the diagram. These horizontal portions show an offset at about 53 pct V. The results of the solidus temperature determinations plotted in Fig. 4 are given in Table III.

Several precautions were taken to guard against errors which might have occurred in these determinations, particularly in the determination of the temperature of the peritectic reaction. Two pyrometers calibrated against a Bureau of Standards

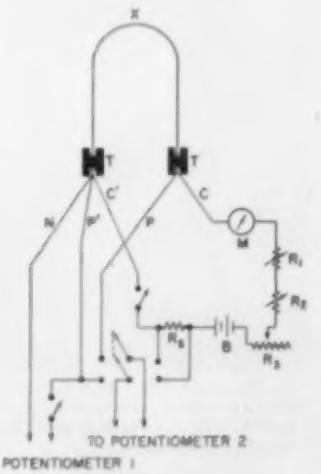

Fig. 3—Electrical circuit for measurement of resistance of wire. *B* is storage battery; *C* and *C'*, chromel current leads; *M*, 0 to 100 dc milliammeter; *N*, alumel wire; *P* and *P'*, chromel potential leads; R_1, coarse current control, 0 to 10 ohm; R_2, fine current control, 0 to 5 ohm; R_3, 0 to 500 ohm; R_s, 0.1 ohm standard resistance, *T*, ⅜ in. lengths of ⅛ in. diam Ta rod; and *X*, specimen.

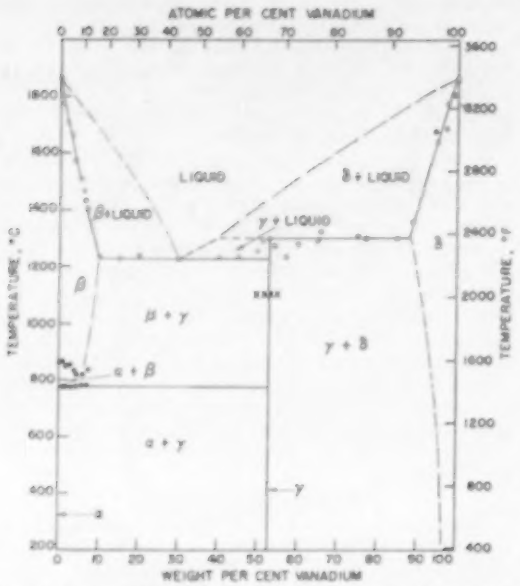

Fig. 4—The equilibrium diagram for the V-Zr system. Open circles are solidus determinations; closed circles, electrical resistance changes; and X, two-phase microstructure.

certified lamp were used throughout the work and the empirical method of correcting pyrometer readings was employed as a safeguard against calibration shifts. Temperature gradients in the region of the hole upon which the pyrometer was sighted were never found to be more than 35°C and were usually about 20°. They would have made observed values slightly low. Repeated observations of the melting point of pure zirconium showed that these sources gave rise to small errors at the most. No value for this melting point differed from 1860°C by more than 10°.

To ensure that the liquid first observed in the vanadium-rich alloys was produced by the peritectic reaction rather than the eutectic reaction, a slow heating rate was employed. The rate used was slow enough so that the eutectic mixture of phases in these alloys reacted to give γ and δ before melting occurred, as Fig. 5 shows. This is a picture of the area adjacent to the hole in a melting point specimen of the 53.02 pct V alloy. Melting had not taken place in this region, but there is no evidence of the eutectic mixture of phases.

Table V. Transformation Ranges in Some V-Zr Alloys from Dilatometric Curves

Composition, Wt Pct V	Temperature Range of Transformation, °C
0.29	812 to 871
0.54	785 to 841
1.03	761 to 849
1.97	788 to 824
3.00	783 to 815
3.88	785 to 810
4.87	790 to 808
5.36	778 to 800
5.55	795 to 824
6*	807 to 834
6.5*	785 to 839
7.02	783 to 849

* Calculated composition.

As an added precaution in determining the peritectic temperature, the four specimens listed in Table IV were heated as described previously for 40 hr at about 1290°C before the determination was made. The results obtained on the specially homogenized specimens were the same as those for specimens of the same composition run in the usual fashion.

The horizontal in the solidus at 1230°C obviously represents a eutectic reaction. The eutectic structure is shown in Fig. 6, a micrograph of a 30 pct V ingot. The figure indicates that the eutectic composition must be near 30 pct V. That the other horizontal at 1300°C represents a peritectic reaction is shown by the micrograph of a 53.02 pct V alloy, Fig. 7. The area shown here is that portion of a specimen heated to melting in a solidus temperature determination. The white layer of V_2Zr surrounding the gray δ phase is clearly defined. Black areas are unresolved eutectic.

The Eutectoid: Preliminary thermal analysis of several alloys containing from 1 to 40 pct V indicated the existence of a transformation in the temperature range from 770° to 850°C. Dilatometric

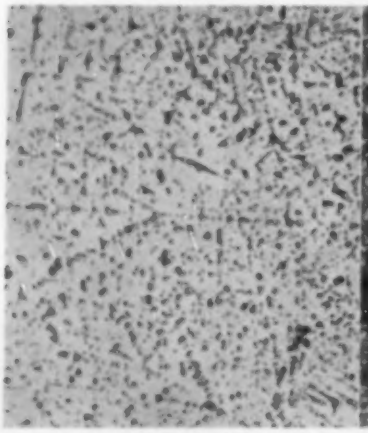

Fig. 5—Area adjacent to hole in melting point specimen of 53.02 pct V alloy. Etched with HF. X120. Area reduced approximately 10 pct for reproduction.

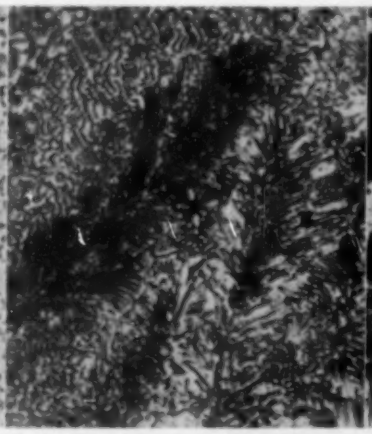

Fig. 6—Eutectic structure of 30 pct V ingot. Etched with HF. X1200. Area reduced approximately 10 pct for reproduction.

Fig. 7—Peritectic structure in partially melted zone of 53.02 pct V alloy melting point specimen. Etched with HF. X1200. Area reduced approximately 10 pct for reproduction.

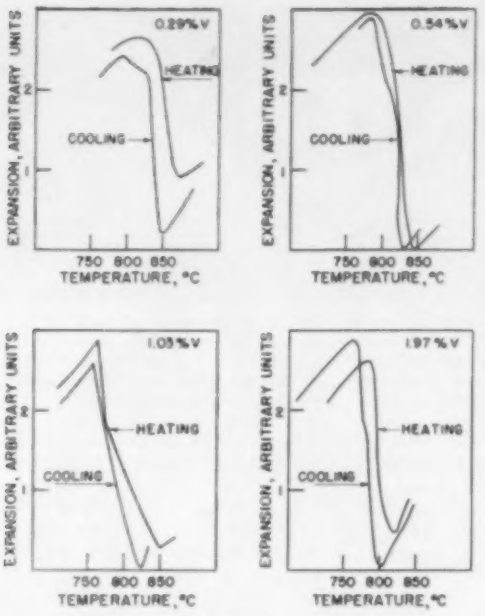

Fig. 8—Dilatometric curves for some V-Zr alloys.

curves for some of these alloys confirmed the existence of this transformation. A sharp decrease in length, interpreted as marking the occurrence of the eutectoid reaction, was observed at about 775°C in each case. The length began to increase again at a temperature which varied with composition and, presumably, corresponded to the entrance into the one-phase β field. Some typical dilatometric curves are shown in Fig. 8. The temperature range over which the dilatometric heating curve showed a decreasing length is given in Table V for each of 12 alloys. The heating curves were chosen because they appeared to be less dependent upon the rate of temperature change than the cooling curves were.

Plots of electrical resistance vs temperature were similar to the dilatometric curves, except that the electrical resistance data were a better representation of equilibrium conditions in the alloys than the dilatometric results. Points for heating and cooling cycles fell on the same curve for the resistance measurements, but they did not on the dilatometric curves. Typical examples of the resistance vs temperature curves are shown in Fig. 9. The temperature range over which the resistance decreased is listed for 10 alloys in Table VI. The common value of 777±5°C for the lower temperature of this range was taken as the eutectoid temperature. The higher temperature listed in Table VI for the transformation range for a particular composition was taken to be the lower boundary of the β region for that composition. The interpretation seems reasonable, since both dilatometric and resistance curves gave roughly the same indications.

Table VI. Transformation Ranges in Some V-Zr Alloys from Electrical Resistance Changes

Composition, Wt Pct V	Temperature Range of Transformation, °C
0.29	802 to 900
0.54	790 to 890
1.03	775 to 865
1.97	777 to 845
3.00	777 to 852
3.80	772 to 830
4.57	777 to 822
5.38	780 to 822
5.55	780 to 830
7.02	782 to 835

It should be noted that three of the ten resistance curves do not fit the foregoing interpretation well. The upper temperature of transformation given for the 7.02 pct V alloy in Table VI is much too low to be the boundary between the β and $\beta+\gamma$ regions, but even up to 1140°C this alloy showed no other resistance anomalies. On the other hand, the upper temperature of transformation for both the 0.29 and 0.54 pct V alloys is too high. It was above 862°C, the temperature of the transformation in zirconium, in both cases. The behavior of the 7.02 pct V alloy was expected, since the boundary between the β and $\beta+\gamma$ regions is so steep as to make its detection by these methods doubtful, but the behavior of the other two alloys was somewhat disturbing. It may indicate contamination of the alloys, perhaps by oxygen.

The rate at which the eutectoid transformation takes place was found to be very high. Large changes in electrical resistance were observed at cooling rates of more than 200°C per min, and X-ray diffraction patterns from alloys quenched from temperatures above the eutectoid invariably showed the presence of the α phase but almost no β.

The γ Phase: The form of the solidus implies the existence of an intermediate phase with a composition near 50 pct V. Figs. 10 through 13 serve to fix the composition limits of this phase more closely. The 51.58 pct V alloy shown in Fig. 11 and the 53.02 pct V alloy shown in Fig. 12 are very nearly single phase. The 49.66 pct V alloy shown in Fig. 10 and the 54.10 pct V alloy shown in Fig. 13 contain larger amounts of a second phase. The structure of the primary constituent in the latter alloys could not be clearly revealed with the etchants used. It is clear from these pictures that the intermediate phase must have very nearly the stoichiometric composition for V,Zr, 52.8 pct V.

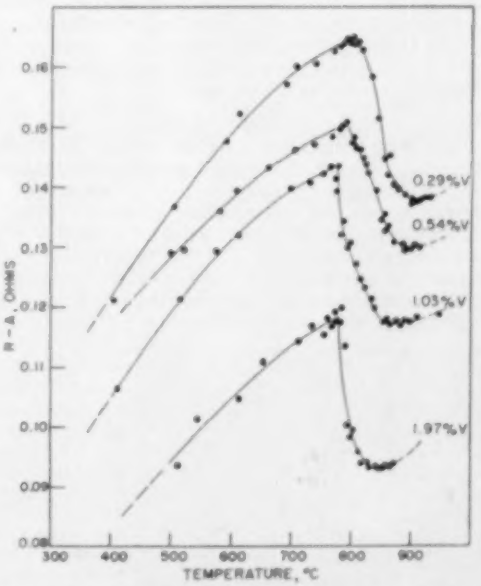

Fig. 9—Electrical resistance vs temperature curves for some V-Zr alloys. *R* is specimen resistance and *A*, arbitrary constant.

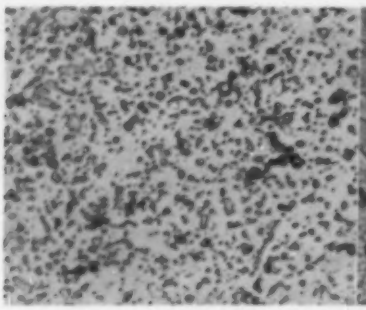

Fig. 10—Microstructure of 49.66 pct V alloy quenched from 1100°C. Etched with HF. X190. Area reduced approximately 25 pct for reproduction.

Fig. 11—Microstructure of 51.68 pct V alloy quenched from 1100°C. Etched with 10 g $(NH_4)HF_2$ to 5 cc glacial acetic acid + 50 cc water. X680. Area reduced approximately 25 pct for reproduction.

Fig. 12—Microstructure of 53.02 pct V alloy quenched from 1100°C. Etched with 10 g $(NH_4)HF_2$ to 5 cc glacial acetic acid + 50 cc water. X680. Area reduced approximately 25 pct for reproduction.

X-ray diffraction results support the conclusions drawn from the microstructures of these alloys and, in addition, indicate that there is no transformation in the intermediate phase. The pattern from the 49.66 pct V alloy quenched from 1100°C was identical to that for the same alloy quenched from 600°C. Both showed very weak lines due to the α phase. The patterns from the 54.10 pct V alloy quenched from 1100°C and from 600°C were identical. They contained very weak δ phase lines. With the exception of the α and δ phase lines, all four of these patterns appeared to be the same.

X-ray diffraction patterns from powders made by crushing the lump of the 53.02 pct V alloy quenched from 1100°C were not successfully indexed. The patterns were not particularly good, showing a high background intensity and lacking resolution in the back-reflection region, but lines were visible which did not seem to be reasonably accounted for by the terminal solid solutions or by the structure assigned to V_2Zr by Wallbaum.

The δ Region: The limit of solubility of zirconium in vanadium indicated by microscopic examination of quenched specimens was not completely certain because of the presence of foreign inclusive matter in the alloys. The best estimate which could be made from the evidence obtained was that vanadium dissolves about 5 pct Zr at 600°C.

Summary

Four solid phases occur in the V-Zr alloy system. These are α zirconium, a solid solution of vanadium in β zirconium, a solid solution of zirconium in vanadium, and the intermetallic compound V_2Zr.

The compound and the β solid solution take part in a eutectic reaction at 1230°C. The eutectic composition is estimated to be 30 pct V. Decomposition of V_2Zr into liquid and the vanadium-rich solid solution takes place at 1300°C.

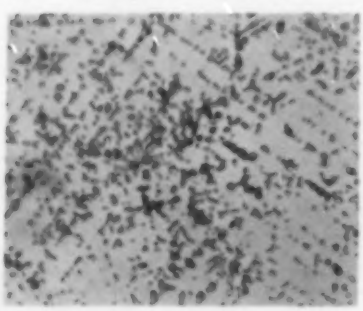

Fig. 13—Microstructure of 54.10 pct V alloy quenched from 1100°C. Etched with HF. X180. Area reduced approximately 25 pct for reproduction.

There is a eutectoid reaction between α zirconium and V_2Zr at 777°C. The eutectoid composition is 5 pct V.

The evidence obtained concerning the limits of the vanadium-rich solid solution is not as good as was desired. This limit is estimated to be 5 pct Zr at 600°C.

The temperatures assigned to the eutectic and peritectic horizontals differ considerably from those given by Rostoker and Yamamoto[5] although the composition of the intermetallic compound is the same. The estimate for the solubility limit of zirconium in vanadium given here is somewhat higher than that proposed by Rostoker and Yamamoto.

Acknowledgment

Contribution No. 346 from the Institute for Atomic Research and Dept. of Chemistry, Iowa State College. Work was performed in the Ames Laboratory of the United States Atomic Energy Commission.

Discussion of this paper, if any, will appear in JOURNAL OF METALS, November 1955, and in AIME Metals Branch *Transactions*, Vol. **203**, 1955.

References

[1] H. J. Wallbaum: Über Weitere Zirkoniumverbindungen mit Übergangselementen. *Naturwissen* (1942) **30**, p. 149.

[2] C. T. Anderson, E. T. Hayes, A. H. Roberson, and W. Kroll: A Preliminary Survey of Zirconium Alloys. *Report of Investigation No. 4658* United States Bureau of Mines (1950) 48 pp.

[3] P. C. L. Pfeil: A Critical Review of the Alloying Behaviour of Zirconium. *Atomic Energy Research Establishment Report No. AERE M/TN 11* (May 1952) Atomic Energy Research Establishment, Harwell, Berkshire, England.

[4] W. Rostoker and A. Yamamoto: A Survey of Vanadium Binary Systems. *Trans.* ASM (1954) **46**, pp. 1136-1163.

[5] G. A. Geach and D. Summers-Smith: A Laboratory Arc-Melting Furnace for Melting Alloys Containing the Refractory Transition Metals. *Metallurgia* (1950) **42**, pp. 153-156.

[6] C. M. Craighead, O. W. Simmons, and L. W. Eastwood: Titanium Binary Alloys. *Trans.* AIME (1950) **188**, pp. 485-513; JOURNAL OF METALS (March 1950).

[7] M. Pirani and H. Alterthum: Über eine Methode zur Schmelzpunktbestimmung an Hochschmelzenden Metallen. *Ztsch. für Elektrochemie* (1923) **29**, pp. 5-8.

[8] H. A. Wilhelm, O. N. Carlson, and H. E. Lunt: Thorium-Titanium Alloy System. *Atomic Energy Commission Report No. AECD-3603* (June 1953).

[9] M. E. Dooley and D. F. Atkins: A New Electronic Vacuum Dilatometer. *Atomic Energy Commission Report No. ISC-482* (1954).

Gallium-Antimony System

by I. G. Greenfield and R. L. Smith

The binary system Ga-Sb has been investigated by thermal, X-ray, and metallographic methods. The intermetallic compound GaSb melts at 705.9°C and forms a eutectic with antimony at 11.8 atomic pct Ga. This eutectic melts at 589.8°C. A eutectic appears to be formed at 29.8°C but is too close to the composition of pure gallium to be detected.

IN the course of an investigation of the semiconducting properties of the intermetallic compound, GaSb, the phase equilibrium between gallium and antimony has been investigated. Recently, the phase diagram of similar systems, such as In-Sb,[1] In-As,[2] and Bi-As[3] have been determined. These diagrams have the same general appearance in that an intermetallic compound is formed at 50 atomic pct and a eutectic is formed on both sides of the intermetallic compound. Jenny,[4] who has been investigating the semiconducting properties of intermetallic compounds, has concluded from thermal data of several alloys that the phase diagram of the Ga-Sb system resembles those mentioned previously. This paper represents a more detailed study of the Ga-Sb equilibrium.

Experimental Procedure

The gallium that was used to prepare the alloys was obtained from A. D. Mackay Inc. and the Aluminum Co. of America; the latter reported the purity as 99.95 pct. The antimony was obtained from Bradley Mining Corp. who specified a purity of 99.997 pct. Since the intermetallic compound of GaSb was prepared primarily to be used for further studies of the semiconducting properties, additional purification by a standard zone-melting technique under an atmosphere of hydrogen was performed. Hall-effect measurements on this material indicated an impurity content of less than 3 ppm.[5] The antimony also was purified by zone melting and used in conjunction with the compound GaSb to make the necessary alloys for the determinations of the antimony-rich side of the phase diagram.

The antimony-rich alloys were chill cast in Vycor tubes which were evacuated to a pressure of less than one micron. Since these alloys expand on freezing, precautions were taken to prevent oxidation of the ingot in the event the tube fractured. To insure homogeneity, the brittle alloys were ground and then placed in the furnace for the thermal-arrest determinations.

I. G. GREENFIELD, Student Associate AIME, and R. L. SMITH, Member AIME, are associated with Solid State Physics Div., The Franklin Institute Laboratories for Research and Development, Philadelphia.

Discussion of this paper, TP 3935E, may be sent, 2 copies, to AIME by Apr. 1, 1955. Manuscript, July 23, 1954. Chicago Meeting, February 1955.

This paper is based on a thesis by I. G. Greenfield, submitted, in partial fulfillment of the requirements for the degree of Master of Science, to the Graduate School, University of Pennsylvania.

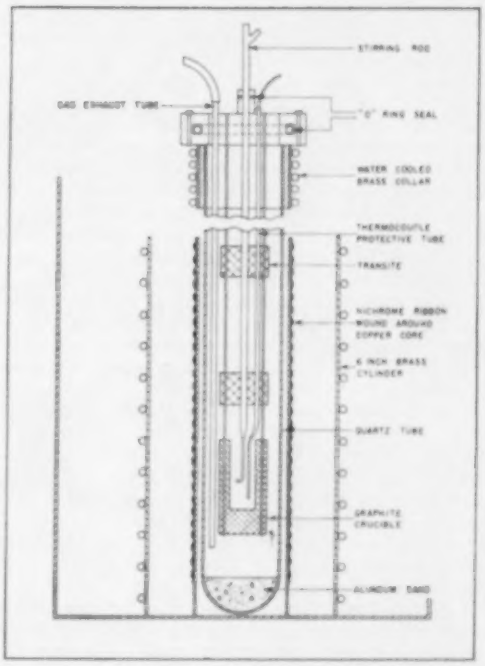

Fig. 1—Furnace for thermal analysis.

Since the cost of gallium is high, the experimental procedure was complicated somewhat because of the necessarily limited sizes of the melts. In order to economize, the gallium-rich side of the diagram was determined by using a 35 g ingot of pure gallium initially and adding increasing amounts of antimony in order to obtain additional alloys.

The furnace used in the determination of the cooling curves is illustrated in Fig. 1. A 2¼ in. quartz tube, sealed at one end, was fitted with a brass flange which was attached with DeKhotinsky cement. The brass collar was water cooled to prevent the cement from softening. An "O" ring was used to provide a seal between the brass collar and the furnace cover. Nichrome ribbon was wound around a 2½ in. asbestos-covered copper core which was used to reduce the thermal gradient in the furnace. The insulation consisted of alternate layers of asbestos and aluminum foil surrounded by sil-o-cel refractory and

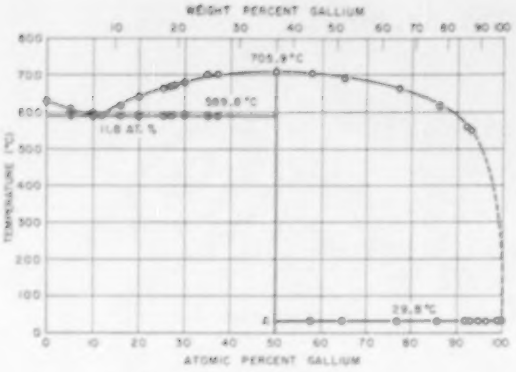

Fig. 2—Ga-Sb phase diagram.

encased in a 6 in. brass cylinder. This cylinder was cooled by water circulated through the attached copper coil. Since it was necessary to obtain temperatures below and in the vicinity of room temperature, special consideration had to be given to the design of the furnace. The present design allowed a controlled cooling rate to be used from 800° to 0°C. The extension of the cooling curves to lower temperatures was accomplished by effectively lowering the ambient conditions of the furnace by means of dry ice placed around the brass cylinder walls. For this reason, the furnace insulation had to be kept at a minimum. The brass cylinder walls were cooled by water at the higher temperatures.

All thermal-arrest determinations were made under an atmosphere of argon which was introduced into the furnace from the top. The gas was allowed to escape through a Vycor tube which extended from the top of the furnace to a point below the crucible.

A calibrated iron-constantan thermocouple in a Vycor protection tube extended into the graphite crucible. Stirring was accomplished by a Vycor stirring rod which vibrated vertically and gave a more effective mixing than a rotating motion. The shaft of the stirring rod was 7 mm Vycor tubing through which powdered material could be introduced for the purpose of seeding the melt in order to prevent undercooling.

A Celect-Ray photoelectric controller was used on which the temperature control knob was removed and replaced by a geared programming device that enabled a decrease or increase in temperature at rates of 1/20° to 10°C per min. The control thermocouple to the Celect-Ray was placed adjacent to the heating coil of the furnace.

The temperature of the melt was recorded by two instruments; 1—a Rubicon Portable Precision potentiometer, and 2—a Minneapolis-Honeywell recording potentiometer. Both instruments could be read to 0.01 mv. The recording potentiometer had a range from 0 to 10 mv; however, by an external circuit, the zero point could be placed at any desired potential. The Rubicon potentiometer which was connected directly into the circuit was used to calibrate the recording potentiometer periodically.

The iron-constantan thermocouple was calibrated directly in the furnace against the secondary standards, antimony, aluminum, zinc, and tin.

Metallography

On the antimony-rich side of the phase diagram both the compound, GaSb, and antimony are extremely brittle; therefore, the preparation of the metallographic specimens required special techniques. No etching was needed with these alloys, since the structure appeared during the polishing operation. However, several etches (Vilella's etch, aqua regia) were used in an effort to detect other microscopical differences that may not have been revealed by polishing. The only effect was an etching of the constituents present without any delineation of other structural features.

Since the eutectic on the gallium-rich side has a melting point in the vicinity of room temperature, the polishing of these specimens had to be conducted under refrigerated conditions. While photographing these alloys, a continuous blast of cold dry nitrogen was concentrated on the surface of the specimen to prevent melting and condensation of water droplets.

Several X-ray diffraction patterns were made to determine if solid solubility of gallium in antimony existed. Since no change in lattice parameter was detected, the solubility of gallium in antimony, if it exists at all, could not be determined with this method.

Results

A cooling rate of 1°C per min was used for the majority of the alloys, but in several instances a rate as slow as 1/20°C per min was used. Undercooling was a problem in the eutectic freezing for the gallium-rich portion of the phase diagram but was almost entirely eliminated by seeding the material with crystallites of pure gallium.

The phase diagram obtained from the cooling curves is illustrated in Fig. 2.

The melting point of the intermetallic compound GaSb was found to be 705.9±1.0°C. Welker[6] reports that Koster has observed a melting point of 702°C. The eutectic composition of the antimony-rich alloy is 11.8 atomic pct Ga and the eutectic temperature is 589.8±0.5°C. Micrographs show the eutectic as a fine structure of both GaSb and antimony in a "Chinese-script" configuration (Fig. 3).

The 5 and 10 atomic pct Ga alloys contain primary antimony grains which appear white against the eutectic matrix (see Fig. 4). The hypereutectic alloys contain dark crystals of the intermetallic compound, GaSb (Fig. 5).

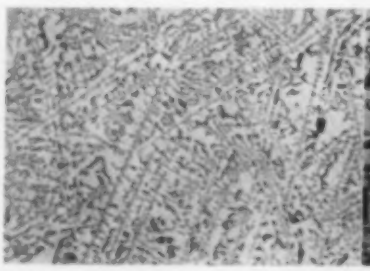

Fig. 3—Antimony-rich eutectic. X100. Area reduced approximately 35 pct for reproduction.

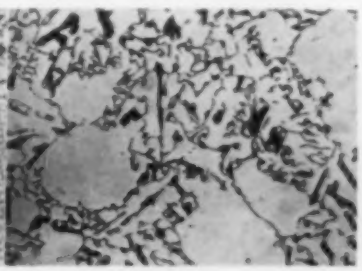

Fig. 4—10 atomic pct Ga. X100. Area reduced approximately 35 pct for reproduction.

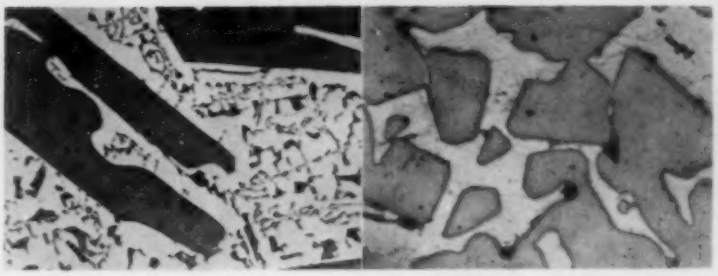

Fig. 5—27 atomic pct Ga. X100. Area reduced approximately 35 pct for reproduction.

Fig. 6—86 atomic pct Ga. X100. Area reduced approximately 35 pct for reproduction.

In the gallium-rich portion, the darker constituent is GaSb; whereas the lighter material is the eutectic structure (Fig. 6). It was difficult to remove all scratches from the surface of the gallium-rich alloys because of the soft nature of the eutectic structure. In fact, when removing the abrasive from the surface with alcohol-saturated cotton, the eutectic matrix became distorted. Therefore, only a light swabbing action was used which did not remove all of the alumina efficiently.

The eutectic composition for the gallium-rich side could not be determined because of the relatively small amounts of antimony present. In fact, the eutectic temperature was found to be the same as the melting point of gallium. The microstructure does not show any eutectiferrous structure but exhibits only grains of GaSb and gallium.

Conclusions

1—The Ga-Sb phase diagram consists of one intermetallic compound of GaSb with a eutectic on either side.

2—The eutectic composition on the antimony-rich side is 11.8 atomic pct Ga; the eutectic temperature is 589.8±0.5°C.

3—The eutectic composition on the gallium-rich side could not be determined. However, the eutectic temperature was found to be the same as the melting point of gallium.

4—No solubility of gallium in antimony was found.

5—The melting point of GaSb was found to be 705.9±1°C.

Acknowledgments

This work was performed at The Franklin Institute Laboratories for Research and Development and forms part of a larger program sponsored by the Air Research and Development Command under Contract AF 18(600)-465. The financial assistance and permission to publish is gratefully acknowledged. The authors also wish to express their appreciation to Dr. D. P. Detwiler, Project Leader, and Dr. R. M. Brick, Director, Dept. of Metallurgy, University of Pennsylvania, for their continued interest in this work.

Discussion of this paper, if any, will appear in JOURNAL OF METALS, November 1955, and in AIME Metal Branch *Transactions*, Vol. **203**, 1955.

References

[1] T. S. Liu and E. A. Peretti: *Trans.* ASM (1952) **44**, p. 539.

[2] T. S. Liu and E. A. Peretti: *Trans.* ASM (1953) **45**, p. 677.

[3] E. A. Peretti and S. C. Carapella, Jr.: *Trans.* ASM (1949) **41**, p. 947.

[4] D. A. Jenny: Private communication and from a slide presented at a meeting of the Electrochemical Society, Chicago (May 26, 1954).

[5] D. P. Detwiler: *Physical Review* (1954) **94**, p. 1431.

[6] H. Welker: *Ztsch. für Naturforschung* (1953) **8a**, p. 248.

Technical Note

Effect of Boron on the Relative Interfacial Tension of Gamma Iron

by A. M. Adair, J. W. Spretnak, and Rudolph Speiser

THERE are sufficient arguments and evidence to indicate that boron should be adsorbed to existing austenite grain boundaries during the austenitizing treatment. Accordingly, it is possible that boron contributes to the hardenability of heat-treatable steels by the reduction of the interfacial energy of austenite grain boundaries, at which sites are nucleated heterogeneously the decomposition products of austenite. Such a reduction in interfacial energy would reduce the total energy that can be borrowed in these heterogeneous nucleation processes and thus retard the initiation of transformation.

This investigation was undertaken in an attempt to determine the effect of boron on this interfacial

Table I. Steel Compositions

Type	C	Mn	P	S	Si	Ni	Cr	Mo	B
AISI 8740	0.390	0.89	0.015	0.019	0.31	0.54	0.47	0.23	0.00
AISI 87B40	0.396	0.89	0.015	0.019	0.31	0.54	0.48	0.23	0.0013
AISI TS 8117	0.190	0.81	0.018	0.029	0.23	0.36	0.41	0.11	0.00
AISI TS 81B17	0.200	0.81	0.018	0.029	0.23	0.36	0.41	0.11	0.0011

tension in commercial steels. It was realized that, in the present state of knowledge, only relative values of the interfacial tension of γ iron could be estimated with the technique employed. However, it is believed that such a study, despite its deficiencies, is justified to determine if boron produces a measurable effect on the interfacial tension and the relative magnitude of this effect, thus establishing whether or not boron is "surface active" in iron (i.e., if boron is significantly adsorbed to grain boundaries).

In this investigation, two sets of steels were used to obtain the requisite data. The matching steels were produced by splitting the heat, i.e., the base steel was divided and boron was added to half the heat in the form of Grainal No. 79. The compositions of the steels, supplied by the Republic Steel Corp., are listed in Table I.

The interfacial tension of the austenite grain boundaries relative to the surface tension of austenite was determined by the technique of heat etching in vacuum. After a sufficiently long etching to develop the grain boundary grooves, the surface was nickel plated to protect the grooves during polishing. The groove angles were determined by directly measuring the width and depth of the groove with a filar eyepiece on a profile section of the heat-etched surface. After measuring the groove angles exposed by a given profile surface, the specimen was ground repeatedly and polished to expose many grain boundary grooves for measurement. One hundred grooves were measured for each specimen to establish the distribution curves of groove angles. Most of the curves obtained were essentially normal, clustering about the true groove angle. The interfacial tension relative to the surface tension was calculated from the average groove angle.

The results obtained are summarized in Table II.

A. M. ADAIR, formerly Graduate Student, The Ohio State University, is Lieutenant, United States Air Force, Aeronautical Research Laboratory, Wright Air Development Center, Wright-Patterson Air Force Base, Ohio, J. W. SPRETNAK, Member AIME, and R. SPEISER, Associate Member AIME, are Associate Professors of Metallurgy, The Ohio State University, Columbus, Ohio.

TN 247E. Manuscript, Sept. 15, 1954.

This note is based on a thesis by A. M. Adair submitted, in partial fulfillment of the requirements for the degree of Master of Science, to The Ohio State University.

Table III. Estimated Values of the Interfacial Tension in Austenite

Steel	Temperature of Heat Etching, °F	Interfacial Tension Estimated, Dynes per Cm	Pct Reduction
AISI 87B40	1830	873	3.5
AISI 8740	1830	904	
AISI 87B40	1600	949	1.9
AISI 8740	1600	967	
AISI TS 81B17	1650	947	2.30
AISI TS 8117	1650	969	

It is of interest to note that in all cases, boron appears to reduce the interfacial energy (increases groove angles), although in none of the cases is the difference in average groove angles statistically significant, since the difference of the means is less in each case than three times the standard deviation of the means. It is interesting also to compare the average angles for AISI 87B40 steels for 1600° and 1830°F. Increasing the temperature apparently decreases the relative interfacial energy, indicating a positive temperature coefficient of adsorption of boron in γ iron. Solely for the purpose of assigning numbers to the relative interfacial tensions of γ iron, Van Vlack's[1] value of 850 dynes per cm for the interfacial tension of γ iron saturated with copper and sulphur at 1105°C was used. The mean groove angle for the AISI 8740 steel at 1105°C was estimated to be 148°. From these data, the surface tension of γ iron was calculated. Assuming this surface tension remains constant in the various experiments, the interfacial energies were estimated from the mean groove angles measured. These estimated values are given in Table III.

Since the question of effect of boron on the surface tension of γ iron is not resolved in this experiment, the results probably should be interpreted as qualitative indications. It does not appear that boron sufficiently reduces the interfacial energy to explain the hardenability effect directly on this basis. It is important that there is a consistent indication of adsorption of boron to the austenite grain boundaries and, in the case of AISI 87B40 steels, an indication that more boron is forced to the grain boundary as the austenitizing temperature is increased.

Acknowledgment

This work on the boron hardenability effect is sponsored by the Aeronautical Research Laboratory, Wright Air Development Center under Contract AF18(600)-94.

[1] L. H. Van Vlack: Intergranular Energy of Iron and Some Iron Alloys. Trans. AIME (1951) 191, p. 251; JOURNAL OF METALS (March 1951).

Table II. Data on Grain Boundary Grooves Developed by Heat Etching

Steel	Temperature of Heat Etching, °F	Mean Groove Angle	Standard Deviation	Standard Deviation of Means	Three Times Standard Deviation of Means	Difference of Mean Groove Angles
AISI 87B40	1830	147.13°	4.349	0.689	2.067	1.20
AISI 8740	1830	145.93°	3.345			
AISI 87B40	1600	144.20°	4.783	0.573	1.719	0.71
AISI 8740	1600	143.49°	3.184			
AISI TS 81B17	1650	144.29°	2.770	0.427	1.281	0.86
AISI TS 8117	1650	143.43°	3.274			

Magnesium-Rich Corner of The Magnesium-Lithium-Aluminum System

by J. A. Rowland, Jr., C. E. Armantrout, and D. F. Walsh

The magnesium-rich corner of the 375°, 200°, and 100°C isothermal sections of the Mg-Li-Al system as developed by metallographic and X-ray diffraction studies is presented in this paper.

THE close-packed-hexagonal structure of magnesium is converted to a ductile and malleable body-centered-cubic lattice by the addition of lithium in excess of 10 pct. Further, the density of magnesium or magnesium-base alloys is decreased by additions of lithium. The practical possibilities of such alloys as a basis for uniquely light, malleable, and ductile structural materials were pointed out by Dean in 1944[1] and by Hume-Rothery in 1945.[2] It was apparent to these investigators, however, that more complex compositions would be required if strengths sufficient for structural applications were to be developed in these alloys. In a search for strengthening additions, various investigators [3-6] have examined a number of the ternary and more complex alloys containing magnesium and lithium. An investigation of the fundamental characteristics of these alloys was undertaken by the Bureau of Mines.

The investigation was initiated with a study of the magnesium-rich corner of the equilibrium diagram for the ternary system, Mg-Li-Al. The following data from published investigations of Mg-Li-Al alloys were available: 1—a description of isothermal sections at 20° and 400°C through the Mg-Li-Al constitution diagram by F. I. Shamrai;[6] 2—a diagram by P. D. Frost et al.[5] showing approximate phase relationships at 700°F for a number of the Mg-Li-Al alloys; and 3—diagrams showing the constitution at 500° and 700°F for the Mg-Li-Al alloy system published by A. Jones et al.[7]

Where compositions and temperatures permit comparison, these diagrams show disagreement. The 700°F isotherms of Frost and Jones differ only in the placement of the phase boundaries. But Shamrai's 400°C (752°F) isotherm shows a variation in phases as well as in phase boundaries. Although rigid comparison of these different isothermal sections might not be justifiable, it seems impossible to reconcile Shamrai's construction with the isotherms of Frost or Jones.

The isothermal sections presented in this paper were prepared to determine compositions which might be suitable for age hardening and to develop the general slope and placement of the various phase boundaries in the magnesium-rich corner of the diagram. Sections at 375°, 200°, and 100°C were selected for investigation.

In constructing these sections, the solubility of aluminum in magnesium, as reported by W. L. Fink and L. A. Willey[8] in 1948, was used at the binary Mg-Al boundary and the solubility of lithium in magnesium was obtained from the equilibrium diagram for that system as reported by G. F. Sager and B. J. Nelson[9] in the same year. The solubility of magnesium in lithium was determined experimentally and conforms in general to data reported by P. Saldau and F. Shamrai.[10] Parameters for AlLi and $Mg_{17}Al_{12}$ were taken from American Society for Testing Materials X-ray diffraction data cards.

J. A. ROWLAND, JR., Member AIME, C. E. ARMANTROUT, and D. F. WALSH, Member AIME, are Metallurgists, Minerals Technology Div., Region VI, Bureau of Mines, Rolla, Mo.

Discussion of this paper, TP 3887E, may be sent, 2 copies, to AIME by Apr. 1, 1955. Manuscript, May 19, 1954. Chicago Meeting, February 1955.

Papers by authors on the Bureau of Mines Staff are not subject to copyright.

Experimental Procedures

Although the isothermal sections presented in this paper are not unusually complex, the experimental techniques involved in their construction are made extremely difficult by the relatively high vapor pressure of lithium and the great chemical activity of both magnesium and lithium. Because of these characteristics, which make precise control of the composition of equilibrium-treated filings practically impossible, the disappearing phase method was used in preference to the parametric method in conjunction with metallographic studies.

The alloys used in this investigation were melted and cast in an atmosphere of helium using a tilting-type furnace which enclosed a steel crucible and mold in a single unit.

Each portion of the charge (500 to 600 g) was cleaned carefully just before placing it in the crucible; and the charge, crucible, and entire melting apparatus were evacuated and then washed with grade A helium while preheating to approximately 100°C. The alloys were melted and chill cast in an atmosphere of helium. Alloys prepared in this way were relatively free from inclusions and a fluxing treatment was considered unnecessary. The cylindrical ingots obtained were scalped and then reduced 96 pct in area by direct extrusion, yielding ⅜ in. diam rod. Sections of the rod, approximately 3 in. long, were given equilibrium heat treatments and then sampled for metallographic examination, X-ray diffraction study, and chemical analysis. The surface of each equilibrium-treated rod was machined to a depth sufficient to insure removal of contaminated material before samples for chemical analysis or X-ray diffraction study were obtained, and all decisions on microstructure were based on the examination of the central portion of the metallographic specimen.

All specimens homogenized at 375°C were analyzed after this equilibrium heat treatment. When the composition of an alloy placed it in a critical area of the 200° or 100°C isothermal section, a check chemical analysis was made on a sample taken from the alloy specimen as-heat-treated at the particular temperature.

Standard chemical procedures of gravimetric analysis were used in the determination of magnesium and aluminum; lithium, potassium, and sodium were determined by flame photometer methods

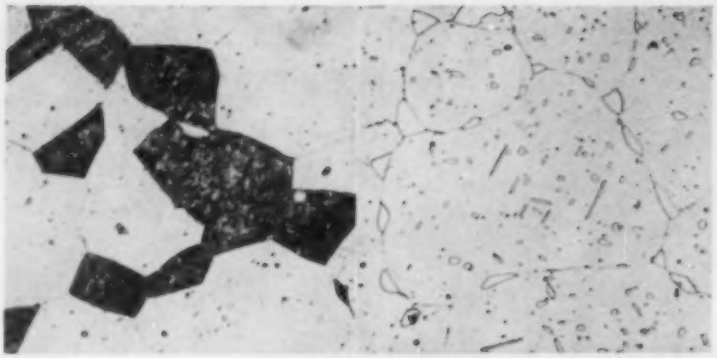

Fig. 1—6.7 pct Li, 3.6 pct Al; quenched from 375°C; $\alpha+\beta$ structure. Phosphopicral etch. X500. Area reduced approximately 30 pct for reproduction.

Fig. 2—0.01 pct Li, 11.4 pct Al; quenched from 375°C; α matrix containing $Mg_{17}Al_{12}$. Phosphoric-glycol etch. X500. Area reduced approximately 30 pct for reproduction.

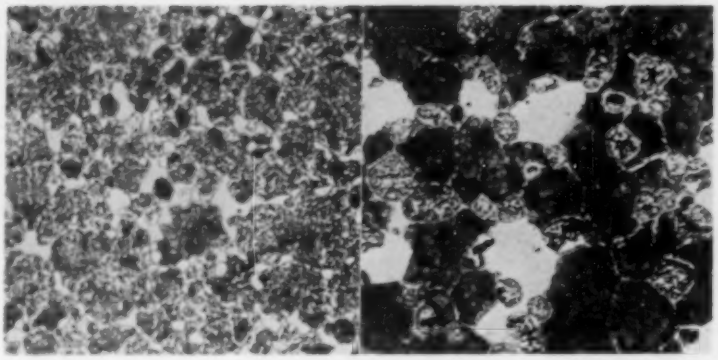

Fig. 3—0.03 pct Li, 14.7 pct Al; 500 hr at 200°C after homogenizing at 375°C; "eutectoidal" areas of α and $Mg_{17}Al_{12}$ + massive areas of $Mg_{17}Al_{12}$. Citric-nitric-glycerine etch. X500. Area reduced approximately 30 pct for reproduction.

Fig. 4—10.4 pct Li, 20.8 pct Al; quenched from 375°C; α grains and AlLi globules in β matrix. Acetic-glycol etch. X500. Area reduced approximately 30 pct for reproduction.

as developed by E. E. Strange[11] in the Bureau laboratories.

In addition to determining the three major elements contained, about half of the alloys used were also analyzed for sodium and potassium, the combined content of which averaged 0.027 pct.

While the total analytical percentages of all component elements indicated less accuracy than would be desired, the data as transcribed to various isothermal sections show no serious inconsistencies. A large number of compositions were prepared and several specimens of each composition were heat treated to obtain equilibrium conditions at the various temperature levels. Thus, although each symbol on the three isotherms represents a specific alloy specimen, the location and structure of that specimen have, in most cases, been verified by duplicate results.

The 375°C Equilibrium Heat Treatment: At 375°C, which is a relatively high heat treating temperature for the Mg-Li-Al alloys, equilibrium is approached rapidly; and both metallographic and X-ray data obtained on specimens annealed for periods of time varying in the range of 20 to 500 hr indicated that equilibrium conditions for the temperature were closely approximated after a 24 hr anneal. The specimens shown on the 375°C section were annealed for not less than 46 hr with a temperature control of ±2°C. Annealing was carried out in helium under an estimated pressure of 1½ atm in sealed glass containers to minimize lithium loss and surface chemical attack.

Quenching in agitated cold water gave an adequate rate of cooling and resulted in an insignificant surface attack on specimens used.

The 200°C Equilibrium Heat Treatment: In general, heat treating techniques for the 200°C isotemperature were similar to the procedures for the 375°C level. Metallographic and X-ray examination of specimens after various periods of heat treatment extending up to 500 hr indicated that equilibrium conditions existed after 200 hr at 200°C. The specimens used in establishing the 200°C isotherm received a treatment of not less than 200 hr at temperature. As an additional assurance that the data employed in constructing this section represented equilibrium conditions, the isotemperature was approached from a homogenizing temperature of 375°C, using one series of specimens, and from room temperature using a duplicate series. Results obtained by the two heat treating procedures were practically identical except for the dispersion of the various phases present. These results and the data obtained from specimens heat treated for various intervals of time combined to give evidence that the 200°C isothermal section as constructed represents equilibrium conditions at the temperature.

Equilibrium Heat Treatment at 100°C: The equilibrium heat treatment for the 100°C isothermal section was tested by methods similar to those used for the 200°C section. These tests revealed that, for many compositions, annealing treatments extending up to 500 hr were inadequate for complete phaseal equilibrium. However, specimens cooled gradually from a homogenizing treatment at 375° to 100°C and maintained at this lower temperature for 200 hr reached phaseal equilibrium; extended heating up to 500 hr showed no further phase changes. Therefore, construction of the 100°C isothermal section was based on results obtained from specimens held at that temperature for 200 hr after being slowly cooled from a 24 hr homogenizing treatment. The cooling rate averaged 3° per hr to 175°C and 2°C per hr to the isothermal temperature at which the specimens were maintained within ±0.5°C for a period of not less than 200 hr.

Electrical Resistivity Measurements: Electrical resistance measurements were made on a number of alloys in an attempt to locate phase boundaries by breaks in the temperature coefficient of resistivity curve. Results obtained were not consistent and the method was abandoned.

Discussion of Results

Microstructures: Four phases in various combinations make up the eight phase regions occupying the magnesium-rich corner of the three isothermal sections investigated. These phases are the magnesium-rich (α) solid solution, the lithium-rich (β) solid solution, and the two binary compounds $Mg_{17}Al_{12}$ and AlLi. The phases when present in sufficient quantity to take a massive form during isothermal treatment are easily distinguished under the microscope. The α and β solid solutions, one of which forms the matrix of each of the alloys studied, are widely different in etching characteristics. The lithium-rich solid solution is very active chemically and even a rinse in ordinary tap water will generally develop a distinctive brown film on this phase, while leaving the magnesium-rich solid solution unattacked. Many of the standard etching reagents for magnesium are excellent for differentiating between these phases and for revealing the general structure of the various alloys. Typical structures, as revealed by one of these standard etchants, are shown in Figs. 1 through 4. Fig. 1 shows the two-phase α-β structure. In Fig. 2, the α phase appears as a matrix containing massive, slightly angular grains of the compound $Mg_{17}Al_{12}$. These irregularly shaped particles which generally tend to polish in relief are the typical form in which this compound appears. With very dilute acid etches, the compound has a blue-white color under green light which contrasts with the grayer tones of α solid solution matrix. The compound also precipitates in a "eutectoidal" form when specimens previously homogenized at 375°C and quenched are heat treated at 100° or 200°C. This structure (Fig. 3) persists even after 500 hr at 200°C.

Fig. 4 shows massive globules containing the compound AlLi, with α grains in a matrix of β solid solution. The peculiar appearance of these globules has not been explained in a completely satisfactory manner. The intensity of the AlLi diffraction lines increases with the amount of globular material, and no additional lines appear in the pattern. From this, it can be reasoned that the duplex structure is the result of a decomposition involving the matrix and AlLi. A simpler explanation of the structure might attribute the duplex appearance to shattering of the globules during polishing or etching. But the structure is evident in the unetched specimens in which the globules are apparent because of their relative hardness, and attempts to shatter the globules by scratching with a microcharacter were unsuccessful. On the other hand, some evidence indicating that the globules are actually a duplex of AlLi and the matrix has been found in an electron micrograph, Fig. 5, obtained from one of these globular formations, and this explanation is compatible with the apparent form of the equilibrium diagram for this system. The AlLi phase, like the $Mg_{17}Al_{12}$ phase, sometimes precipitates as lamellae from the α solid solution. Fig. 6 shows AlLi occurring in both globular and lamellar form in a matrix of α containing islands of β. While the $Mg_{17}Al_{12}$ and AlLi lamellae have very similar microstructures, they are readily distinguished by X-ray diffraction.

X-Ray Diffraction Data: X-ray diffraction patterns for each of the four phases observed check closely with published data and with patterns obtained from laboratory melts with nominal compositions corresponding to the theoretical composition of each phase. Additional lines, usually very faint, were found in an occasional pattern; these could be attributed to nitrides or carbonates on the basis of published data. Four of the additional lines, however, were more intense. They occurred frequently, but not consistently, in alloys containing substantial amounts of β. These lines corresponded closely in both angle and intensity to the four principal lines reported for the ternary compound $MgLi_2Al$, as mentioned by Jones et al.[1] and credited to the Dow Chemical Co. Therefore, several alloys approximating the composition $MgLi_2Al$ were prepared in the laboratory and diffraction patterns on these alloys were obtained immediately after equilibrium heat treatments in a purified helium atmosphere at 400°, 375°, and 100°C. In every case, the alloys were found to contain the compound AlLi with β or with α and β, and there was no trace of the four additional lines in any of the patterns obtained. From this it must be assumed that an equilibrium compound $MgLi_2Al$ does not exist in the temperature range 100° to 400°C. Diffraction patterns were also obtained from a number of alloys in the range of 4 to 15 pct Li and 12 to 30 pct Al after homogenizing treatments at temperatures of 400°, 375°, and 100°C. These patterns also failed to reveal any evidence of the four lines which were initially attributed to $MgLi_2Al$. Further analysis of the data revealed that the four additional lines occurred only in the region near the β corner of the α-β-AlLi and β-AlLi areas. These lines, when encountered, were from specimens which had been homogenized at 375°C and then aged at either room temperature or 100°C for a considerable period of time. Therefore, although

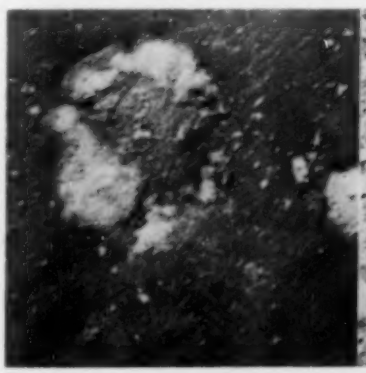

Fig. 5—Electron micrograph showing AlLi in globular formation in a β matrix. Unetched. X25,000. Area reduced approximately 30 pct for reproduction.

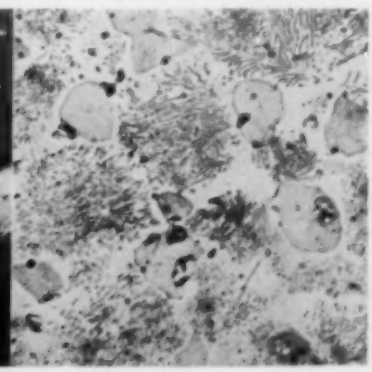

Fig. 6—7.2 pct Li, 5.5 pct Al; 100 hr at 375°C, cooled slowly over 100 hr to 100°C, held 200 hr at 100°C, and then quenched. AlLi occurring in both globular and lamellar form in a matrix of α containing islands of β. Phosphoric-glycol etch. X500. Area reduced approximately 30 pct for reproduction.

the lines could not be reproduced consistently even with specimens of the same alloy, it is believed that the four diffraction lines are from a transitional structure. In any case, it was possible to eliminate the four excess lines from the diffraction patterns by careful control of the heat treating practice to insure equilibrium conditions and by minimizing delays in the X-ray diffraction analysis of the heat treated specimens.

Construction of the Isothermal Sections: Results for the 375°C isothermal section are shown in Fig. 7. At this temperature, the α and β regions extend well into the ternary triangle and the three-phase (α-β-AlLi) field occupies a large part of the central section. The three-phase (α-AlLi-$Mg_{17}Al_{12}$) field is extremely narrow at this temperature and only two of the alloys examined contained considerable amounts of both binary compounds. A micrograph of one of these alloys showing AlLi globules and angular particles of $Mg_{17}Al_{12}$ in an α matrix is reproduced in Fig. 8. Fortunately, very small quantities of the AlLi phase can be detected by X-ray diffraction and it is, therefore, possible to establish the presence of this compound by diffraction methods even when it is not identifiable by ordinary microscopical examination. When the results are described in terms of weight percentages, the solubility of aluminum in magnesium first decreases and then increases slightly until the $\alpha/Mg_{17}Al_{12}$ boundary meets the corner of the ternary area for the α solid solution and the two binary compounds. Above this point, the aluminum solubility again decreases. Apparently, the aluminum content of α magnesium has very little effect on the solubility of lithium, but the solubility of magnesium in β lithium decreases perceptibly with increasing aluminum content. The exact direction taken by the β/β-AlLi boundary which has been extended as a dotted line cannot be established from the data now available, but it is apparent that it will extend to the solidus from the corner of the ternary triangle.

The 200°C isotherm is shown in Fig. 9. No additional phases appear at this temperature. The α, β, α-β, and α-$Mg_{17}Al_{12}$ fields, however, have retracted abruptly toward the binary surfaces, permitting a marked expansion of the four fields containing AlLi. Although the data do not establish the slope of the α-β/α-β-AlLi boundary with decreasing temperature, it is apparent that this slope would increase with decreasing temperature.

With a further decrease in temperature to 100°C, retraction of the α, β, α-β, and α-$Mg_{17}Al_{12}$ areas continues at a much slower rate. At the 100°C isotherm (Fig. 10), these fields are slightly smaller than at the 200°C level and the central areas containing AlLi are expanded proportionately. Otherwise, the 200° and 100°C isothermal sections are very similar.

Summary

The principal results of this investigation are summarized in the three isothermal sections, Figs. 7, 9, and 10. It is evident that the first requisite for an age-hardening alloy is present in a wide range of the compositions investigated. As the β solid solution is the most ductile phase in the Mg-Li-Al system, the portions of the equilibrium diagram of greatest interest, from the practical standpoint of developing alloys combining good workability and strength, adjoin the α-β/α-β-AlLi phase boundary. It is evident that β and α-β alloys supersaturated with AlLi can be obtained by quenching from a homogenizing temperature in the vicinity of 375°C.

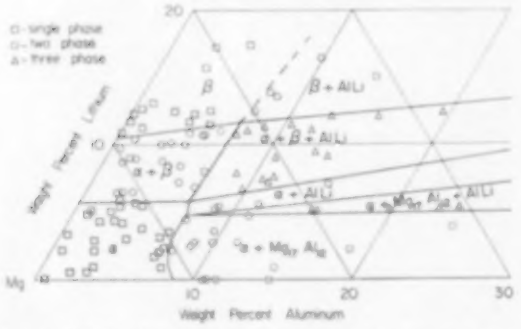

Fig. 7—375°C isothermal section of magnesium-rich corner of the Mg-Li-Al system.

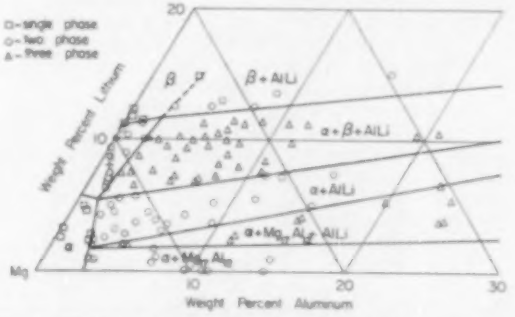

Fig. 9—200°C isothermal section of magnesium-rich corner of the Mg-Li-Al system.

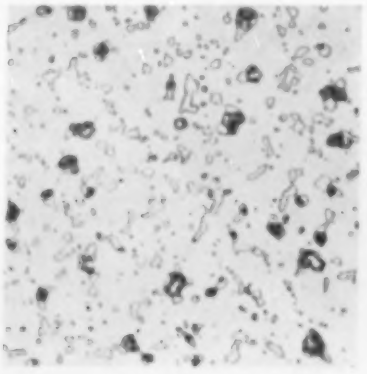

Fig. 8—5.2 pct Li, 15.0 pct Al; quenched from 375°C; AlLi and $Mg_{17}Al_{12}$ in an α matrix. Citric-nitric-glycerine etch. X500. Area reduced approximately 30 pct for reproduction.

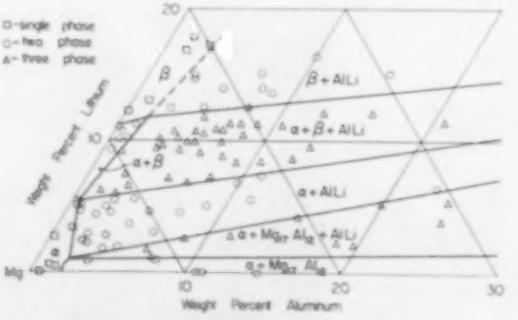

Fig. 10—100°C isothermal section of magnesium-rich corner of the Mg-Li-Al system.

It also seems probable from the tendency of the metastable condition to persist after 500 hr at 100°C that a massive precipitation of the AlLi can be avoided by suitable aging treatment. However, it remains to be positively demonstrated whether precipitation hardening of a sufficiently permanent type can be developed in this region.

Discussion of this paper, if any, will appear in JOURNAL OF METALS, November 1955, and in AIME Metals Branch *Transactions*, Vol. **203**, 1955.

References

[1] R. S. Dean: The Present Status of Electrolytic Manganese and Its Alloys. *Trans.* AIME (1944) **156**, p. 301; METALS TECHNOLOGY (June 1944).

[2] W. Hume-Rothery: Equilibrium Relations and Some Properties of Magnesium-Lithium and Magnesium-Silver-Lithium Alloys. *Journal* Institute of Metals (1945) **71**, pp. 581-601.

[3] J. H. Jackson, P. D. Frost, A. C. Loonam, L. W. Eastwood, and C. H. Lorig: Magnesium-Lithium Base Alloys. *Trans.* AIME (1949) **185**, pp. 149-168; JOURNAL OF METALS (February 1949).

[4] R. S. Busk, D. L. Leman, and J. J. Casey: The Properties of Some Magnesium-Lithium Alloys Containing Aluminum and Zinc. *Trans.* AIME (1950) **188**, pp. 945-951; JOURNAL OF METALS (July 1950).

[5] P. D. Frost, J. G. Kura, and L. W. Eastwood: Aging Characteristics of Magnesium-Lithium Base Alloys. *Trans.* AIME (1950) **188**, pp. 1277-1282; JOURNAL OF METALS (October 1950).

[6] F. I. Shamrai: The Ternary System Al-Mg-Li: Part III Description; Projection of the Surface of the Liquidus; Isotherms at 400°C and 20°C; and Process of Crystallization. *Izvestiya Akademii Nauk SSSR* Otdelenie Khimicheskikh Nauk (May-June 1948) pp. 290-301.

[7] A. Jones, J. H. Lennon, R. R. Nash, W. H. Chang, and E. G. MacPeek: Magnesium Alloy Research Studies. *Technical Report 52-169* (September 1952) 125 pp. United States Air Force, Air Research and Development Command, Wright Patterson Air Force Base.

[8] W. L. Fink and L. A. Willey: Aluminum-Magnesium. *Metals Handbook*. (1948) p. 1163. Cleveland. ASM.

[9] G. F. Sager and B. J. Nelson: Lithium-Magnesium. *Metals Handbook*. (1948) p. 1224. Cleveland. ASM.

[10] P. Saldau and F. Shamrai: Equilibrium Diagrams of the System Magnesium-Lithium. *Ztsch. Anorg. Allgem. Chemie* (1935) **224**, pp. 388-398.

[11] E. E. Strange: The Determination of Lithium in a Magnesium Alloy by Use of the Flame Photometer. *Analytical Chemistry* (1953) **25**, p. 650.

Technical Note

Magnetic Properties of Manganese-Germanium Alloys

by R. J. Quigg, G. P. Conard, and J. F. Libsch

IN a recent investigation of the Mn-Ge system by Zwicker et al.,[1] it was reported that two intermetallic compounds in this system, Mn_3Ge_2 and Mn_5Ge_3, exhibited ferromagnetic properties. Of these, Mn_3Ge_2 was reported as "strongly magnetic" and Mn_5Ge_3 was said to be "weakly magnetic" but no actual values were given. In a study of magnetic alloys of nonmagnetic elements sponsored by the United States Army Signal Corps at Lehigh University, test bars having the nominal composition of these compounds were prepared by pressing elemental powders and sintering them in a purified helium atmosphere. Magnetic values obtained on these compounds are reported in Tables I and II.

It should be cautioned that the test bars were somewhat porous and that X-ray patterns run on these materials indicated that the homogenization in the samples was not complete, but that in each case the compound reported on was the dominant phase. The $(B\text{-}H)$ max and particularly the Br values for pure dense Mn_3Ge_2 can, therefore, be expected to be somewhat higher than those reported herein, while those for Mn_5Ge_3 may be in error in either direction.

Further details on this investigation are available in previous publications.[2,3]

References

[1] V. Zwicker, E. Jahn, and K. Schubert: The Manganese-Germanium System. *Ztsch. für Metallkunde* (1949) **40**, p. 433.

[2] Research Study on the Improvement of Magnetic Materials. *First Quarterly Progress Report* United States Army Signal Corps Contract No. DA-36-039-SC-42580 with Lehigh University (October 1953).

[3] Research Study on the Improvement of Magnetic Materials. *Fourth Quarterly Progress Report* United States Army Signal Corps Contract No. DA-36-039-SC-42580 with Lehigh University (July 15, 1954).

Table I. Induction Values of Mn_3Ge_2 (Nominal*)

Bar No.	$(B\text{-}H)$ max H = 4000, Gauss
34	213
39 B	200
36	222
36 retest	209
Apparent average	235

* Values of Br and Hc were found to be unreliable in view of the low $(B\text{-}H)$ max. Br was estimated as less than 100 gauss and Hc estimated as 30 to 40 oersteds.

Table II. Magnetic Values of Mn_5Ge_3

Bar No.	$B\text{-}H$ max H = 4000, Gauss	Br, Gauss	Hc, Oersteds
37 A	1450 +	90 --	29
37 B	1160	60 +	24
37 B (H = 3000)	1240	30	24
Apparent average	1300	60	25

R. J. QUIGG, formerly Graduate Student, Lehigh University, is associated with Rem-Cru Titanium Co., Midland, Pa., G. P. CONARD, and J. F. LIBSCH, Members AIME, are Assistant Professor of Metallurgy and Associate Director, and Professor of Metallurgy and Director, respectively, Magnetic Materials Laboratory, Lehigh University, Bethlehem.

TN 258E. Manuscript, Nov. 1, 1954.

This note is based on a portion of a thesis by R. J. Quigg submitted, in partial fulfillment of the requirements for the degree of Master of Science, to the Graduate Faculty, Lehigh University.

Structure and Magnetic Properties of Some Transition Metal Nitrides

by George W. Wiener and J. Aldred Berger

Several transition metal nitrides have been prepared and their saturation magnetization determined. On the basis of an atomic model of ferromagnetism involving a consideration of nearest neighbor interactions and the assumption that all atomic moments of the metal point in the same direction, it appears that the nitrogen interacts with *d*-shell of the transition metal in such a way as to reduce the magnetic moment.

THERE is a large class of materials having metallic properties which are formed by a combination of hydrogen, boron, carbon, oxygen, or nitrogen with the transition metals. Several attempts have been made to establish the type of metal-nonmetal bonding in these interstitial alloys because it is believed that many of the physical properties of these materials are determined by the characteristics of this bond. Several of these alloys are ferromagnetic, and thus a powerful method is available for investigating the structures in a direct manner by measuring the saturation magnetization. The latter is a fundamental property of ferromagnetic metals and alloys which depends primarily on the electron distribution surrounding the atom. For the first row of transition metals, this refers specifically to the 3*d*-shell. Since bonding involves the electronic configuration between atoms, there is reason to suppose that a relationship exists between ferromagnetism and bond type. In the case of the interstitial structures studied in this work, bonding will refer to the distribution of electrons between the transition metal and the nonmetal. Since these alloys have metallic properties, it is further proposed that any bonding interactions will involve the outer *p*-shell of the interstitial element and the incomplete *d*-shell of the transition metal. If this is the case, then the relationship between ferromagnetism and metal-nonmetal bonding is established qualitatively.

In order to investigate the subject quantitatively, certain transition metal nitrides were chosen because they have simple crystal structures, are ordered alloys, and are ferromagnetic. They also have sufficiently high saturation magnetization to be of technical interest.

Currently there are two major theories of ferromagnetism, each of which has been applied to the interpretation of the saturation magnetization in terms of atomic structure. They are usually referred to as the band theory and the atomic theory. The former has found widespread application to the study of pure metals and certain solid-solution alloys. However, it has not been applied to the interstitial structures or ordered alloys because it does not interpret the properties directly in terms of the crystal structure. The atomic theory on the other hand is especially suited to the study of interstitial structures because it permits an interpretation of ferromagnetic phenomena in terms of the crystal geometry. As has been pointed out previously, the nitrides have simple ordered crystal structures and, therefore, the choice of the atomic theory for the interpretation of the data is a natural one. One of the prime difficulties with the atomistic theory is that its mathematical justification is much more difficult, and for this reason its general acceptance will depend to a large extent on the value it has in explaining and predicting the results of experiment.

Before the presentation of the theoretical basis for understanding the metal-nonmetal bond, it is useful to review the ideas existing prior to this work.

Four different interpretations have been given to the metal-nonmetal bond. These are summarized as follows: 1—acceptance of electrons by the nonmetal from the incomplete *d*-shell of the transition metal, 2—transfer of electrons from the nonmetal to the incomplete shell of the transition metal, 3—no exchange of electrons between the two atoms, and 4—a resonating type of bond involving the *p* electrons of the interstitial atom giving rise to half bonds.

Zener[1-4] in a recent series of papers has proposed a new theory of ferromagnetism and has developed an explanation of the observed saturation magnetization of iron nitride (Fe,N) using the concept that nitrogen accepts electrons from the 3*d*-shell of iron. Jack,[5] on the basis of atom size considerations in iron carbonitrides, has proposed that nitrogen transfers or donates electrons to the inner 3*d*-shell. He found that the effective size of the carbon atom was less than that of nitrogen and thus suggested that the interstitial atoms give up electrons. Kiessling[6] has studied the borides of several transition metal atoms and proposed that boron loses one *p* electron to the transition metal. He postulated that the additional electron added to the metal lattice compensates for the loss in metallic properties which results from the increased metal-metal atom separation. Guillaud[7,8] has proposed similar arguments from some recent magnetic studies he had made on manganese nitride. However, he did not base his conclusions on a quantitative argument. Pauling,[9] in a recent paper, discussed electron transfer in intermetallic compounds. He classified nitrogen as a hyperelectronic atom which can increase its valence by giving up electrons. He classified the transition metals as buffer atoms which are capable of either accepting or giving up an electron. He pointed out that two factors are operating which promote electron transfer because they lead to increased stability. The first is an increase in the number of bonds, and the second is a decrease in the electric charges on the atoms. These ideas when applied to the interstitial nitrides would indicate a viewpoint favoring electron transfer by nitrogen to the transition metal. Hagg's arguments in favor of no exchange are adequately summarized by Wells.[10] Implicitly, Hagg

G. W. WIENER, Member AIME, is associated with Research Laboratories, Westinghouse Electric Corp., East Pittsburgh, Pa., and J. A. BERGER, Member AIME, is Professor and Head, Metallurgical Engineering Dept., University of Pittsburgh, Pittsburgh.

Discussion of this paper, TP 3914E, may be sent, 2 copies, to AIME by Apr. 1, 1955. Manuscript, May 19, 1954. Chicago Meeting, February 1955.

This paper is based on a thesis by G. W. Wiener submitted, in partial fulfillment of the requirements for the degree of Doctor of Philosophy, to the University of Pittsburgh.

regarded the nitrides as interstitial solutions without any *Me*-N interaction.

Rundle[11] has proposed a resonating type of bond involving the three *p* electrons of nitrogen. He called them half bonds because the nonmetal forms more bonds than it has bonding orbitals. He further assumed that the extreme brittleness of these materials is an indication of directed valence. It was also suggested that the interstitial compounds formed with the transition metals to the left of chromium have high melting points because of strong metal to nonmetal bonds. Although Rundle confined his ideas primarily to interstitial alloys of equal atomic composition, he suggested that a similar picture applies to the lower nitrides of the type Me_4N. In this case he suggested that the metal-metal bonding also must be important.

So far in the discussion, the evidence for each of the proposed bonding mechanisms has been inconclusive. Properties such as atom size, electrical conductivity, brittleness, and melting point do not yield a quantitative picture of the actual electron configuration. Although it is possible to establish the electron configuration of the incomplete 3*d*-shell from magnetic data, the diametrically opposite views of Zener and Guillaud could not be resolved from the data which existed at the time this research was begun. In spite of this disagreement, the measurement of magnetic saturation is considered one of the most promising methods of attacking the problem. In the next section there are presented certain theoretical ideas on the basis of which the saturation magnetization can be used to interpret the metal-nonmetal bond.

Theory

For the atom model of a metal, it is generally assumed that, when the free atoms are condensed to the solid state, the electrons originally associated with the free atom are still identified with it in the crystal lattice. This is true for all but the outer 4*s* electrons which are free and are distributed in a band. It must also be recognized even on this picture that the remaining electrons may overlap or interact with nearest neighbor atoms. On the basis of this model of a metal, Zener has postulated the following:

1—The incomplete *d*-shell of the transition metal has the highest net electron spin consistent with the total number of electrons available. This is based on Hund's rule of maximum multiplicity. To illustrate this rule, consider a 3*d* shell containing seven electrons. Each electron has associated with it a spin vector which will be positive or negative depending upon whether, in the examples illustrated, it points to the right or left. In filling up the *d*-shell, the electrons will be added so that spins of one direction will be added first. This has been shown by quantum mechanics to be a state of lowest energy. Therefore, the 3d' configuration can be represented as

$$\begin{matrix} \rightarrow & \rightarrow & \rightarrow & \rightarrow & \rightarrow \\ \leftarrow & \leftarrow & & & \end{matrix}$$
$$3d^7.$$

It is easily seen from this picture that there is a net spin of +3. Therefore atoms having an incompleted shell have associated with them a net spin vector, and each atom on the crystal lattice can be considered as a small magnet.

2—As a result of the overlap of nearest neighbor atoms, there will be an interaction tending to produce an antiparallel arrangement of the magnetic vectors. The extent of this overlap depends on the radius of the 3*d*-shell. It is known that the radius of the 3*d*-shell increases in going from the right to the left in the periodic table. Therefore in nickel and cobalt the overlap is sufficiently small so that a parallel arrangement may be expected. When iron is reached, however, there is considerable doubt as to the likelihood of a parallel arrangement. Finally, manganese and the elements to the left are no longer ferromagnetic.

3—The interaction opposing the overlap forces is believed to be due to the free or conduction electrons. It is postulated that the 4*s* electrons exert a force which aligns the magnetic vectors in a parallel manner.

Table I. Outer Atomic Configuration of Transition Metals

	Free Atom	Metallic State
Mn	$3d^5\ 4s^2$	$3d^5\ 4s^2$
Fe	$3d^6\ 4s^2$	$3d^7\ 4s^2$
Co	$3d^7\ 4s^2$	$3d^8\ 4s^2$
Ni	$3d^8\ 4s^2$	$3d^9\ 4s^1$

From postulates 1 and 2 just given, it is possible to write an equation representing the magnetic moment of an alloy in terms of the number of metal atoms in the unit cell. This is possible only if the orbital momentum is considered to be quenched, so that the total magnetization results only from the net spin of the unpaired electrons. This is generally the case for cubic alloys and is assumed in the equation given subsequently. Since magnetic moment is a vector, the direction pointing toward the right will be considered as positive throughout the rest of this paper. The net magnetic moment per unit cell of an alloy can be expressed by the equation

$$\mu_T = N_A\mu_A + N_B\mu_B \qquad [1]$$

where μ_T is the saturation moment in Bohr magnetons per unit cell

$$N_A\mu_A = (n_{AR} - n_{AL})\mu_A \qquad [2]$$

$$N_B\mu_B = (n_{BR} - n_{BL})\mu_B \qquad [3]$$

and n_{AR} is the number of A atoms per unit cell having spins pointing to the right, n_{AL} is the number of A atoms per unit cell all having spins pointing to the left, $\mu_A = (10\text{-}d_A)$, and d_A is the number of d electrons ≥ 5. Similar definitions apply to $N_B\mu_B$.

Substitution of 2 and 3 into Eq. 1 leads to

$$\mu_T = (n_{AR} - n_{AL})\,\mu_A + (n_{BR} - n_{BL})\,\mu_B. \qquad [4]$$

The use of Eq. 4 facilitates calculation of the experimental data. Experimentally, only the absolute magnitude of μ_T can be arrived at, but it must be remembered that μ_T can represent only a net moment pointing to the right or to the left. Examples of the use of Eq. 4 will be given in discussing the experimental data.

In using Eq. 4 it is necessary to postulate the configuration of the *d* and *s* electrons when the free atom is condensed into the solid state. It is generally recognized that some of the 4*s* electrons for the transition metals are demoted to the 3*d* band. If it is assumed with Zener[1] that, when the atoms are condensed to the solid state, one of the two 4*s* electrons is demoted to the *d*-shell, then the configuration given in Table I will result.

With the appropriate model, the data in Table I

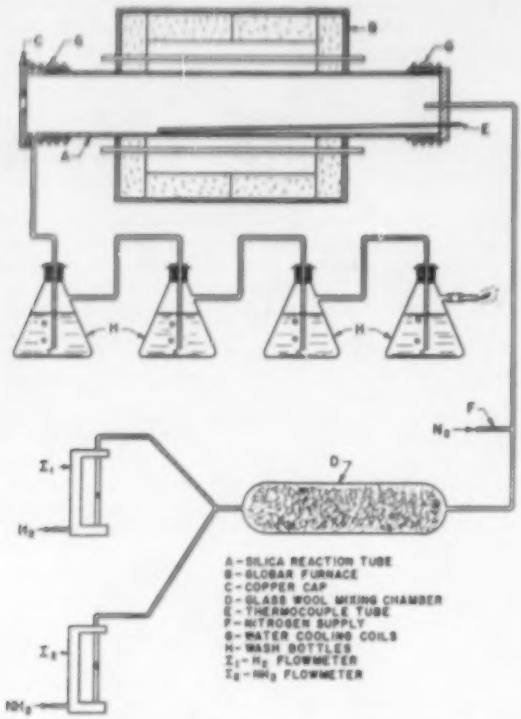

Fig. 1—Schematic diagram of nitriding furnace.

together with Eq. 4 can be used to calculate various values of μ_r.

Prior to this investigation, the only known cubic ferromagnetic nitrides were manganese nitride (Mn_4N) and iron nitride (Fe_4N). Since neither of these nitrides can be analyzed adequately in terms of the theory developed in this paper, it was decided to study additional alloys. These included iron nickel nitride (Fe_3NiN), iron platinum nitride (Fe_3PtN), and a face-centered-cubic alloy of cobalt containing 1 pct N in solid solution.

Experimental Procedure

The experimental procedure described in this section may be divided into three main categories: 1—preparation of the nitrides, 2—structure of the nitrides, and 3—magnetic saturation measurements. The samples were prepared by reaction with ammonia-hydrogen gas mixtures, and crystal structures were determined by the Debye-Scherrer powder method on ground samples. Magnetic measurements were made using a force method.

Preparation of Iron Nickel Nitride (Fe_3NiN): A master Fe-Ni alloy was melted in vacuum with the following analysis: 0.012 wt pct C, 0.0057 wt pct N, 27.5 wt pct Ni, a trace of cobalt, manganese, and copper, aluminum not detected, and the balance iron. The ingot was processed to strip 0.004 and 0.002 in. thick in which form it was ready for nitriding.

Nitriding was carried out in a quartz tube furnace assembled as shown in Fig. 1. The proper NH_3/H_2 ratio in equilibrium with Fe_3NiN was obtained by trial. Fig. 2 shows a typical structure of partial nitriding. In this micrograph the dark etching layer on the sample shows the small nitride penetration. It will be noticed that the nitride has penetrated completely through the grain boundaries of the austenite. It is noteworthy that the nitride layer in this alloy appears black. This is an etching effect due to the presence of the γ Fe-Ni phase. X-ray analysis confirmed the fact that the structure given in Fig. 2 is a mixture of γ (face-centered-cubic) Fe-Ni and Fe_3NiN.

Since it was apparent that the nitride phase forms under these conditions, it was decided to reduce the thickness of the strip. Since it is known that diffusion proceeds more slowly in the γ region, the use of a thinner strip allows the attainment of a homogeneous alloy in a reasonable time. Fig. 3 shows the structure of a 2 mil strip, sample 19b, after 48 hr. This structure is two-phase although the nitriding has apparently proceeded completely through the strip. This alloy was heated an additional 24 hr without further change in composition. In order to obtain complete nitriding, it was decided to use a richer gas mixture. The final ratio of NH_3/H_2 which gave complete nitriding was 1.0, with a linear flow rate of 30 cm per min. The structure of sample 24b, obtained after 48 hr, is given in Fig. 4. Sample 24b was used for extensive magnetic and X-ray investigation. The nitrogen content by weight is 5.82 pct (19.99 atomic pct).

The cracked appearance is due to separation at grain boundaries and the fact that the alloy is glass brittle. Therefore, during polishing and mounting it is susceptible to cracking. The metallographic preparation of the nitrides followed conventional procedures. The samples were mounted in lucite and polished mechanically, finishing with a wet wheel on which sapphire dust was the abrasive.

Preparation of Iron Platinum Nitride, (Fe_3PtN): The master alloy was melted in the same manner as for the Fe-Ni alloy. The ingot analysis is as follows: 0.018 wt pct C, 0.004 wt pct N, 55.3 wt pct Pt, a trace of cobalt, manganese, silicon, copper, and aluminum, and the balance iron. The cast ingot was cold rolled directly to 0.002 and 0.001 in. with intermediate anneals at 1000°C in a hydrogen atmosphere whenever necessary.

Initial work with the Fe-Pt strip indicated that diffusion is extremely slow. Fig. 5 shows a 2 mil strip, sample 26a, nitrided at 600°C in an ammonia-hydrogen mixture of 1.32 to 1.65. Note the layer of nitride on the surface with evidence of penetration along grain boundaries. At this point, it was realized that a 2 mil strip would require excessively long times for nitriding, so further nitriding was done on 1 mil strips. At the same time, it was thought that a richer gas mixture together with increased temperature would aid in the nitriding. It is recognized that increasing the temperature also increases the amount of ammonia dissociation. However, from the structures observed metallographically, the formation of

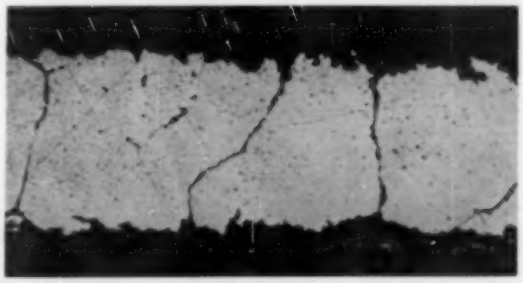

Fig. 2—Partially nitrided Fe-Ni alloy. Etched with 2 pct nital. X500. Area reduced approximately 30 pct for reproduction.

Fig. 3—Partially nitrided Fe-Ni alloy. Etched with 2 pct nital. X500. Area reduced approximately 30 pct for reproduction.

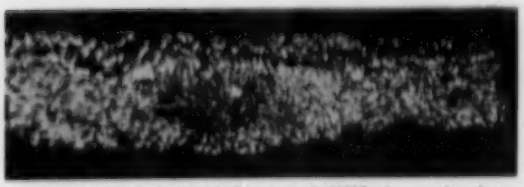

Fig. 4—Fe_4NiN. Etched with 2 pct nital. X500. Area reduced approximately 30 pct for reproduction.

Fig. 5—Partially nitrided Fe-Pt alloy. Etched with HCl plus H_2O_2. X500. Area reduced approximately 30 pct for reproduction.

the nitride phase was proceeding satisfactorily and increasing the reaction rate would be beneficial. Finally a sample identified as 30b, was nitrided for 68 hr in an ammonia-hydrogen ratio of 1.66 at 700°C and then an additional 22 hr at 600°C with a resulting nitrogen content of 3.32 wt pct (18.45 atomic pct). Magnetic and X-ray measurements were carried out on this sample. A second specimen, 32a with 3.15 wt pct N (17.65 atomic pct) was also prepared and used for magnetic measurements.

Structure of the Nitrides: The X-ray diffraction techniques used to determine the crystal structure of the nitrides are briefly described. Strip samples of Fe_4NiN, prepared as described previously, were ground in an agate mortar to pass 200 mesh and analyzed on a Norelco spectrometer using $CoK\alpha$ radiation. The observed intensities were measured by noting the number of counts recorded on a Geiger-counter as the spectrum was scanned at very slow speeds. Several runs were made to reduce the effect of background; this is particularly important in the case of the weak superlattice lines.

The structure of Fe_3PtN was determined, using a single crystal monochromator. The sample was ground as described for the Fe_4NiN. The pattern was obtained using a 9 cm diam camera with $FeK\alpha$ radiation and a flat crystal of lithium fluoride arranged so that the reflections from the (200) plane would strike the sample.

A reproduction of the X-ray pattern is given in Fig. 6. The superlattice lines as well as the principal lattice lines are indicated on the figure. It will be noted that the superlattice lines are strong and give unmistakable evidence of ordering. A Leeds and Northrup nonrecording microphotometer was used to measure the intensity of the lines.

Crystal Structure Data: Both Fe_3PtN and Fe_4NiN are fully ordered structures. They are described by the following coordinates: platinum or nickel at (0, 0, 0), iron at (½, ½, 0) (½, 0, ½) (0, ½, ½), and nitrogen at (½, ½, ½). The lattice parameters for each are included in Tables II and III giving the results of the structure determination.

Table II summarizes the information for Fe_3PtN. It will be noted that structure I agrees best with the observed values.

In Table III are the data for Fe_4NiN. The calculated intensities were carried out in the same manner as for the Fe_3PtN with the exception that no absorption correction had to be made. This is due to the fact that the sample thickness in the cassette was sufficient to eliminate the need for the correction. The structural and magnetic data for Fe_4NiN are given in Table V.

Magnetic Saturation Measurements: Early in this work it became apparent that samples of suitable size and ductility for conventional ballistic measurements could not be prepared. It was decided therefore to use a force method for determining the saturation magnetization. It is well known that, when a ferromagnetic is placed in an inhomogeneous magnetic field, the force experienced by the sample is given by the equation

$$F = m\sigma \frac{dH}{dX} \qquad [5]$$

where F is force $= g(M' - m)$, dynes; g is the acceleration due to gravity, 980 cm per sec^2; M' is the increase in weight experienced on application of field; m is the mass of sample, grams; σ is the saturation moment per gram, emu per gram; and dH/dX is the field gradient perpendicular to field.

Apparatus Employed for Making Magnetic Measurements: A diagram of the apparatus used is shown in Fig. 7. An ordinary analytical balance A was used for making the force measurements. To the balance arm a copper wire B is attached which in turn is connected to a quartz tube C. This suspension is located so that the end containing the sample is in the region of maximum gradient. For other than room temperature measurements, the sample is surrounded by a furnace or Dewar flask D. This is supported on a wooden pedestal E. Finally, a guide F is used to prevent lateral motion. The helium gas enters a flow meter H and is dried through a liquid nitrogen trap G. The sample is placed either in a brass or plastic holder as indicated by I and J. The sample holder I is a cylindrical container capped at both ends for use with powder samples. Holder J is simply a cap which can be slipped over the quartz tube C and is used for strip samples. The thin section of sample is placed in the slit shown in the figure. The design of the pole faces is due to Sucksmith.[12] The apparatus is calibrated by using pure iron. This is necessary to determine accurately the field gradient. Generally fields of the order of 12,000 oersteds were used for the iron-base nitrides and 19,000 oersteds for the cobalt samples.

The initial measurements were made on solid sections of the nitrided strip. These were supported in

Fig. 6—X-ray photograph of Fe_3PtN. Sample 30b,.

Table II. Structure of Fe_2PtN Lattice Parameter $a = 3.857$A

H KL	Obs. Intensity	I. Calc. Intensity Structure with N at (½ ½ ½)	II. Calc. Intensity Structure with N at (0 0 ½)	Pct Deviation of Structure I	Pct Deviation of Structure II
100 S	530	988	795	+6.9	+54.0
110 S	1130	1089	985	−1.9	−11.0
111	2630	2537	2537	−3.1	−3.1
200	1990	1873	1873	−5.9	−5.9
210 S	980	1048	1202	+6.0	+20.0
211 S	1200	1313	1109	+9.4	−7.6
220	2750	2606	2606	−5.2	−5.2
221	1190	1184	1407	+2.9	+22.0
300					
310 S	1230	1353	1076	+9.2	−14.0
311	6050	5122	5122	−15.3	−15.3
222	2100	2160	2160	+2.9	+2.9
320 S	1380	1470	1719	+6.5	+25.0
321 S	4600	4790	4147	+4.1	−9.8

a groove as shown in Fig. 7. Since the suspension holding the sample was free to rotate, on application of a field the sample would orient itself with the thickness parallel to the field. This orientation minimizes the demagnetization factor. Calculations based upon ellipsoidal formulae show that for this orientation the demagnetization factor is negligible. Later measurements were carried out with powders because larger sample weights could be used. No differences in the saturation values at room temperature could be found. This indicates that the magnetic hardness due either to shape or crystalline anisotropy is not sufficiently great to cause difficulty in obtaining saturation of the nitride powders. Figs. 8, 9, and 10 summarize the data obtained on the nitrides of Fe-Ni and Fe-Pt. As stated earlier, a sample of Co-N alloy was studied also, and the measurements are summarized in Table IV. Jack,[11] who has prepared this material, determined the structure and found it to be face-centered-cubic witn a lattice constant equal to 3.560A.

Since there is less than a 1 pct change in the saturation magnetization of cobalt extrapolated to absolute zero, the precision of the method did not warrant measurements at low temperature.

Correlation of Theory and Experimental Results

In this section the magnetic data together with the results of structural investigations are discussed. For convenience, the structural and magnetic data are summarized in Table V.

It will be shown that a single atomic model can

Table III. Crystal Structure of Fe_4NiN Lattice Parameter $a = 3.790$A

H KL	Obs. Intensity	I. Calc. Intensity Structure with N at (½ ½ ½)	II. Calc. Intensity Structure with N at (0 0 ½)	Pct Deviation of Structure I	Pct Deviation of Structure II
100 S	33	34	299	+3.0	+806
110 S	256	371	125	+39.4	−55.0
111	7191	7276	7276	+1.2	+1.2
200	4225	4236	4236	+0.3	+0.3
210 S	—*	0.030	94	—†	—
211 S	84	127	36	+51.0	−56.0
220	2231	2203	2203	−1.3	−1.3
221	—*	0.33	41	—†	—
300 S					
310 S	30	40	28	+33.0	−6.7
311	2256	2190	2190	−3.4	−3.4
222	851	884	884	+3.8	+3.8

* Line not detected on the spectrometer under the experimental conditions used.
† The fact that this line is not detected supports the view that structure I is the more correct configuration, as the calculated intensity for this structure is very low.

Table IV. Magnetic Properties of Cobalt

Sample	Atomic Pct N	Experimental (This Investigation)	Literature
Pure cobalt	Nil	160.8	161.0[16]
Face-centered-cubic cobalt	2.72	153.5	—
Face-centered-cubic cobalt	Nil	—	164.0[16]

Table V. Structure and Magnetic Data of Nitrogen Alloys

Alloy	Structure	Lattice Constant in A	Nearest Me-Me Distance in A	σ cgs	Curie Point
Fe_4N*	Cubic	$a_0 = 3.795$	2.683	208.5	488°C
Mn_4N*	Cubic	$a_0 = 3.857$	2.727	24.2	465°C
Fe_3NiN	Cubic	$a_0 = 3.790$	2.680	166	487°C
Fe_2PtN	Cubic	$a_0 = 3.857$	2.727	119	309°C
$Co_{3.28}N_{0.44}$	Cubic	$a_0 = 3.560$	2.517	153.5†	—

* Magnetic data from Guillaud.
† Room temperature saturation magnetization.

be used to explain the five cubic nitrogen alloys investigated.

Interpretation of Cubic Nitrides: From the model shown in Fig. 11, it will be recognized that two basic assumptions have been made. The first of these is that there is inherently an antiferromagnetic arrangement of the iron atoms and the second is that nitrogen acts as an acceptor of electrons. On the basis of experimental evidence prior to this research, arguments for this point of view depend primarily on theoretical considerations. As will be shown subsequently, this viewpoint also explains the observed data for the face-centered alloy Mn,N. However, in the light of the present experiments certain modifications of the original model seem to be required.

In Table V, the saturation magnetization per gram of Fe,N is given as 208.5. Thus, the net number of Bohr magnetons per unit cell is calculated to be 8.86 by application of Eq. 6

$$\mu_0 = \frac{M.W. \times \sigma}{A \times \beta} \qquad [6]$$

where μ_0 is the number of Bohr magnetons per unit cell, $M.W.$ is molecular weight, σ is the saturation moment per gram, A is Avagadro's number $= 6.025 \times 10^{23}$ atoms per mol, and β is Bohr magneton $= 0.927 \times 10^{-20}$ erg per gauss. If the net magnetization per atom is required, then for Fe,N the number of Bohr magnetons per atom, $\mu_N = 1.77$, where $\mu_N = \mu_0/5$. If the orbital moment is considered to be quenched, then the value μ_0 must be interpreted as

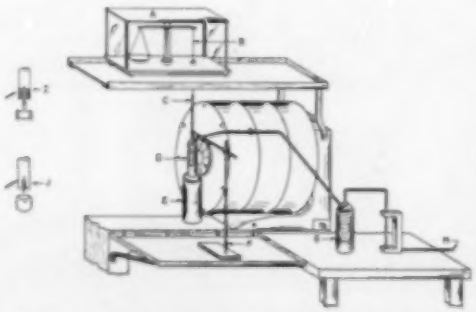

Fig. 7—Diagram of apparatus for magnetic measurements.

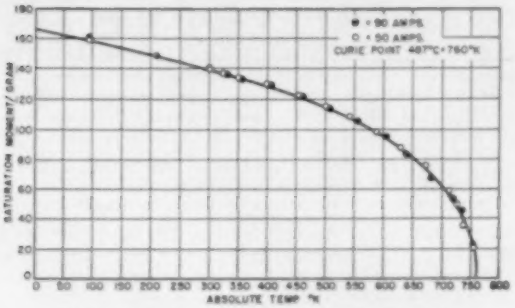

Fig. 8—Magnetization curve of Fe_4NiN sample 24B.

arising from the unpaired *d* electrons existing in the alloy. Then on the basis of a simple model, it is possible to postulate certain spin arrangements and calculate the magnetic moment, using Eqs. 1 or 4 presented in the section on theory. Consider the case for Fe,N where the atoms have the arrangement given in Table VI. The theoretical value μ_T is in good agreement with the experimental value μ_0 given previously. It will be recognized that this configuration with an antiparallel arrangement of iron atoms requires nitrogen to act as an acceptor of electrons. However, it is immediately obvious that a certain ambiguity exists, for if nitrogen is considered a donor of electrons the configuration in Table VII may exist.

This value of μ_T depends on having all iron atoms parallel. The major objection to this second interpretation is that the overlap of the metal atoms would be a factor favoring the antiparallel arrangement. However, it must be pointed out that the addition of nitrogen to the lattice expands it so that nearest neighbors are 6 pct farther apart than in normal face-centered-cubic iron. Since this model is the one considered as a result of this investigation to be the most desirable interpretation of not only the magnetic properties but also the metal-nitrogen bond, it is given in Fig. 12. The configuration follows the notation used earlier.

Now consider the case for manganese nitride (Mn,N) when the atoms have the arrangement given in Table VIII.

Since the normal state for manganese metal (solid) has been chosen as $3d^5\,4S^1$, it will be recognized that the configuration in Table VIII represents nitrogen acting as an acceptor of electrons. Furthermore, this has an antiparallel arrangement to conform with the large size of the manganese atom and the resulting overlap. However, more detailed examination shows that this case is not unique; case II given in Table IX gives the identical value of μ_T. Calculating μ_T as in Table IX gives a value of −1.0. The minus sign, of course, originates from the coordinate system chosen. Experimentally, only the magnitude of the magnetic moment is measured, so

Table VI. Atom Arrangements for Fe,N for Nitrogen as an Acceptor of Electrons

Atom Type	Coordinates	No., *d* electrons	μ	$n_\uparrow$	$n_\downarrow$
Fe	(0, 0, 0)	7	3	0	1
Fe	(½, ½, 0)	6	4	1	0
Fe	(0, ½, ½)	6	4	1	0
Fe	(½, 0, ½)	6	4	1	0

$\mu_T = (n_{A\uparrow} - n_{A\downarrow})\,\mu_A + (n_{B\uparrow} - n_{B\downarrow})\,\mu_B$ (Case I).
$\mu_T = (2)_4 + (0 - 1)3 = 9.0$.

Table VII. Atom Arrangements for Fe,N for Nitrogen as a Donor of Electrons

Atom Type	Coordinates	No., *d* electrons	μ	$n_\uparrow$	$n_\downarrow$
Fe	(0, 0, 0)	7	3	1	0
Fe	(½, ½, 0)	8	2	1	0
Fe	(0, ½, ½)	8	2	1	0
Fe	(½, 0, ½)	8	2	1	0

$\mu_T = (3)2 + 1(3)$.
$\mu_T = 9.0$.

that agreement of the experimental results with the two models is excellent.

Although the manganese data are ambiguous, they do give rise to an important concept, namely that unbalanced spins result from the introduction of the nitrogen to the face-centered-cubic lattice. It has been shown that, in both configurations of manganese nitride, equal numbers of manganese atoms are pointing to the right and left. If all atoms were equivalent, Mn,N would show no net magnetic moment. The face-centered atoms are closer to the nitrogen, and it is suggested that these atoms interact with the nitrogen atom so as to give the unbalance in spins required to agree with experiment. A picture of these configurations is given in Fig. 13. It is suggested that the argument just presented for nitrogen interaction with nearest neighbors in Mn,N applies equally well to Fe,N and the ternary alloys discussed subsequently. The discussion of Fe_4NiN parallels to that for Fe,N. The observed saturation

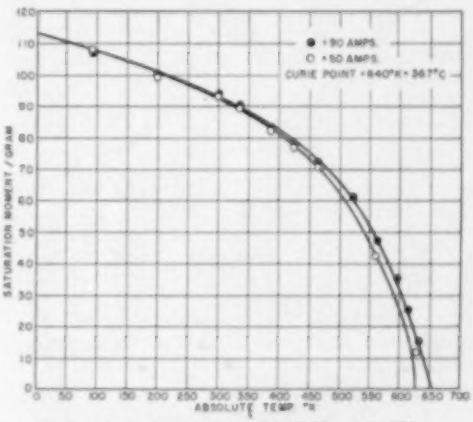

Fig. 9—Magnetization curve of Fe_4PtN sample 30b.

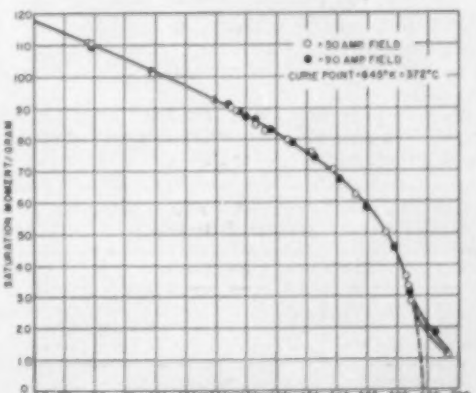

Fig. 10—Magnetization curve of Fe_4PtN sample 32A.

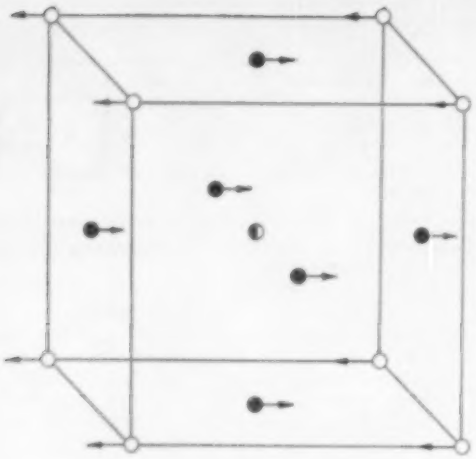

◐ Nitrogen Atom ($\uparrow\downarrow\uparrow\downarrow\uparrow$) $2p^6$
● Fe Atom ($\uparrow\downarrow\uparrow\uparrow\uparrow$) $3d^6$
○ Fe Atom ($\uparrow\downarrow\uparrow\downarrow\uparrow$) $3d^7$

Fig. 11—Structure of iron nitride (Fe_4N).

magnetization per gram is 166 corresponding to a μ_0 of 7.15. Case I is given the arrangement in Table X.

If the μ_T given in Table X is compared to the observed value μ_0, the disagreement is at once apparent. The choice of a parallel arrangement is based primarily on the smaller size of the nickel atom as compared to the iron atom. It is further assumed that nitrogen acts as an acceptor of electrons. If the antiparallel condition of Mn_4N or Fe_4N is chosen, agreement with experiment is still poor.

Now consider Case II given in Table XI. In this case a parallel arrangement is chosen, and nitrogen is considered to donate electrons.

The last alloy of this group to consider is the Fe_3PtN. The X-ray data give the detailed crystal structure and, as with the Fe-Ni-N alloy, it is ordered. From the saturation moment per gram of 115 given in Table V, μ_0 is calculated to be 7.90. The configuration analogous to that given under case II for the Fe_3NiN yields a value of μ_T equal to 7.0. It is recognized that this deviates from the experimental value by 12 pct. A consideration of the atomic size of platinum (1.38Å) and the atomic size of nickel (1.24Å) does not offer a reasonable explanation because the nearest neighbor distance also increases. It should be noted, however, that this alloy contains about 10 pct less nitrogen than the Fe_3NiN.

By way of review, these data have been discussed in the framework of Zener's theory with two principal exceptions: 1—parallel or a ferromagnetic

Table VIII. Atom Arrangements for Mn_4N for Nitrogen as an Acceptor of Electrons

Atom Type	Coordinates	No., d electrons	ρ	$n_\uparrow$	$n_\downarrow$
Mn	(0, 0, 0)	6	4	0	1
Mn	(½, ½, 0)	5	5	0	1
Mn	(0, ½, ½)	5	5	1	0
Mn	(½, 0, ½)	5	5	1	0

μ_0, calculated from the data in Table V, is 1.09.
$\mu_T = (n_{\uparrow\Gamma} - n_{\downarrow\Gamma})\,\mu_B + (n_{\uparrow\Gamma'} - n_{\downarrow\Gamma'})\,\mu_B$ (Case I).
$= (2 - 1)3 + (0 - 1)4)$.
$\mu_T = 1.0$.

Table IX. Atom Arrangements for Mn_4N for Nitrogen as a Donor of Electrons

Atom Type	Coordinates	No., d electrons	ρ	$n_\uparrow$	$n_\downarrow$
Mn	(0, 0, 0)	6	4	0	1
Mn	(½, ½, 0)	7	3	0	1
Mn	(0, ½, ½)	7	3	1	0
Mn	(½, 0, ½)	7	3	1	0

$\mu_T = 3\text{-}4 = -1.0$ (Case II).

alignment of the spins in all the alloys of iron, and 2—nitrogen interaction in such a way as to donate electrons to the 3d-shell. In order to verify either of these premises would require extensive quantum mechanical calculations for the alloy or neutron diffraction experiments.

There is a certain amount of experimental evidence in the literature pointing to the fact that an interstitial element exists as a positive ion in the metal. Dayal and Darken[14] have shown in some experiments on the mobility of carbon that it behaves approximately as an ion with a +4 charge. Jack[4] also has postulated this behavior for nitrogen on the basis of structural data and size consideration in iron carbonitrides. A weaker but additional argument from this point of view may be derived from considering the structural data of the nitrides themselves. The lattice parameter of Fe_3NiN, for example, is 3.790Å. Since the normal radius of the iron atom is 1.26Å, it is easily calculated that the interstitial hole for the nitrogen atom is 0.635Å. The normal covalent radius for nitrogen is given as 0.77; hence, accommodation of nitrogen in the iron lattice requires a smaller size for nitrogen (loss of electrons).

On the basis of the model developed previously, it may be postulated that nitrogen can reduce the saturation magnetization by more than just dilution. That is, it can interact with the 3d-shell contributing up to approximately 3 electrons per atom of nitrogen. Unfortunately, this effect can be verified in very few metals because of the low solubility. However, the face-centered phase of cobalt is useful for studying this effect. In Table XII are given data from which the effect of nitrogen on the saturation moment of cobalt can be determined. The sample measured may be represented by the formula ($Co_{0.96}N_{0.04}$). It is an alloy with nitrogen in solid solution. Using Eq. 6, the average number of Bohr

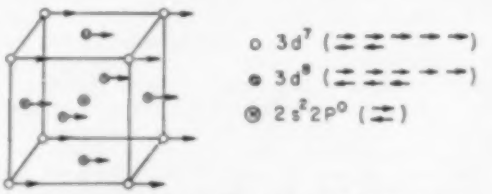

○ $3d^7$ ($\uparrow\downarrow\uparrow\downarrow\uparrow\uparrow\uparrow$)
● $3d^8$ ($\uparrow\downarrow\uparrow\downarrow\uparrow\downarrow\uparrow$)
⊗ $2s^2 2p^0$ ($\uparrow\downarrow$)

Fig. 12—Atomic model considered as a result of this investigation to be most desirable interpretation of not only magnetic properties but also metal-nitrogen bond.

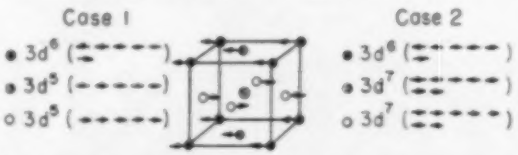

Fig. 13—Configurations for concept that unbalanced spins result from introduction of nitrogen to face-centered-cubic lattice.

magnetons per unit cell, μ_m, is calculated, and the effective number of Bohr magnetons per cobalt atom, μ_a, also can be evaluated, since all the magnetism can be considered as arising from the metal atoms. Furthermore, if the orbital momentum is to be considered quenched, then the average number of unpaired *d* electrons can be calculated also, and the effective contribution of the nitrogen can be estimated. This information is summarized in Table XII.

The value μ_a in Table XII was calculated from the most recent data of Myers and Sucksmith[10] for pure face-centered-cubic cobalt. They obtained an extrapolated value for the saturation magnetization of 167.3 at −273°C. The foregoing data support the viewpoint that nitrogen interacts with the *d*-shell in such a way as to reduce the moment.

Throughout this paper arguments have been advanced to show that nitrogen donates electrons to the metal and therefore may exist as a positive ion. However, it is not meant to imply that a typical ionic bond exists; the structures formed have the characteristics of metallic crystal lattices and not of ionic lattices of the NaCl type. Furthermore, the interaction proposed in this paper is between the *d* electrons of the metal and the *p* electrons of nitrogen, leaving the valence or conduction electrons essentially unchanged. It is recognized that, on the basis of the magnetic data presented, no unique choice between a covalent bond and the donation concept can be made, if the covalent bond is one between the nitrogen atom and the unpaired electrons of the metal *d*-shell. A covalent bond has already been proposed by Rundle[11] to explain the transition metal carbide and nitrides of the NaCl structures, and it may be that the characteristics of this bond persist in the materials studied here. However, the strong metallic character of the lower nitrides may modify this interpretation.

Conclusions

Magnetic and X-ray investigations have been completed on several transition metal nitrides. The relationship between structure and magnetic properties has been discussed in terms of a simple atomic model. Specifically, the following have been presented:

1—Iron platinum nitride (Fe_3PtN) has been prepared and its structure determined. It is a face-centered-cubic crystal with five atoms per unit cell. The nitrogen occupies an octahedral position in the center of the cell. The atom coordinates are Pt(0, 0, 0), Fe(½, ½, 0) (½, 0, ½) (0, ½, ½), and N(½, ½, ½).

2—Iron nickel nitride (Fe_3NiN) has been prepared and its structure is identical to the Fe-Pt alloy given in conclusion 1.

3—Complete magnetic data have been obtained on the foregoing two nitrides. Fe_3PtN has a saturation moment per gram of 115 (electromagnetic units) and a Curie temperature of 369°C. Fe_3NiN has a saturation moment of 166 (electromagnetic units) and a Curie temperature of 487°C. The curves showing variation of magnetization vs temperature of both alloys have been given. The values of the saturation moment reported were obtained by extrapolation to absolute zero.

4—The saturation moment per gram of a sample of cobalt metal containing nitrogen in solid solution was measured at room temperature and has a value of 153.5 (electromagnetic units). This represents a greater decrease in magnetic moment than could be expected on the basis of simple dilution.

5—A self-consistent hypothesis has been utilized to explain the effects observed for the three cubic nitrogen alloys studied in this research as well as for two previously reported cubic nitrogen alloys, iron nitride (Fe,N) and manganese nitride (Mn,N). This model is based upon three fundamental concepts: 1—Each metal atom can be considered as having its own shell of *d* electrons associated with it. 2—Magnetization results from electron spin only. 3—Nitrogen acts as a donor of three electrons to the 3*d*-shell of the metal; it may be considered either as a positive ion or alternately as forming a covalent bond involving interaction of the *p* electrons of the nitrogen with the unpaired *d* electrons of nearest neighbor metal atoms.

Table X. Atom Arrangements for Fe_3NiN for Nitrogen as an Acceptor of Electrons

Atom Type	Coordinates	No., *d* electrons	μ	$n_\uparrow$	$n_\downarrow$
Ni	(0, 0, 0)	9	1	1	0
Fe	(½, ½, 0)	6	4	1	0
Fe	(0, ½, ½)	6	4	1	0
Fe	(½, 0, ½)	6	4	1	0

$\mu_T = 12 + 1 = 13$ (Case I).

Table XI. Atom Arrangements for Fe_3NiN for Nitrogen as a Donor of Electrons

Atom Type	Coordinates	No., *d* electrons	μ	$n_\uparrow$	$n_\downarrow$
Ni	(0, 0, 0)	9	1	1	0
Fe	(½, ½, 0)	5	2	1	0
Fe	(0, ½, ½)	5	2	1	0
Fe	(½, 0, ½)	5	2	1	0

$\mu_T = 6 + 1 = 7.0$ (Case II).

Table XII. Magnetic Moments of Cobalt and Cobalt Containing Nitrogen in Solid Solution

Sample	μ_m	μ_a	No. of N Atoms per 100 Co Atoms	No. of Electrons per N Atom Donated
Nitrogen-cobalt (face-centered-cubic)	1.572	1.633	3.86	2.5
Pure cobalt (face-centered-cubic)	1.730	1.730	0	0

Acknowledgments

The authors would like to thank Dr. Clarence Zener, Associate Director of Research of the Westinghouse Research Laboratories, for his suggestions and guidance throughout this work. Acknowledgment is also due to Dr. W. J. Carr, Dr. K. H. Jack, and Miss J. Von Hoene, as well as to other members of the Westinghouse Research Laboratories for their help and cooperation.

Discussion of this paper, if any, will appear in JOURNAL OF METALS, November 1955, and in AIME Metals Branch *Transactions*, Vol. **203**, 1955.

References

[1] C. Zener: Interaction Between the d-Shells in the Transition Metals. *Physical Review* (1951) **81**, pp. 440-444.

[2] C. Zener: Part II Ferromagnetic Compounds of Manganese with Perovskite Structure. *Physical Review* (1951) **82**, pp. 403-405.

[3] C. Zener: Part III Calculation of the Weiss Factors in Fe, Co, Ni. *Physical Review* (1951) **83**, pp. 299-301.

[4] C. Zener: Part IV The Intrinsic Antiferromagnetic Character of Iron. *Physical Review* (1952) **85**, pp. 324-328.

[8] K. H. Jack: Binary and Ternary Interstitial Alloys II. *Proceedings* Royal Society (1948) **195A**, pp. 41-45.
[9] R. Kiessling: The Borides of Some Transition Metals. *Journal* Electrochemical Society (1951) **98**, pp. 166-169.
[10] C. Guillaud and J. Wyart: Propriétés magnetiques des Azotures de Manganese. *Comptes Rendus* (1946) **222**, pp. 71-73.
[11] C. Guillaud: Variation Thermique de l'Aimantation Spontanée. *Comptes Rendus* (1946) **223**, pp. 1110-1112.
[12] L. Pauling: Electron Transfer in Intermetallic Compounds. *Proceedings* National Academy of Sciences (1950) **36**, pp. 533-538.
[13] A. F. Wells: *Structural Inorganic Chemistry*. (1950) Oxford. Clarendon Press.
[14] R. E. Rundle: A New Interpretation of Interstitial Compounds—Metallic Carbides, Nitrides, and Oxides of Composition MX. *Acta Crystallographica* (1948) **I**, pp. 180-187.
[15] W. Sucksmith: The Measurement of Magnetic Saturation Intensities at Different Temperatures. *Proceedings* Royal Society (1939) **170A**, pp. 551-560.
[16] K. H. Jack: Unpublished research.
[17] P. Dayal and L. S. Darken: Migration of Carbon in Steel Under the Influence of Direct Current. *Trans.* AIME (1950) **188**, pp. 1156-1158; JOURNAL OF METALS (September 1950).
[18] H. P. Myers and W. Sucksmith: Spontaneous Magnetization of Cobalt. *Proceedings* Royal Society (1951) **A207**, pp. 427-446.
[19] R. M. Bozorth: *Ferromagnetism*. (1951) p. 867. New York. D. Van Nostrand Co. Inc.

Technical Note

Preliminary Investigation of the System Ti-Mg

by J. W. Fredrickson

VERY little information is available in the literature concerning the solubility of magnesium in titanium. Aust and Pidgeon[1] report the solubility of titanium in magnesium to be 0.0025 pct at 650°C and 0.015 pct at 850°C. X-ray diffraction studies failed to detect any evidence of solid solubility. Based on the fact that the addition of titanium to magnesium increases the c/a ratio of magnesium, Busk[2] suggested that the Mg-Ti system, like the Mg-Zr, is a peritectic. Eisenreich[3] reported the solubility of titanium in magnesium to be 0.003 pct at 655°C and 0.064 pct at 760°C. Removal of hydrogen from the melt increased the solubility of titanium to 0.115 pct at 800°C. Eisenreich proposes a peritectic-type diagram for the high magnesium side of the system. Recent work[4] with Ti-Mg diffusion couples indicate that the solid solubility of titanium in magnesium is extremely small and that there is limited solid solubility of magnesium in titanium.

Experimental work on the Ti-Mg system is complicated by the fact that the boiling point of magnesium is considerably below the melting point of titanium. Consequently, the usual alloying methods are impractical. Alloying was accomplished in this investigation by sheath-rolling compressed compacts.[5]

The alloys were made from titanium sponge and high purity magnesium. Chemical analysis of the sponge showed 0.04 pct Mg, <0.005 pct Al, <0.001 pct Cu, 0.05 pct Fe, 0.022 pct Mn, <0.0025 pct Ni, 0.007 pct Si, <0.005 pct V, and <0.01 pct Zn.

All heat treating was conducted in a protective atmosphere by encapsulating the specimens in fused silica ampules under a partial pressure of helium. Equilibrium was achieved by holding the specimens at temperature for periods of 24 to 120 hr. The alloys were hot rolled, cold rolled, and annealed prior to solution heat treatment.

Fig. 1 shows the constitutional diagram obtained for the Ti-Mg system up to 1.5 pct Mg. Oxygen was known to be present in the alloys; therefore, it is necessary to consider the alloys as ternary rather than binary and the diagram should be viewed as a plot of a section through the Ti-Mg-O system. Other investigators[6] have shown that the addition of oxygen to titanium stabilizes the α phase. The data presented in Fig. 1 indicate that the addition of magnesium to titanium tends to stabilize the β phase. Armour Research Foundation[7] has shown that the addition of magnesium to zirconium lowers the α transus and is classified as a β stabilizer in that system.

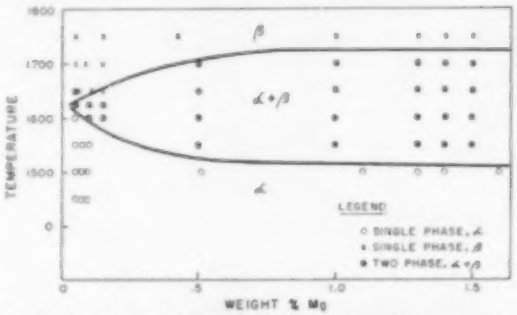

Fig. 1—Constitutional diagram obtained for the Ti-Mg system indicates that the addition of magnesium to titanium tends to stabilize the β phase.

Magnesium is soluble in solid titanium to the extent of at least 1.5 pct in both the α and β phases. No intermetallic compounds or magnesium-rich phases were observed either by light microscopy or X-ray diffraction. However, this does not negate the possibility that such phases exist at higher alloy concentrations.

References

[1] W. F. Aust and L. M. Pidgeon: *Trans.* AIME (1949) **185**, pp. 585-587; JOURNAL OF METALS (September 1949).
[2] R. S. Busk: *Trans.* AIME (1950) **188**, pp. 1460-1464; JOURNAL OF METALS (December 1950).
[3] H. Eisenreich: *Metall* (1953) **7**, pp. 1003-1006.
[4] Rensselaer Polytechnic Institute. Progress Report No. 1 to Wright Air Development Center, Wright-Patterson Air Force Base. Contract No. AF 33(616)-2312 (Feb.-Apr. 1954).
[5] J. R. Long: *Titanium, Report of Symposium, Dec. 16, 1948*. Sponsored by ONR (March 1949) pp. 27-46.
[6] E. S. Bumps, H. D. Kessler, and M. Hansen: *Trans.* ASM (1953) **45**, pp. 1008-1024.
[7] Armour Research Foundation, Final Report to Atomic Energy Commission, Contract No. AT (11-1)-149 (Apr. 14, 1952).

J. W. FREDRICKSON, Member AIME, is associated with Metallurgical Laboratories, The Dow Chemical Co., Midland, Mich.
TN 259E. Manuscript, Oct. 29, 1954.

Recrystallization Characteristics of Superpurity Base Al-Mg Alloys Containing 0 to 5 Pct Mg

by E. C. W. Perryman

The recrystallization characteristics of superpurity Al-Mg alloys containing 0 to 5 pct Mg, cold worked 20 to 80 pct, have been investigated by determining isothermal softening curves and by micrographic examination. The effect of magnesium on the rate of nucleation and growth has been determined using the micrographic method.

IN spite of the large amount of work which has been carried out on the recrystallization of aluminum and its alloys, there has been no complete investigation of the recrystallization characteristics of Al-Mg alloys. The most complete investigation is that reported by Bungardt and Osswald[1] who, working with commercial-purity materials, found that the temperature both of beginning and of complete recrystallization increased with magnesium content up to about 2 pct Mg, then decreased with a further increase in magnesium up to 5.0 pct, and thereafter increased again. Michaud and Segol[2] working with 99.93 pct Al also found the temperature of beginning of recrystallization to decrease as the magnesium content increased from 2.13 pct to about 4.5 pct. Chossat[3] using aluminum of 99.99 pct purity found that 0.12 pct Mg had no effect but that 0.4 pct Mg increased the recrystallization temperature by about 30°C. That no effect was found for 0.12 pct Mg does not agree with the later results reported by Demer and Beck[4] who found that 0.025 pct Mg in 99.99 pct Al increased the time for complete recrystallization and furthermore increased the activation energy for the recrystallization process. Kratz[5] using 99.997 pct Al found that 0.5 pct Mg increased both the temperature of beginning and of complete recrystallization by 100°C. Chadwick and Hooper[6] working with commercial-purity material found that 1 pct Mg increased the temperature of complete recrystallization by about 40°C for cold reductions in the range 17 to 72 pct. With smaller amounts of cold work produced by stretching (10 pct strain), they found no significant effect of magnesium. The latter result agrees with that obtained by Williams and Eborall[7] who found no effect of 2 pct Mg on the recrystallization temperature of commercial-purity aluminum strained 10 pct or less by stretching.

Experimental Procedure

Material Used: The chemical analyses of the materials used throughout this investigation are given in Table I.

E. C. W. PERRYMAN is Physical Metallurgist, Div. of Physics and Physical Metallurgy, Aluminium Laboratories Ltd., Kingston, Ont., Canada.

Discussion of this paper, TP 3925E, may be sent, 2 copies, to AIME by Apr. 1, 1955. Manuscript, July 6, 1954. Chicago Meeting, February 1955.

Table I. Composition of Alloys

Mg	Fe	Si	Cr	Mn	Cu
<0.001	0.003	0.002	<0.002	<0.001	0.002
0.48	0.003	0.001	<0.002	<0.001	0.002
0.99	0.002	0.001	<0.002	<0.001	0.002
1.98	0.004	0.001	<0.002	<0.001	0.002
2.54	0.004	0.002	<0.002	0.001	0.002
4.09*	0.003	0.002	<0.002	0.001	0.002
5.08*	0.004	0.002	<0.002	0.001	0.003

* Determined by wet analysis; all others determined spectrographically.

Fabrication: The alloys were cast in iron molds which had been washed thoroughly with alumina. After scalping, the ingots were annealed for 16 hr at 450°C, pressed, annealed at 450°C for 16 hr and hot rolled to 0.25 in. After hot rolling, the slabs were alternately annealed and cold rolled to 0.036 in. Cold-rolling reductions between intermediate anneals were kept at about 30 pct and a high intermediate annealing temperature of 450°C was used so as to obtain, as nearly as possible, similar starting grain sizes for the different materials. All intermediate anneals were done in a salt bath and were followed by cold-water quenching so as to retain all the magnesium in solid solution. The final cold reductions investigated were 20, 30, 40, 50, 60, and 80 pct. The initial grain sizes, that is, the grain size before the final cold reduction, were all very similar.

Annealing Procedure: Specimens, 1 in. sq, were cut from the 0.036 in. sheet and annealed in a salt bath, the temperature of which was controlled to ±2°C. Separate specimens were annealed for different times at 350°, 375°, 400°, and in one or two cases at 415°C and after annealing were quenched in cold water. The time taken for a specimen to reach temperature was approximately 5 sec. Metallographic examination after annealing showed that no precipitation of Mg_2Al_3 occurred during cooling.

Procedures Used for Determining Recrystallization Characteristics: All specimens were electrolytically polished and etched by the method described previously[8] and polishing was continued until about 0.002 in. had been removed from each side of the specimen. Using this technique, the smallest recrystallized grain which could be observed with cer-

Fig. 1—Al-1 pct Mg alloy cold worked 60 pct. Held 1 min at 350°C. X100. Area reduced approximately 35 pct for reproduction.

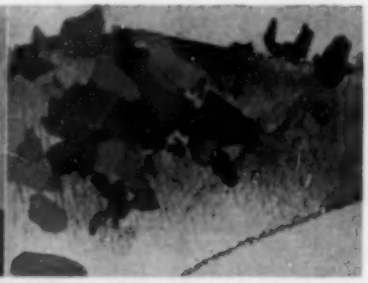

Fig. 2—Al-1 pct Mg alloy cold worked 60 pct. Held 2 min at 350°C. X100. Area reduced approximately 35 pct for reproduction.

Fig. 3—Al-1 pct Mg alloy cold worked 60 pct. Held 10 min at 350°C. X100. Area reduced approximately 35 pct for reproduction.

Fig. 4—Al-1 pct Mg alloy cold worked 60 pct. Held 30 min at 350°C. X100. Area reduced approximately 35 pct for reproduction.

tainty was about 2×10^{-4} cm. Grain size measurements were carried out using the intercept method. After microscopical examination, the VHN of each sample was determined.

Measurement of Percentage Recrystallization, Rate of Nucleation, and Rate of Growth: Using the same electropolishing and etching technique, five photographs were taken from each sample at X50 and the percentage of recrystallization, rate of nucleation, N, and rate of growth, G, measured by the method described by Anderson and Mehl.[8]

Results

Determination of Time for Complete Recrystallization: It is well known that the rate of recrystallization decreases rapidly towards the end of the process. Thus, at annealing times near that for complete recrystallization, the major part of the specimen is recrystallized but there still remains a small part which has only recovered. A hardness test will not be sensitive to these very small amounts of unrecrystallized material, so that the time for complete recrystallization determined by hardness testing alone is likely to be smaller than that determined by microscopical examination. In drawing the isothermal softening curves, both hardness and metallographic results have been taken into account. Figs. 1 through 4 show the progress of recrystallization in an Al-1 pct Mg alloy cold worked 60 pct and annealed at 350°C. The tendency for new recrystallized grains to nucleate at grain boundaries can be seen clearly from this series of photographs, especially Fig. 1. It will be seen also that there is a large tendency for groups of new grains to form. This was a common characteristic observed throughout this work. Typical isothermal softening curves for the different alloys cold worked 60 pct and annealed at 350°C are shown in Fig. 5. For comparison purposes, the hardness of the cold-worked material has been plotted at an annealing time of 1 sec. Wherever possible, the beginning of recrystallization is indicated on the curves; this corresponds to the time at which one or two nuclei about 2 to 5 microns in size could be observed. Thus, although recrystallization has started at the times indicated on the curves, the effect of this amount of recrystallization on the hardness would probably be negligible. It will be seen, however, that by the time this point has been reached there has been an appreciable decrease in hardness, the magnitude of which increased with increasing magnesium content and cold work. If the percentage of softening up to the beginning of recrystallization is determined, it is found that this is independent of magnesium content and percentage cold reduction and has a value of about 30 pct. This value of 30 pct and its independence of cold work has been confirmed in more recent work[9] in which the recovery process has been investigated more thoroughly. The percentage of softening is given by

$$\frac{H_{cw} - H_t}{H_{cw} - H_{cr}} \times 100$$

where H_{cw} is the hardness of cold-worked material, H_t is the hardness after annealing time t, and H_{cr} is the hardness of completely recrystallized material. It should be noted that, while the percentage of sof-

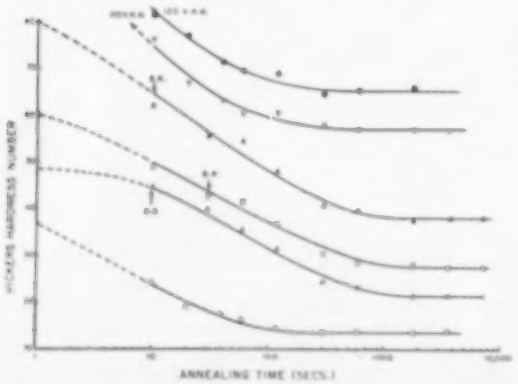

Fig. 5—Isothermal softening curves of Al-Mg alloys cold worked 60 pct and annealed at 350°C. Open circle represents superpurity aluminum; open upright triangle, Al-0.5 pct Mg; square, Al-1.0 pct Mg; closed triangle, Al-2.0 pct Mg; open inverted triangle, Al-4.0 pct Mg; and closed circle, Al-5.0 pct Mg.

tening mentioned previously is due to recovery, it has been shown by Perryman[9] that in superpurity aluminum further softening due to recovery takes place at the same time as recrystallization and it will be shown later that this also occurs for Al-Mg alloys.

The time for complete recrystallization was found to increase with magnesium content up to about 1.5 pct Mg and then decrease. A typical set of curves is shown in Fig. 6 for an annealing temperature of 350°C; similar curves were obtained at 375° and 400°C. Fig. 7 shows typical curves obtained by plotting the logarithm of the time for complete recrystallization against percentage of cold reduction; similar curves were obtained for the other alloys investigated. The linear relationship at large amounts of cold work agrees with Cook and Richards[10] results on copper.

At times for which the amounts of reaction are equal, the dependence of rate, r, on temperature can be expressed by the Arrhenius equation

$$r = ae^{-Q/RT}.$$

Using this equation, the logarithm of the reciprocal of the time for complete recrystallization was plotted against the reciprocal of the absolute temperature. Typical plots are shown in Fig. 8 for an Al-2.5 pct Mg alloy. From these plots, the activation energy and the recrystallization temperature for a 30 min anneal were determined. Figs. 9 and 10 show the activation energy as a function of magnesium content and cold work, respectively. Similar curves were obtained for the recrystallization temperature. For superpurity aluminum, it appears that both these parameters are proportional to the amount of cold work. However, consideration of these results and those of Williams and Eborall[7] shows that the curve departs from linearity at about 10 pct cold work. The curves for the 0.5, 1, and 2 pct Mg alloys depart from linearity at about 30 to 40 pct cold reduction. It appears from Fig. 10 that the activation energy of the Al-Mg alloys increases with decreasing cold work more rapidly than with superpurity aluminum.

The activation energy which has so far been determined is that for the complete annealing process. From the isothermal softening curves, the activation energy was determined also at low degrees of softening where it was known by microscopical examination that recrystallization had not started; this would be the activation energy for recovery. For material cold worked 20 pct, the activation energy was found to be 33,000 and 25,000 cal per gram-

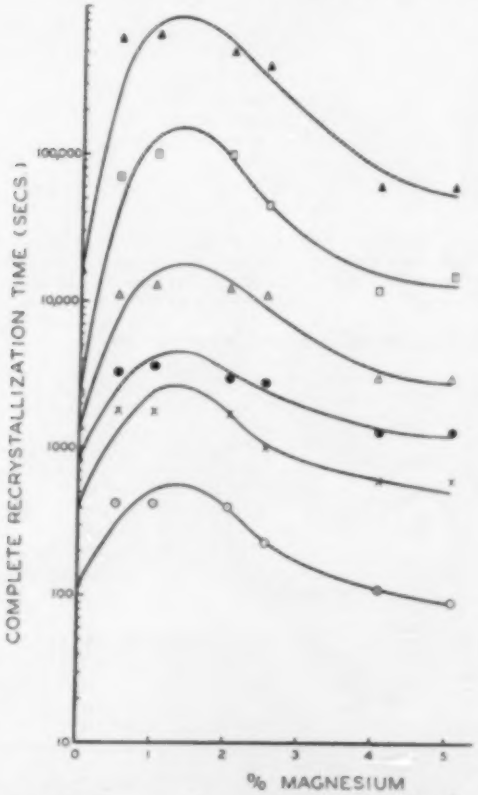

Fig. 6—Time for complete recrystallization of Al-Mg alloys containing 0 to 5 pct Mg at 350°C. Closed triangle represents 20 pct cold work; square, 30 pct cold work; open triangle, 40 pct cold work; closed circle, 50 pct cold work; X, 60 pct cold work; and open circle, 80 pct cold work.

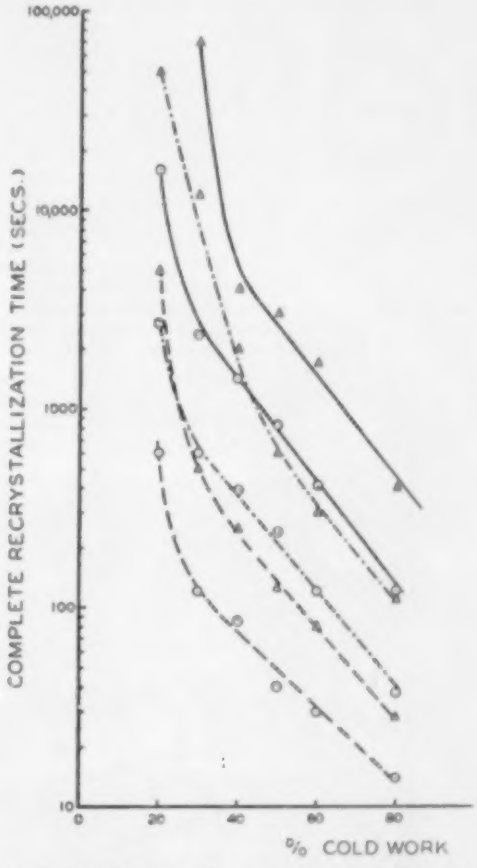

Fig. 7—Variation of time for complete recrystallization with percentage of cold reduction. Solid line and circle represent superpurity aluminum annealed at 350°C; solid, dashed line and circle, superpurity aluminum annealed at 375°C; dashed line and circle, superpurity aluminum annealed at 400°C; solid line and triangle, Al-2.0 pct Mg annealed at 350°C; solid, dashed line and triangle, Al-2.0 pct Mg annealed at 375°C; and dashed line and triangle, Al-2.0 pct Mg annealed at 400°C.

grain size was investigated using the 2.5 pct Mg

atom for superpurity aluminum and a 1 pct Mg alloy, respectively. Thus, it appears that 1 pct Mg decreases the activation energy for recovery but increases the activation energy for recrystallization which is in agreement with the work of Varley.[18]

Grain Size: The as-recrystallized grain size decreased with increasing magnesium content and

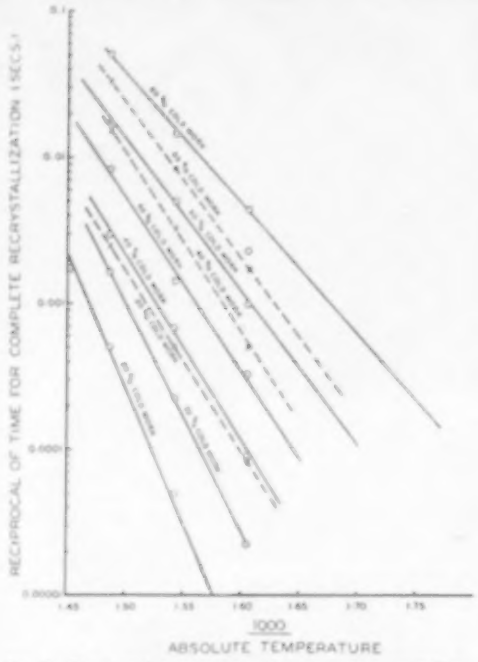

Fig. 8—Times and temperatures for complete recrystallization, Al-2.5 pct Mg alloy. Solid line and circle represent initial grain size ≏ 250μ; and dashed line and X, initial grain size ≏ 60μ.

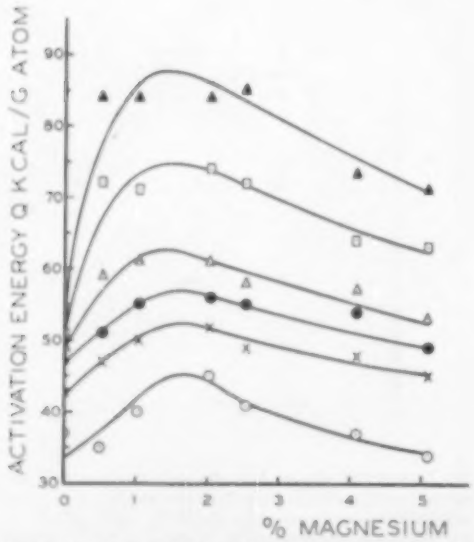

Fig. 9—Activation energy for the complete recrystallization process as a function of magnesium content. Closed triangle represents 20 pct cold work; square, 30 pct cold work; open triangle, 40 pct cold work; closed circle, 50 pct cold work; X, 60 pct cold work; and open circle, 80 pct cold work.

percentage of cold reduction and, within the experimental error, was independent of the annealing temperature. This independence of temperature agrees with the results of Eastwood et al.[19] but contradicts those of Demer and Beck.[4] Fig. 11 shows the grain size as a function of magnesium content. No sharp change in the curves at 30 to 40 pct cold reduction was observed as was found for recrystallization time, recrystallization temperature, and activation energy. Figs. 12 through 15 show the variation of grain size with magnesium content and also reveal the tendency for the grain structure to become more equiaxed with increasing magnesium content.

Channon and Walker[16] have shown that for α brass the logarithm of the as-recrystallized grain size is proportional to the square root of the percentage of cold reduction. Within the limits of experimental error either this relation or the simpler one, logarithm of the grain size is proportional to percentage of cold reduction, can be fitted to the experimental results reported here, see Fig. 16.

Effect of Initial Grain Size: The effect of initial

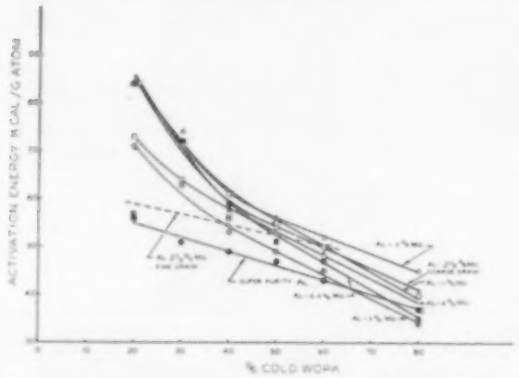

Fig. 10—Activation energy as a function of percentage of cold reduction. Closed circle represents superpurity aluminum; closed square, Al-0.5 pct Mg; open circle, Al-1 pct Mg; open triangle, Al-2 pct Mg; X, Al-2.5 pct Mg (large initial grain size); dashed line and half-closed circle, Al-2.5 pct Mg (fine initial grain size); open square, Al-4 pct Mg; and encircled cross, Al-5 pct Mg.

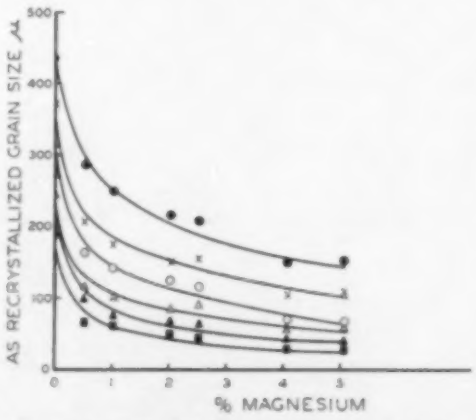

Fig. 11—As-recrystallized grain size as a function of magnesium content. Closed circle represents 20 pct cold work; X, 30 pct cold work; open circle, 40 pct cold work; open triangle, 50 pct cold work; closed triangle, 60 pct cold work; and closed square, 80 pct cold work.

grain size was investigated using the 2.5 pct Mg alloy. Isothermal annealing curves were obtained as before and the time for complete recrystallization determined, and the activation energy and recrystallization temperature calculated. The results are given in Table II and are included in Figs. 8 and 10.

The time for complete recrystallization, recrystallization temperature, activation energy, and as-recrystallized grain size are all smaller for the material with a fine initial grain size. It appears also from Table II that this effect of initial grain size increases with decreasing percentage of cold reduction, it being small at 60 pct. These results are in agreement with those of Channon and Walker[14] on brass, of Laurent and Batisse[15] on aluminum, and of Williams and Eborall[1] on aluminum and its alloys.

Micrographic Measurements of Percentage of Recrystallization, Rate of Nucleation, N, and Rate of Growth, G: From the electrolytically etched samples, five photographs were taken at random from each sample at a magnification of either X50 or X100. The new recrystallized grains were slightly lenticular in shape and so both the maximum and minimum diameter of the largest grain visible, which had not impinged upon another growing grain, was measured. Next, the number of recrystallized grains per unit area was counted and then the combined area of the recrystallized grains was measured using a planimeter. Measurements were made on superpurity aluminum and the 0.5, 1.0, and 4.0 pct Mg alloys cold worked 20 and 60 pct and annealed at 350°C.

Measurement of Percentage of Recrystallization—The isothermal recrystallization curves are shown in Fig. 17. It is interesting to note that the slopes of all these curves are very similar and can be superimposed simply by a shift along the time axis. The percentage of softening as a function of percentage of recrystallization is shown in Fig. 18. As observed for superpurity aluminum,[9] the softening is more rapid in the early stages of recrystallization which is probably due to the fact that recovery and recrystallization are proceeding together; once recovery has finished, there is a linear relationship. These results do not support the conclusions of Varley[16] who found that the percentage of softening was a linear function of percentage of recrystallization right from the beginning. The discrepancy between Varley's results and those presented here is probably because of the relatively inaccurate X-ray method he used for determining the percentage of recrystallization.

Table II. Effect of Initial Grain Size on Recrystallization of Al-2.5 Pct Mg Alloy

Pct Cold Reduction	Initial Grain Size, Microns	Recrystallization Temperature, °C	Activation Energy, Kcal per Gram-Atom	As-Recrystallized Grain Size, Microns
20	262	401	85	205
40	210	375	58	120
60	281	340	49	80
20	58	378	57	110
40	63	360	56	60
60	72	333	50	50

Measurement of Growth Rate, G—Fig. 19 shows the longest dimension of the largest grain as a function of annealing time at 350°C for superpurity aluminum and the alloys containing 0.5, 1.0, and 4.0 pct Mg. Curves of similar shape were obtained when the shortest dimension of the largest grain was plotted. It is interesting to note that there is no measurable incubation period and that the departure from linearity occurs at very small amounts of recrystallization, in general, at less than 10 pct recrystallization. These observations have been confirmed in more recent work[9] on superpurity aluminum. It is commonly supposed that the departure from linearity is because of impingement with other grains; this seems rather doubtful considering the very small amount of recrystallization which has occurred when this takes place. The growth rate measurements are summarized in Table III.

For a given amount of cold work, 0.5 pct Mg decreases the rate of growth considerably but further additions of magnesium have little effect. It does appear that the rate of growth is larger for the 4 pct than the other Al-Mg alloys. This will be discussed later. Increasing amounts of cold work in-

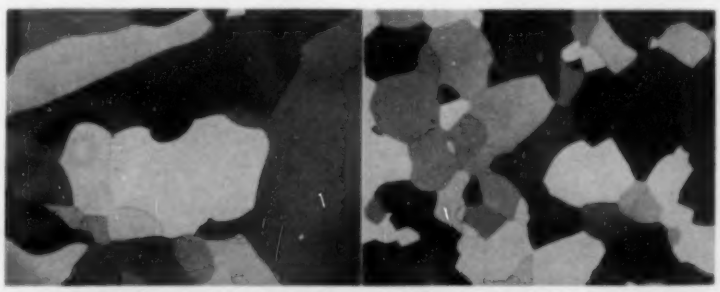

Fig. 12—Effect of magnesium on as-recrystallized grain size of Al-Mg alloys. Superpurity aluminum; 40 pct cold reduction and annealed at 350°C. X50. Area reduced approximately 35 pct for reproduction.

Fig. 13—Effect of magnesium on as-recrystallized grain size of Al-Mg alloys. Al-1.0 pct Mg; 40 pct cold reduction and annealed at 350°C. X50. Area reduced approximately 35 pct for reproduction.

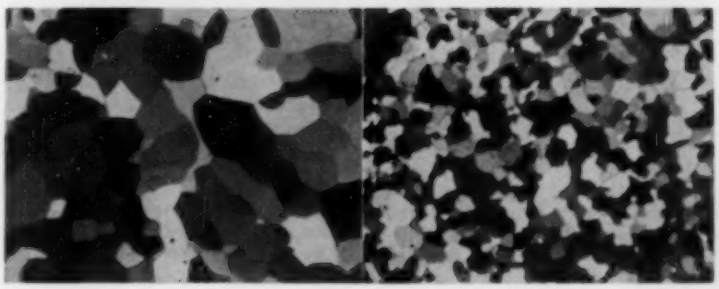

Fig. 14—Effect of magnesium on as-recrystallized grain size of Al-Mg alloys. Al-2.5 pct Mg; 40 pct cold reduction and annealed at 350°C. X50. Area reduced approximately 35 pct for reproduction.

Fig. 15—Effect of magnesium on as-recrystallized grain size of Al-Mg alloys. Al-5.0 pct Mg; 40 pct cold reduction and annealed at 350°C. X50. Area reduced approximately 35 pct for reproduction.

crease the rate of growth G. It is interesting to note that the rate of growth in the short direction is in all cases smaller than that in the long direction but that the difference is much greater for superpurity aluminum than for the Al-Mg alloys. Also, the difference is smaller for 20 pct cold reduction than for 60 pct cold reduction. These results help to explain why the grain structures in the Al-Mg alloys were more equiaxed. To investigate this point a little further, glancing-angle X-ray photographs were taken from the cold-worked specimens. For any given material, it was found that the texture was stronger for high than low amounts of cold work and furthermore was much stronger for superpurity aluminum than the Al-Mg alloys. The foregoing results therefore can be explained by orientation effects.

Measurement of Nucleation Rate—The measurement of N is a very difficult and time-consuming process for three-dimensional recrystallization, that is, when the thickness of the sheet is greater than the recrystallized grain size. However, Phillips and Phillips[11] working with heavily cold-worked copper found that the ratio of the number of spherical grains per unit volume to the number of grains per unit area was almost constant for all the materials they investigated which indicates that, for a quali-

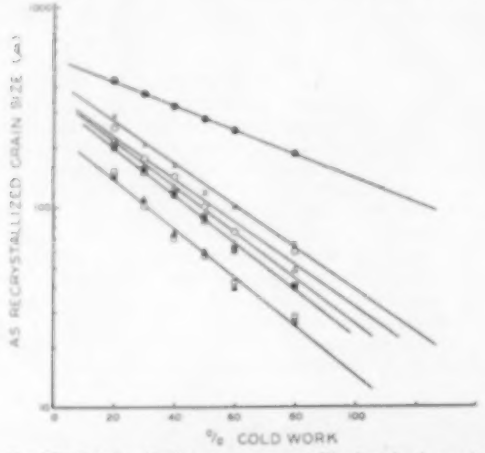

Fig. 16—Relationship between as-recrystallized grain size and percentage of cold reduction. Closed circle represents superpurity aluminum; X, Al-0.5 pct Mg; open circle, Al-1.0 pct Mg; open triangle, Al-2.0 pct Mg; closed square, Al-2.5 pct Mg; open square, 4.0 pct Mg; and open triangle, Al-5.0 pct Mg.

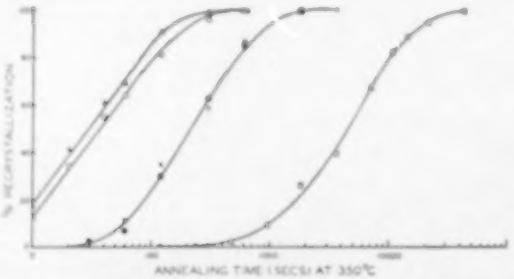

Fig. 17—Isothermal recrystallization curves at 350°C. Open triangle represents superpurity aluminum, cold worked 60 pct; closed circle, Al-0.5 pct Mg cold worked 60 pct; X, Al-1 pct Mg cold worked 60 pct; open square, Al-1 pct Mg cold worked 20 pct; and open circle, Al-4 pct Mg cold worked 60 pct.

Table III. Growth Rate Measurements on Al-Mg Alloys Cold Worked 20 and 60 Pct and Annealed at 350°C

Alloy	Percentage of Cold Reduction	G_{LL} Long Direction, Cm per Sec	G_{LS} Short Direction, Cm per Sec
Superpurity aluminum	60	18×10^{-4}	2.3×10^{-4}
Superpurity aluminum	20	2.6×10^{-4}	1.0×10^{-4}
Al-0.5 pct Mg	60	1.8×10^{-4}	1.1×10^{-4}
Al-1.0 pct Mg	60	1.2×10^{-4}	0.7×10^{-4}
Al-1.0 pct Mg	20	0.2×10^{-4}	0.2×10^{-4}
Al-4 pct Mg	60	2.5×10^{-4}	—

tative comparison, it is sufficient to measure the planar rate of nucleation. Furthermore, Reiter[30] has recently shown that for a low carbon steel a quantitative comparison can be made using the planar rate of nucleation.

The number of new recrystallized grains per square centimeter as a function of annealing time is shown in Fig. 20. Straight lines have been drawn through the initial points because later work[9] has shown that this part of the curve is linear. It is interesting to note the decrease in the number of grains per square centimeter which occurs at about 50 to 60 pct recrystallization. As can be seen micrographically, this is due to primary grain growth within the recrystallized areas. To determine the rate of nucleation, the slopes of the curves in Fig. 20 at any time period was determined and this divided by the fractional area of unrecrystallized matrix at the same time period gave the rate of nucleation N. N as a function of annealing time at 350°C is shown in Fig. 21. The rate of nucleation is high from the very beginning of recrystallization and then either remains constant for a short time and decreases or decreases immediately. Similar results have been obtained on superpurity aluminum cold worked 20 pct[9] and also by Phillips and Phillips[11] on copper. It is interesting to note that additions of magnesium up to 1 pct have only a very small effect on the rate of nucleation compared with that of a 4 pct Mg addition.

Kinetics of Recrystallization—A complete discussion of the kinetics of recrystallization has been given recently by Burke and Turnbull[29] and it is only intended here to refer briefly to the various theories. Johnson and Mehl[26] and Avrami[31] have presented equations based on the nucleation and growth hypothesis. These two treatments differ only in their assumptions as to how the rate of nucleation N varies with time. Anderson and Mehl[9] showed that, for lightly strained aluminum, $N = at^b$ where a and b are constants. Avrami, on the other

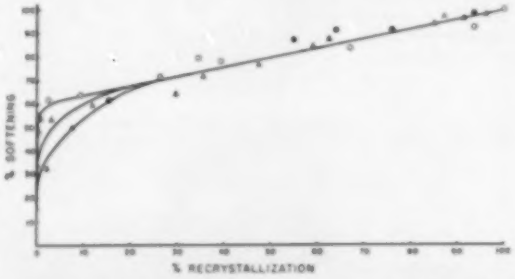

Fig. 18—Percentage of softening as a function of percentage of recrystallization. Closed triangle represents Al-0.5 pct Mg cold worked 60 pct, 350°C; open triangle, Al-1 pct Mg, cold worked 60 pct, 350°C; open circle, Al-1 pct Mg cold worked 20 pct, 350°C; and closed circle, Al-4 pct Mg cold worked 60 pct, 350°C.

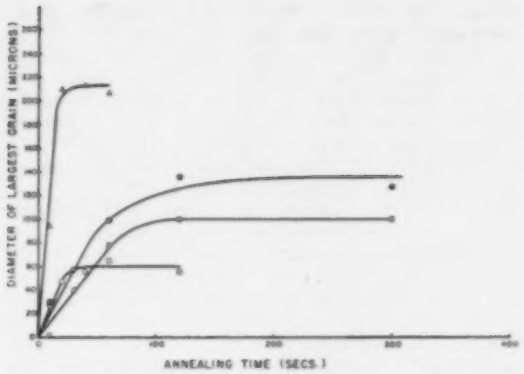

Fig. 19—Diameter of largest grain as a function of annealing time at 350°C, 60 pct cold work. Open triangle represents superpurity aluminum; encircled cross, Al-0.5 pct Mg; square, Al-1 pct Mg; and open circle, Al-4 pct Mg.

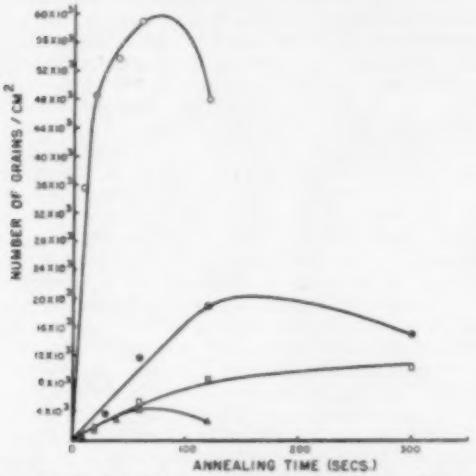

Fig. 20—Number of grains as a function of annealing time at 350°C, 60 pct cold work. Triangle represents superpurity aluminum; square, Al-0.5 pct Mg; encircled cross, Al-1 pct Mg; and open circle, Al-4 pct Mg.

hand, says that there pre-exists in the cold-worked material a certain number of preferred nucleation sites which may be suitably oriented subgrains or areas of high lattice curvature. During recrystallization, these sites are used up and he concludes that the rate of nucleation decreases with time. Assuming that the rate of growth is isotropic, this leads Avrami to the following equation for the kinetics of recrystallization

$$x = 1 - e^{-Bt^k} \qquad [1]$$

where B and k are constants and x is the fraction recrystallized. k depends upon the shape of the recrystallization nuclei and should have the following values

Three dimensional	$3 \leq k \leq 4$
Two dimensional	$2 \leq k \leq 3$
One dimensional	$1 \leq k \leq 2$.

By plotting loglog $1/1-x$ against log t, the values of k can be determined from the slope of the resultant straight line. This has been done for the isothermal recrystallization curves determined micrographically and also for some of the isothermal softening curves,

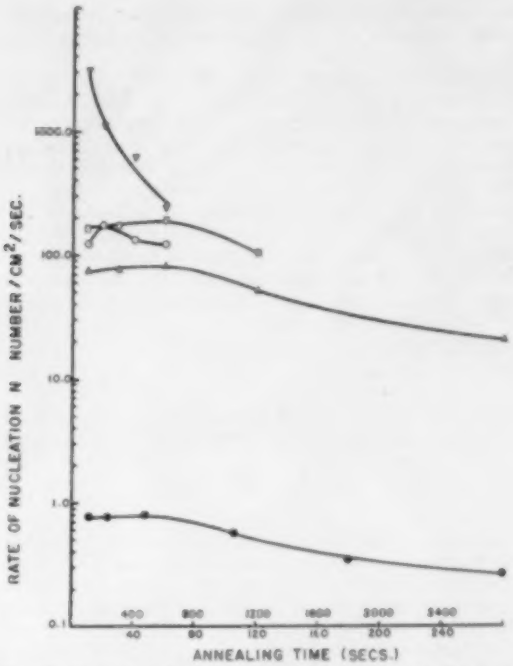

Fig. 21—Rate of nucleation as a function of annealing time at 350°C. Note change of time scale for 1 pct Mg cold worked 20 pct. Open circle represents superpurity aluminum cold worked 60 pct; upright triangle, Al-0.5 pct Mg cold worked 60 pct; square, Al-1.0 pct Mg cold worked 60 pct; inverted triangle, Al-4.0 pct Mg cold worked 60 pct; and closed circle, Al-1.0 pct Mg cold worked 20 pct.

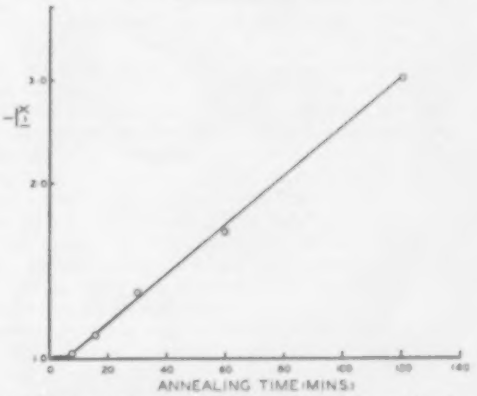

Fig. 22—Log $1/1-x$ as a function of t for Al-1 pct Mg alloy cold worked 20 pct and annealed at 350°C.

using Fig. 26 to convert the hardness value into percentage of recrystallization. The results from the isothermal recrystallization curves are given in Table IV.

Using the isothermal softening curves, values of k varying between 1.2 and 1.8 were obtained. These values agree with later work[9] and also with that of other workers who have used rolled material, see Table V.

The values of k for rolled material are lower than would be expected from Avrami's theory but are consistent if N and/or G decrease with time. Two alternative theories both of which are independent of N and G have been proposed by Krupkowski and Balicki[10] and Cook and Richards.[11] The first is based

on the assumption that recrystallization is a first-order reaction and gives Avrami's equation with $k = 1$.

Cook and Richards have postulated a two-stage process such that recovery must occur first and that when recrystallization starts it is confined to the part of the material which has recovered. It is assumed that recovery is a first-order rate process and for short times the fraction recovered is directly proportional to annealing time. This leads to the same equation as Avrami's with $k = 2$. Thorley[28] has used the same basic concepts as Cook and Richards but without assuming that the fraction recovered is proportional to annealing time. This leads to the following equation

$$\ln \frac{1}{1-x} = A\left[t + \frac{1}{\beta}\left(e^{-\beta t} - 1\right)\right] \qquad [2]$$

where A and β are constants both dependent on temperature. If t is large, $e^{-\beta t} \to 0$ and Eq. 2 becomes

$$\ln \frac{1}{1-x} = A\,(t - t_0) \qquad [3]$$

where $t_0 = 1/\beta$. Thus by plotting log $1/1-x$ against t, the constants A and t_0 can be determined. A typical plot is shown in Fig. 22. The theoretical curves calculated from Avrami's Eq. 1 and Thorley's Eq. 2 are shown in Fig. 23. The agreement with the experimental results is reasonably good. A more complete investigation[7] of the kinetics of recrystallization of superpurity aluminum has shown that the agreement between the foregoing two theoretical equations and the experimental results is much better than Fig. 23 would indicate.

Discussion of Results

The results show that, for any percentage of cold reduction between 20 and 80 pct, the time for complete recrystallization, recrystallization temperature, and activation energy increases from 0 to about 1.5 pct Mg and then decreases from 1.5 to 5.0 pct Mg. This agrees with the observations on commercial-purity base alloys made by Bungardt and Osswald[1] who found a maximum in the curve at about 1.5 pct Mg. Beck[4] who investigated superpurity base alloys containing 0.025, 0.12, and 2.05 pct Mg also found that magnesium increased the time for complete recrystallization and that the activation energy was increased from 44 to 51.5 kcal per gram-atom by 0.12 pct Mg. The maximum difference in recrystallization temperature between superpurity aluminum and the 1 pct Mg alloy was found to be about 45°C. This should be compared with a difference of about 10°C found by Bungardt and Osswald[1] for 50 pct cold reduction and 100°C found by Kratz[2] for a 0.5 pct Mg alloy cold worked 70 and 90 pct. In both cases, the percentages of cold reduction is sufficiently high for the results to be little affected by variations in initial grain size. This difference in magnitude of the effect of magnesium on the recrystallization temperature can be accounted for by the difference in base metal purity used in the different investigations. Bungardt and Osswald[1] used commercial-purity (0.37 pct Fe and 0.20 pct Si) aluminum, Kratz[2] used 99.997 pct Al, and throughout the work described here 99.993 pct purity aluminum was used. It is well known that very small amounts of impurities in solid solution increase the recrystallization temperature, so that if an element, such as magnesium which increases the recrystallization temperature, is used, it is evident that its effect will be far more marked when the impurity content of the base metal is low than when it is high.

The decrease in recrystallization temperature over the range 1.5 to 5.0 pct Mg has been attributed to the increased strain hardening resulting from the magnesium additions. On the other hand, the strain hardening also increases from 0 to 1.5 pct Mg in which range the recrystallization temperature increases. This suggests that there are two effects working in opposition to one another. If strain hardening is the effective agency in decreasing the recrystallization temperature, then, by comparing the effect of magnesium at the same hardness value instead of at the same percentage of cold reduction, an increase in the recrystallization temperature over the complete range of magnesium content should be found. That this is so is shown by Fig. 24 where the recrystallization temperature is plotted against the hardness of the as-cold-worked material. Similar curves were obtained for the activation energy. The same type of observation was made by Laurent and Batisse[29] who found that, if aluminum was strained in liquid nitrogen to the same amount as at room temperature, the material treated at low temperature recrystallized first; if, however, the material was strained in liquid nitrogen to the hardness attained by straining at room temperature, then the low temperature material recrystallized last. Thus it appears that strain hardening is playing an important role in the recrystallization of alloys containing more than 1.5 pct Mg and that some other factor is overcoming this at smaller magnesium contents. From the nucleation and growth measurements, it will be seen that the rate of growth, G, is reduced by a factor of about 6 by the addition of 0.5 pct Mg but is little affected by further increase in magnesium. On the other hand, the rate of nucleation at 20 pct recrystallization is little affected by magnesium up to 1 pct Mg but increases markedly with larger magnesium contents, increasing by a factor of about 18 for 4 pct Mg, see Fig. 25. Thus, at about 1.5 pct Mg the rates of growth and nucleation are at a minimum, thus explaining the maximum in time for complete recrystallization etc. at 1.5 pct Mg. The small increase in rate of growth, G, with magnesium contents greater than 1.5 pct Mg is probably a result of the increased strain hardening. Why adding magnesium decreases G is not clear. It is well known that the rate of strain hardening increases with increasing magnesium and if, as is generally assumed, the strain energy is the driving force for grain growth, this would lead to an increase in growth rate with magnesium content. Therefore, there must be some other factor which is having a greater effect than that of strain energy and in the opposite sense. There is practically no information on the effect of foreign atoms in solid solution on G and so any explanation must be hypothetical. The fact that G is affected by very small additions does suggest the possibility that segregation of solute

Table IV. Values of Avrami's Constant *k*

Alloy	*k*
Superpurity aluminum, 60 pct CW*	1.14
Al-0.5 pct Mg, 60 Pct CW	1.60
Al-1 pct Mg, 60 pct CW	1.43
Al-4 pct Mg, 60 pct CW	1.30
Al-1 pct Mg, 20 pct CW	1.55
Superpurity aluminum, 20 pct CW	1.60

* CW stands for cold worked.

Table V. Summary of Avrami's Constant *k*

Reference	Purity, Pct	Method of Observation	Method of Deformation	Number of Curves	k
Anderson and Mehl[3]	99.95	Micrographic	5,10,15 pct strain	3	4.5 to 7.5
Anderson and Mehl[3]	99.97	Micrographic	2 to 10 pct strain	6	4.5 to 5.5
Anderson and Mehl[3]	99.97	Micrographic	Rolled 90 pct	1	1.7
Anderson and Mehl[3]	99.98	Micrographic	5 pct strain	3	3.3
Varley[16]	99.4	Tensile strength	Rolled	3	1.3 to 1.5
Laurent and Batisse[15]	99.35	Hardness	10 to 30 pct strain	24	0.95 to 1.35
Laurent and Batisse[15]	99.991	Hardness	10 to 25 pct strain	14	1.65 to 2
Perryman[5]	99.993	Micrographic	Rolled 20 pct	4	1.40 to 1.43
Marchand[22]	Al-Mn	Micrographic	Rolled 30 and 40 pct	1	1.66

atoms at the advancing boundary may be playing a part. To explain the effect of magnesium on the rate of nucleation is even more difficult, for what constitutes a nucleus is still unknown. It has been suggested that the subgrains which are observed directly after cold working may represent the germ nuclei. The results here do not seem to support this contention, for Perryman[5] has shown that 1 pct Mg markedly reduces the subgrain size which, on the foregoing hypothesis, would lead to increased rate of nucleation. It would seem that the increase in strain hardening brought about by magnesium is the more likely explanation. Thus, it would seem that regions of high lattice curvature are the more likely sites for nucleation which is in keeping with the fact that recrystallization nuclei are preferentially formed at grain boundaries and that there is no incubation period.

Decreasing amounts of cold work have been shown to increase the recrystallization temperature, time for complete recrystallization, and activation energy, the increase being linear down to 20 pct cold reduction for superpurity aluminum and 30 to 40 pct cold reduction for Al-Mg alloys. With lower amounts of cold work, these same parameters increase much more rapidly than the straight-line relationship would indicate. The measurements of N and G have shown that for a 1 pct Mg alloy N is lowered by a factor of about 330 times when the percentage of cold reduction is decreased from 60 to 20 pct while G only decreases by a factor of about 6 times. This indicates that the rapid increase in recrystallization temperature at low amounts of cold work is a result of the large decrease in N. Support for this is given by the fact that, if the initial grain size is decreased thus increasing the grain boundary area and so the rate of nucleation, the rapid rise in recrystallization temperature occurs at smaller amounts of cold work, see Fig. 10.

The results reported here on the effect of initial grain size are in agreement with those of other workers in that a reduction in initial grain size decreases the recrystallization temperature. It has been shown[21, 22] that, when a polycrystalline aggregate is plastically deformed, a shear gradient exists at the grain boundaries. This explains why recrys-

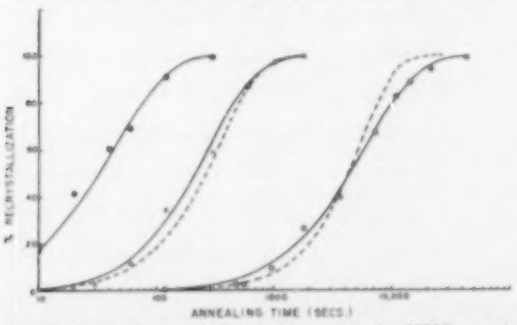

Fig. 23—Calculated recrystallization-time curves for 350°C anneal. Dotted line represents data calculated from Avrami's equation $x = 1 - e^{-kt^n}$; solid line, data calculated from Thorley's equation $\log 1/1 - x = A[t + (1/\beta)(e^{-\beta t} - 1)]$; X, experimental points Al-1 pct Mg alloy rolled 60 pct and annealed at 350°C; encircled cross, experimental points Al-1 pct Mg alloy rolled 20 pct and annealed at 350°C; and closed circle, experimental points superpurity aluminum alloy rolled 60 pct and annealed at 350°C.

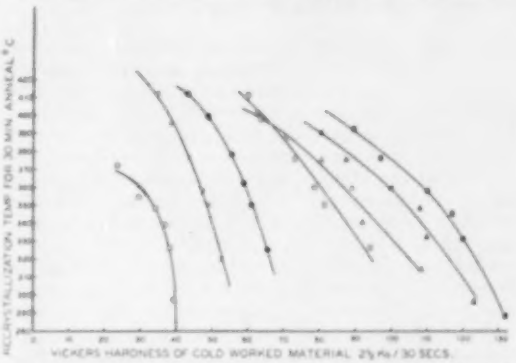

Fig. 24—Recrystallization temperature as a function of hardness of cold-worked material. Open circle represents superpurity aluminum; X, Al-0.5 pct Mg; closed circle, Al-1.0 pct Mg; open square, Al-2.0 pct Mg; open triangle, Al-2.5 pct Mg; closed triangle, Al-4.0 pct Mg; and closed square, Al-5.0 pct Mg.

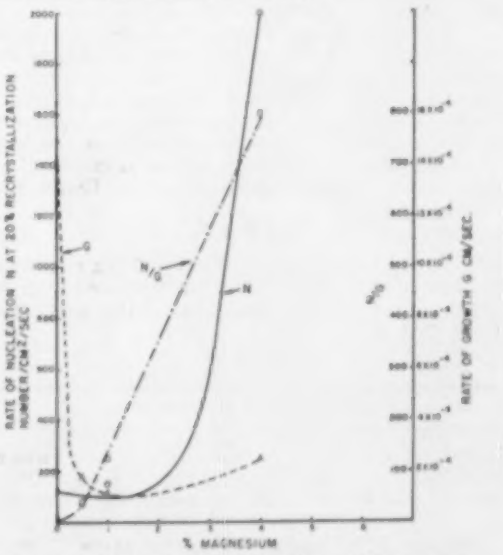

Fig. 25—Rate of nucleation and growth as a function of magnesium content. Triangle represents rate of growth G; circle, rate of nucleation N; and square, N/G.

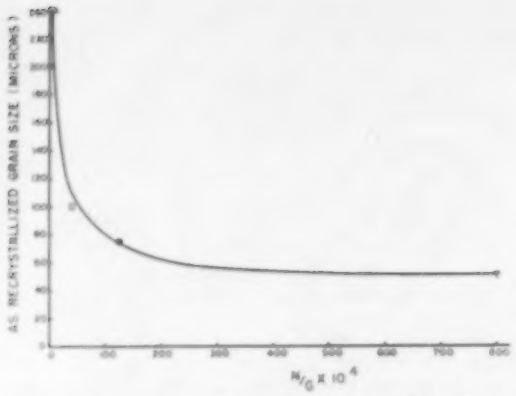

Fig. 26—*N/G* as a function of grain size for Al-Mg alloys. Upright triangle represents superpurity aluminum cold worked 60 pct; square, Al-0.5 pct Mg cold worked 60 pct; closed circle, Al-1 pct Mg cold worked 60 pct; inverted triangle, Al-4 pct Mg cold worked 60 pct; and open circle, Al-1 pct Mg cold worked 20 pct.

tallization nuclei are formed preferentially at these boundary regions. If the grain boundary surface area is increased by decreasing the initial grain size, then clearly the rate of nucleation will be increased, thus leading to a smaller time for complete recrystallization. For high amounts of cold work, the difference in the state of deformation between grains and grain boundary will probably be less and so the effect of initial grain size will not be so great. It is interesting to note that Williams and Eborall[7] observed that the effect of initial grain size is much greater for superpurity aluminum than for commercial-purity aluminum which suggests that the second phases present in the latter material increased the rate of nucleation. Reiter[25] has shown that pearlite in steel increases N and Perryman[9] has shown that insoluble intermetallic compounds in Al-Mg alloys increase the nucleation rate N. All the foregoing arguments support the idea that regions of high lattice curvature are the more likely sites for nucleation.

It has been shown in this work that for large amounts of cold work the logarithm of the time for complete recrystallization is proportional to the percentage of cold reduction S. Phillips and Phillips[26] have recently shown for copper that the logarithm of the nucleation rate is proportional to the half softening time which in turn will be proportional to the time for complete recrystallization. Hence it is found that

$$\text{Log } N \propto S.$$

Since, at high degrees of cold work, G is a relatively insensitive function of cold work compared with N, the grain size will be almost completely controlled by N, that is

$$D_s \propto N$$

where D_s is the as-recrystallized grain size. Thus the logarithm of the grain size should be proportional to the percentage of cold reduction for high degrees of cold work.

Table VI gives a summary of the rate of nucleation and growth measurements together with the as-recrystallized grain size.

The as-recrystallized grain size as a function of N/G is shown in Fig. 26. Although the grain size decreases with increasing N/G, the two parameters are not proportional. This is not surprising, since, as mentioned earlier, primary grain growth occurs in the recrystallized areas at the same time as recrystallization is proceeding. Clearly this effect will be more marked with superpurity aluminum than with the Al-Mg alloys because of the effect of magnesium in reducing the rate of primary grain growth.[4]

Table VI. *N* and *G* for Al-Mg Alloys

Alloy	Pct Cold Reduction	G_{11} Long Direction, Cm per Sec	*N* at 20 Pct Recrystallization, No. per Sq Cm per Sec	*N/G*	Recrystallized Grain Size, Microns
Superpurity aluminum	60	15×10^{-4}	122	8.1×10^{5}	240
Al-0.5 pct Mg	60	1.8×10^{-4}	68	38×10^{5}	100
Al-1 pct Mg	60	1.2×10^{-4}	190	135×10^{5}	75
Al-4 pct Mg	60	2.5×10^{-4}	2000	800×10^{5}	50
Al-1 pct Mg	20	0.2×10^{-4}	0.4	2×10^{5}	250

Acknowledgments

The author wishes to express his thanks to G. Marchand for many helpful discussions and to W. Marsh who assisted with the experimental work.

Discussion of this paper, if any, will appear in JOURNAL OF METALS, November 1955, and in AIME Metals Branch *Transactions*, Vol. **203**, 1955.

References

[1] W. Bungardt and E. Osswald: *Ztsch. für Metallkunde* (1938) **30**, p. 202.
[2] R. Michaud and E. Segol: *Comptes Rendus* (1937) **204**, p. 980.
[3] H. Chossat: *Revue de Métallurgie* (1950) **47**, pp. 167, 306, and 343.
[4] L. J. Demer and P. A. Beck: *Trans.* AIME (1949) **180**, p. 147; METALS TECHNOLOGY (June (1948).
[5] E. Kratz: *Aluminium Archiv* (1937) **6**, 25 pp.
[6] R. Chadwick and W. H. L. Hooper: *Journal* Institute of Metals (1948-1949) **75**, p. 609.
[7] W. M. Williams and R. Eborall: *Journal* Institute of Metals (1953) **81**, p. 501.
[8] W. A. Anderson and R. F. Mehl: *Trans.* AIME (1945) **161**, p. 140.
[9] E. C. W. Perryman: Unpublished work.
[10] E. C. W. Perryman: *Acta Metallurgica* (1954) **2**, p. 26.
[11] M. Cook and T. L. E. Richards: *Journal* Institute of Metals (1947) **73**, p. 1.
[12] P. C. Varley: *Journal* Institute of Metals (1948-1949) **75**, p. 1037.
[13] L. W. Eastwood, R. W. James, and M. F. Bell: *Trans.* AIME (1939) **133**, p. 124.
[14] S. L. Channon and H. L. Walker: *Reprint No. 8* ASM (1952).
[15] P. Laurent and N. Batisse: *Revue de Métallurgie* (1952) **49**, pp. 485, 593.
[16] P. C. Varley: *Journal* Institute of Metals (1948-1949) **75**, p. 185.
[17] V. A. Phillips and A. Phillips: *Journal* Institute of Metals (1952-1953) **81**, p. 185.
[18] S. F. Reiter: *Trans.* AIME (1952) **194**, p. 972; JOURNAL OF METALS (September 1952).
[19] J. E. Burke and D. Turnbull: *Progress in Metal Physics* (1951) **3**, p. 220.
[20] W. A. Johnson and R. F. Mehl: *Trans.* AIME (1939) **135**, p. 416.
[21] M. Avrami: *Journal of Chemical Physics* (1939) **7**, p. 1103; (1940) **8**, p. 212; (1941) **9**, p. 177.
[22] G. Marchand: Unpublished work.
[23] A. Krupkowski and M. Balicki: *Ann. Akad. Sci. Tech. Varsovie* (1937) **4**, p. 270.
[24] N. Thorley: *Journal* Institute of Metals (1950) **77**, p. 141.
[25] W. Boas and M. Hargreaves: *Proceedings* Royal Society (1948) **193A**, p. 89.
[26] G. B. Greenough: *Nature* (1947) **160**, p. 258.

Some Aspects of the Crystallization and Recrystallization of Vapor-Deposited Vitreous Selenium

by N. E. Brown and F. L. VerSnyder

Observations of the microstructural changes on metallographically prepared cross-sectional specimens of brominated vapor-deposited vitreous selenium, as well as free-surface specimens, as a function of heat treatment have been made. Comments on the microstructural mode of crystallization of vitreous selenium and on the recrystallization phenomenon of hexagonal selenium as observed are advanced.

THE apparent dependency of the electrical characteristics of hexagonal crystalline selenium on microstructure has aroused much interest in microscopical studies of selenium. Microscopic observations on the crystallization of selenium have been made by Escoffery and Halperin,[1] P. H. Keck,[2] and other investigators. It is the purpose of this paper to discuss the microstructural changes observed on polished cross-sections of single layers of selenium after various heat treatments. Observations were also made on crystallization of the free-surface layer of these deposits. In general, all of the transformations studied were either transformations of the vitreous selenium to hexagonal selenium or microstructural transformation of the hexagonal selenium itself.

Procedure

The selenium used in this work was obtained from the American Smelting and Refining Co. and was approximately 99.96 pct pure. An intentional impurity of 1 part per 2,000 of bromine was added to the material prior to evaporation.

A thickness of approximately 0.002 in. of this selenium was vapor deposited on an aluminum base plate. The maximum plate temperature during the vacuum vapor deposition was 140°C.

Mounting of the cross-sectional specimens for metallographic study could not be done in plastic mounting media, as is customary, since temperatures in excess of 50°C would cause unwanted transformations. Consequently, a simple clamp-type device was used to mount the specimens for preparation.

All grinding operations were then done carefully by hand in order that the specimen not become heated during this operation.

Wet polishing was done on the conventional metallographic polishing laps, using successively finer grinding powders. An extremely careful polish is necessary, since observation and micrography of the specimens are done in the unetched condition under polarized light.

The two observations of crystallization made on the free surface of vitreous selenium deposits (Figs. 4 and 5) were made on surfaces which were perpendicular to the cross-sections studied. These free-surface layers were examined directly, i.e., no previous metallographic preparation, as obtained from the vacuum vapor deposition.

N. E. BROWN and F. L. VERSNYDER are associated with Metallographic Section, Thomson Laboratory, and Metallography and High Temperature Testing Unit, Small Aircraft Engine Laboratory, respectively, General Electric Co., West Lynn, Mass.

Discussion of this paper, TP 3939E, may be sent, 2 copies, to AIME by Apr. 1, 1955. Manuscript, Nov. 5, 1953. Chicago Meeting, February 1955.

Microscopic Observations

A study was made of polished cross-sections of the vitreous selenium as-deposited. It was noted that in all cases there was columnar crystallization adjacent to the base plate, which appeared to occur during the vacuum deposition process. This observation has also been made by Keck.[2] It also was observed that vagrant spherulitic crystallization occurred in the vitreous selenium. The term "vagrant" is used, since these spherulitic grains appear to crystallize at random throughout the vitreous selenium during the vacuum deposition process. Columnar crystallization at the Al-Se interface and a typical spherulite observed in a polished cross-section of "as-deposited" vitreous selenium may be seen in Fig. 1.

Cross-sectional samples of vitreous selenium studied after heat treating individual samples for 20 min in 10° steps from 80° to 220°C revealed that crystallization—in this case, columnar crystal growth—proceeds from the aluminum base plate to the surface of the specimen (Fig. 2). Crystallization was microscopically observed to be complete after the 130°C heat treatment. Visual examination of the free surface of the specimen after the 130°C heat treatment revealed the readily recognizable grey appearance of the completely crystallized selenium, in corroboration of the microstructural observations. No microstructural transformations then appeared to take place between 130° and 190°C. At 190°C the beginning of recrystallization appeared and proceeded until the columnar grain structure had been completely transformed to equiaxed grains between 210° and 220°C (Fig. 3). Naturally, the grain size of the recrystallized grains at the lower temperatures (190° to 210°C) was smaller than is illustrated in Fig. 3.

In addition, polished cross-sections of deposits heat treated at 140°C for 10 min to cause complete crystallization and, subsequently, heat treated in 10° steps from 80° to 220°C for 20 min were studied. As expected, no microstructural transformations took place until the beginning of recrystallization was observed at 190°C. A comparison with the previously studied specimens revealed that recrystallization proceeded almost identically in the two experiments although in the first case the deposits were vitreous prior to the series of heat treatments and in the second case they had been crystallized by a previous heat treatment. By heat treating for longer times (180 min) at lower temperatures, the

Fig. 1—Unetched. Polarized light. X500. Area reduced approximately 25 pct for reproduction.

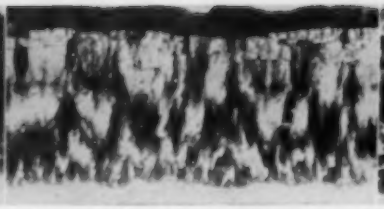

Fig. 2—Columnar growth proceeding from aluminum base plate towards free surface of specimen. Heat treated at 110°C for 20 min. Polished cross-section, polarized light. X500. Area reduced approixmately 25 pct for reproduction.

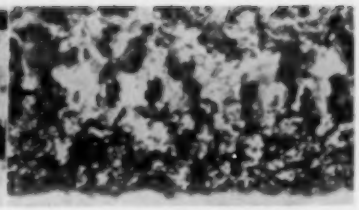

Fig. 3—Recrystallized structure after heat treatment of vitreous selenium at 220°C for 20 min. Polished cross-section, polarized light. X500. Area reduced approximately 25 pct for reproduction.

beginning of recrystallization was noted at the lowest temperature studied (180°C).

Crystallization in the free-surface layer of a vitreous deposit was induced on the metallographic stage by utilizing the heat from the illuminating source, after it had passed through the optics of the metallograph, and by controlling its intensity by opening and closing the aperture diaphragm. The illuminating source employed was a 10 amp approximately 3820°K color temperature carbon-arc lamp, standard equipment of the Bausch and Lomb research metallograph. No exact determination of the temperature of the area heated in this manner was attempted. On a specimen whose free surface was as-deposited, spherulitic crystals nucleated and grew. The micrographs of Fig. 4, taken at several cumulative time periods, illustrate this spherulitic germination and growth.

Subsequently, the free surface of a vitreous sample "as-deposited" was disturbed by drawing a forefinger across the surface and then inducing crystallization on the microscope stage. Micrographs were taken again at several cumulative time periods, four of which are shown in Fig. 5. In this case, many small nuclei were formed and the grains grew in a rather uniform fashion so that the resulting granular structure was composed of rather uniform grains. It is interesting to note the directional bands of grains, readily observable in the early time periods, which are the result of disturbing the surface. In this case, the only spherulitic grain shown was one already present in the "as-deposited" material and which was included in the field of observation as a reference point.

Discussion

It was observed that a layer of columnar crystals was present in most of the vitreous selenium deposits. It was observed also that during crystallization the grains grew in a columnar fashion from the base plate to the surface. The presence of the columnar crystals at the Al-Se interface is in agreement with the explanation by Keck[5] that this crystallization is a function of the time-temperature conditions of deposition. Since, in most deposits, there is a columnar crystallization at the Al-Se interface in the vitreous state, it would be expected that the growth of the crystals would proceed predominantly in a columnar fashion from the base plate to the surface. Growth of the vagrant spherulitic crystals also occurs during the heat treatment for crystallization of the vitreous selenium; therefore, the crystallization of vitreous selenium is not solely columnar growth from base plate to surface.

In order that recrystallization of the columnar structure may occur, it is necessary for a certain amount of strain to be present in the granular system. In this case, then, there must be strains which provide sites of high energy in the columnar formation in order that it may recrystallize on subsequent heat treatment. It is visualized that this strain is induced in the columnar grain formation during the crystallization and growth of these columnar grains. Since there is a constant volume of vitreous selenium, there must be an unequal change in volume from the Al-Se interface to the surface of the selenium during crystallization. It is known that the crystallization of vitreous selenium causes a marked volume change;[6] and since the selenium is firmly affixed to the aluminum plate, the volume change must spread throughout the bulk of the selenium layer, perhaps becoming greatest at the surface. The strain then provides the sites for the nucleation of the strain-free or recrystallized grains.

This view is strongly supported by the evidence of the sensitivity of vitreous selenium to disturbance and its subsequent effect on crystallization characteristics. This is illustrated by the two studies made on the surface crystallization of vitreous selenium,

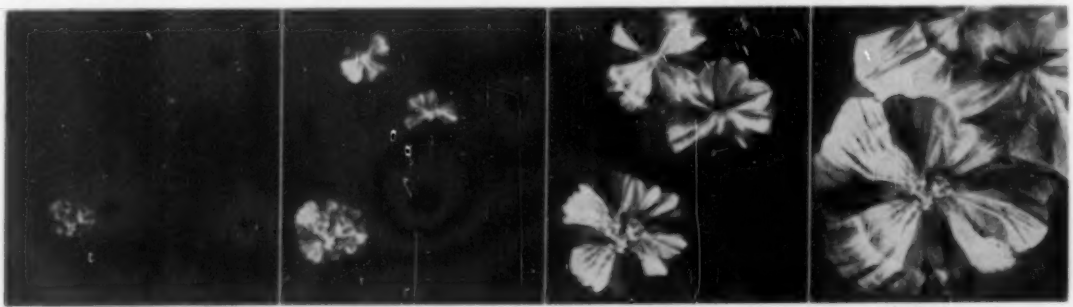

a—As deposited b—30 sec. c—1.5 min. d—4 min.

Fig. 4—Crystallization on free surface of undisturbed vitreous selenium. Polarized light. X500. Area reduced approximately 10 pct for reproduction.

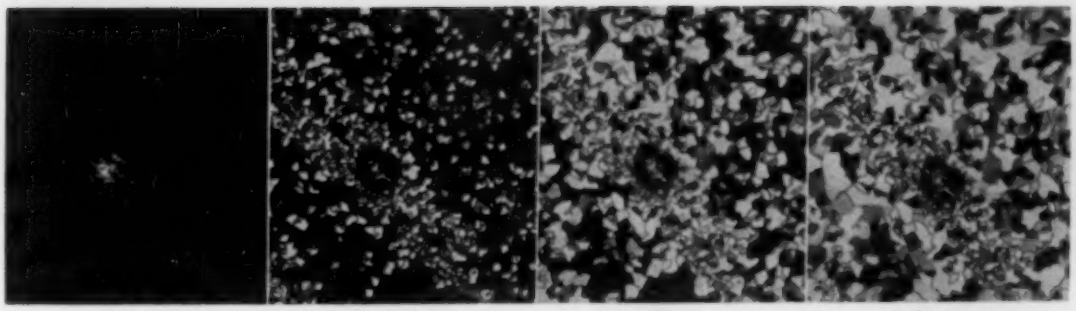

a—As deposited. b—15 sec. c—30 sec. d—1 min.

Fig. 5—Crystallization on free surface of disturbed vitreous selenium. Polarized light. X500. Area reduced approximately 10 pct for reproduction.

where spherulites grew in the undisturbed; but many fine equiaxed grains nucleated and grew in the disturbed surface.

Conclusions

From the foregoing microscopic observations on vacuum vapor-deposited vitreous selenium, under the conditions stated, the following statements may be made:

1—Columnar crystallization of the brominated, vapor-deposited vitreous selenium proceeds predominantly, but not exclusively, from the Al-Se interface to the surface of the deposit.

2—It is suggested that the strain induced from crystallization of the brominated vitreous selenium deposits can result in recrystallization of the selenium layer if the recrystallization temperature is subsequently exceeded.

3—An indication of the temperature at which the recrystallization of brominated selenium began was observed as 190°C at 20 min.

Acknowledgment

The authors wish to express their appreciation to Mr. John Tyndall for the preparation of the many selenium deposits.

Discussion of this paper, if any, will appear in JOURNAL OF METALS, November 1955, and in AIME Metals Branch *Transactions*, Vol. **203**, 1955.

References

[1] C. A. Escoffery and S. Halperin: Studies on the Polymorphic Transformation of Selenium. *Preprint* 90-7 Electrochemical Society (1946).

[2] P. H. Keck: Photoconductivity in Vacuum-Coated Selenium Films. *Journal of Optical Society of America*. (April 1952) **42**, No. 4, p. 221.

[3] C. F. Rammelsberg: *Ber.* (1874) **7**, p. 669.

On the Relationship of Texture Changes of Cold-Rolled Face-Centered-Cubic Metals During Recrystallization

by Y. C. Liu and W. R. Hibbard, Jr.

An analysis of the relationship between the deformation and recrystallization textures in face-centered-cubic metals is presented. The analysis assumes that orientations of the secondary as well as the primary textures are related to the deformation texture. The effect of alloying elements on the recrystallization texture of copper-base alloys is also discussed.

Y. C. LIU, Junior Member AIME, is Research Associate, New York University, New York, and W. R. HIBBARD, Jr., Member AIME, formerly Associate Professor of Metallurgy, Yale University, New Haven, Conn., is associated with Metallurgy Research Dept., Research Laboratory, General Electric Co., Schenectady.

Discussion of this paper, TP 3975E, may be sent, 2 copies, to AIME by Apr. 1, 1955. Manuscript, Dec. 1, 1953. Chicago Meeting, February 1955.

This paper is based on a portion of a thesis by Y. C. Liu submitted, in partial fulfillment of the requirements for the degree of Doctor of Engineering, to the Faculty of Yale University.

ROTATIONAL relationships based on prior orientations have been used to derive both the primary and secondary recrystallization textures.[1-4] This similarity suggests that, if the secondary texture arises from grains formed during primary recrystallization, as proposed by Dunn,[5] and if primary recrystallization derives its lineage from the deformation structure, then the orientations obtained in secondary recrystallization as well as those obtained in primary recrystallization should be related to the deformation texture. The following discussions are

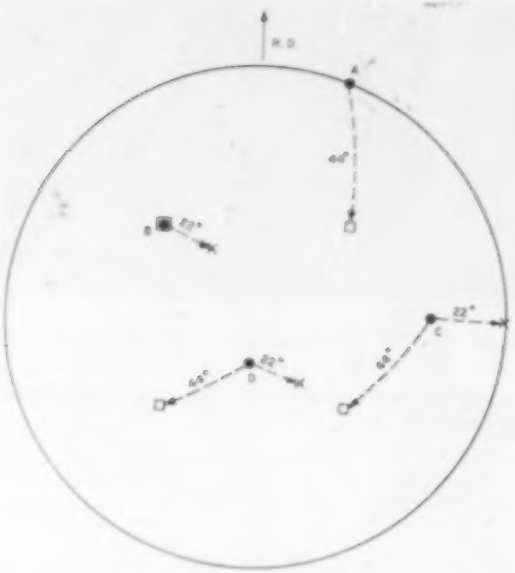

Fig. 1—"Operation" of modified (358) [$3\bar{5}2$] deformation texture. Octahedral poles: closed circle represents modified (358) [$3\bar{5}2$] orientation; square, (100) [001], X, (110) [$1\bar{1}2$].

intended to present an analysis* supporting this relationship.

* This analysis is not a theory.

Method of Analysis

It has been found for copper[7] that the cubic texture is not obtained from the recrystallization of a single (110) [$1\bar{1}2$] deformation texture. Since the texture of cold-rolled polycrystalline copper is a double (110) [$1\bar{1}2$] texture,† the cubic recrystallization texture which is found for this material may be influenced by the differences between the double and single (110) [$1\bar{1}2$] deformation textures. The following possibilities can be considered: The deformation texture of cold-rolled polycrystalline copper is not (110) [$1\bar{1}2$] as previously supposed;[8] or, in addition, there is a cubic-texture-developing component[7] of the deformation texture similar to (358) [$3\bar{5}2$]* included in the spread of the pole figure.

† "Double texture" is defined in the present paper as component orientations which are symmetrical with respect to both rolling and transverse directions.

* Hu, Sperry, and Beck[2] proposed several orientations of the (123) [$1\bar{2}1$] type. (358) [$3\bar{5}2$] is selected as the one best fitting the rationalization in this paper.

Only the latter possibility is considered in the present analysis.

For purposes of this discussion, the indices of the cubic-texture-developing component of the deformation texture in face-centered-cubic metals may be considered as similar to (358) [$3\bar{5}2$] previously proposed,[7] with the modification that one of the octahedral poles is located exactly on the site of an octahedral pole of cubic orientation and another on the primitive circle of the stereographic projection 20° away from the rolling direction. Using this modified (358) [$3\bar{5}2$] orientation and the (110) [$1\bar{1}2$] orientation, it is possible to derive by simple rotation and twinning the major recrystallization textures reported in the literature for face-centered-cubic metals. It is now proposed to describe these derivations without implications as to mechanisms.

Copper

Cook and Richards[10] observed that the recrystallization texture of copper strip depends upon the reduction during rolling; a (110) [$1\bar{1}2$] recrystallization texture was obtained for copper rolled 85 pct reduction in thickness and cubic recrystallization texture for 97 pct reduction. As shown in Fig. 1, a 22° rotation of the modified (358) [$3\bar{5}2$] orientation about the octahedral pole *A* yields the (110) [$1\bar{1}2$] orientation, while a 44° rotation about pole *B* produces the cubic orientation.

Secondary Grains in Copper

The observed orientations of secondary grains in copper related to the cubic or primary texture may be summarized as follows: a 30° or 38° rotation about all the four (111) poles[1, 9] and a 19° rotation about all cubic poles.[8, 11]

It was found that all the orientations of the secondary grains can be related to the twin orientation† of (358) [$3\bar{5}2$] about pole *B*, Fig. 2, which is common to both the cubic and modified (358) [$3\bar{5}2$] orientations. Fig. 2 shows the modified (358) [$3\bar{5}2$] orientation in dotted lines and the twin from the octahedral pole *B* in solid lines. Fig. 3 shows the four orientations generated by a 16° rotation about each of the octahedral poles of this twin. The resulting orientations fit all the observed orientations very well. Theoretically, these orientations lead to a 32° rotational difference between primary and secondary orientations as reported in Sharp and Dunn's data.[11]

† This orientation is contained within the spread of the pole figure of the copper deformation texture.[12]

Aluminum

Hu, Sperry, and Beck[2] proposed (7 12 22) [8 4 $\bar{5}$] indices for the orientation of cold-rolled polycrystal-

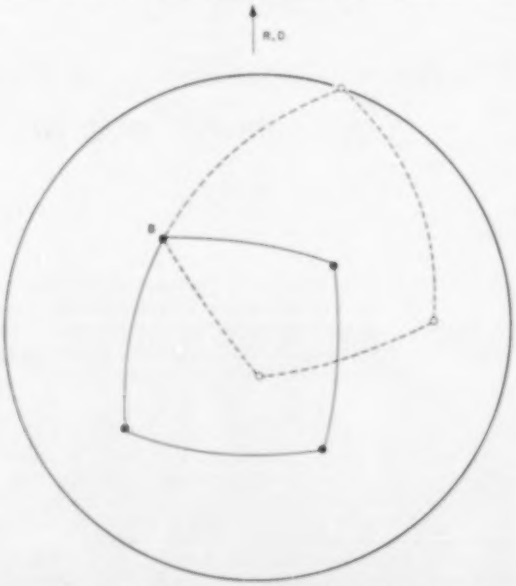

Fig. 2—Octahedral poles of the orientation related to secondary grains in copper. Open circle represents modified (358) [$3\bar{5}2$]; closed circle, orientation of twin of modified (358) [$3\bar{5}2$] about (111) *B*.

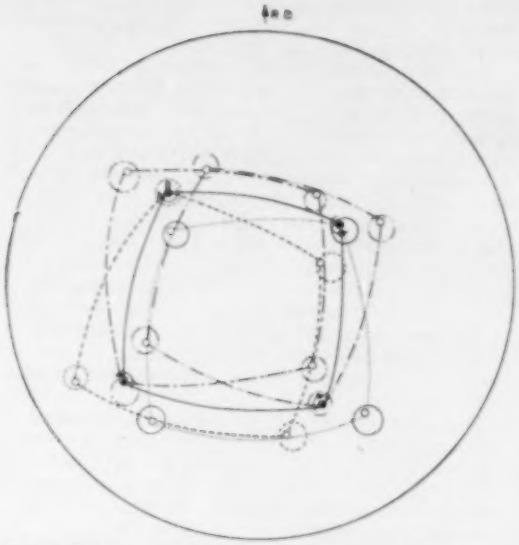

Fig. 3—Rotations generating the orientations of secondary grains in copper. Octahedral poles (small circles): closed circle represents twin of modified (358) [$3\bar{5}2$] orientation about pole *B* (see Fig. 2); open circle, 16° rotation about each of the four (111) poles of twin orientation. Fitted to experimental observations described by various investigators, the larger circles represent as follows: solid and dashed-line circle, 19° about ($\bar{1}00$), Sharp and Dunn;[11] solid-line circle, 19° about (010), Sharp and Dunn;[11] solid and dotted-line circle, 19° about (001), Sharp and Dunn;[11] and uniformly dashed-line circle, 30° about (111), Sharp and Dunn,[11] Bowles and Boas,[1] and Kronberg and Wilson.[2] Circles are drawn with 5° radius. Actual spread is 10° radius, see Sharp and Dunn.[11]

line aluminum strip after 95 pct reduction in thickness. A comparison of their pole figures shows a close similarity between aluminum and copper. Since the orientation of (7 12 22) [8 4 $\bar{5}$] is close to the modified (358) [$3\bar{5}2$] indices, it can be assumed for the purpose of this discussion that the modified (358) [$3\bar{5}2$] component is included in cold-rolled aluminum. The recrystallization texture of aluminum as reported by Beck and Hu[9] is a combination of cubic orientation and the same orientation as the deformation texture.

As shown in Fig. 4, a 44° rotation about octahedral pole *A* of the modified (358) [$3\bar{5}2$] deformation texture results in an orientation which is almost the same as the modified (358) [$3\bar{5}2$] orientation.‡

‡ 44° rotations about the other two octahedral poles in the directions shown in Fig. 3 will also yield the modified (358) [$3\bar{5}2$] orientation.

As previously described for copper, a 44° rotation about the octahedral pole *B* yields the cubic orientation (center dot).

Brass and Silver

There is evidence that the recrystallization temperature could be dependent on the deformation texture.* For example, Brick and Williamson[29] report that copper rolled 99 pct to produce different deformation textures (straight vs cross-rolled) correspondingly recrystallized at different temperatures to different textures. The material forming the simple cubic texture had the lower recrystallization temperature.

* It is well known that strain produced in single crystals is a function of the orientation of the stress axis. Therefore, it is not inconceivable that different components of the deformation texture may be in different conditions of strain (and strain energy), leading to differences in recrystallization temperatures.

Thus, the modified (358) [$3\bar{5}2$] component of the deformation texture which is associated with the cubic recrystallization texture might have a lower recrystallization temperature than the (110) [$1\bar{1}2$] component. By introducing this variable during the annealing of a specimen having both (110) [$1\bar{1}2$] and modified (358) [$3\bar{5}2$] orientations in the deformation texture, the latter may recrystallize at lower annealing temperatures while the (110) [$1\bar{1}2$] deformation component thus can be considered as affecting the primary recrystallization process only in the presence of a limited or undetectable amount of the modified (358) [$3\bar{5}2$] deformation component, e.g., the copper single crystal specimens,[1] or in silver.[12] A possible means of suppressing the modified (358) [$3\bar{5}2$] deformation component found in copper may be by the introduction of an alloying element, such as in brass.[14, 28]

It is proposed that the effect of alloying elements in copper is to suppress† the orientations derived from the (358) [$3\bar{5}2$] component of the deformation texture and to enhance the orientations derived from the (110) [$1\bar{1}2$] orientations, resulting in the disappearance of the cubic-texture and the appearance of these (113) [$2\bar{1}1$] type textures.[5, 14-18]

† Suppress but not eliminate. This component may exist in weak amounts below the sensitivity of X-ray film pole figure techniques, but subsequently become operative (analogous to the case of silicon iron[5, 18]) to produce the secondary texture (as suggested in a subsequent paragraph).

Both 70:30 brass and silver have a double (110) [$1\bar{1}2$] deformation texture[5, 9, 18] and a (113) [$2\bar{1}1$] recrystallization texture.[5] The (113) [$2\bar{1}1$] orientation, as suggested by many investigators, can be related by a 30° rotation about a (111) pole of the (110) [$1\bar{1}2$] deformation texture (pole *A* in Fig. 1).[5, 9]

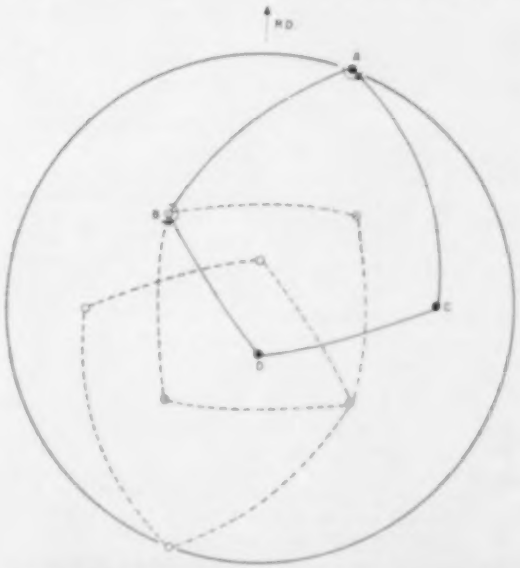

Fig. 4—Recrystallization reorientation in aluminum by 44° rotations about octahedral poles of modified (358) [352] orientation. Octahedral poles: closed circle represents modified (358) [352] orientation; open circle, 44° rotations about poles *A* and *B*. Dots indicate poles obtained by rotation about *B*.

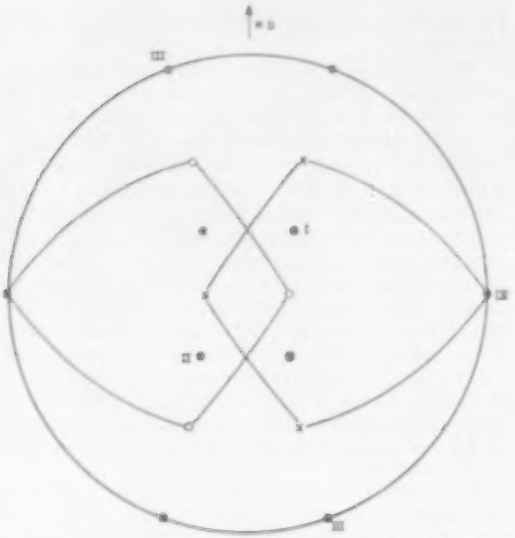

Fig. 5—Deformation texture in 70:30 brass and silver. Octahedral poles: encircled cross represents twin (110) [1$\bar{1}$2] orientation; open circle, X, 30° rotation of twin (110) [1$\bar{1}$2] orientation about pole IV.

It is proposed that the (110) [1$\bar{1}$2] secondary grains in brass and silver[17, 18] are related to the modified (358) [35$\bar{2}$] deformation texture. Consistent with the analysis in the case of copper, the (110) [1$\bar{1}$2] orientation of the secondary grains in brass and silver can be derived as shown in Fig. 1 from a 22° rotation of the modified (358) [35$\bar{2}$] orientation about the (111) pole *A*.

Discussion and Summary

In the following paragraphs, an attempt is made to point out the features of the "oriented growth" and "oriented nucleation" processes in relation to this analysis.

The recrystallization reorientation observed for a single (110) [1$\bar{1}$2] deformation texture can be described as a 30° rotation clock and counterclockwise about each of the four (111) poles of the matrix.[7] For a double (110) [1$\bar{1}$2] deformation texture, if a 30° orientation rotation about a (111) pole of the deformed matrix is retained between the orientation of the deformed matrix and the recrystallized grains,[8] then, according to the "oriented growth" hypothesis, the orientation of the recrystallized grains should fulfill the prescribed relations with respect to both components of the double (110) [1$\bar{1}$2] texture. Fig. 5 shows the (111) poles of double (110) [1$\bar{1}$2] texture. The only (111) pole which is common to both of these two {110} <112> type components is (111) pole IV. A 30° rotation about this pole in either direction results in an orientation which will satisfy the prescribed condition for both components of the double {110} <112> deformation texture. The resulting two orientations, as indicated by the connected poles in Fig. 5, are *not* the recrystallization texture of either 70:30 brass or silver, which have a deformation texture of double (110) [1$\bar{1}$2] type.

Should the rotational reorientation be related to oriented nucleation, the rotations should be based on the deformation texture. During the course of the present analysis, it was found that there are relations between the orientation of the deformation texture and the various recrystallization textures by rotations, and in the case of copper by twinning, about (111) poles.

It is not proposed that the analysis presented here is a new or unique solution relating the various textures. It is, however, proposed that this analysis is reasonably consistent in terms of the selection of axis of rotation or twinning (poles *A* or *B* of Fig. 1), the direction of rotation (Fig. 4), and the amount of rotation (16°, 22°, 30°, or 44°). The shift in the axis of rotation can be rationalized on the basis of single-crystal studies[20-24] where it was found that the pole of rotation relating orientations is usually the pole of the octahedral planes on which slip occurred during the deformation process. In the case of cold-rolled specimens, the axis of rotation thus can be shifted from one (111) pole to another because of the multiple slip systems and complexity of increasing deformation.

The existence of the relationships described in this paper does not prove the existence of oriented nucleation. However, it permits the rationalization of primary and secondary recrystallization textures in terms of oriented nucleation as well as in terms of oriented growth.

Discussion of this paper, if any, will appear in JOURNAL OF METALS, November 1955, and in AIME Metals Branch *Transactions*, Vol. **203**, 1955.

References

[1] J. S. Bowles and W. Boas: *Journal* Institute of Metals (1948) **74**, p. 501.

[2] M. L. Kronberg and F. H. Wilson: *Trans.* AIME (1949) **185**, p. 501; JOURNAL OF METALS (August 1949).

[3] G. W. Rathenau and J. F. H. Custer: *Philips Research Reports* (1949) **4**, p. 241.

[4] P. A. Beck and H. Hu: *Trans.* AIME (1949) **185**, p. 627; JOURNAL OF METALS (September 1949).

[5] H. Hu, P. R. Sperry, and P. A. Beck: *Trans.* AIME (1952) **194**, p. 76; JOURNAL OF METALS (January 1952).

[6] P. A. Beck and H. Hu: *Trans.* AIME (1952) **194**, p. 83; JOURNAL OF METALS (January 1952).

[7] Y. C. Liu and W. R. Hibbard, Jr.: *Trans.* AIME (1953) **197**, p. 672; JOURNAL OF METALS (May 1953).

[8] C. G. Dunn: *Acta Metallurgica* (1953) **1**, p. 163.

[9] C. S. Barrett: *Structure of Metals.* (1952) New York. McGraw-Hill Book Co.

[10] M. Cook and T. L. Richards: *Journal* Institute of Metals (1940) **66**, p. 1.

[11] M. Sharp and C. G. Dunn: *Trans.* AIME (1952) **194**, p. 43; JOURNAL OF METALS (January 1952).

[12] R. M. Brick and M. A. Williamson: *Trans.* AIME (1941) **143**, p. 84; METALS TECHNOLOGY (February 1941).

[13] R. Glocker: *Ztsch. für Metallkunde* (1924) **16**, p. 377; (1925) **17**, p. 353; (1927) **19**, p. 41; *Ztsch. für Ange. Physik* (1925) **31**, p. 368.

[14] D. L. Martin: *Graduate Thesis*, Yale University (1942).

[15] R. M. Brick, D. L. Martin, and R. P. Angier: *Trans.* ASM (1943) **31**, p. 671.

[16] F. von Göler and G. Sachs: *Ztsch. für Physik* (1929) **56**, p. 485.

[17] F. H. Wilson and R. M. Brick: *Trans.* AIME (1945) **161**, p. 173.

[18] F. D. Rosi, B. H. Alexander, and C. A. Dube: *Trans.* AIME (1952) **194**, p. 189; JOURNAL OF METALS (February 1952).

[19] R. Maddin, C. H. Mathewson, and W. R. Hibbard, Jr.: *Trans.* AIME (1949) **185**, p. 655; JOURNAL OF METALS (October 1949).

[20] N. K. Chen and C. H. Mathewson: *Trans.* AIME (1952) **194**, p. 501; JOURNAL OF METALS (May 1952).

[21] J. J. Becker and J. N. Hobstetter: *Trans.* AIME (1953) **197**, p. 1235; JOURNAL OF METALS (September 1953).

[22] C. G. Dunn: *Acta Metallurgica* (1954) **2**, p. 173.

Effect of Zinc Content on the Rolling Texture And Annealing Texture of Alpha Brass

by Alfonso Merlini and Paul A. Beck

Quantitative texture determinations were made for rolled and for rolled and annealed strips of 3, 6, and 10 pct Zn brasses. The main components of the rolling texture gradually shift over a wide composition range from the orientation characteristic of copper to that of 70-30 brass. At least the main features of the corresponding gradual changes in the annealing texture may be accounted for qualitatively on the basis of the oriented growth theory of annealing textures. All the oriented nucleation-type theories are notably less successful in accounting for the observed textures.

EARLIER investigations by von Goeler and Sachs,[1] Dahl and Pawlek,[2] and Brick, Martin, and Angier[3] suggested that the annealing texture of copper is more sensitive to the addition of solute elements than the rolling texture. It was reported[3] that the cube texture changes over into a brass-type recrystallization texture on addition of about 1 pct Zn, while the deformation texture changes only at about 5 pct Zn. Such behavior would be difficult to reconcile with any theory of annealing texture formation that relates the annealing texture to the deformation texture. In particular, the oriented growth theory of the cube texture[4] is based on a certain orientation relationship between the cube texture and the main components of the deformation texture which could not be reconciled with the reported behavior of low brasses. It was, therefore, of interest to re-examine these textures by means of the quantitative methods now available. The deformation and annealing textures of rolled α brasses with approximately 3, 6, and 10 pct Zn have been determined in terms of (111) and (200) pole figures.

Experimental Methods

The chemical analyses of the Cu-Zn alloys of commercial purity used in the present work are given in Table I. Chill-cast bars of the tabulated compositions were rolled and annealed according to the following schedule: 1—rolling from 1.2 to 1.02 in. thickness, 15 pct reduction area, annealing 15 min at 450°C; 2—rolling from 1.02 to 0.867 in. thickness, 15 pct reduction area, annealing 15 min at 450°C; 3—rolling from 0.867 to 0.600 in. thickness, 31 pct reduction area, annealing 2 hr at 540°C; 4—rolling from 0.600 to 0.400 in. thickness, 33 pct reduction area, annealing 2 hr at 480°C. In the final straight rolling of 96.25 pct reduction area, the strips were reversed end to end after each pass.

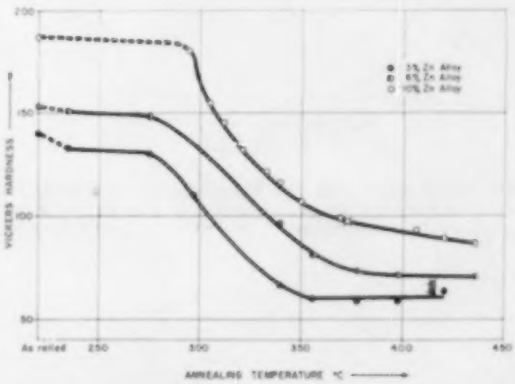

Fig. 1—Vickers hardness vs annealing temperature for 3, 6, and 10 pct brasses, rolled 96 pct. Annealing period 5 min in salt bath. Annealing temperatures adopted for study of annealing textures are marked with a barred cross.

The final annealing temperature was determined for each alloy by annealing specimens of the cold-rolled strips in salt bath for 5 min at varying temperatures. The results of the hardness measurements are given in Fig. 1, where the final annealing temperature used for each alloy in determining the annealing texture is indicated by a cross.

A. MERLINI, Student Associate AIME, and P. A. BECK, Member AIME, are associated with Dept. of Physical Metallurgy, University of Illinois, Urbana, Ill.

Discussion of this paper, TP 3945E, may be sent, 2 copies, to AIME by Apr. 1, 1955. Manuscript, July 6, 1954. Chicago Meeting, February 1955.

This paper is based on a portion[7] of a thesis by A. Merlini submitted, in partial fulfillment of the requirements for the degree of Doctor of Philosophy, to the Graduate College of the University of Illinois.

The X-ray specimens were etched to a thickness of approximately 0.002 in. in an etchant consisting of 30 pct nitric acid, 20 pct acetic acid, and the balance water. This etchant gave smooth surfaces and uniform specimen thickness.

Texture determinations were carried out by using CuKα radiation, filtered through two or three layers of 0.00035 in. thick nickel sheet. The central portion of each pole figure, up to 50° or 60° from the center, was determined with the Schulz[3] reflection method. The peripherial portion of the pole figures, from 40° or 50° to 90° from the center, was determined by using the transmission method of Decker, Asp, and Harker.[4] Intensity determinations were made at 5° tangential and radial intervals. Near maxima and at other interesting locations, measurements were made at 2° intervals. Determinations were made over more than a quadrant of each pole figure and, in some cases, half of the pole figure was determined. In order to establish with sufficient accuracy the position of some of the important intensity maxima, the exact location of these maxima was determined in at least two quadrants. Care was taken to make the determinations in the same quadrant of the pole figure with both the reflection and the transmission method in order to obtain good match between the peripherial and the central portions. In order to assure comparable intensity values in all pole figures, identical slit widths and operating conditions were used throughout the investigation, and all the measured transmission intensities were corrected to conform to the corresponding reflection intensities. The method of procedure and the corrections used were essentially the same as those described in earlier publications.[5] Both the reflection and the transmission specimen holders were built so as to provide integration over a considerable specimen area. This feature was found to be particularly important in determining pole figures for recrystallized specimens.

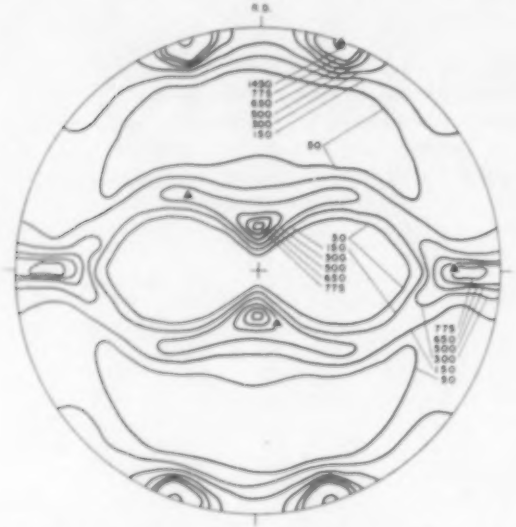

Fig. 2—Pole figure, (111), for 3 pct brass, as rolled to 96 pct reduction area. Symbols indicate location of poles for one of four equivalent "ideal orientations."

Experimental Results

The (111) and (200) pole figures for the three rolled alloys are given in Figs. 2 through 7. Comparison of these pole figures with each other and with those previously determined by Hu, Sperry, and Beck[6] for copper and for 70-30 α brass indicates a number of gradual changes taking place with increasing zinc content.*

* The photographically determined (111) pole figure for a copper alloy with 0.05 pct Cd, given by Phillips and Phillips[10] is very similar to that for the 10 pct Zn brass (Fig. 6), suggesting that the textural changes effected by cadmium are similar to those due to zinc.

The strong peripherial maxima in the (111) pole figures, Figs. 2, 4, and 6, approximately 37° to 40° from each other on either side of the rolling direction, retain their position quite well from 0 to 30 pct Zn. On the other hand, the strong (111) maxima near the transverse direction are clearly inside the

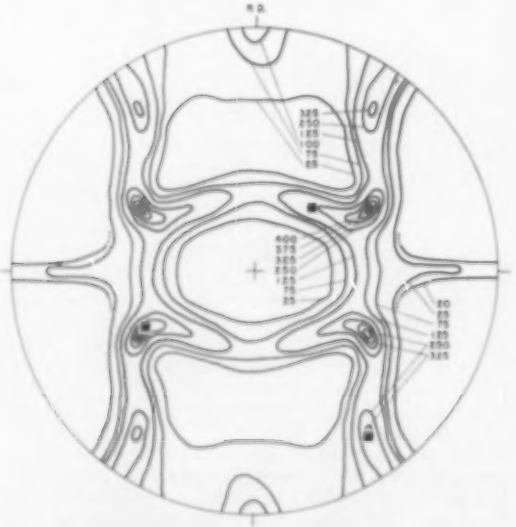

Fig. 3—Pole figure, (200), for 3 pct brass, as rolled to 96 pct reduction area. Symbols indicate location of poles for one of four equivalent "ideal orientations."

Fig. 4—Pole figure, (111), for 6 pct brass, as rolled to 96 pct reduction area. Symbols indicate location of poles for one of four equivalent "ideal orientations."

and the intensity relationships are also different

the rolling direction, was found[7] previously in the

Table I. Analyses of 3, 6, and 10 Pct Brasses

	3 Pct	6 Pct	10 Pct
Pct Cu	96.81	93.83	89.73
Pct Zn	3.19*	6.17*	10.27*
Pct Fe	0.002	0.001	0.006
Pct Pb	0.0007	0.0007	—

* Determined by difference.

pole figure in the case of copper and of the 3 and 6 pct Zn alloys, while they merge into a single maximum at the periphery of the pole figure for the 10 and 30 pct Zn alloys. Correspondingly, the strong (111) maxima near the normal direction, which are very intense in the case of copper, gradually decrease in intensity and become less sharp up to 6 pct Zn, and finally separate into two distinct maxima in the case of the 10 and 30 pct brasses. Corresponding changes occur also in the (200) pole figures. In determining the "ideal orientations" of the main components for each rolling texture, the location of the strong and well defined peripherial (111) maxima near the rolling direction and the fairly sharp (200) maxima near the normal direction were chosen as the basis. The main components of the rolling textures of the 3 and 6 pct brasses may be described by four ideal orientations approximately corresponding to (145) $[94\bar{5}]$ and for the 10 pct brass by four ideal orientations approximately (156)$[10,5,\bar{6}]$. One of the four crystallographically equivalent ideal orientations is shown in each pole figure, Figs. 2 through 7, by filled triangles and squares. These orientations can be derived from the (011)$[2\bar{1}1]$ ideal orientation by rotation around the two peripherial (111) poles near the rolling directions. (See Fig. 16.) The angle of rotation is approximately 12°, 10°, and 5°, respectively, for the 3, 6, and 10 pct brasses. In accordance with the foregoing interpretation of the gradual shifting of the ideal orientations of the main components of α brasses as a function of the zinc content, the (220) intensities, measured along the radius of the pole figure from the normal direction toward the transverse direction, showed increasing displacement of high intensities away from the normal direction with decreasing zinc content. For the 3 pct Zn alloy a fairly well defined relative maximum of the (220) intensity was found 30° away from the normal direction.

The rolling texture of 70-30 brass is usually described by means of two main components of the (011)$[2\bar{1}1]$ type. That this interpretation is somewhat arbitrary is apparent in the (111) pole figure for the rolling texture of 70-30 brass;[6] the positions of several of the intensity maxima in the (111) and (200) pole figures do not correspond exactly to the positions required by the (011)$[2\bar{1}1]$ interpretation,

Fig. 6—Pole figure, (111), 10 pct brass, as rolled to 96 pct reduction area. Symbols indicate location of poles for one of four "ideal orientations."

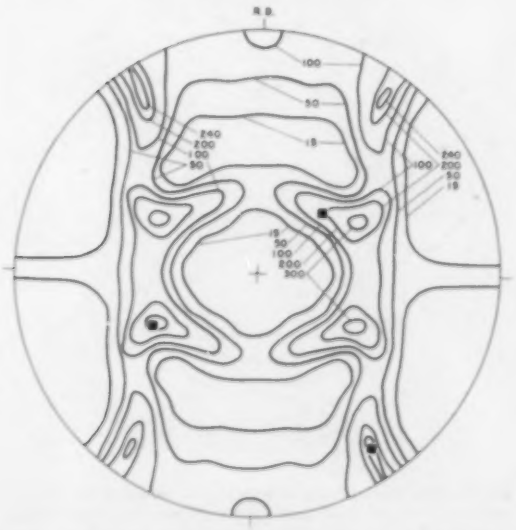

Fig. 5—Pole figure, (200), for 6 pct brass, as rolled to 96 pct reduction area. Symbols indicate location of poles for one of four equivalent "ideal orientations."

Fig. 7—Pole figure, (200), for 10 pct brass, as rolled to 96 pct reduction area. Symbols indicate location of poles for one of four equivalent "ideal orientations."

this "brass-type" spread with increasing zinc con- ima were used as the basis for all three brasses for

and the intensity relationships are also different from those expected. Using the same basis as in the 3, 6, and 10 pct Zn alloys, the rolling texture of 70-30 brass may be described also by four rather than two ideal orientations; these four orientations are identical with the corresponding ones for 10 pct brass, since the location of the intensity maxima is the same for both alloys.

A minor texture component, that may be described as a [100] fiber texture with the fiber axis in the rolling direction, was found[7] previously in the rolling texture of copper. As seen in the (200) pole figures of the α brasses, Figs. 3, 5, and 7, in the present work a similar fiber texture was found to persist, although with decreasing intensity, up to 10 pct Zn.

In all three brass rolling textures investigated, the most intense orientation spread is the one centered around the (011)[$2\bar{1}1$] orientation. The same orientation spread is also present with very high intensity in the rolling texture of copper and that of 70-30 brass.[6] In first approximation, the relative intensity of this spread is not dependent on the zinc content. In the rolling texture of copper[7] there is, in addition, a second very intense orientation spread, which is characterized by high intensities between the two peripherial (111) poles near the rolling direction and between pairs of (200) poles near the center of the pole figure. Two ideal orientations of the type (112)[$11\bar{1}$], around which the two crystallographically equivalent spreads in the pole figures are centered, may be considered as representatives of these spreads. As seen in the pole figures, Figs. 2 through 7, the intensity of these spreads decreases strongly with increasing zinc content. In the rolling texture of 70-30 brass this orientation spread, if still present, is certainly very low. Even in the 10 pct Zn alloy, Figs. 6 and 7, the relative intensity of these "copper-type" spreads is rather low. A very strong orientation spread, characteristic of 70-30 brass, centers around the (011)[100] "ideal orientation." The corresponding high intensities in the (111) pole figures adjoin the peripherial (111) poles near the rolling direction, extending from these poles peripherially toward the transverse direction. In the (200) pole figure, this orientation spread is very conspicuous as a strong intensity band connecting the pair of the four (200) maxima to the left and also the pair to the right of the normal direction. Figs. 2 through 7 clearly show the gradual increase of the intensity of

Fig. 8—Pole figure, (111), 3 pct brass, rolled 96 pct and soft annealed. Poles of one *A* component are marked by empty symbols, those of a *B* component by filled symbols. Poles of the *C* component are indicated by half-filled symbols. One of the *F* components is designated by empty symbols with stems. One of the M components is marked by half-filled symbols with stems.

Fig. 9—Pole figure, (200), for 3 pct brass, rolled 96 pct and soft annealed. Poles of one *A* component are marked by empty symbols, those of a *B* component by filled symbols. Poles of the *C* component are indicated by half-filled symbols. One of the *F* components is designated by empty symbols with stems. One of the M components is marked by half-filled symbols with stems.

Fig. 10—Pole figure, (111), of 6 pct brass, rolled 96 pct and soft annealed. Poles of one *A* component are marked by empty symbols, those of a *B* component by filled symbols. Poles of the *C* component are indicated by half-filled symbols. One of the *F* components is designated by empty symbols with stems. One of the M components is marked by half-filled symbols with stems.

this "brass-type" spread with increasing zinc content. A quantitative expression that may be used as an indicator of the relative changes in the brass-type and copper-type spreads with varying zinc content may be defined as the ratio of the intensity maximum in the (200) pole figure measured along the radial section from the normal direction toward the transverse direction on the one hand, and the maximum measured along the radial section from the normal direction toward the rolling direction on the other. This ratio, which is only 0.18 for 92.5 pct rolled Cu, increases to 1.4, 4.8, and 9.9 for the 96 pct rolled 3, 6, and 10 pct brasses, respectively. It is interesting that the greatest relative change in the ratio of the two types of orientation spread occurs between 0 and 3 pct Zn.

The results of the annealing texture determinations are shown in the (111) and (200) pole figures for the three brasses, Figs. 8 through 13. In spite of the complexity of these pole figures and of the considerably smaller intensity variations from minimum to maximum value than those occurring in the deformation textures, it was possible to interpret the various maxima in each pair of pole figures with a fair degree of accuracy in terms of certain "ideal orientations." The main components in all three annealing textures are of five types, designated by the letters *A*, *B*, *C*, *F*, and *M*. In the pole figures, one ideal orientation of each type is indicated by the location of the corresponding poles. The poles for the *A* orientation are designated by empty symbols, for the *B* orientation by filled symbols, for the *C* orientation by half-filled symbols, for the *F* orientation by empty symbols with stems, and for the *M* orientation by half-filled symbols with stems. The selection of the maxima from which these ideal orientations were determined was based on the following criteria: the sharpness of the maximum and the fact that it corresponds, as far as possible, to one orientation only. For each component, corresponding maxima were used as the basis for all three brasses for determining the ideal orientations. Table II gives the coordinates of these maxima for the 6 pct brass. The orientation designated as *S*, included in Table II, corresponds to the center of an important orientation spread that appears in both the (111) and (200) pole figures. The indices of the ideal orientations for each type of annealing texture component for the 3, 6, and the 10 pct brasses are given in Table III.

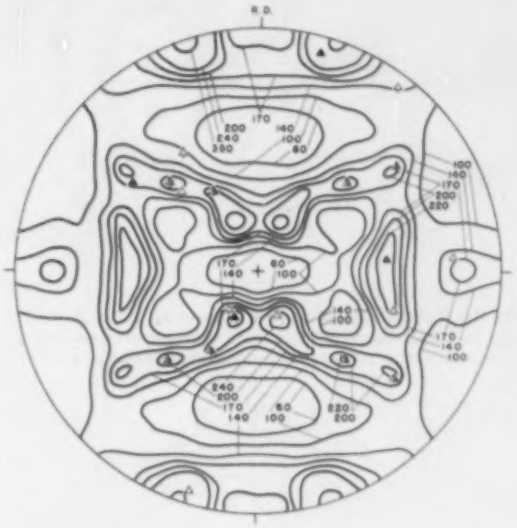

Fig. 12—Pole figure, (111), 10 pct brass, rolled 96 pct and soft annealed. Poles of one *A* component are marked by empty symbols, those of a *B* component by filled symbols. Poles of the *C* component are indicated by half-filled symbols. One of the *F* components is designated by empty symbols with stems. One of the *M* components is marked by half-filled symbols with stems.

Fig. 11—Pole figure, (200), 6 pct brass, rolled 96 pct and soft annealed. Poles of one *A* component are marked by empty symbols, those of a *B* component by filled symbols. Poles of the *C* component are indicated by half-filled symbols. One of the *F* components is designated by empty symbols with stems. One of the *M* components is marked by half-filled symbols with stems.

Fig. 13—Pole figure, (200), 10 pct brass, rolled 96 pct and soft annealed. Poles of one *A* component are marked by empty symbols, those of a *B* component by filled symbols. Poles of the *C* component are indicated by half-filled symbols. One of the *F* components is designated by empty symbols with stems. One of the *M* components is marked by half-filled symbols with stems.

Fig. 14—Relative orientation of an *A* component (filled symbols) in the annealing texture of 6 pct brass with respect to the four deformation texture components (empty symbols), (111) poles.

Fig. 15—Relative orientation of a *B* component (filled symbols) in the annealing texture of 6 pct brass with respect to the four deformation texture components (empty symbols), (111) poles.

The *A*, *B*, *F*, and *S* types of orientations have a multiplicity of four and, correspondingly, four orientations of each type appear in the annealing textures. The orientations of the type *M* have a multiplicity of two, and both orientations appear in the annealing textures. *C* designates the cube texture, which has a multiplicity of one and which is represented by measurable intensities in each pole figure. The total number of main components in each of these annealing textures is 15.

The orientations of the *A* components do not vary appreciably from 3 to 6 pct Zn. The *A* orientations are very close to the ideal orientations of the main deformation texture components for copper, which may be retained in the annealing texture of copper if the penultimate grain size is sufficiently large and the final rolling reduction is not too great. Even in the annealing textures of 3 and 6 pct brasses, the *A* components are not very far removed from the orientations of the main rolling texture components, Fig. 14. However, some amount of material appears to be present in *A*-type orientations even in the annealing texture of 70-30 brass where the main deformation texture components have a distinctly different orientation, so that the foregoing similarity no longer holds. The intensity of the *A* components appears to decrease gradually with increasing zinc content.

The orientation of the *B* components is gradually shifted with the zinc content in such a way that each *B* component retains its orientation relationship of approximately 30° rotation around the peripherial (111) pole with respect to one of the main deformation texture components, Fig. 15. In the pole figure of the 10 pct brass, the poles of the four *B* components are fairly close to the corresponding maxima for the annealing texture of 70-30 brass. This is also clearly expressed in the similarity of the indices of these orientations, namely (438)[63$\bar{4}$] for the *B* component in 10 pct brass, vs (225)[73$\bar{4}$] for the annealing texture of 70-30 brass. It appears then that the *B* components of the annealing texture change over continuously with increasing zinc content into the four annealing texture components of 70-30 brass. Correspondingly, the intensity of the *B* components increases distinctly with increasing zinc content.

The orientation of the *F* components does not vary appreciably with the zinc content. These components, which appear in the annealing texture of the 3, 6, and 10 pct brasses, are apparently absent in the annealing texture of copper and of 70-30 brass. The two *M* components are fully developed with clear-cut maxima in the annealing texture of 10 pct brass. Some of these maxima are also clearly visible in the pole figures of annealed 70-30 brass, so that it is probable that the *M* components also are present in this alloy. However, in the annealing textures of the 3 and 6 pct brasses, the *M* components are not represented by separate maxima, only as spreads. The orientations for the *M* components in these alloys, given in Table IV, correspond to the two ends of this spread, which centers around the cube orientation. In the annealing texture of the 3 and 6 pct brasses, the cube texture is much stronger than the *M* components. The decrease in the amount of cube texture is very great between 0 and 3 pct Zn, and it is also quite considerable between 3 and 6 pct Zn. In the

Table II. Coordinates of the Maxima Used as Basis to Determine the Ideal Orientations of the Annealing Texture Components for 6 Pct Brass

Type of Component	Coordinates to the Maxima		Pole Figure
	ϕ	α	
A	55°	63°	(200)
	Best fit with the other (111) and (200) intensity maxima		
B	50°	82°	(111)
	60°	31°	(200)
F	90°	38°	(111)
	62°	72°	(111)
	70°	13°	(200)
M	80°	0°	(200)
	66°	90°	(200)
S	60°	0°	(111)
	62°	73°	(111)

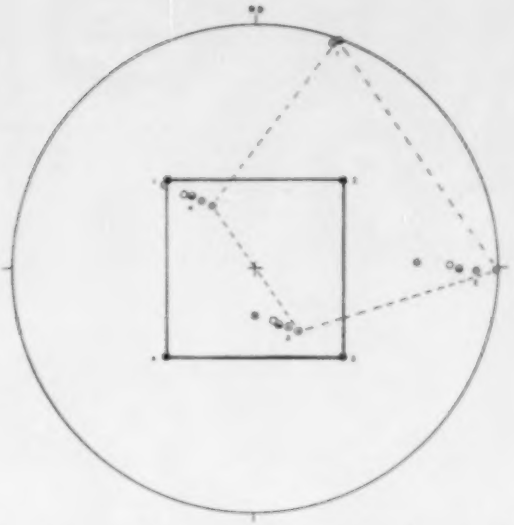

Fig. 16—Relative orientation of the *C* component (filled symbols) in the annealing texture with respect to a deformation texture component of each copper (encircled X), 3 pct brass (open circle), 6 pct brass (half-filled circle), 10 pct brass (encircled dot), and 30 pct brass (encircled +).

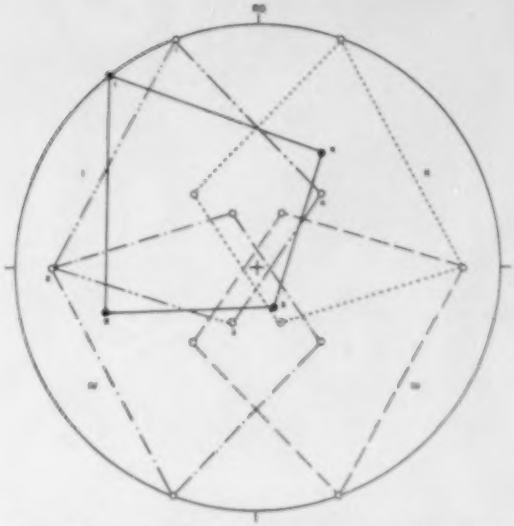

Fig. 17—Relative orientation of an *F* component (filled symbols) in the annealing texture of 6 pct brass with respect to the four deformation texture components (empty symbols), (111) poles.

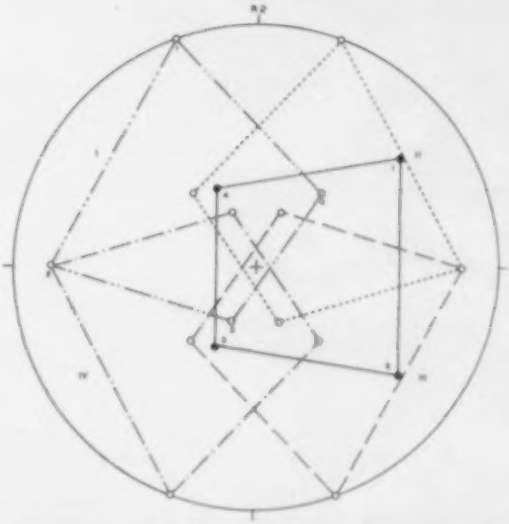

Fig. 18—Relative orientation of an *M* component (filled symbols) in the annealing texture of 6 pct brass with respect to the four deformation texture components (empty symbols), (111) poles.

10 pct Zn alloy, the amount of material in the cube texture is fairly small (although definitely present), while the intensity of the *M* components is larger.

The relative orientations of each one of the five different types of annealing texture components with respect to the four main components of the deformation texture in the case of 6 pct Zn brass are given in Figs. 14 through 18.

Discussion of Results

It has been pointed out[9] that, in cases where the matrix texture consists essentially of a single orientation, the recrystallization texture in face-centered-cubic metals usually consists of eight components corresponding to all possible orientations having a 30°, respectively 40°, [111] rotational relationship with the matrix orientation, as may be expected on the basis of the oriented growth theory of annealing textures.[10] On the other hand, in the more general case of complex matrix textures, comprising several main deformation texture components and orientation spreads, the orientation most favorable for growth would not be necessarily expected to have a 30° [111] rotational relationship with any of the matrix components.[11] At present there are no reliable quantitative data on boundary mobility as a function of the disorientation across the boundary. Even when such data become available, the prediction of annealing textures in complex matrices will be possible only if both the proposed inhibiting effect of minor amounts of matrix material in orientations unfavorable for the growth of the new grains and the effect of the geometrical arrangement (such as size) of matrix elements in various orientations[9] can be taken into account quantitatively.

In view of these complexities, it is interesting that a 30° [111] rotational relationship between an annealing texture component and of the components of a complex matrix is actually often found, at least approximately.[7, 10] It has been pointed out[8, 11] that, on the basis of the oriented growth theory, it is certainly to be expected that the various orientations ideally related for growth with respect to *one* of the matrix components will, in general, have different orientation relationships with the other matrix components and orientation spreads. Consequently, the various orientations ideally related to one of the matrix components will not be equivalent to each other in regard to boundary mobility with respect to the complex matrix as a whole. It has been shown that, in cross-rolled copper[5] and in the case of straight-rolled 70-30 brass,[11] the "missing orientations" may be accounted for, at least qualitatively, by considering their relations with the various matrix components and orientation spreads.

The most conspicuous change taking place in the annealing texture of α brass with increasing zinc content is the decrease in the intensity of the cube

Table III. Indices of the Ideal Orientation for Each Type of Annealing Texture Component for the 3, 6, and 10 Pct Brasses

Type of Component	3 Pct Brass	6 Pct Brass	10 Pct Brass
A	(308) [43$\bar{3}$]	(308) [43$\bar{3}$]	(236) [946]
B	(314) [53$\bar{2}$]	(427) [43$\bar{2}$]	(438) [63$\bar{4}$]
C	(001) [100]	(001) [100]	(001) [100]
F	(113) [20$\bar{1}$]	(113) [20$\bar{1}$]	(112) [20$\bar{1}$]
M	(047) [100]	(037) [100]	(038) [100]
S	(125) [563]	(125) [332]	(238) [443]

texture. A satisfactory qualitative explanation for this change may be given on the basis of the oriented growth theory. As seen in Fig. 16, with increasing zinc content the main deformation texture components are gradually changing their orientation in such a way as to become further and further removed from a [111] rotational relationship with respect to the cube orientation. On this basis, it would be expected that the advantage of the cube-oriented grains over grains in other orientations in regard to boundary mobility in the matrix is more and more suppressed. In addition, the strong increase of the "brass-type spread" in the deformation texture with increasing zinc content, particularly between 0 and 6 pct Zn, may also contribute significantly to the suppression of the cube texture, since the orientation representative of this spread and corresponding to its center is very far removed from a [111] rotational relationship with respect to the cube orientation. The fact that, despite the loss of a [111] rotational relationship with respect to the cube orientation, a cube texture component does appear in annealed low α brasses is rather significant. Although the "cube grains" in these alloys are not very close to an ideal orientation relationship for maximum boundary mobility with respect to any one of the main components of the deformation texture, they are at least fairly favorably oriented for growth with regard to *all four* matrix components. In these alloys much more obviously than in copper, the cube component appears as a "compromise texture," corresponding to relatively high boundary mobility in the matrix as a whole, rather than to maximum boundary mobility in one component.

With increasing zinc content, the *M* orientations, Fig. 18, come progressively nearer to a [111] rotational relationship with all four main rolling texture components. In view of this, the increasing intensity with increasing zinc content of the orientation spread extending between the cube texture and the *M* orientations and, finally, the emergence of distinct and well defined *M* components at 10 pct Zn is consistent with the oriented growth theory.

The present results may serve to illustrate the fact that in the case of complex matrix textures the annealing texture components can not be predicted in full detail on the basis of the oriented growth theory without more quantitative knowledge of the orientation dependence of boundary mobility, and of the "inhibition effect" and "size effect" mentioned previously, than that available at the present time. This is particularly true with regard to the *A* and *F* components encountered in annealed 3, 6, and 10 pct brasses.

Since each *B* component is approximately ideally oriented with respect to one of the deformation texture components, Fig. 15, and since this orientation relationship is preserved as the deformation texture varies with the zinc content, it may be concluded that the *B* component is nearly ideally oriented for growth at least with respect to one deformation texture component. The fact that the intensity of the *B* components increases with increasing zinc content also may be explained qualitatively on the basis of the oriented growth theory, since each *B* component becomes further and further removed from having a twin orientation relationship with another one of the main deformation texture components.

It appears that none of the various oriented nucleation theories of annealing textures is very promising in explaining the experimentally found annealing textures for 3, 6, and 10 pct brasses. None of these theories offers any explanation for the formation of the *A* and *F* texture components. An oriented nucleation theory based on a [111] rotational relationship between the nucleus orientations and the matrix orientation, as the one recently proposed by Liu and Hibbard,[6] could account for the formation of the *B* annealing texture components, but it could not explain without new hypotheses the increase in the intensity of the *B* components with increasing zinc content. Such a theory would certainly have difficulty in accounting for the formation of the cube texture, even in decreasing amounts, when the main deformation texture components become further and further removed from a [111] rotational relationship from the cube orientation. Furthermore, this theory does not account for the typical sharpness of the cube texture which forms in copper on annealing from a rolling texture that includes very considerable orientation spreads. If it is assumed that the nuclei possess a definite orientation relationship with the matrix, it might be expected that each nucleus is so related with respect to a microscopic portion of the matrix directly adjacent to it. The spread of nucleus orientations then should correspond approximately to the spread of matrix orientations, in contradiction with experimental fact. On the other hand, the oriented nucleation theory of Burgers[4] could account for the formation of the cube texture in spite of the shifting of the main deformation texture components, since it relates the formation of the cube texture to the high rate of polygonization of cube-oriented minor matrix elements which it assumes to serve as nuclei, regardless of the orientation of the main matrix texture components. On this picture, the decrease in the amount of cube texture formed with increasing zinc content presumably would have to be explained on the basis of a decrease in the amount of cube-oriented matrix elements. Actually, the amount of cube-oriented material in the rolled strips does decrease with increasing zinc content. However, quantitatively the correlation is not very good. The deformation texture indicates little change in the amount of cube-oriented material between 3 and 6 pct Zn, whereas the intensity of the cube component in the annealing texture decreases very sharply in that composition range. It has been shown in a previous publication[7] that this theory leads to the prediction that cross-rolled copper should recrystallize in the cube orientation, while the experimentally determined recrystallization texture does not comprise a cube component. Burgers' theory offers no help in explaining the formation of any of the other annealing texture components encountered in low brasses.

The results of the present investigation show that the changes with increasing zinc content in both the deformation texture and the annealing texture of Cu-Zn alloys take place progressively over a wide

composition range. The evidence does not support the view, attained by previous investigators on the basis of photographic texture determinations, that the annealing texture is more sensitive to compositional changes than the deformation texture. In particular, it appears that the decrease in the intensity of the cube component in the annealing texture with increasing zinc content may be explained on the basis of the oriented growth theory by the changes in the deformation texture resulting from increasing zinc content.

Conclusions

1—The rolling texture of low brasses may be described in first approximation by four main components with "ideal orientations" gradually shifting from approximately (145)[94$\bar{5}$] for 3 pct Zn to approximately (156)[10,5,$\bar{6}$] for 10 pct Zn.

2—The three principal orientation spreads present in rolled low brasses center around orientations of the following types: (011)[2$\bar{1}$1], (112)[11$\bar{1}$], and (011)[100]. The spread represented by (011)[2$\bar{1}$1] is present in large amounts for any zinc content between 0 and 30 pct. The spread represented by (112)[11$\bar{1}$] is typical of copper and decreases in intensity with increasing zinc content. The spread represented by (011)[100] is typical of 70-30 brass and decreases in intensity with decreasing zinc content.

3—The minor texture component previously found in rolled copper, which may be described as a [100] fiber texture with the rolling direction as fiber axis, occurs also in low brasses. Its intensity decreases with increasing zinc content.

4—The annealing texture of rolled low brasses consists of 15 main components, which fall into five types, designated as *A*, *B*, *C*, *F*, and *M*. The four *A* components correspond approximately to the orientation of the retained deformation texture components in annealed copper, and this orientation is little affected by the zinc content. Each one of the four *B* components is related to one of the main rolling texture components by a 30° rotation around the peripherial [111] axis and retains this relative orientation as the deformation texture components shift with increasing zinc content; the four *B* components go over into the four main components of the recrystallization texture of 70-30 brass. *C* is the cube texture component. The four *F* components correspond to the (112)[20$\bar{1}$] type, regardless of zinc content. The two *M* components in annealed 10 pct brass have ideal orientations of the type (038)[100].

5—The amount of the cube texture decreases with increasing zinc content, particularly sharply up to 3 pct Zn. However, a measurable amount of material in cube orientation appears to be present even in the annealing texture of 10 pct brass. The *M* components, which are not present in the annealing texture of 96 pct straight-rolled copper, increase in amount with increasing zinc content. Most likely, *M* components are present in the annealing texture of 70-30 brass. *B* components are not present in the annealing texture of 96 pct straight-rolled copper and their amount increases gradually with the zinc content. Minor variations in the orientation and in the amount of the *A* and *F* components have been observed from 3 to 10 pct Zn content. There is no indication of the presence of *F* components in the annealing texture of either rolled copper or 70-30 brass.

6—The conclusion of previous investigators that the change in the rolling texture from the copper to the brass type occurs at a zinc content different from that necessary to produce corresponding changes in the annealing texture is not confirmed by the present work. The orientation of the main rolling texture components and the intensity of the various orientation spreads of the rolling texture change gradually with increasing zinc content. Corresponding gradual changes take place in the orientation and in the amount of most annealing texture components.

Acknowledgments

This work was supported by the United States Atomic Energy Commission, Contract No. AT(11-1)-67, Project No. 9. One of the authors is indebted to Professor A. Scortecci and to Società Siderurgica Finsider for financial assistance. The authors wish to express their appreciation to W. E. Heitman and V. Y. Doo for their assistance in the experimental work and to Dr. F. H. Wilson and the American Brass Co. for kindly supplying the brass ingots and their analyses.

Discussion of this paper, if any, will appear in JOURNAL OF METALS, November 1955, and in AIME Metals Branch *Transactions*, Vol. **203**, 1955.

References

[1] von Goeler and G. Sachs: Walz- und Rekristallisationstextur regulaerflaechenzentrierter Metalle. II. *Ztsch. für Physik* (1927) **41**, p. 889.

[2] O. Dahl and F. Pawlek: Kornordnung und Kornwachstum bei Walzblechen. *Ztsch. für Metallkunde* (1936) **28**, p. 262.

[3] R. M. Brick, D. L. Martin, and R. P. Angier: Effects of Various Solute Elements on the Hardness and Rolling Textures of Copper. *Trans.* ASM (1943) **31**, p. 675.

[4] P. A. Beck: Origin of the Cube Texture in Face-Centered Cubic Metals. *Trans.* AIME (1951) **191**, p. 474; JOURNAL OF METALS (June 1951).

[5] L. G. Schulz: A Direct Method of Determining Preferred Orientation of a Flat Reflection Sample Using a Geiger Counter X-ray Spectrometer. *Journal of Applied Physics* (1949) **20**, p. 1030.

[6] B. F. Decker, E. T. Asp, and D. Harker: Preferred Orientation Determination Using a Geiger Counter X-ray Diffraction Goniometer. *Journal of Applied Physics* (1948) **19**, p. 388.

[7] A. Merlini and P. A. Beck: Study of the Origin of the Cube Texture. *Acta Metallurgica* (1953) **1**, p. 598.

[8] H. Hu, P. R. Sperry, and P. A. Beck: Rolling Textures in Face-Centered Cubic Metals. *Trans.* AIME (1952) **194**, p. 76; JOURNAL OF METALS (January 1952).

[9] P. A. Beck: Notes on the Theory of Annealing Textures. *Acta Metallurgica* (1953) **1**, p. 230.

[10] P. A. Beck: Theory of Annealing Textures. *Trans.* AIME (1951) **191**, p. 475; JOURNAL OF METALS (June 1951).

[11] P. A. Beck: Annealing of Cold Worked Metals. *Advances in Physics* (1954) **3**, p. 245.

[12] P. A. Beck and H. Hu: Annealing Textures in Rolled Face-Centered Cubic Metals. *Trans.* AIME (1952) **194**, p. 83; JOURNAL OF METALS (January 1952).

[13] Y. C. Liu and W. R. Hibbard, Jr.: On the Relationship of Texture Changes of Cold-Rolled Face-Centered-Cubic Metals During Recrystallization. *Trans.* AIME (1955) **203**, p. 381; JOURNAL OF METALS (February 1955).

[14] W. G. Burgers, Y. H. Liu, and T. J. Tiedema: The Influence of Crystal Orientation on Polygonization of Aluminum Single Crystals. *Proceedings* Koninkl. Nederl. Akad. van Wetenschappen (1951) **94**, p. 459.

[15] V. A. Phillips and A. Phillips: The Effect of Certain Solute Elements on the Recrystallization of Copper. *Journal* Institute of Metals (1952-1953) **81**, p. 185.

Technical Note

Crystal Structure and Some Properties of the Compound, Zr_2Al

by J. H. Keeler and J. H. Mallery

THE crystal structure of Zr_2Al, the compound richest in zirconium (91.03 pct Zr by weight) in the system Zr-Al, has been found to be ordered face-centered-cubic. This compound is of particular interest, since it is encountered as the precipitated phase in potentially useful zirconium-rich alloys. It forms peritectoidally from body-centered-cubic zirconium and Zr_2Al at about 975°C. The Zr-Al constitution diagram has been reported by McPherson and Hansen.[1]

For the primary determination a 100 g ingot was prepared by arc-melting in a water-cooled copper crucible under purified argon. The raw materials were crystal-bar zirconium (a purity of better than 99.7 pct) and spectroscopically pure aluminum. The ingot was double melted, examined metallographically, and found to be quite uniform as shown in Fig. 1. The hardness of the as-cast button was VHN 390 to 445.

A 20 mil diam specimen was prepared from annealed (900°C) filings of Zr_2Al. The specimen was mounted in a 5 cm radius powder camera and an 8 hr exposure was taken using copper radiation with a nickel filter.

The structure of the compound Zr_2Al was found to be ordered face-centered-cubic of the Cu_2Au type, with an a_o value of 4.372±0.003A. Its calculated density is 5.976±0.013 g per cu cm. The relative intensities for the lines were calculated using the formula

$$I \propto \frac{1 + \cos^2 2\theta}{\sin^2 \theta \cos \theta} \cdot p \cdot |F^2|$$

where $\frac{1 + \cos^2 2\theta}{\sin^2 \theta \cos \theta}$ is the Lorentz polarization factor, p is the multiplicity factor, and F is the structure factor. The X-ray data are given in Table I.

Table I. X-Ray Data for Compound Zr_2Al

hkl	Calculated d	Observed d	Calculated Intensity	Observed Intensity
100	4.372	4.38	227	Medium
110	3.091	3.09	186	Medium
111	2.524	2.52	1543	Very strong
200	2.186	2.18	760	Strong
210	1.955	1.95	97	Weak
211	1.785	1.78	71	Weak
220	1.546	1.54	470	Strong
300,221	1.457	1.46	9 to 35	Weak
310	1.383	1.38	57	Weak
311	1.318	1.32	517	Strong
222	1.262	1.26	154	Medium to strong
320	1.212	1.22	38	Very weak
321	1.168	1.17	39	Weak
400	1.093	1.09	79	Medium
410,322	1.060	1.06	14 to 14	Very weak
411,330	1.030	1.03	13 to 7	Very weak
331	1.003	1.003	276	Medium to strong
420	0.9776	0.977	287	Medium to strong
421	0.9540	0.953	26	Very weak
332	0.9321	0.931	14	Very weak
422	0.8924	0.892	279	Strong
500,430	0.8744	0.873	4 to 15	Very very weak
510,431	0.8574	0.857	16 to 31	Very weak
511,333	0.8414	0.841	336 to 112	Strong
520,432	0.8119	0.812	45 to 45	Weak
521	0.7982	0.798	55	Weak

The compound has exhibited plasticity when present as particles in a matrix of α zirconium. During hot working at about 900°C, the compound has been found to deform plastically to the extent that some of the particles exhibit a length-to-width ratio greater than 4:1 as shown in Fig. 2. In answer to the discussion of ref. 1, McPherson and Hansen pointed out that the compound may be cold rolled and reduced as much as 33 pct.

Zr_2Al has also been found[2] under certain conditions to precipitate in lamellar form at grain boundaries of the α phase of hexagonal-close-packed zirconium.

Acknowledgment

This work was carried out under Contract W-31-109-Eng 52 for the United States Atomic Energy Commission.

J. H. KEELER, Member AIME, and J. H. MALLERY are associated with Alloy Studies Research, Research Laboratory, General Electric Co., Schenectady.

TN 257E. Manuscript, Oct. 22, 1954.

[1] D. J. McPherson and M. Hansen: *Trans.* ASM (1954) 46, p. 354.
[2] J. H. Keeler: *Trans.* ASM (1954) 46, p. 373.

Fig. 1—Micrograph of as-cast Zr_2Al shows a fairly uniform structure. Bright field, etched in HNO_3, HF, and glycerine. X100. Area reduced approximately 20 pct for reproduction.

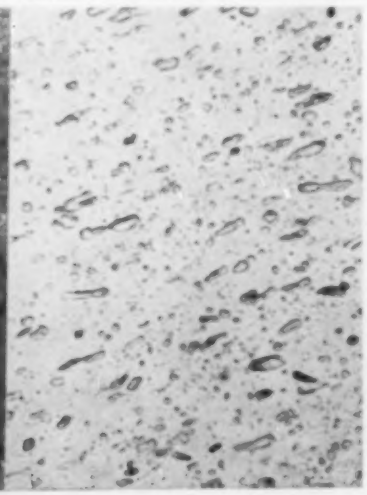

Fig. 2—Micrograph of specimen shows elongated particles of Zr_2Al in a matrix of α zirconium. The specimen of 10 atomic pct Al in zirconium was hot rolled at 900°C and then annealed 1 hr at 850°C. Bright field, etched in HNO_3, HF, and H_2O. X500. Area reduced approximately 20 pct for reproduction.

Preferred Orientations in Beta-Annealed Zirconium

by J. H. Keeler and A. H. Geisler

Preferred orientations in unalloyed zirconium were determined by the Geiger-counter spectrometer X-ray diffraction technique. With increasing β-annealing temperature the following textures were obtained: 1—a retained α-annealing texture, 2—additional orientations predictable from the α-β (Burgers) relationship, and 3—a texture derived from a cube texture in the β phase. Earlier work on cold-worked and α-annealed zirconium was reappraised to show a quantitative dependence of rotations on temperature and to identify spurious areas of some of the pole figures.

IN a previous paper,[1] the preferred orientations of high purity zirconium sheet were described for cold-rolled and annealed samples. Annealing temperatures up to 900°C, which is slightly above the allotropic transformation temperature, were explored. Of interest was the observation that the orientation of the hexagonal-close-packed material after annealing in the temperature range of the stable body-centered-cubic phase was similar to that of the material which had been annealed in the α temperature region, although a change in texture would be expected because of the many new orientations based on an orientation relationship between the two forms of zirconium. The reversion to an original orientation after an allotropic transformation cycle is not unusual. It has been found for titanium,[2-3] for thallium,[4] and for cobalt[5] among the hexagonal metals. Burgers found in his original work[1] that, when zirconium was cooled through the allotropic transformation and then reheated, the body-centered-cubic phase reverted to the original orientation. Additional experimental work has been carried out to further explore the textures of zirconium after annealing in the temperature range above the allotropic transformation. In addition, a reappraisal was made of the earlier results for zirconium[1] in light of recent work on titanium[3] which has shown that the texture type depends quantitatively on the temperature of annealing and that spurious areas may be encountered in the pole figures of hexagonal metals determined by the X-ray spectrogoniometer technique of analysis.

J. H. KEELER, Member AIME, is Research Associate, and A. H. GEISLER, Member AIME, deceased, was Research Associate, Research Laboratory, General Electric Co., Schenectady.

Discussion of this paper, TP 3973E, may be sent, 2 copies, to AIME by Apr. 1, 1955. Manuscript, Aug. 23, 1954. Chicago Meeting, February 1955.

Table I. Composition of Crystal-Bar Zirconium

Element	Wt Pct
Hafnium	0.3 maximum
Iron	0.02 to 0.1
Aluminum	0.005 to 0.02
Chromium	0.02 to 0.1
Copper	0.001 to 0.005
Nickel	0.005 to 0.02
Magnesium	0.001 to 0.005
Molybdenum	0.01
Nitrogen	0.007*

* Chemical analysis (oxygen and carbon are estimated at 0.02 pct).

Experimental Procedure

Crystal-bar zirconium prepared by the iodide process was the material used in this investigation. The major impurity was hafnium which was less than 0.3 pct. The composition obtained by spectrographic analysis is given in Table I.

Cold-rolled specimens were prepared from crystal bar by a series of reductions of approximately 0.010 in. until the sheet reached a thickness of 0.010 in., after which it was cold rolled to 0.001 in. thickness between sheets of alloy steel. The total cold reduction amounted to about 99.8 pct. Specimens were annealed for ½ hr at 1000° to 1100° to 1200°C or 1 hr at 1400°C in an evacuated Vycor or quartz tube.

The transmission pole figures were obtained by

RD

came less pronounced with increased annealing tem-

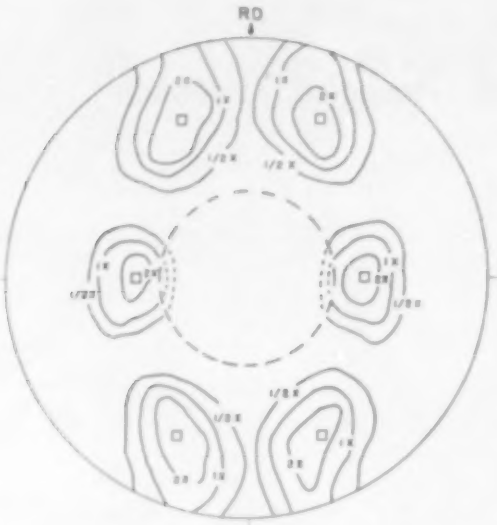

Fig. 1—(10$\bar{1}$0) pole figure of 99.8 pct cold-reduced zirconium sheet annealed at 600°C for 30 min and then at 900°C for 30 min. The orientations of (10$\bar{1}$0) poles for the texture (0001)[11$\bar{2}$0] with a tilt of ±40° about the rolling direction are indicated by squares.

the quantitative method of Decker, Asp, and Harker[5] modified by Geisler[6] using an X-ray spectrogoniometer with CuKα radiation. Many of the pole figures prepared during the latter part of this investigation were made with the automatic pole-figure recorder reported recently by Geisler.[7] Unless otherwise specified, all four quadrants were examined with 5° increments along the radius of the pole figure. Absorption corrections were made for changes in length of the X-ray path through the sample as inclination of the sample to the beam changed. During examination, the specimen was translated back and forth in its plane through a 1 in. distance in order to increase the total number of grains contributing to the measured X-ray intensity. The intensity contours were expressed in multiplicities of the intensity of a comparable sample, but with randomly oriented crystallites.

Usually the inner 40° of the pole figure was not determined because the specimen holder interfered with the passage of the X-ray beam. In most instances, it was not necessary to examine this area, since consistent pole figures of [10$\bar{1}$0] poles (which were confirmed by making (0002) pole figures for most samples) were obtained in the outer 50°, thus defining the textures. However, the inner 40° was determined for several pole figures and this work was performed at the Knolls Atomic Power Laboratory with a spiral-scanning X-ray reflection goniometer previously described by Holden.[8] As in the other zirconium work reported here, CuKα radiation was used. Since these results were not calibrated as multiples of random intensity, the contours thus obtained are included in the pole figures as broken lines.

Results and Discussion

β-annealing Textures: When zirconium sheet was annealed for ½ hr at 900°C (about 45° above the nominal transformation temperature), the relatively simple texture reproduced in Fig. 1 from previous work[1] was obtained.* This texture was described by (0001) tilted 40° to the rolling plane about the [11$\bar{2}$0] which was in the rolling direction. The (0002) pole figure exhibited only two intense areas which were spread along the transverse direction. Although the combined effect of a 600° and a 900°C anneal was required to develop this texture, it may be regarded as the end state of a series characteristic of annealing in the α temperature region. It may be used for evaluation of β-annealing texture, since there are no new areas which can be attributed to the transformation.

Results obtained recently when severely cold-reduced sheets of zirconium were annealed at 1000°,

* In a very recent study,[13] Glen and Pugh discuss the possible orientations which can arise from several transformations. They suggest that dislocations in the parent phase may be responsible for a reversion to the original texture after a transformation cycle.

Fig. 2—(10$\bar{1}$0) pole figure of 99.8 pct cold-reduced zirconium sheet heated in the furnace from 900° to 1100°C and held ½ hr at 1100°C.

Fig. 3—(0002) pole figure of 99.8 pct cold-reduced zirconium sheet heated in the furnace from 900° to 1100°C and held ½ hr at 1100°C.

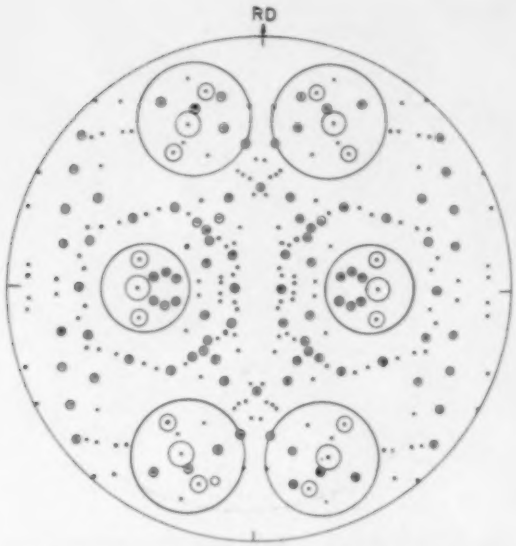

Fig. 4—Predicted orientations for (10$\bar{1}$0) poles from an original texture, (0001) at 40° from the rolling plane and [11$\bar{2}$0] in the rolling direction, heated above the transformation temperature. The encircled points indicate superposition of 2, 3, or 6 poles with the number increasing with the size of circle. Poles clustered in the big circles agree with observed high intensity areas.

1100°, and 1200°C show new areas in the (10$\bar{1}$0) pole figures as illustrated in Fig. 2. On comparison with Fig. 1, these areas were particularly noticeable on the basic great circle at approximately 40° to 45° from the rolling direction and in the transverse direction.† Although the preferred orientation became less pronounced with increased annealing temperature, the dominant component would appear to be still (0002) about 40° to the rolling plane with [11$\bar{2}$0] in the rolling direction like Fig. 1. However, inspection of the (0002) pole figures as illustrated by Fig. 3 and the (10$\bar{1}$0) poles predicted in Fig. 4 indicates that what appears to be a single component comes about from the superposition of a number of different orientations.

The new areas are related to the initial texture by the Burgers orientation relationship, as shown most simply by comparing the predicted pole locations of Fig. 5 with the (0002) pole figure in Fig. 3. This relationship is one in which the (0001) plane of the hexagonal modification is parallel to one of the {110}cubic planes with a [11$\bar{2}$0] hexagonal direction parallel to one of the <111> cubic directions. The points in Fig. 5 represent (0002) poles predicted for the hexagonal product formed on cooling the cubic product arising from heating the hexagonal material with the nominal texture (0002) 40° to the rolling plane, [11$\bar{2}$0], in the rolling direction. Each of the two initial hexagonal orientations produce six orientations of the cubic form on heating, and each of these could provide six orientations of basal poles on cooling for an increase from two to a total of 72 orientations of basal poles.** Superposition of some, shown by circles in Fig. 5, and grouping of others adequately explain the locations and shapes of the high intensity areas of the observed (0002) poles in Fig. 3. Planes of the (10$\bar{1}$0) type involve a further multiplicity of six, or a total of 432, poles and in the absence of significant grouping might merely contribute to the background and spread of the pole figure. The effect of temperature in the range 1000° to 1200°C is not clearly recognized in the (10$\bar{1}$0)

† New peaks were also observed in the rolling direction about 50° from the normal to the rolling plane, but the maximum intensity was slightly less than the lowest intensity recorded in these figures.

** McGeary and Lustman[12] had evidently neglected to consider five of the six possible cubic orientations from each original hexagonal orientation since their predicted pole figure (their Fig. 6a) shows only one sixth the number of poles as the authors' Fig. 5. The predicted orientations in this report include the three [1120] directions in the basal plane to which each of two [111] directions in the single (110) plane of the cubic form can be parallel.

Fig. 5—Predicted orientations for (0002) poles from an original texture, (0001) at 40° from the rolling plane and [11$\bar{2}$0] in the rolling direction, heated above the transformation temperature. The encircled points indicate superposition of 2, 3, or 6 poles with the number increasing with the size of circle.

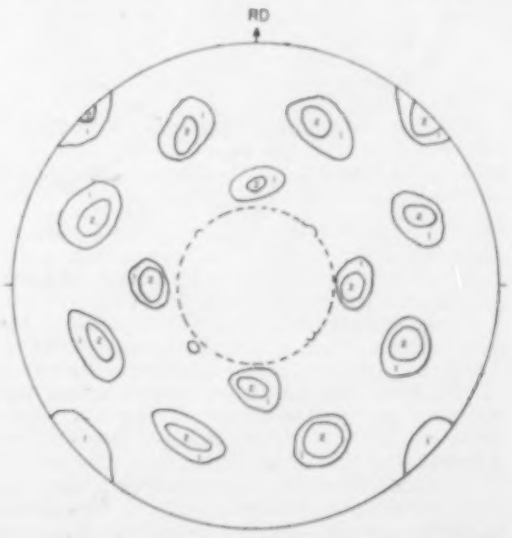

Fig. 6—(10$\bar{1}$0) pole figure of 99.8 pct cold-reduced zirconium sheet annealed 1 hr at 1400°C.

Fig. 7—(0002) pole figure of 99.8 pct cold-reduced zirconium sheet annealed 1 hr at 1400°C.

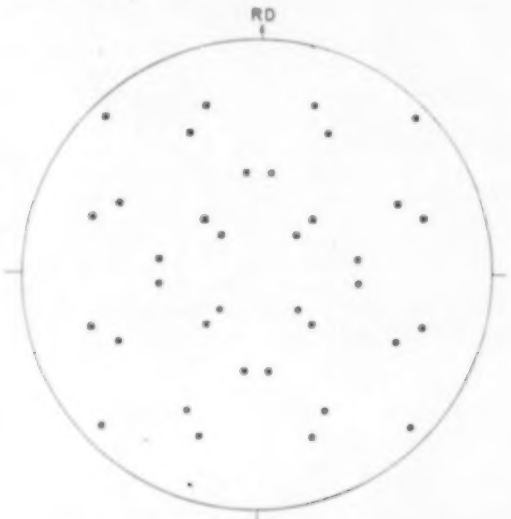

Fig. 8—Predicted $(10\bar{1}0)$ poles for α-zirconium transformed from a cube texture of β.

texture. Nevertheless, the outstanding feature for zirconium sheet annealed at temperatures up to 1200°C is a pole figure which recembles the nominal recrystallization texture, but the prominent difference is apparent on the (0002) pole figure. Fig. 4 shows the positions of $(10\bar{1}0)$ poles predicted from a heat treatment in the β region, followed by cooling again into the hexagonal-close-packed temperature region, assuming the texture before the β-heat treatment was that of a symmetrical texture about a $[11\bar{2}0]$ direction in the rolling direction and the basal planes tilted 40° to the rolling plane. The good correlations of these predicted (0002) and $(10\bar{1}0)$ poles with the experimental results suggests that the cold-rolled hexagonal sheet recrystallized during heating before transforming.

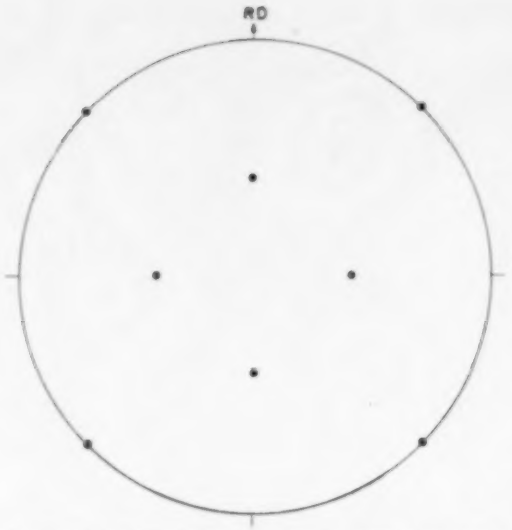

Fig. 9—Predicted (0002) poles for α-zirconium transformed from a cube texture of β.

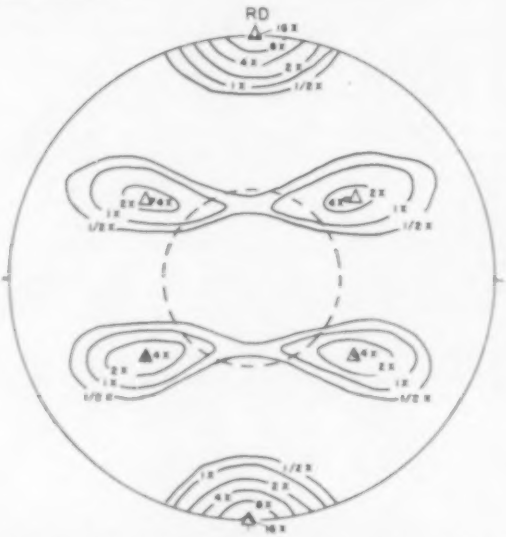

Fig. 10—$(10\bar{1}0)$ pole figure for 99.8 pct cold-reduced zirconium sheet. The spurious reflections originally in the transverse direction from (0002) planes have been removed. The orientations of $(10\bar{1}0)$ poles for the deformation texture (0001) $[10\bar{1}0]$ with a tilt $\pm 40°$ about the axis of the rolling direction are indicated by triangles.

The presence of preferentially distributed impurity particles or the presence of lattice strain remaining after the transformation could account for the ability of the β zirconium to return its original α orientation during cooling after annealing below 1000°C in the β range in preference to the alternate orientations possible through the Burgers orientation relationship for the α and β phases. Increasing the β-annealing temperature to 1000°C and above would reduce the influence of both possibilities by allowing greater solution of the impurity and by permitting relief of the lattice strain. The results of this investigation do not distinguish between the two possibilities.

An annealing treatment of 1400°C for 1 hr pro-

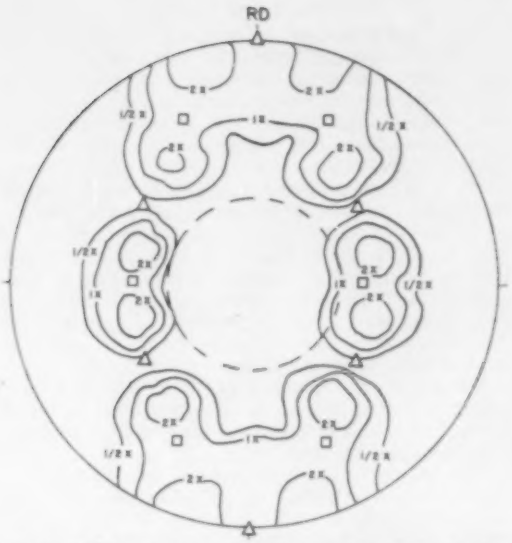

Fig. 11—(10$\bar{1}$0) pole figure for 99.8 pct cold-reduced zirconium sheet annealed 1 hr at 500°C. The spurious reflections originally in the transverse direction from (0002) planes have been removed. The squares indicate the orientations of (10$\bar{1}$0) poles for a texture with a 38° angle between the rolling plane and the basal plane, a 14° angle between the axes of tilt and the rolling direction, and an angle of 14° between the [10$\bar{1}$0] direction and the rolling direction.

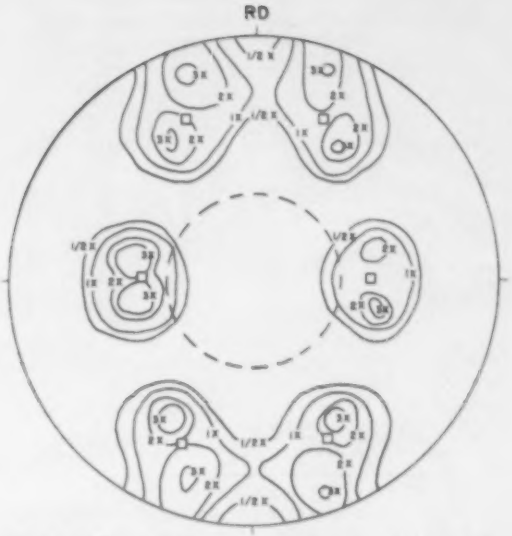

Fig. 12—(10$\bar{1}$0) pole figure of 99.8 pct cold-reduced zirconium sheet annealed 30 min at 600°C. The squares indicate the orientations of (10$\bar{1}$0) poles for a texture with a 35° angle between the rolling plane and the basal planes, a 7° angle between the axis of tilt and the rolling direction, and an angle of 20° between the rolling direction and the [10$\bar{1}$0] direction.

duced another new texture in the α-zirconium, as shown by Figs. 6 and 7. Rather than being based on an α-annealing texture, this new texture could be predicted from a cube texture (the (100) planes parallel to the rolling plane and the [100] direction parallel to the rolling direction in the β-phase). In Fig. 8 are plotted the (10$\bar{1}$0) poles that would be predicted by the Burgers transformation orientation relationship from a cube texture of the body-centered-cubic phase. Fig. 9 shows the locations of (0002) poles similarly predicted from a cube texture of β-zirconium. Comparison of Fig. 8 with 6 and Fig. 9 with 7 shows that a cube texture was present in the zirconium at 1400°C. The α-annealing texture ([11$\bar{2}$0] in the rolling direction and basal planes tilted ±40° about the rolling direction) no longer predominates in the high temperature β-annealed texture.

The results for β-annealed zirconium are very similar to those obtained for β-annealed titanium.[4] In both instances, annealing just above the allotropic transformation temperature resulted in an essentially complete return to the α-annealing texture during cooling. Also, for both metals, annealing at higher temperatures in the β region caused new orientations to appear; first, those that could be predicted from the α annealing texture using the β-α orientation relationships and secondly, a new texture resulted from annealing at the very highest temperatures where a cube orientation of the body-centered-cubic β phase developed during annealing. It was necessary to anneal zirconium at 1400°C for 1 hr to develop the cube texture, whereas 1 hr at 1200°C developed the cube texture in titanium.

Reappraisal of Cold-Reduced and α-Annealing Textures: On the basis of spurious reflections encountered in a recently completed study of the preferred orientations of titanium,[4] cold-reduced zirconium and cold-reduced zirconium annealed at temperatures up through 500°C were re-examined to see if the minor intensity peaks observed in the transverse direction of these pole figures[1] were real. These areas were removed when the Kα component of the copper radiation was eliminated with a cobalt filter. This behavior showed that the reflections were reflections of Kα radiation and not components of the white radiation which have produced spurious areas in pole figures of iron and nickel alloys.[14] When the resolution of the spectrometer was improved by substituting a 1° source slit for the normally used 3° source slit, the spurious areas completely disappeared as shown in Figs. 10 and 11. The spurious areas were apparently caused by lack of resolution of the (10$\bar{1}$0) and (0002) reflections which are only 2.9° apart in 2θ. On this basis, the minor areas in the transverse direction of previously published pole figures for zirconium (Figs. 1, 4, and 5 of ref. 1) should be disregarded.

Further reappraisal of previous work on the α-annealing textures concerns the quantitative changes of the textures when described relative to the cold-rolled texture. The recrystallized texture for annealing at 600°C which is reproduced as Fig. 12 was described as being related to the original cold-rolled texture by a nominal rotation of 30° about the basal poles in agreement with earlier work based on the film technique.[10] It was also pointed out[1] that a more detailed examination showed, however, that the rotations appeared to be combinations of a small rotation of the range 16° to 24° and a larger rotation of the range of 34° to 46°. From these relations, the conclusion was warranted that the [11$\bar{2}$0] directions were not in the rolling direction, but tilted about 10° from the rolling direction (and out of the rolling plane).

Further examination provides the more precise results of texture analysis of zirconium using the Geiger-counter spectrometer technique which are summarized in Table II. The summary shows that

Table II. Results of Texture Analysis on Zirconium Using Geiger-Counter Spectrometer

Treatment	Angle Between *RP* and (0001)	Angle Between Axis of Tilt and *RD*	Smallest Angle Between *RD* and [10$\bar{1}$0]	Reference
Cold rolled	30°	0	0	13
Cold rolled	40°	0	0	1
Annealed at 300°C	38°	0	0	1
Annealed at 400°C	45°	0	0	1
Annealed at 500°C	38°	14°	14°	1
Annealed at 600°C	30°	7°	30°*	13
Annealed at 600°C	35°	7°	30°*	1
Annealed at 800°C	40°	8°	32°*	—
Annealed at 900°C	40°	3°	34°*	1
Annealed at 600°C + 800°C	40°	0	30°*	1
Annealed at 1000°C	40°†	0	30°*	—
Annealed at 1100°C	40°†	0	30°*	—
Annealed at 1200°C	30°†	0	30°*	—
Annealed at 1400°C	45°, 90°‡	0, 90°	32°	—

* (10$\bar{1}$0) not in rolling plane. For the cases when this angle is 30°, the (11$\bar{2}$0) is in the rolling direction.
† New components are due to transformation also present.
‡ A result of a cube texture in the β phase during annealing.

the angle of tilt between the rolling plane (*RP*) and the (0001) plane varies somewhat with annealing temperature. More significantly, however, the axis of tilt is not parallel to the rolling direction (*RD*) on annealing in the range 500° to 900°C, but starts at a higher angle to the rolling direction which gradually decreases with increasing annealing temperature as the [10$\bar{1}$0] poles move away from the rolling direction. A simple rotation of 30° about the basal poles of the cold-rolling texture can nominally describe these annealing textures, but the actual textures obtained at intermediate annealing temperatures indicate a more precise description would involve a complex series of orientation changes. The two types of splitting of the intense areas of the pole figures for samples annealed in the range 500° to 900°C (compare Figs. 11 and 12 with 1) can be described as 1—about the rolling direction and 2—about the normal to the rolling plane (500°C) or normal to the basal plane (600° to 900°C). These rotations depend quantitatively on annealing temperature and the [11$\bar{2}$0] direction approaches the rolling direction only when the anneal temperature approaches 900°C. The agreement of the results in Table II for two different determinations[1,10] of the 600°C annealing texture is noteworthy. Results for 800°C annealing were determined in the present work to provide data for a temperature intermediate between 600° and 900°C.

The results for α-annealed textures of zirconium when precisely appraised are similar to those for titanium[7] the quantitative description relative to the cold-rolled texture is dependent on annealing temperature. In the case of titanium, the second axis of tilt was about the normal to the sheet surface with the [10$\bar{1}$0] direction remaining in the rolling plane on annealing at 500° to 950°C, whereas this axis served only for the description of the 500°C annealing texture of zirconium. With both materials the change in orientation increased with annealing temperature in the range below that at which the transformation texture dominated. These results provide the conclusions that the "recrystallization texture" cannot be specified categorically and that possibly a temperature dependence of the relationship between interfacial energy and orientation should be included in theories that purport to explain the origin of recrystallization textures.

Conclusions and Summary

The transformation textures in unalloyed zirconium are strongly dependent upon the β-annealing temperature and these textures can be placed in three categories: 1—Annealing at 900°C, just above the allotropic transformation, permits essentially total reversion to the α-annealing texture. 2—Annealing in the range 1000° to 1200°C produces new areas in the pole figures that can be explained by the Burgers orientation relations, using the nominal α-annealing texture as a basis. 3—Annealing at 1400°C, about 525°C above the allotropic transformation temperature, produces a new series of hexagonal orientations that are shown to arise from a cube orientation of the β zirconium during annealing. The nominal α-annealing texture is no longer predominant after annealing at 1400°C.

Certain minor intensity peaks which have been reported in the transverse direction of pole figures for zirconium have been identified as spurious and should be disregarded.

The change in orientation from that of the cold-rolled material to that of the α-annealed texture, although nominally described as a 30° rotation about the basal poles, is actually a more complex series of changes, as shown in Table II.

Acknowledgments

The authors wish to thank Mrs. Anne S. Cooper who obtained most of the X-ray data and also other members of the Metallurgy Research Dept. who assisted in the experimental portions of this research. The authors are also obligated to Dr. W. E. Seymour and Mr. John Duffy of the Knolls Atomic Power Laboratory for the use of the spiral scanning X-ray reflection goniometer and the data obtained therefrom. This work was supported by the United States Atomic Energy Commission under Contract No. W-31-109-Eng-52.

Discussion of this paper, if any, will appear in JOURNAL OF METALS, November 1955, and in AIME Metals Branch *Transactions*, Vol. **203**, 1955.

References

[1] J. H. Keeler, W. R. Hibbard, Jr., and B. F. Decker: *Trans.* AIME (1953) **197**, p. 932; JOURNAL OF METALS (July 1953).
[2] C. J. McHargue and J. P. Hammond: *Trans.* AIME (1953) **197**, p. 57; JOURNAL OF METALS (January 1953).
[3] J. B. Newkirk and A. H. Geisler: *Acta Metallurgica* (1953) **1**, p. 370.
[4] J. H. Keeler and A. H. Geisler: To be published.
[5] U. Dehlinger: *Metallwirtschaft* (1952) **11**, p. 223.
[6] U. Dehlinger, E. Osswald, and H. Bumm: *Ztsch. für Metallkunde* (1933) **25**, p. 62.
[7] W. G. Burgers: *Physica* (1933-1934) **1**, p. 561.
[8] B. F. Decker, E. T. Asp, and D. Harker: *Journal of Applied Physics* (1948) **19**, p. 388.
[9] A. H. Geisler: *Modern Techniques in Physical Metallurgy.* (1953) p. 131. Cleveland. ASM.
[10] A. H. Geisler: To be published in *Review of Scientific Instruments; Report No. RL-963* General Electric Research Laboratory, available on request.
[11] A. N. Holden: *Review of Scientific Instruments* (1953) **24**, No. 1, pp. 10-12.
[12] R. K. McGeary and B. Lustman: *Trans.* AIME (1951) **191**, p. 994; JOURNAL OF METALS (November 1951).
[13] R. K. McGeary and B. Lustman: *Trans.* AIME (1953) **197**, p. 284; JOURNAL OF METALS (February 1953).
[14] A. H. Geisler: To be published in *Journal of Applied Physics; Report No. RL-971A* General Electric Research Laboratory, available on request.
[15] J. W. Glen and S. F. Pugh: *Acta Metallurgica* (1954) **2**, p. 520.

Cold-Rolled Textures of Silicon-Iron Crystals

by P. K. Koh and C. G. Dunn

Si-Fe single crystals in a number of selected orientations were cold rolled 70 pct and analyzed to obtain quantitative (110) pole figures. Stable end orientations were determined, and the effect of orientation on deformation behavior was investigated.

WHEN single crystals are cold rolled sufficiently, they rotate into end orientations that are stable or unchanged in position with additional deformation. The end orientations of heavily cold-rolled iron crystals, positioned in holes in copper to limit lateral flow and to simulate polycrystalline conditions during deformation, were determined by Barrett and Levenson.[1] They found that the sum of the end orientations, a pole figure for all the crystals studied, reproduced the essential features of the cold-rolled texture of polycrystalline iron. In an investigation of Fe-Si alloys, Barrett, Ansel, and Mehl[2] observed little effect of silicon content on the textures of heavily cold-rolled samples. Since alloys with less than 4 pct Si are known to have the same slip systems as iron,[3] it seems logical to expect that they would also have the same end orientations as those for iron.

Whereas Barrett and Levenson in their study of single crystals were interested in the problem of the origin of the cold-rolled texture of polycrystalline iron, the present authors are more interested in the final cold-rolled textures of single crystals of Si-Fe from the point of view of their relationship to subsequent recrystallization phenomena which will be reported in another paper. Nevertheless, such points as the tendency of an end orientation not to rotate (stability), the tendency of a pole concentration to spread out, and the tendency of the crystal to widen during cold rolling become interesting separately when the initial orientations are selected already in end orientations. Also the initial orientations having a [110] axis parallel with the transverse direction, which include the two end orientations (111) [$\bar{1}\bar{1}2$] and (001) [110], comprise a series that needs further clarification regarding the way such crystals rotate during deformation. Finally the present use of quantitative pole figure methods[4] represents an advance over the X-ray photographic method employed by Barrett and Levenson in their work on end orientations.

The present investigation provides information on the cold-rolling behavior of two groups of Si-Fe crystals: 1—crystals initially oriented in recognized end orientations for iron crystals with a [110] direction parallel with the rolling direction, and 2—crystals initially oriented with a [110] direction 90° to the rolling direction and in the rolling plane. For the second group, there is a 90° range between the (001) [110] orientation and the (110) [001] orientation. Since the 35° portion of this range from (110) [001] to (111) [$\bar{1}\bar{1}2$] was included in a previous investigation,[5] only the remaining 55° portion from (111) [$\bar{1}\bar{1}2$] to (001) [110] needs further consideration. Also, since both (111) [$\bar{1}\bar{1}2$] and (001) [110] are end orientations for iron crystals,[1] there might be a critical orientation* or orientation range between them such that early in the deformation an orientation within this critical range splits into two orientations. Upon further deformation, these two orientations rotate to produce a final texture consisting of (001) [110] and (111) [$\bar{1}\bar{1}2$] components.

The end orientations obtained are discussed in connection with the work of Barrett and Levenson, while the observed tendency for lateral flow of crystals in these orientations is treated in terms of the theory of Hibbard and Yen.[7] Lateral flow according to the theory increases with deviation of the plane containing the rolling direction and the slip direction from a position perpendicular to the plane of rolling.

Experimental Procedure

Single crystals in sheet form with preselected orientations were prepared by methods that have been described elsewhere.[6]† Three lots designated *A*, *B*, and *C* with 3.25 pct Si, 0.004 pct C, 0.009 pct P, 0.010 pct S, 0.035 pct Mn, 0.070 pct Ni, 0.090 pct Cu, 0.009 pct Sn, and only traces of aluminum and chromium were used. Depending on lot, initial thickness varied between 0.025 and 0.030 in., but the reduction in thickness was held as closely as possible to 70 pct to make present data comparable with those obtained in an investigation of recrystallization phenomena.[5] Specimens approximately 1.25 in. wide were cold rolled without auxiliary constraining devices on an 8 in. diam mill.

* W. W. Martin and C. G. Dunn[6] noted that (112) ($\bar{1}\bar{1}1$) was such a critical orientation.

† Martindale and Langford[6] describe a similar procedure for preparing single crystals of Si-Fe of lower silicon content than that used here.

P. K. KOH is associated with Research Laboratories, Allegheny Ludlum Steel Corp., Brackenridge, Pa., and C. G. DUNN, Member AIME, is associated with General Electric Co., Pittsfield, Mass.

Discussion of this paper, TP 3944E, may be sent, 2 copies, to AIME by Apr. 1, 1955. Manuscript, Sept. 13, 1954. Chicago Meeting, February 1955.

Table I. Description of Specimens

Specimen	Group	Initial Orientation		Cold-Rolled Texture		Pct Widening During Rolling	Primary* Recrystallization Tendency
		Rolling Plane	Rolling Direction	Rolling Plane	Rolling Direction		
A1	II	(338)	[$\bar{9}\bar{6}\bar{6}$]	(111)	[$1\bar{1}\bar{2}$]	20	Strong
A2	I	(338)	[$\bar{1}10$]	(338)	[$\bar{1}10$]	9	Weak
A3	II	(112)	[$\bar{1}\bar{1}1$]	(111)	[$\bar{1}\bar{1}2$]	10	Strong
				plus			
				(001)	[110]		
A4	I	(112)	[$1\bar{1}0$]	(112)	[$1\bar{1}0$]	8	Weak
B1	II	(111)	[$\bar{1}\bar{1}2$]	(111)	[$\bar{1}\bar{1}2$]	31	Strong
B2	I	(111)	[$1\bar{1}0$]	(111)	[$1\bar{1}0$]	9	Strong
C1	II	(113)	[$\bar{3}\bar{3}2$]	(001)	[110]	3	Very weak
C2	I	(114)	[$\bar{1}10$]	(114)	[$\bar{1}10$]	3	Very weak
C3	II	(1,1,16)	[$\bar{8}\bar{8}1$]	(001)	[110]	3	Weak
B3	II	(112)	[$\bar{1}\bar{1}1$]				
B4	—	(111)	[15° from $\bar{1}10$]				
C4	II	(225)	[$\bar{5}\bar{5}4$]				
C5	I	(1,$\bar{1}$,16)	[110]				

* The column showing tendency to recrystallize on annealing has been included as a qualitative correlating item having the following meanings for annealing at temperatures near 1000°C: strong, recrystallizes within less than 1 min to a fine grained structure; weak, recrystallizes within 1 hr to a coarse-grained structure; and very weak, recrystallizes in a matter of hours to a very coarse-grained structure.

Table I gives a summary of rolling data for the 13 specimens studied. Some of the specimens were used only in a qualitative way, but the first 9 of the table were analyzed to give quantitative pole figures.

X-ray specimens 0.002 in. thick were taken from the central portion of the cold-rolled crystals. X-ray data were obtained by a transmission method[4] using an integrating specimen holder in conjunction with a Geiger-counter diffractometer. MoKα radiation was obtained at 40 kv and 20 ma. A 1° slit was used to define the incident beam and a soller slit and a 0.3° detector slit, for the diffracted beam. To eliminate white radiation and fluorescence effects, a 0.0015 in. thick zirconium foil was inserted immediately before the Geiger-counter window. Diffraction was from (110) planes. Scanning of each specimen included a rotation angle of 360° and tilt angles of 5° steps to cover the area of the stereogram from 30° of the center to the basic circle. Chart records were calibrated in counts per second and then converted into pole density units.[5,6] Only one random orientation specimen (made with iron powder) was used in establishing these units; the Decker-Asp-Harker[5] correction formula was used for specimens of different μt values and for specimens at various tilt angles.

Contour lines in each stereogram were taken as a geometric series of pole density values, namely, 1.5, 3, 6, 12, 24, 48, 96, etc. pole density units, except in those stereograms where these lines fell too close together due to the extreme sharpness of the pole concentrations. In such cases the sequence used was the following: 1.5, 6, 24, 96, 384, etc. pole density units. For those more familiar with "times random" units, the present pole density units may be reconverted to "times random" units by dividing by a factor of 6.

Results

The stereograms giving the cold-rolled textures of the nine specimens studied are shown in Figs. 1 through 9. The six black dots in each stereogram

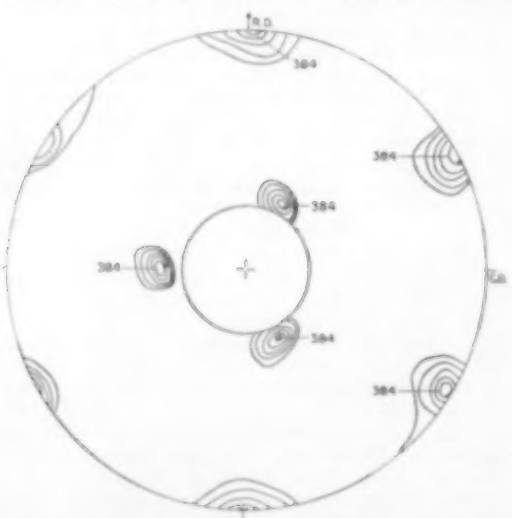

Fig. 1—Pole density stereogram of (110) poles of specimen B2 cold rolled 70 pct. Contour lines are a 1.5, 6, 24, 96, 384 pole density unit sequence. Black dots give the initial orientation (111) [$\bar{1}10$].

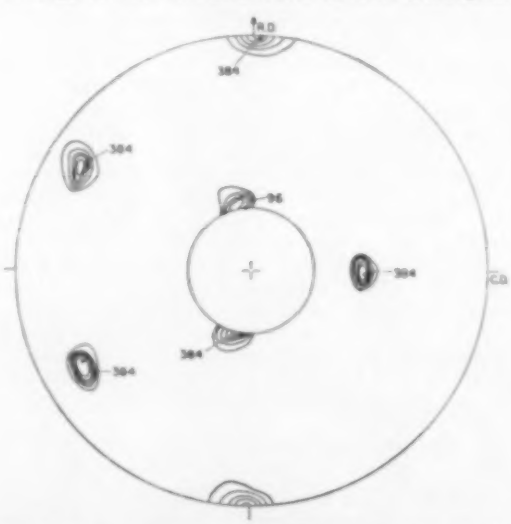

Fig. 2—Pole density stereogram of (110) poles of specimen A2 cold rolled 70 pct. Contour lines are a 1.5, 6, 24, 96, 384 pole density unit sequence. Black dots give the initial orientation (335) [$\bar{1}10$].

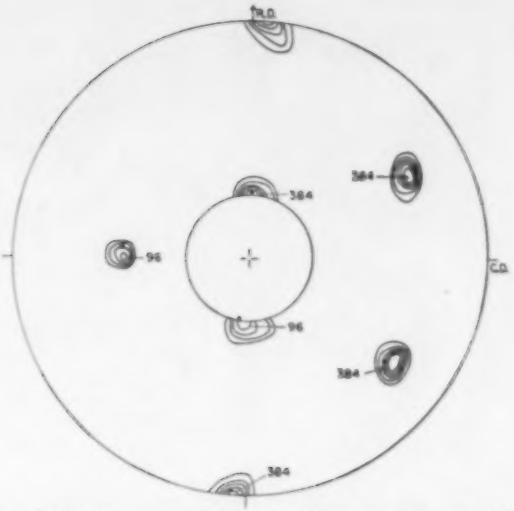

Fig. 3—Pole density stereogram of (110) poles of specimen A4 cold rolled 70 pct. Contour lines are a 1.5, 6, 24, 96, 384 pole density unit sequence. Black dots give the initial orientation (112) [$\bar{1}10$].

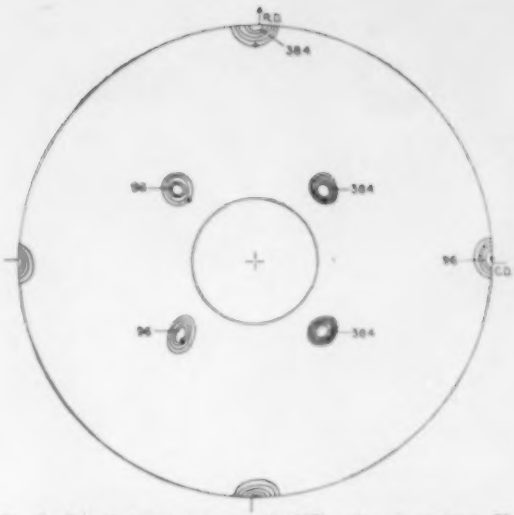

Fig. 5—Pole density stereogram of (110) poles of specimen C3 cold rolled 70 pct. Contour lines are a 1.5, 6, 24, 96, 384 pole density unit sequence. Black dots give the initial orientation (1,1,16) [88$\bar{1}$] or a 5° tilt from (001) [110].

locate the (110) poles of each original crystal. The numbers opposite pole concentrations refer to the highest pole density levels plotted and not to peak heights. The lowest level plotted is always 1.5 pole density units. Fig. 10 gives a Lauegram of specimen C5.

In Figs. 1 through 5 and Fig. 10 for specimens B2, A2, A4, C2, C3, and C5, respectively, representing specimens of the first group with a [110] direction parallel to the rolling direction, it can be seen that the orientations remained essentially unchanged during deformation. Only after a 5° rotation is specimen C3 an ideal member of the first group. The qualitative information on specimen C5, with initial and final Lauegrams showing no rotation above an error of two degrees, also establishes the stability of the (1,1,16) [110] orientation, which is 5° from (001) [110].

In the second group with a [110] direction 90° to the rolling direction, all but one orientation rotated during deformation. Specimen C3 (Fig. 5) rotated 5° and specimen C1 (Fig. 6) rotated 25° to the stable end orientation (001) [110]. On the other hand, specimen B1 (Fig. 7) maintained the (111) [$\bar{1}\bar{1}2$] end orientation, while specimen A1 (Fig. 8) initially in a (335) [55$\bar{6}$] orientation rotated 15° into the (111) [11$\bar{2}$] end orientation. Fig. 9, however, shows that specimen A3, which was initially in the (112) [$\bar{1}\bar{1}1$] orientation, developed a texture with two components, the (001) [110] and (111) [$\bar{1}\bar{1}2$] end orientations. According to qualitative information,

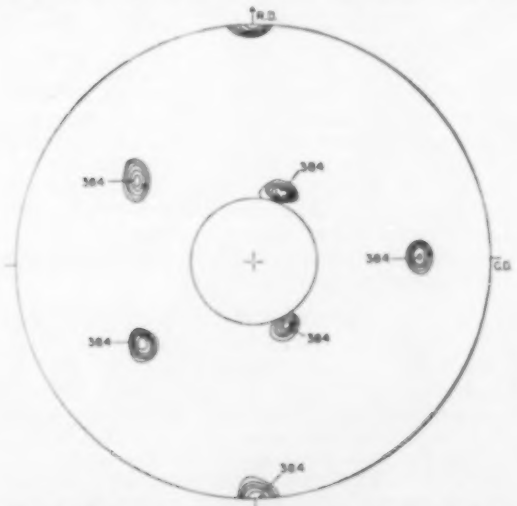

Fig. 4—Pole density stereogram of (110) poles of specimen C2 cold rolled 70 pct. Contour lines are a 1.5, 6, 24, 96, 384 pole density unit sequence. Black dots give the initial orientation (114) [$\bar{1}10$].

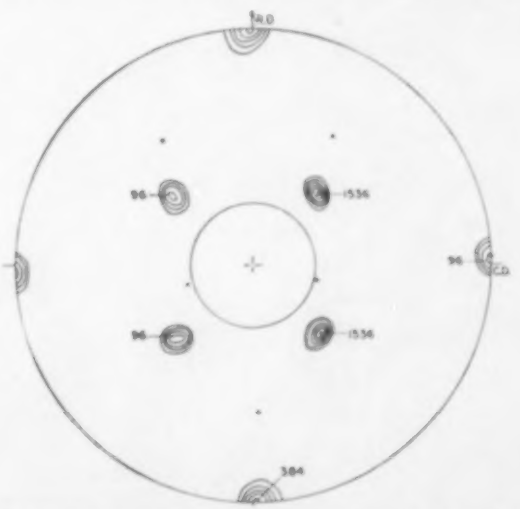

Fig. 6—Pole density stereogram of (110) poles of specimen C1 cold rolled 70 pct. Contour lines are a 1.5, 6, 24, 96, 384, 1536 pole density unit sequence. Black dots give the initial orientation (113) [$\bar{3}\bar{3}2$].

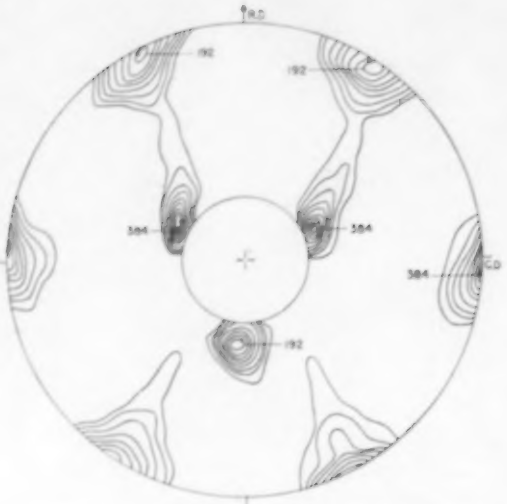

Fig. 7—Pole density stereogram of (110) poles of specimen B1 cold rolled 70 pct. Contour lines are a 1.5, 3, 6, 24, 98, 192, 384 pole density unit sequence. Black dots give the initial orientation (111) [$\bar{1}12$].

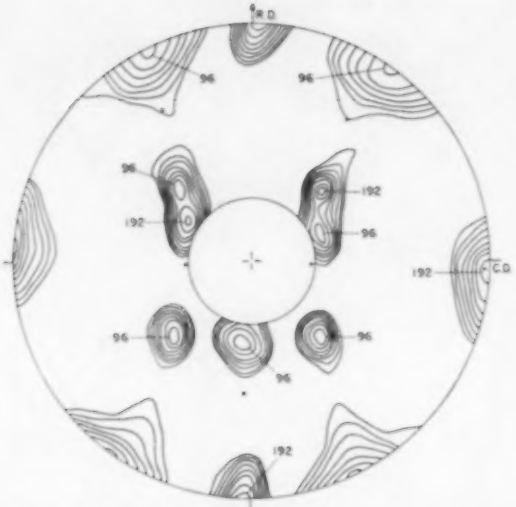

Fig. 9—Pole density stereogram of (110) poles of specimen A3 cold rolled 70 pct. Contour lines are a 1.5, 3, 6, 12, 24, 48, 192 pole density unit sequence. Black dots give the initial orientation (112) [$\bar{1}\bar{1}1$].

this situation was duplicated in specimen B3, which has the same orientation as specimen A3, and in specimen C4 in the (225) [$55\bar{4}$] orientation. Under the experimental conditions employed, there is therefore a 5° to 15° range of initial orientations that develop both end orientations simultaneously.

Assuming a continuous variation in this critical range, the relative amounts of the final components would be expected to depend on the initial position in this range. The position of equality of components should not be far from the (112) [$\bar{1}\bar{1}1$] orientation according to the distribution obtained in Fig. 9. Regarding the origin of the two components, it was observed that specimens A3, B3, and C4 developed macrodeformation bands in the cold-rolling process; so it was thought that these bands probably led to the production of the two components found in the texture. A simple proof of this was obtained by taking Lauegrams of individual bands; these showed one or the other of the end orientations.

Finally, the qualitative study made on specimen B4, the (111) [15° from $1\bar{1}0$] orientation, indicated its being an end orientation (rotation estimated at less than 2°), and this is similar to the behavior of the (111) [$1\bar{1}0$] and (111) [$\bar{1}12$] orientations of groups I and II, respectively.

The stereograms also show the sharpness of the various (110) pole concentrations and hence the sharpness of the textures developed.* In group I (Figs. 1 through 5), which have sharp textures, it can be seen that orientations near (001) [110] are sharper than those near (111) [$1\bar{1}0$]. This appearance correlates to a degree with the percentage of widening and the tendency to recrystallize shown in Table I. In group II (Figs. 6 through 9), the (001) [110] end orientations are considerably sharper than the (111) [$\bar{1}\bar{1}2$] end orientations, and this appearance also correlates with percentages of widening and tendency to recrystallize.

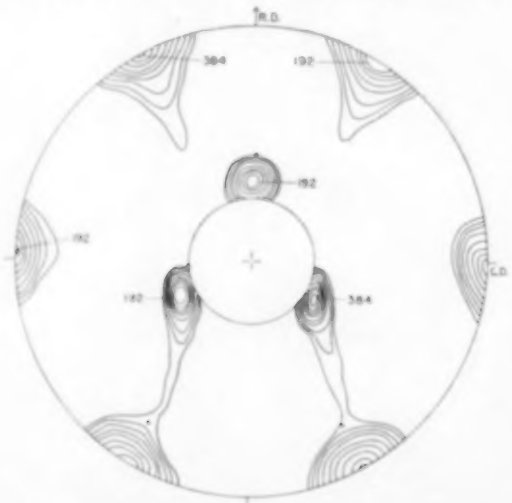

Fig. 8—Pole density stereogram of (110) poles of specimen A1 cold rolled 70 pct. Contour lines are a 1.5, 3, 6, 12, 24, 48, 192, 384 pole density unit sequence. Black dots give initial orientation (335) [$55\bar{6}$].

* In an ideal quantitative pole figure with sharp single orientation texture, the integral taken over an isolated pole concentration is one.[10] In the present data, there are cases of pole concentrations that fall short on this score, but otherwise they appear reasonably accurate.

Discussion of Results

The results for group I crystals after a 70 pct cold-rolling reduction show that all orientations investigated between (001) [110] and (111) [$1\bar{1}0$] are stable. Therefore, lacking any significant rotation about a [110] axis or lateral tilting, it may be concluded that the entire range is a continuous one of stable end orientations, which agrees with the conclusion reached by Barrett and Levenson[1] in their work on iron crystals. The more quantitative aspects disclosed in the present work, however, establish the nature of the stable end orientations to a greater degree of certainty. It was also pointed out

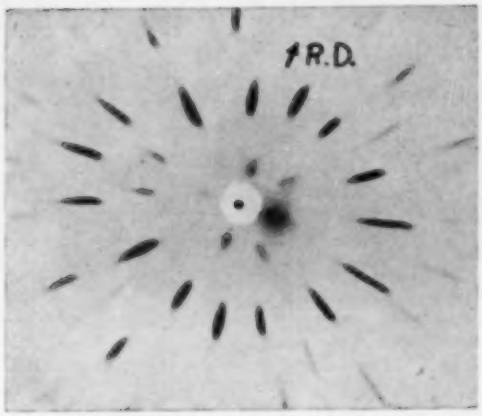

Fig. 10—Transmission Lauegram of specimen C5 cold rolled 70 pct. Initial orientation (1,$\bar{1}$,16) [110] or a (001) [110] 5° lateral tilt from (001) [110].

previously that there is a trend of decreasing sharpness of the texture as the orientation of the crystal is taken further from the (001) [110] orientation.

Considering Figs. 1 and 7 for crystals initially oriented with a (111) plane parallel with the plane of rolling and also the qualitative information obtained for specimen B4, which was cold rolled along a direction 15° from a [1$\bar{1}$0] direction, it can be seen that these orientations form a stable set. Since a 30° range covers all the possibilities and the authors' three specimens cover this range, it appears quite definite that all orientations having a (111) plane in the plane of rolling are stable; this checks another conclusion reached by Barrett and Levenson.[1] It is apparent, however, that the (111) [1$\bar{1}$0] orientation suffers less spread than the (111) [$\bar{1}$12] orientation in a 70 pct reduction.

The present results for the group II crystals together with those already published[2] show that crystals cold rolled 90° to a [110] direction rotate either to the (111) [$\bar{1}$12] or the (001) [110] stable end orientation except for crystals in a narrow range near the (112) [$\bar{1}\bar{1}$1] orientation. Crystals near the (112) [$\bar{1}\bar{1}$1] orientation develop macrodeformation bands, which rotate individually. The cold-rolled textures for these crystals consist of both (111) [$\bar{1}\bar{1}$2] and (001) [110] end orientations. Fig. 11 summarizes the main rotation behavior of group II crystals. The two-dimensional diagram shows the position of atoms in a (1$\bar{1}$0) plane for various orientations between (001) [110] and (110) [001]. The normal to specimen surface or rolling plane is vertical in the drawing and the rolling direction is to the right. The arrows indicate the direction and amount of rotation as a result of the cold-rolling reductions employed, while the captions for each figure indicate whether the final cold-rolled texture has one or two components. Absence of an arrow indicates no reorientation and thus a stable end orientation.

Although the question of active slip planes arises in every deformation process, the complexity of this problem precludes a fruitful treatment of the present data. Nevertheless, the data may be of value for checking predicted textures or the behavior of end orientations. (Calnan and Clews[10] have recently treated body-centered-cubic lattices.) On the other hand, it is of interest to consider the orientation requirements postulated by Hibbard and Yen[7] for obtaining cold-rolling reductions without appreciable widening because the present data bear on this problem.

Although the slip plane is of importance in the Hibbard-Yen theory, the slip direction is of special importance. This direction may be taken as [111] in the body-centered-cubic lattice. Hibbard and Yen state that the active [111] slip directions should lie in the plane containing the rolling direction and the normal to the rolling plane if lateral flow is to be avoided (it is realized, of course, that constraints can prevent widening and that as many as five slip systems may have to become active in order to maintain continuity between neighboring grains[10, 11]). Let ω be the amount of rotation about the rolling direction as an axis for a plane that starts normal to the rolling plane and ends containing the active [111] slip direction. In the absence of constraints, lateral flow, according to Hibbard and Yen, should increase as ω increases.

In all of the group I crystals, there are two symmetrically positioned [111] directions 35° from the rolling direction; these should be active for flow in the rolling direction. The angle ω is zero for a (001) [110] orientation; it increases with rotations away from (001) [110] and reaches 55° in the (111) [1$\bar{1}$0] orientation. Since widening also increases in this sequence according to Table I, it can be seen that widening correlates reasonably well with ω, being small when ω is small and appreciably larger when ω is large. Other slip directions no doubt have to be active to account for no noticeable lateral rotation of orientations (i.e., movement of peak positions in the stereograms).

In the group II crystals, it can be seen that ω is 69° for two [111] slip directions and zero for a third [111] direction, which should be active in the (111) [$\bar{1}$12] stable end orientation for producing flow in the rolling direction. The large values of ω correlate well with the fairly large amount of widening observed for specimen B1. (Very recent results also

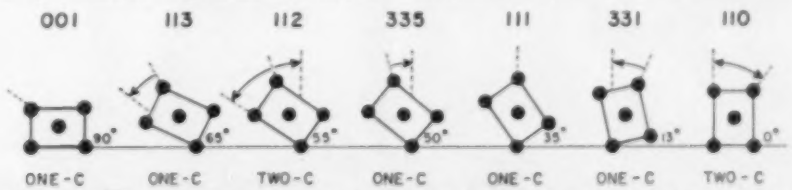

Fig. 11—A (1$\bar{1}$0) layer view showing nature of rotation produced by cold rolling 7 initial orientations in a 90° range. The direction normal to the plane of the drawing is the [1$\bar{1}$0] axis of each crystal that lies parallel to the transverse direction C.D. of the stereograms. Miller indices of directions that are normal to the plane of rolling appear over each illustration. Approximate angles between [001] and the rolling direction are indicated. One *C* or two *C* refers to one component or two components in the texture produced by cold rolling.

show a marked effect of initial thickness, thus indicating further complexities.)

Summary and Conclusions

Si-Fe crystals grown to preselected orientations were cold rolled to a reduction in thickness of 70 pct to obtain specimens for quantitative pole figure data. The cold-rolled textures showed the following:

1—Initial orientations in a (001) [110] to (111) [$\bar{1}$10] series are stable end orientations.

2—Initial orientations having a (111) plane parallel to the plane of rolling, such as (111) [$\bar{1}\bar{1}$2], (111) [$\bar{1}$10], and others, are stable end orientations.

3—Initial orientations in a series from (001) to (111) parallel to the rolling plane and with [110] always 90° to the rolling direction either rotate to or maintain one or the other of two end orientations—namely, (001) [110] or (111) [$\bar{1}\bar{1}$2]—except for a narrow range near (112) [$\bar{1}\bar{1}$1]. Orientations near (112) [$\bar{1}\bar{1}$1] develop a texture with two components—(001) [110] + (111) [$\bar{1}\bar{1}$2]—via the development of macrodeformation bands.

4—Sharpness of texture is dependent on initial orientation and correlates qualitatively with tendency to recrystallize upon annealing.

5—Widening during deformation correlates with the position of [111] slip directions in agreement with the theory of Hibbard and Yen.

Acknowledgments

The authors thank Dr. W. R. Hibbard for a critical reading of the manuscript, H. T. Sagendorph for aid in the preparation of specimens, and Miss B. Caugherty for aid in the X-ray work.

Discussion of this paper, if any, will appear in JOURNAL OF METALS, November 1955, and in AIME Metals Branch *Transactions*, Vol. **203**, 1955.

References

[1] C. S. Barrett and L. H. Levenson: *Trans.* AIME (1941) **145**, p. 281.

[2] C. S. Barrett, G. Ansel, and R. F. Mehl: *Trans.* AIME (1937) **125**, p. 516.

[3] C. S. Barrett: *Structure of Metals* (1952) 2nd ed., p. 388. New York. McGraw-Hill Book Co. Inc.

[4] A. H. Geisler: *Modern Research Techniques in Physical Metallurgy.* (1953) p. 131. Cleveland. ASM.

[5] C. G. Dunn: *Acta Metallurgica* (1954) **2**, p. 173.

[6] W. W. Martin: *Research Laboratory Publications* (1947) Metallurgy Symposium, Research Laboratory, Schenectady.

[7] W. R. Hibbard and Ming-Kao Yen: *Trans.* AIME (1948) **175**, p. 126.

[8] C. G. Dunn and G. C. Nonken: *Metal Progress* (1953) **64**, No. 6, p. 71.

[9] R. G. Martindale and D. A. Langford: *Proceedings* Institute of Electrical Engineers (1953) **100**, No. 76, p. 417.

[10] C. G. Dunn: *Journal of Applied Physics* (1954) **25**, p. 233.

[11] B. F. Decker, E. T. Asp, and D. Harker: *Journal of Applied Physics* (1948) **19**, p. 388.

[12] E. A. Calnan and C. J. B. Clews: *Philosophical Magazine* (1951) **42**, p. 616.

[13] R. vonMises: *Ztsch. Angew. Math. Mech.* (1928) **8**, p. 161.

[14] G. I. Taylor: *Journal* Institute of Metals (1938) **62**, p. 307.

Technical Note

Cellular Structure in High Purity Zinc

by R. P. Steijn

IT has been observed by a number of investigators that under certain conditions metals freeze into an aggregate of small hexagonal strands, parallel to one another and with their axes approximately in the direction of growth.[1-4] This structure has been termed "cellular structure" and is explained in various ways by different workers, notably by Rutter and Chalmers.[5] These investigators attribute the phenomenon to the presence of minute quantities of solute atoms which induce constitutional supercooling. However, if this is true, observations of the cellular structure in extremely pure substances, like frozen distilled water[6] and germanium of less than 0.0001 atomic pct metallic solute,[8] are difficult to comprehend.

The purpose of this communication is to describe several observations made of the prismatic structure in zinc of 99.99 pct purity.

Zinc single and bicrystals grown in a constant gradient electrical resistance furnace exhibit the cellular structure after etching in 15 pct HCl. (See Figs. 1 and 2.) It is noticed that the hexagonal substructure sometimes continues unbroken across the bicrystalline grain boundary.

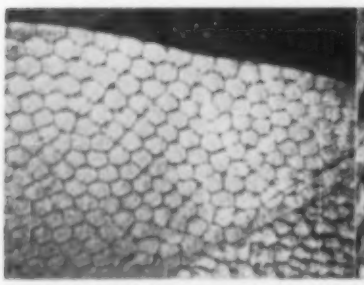

Fig. 1—Etched section, perpendicular to direction of growth. X11. Area reduced approximately 40 pct for reproduction.

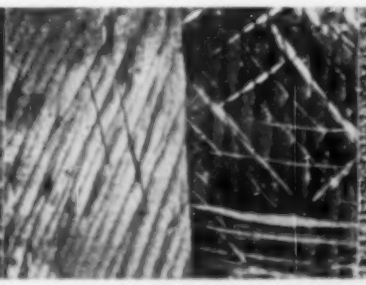

Fig. 2—Etched section, parallel to direction of growth. X11. Area reduced approximately 40 pct for reproduction.

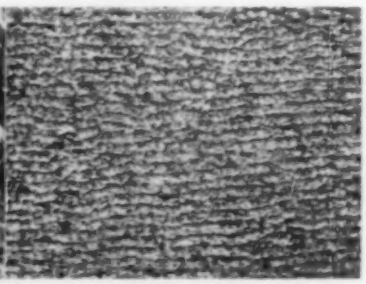

Fig. 3—Perpendicular to growth direction. X50. Area reduced approximately 40 pct for reproduction.

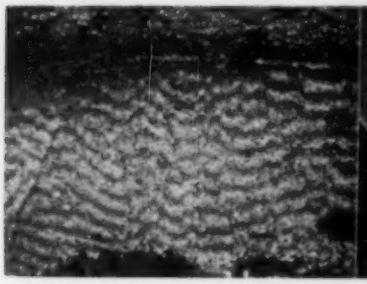

Fig. 4—Parallel to growth direction. X25. Area reduced approximately 40 pct for reproduction.

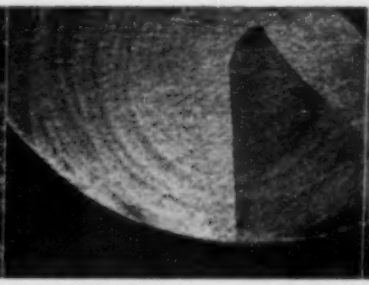

Fig. 5—Perpendicular to growth direction. X11. Area reduced approximately 40 pct for reproduction.

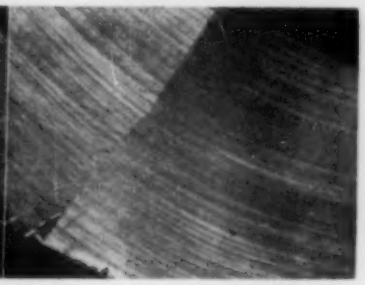

Fig. 6—Parallel to growth direction. X11. Area reduced approximately 40 pct for reproduction.

Zinc crystals, grown by a modified Czochralski technique using a seed crystal rotating around a vertical axis at a speed of 150 rpm, show after etching a pattern of undulations and etch figures akin to the cell structure. (See Figs. 3 and 4.) In terms of the Rutter-Chalmers mechanism, this observation can be explained as follows: the constant stirring of the melt by the rotating crystal rod tends to eliminate concentration gradients in the liquid near the interface, thereby making constitutional supercooling less likely. The result is an incomplete cell structure.

Bicrystals and large columnar crystals of zinc, grown by the Bridgeman method in a high frequency induction furnace, show after etching concentric rings on sections perpendicular to the growth direction (Fig. 5), and an array of concave bands on longitudinal cuts (Fig. 6). This happens in spite of the vigorous stirring of the melt by the induced eddy currents. The observation suggests that even under these conditions freezing is a steplike process.

The hexagonal strands form small angle boundaries with one another. Orientation differences up to 15 min are recorded in the literature.[5] Therefore, a longitudinal cut through the prismatic structure should contain lineage boundaries. If proper conditions in terms of the plane of cut and angle of misfit prevail, these boundaries after etching may be resolved optically as a row of etch pits at the sites of Taylor-Orowan dislocations. This was shown convincingly by Vogel et al.[6] for the lineage boundary in a germanium single crystal.

The etch pits, revealed by careful etching of polished sections parallel to the hexagonal strands in a zinc single crystal, are shown in Figs. 7, 8, and 9. The etchant was a chromic acid-sodium sulphate solution. Repolishing and re-etching makes the row of pits reappear; some vanish after repolishing twice, others persist over a considerable depth. Microradiographs of thin wafers showed that the row of dots was not of globular lead inclusions as was first thought. The average spacing between the etch pits of Fig. 9 is 1.35×10^{-4} cm which corresponds to an angle of misfit of approximately 75 sec or less. It is felt that this observation gives additional evidence to the general belief that the low angle boundary consists of a series of equally spaced edge dislocations.

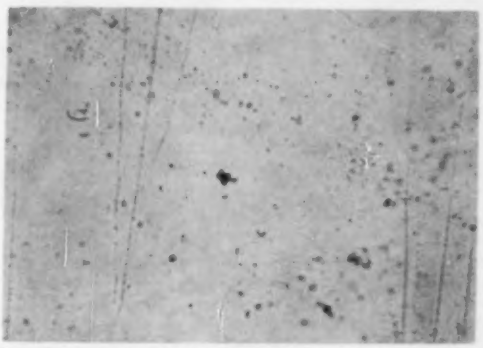

Fig. 7—Lineage boundaries after etching. X145. Area reduced approximately 25 pct for reproduction.

Fig. 8—Lineage boundaries after etching. X170. Area reduced approximately 25 pct for reproduction.

Fig. 9—Lineage boundaries after etching. X550. Area reduced approximately 30 pct for reproduction.

Acknowledgment

This work was perfomed at The Franklin Institute Laboratories for Research and Development and forms part of a larger program sponsored by the Air Research and Development Command under Contract AF 18(600)-465. The financial assistance and permission to publish are gratefully acknowledged.

References

[1] F. Blaha: *Nature* (1953) **171**, p. 650.
[2] R. B. Pond and S. W. Kessler: *Trans.* AIME (1951) **191**, p. 1157; JOURNAL OF METALS (December 1951).
[3] J. W. Rutter and B. Chalmers: *Canadian Journal of Physics* (1953) **31**, p. 15.
[4] Discussion of ref. 2. *Trans.* AIME (1952) **194**, p. 1185; JOURNAL OF METALS (November 1952).
[5] Ajit Ram Verma: *Proceedings* Physical Society (1954) **67B**, p. 359.
[6] F. L. Vogel, W. G. Pfann, H. E. Corey, and E. E. Thomas: *Physical Review* (1953) **90**, p. 489.

R. P. STEIJN, Associate Member AIME, was formerly Senior Research Metallurgist, Solid State Physics Div., Laboratories for Research and Development, The Franklin Institute of the State of Pennsylvania, Philadelphia.

TN 241E. Manuscript, Aug. 30, 1954.

Formation of Cold-Worked Regions in Fatigued Metal

by Rayjor Webeler

In order to study the role of work hardening in the fatigue process, use was made of the great sensitivty of the resistivity of AuCu to cold work. A change of the resistivity of AuCu of the order of 1 to 2 pct at the temperature of liquid nitrogen was found to occur as a consequence of severe fatigue.

ACCORDING to Orowan's theory,[1] the process of fatigue in metals is associated with the production of a number of small regions which have undergone strain hardening. This phenomenon is supposed to occur even if the stress applied during fatiguing is always smaller than the yield stress. In an attempt to verify the existence of such regions, Welber and Webeler[2] undertook to detect the stored energy associated with severe fatigue in copper. Previous experiments[3] had shown that the energy stored in a sample of copper which has been cold worked by torsion is released in the temperature range between 150° and 250°C when the sample is heated from room temperature and that no more energy is released (or absorbed) between 250° and 450°C. In particular the stored energy amounted to 0.41 cal per g for a case in which the mechanical energy expended in twisting the sample was 11.9 cal per g. In the case of fatigued copper, however, no release of stored energy could be detected between 150° and 250°C, so that the experimental error of ±0.02 cal per g represents an upper limit for the amount of energy stored in strain hardening.*

* The absorption of energy in the temperature range between 250° and 350°C reported by these investigators in the case of fatigued copper is not observed in cold-worked copper and presumably has no connection with strain hardening.

It seemed desirable to attack the problem in a new fashion. For this purpose, it was decided to make use of the fact that, if an alloy capable of undergoing the order-disorder transition is ordered and then cold worked, the resistivity, ρ, increases very greatly above the value for the ordered state even if the deformation is very small. Some insight into the nature of the fatigue process may be obtained then by measuring the resistivity of an ordered sample before and after subjecting it to fatigue. For reasons which will become apparent from the following remarks, considerably more can be learned by carrying out the resistivity measurements at two different temperatures.

In the case of a material containing impurities, vacancies, dislocations, or other imperfections of essentially atomic dimensions, the resistivity, ρ, according to Matthiessen's rule, can be represented as a sum of two terms $\rho = \rho_T + \rho_i$, where ρ_T is the (temperature dependent) resistivity of the pure metal, and ρ_i is the temperature independent contribution of the imperfections. Briefly, the physical basis for this rule is the following: The main contribution of the impurities in question to the resistivity results from the fact that they interrupt the periodicity of the lattice and thus scatter the conduction electrons with a probability which is almost independent of temperature. In order that this be the case, it is necessary that the extension of the impurities be small enough—roughly less than one electron mean free path—so that their main effect on the resistivity occurs for the foregoing reason. If an alloy like AuCu is partly or completely disordered by quenching from an appropriate temperature, Matthiessen's rule also applies to a very good approximation* with ρ_T representing in this case the resistivity ρ_0 of the ordered sample and ρ_i the additional (temperature independent) resistivity due to the disorder. In general, the disorder can be represented in terms of atoms which are displaced from their "proper" positions in the superlattice and which thus qualitatively represent the imperfections in the superlattice responsible for the term ρ_i. Since the misplaced atoms are distributed at random throughout the superlattice, their contribution to the resistivity still can be considered in terms of the scattering of conduction electrons by lattice defects. The situation is somewhat more complex in the case of an alloy disordered by cold work because the process of disordering here does not involve a random redistribution of the atoms; however, Matthiessen's rule also holds in this case. Whenever Matthiessen's rule does apply, the values of the quantity $\beta = (\rho_2 - \rho_1)/(T_2 - T_1)$, where ρ_1 and ρ_2 are the values of the resistivity at two fixed temperatures, T_1 and T_2, respectively, is constant (independent of ρ_i) for a given alloy or metal. In particular, if a sample of AuCu is subjected to ordinary cold work, the value of β remains equal to β_0, the value for the ordered material.

* The change in the vibrational spectrum occurring as a result of the alteration of the elastic properties of the alloy during the order-disorder transformation should make Matthiessen's rule inexact in this case. Such a deviation would be indicated by a change in the Debye temperature with the degree of order. E. Passaglia and W. F. Love[4] were unable to detect such a change at all and Dr. David Kahn of this laboratory, who has observed a change of this quantity, found it of a magnitude much too small to affect the applicability of Matthiessen's rule in the analysis of the present experiment.

According to Orowan's theory,[1] as remarked before, a fatigued sample contains a large number of isolated severely cold-worked regions, which make up only a small proportion of the metal. Thus, if a sample of AuCu initially in the ordered state is fatigued, more or less disordered regions will be produced within the ordered material. If these regions are small enough so that Matthiessen's rule applies, then it follows from the previous discussion that β again will remain equal to β_0. If the effect of fatigue is to produce cold-worked regions which are macroscopic—of the order of at least several electron mean free paths—the effective resistivity, ρ, has to be computed by use of the ordinary laws of large-scale electrodynamics. For the sake of simplicity, it will be assumed here that the cold-worked regions are completely disordered and have a resistivity, ρ_D. For a given proportion λ of disordered regions the effective resistivity, ρ, for the current in a given direction depends on the geometrical configuration of these regions. In any case, the value of ρ for such

R. WEBELER is associated with Lewis Flight Propulsion Laboratory, National Advisory Committee for Aeronautics, Cleveland.

Discussion of this paper, TP 3949E, may be sent, 2 copies, to AIME by Apr. 1, 1955. Manuscript, July 21, 1954. Chicago Meeting, February 1955.

a sample lies between two extremes $\rho_{s\infty}$ and ρ_{s0} given by

$$\rho_{s\infty} = (1-\lambda)\rho_0 + \lambda\rho_0 \quad [1]$$

and

$$1/\rho_{s0} = (1-\lambda)/\rho_0 + \lambda/\rho_0. \quad [2]$$

The two limits correspond, respectively, to the cases where the ordered and disordered regions are electrically in series and in parallel. The quantity β, in the first case, is given by

$$\beta_{s\infty} = \beta_0 \quad [3]$$

and, in the second, for the values of ρ_0 and ρ_0 encountered here and $\lambda << 1$, by

$$\beta_{s0} = \beta_0(1 + 3\lambda/5). \quad [4]$$

If the disordered regions are regularly shaped and are randomly distributed throughout the sample, then it follows from calculations of Landauer[4] that the effective resistivity, for $\lambda << 1$, is

$$\rho_{m1} = \rho_0[1 + 3\lambda(\rho_0 - \rho_0)/(2\rho_0 + \rho_0)] \quad [5]$$

and that the value of β for the present values of ρ_0 and ρ_0 is given by

$$\beta_{m1} = \beta_0(1 + 2\lambda/3). \quad [6]$$

It follows from the discussion that in the present study it is useful not only to measure the value of ρ at a single temperature but also to determine the value of β. The extent to which the value of β obtained remains constant for cold-worked samples provides an estimate of the accuracy of the determination of ρ; in addition, from the behavior of β when the sample is fatigued, conclusions can be drawn concerning the configuration of the cold-worked regions in such a sample.

The experiments were done with six AuCu wires 0.050 in. in diameter and 28 in. long. To serve as potential leads in the subsequent resistivity measurements, a pair of 0.020 in. diam AuCu wires was spot welded to each of these samples on either side of its center. The samples then were brought into a fairly well ordered state by annealing 18 hr at 290°C. The average grain diameter of the alloy was 0.035 mm (ASTM 6). The length (approximately 9.5 cm) and diameter of the portion of each wire located between the potential leads were measured and the resistance of this section then determined at 77.4°K (liquid nitrogen temperature) and at 298.2°K by means of a Kelvin bridge. The way in which the rest of the study was carried out can be explained best by describing in detail an individual experiment done with two of the samples, *a* and *b*. Sample *a* was placed in a Krouse fatigue machine with the aid of a pair of adapters like that shown in Fig. 1. Each end of the wire *W* was fastened to the cylindrical surface of an aluminum drum *D*, which was 1½ in. in diameter, by a clamp *C*, and two turns of the wire were taken around the drum. The fixture *B* consisted of a pair of rubber-covered metal pieces which were pressed against the wire and served to diminish its motion relative to the drum *D* during the operation of the fatigue machine. The adapters in turn were attached rigidly to the jaws of the fatigue machine in such a way that the sample was aligned properly between them. The wire was then subjected to an alternating tension which varied between 12,000 and 45,800 lb per sq in. for 290,000 cycles (145 min) after which it broke at the point between one of the drums and the adjacent voltage lead. Sample *b* was used as a control to set an upper limit for the effects of any plastic deformation that might result from the pure tension effects in sample *a*. It was subjected to a static load of 47,000 lb per sq in. for 165 min, a length of time approximately equal to that during which sample *a* was subjected to fatigue. Subsequently, the resistances and dimensions of the samples were measured. As far as could be ascertained neither the fatiguing nor the static loading induced any change in the dimensions of the wires.

Results and Discussions

Table I gives the values of ρ_0, ρ_0 and β obtained for each sample as well as $\Delta\rho_i$ and $\Delta\rho_0$, the change in the quantities in question as the result of the fatiguing process. Table II gives $\Delta\rho_i/\rho_i$ and $\Delta\beta/\beta$, the relative changes in ρ_i and β, respectively, for three samples fatigued to failure and three samples subjected to static loading experiments of the type described, including those referred to in Table I. It can be seen that both static loading and fatiguing change the resistivity of the samples but that the change produced by the fatiguing is considerably greater for a given maximum tension. The quantity $\Delta\beta/\beta$, however, is nearly zero for all the samples. This result is to be expected for the samples subjected to static loading, so that the observed scatter of ±0.01 pct provides an estimate of the error involved in the measurement of ρ and β. In so far as the fatigued samples are concerned, the constancy of β means either that Matthiessen's rule applies, i.e., the regions disordered by cold working are of dimensions less than one mean free path of the electrons in AuCu (about 1000A) or that they are rather larger than this and are disposed in such a way as to be electrically in series with the ordered regions. This latter situation would hold if the regions were of considerably greater extent in the direction perpendicular to the axis of a wire than in the direction along the axis. Such a disk-shaped disordered region would be found, e.g., if slip occurs along a large area of a plane[5] resulting in an antiphase boundary.

From the observed constancy of β, the possibility that the disordered regions are roughly spherical and

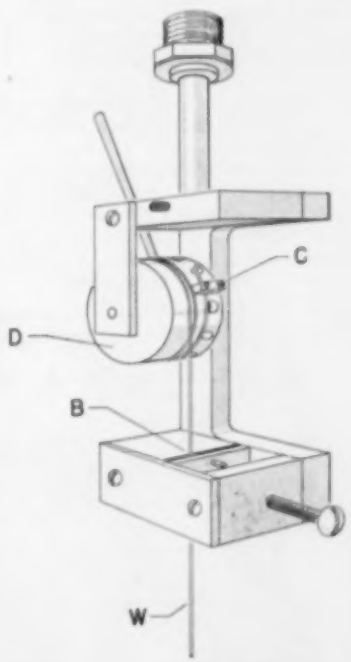

Fig. 1—Adapter employed to test wires in Krouse fatigue machine.

Table I. Effects of Fatigue and Static Tension on the Electric Resistivity ϱ of AuCu at the Temperatures $T_1 = 77.7°K$ and $T_2 = 298.2°K$ and on its Average Rate of Change with Temperature, $\beta = \frac{\varrho_2 - \varrho_1}{T_2 - T_1}$

		Sample a		Sample b	
		As ordered	Subjected to fatigue: max. tensile, 45,800 lb per in.; min. tensile, 12,000 lb per in.; 290,000 cycles in 145 min	As ordered	Subjected to static tension: 46,900 lb per in. for 165 min
ϱ_1 in (77.4°K)	$\mu\Omega$ cm	2.368	2.364	2.051	2.058
ϱ_2 in (298.2°K)	$\mu\Omega$ cm	4.791	4.810	4.554	4.563
$\Delta\varrho_1$ in	$\mu\Omega$ cm	0.022		0.007	
$\Delta\varrho_2$ in	$\mu\Omega$ cm	0.019		0.009	
β in	$\mu\Omega$ cm per °K	1.136x10^{-2}	1.135x10^{-2}	1.134x10^{-2}	1.135x10^{-2}

of dimensions large compared to the mean free path can be excluded as follows: * If they are assumed to be of this size and shape and, therefore, Eq. 5 is applied to the measured change of ρ_1 for sample *a*, for example, λ is found to be 1.1 pct which means according to Eq. 6 that contrary to the results of the experiments, $\Delta\beta/\beta$ should change by 0.7 pct. The same conclusion follows from the results obtained from the other fatigued samples. Similar considerations also exclude the possibility that the disordered regions are effectively electrically in parallel to the ordered ones. Finally, it should be remarked that, if microcracks were responsible for the change in the measured ρ, the relation β/ρ = constant would hold, so that $\Delta\beta/\beta$ would equal $\Delta\rho/\rho$. This is not the case, $\Delta\rho/\rho$ being at least 20 times as large as $\Delta\beta/\beta$ so that none of the effects found here can be due to microcracks.

* In this consideration, it was assumed that the increase in resistivity is entirely due to fatigue effects. There is, as mentioned above, an effect due to static tensions which is, however, so small that it can be neglected here.

It can be seen from Table II that the relative change in ρ_1, in the case of samples fatigued to failure, ranges from 0.7 to 2.3 pct while the change in ρ_1 due to static loading is 0.2 to 0.3 pct. The change in the resistivity of the fatigued samples due to effects connected specifically with the cyclic loading must be at least as great as the difference between the $\Delta\rho_1/\rho_1$ for the fatigued samples and the $\Delta\rho_1/\rho_1$ for the statically loaded samples, which difference lies between 0.5 and 2.0 pct for the samples studied here. As mentioned before, the results are consistent with the existence of macroscopic disordered regions effectively in series electrically with the rest of the material. On the basis of this assumption, the fraction λ of the material which is disordered can be calculated from Eq. 2 and the results for each fatigued sample are given in Table II using value of $\rho = 12\mu\Omega$ cm for ρ_0 at the temperature $T_1 = 77.4°K$. It can be seen that the fraction of disordered material is always less than ½ of 1 pct. If the disordered regions have dimensions smaller than the electron mean free path, it is reasonable to compare the change in resistivity upon fatiguing with that due to static loading with the same maximum stress applied for the same length of time as the sample is fatigued. The ratio of these two quantities lies between 3 and 10. In order to convey some idea of the size of the effect, it should be remarked that a reduction in area of between 0.05 and 0.19 pct by swaging[5] produces the same increase in resistivity of AuCu as did severe fatigue.

In any event, the amount of cold working produced by fatigue is so minute that the associated stored energy could not have been detected by calorimetric experiments of the type described previously.[2]

Summary

In order to determine the extent to which cold-worked regions are formed during fatiguing, wires of ordered copper gold were fatigued to fracture at room temperature under tensile stresses of the order of 5x10^4 lb per sq in. It was found that the resistivity at liquid nitrogen temperature increased by 1 or 2 pct as a consequence of the fatiguing while β, the average rate of change of resistivity with temperature between liquid nitrogen and room temperature, was unaffected. Analysis of the results showed that these effects could not be explained either by the formation of microcracks or of small macroscopic uniformly distributed regions of cold-worked material which either are roughly spherical or have their longest dimension parallel to the axis of the wire. The affected regions must be either of microscopic size (less than an electron mean free path) or of macroscopic size with the longest dimension perpendicular to the axis (disk-shaped with axis parallel to that of the wire).

Table II. Effect of Fatigue and of Static Tension on the Resistivity, ϱ_1, of AuCu at the Temperature $T_1 = 77.4°K$ and on the Average Rate of Change of ϱ with Temperature, $\beta = \frac{\varrho_2 - \varrho_1}{T_2 - T_1}$, Between the Temperatures T_1 and $T_2 = 298.2°K$

Number of Cycles	Minimum Tension, Psi	Maximum Tension, Psi	Time, Min	$\frac{\Delta\varrho_1}{\varrho_1}$, Pct	$\frac{\Delta\beta}{\beta}$, Pct	λ, Pct
		Samples Fatigued				
70,000	11,600	53,500	39	2.3	0.1	0.45
290,000	12,000	45,800	145	1.9	0.1	0.22
330,000	13,200	46,900	165	0.7	0	0.16
		Samples Subjected to Static Tension				
		53,500	39	0.2	0	
		46,900	165	0.2	0.1	
		50,900	88	0.2	0	

Acknowledgment

Thanks are due to Drs. G. Groetzinger and Philip Schwed for valuable discussions.

Discussion of this paper, if any, will appear in JOURNAL OF METALS, November 1955, and in AIME Metals Branch *Transactions*, Vol. **203**, 1955.

References

[1] E. Orowan: *Proceedings* Royal Society (1939) **171**, p. 79.

[2] B. Welber and R. Webeler: JOURNAL OF METALS (1953) **5**, p. 1558.

[3] B. Welber: *Journal of Applied Physics* (1952) **23**, p. 876.

[4] R. Landauer: *Journal of Applied Physics* (1952) **23**, p. 779.

[5] B. Wiener, G. Groetzinger, and P. Schwed: Private communication; *Physical Review* (1954) **93**, p. 922.

[6] P. J. E. Forsyth: *Journal* Institute of Metals (1954) **82**, p. 449.

[7] E. Passaglia and W. F. Love: *Physical Review* (1954) **95**, p. 666.

Technical Note

Crystal Structure of Neodymium Metal

by F. H. Ellinger

THE crystal structure of neodymium has been reported by Quill[1] and by Klemm and Bommer[2, 3] to be hexagonal-close-packed, Strukturbericht-type A3, with $a_o = 3.650$Å, $c_o = 5.890$Å, $c/a = 1.614$. Klemm and Bommer,[3] however, pointed out that the observed intensities of the lines of the neodymium powder pattern agreed only in part with the intensities calculated for the type A3 structure, and that the neodymium powder pattern showed extra lines which could not be traced to impurities. They found that these extra lines could be accounted for by doubling the c-axis, but apparently they did not consider their evidence to be sufficiently conclusive to justify reporting the doubled c-axis. In the present work, the structure of neodymium was found to be double hexagonal-close-packed.

The neodymium metal used in the present investigation was obtained through the courtesy of F. H. Spedding of the Ames Laboratory. Its major impurity was stated to be 0.03 pct Ca. The author's spectrographic analysis indicated high purity and carbon was determined to be less than 30 ppm. X-ray powder specimens were prepared from filings stress relieved in vacuum at 200°C for 50 hr. Powder photographs were taken in an 114.6 mm diam camera (Straumanis film mounting) at room temperature and in a 19 cm diam Unicam high temperature camera at elevated temperatures. Copper x-radiation was used for all the photographs.

The powder pattern of neodymium was found to index to a hexagonal unit cell with dimensions, as determined from the high angle $K\alpha$ doublets, of: $a_o = 3.655 \pm 0.001$Å; $c_o = 11.796 \pm 0.004$Å; and $c/a = 3.227$ at room temperature. The measured density of neodymium shows that this cell contains 4 atoms, the calculated density is accordingly $D_x = 7.02$ g per cu cm. The diffraction data for the first 15 lines of the powder pattern are listed in Table I. In a double hexagonal-close-packed unit cell, the 4 atoms would be in the positions (0,0,0), (0,0,½), (1/3, 2/3, ¼), and (2/3, 1/3, ¾) of space group $P\ 6_3/m\ m\ c$. On the basis of these positions, the relative intensities of the reflections were calculated using the expression:

$$I \propto |F|^2 p \frac{1 + \cos^2 2\theta}{\sin^2 \theta \cos \theta}$$

where F is the structure factor and p is the multiplicity factor. Since absorption was not taken into consideration, comparison of observed and calculated intensities should be made only for neighboring reflections.

Table I. X-Ray Diffraction Data for Neodymium Metal, Radiation: Cu $K\alpha$

HK L	Observed		Calculated Intensity
	d, A	Intensity*	
10.0	3.136	w	48
10.1	3.032	m	262
00.4	2.921	m	314
10.2	2.767	s	614
10.3	2.452	mw	148
10.4	2.141	vw	37
10.5	1.863	w	65
11.0	1.820	mw	86
10.6	1.664	m	130
20.0	nil	nil	0
20.1	1.563	vw	36
11.4	1.549	mw	185
20.2	1.525	mw	97
10.7	1.483	w	29
00.8 } 20.3 }	1.469	w +	25 29

* s is strong; m, medium; w, weak; and v, very.

Each atom has 12 neighbors, 6 in the basal plane at a distance of 3.655Å and 3 above and 3 below at the closer distance of 3.626Å. These distances correspond to an average radius of the neodymium atom of 1.820Å.

The description of this structure in terms of A, B, and C close-packed layers of atoms is $ABACABAC\cdots\cdots$. The structure repeats every fourth layer and the stacking sequence of the second, third, and fourth layers corresponds to cubic-close-packing of atoms.

A series of powder photographs taken at successively increasing temperatures up to 680±10°C revealed that the double hexagonal-close-packed structure is stable up to this temperature.

Acknowledgments

The author wishes to thank W. H. Zachariasen and A. S. Coffinberry for their helpful comments on this work and also Marion Gibbs for measuring the diffraction films. This work was sponsored by the United States Atomic Energy Commission.

F. H. ELLINGER, Member AIME, is associated with Los Alamos Scientific Laboratory, University of California, Los Alamos, N. M.

TN 208E. Manuscript, Dec. 7, 1953.

[1] L. L. Quill: *Ztsch. anorg. allgem. Chemie* (1932) **208**, p. 272.

[2] W. Klemm and H. Bommer: *Ztsch. anorg. allgem. Chemie* (1937) **231**, p. 138.

[3] W. Klemm and H. Bommer: *Ztsch. anorg. allgem. Chemie* (1939) **241**, p. 264.

Technical Note

Temper Brittleness of Some Fe-Ni-Cr Alloys

by L. D. Jaffe

IN 1945-1946, the author measured temper brittleness in ingots of varying composition prepared by remelting SAE 3135 bar stock under vacuum. Since other investigators[1-6] have been referring to this hitherto unpublished work, belated publication seems worthwhile.

Steel in 7 lb batches[7] was induction melted with nickel additions in a magnesia crucible under a pressure of 10 microns of Hg or less and cast into a 2 in. diam chill mold. The compositions of ingots *A*, *B*, and *C* prepared in this way are shown in Table I; the vacuum melting lowered carbon, manganese, sulphur, and nitrogen content. Ingot *B* was homogenized 24 hr at 1095°C; ingots *A* and *C* were not homogenized. Blanks, ½ in. square, were cut from each ingot, austenitized 1 hr at 870°C, water quenched, tempered 1 hr at 595°C, and water quenched. Half the blanks from each ingot were given an embrittling treatment of 50 hr at 455°C and water quenched. A few specimens, embrittled and unembrittled, were finally heated 1 hr at 580°C and water quenched.

Charpy specimens machined from the blanks were *V*-notched on the side closest to ingot mid-radius and paired as to radial position in the ingot, one of each pair having received the embrittling treatment and the other not. Specimens were broken in a standard impact machine at various temperatures, the same temperature, in general, being used for both bars of a pair. Fig. 1 shows the results. It is evident that temper brittleness, as measured by the increase in temperature of transition from brittle to tough failure introduced by the 455°C treatment, was decreased but not eliminated by reducing carbon to 0.006 pct, manganese to < 0.004 pct, and nitrogen to 0.001 pct. In another study,[3] temper brittleness was apparently eliminated by reducing carbon to 0.003 pct, with 0.80 pct Mn and 0.0015 pct N (ingot *D*).*

* Analyses given for carbon below 0.02 pct were made by Jensen method; for nitrogen, by Kjehldahl method. Values quoted elsewhere[1-4,7] for carbon content of ingot *C* and for nitrogen content of ingot *D* were obtained by conventional combustion and by vacuum fusion methods, respectively, and are considered much less accurate.

The 580°C final treatment removed previous embrittlement (ingot *B* particularly), indicating that this was "reversible embrittlement."[5]

Metallographic examination of ingot *C* with 1 pct nital etch revealed only ferrite; ingot *A* had carbide spheroids uniformly distributed in a ferrite matrix. With ethereal picric acid plus zephiran chloride etchant,[7] no differences between embrittled and unembrittled specimens of ingots *A*, *B*, or *C* were noted. Fracture of *C* and *D* below the transition temperature was predominantly transcrystalline, with traces of intercrystalline, in both embrittled and unembrittled conditions. The corresponding fracture of unembrittled *B* was mixed transcrystalline and intercrystalline; of embrittled *B*, predominantly intercrystalline with some transcrystalline areas.

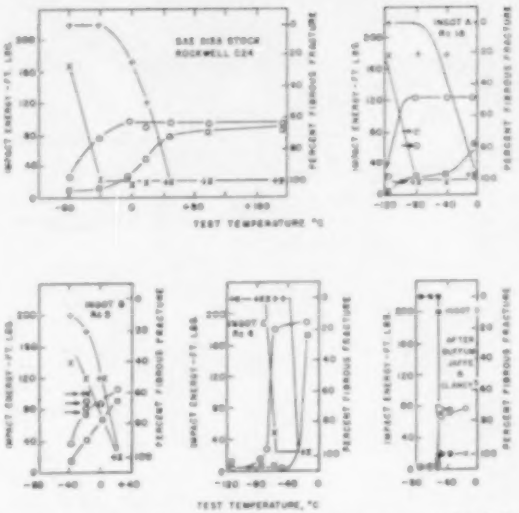

Fig. 1—Experimental data. Circle is impact energy, unembrittled; square, impact energy, embrittled; ×, percent fibrous fracture, unembrittled; +, percent fibrous fracture, embrittled; and arrow designates specimens reheated to 580°C and water quenched.

L. D. JAFFE, Member AIME, formerly associated with Watertown Arsenal, Watertown, Mass., is Chief, Materials Section, Jet Propulsion Laboratory, California Institute of Technology, Pasadena, Calif.

TN 255E. Manuscript, Feb. 2, 1954.

Acknowledgment

The efforts of J. C. Leschen, formerly of National Research Corp., in preparing the ingots are acknowledged with thanks.

References

[1] A. P. Taber, J. F. Thorlin, and J. F. Wallace: *Trans.* ASM (1950) **42**, pp. 1033-1056.
[2] B. C. Woodfine: *Journal* Iron and Steel Institute (1953) **173**, pp. 229-240.
[3] R. Hultgren and J. C. Chang: *Trans.* ASM (1954) **46**, pp. 1298-1317.
[4] J. H. Hollomon, L. D. Jaffe, D. E. McCarthy, and M. R. Norton: *Trans.* ASM (1947) **38**, pp. 807-847.
[5] D. C. Buffum, L. D. Jaffe, and W. P. Clancy: *Trans.* AIME (1949) **185**, pp. 499-500; JOURNAL OF METALS (August 1949).
[6] J. F. Libsch, A. E. Powers, and G. Bhat: *Trans.* ASM (1952) **44**, pp. 1058-1075.
[7] J. B. Cohen, A. Hurlich, and M. Jacobson: *Trans.* ASM (1947) **39**, pp. 109-138.

Table I. Compositions, Pct; Balance Nominally Fe

Heat	C	Mn	Si	S	P	Cr	Ni	Mo	V	Al	Mg	Sb	B	N	O	H
3135 melting stock	0.35	0.87	0.22	0.020	0.020	0.50	1.16	0.005	0.003	0.020	—	—	0.0005	0.005	—	—
A	0.11	0.004	<0.31	0.006	0.028	0.40	5.55	—	0.003	0.007	<0.001	<0.01	0.001	0.002	—	—
B	0.04	0.004	<0.32	0.006	0.033	0.40	5.24	—	—	0.021	<0.001	<0.01	0.0027	0.001	—	—
C	0.006	0.004	<0.35	0.004	0.034	0.27	4.92	—	—	0.009	<0.001	<0.01	0.0029	0.0015	—	—
D	0.003	0.80	0.02	0.005	0.002	0.61	1.49	0.002	—	—	—	—	—	0.0015	0.017	0.00006

Decomposition of Beta Titanium

by Franz R. Brotzen, Edward L. Harmon, Jr., and Alexander R. Troiano

Precipitation processes leading to drastic property changes are a frequent occurrence in titanium alloys containing large amounts of the retained high temperature β phase. In order to establish the kinetics and nature of these precipitation processes, a series of Ti-V alloys was studied. Time-temperature-transformation diagrams were obtained for 12.5 and 15 pct V-Ti alloys. These diagrams consisted of two intersecting C-shaped curves: one in the high temperature region for the equilibrium transformation $\beta \rightarrow \alpha + \beta$, and another at lower temperatures depicting the formation of the metastable transition phase, ω. Presence of the transition phase retarded the precipitation of the equilibrium α phase. Deformation of retained β resulted in the formation of the ω phase. Reversion and retrogression phenomena of the transition phase were observed. A negative temperature coefficient of resistance was found in quenched alloys containing from 15 to 20 pct V.

CERTAIN titanium-base alloys can be heat treated to produce appreciable changes in properties. For example, remarkably high hardness values may be obtained by aging or isothermal quenching treatments. Most of the information available to date on the hardening of titanium-base alloys has been systematized recently in an article by L. D. Jaffe.[1] It was pointed out by that author that the hardening was the result of the decomposition of the retained β phase to the equilibrium constituents, α and β, and that this decomposition had many of the characteristics of an age-hardening reaction. Recent work by Frost et al.[2, 3] has contributed much to the fundamental understanding of the hardening mechanism in titanium-base systems. These authors established the presence of a transition phase in the transformation from β to $\alpha + \beta$, which they designated ω. The transition phase, in their opinion, was at least partially responsible for the hardening and embrittling effects which accompanied low temperature aging.

The present investigation of the mechanism and kinetics of the hardening reaction was carried out for the Ti-V system. Ti-V alloys were ideally suited for a study of the decomposition of β, since age hardening was known to occur readily in this system.[4] Moreover, no intermetallic compounds occur in this system, Fig. 1, thus simplifying the interpretation of the results.

F. R. BROTZEN, formerly Senior Research Associate, Case Institute of Technology, is Assistant Professor, Rice Institute, Houston, E. L. HARMON, JR., Junior Member AIME, and A. R. TROIANO, Member AIME, are Research Assistant, and Professor of Physical Metallurgy and Head, Dept. of Metallurgical Engineering, respectively, Case Institute of Technology, Cleveland.

Discussion of this paper, TP 3969E, may be sent, 2 copies, to AIME by Apr. 1, 1955. Manuscript, Sept. 13, 1954. Chicago Meeting, February 1955.

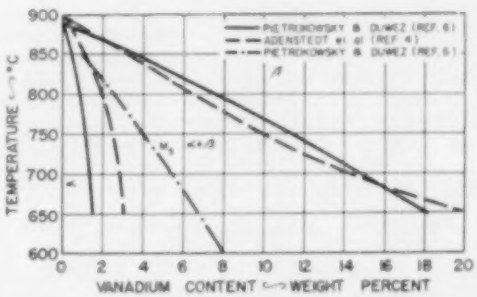

Fig. 1—Partial Ti-V diagram, showing also M_s as a function of vanadium content.

Material and Procedure

Alloys containing 12.5 and 15 pct V were prepared by Battelle Memorial Institute from iodide titanium furnished by Watertown Arsenal and vanadium of 99.8 pct purity. Ingots of 8 lb each were prepared by arc melting in an inert atmosphere with a tungsten electrode and water-cooled copper crucible. Each of the ingots was melted once, forged at 1600°, and rolled at 1400°F. Following this, the ingots were remelted, forged, and then rolled to ½ in. sq bars, which were subsequently grit blasted, pickled, and wire brushed.

Another set of alloys containing nominally 17.5 and 20 pct V was produced by the Research Div., New York University. These alloys were arc melted in an inert atmosphere in lots of 20 g each.

Heat-Treating Procedure: Whenever feasible, specimens were heat treated in high vacuum resistance furnaces at pressures below 5×10^{-4} mm of Hg. Aging and isothermal quenching treatments were generally carried out in salt baths. Specimens were not attacked by the salt, provided the tempera-

Table I. X-Ray Diffraction Lines Observed in a Titanium Specimen Containing 15 Pct V*

Reflection Angle, 2θ	Interplanar Distance, A	Identification
32.4	2.74	ω
39.3	2.28	ω
39.7	2.26	β (110)
56.48	1.624	ω
57.22	1.607	β (200)
66.18	1.398	ω
70.68	1.317	ω
71.45	1.305	β (211)
79.55	1.202	ω
83.80	1.151	ω
85.05	1.133	β (220)
98.55	1.033	β (310)
105.40	0.987	ω
109.50	0.963	β (222)
114.45	0.915	ω
119.05	0.894	ω
123.90	0.871	ω
126.45 (?)	0.860	β (321)
129.30	0.850	ω
149.90	0.799	ω

* Radiation was CuKα; filter, nickel; camera, Debye 57.3 mm radius. Heat treatment consisted of 20 min at 975°C, brine quench; aged 30 min at 444°C, water quench.

ture did not exceed about 575°C. Lead baths were employed for isothermal quenching of metallographic specimens.

Metallography and Hardness Measurements: Specimens used for hardness measurements and metallographic purposes were ¼x¼x1/32 in. in size. The thin section made it possible to quench the specimens at a very high cooling rate.

Metallographic specimens were polished electrolytically. The etching reagent employed contained 1 part HF, 1 part HNO_3, and 4 parts glycerine.

Dilatometric Studies: The kinetics of the β decomposition at temperatures up to 600°C were investigated with a quenching dilatometer similar in design to that described by Flinn, Cook, and Fellows.[5] Dilatometric specimens measured 1½x¼x1/32 in. Dimensional changes were detected by a differential transformer coupled to a high speed recorder.

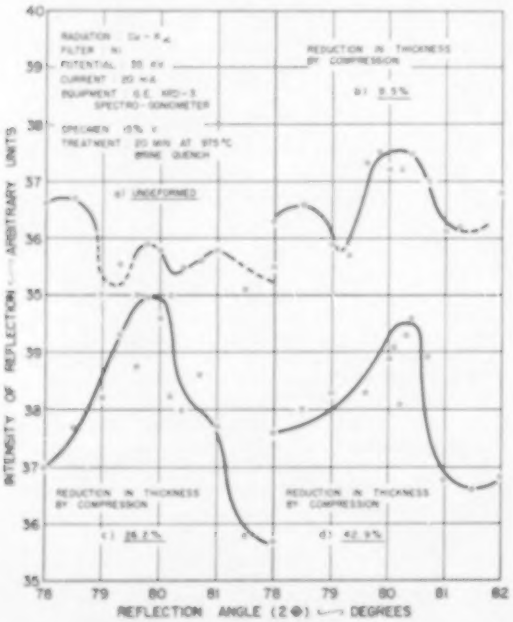

Fig. 2—Scaled intensity of an X-ray diffraction line of the transition lattice produced by deformation.

Electrical Resistance Measurements: Specimens used for electrical resistance measurements were 1½x1/32x1/32 in. in size. The quenched specimens were suspended in a manner that allowed aging in a salt bath or cooling to testing temperatures without disconnecting the leads. The voltage drop across a constantan standard resistance, which corresponded to the current through the specimen, and the voltage drop across the specimen were measured with the same potentiometer. The temperature was determined with copper constantan thermocouples at each end of the specimen. The thermocouple wires also served as potential leads in the measuring circuit. This yielded reproducible results of relative resistance within about 0.05 pct, but did not lend itself to absolute resistivity measurements. From the data collected by this method, variations in resistance and temperature coefficient of resistance were determined.

X-Ray Diffraction: X-ray diffraction studies employed small slivers of polycrystalline material in all cases. The heat-treated specimens, approximately 0.010 in. in diameter, were polished electrolytically in a solution designed to prevent hydrogen absorption.*

* The electrolyte contained 6 g $AlCl_3$, 28 g $ZnCl_2$, 90 cc methyl alcohol, and 10 cc glycerine. This is a modification of a solution used by Frost et al.[4]

Results and Discussion

Nature of β Decomposition: X-ray diffraction studies provided evidence for the existence of a transition phase, ω, which could not be detected by optical metallography. Debye diffraction lines of an aged 15 pct V-Ti alloy containing the transition phase were found at the angles listed in Table I. With exception of one line,* all were in good agreement with those reported for other alloys.[6] This indicates that the transition phase in Ti-V alloys is structurally identical with that in other β-stabilized systems.

* The angular position of this line at $\theta = 15°$, as listed in ref. 3, may well be a typographical error. The stated interplanar distance does not fit the given reflection angle.

The as-quenched structure is particularly sensitive to vanadium content in the range from 12 to 15 pct. For example, when a 15 pct V-Ti alloy was rapidly quenched from 975°C, i.e., above the transformation temperature, it contained small amounts of ω along with retained β.† The 12.5 pct V alloy, when quenched, consisted of retained β, supersaturated α, and quantities of ω slightly greater than those observed in the 15 pct V alloy.

† M_s for a 15 pct V-Ti alloy is below room temperature.[6]

Low temperature aging of the quenched alloys promoted further precipitation of ω. As this trans-

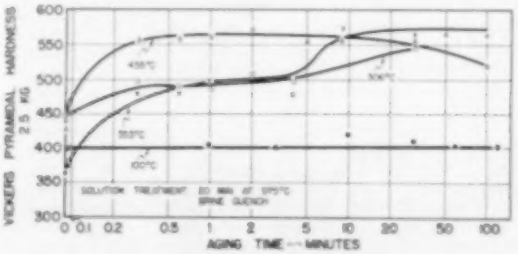

Fig. 3—Hardness curves for a titanium alloy containing 12.5 pct V, aged at various temperatures.

formation progressed, each of the β-titanium diffraction lines broadened and eventually developed a split. The low angle components of the split β lines were probably part of the ω pattern, since their positions, like those of the lines which unequivocally pertained to ω, were virtually unaffected by aging time and temperature. Furthermore, the intensities varied with aging time in both the low angle components of the split and in the ω lines in a like manner. Visual comparison of the intensities of the ω and β lines indicated that in some cases large amounts of ω were present, perhaps more than 50 pct. The ω lines broadened and the split in the β lines became less pronounced as the aging temperature was lowered.

Since the alloys were relatively coarse grained, the diffraction lines were not continuous but consisted of distinct spots. For each spot in the high angle portion of the β-titanium split, there was a "parallel" spot in the low angle component. This was indicative of the existence of a lattice relationship between the β matrix and the transition phase, ω. Upon prolonged aging, especially at higher temperatures, the spottiness of the ω lines gave way to more continuous circles.

X-ray diffraction data for a 15 pct V alloy indicated that during the precipitation of ω the composition of the β matrix increased continuously. Neglecting possible effects of strains upon the lattice, the vanadium contents of the β matrix at two different aging temperatures were estimated from the observed parameters, Table II. The composition of the β phase remained constant after it had reached a certain value; this value increased with lower aging temperatures.

Precipitation of α titanium and simultaneous disappearance of ω were noticed after prolonged aging. In the 15 pct V alloy, for example, this reaction was first observed by X-ray diffraction after 75 min at 444°C. As the α-titanium lines became more intense, the ω lines, including the low angle portion of the split, became fainter and eventually vanished. Thereafter, the patterns contained only α-titanium lines and the high angle β-titanium lines of the former split.

Omega was obtained not only by aging but also by deformation of metastable β. When a quenched 15 pct V alloy was severely deformed by compression, the ω diffraction lines, initially very faint, appeared strong and diffuse. Fig. 2 demonstrates the effect of deformation on the generation of ω. Strain-induced formation of the transition phase may be indicative of a shear-type process, akin to the formation of martensitic α, or of a process in which nucleation is greatly enhanced by strain. The development of brittle ω during room temperature deformation may have deleterious effects on the ductility and formability of β-titanium alloys.

Kinetics of β Decomposition: The decomposition of metastable β titanium can be represented by the reaction sequence

$$\beta \rightarrow \omega + \beta \rightarrow \omega + \alpha + \beta \rightarrow \alpha + \beta.$$

At high reaction temperatures, the first and second steps are bypassed. At low temperatures, on the other hand, the reaction is so slow that the last two steps are not operative within practical time limits. In an intermediate temperature range, all stages in the β decomposition can be observed. For alloys containing 12.5 and 15 pct V, this intermediate range extends approximately from 360° to 500°C.

At low aging temperatures, the hardness increase closely parallels the formation of the transition

Table II. X-Ray Diffraction Lines of β Titanium Evaluated in Terms of Apparent Vanadium Content*

Aging Time in Min	Apparent Vanadium Content, Pct
Aged at 444°C	
0.25	15
10	27
30	25
70	27
Aged at 353°C	
10	38
20	38

* Alloy, 15 pct V-Ti. Heat treatment consisted of 20 min at 975°C, brine quench.

structure, ω. There was a tendency for the alloys to reach higher hardness values at lower aging temperatures, although peak hardnesses were attained more rapidly at the higher temperatures, Figs. 3 to 6. This was in agreement with observations made in the Ti-Al-Cr system.[1]

The precipitation of ω was associated with a decrease in volume which, on occasion, was as large as 10^{-3} cu in. per cu in. This phenomenon allowed the dilatometric observation of the isothermal decomposition of retained β to ω. A discrepancy between heating and cooling curves for thermal expansion had been observed earlier in certain titanium-base alloys.[4,5] This unusual behavior, which was also observed in a 15 pct V alloy, was undoubtedly caused by the formation of ω, since it occurred only in the temperature region where ω was known to form. The curves of Fig. 7 clearly indicate a correlation between hardening and contraction. The general aspect of the dilatometric curves was the same for isothermal quenching as for aging, except for the significant observation that isothermal quenching to temperatures near 400°C revealed clearly the presence of an incubation period, Fig. 8. This was the case for both the 12.5 and 15 pct V alloys. Hardness curves for a 20 pct V alloy, Fig. 6, showed an incubation period also upon aging. As mentioned earlier, in the 12.5 and 15 pct V alloys

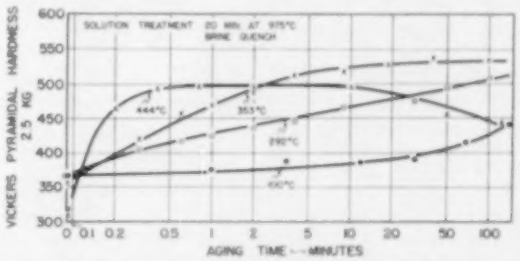

Fig. 4—Hardness curves for a titanium alloy containing 15 pct V, aged at various temperatures.

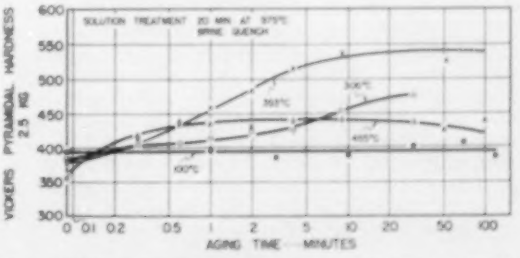

Fig. 5—Hardness curves for a titanium alloy containing 17.5 pct V, aged at various temperatures.

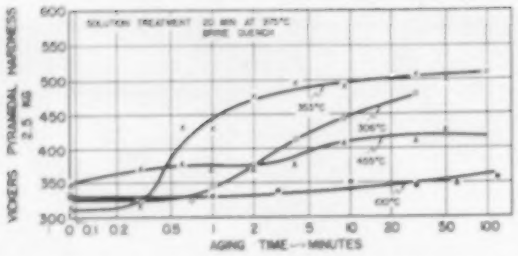

Fig. 6—Hardness curves for a titanium alloy containing 20 pct V, aged at various temperatures.

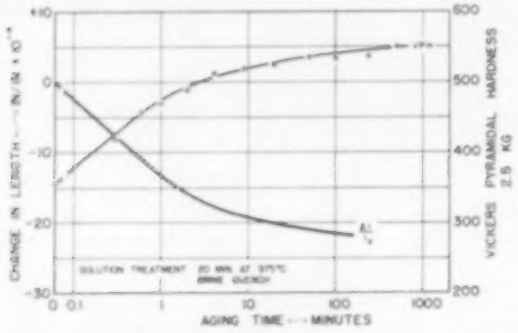

Fig. 7—Dilatometric and hardness values as a function of time for a titanium alloy containing 15 pct V, aged at 353°C.

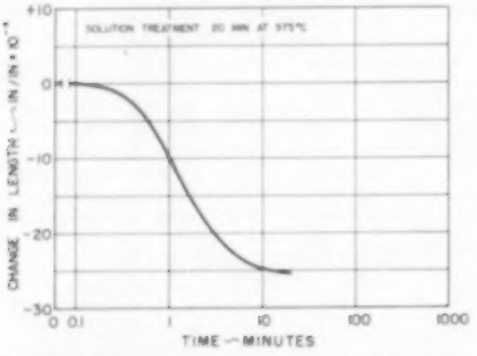

Fig. 8—Dilatometric values as a function of time for a titanium alloy containing 15 pct V, isothermally quenched to 396°C.

the transition phase was present even after very rapid quenching, thus indicating that the minimum incubation time for the formation of ω was extremely short.

Electrical resistance measurements added materially to the analysis of the decomposition of metastable β. A negative temperature coefficient of resistance observed in β-titanium alloys containing approximately 15 to 20 pct V was particularly helpful in following the transformations. This unusual phenomenon, Fig. 9, may be associated with an energy overlap across the {200} of the second Brillouin zone for body-centered-cubic structures at an electron:atom ratio of 4.1899.* The effect of aging of quenched Ti-V alloys upon the electrical resistance at various temperatures is demonstrated in Figs. 10

* Assuming the electron contributions to be those of free atoms, the foregoing electron:atom ratio would correspond to that of titanium alloy containing 20.2 pct V by weight.

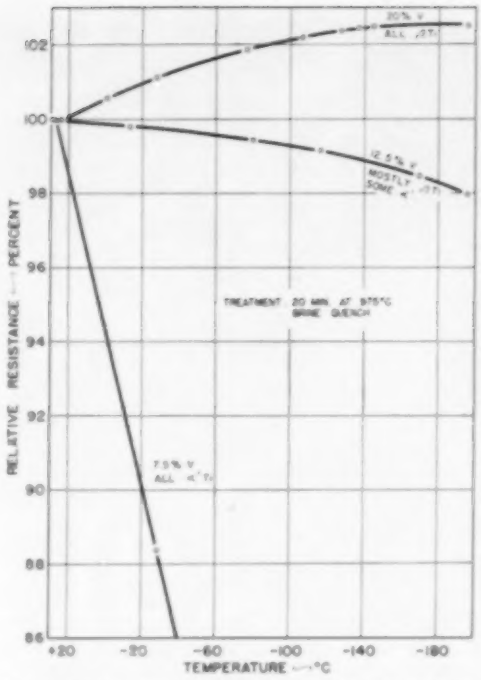

Fig. 9—Relative electrical resistance of quenched Ti-V alloys.

and 11. The coefficient of resistance, initially negative, became more negative during the early stages of the aging process and, after reaching a minimum, increased rapidly, Fig. 12. This behavior was typical for the alloys containing 15 to 20 pct V and may be indicative of the existence of a critical composition of β, probably above 20 pct V, at which the coefficient is a minimum. This is in line with the Brillouin zone effect mentioned earlier and implies a continuous change in the composition of the β matrix during aging, which was corroborated by X-ray parameter measurements. Fig. 12 reveals also that the hardness changes during aging preceded the increase in temperature coefficient. Alloys containing 15 and 17.5 pct V behaved in the same manner.

Precipitation of α accompanied by rapid disappearance of ω took place within reasonable times at sufficiently high aging temperatures. The appearance of α signified the beginning of overaging concurrent with a typical reduction of hardness, Fig. 13. Since a slight increase in volume was associated with the formation of α, dilatometric measurements again were useful in determining the kinetics of the reaction. A typical time-dilation curve for a quenched and aged alloy is given in Fig. 13. The only apparent difference between the dilation curves for aging and those for isothermal quenching was that the latter exhibited an incubation period prior to ω precipitation, Fig. 14. The formation of α was preceded by an incubation period upon aging, Fig. 13, and upon isothermal quenching, Fig. 14.

Above the highest temperatures at which ω was found, equilibrium α formed directly from β. Again, the precipitation of α was accompanied by an expansion. After a short time at temperatures between 550° and 700°C, grain-boundary α was apparent in both the 12.5 and 15 pct V alloys. This initial grain-boundary precipitation was followed immediately by

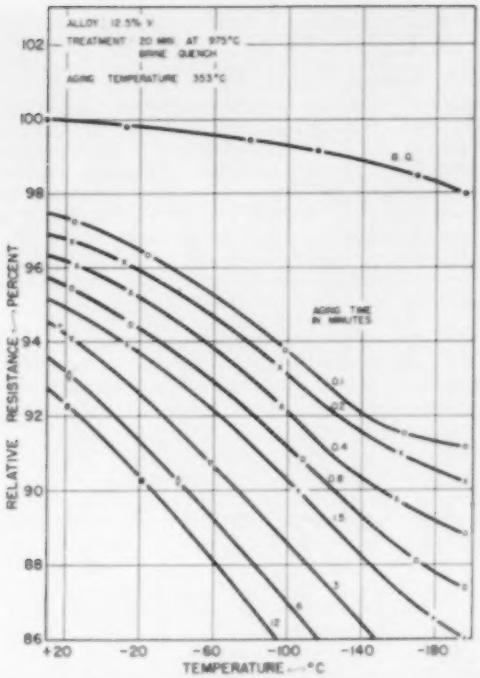

Fig. 10—Relative electrical resistance of an aged titanium alloy containing 12.5 pct V, as a function of testing temperature, for various aging times.

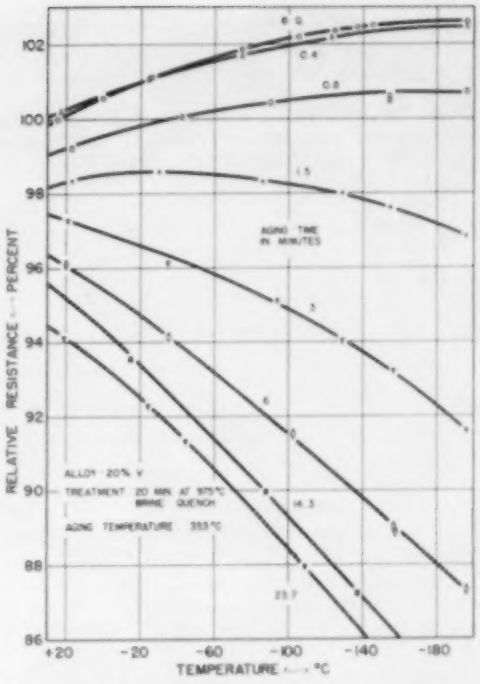

Fig. 11—Relative electrical resistance of an aged titanium alloy containing 20 pct V, as a function of testing temperature, for various aging times.

general precipitation, resulting in a fine dispersion of α in the β matrix. Below approximately 550°C, precipitation appeared to start in a uniform manner throughout the grain.

The time-temperature-transformation (*TTT*) diagrams, Figs. 15 and 16, for the decomposition of β to α and ω consist of *C*-shaped curves. The effect of increasing vanadium content was to shift the *C*-curves to longer times and lower temperatures. The maximum temperature at which ω formed was higher in the 12.5 than in the 15 pct V alloy. A continuous depression of this maximum temperature would imply a concentration beyond which there is no appreciable formation of ω. This was borne out by earlier investigations of the Ti-V,[3] Ti-Mn,[4] and Ti-Fe[10] systems.

The decomposition of β retained in quenched specimens could be followed upon aging in much the same fashion as upon isothermal quenching. Quenching and aging displaced the *TTT* curve, Fig. 17, for the formation of α in the 15 pct V alloy to longer times than those for the same alloy isothermally quenched. It should be noted that isothermal quenching of a 15 pct V alloy to temperatures above 430°C did not produce ω, while brine quenching and reheating to this range caused the formation of considerable amounts of the transition phase. This indicates that the presence of ω was responsible for the retardation in the aged specimens.

Isothermal step quenching may cause partial or complete suppression of martensitic α.[11] Step quenching of a 12.5 pct V alloy to 353°C and holding for 15 min prior to brine quenching produced a hardened matrix without any visible α precipitate. After direct brine quenching, however, the same alloy contained large amounts of martensitic α. The suppression of the martensitic transformation by low

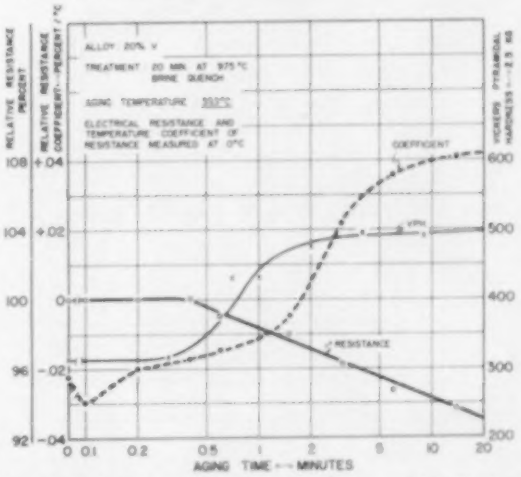

Fig. 12—Electrical properties and hardness of a quenched titanium alloy containing 20 pct V, aged at 353°C.

temperature step quenching may be attributed to the increase in vanadium content in the β matrix, concurrent with the formation of ω.

Reversion and Retrogression of ω: The ω transition phase, formed upon aging or isothermal quenching, reverted to β when heated briefly to temperatures above the ω range, i.e., above about 500°C. This was readily observed in a Debye pattern of an isothermally quenched (403°C for 1 min) 15 pct V alloy. The heavy ω lines in the Debye pattern almost vanished upon subsequent heating to 575°C for 3 sec. The broad diffraction lines for the β matrix became sharp as a result of the high temperature

treatment. The hardness, as expected, was lowered from 557 to 455 VPH by this reversion treatment. The reversion of ω was also observed by changes in the temperature coefficient of electrical resistance, Fig. 18.

These results demonstrate that ω, instead of transforming to α titanium, reverted to the original metastable β at temperatures well below the $\beta/\alpha+\beta$ equilibrium boundary.*

* The equilibrium transformation temperature for this alloy is approximately 700°C.

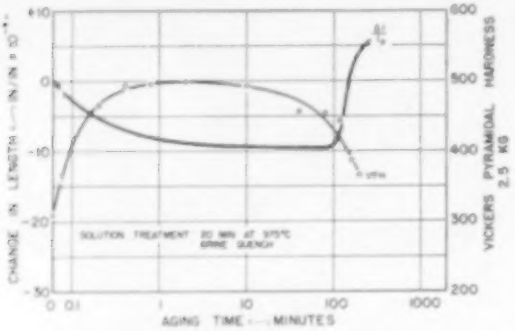
CHANGE IN LENGTH ⟶ ΔL/L × 10⁴
VICKERS PYRAMIDAL HARDNESS 2.5 KG
SOLUTION TREATMENT 20 MIN AT 975°C BRINE QUENCH
AGING TIME ⟶ MINUTES

Fig. 13—Dilatometric and hardness values as a function of time for a titanium alloy containing 15 pct V, aged at 444°C.

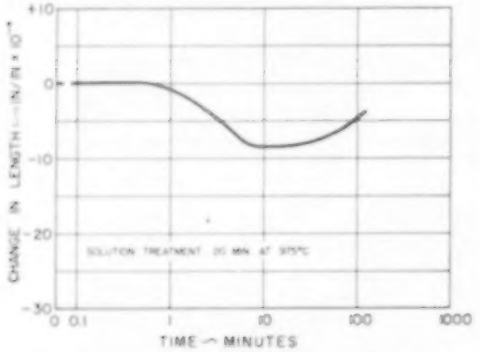

Fig. 14—Dilatometric values as a function of time for a titanium alloy containing 15 pct V, isothermally quenched to 415°C.

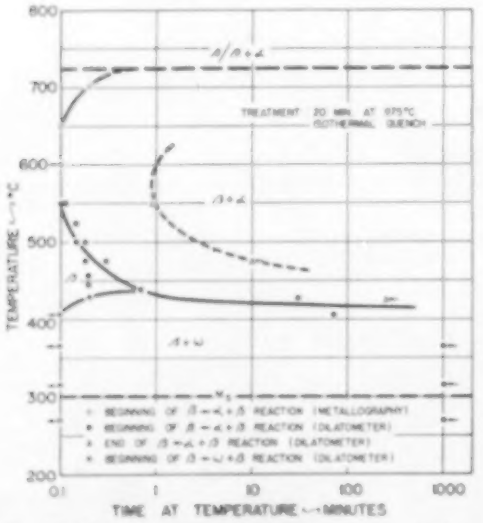
TEMPERATURE ⟶ °C
TREATMENT 20 MIN AT 975°C ISOTHERMAL QUENCH
BEGINNING OF β⟶α+β REACTION (METALLOGRAPHY)
BEGINNING OF β⟶α+β REACTION (DILATOMETER)
END OF β⟶α+β REACTION (DILATOMETER)
BEGINNING OF β⟶ω+β REACTION (DILATOMETER)
TIME AT TEMPERATURE ⟶ MINUTES

Fig. 15—Time-temperature-transformation diagram for isothermal quenching of a titanium alloy containing 12.5 pct V.

Retrogression effects, characteristic of many age-hardening systems, were also observed in Ti-V alloys. When a 15 pct V alloy, hardened by aging for 12 min at 353°C, was up-quenched to a temperature within the ω formation range (455°C), no appreciable change in hardness or electrical resistance was noted, Fig. 19. The temperature coefficient of resistance, on the other hand, decreased rapidly after up-quenching. This indicated an adjustment towards a lower vanadium content of the β matrix, in agreement with the X-ray results in Table II.

Summary and Conclusions

Ti-V alloys are highly responsive to precipitation hardening. The hardening is most pronounced at low reaction temperatures where it is accompanied

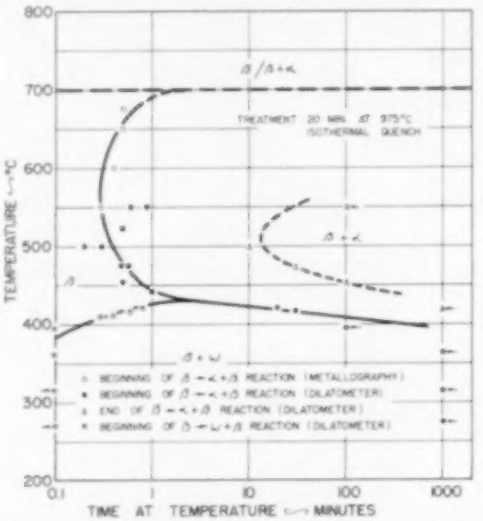
TEMPERATURE ⟶ °C
TREATMENT 20 MIN AT 975°C ISOTHERMAL QUENCH
BEGINNING OF β⟶α+β REACTION (METALLOGRAPHY)
BEGINNING OF β⟶α+β REACTION (DILATOMETER)
END OF β⟶α+β REACTION (DILATOMETER)
BEGINNING OF β⟶ω+β REACTION (DILATOMETER)
TIME AT TEMPERATURE ⟶ MINUTES

Fig. 16—Time-temperature-transformation diagram for isothermal quenching of a titanium alloy containing 15 pct V.

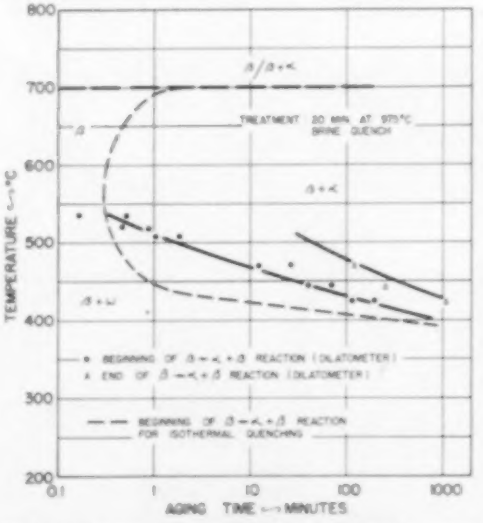
TEMPERATURE ⟶ °C
TREATMENT 20 MIN AT 975°C BRINE QUENCH
BEGINNING OF β⟶α+β REACTION (DILATOMETER)
END OF β⟶α+β REACTION (DILATOMETER)
BEGINNING OF β⟶α+β REACTION FOR ISOTHERMAL QUENCHING
AGING TIME ⟶ MINUTES

Fig. 17—Time-temperature-transformation diagram for aging of a quenched titanium alloy containing 15 pct V.

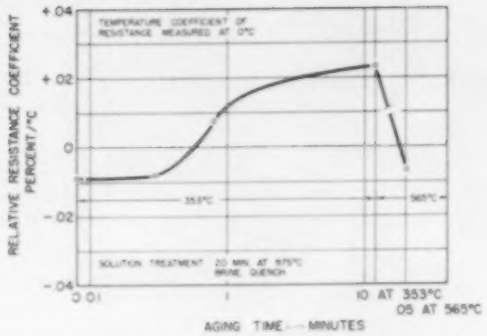

Fig. 18—Temperature coefficient of electrical resistance of a quenched titanium alloy containing 15 pct V, aged at 353°C, and up-quenched to 565°C.

by a decrease in volume. At these temperatures, a metastable phase, ω, forms as an intermediate stage in the decomposition of retained β. During the precipitation of ω the β matrix experiences a continuous parameter change, indicating composition adjustments. Severe compressive deformation of retained β at room temperature also induces the formation of the transition phase. Omega, which may be present in very large quantities in Ti-V alloys, is identical in structure with transition phases observed in several other β-stabilized titanium systems. The viewpoint that ω is a coherent transitional phase formed prior to the precipitation of equilibrium α is favored.

The isothermal formation of ω is preceded by an incubation period which becomes shorter at lower reaction temperatures. Increasing vanadium content retards the formation of ω and depresses the maximum temperature at which it can form.

The eventual formation of equilibrium α is accompanied by a gradual disappearance of the ω phase. This transformation occurs more rapidly at higher temperatures. Above the maximum temperature of ω formation, equilibrium α forms directly from retained β. Time-temperature-transformation diagrams illustrating the transformation kinetics of both α and ω are presented for 12.5 and 15 pct V alloys.

The formation of ω at low temperatures during quenching and reheating inhibits subsequent α precipitation. This results in incubation periods, prior to α precipitation, which are longer for quenching and aging than for direct isothermal quenching.

The transition phase, ω, exhibits a retrogression effect when the temperature is raised during aging. At low temperatures, this effect is slight and is detectable only through changes in the temperature coefficient of electrical resistance. The examination of these changes is facilitated by the fact that β titanium containing 15 to 20 pct V has a negative temperature coefficient of resistance. At higher subcritical aging temperatures, X-ray data reveal the reversion of the transition phase into β titanium of original composition. These effects substantiate the transitional character of the ω phase.

Acknowledgments

This investigation was carried out under contract number DA 33-019-ORD-941 with Army Ordnance Corps, Watertown Arsenal. The authors express their appreciation to the Ordnance Corps of the Army for permission to publish this research. They also gratefully acknowledge the friendly cooperation of Mr. D. C. Buffum of Watertown Arsenal Laboratory.

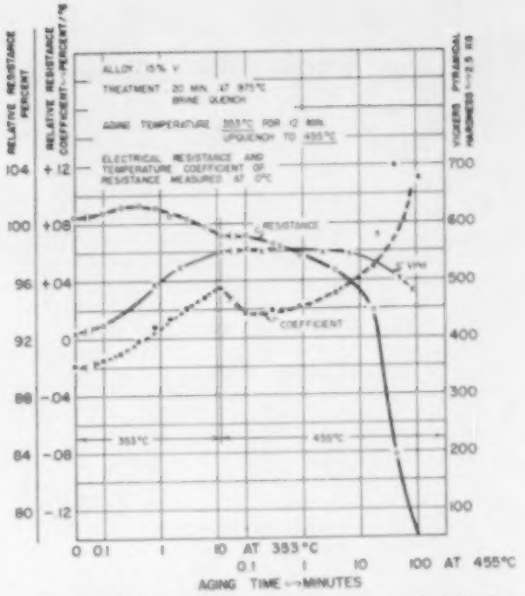

Fig. 19—Electrical properties and hardness of a quenched titanium alloy containing 15 pct V, aged at 353°C, and up-quenched to 455°C.

Discussion of this paper, if any, will appear in JOURNAL OF METALS, November 1955, and in AIME Metals Branch *Transactions*, Vol. **203**, 1955.

References

[1] L. D. Jaffe: Heat Treatment of Titanium Generalized in Terms of Beta Prime. *Trans.* AIME (1954) **200**, p. 210; JOURNAL OF METALS (February 1954).

[2] P. D. Frost, W. M. Parris, L. L. Hirsch, J. R. Doig, and C. M. Schwartz: Isothermal Transformation in Titanium-Chromium Alloys. *Trans.* ASM (1954) **46**, pp. 231-256.

[3] P. D. Frost, W. M. Parris, L. L. Hirsch, J. R. Doig, and C. M. Schwartz: Isothermal Transformation in Titanium-Manganese Alloys. *Trans.* ASM (1954) **46**, pp. 1056-1074.

[4] H. K. Adenstedt, J. R. Pequignot, and J. M. Raymer: The Titanium-Vanadium System. *Trans.* ASM (1952) **44**, pp. 990-1003.

[5] R. A. Flinn, E. Cook, and J. A. Fellows: Quantitative Study of Austenite Transformation. *Trans.* ASM (1943) **31**, pp. 41-70.

[6] P. Pietrokowsky and P. Duwez: Partial Titanium-Vanadium Phase Diagram. *Trans.* AIME (1952) **194**, pp. 627-630; JOURNAL OF METALS (June 1952).

[7] H. D. Kessler and M. Hansen: Transformation Kinetics and Mechanical Properties of Titanium-Aluminum-Chromium Alloys. *Trans.* ASM (1954) **46**, pp. 609-639.

[8] C. W. Phillips and J. C. Tobin: The Phase Transformation and Heat Treatability of Titanium-Base Alloys. *Final Report* University of Michigan to U. S. Army Ordnance (June 1953) Contract DA 20-018-ORD-11456.

[9] R. L. Berry, M. B. Waldron, and G. V. Raynor: Outer Brillouin Zones for the Face-Centered Cubic, Body-Centered Cubic, and Close-Packed Hexagonal Structures. *Research* (1950) **3**, pp. 195-196.

[10] H. W. Worner: Heat Treatment of Titanium-Rich Titanium-Iron Alloys. *Journal* Institute of Metals (1952) **80**, pp. 213-216.

[11] D. J. DeLazaro, M. Hansen, R. E. Riley, and W. Rostoker: Time-Temperature-Transformation Characteristics of Titanium-Molybdenum Alloys. *Trans.* AIME (1952) **194**, pp. 265-269; JOURNAL OF METALS (March 1952).

Technical Note

Sigma Phase in the Molybdenum-Ruthenium System

by D. S. Bloom

RECENTLY a report has been published on an investigation of the Mo-Ru system by E. Raub.[1] In this report it is stated that below approximately 1200°C the system consists of two terminal solid-solution phases and the intervening two-phase field; at 1200°C and above, an intermetallic compound labeled Mo_3Ru_2 makes an appearance.

Along with some other little known systems in which it was considered possible for a σ phase to form, the Mo-Ru system had been under investigation in this laboratory. Since molybdenum and ruthenium have very high melting points and also since ruthenium is expensive, the investigation was confined to X-ray diffraction by sintered powder compacts. The compositions which were studied were (in atomic percentages): 75 Mo-25 Ru, 67 Mo-33 Ru, 50 Mo-50 Ru, and 25 Mo-75 Ru. All compacts were made from the pure powders, and no chemical analyses were attempted. Each compact weighed about 5 g. All annealing was done in evacuated Vycor capsules, and even though the capsules completely collapsed at 1250°C, they still admitted no air.

The results of this investigation in general corroborate the work of Raub. Up to 1150°C the two terminal solutions and the intervening two-phase field were found, and at 1200°C and above an intermetallic compound was found. However, the composition limits of the compound were estimated to lie close to 70 atomic pct Mo rather than 62.5 atomic pct Mo as Raub had reported. At least the X-ray diffraction results indicated that the 75 atomic pct Mo specimen consisted of the molybdenum solid solution plus the compound, while the 67 atomic pct Mo specimen consisted of the ruthenium solid solution plus the compound and the equiatomic composition contained only very little of the compound.

The most interesting observation, however, was that the diffraction pattern of the compound was similar to that of the well known σ phases, except that unusually large lattice constants were indicated. The d-values, or interplanar spacings, of the diffraction lines (as produced by filtered copper $K\alpha$ radiation) of the compound are given in Table I, as determined from specimens annealed at 1250°C for 9 hr and then quenched in water. Also shown are the lines of the Mn-Mo σ phase as given by Decker, Waterstrat, and Kasper,[2] the lines of the Fe-Mo σ as given by Goldschmidt,[3] and the lines of the Mo-Ru phase multiplied by constants in order to make comparison with the Mn-Mo and Fe-Mo patterns easier. These results indicate that the compound in the Mo-Ru system is apparently isomorphous with the other σ compounds.

The rather large lattice constants of the Mo-Ru σ phase are acceptable in view of the comparatively large size of the constituent atoms.

The data in Table I for the Mo-Ru compound check quite well with those given by Raub, not shown here, though there are some discrepancies between the two sets of data in the estimated intensities of a few lines.

Table I. Comparison of Diffraction Patterns of Mn-Mo, Mo-Ru, Fe-Mo σ Phases

Mn-Mo σ		Mo-Ru σ x 0.9551	Mo-Ru σ		Mo-Ru σ x 0.9479	Fe-Mo σ	
d	I*		d	I*		d	I*
2.463	m	2.455	2.570	w	2.44	2.46	w
2.368	m	2.353	2.464	m	2.34	2.35	mw
2.286	s	2.309	2.313	s	2.19	2.21	s
2.144	mw	2.149	2.249	mw	2.13	2.13	m
2.097	mw	2.094	2.192	s	2.08	2.08	m
2.045	s	2.036	2.134	s	2.02	2.04	mw
2.000	m	1.996	2.092	m	1.98	1.99	s
1.952	s	1.950	2.047	mw	1.94	1.93	m
1.907	mw	1.902	1.901	mw	1.89	1.90	w
1.829	mw	1.822	1.908	mw	1.81	1.82	w
—	—	1.791	1.875	w	1.78	—	—
1.697	vvw	—	—	—	—	—	—
1.672	vvw	—	—	—	—	—	—
1.444	mw	1.440	1.508	w	1.43	1.44	vw
1.426	mw	1.434	1.491	w	1.41	1.43	—
—	—	1.418	1.484	w	1.41	—	—
1.385	vw	1.411	1.477	w	1.40	—	—
1.377	mw	1.377	1.442	w	1.37	1.37	w
1.362	vvw	—	—	—	—	—	—
1.304	s	1.303	1.365	m	1.29	1.30	mw
1.286	vw	1.289	1.350	m	1.28	—	—
1.279	m	1.280	1.340	m	1.27	1.28	s
1.272	mw	—	—	—	—	—	—
1.267	m	1.267	1.326	m	1.26	—	—
1.253	s	1.253	1.312	mw	1.24	—	—
1.244	m	1.245	1.304	mw	1.236	1.246	mw
1.232	mw	—	—	—	—	—	—
1.221	mw	—	—	—	—	1.220	m
1.211	mw	1.211	1.268	mw	1.202	1.205	w
1.195	vvw	—	—	—	—	—	—
1.187	s	1.179	1.234	mw	1.170	1.177	m
			1.187	mw	1.125	1.179	m
			1.158	mw	1.098	1.100	m
			1.1273	m	1.069	1.068	s
			1.0893	mw	1.032	1.035	s
			1.0836	m	1.027	1.029	s
			1.0690	mw	1.013	1.020	s

* Standard abbreviations for weak, w; medium, m; strong, s; and very, v.

Although very little is known at present about this σ phase, there are some things which may be pointed out, mainly in comparison with other better known σ phases. Even though molybdenum and ruthenium are in the same columns in the Table of Elements as chromium and iron, respectively, the Mo-Ru σ phase contains much more molybdenum than ruthenium, while the Cr-Fe σ phase centers around or very nearly around the equiatomic composition; furthermore, the Mo-Ru σ is stable only above approximately 1200°C, but the Cr-Fe σ is stable only below about 825°C. With respect to its being unstable below 1200°C, the Mo-Ru σ is similar to the other binary molybdenum σ phases in the Co-Mo and Fe-Mo systems. Similar to the latter two systems, the Mo-Ru σ apparently exists over a rather narrow composition range, whereas the Cr-Fe σ at lower temperatures is stable over a much wider composition range. The Mo-Ru σ thus is closer to the other molybdenum σ phases than to the Cr-Fe σ phase. The most striking feature of the Mo-Ru σ phase, however, is the absence of any of the transition elements of the First Long Period.

D. S. BLOOM is associated with Michelson Laboratory, United States Ordnance Test Station, Inyokern China Lake, Calif.

TN 262E. Manuscript, Nov. 29, 1954.

[1] Ernst Raub: Die legierungen der Platinmetalle mit Molybdan. *Ztsch. für Metallkunde.* (1954) 45, No. 1, p. 23.

[2] B. F. Decker, R. M. Waterstrat, and J. S. Kasper: Formation Sigma Phase in the Mn-Mo System. *Trans.* AIME (1953) 197, p. 1476; JOURNAL OF METALS (November 1953).

[3] H. J. Goldschmidt: A Molybdenum Sigma Phase. *Research.* (1949) 2, p. 343.

A Calorimetric Investigation of the Energy Relations in Alloys of Composition Cu_3Au

by L. R. Rubin, J. S. Ll. Leach, and M. B. Bever

The energies of formation of ordered and disordered solid solutions of composition Cu_3Au and the energy of ordering in this alloy were determined by tin solution calorimetry. The degree of order was measured by X-ray diffraction and electrical resistance and microhardness measurements were made on ordered and disordered specimens.

AMONG the phenomena associated with the order-disorder transformation of a solid solution, the change in internal energy is of special interest because of the part it plays in the various theories of ordering. Published values for the decrease in internal energy accompanying the formation of a superlattice from a disordered solid solution of composition Cu_3Au range from −370 to −2260 cal per gram-atom. Some of these values represent calculations based on theory and others are the results of experimental measurements. The distinction between the change in internal energy, ΔE, and the change in enthalpy, ΔH, can here be neglected, because they are approximately equal for solid-state reactions at normal pressure.

An analysis of ordering by Bragg and Williams[1] predicts an energy change of −605 cal per gram-atom for the formation of a superlattice in the alloy Cu_3Au from a completely random solution. Peierls[2] application to Cu_3Au of Bethe's[3] nearest-neighbor theory yields −560 cal per gram-atom for the formation of a superlattice from a matrix which initially contains short-range order. Cowley[4] extended the nearest-neighbor approach to include as many as five shells of neighbors; on this basis a change in energy of −500 cal per gram-atom is expected. Eguchi,[5] using a quantum-mechanical treatment, calculated a value of −2260 cal per gram-atom for the difference in the energy of completely disordered and completely ordered Cu_3Au.

Sykes and Jones[6] heated a completely ordered alloy and measured its heat capacity as a function of temperature. This measured heat capacity agrees closely with the corresponding value found by the Kopp-Neumann (or mixture) rule up to about 250°C and above this temperature exceeds it, especially near the critical temperature for ordering. The difference between the integrals with respect to temperature of the observed and the Kopp-Neumann heat capacities was considered to be the energy of ordering. By this method Sykes and Jones found a value of −530 cal per gram-atom. This value is not adjusted for the short-range order remaining above the critical temperature. The presence of such short-range order is suggested by the difference between the measured heat capacity and the extrapolated Kopp-Neumann heat capacity immediately above the critical temperature.

Values reported by Weibke and von Quadt[7] and by Hirabayashi, Nagasaki, and Maniwa[8] were obtained in the course of investigations primarily aimed at other objectives. Weibke and von Quadt measured the temperature coefficient of the electromotive force of a Cu-Cu_3Au cell. They obtained a value of −1010 cal per gram-atom for the heat of formation of the alloy at 500°C, at which temperature there is no long-range order. They also obtained −1380 cal per gram-atom as the heat of formation of the ordered alloy at 370°C. Considering the heat of formation of the disordered alloy to be independent of temperature, they estimated the energy of ordering at 370°C as −370 cal per gram-atom. At this temperature long-range order is incomplete and the degree of order changes rapidly with temperature. Hirabayashi, Nagasaki, and Maniwa,[8] using an annealing calorimeter, investigated an alloy containing 23.4 rather than 25.0 atomic pct Au and thus could not obtain complete order. Their value of the energy of ordering was −490 cal per gram-atom.

Oriani[9] has recently investigated the Au-Cu system by the galvanic emf technique. He reports values for the heats of formation of Cu-Au alloys, from which the heat of formation at 427°C of an alloy of composition Cu_3Au may be found by interpolation. This value is −1080 cal per gram-atom.

In the work here reported, disordered and ordered alloys of composition Cu_3Au and corresponding mixtures of gold and copper were dissolved in liquid tin and the heat effects measured. These heat effects are small, since the dissolution of gold in tin is exothermic and the dissolution of copper is endothermic. The method, therefore, yields fairly precise values of the heats of formation of disordered and ordered alloys and of the energy of ordering.

Experimental Procedure

The calorimeter consisted of a long-necked Dewar flask immersed in a constant temperature salt bath and has been described by Ticknor and Bever.[10] The chief changes in this equipment were an improvement in vacuum and the replacement of the mercury thermoregulator by a resistance thermometer control circuit.

The solvent, which was maintained at a constant temperature near 350°C, consisted of 500 grams of 99.99 pct pure tin. The solute samples were mixtures of gold and copper in the proportion corresponding to the composition Cu_3Au or solid solutions

L. R. RUBIN, J. S. LL. LEACH, and M. B. BEVER, Member AIME, are Staff Members, Division of Industrial Cooperation, and Associate Professor of Metallurgy, respectively, Massachusetts Institute of Technology, Cambridge, Mass.

Discussion of this paper, TP 3913E, may be sent, 2 copies, to AIME by Apr. 1, 1955. Manuscript, July 27, 1954. Chicago Meeting, February 1955.

This paper is based in part on a thesis by L. R. Rubin submitted, in partial fulfillment of the requirements of the degree of Master of Science in Metallurgy, to Massachusetts Institute of Technology.

of this composition, analyzing 50.90±0.05 wt pct Au. The alloys in the form of ½ in. lengths of thin ribbon were annealed under vacuum for approximately 12 hr at 480°C and then were water quenched to retain their disordered condition or cooled to approximately 180°C at a rate of about 2°C per hr to form a superlattice. The gold in the mechanical mixtures contained 0.03 pct Ag and Cu. The copper was prepared by the method of Smart, Smith, and Phillips[9] and the impurity limits (less than 0.001 pct) stated by them are assumed.

The calorimetric procedure, described previously in detail,[7] will only be summarized. A weighed sample which was at 0°C was added to the molten tin under vacuum. The resulting change in temperature of the bath was measured as a function of time. Four 5 gram or six 3 gram samples were added during a run. To determine the heat capacity of the calorimeter, a charge of 99.4±0.1 pct W wire, which does not react with tin at the experimental temperature, was added at the end of each run.

The temperature of the calorimeter dropped when the alloy or mixture was added because of the heating and endothermic dissolution of the sample. As the dissolution process neared completion, the temperature began to rise gradually because of the transfer of heat from the constant-temperature salt bath to the calorimeter. The total heat absorbed, therefore, is attributable to the change of state of the sample from its initial condition at 0°C to its final state in the tin solution. The difference in the heat effects for the addition of two chemically identical samples represents the difference of their energy contents in their initial states, that is, at 0°C. Several additions could be made in a single run because the heat of solution is a known function of the concentration of the solute in the tin. The basic methods of calculation have been described[8] and some minor changes recently made will be published.

The samples used in these experiments were prepared in two batches. Specimens suitable for microhardness and electrical resistivity measurements and powder samples for X-ray diffraction work were heat treated simultaneously with the samples for calorimetric measurements. The degree of order in each batch was calculated from the intensities of the fundamental and superlattice lines obtained from the powder samples. The microhardness and electrical resistivity measurements were used as further checks on the degree of order of the samples.

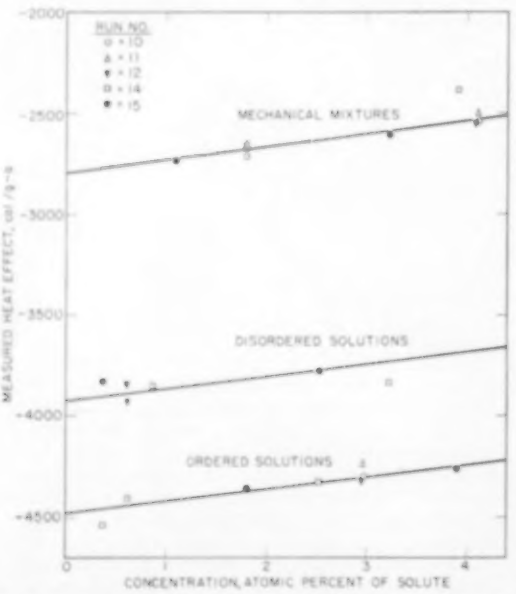

Fig. 1—Heat effects associated with the addition of samples plotted against the average of the solute concentrations in solution before and after each addition.

Experimental Results

Fig. 1 shows the heat effects measured in five calorimetric runs plotted against the average concentration of solute in solution resulting from each addition. The measured heat effect is defined so that heat transferred from the calorimetric system to the sample is negative. The curves for the mixtures, disordered solid solutions, and ordered solid solutions have the same slope, which represents the rate of change of their differential heat of solution in tin. This slope was experimentally found to be +60 cal per gram-atom per atomic pct of solute. The intercepts of these curves with the ordinate give the heat effects at infinite dilution, which have the following values: mechanical mixtures, −2788±21 cal per gram-atom; disordered solid solutions, −3928 ±62 cal per gram-atom; and ordered solid solutions, −4480±42 cal per gram-atom.

The differences in the ordinates of these curves, taken at any concentration, give the heats of formation of the disordered and ordered solid solutions and the energy effect of ordering at 0°C. These values and their root mean square errors are: mixture to disorder, −1140±66 cal per gram-atom; mixture to order, −1692±47 cal per gram-atom; and disorder to order, −552±75 cal per gram-atom.

By an alternative method for evaluating the heat effects, the differences in the ordinates are taken for every run and the results are averaged. The absolute values of the measured heat effects are proportional to the heat capacity of the calorimeter, which is experimentally determined in each run. Errors in the heat capacity appear as corresponding percentage errors in the heat effects and result in larger percentage errors in the differences between the heat effects. The absolute magnitude of the heat effects, when averaged as in the first method, yields a percentage error in the differences larger than if the differences were obtained from each run separately and then averaged. The values obtained by this alternative method of calculation are: mixture to disorder, −1124±55 cal per gram-atom; mixture to order, −1682±30 cal per gram-atom; and disorder to order, −562±59 cal per gram-atom. The latter values are considered to deserve preference.

By the definition of Bragg and Williams, the degree of order of the ordered specimens, as determined by X-ray measurements, was 0.93 for runs 10 through 12 and 0.94 for runs 14 and 15. No trace of superlattice lines was observed for the disordered samples of either batch of specimens.

Knoop hardness measurements, made with a Tukon tester and a 300 gram load, on ordered and disordered specimens show that the hardness of corresponding specimens from the two batches was the same within the experimental error. The ordered and disordered specimens used in calorimetric runs 10 through 12 had average Knoop hardness numbers of 82.8 and 58.1, respectively. The corresponding specimens for runs 14 and 15 had average Knoop hardness numbers of 85.3 and 62.0.

Resistance measurements for the specimens used

in runs 14 and 15 yielded specific resistivities of 4.2×10^{-6} and 11.7×10^{-6} ohm-cm for the ordered and disordered alloys at room temperature as compared with 4.3×10^{-6} and 11.4×10^{-6} ohm-cm obtained by Sykes and Evans.[12] The specific resistivities obtained for the specimens used in runs 10 through 12 were larger in absolute value but were in approximately the same ratio (2.60) as those of Sykes and Evans (2.65).

Discussion

The range of theoretical and experimental values of the energy associated with the order-disorder transformation in Cu_3Au, found in the literature, is considerable. The values obtained by Weibke and von Quadt[7] and by Hirabayashi and coworkers[8] can be expected to be low. The former investigators worked at 370°C, where only partial order can exist, and the alloy composition used by the latter precluded complete ordering. Sykes and Jones[6] found the energy change of ordering from the difference in observed and calculated heat capacities. Their value is based on the assumption that the heat capacity of the disordered solid solution is equal to that of the mechanical mixture of the constituent elements; their measurements below 250°C lend considerable support to this assumption. Sykes and Jones prepared the ordered alloys by cooling at 30°C per hr and also at 1°C per hr; they found that the energy effects observed on heating these alloys varied by less than 1 pct, which suggests that the rate of cooling used in the present work (2°C per hr) was entirely adequate.

The calorimetric method used in the work reported here compares the initial conditions of two sets of samples at 0°C. It is true that the initial state of alloys here called "disordered" involves some short-range order, which is that present at the temperature from which the alloys were quenched (480°C) in addition to any short-range order originating during the quench. The presence of such short-range order in Cu_3Au alloys quenched from above their critical temperature is generally recognized. The energy values measured in this work, therefore, involve the change from a disordered solid solution containing an unknown but probably small amount of short-range order to a solid solution which has nearly complete long-range order. The energy of this transformation, found to be -562 ± 59 cal per gram-atom, is in reasonable agreement with the values predicted by the theories of Bragg and Williams (−605 cal per gram-atom), Peierls (−560 cal per gram-atom) and Cowley (−500 cal per gram-atom). The value of Bragg and Williams also includes the energy effect of the formation of short-range order from the random solid solution. The value reported here is in good agreement with the value of −530 cal per gram-atom measured by Sykes and Jones. They used a different method of measurement but, as already noted, the alloys in both investigations can be expected to have a comparable degree of long-range order.

The heat of formation of the disordered alloy at 0°C was determined at -1124 ± 55 cal per gram-atom which compares with −1010 cal per gram-atom found by Weibke and von Quadt at 500°C and −1080 found by Oriani at 427°C. The ratio of the energy of ordering to the energy of formation of the disordered alloy according to Shockley[15] should have the value of 1/3 at the AB_3 composition. The ratio of the values measured in the present investigation is approximately ½.

The increase in hardness values associated with the formation of a superlattice which was found in this investigation contradicts the results of Sachs and Weerts.[16] These investigators found a decrease in the critical shear stress of single crystals of Cu_3Au upon ordering. Also, according to current opinions only a negligible change in hardness would be expected in the absence of a change in shape of the unit cell.[17]

Summary and Conclusions

The change in internal energy of the transformation of a disordered into an ordered solid solution of composition Cu_3Au was found to be -562 ± 59 cal per gram-atom; the disordered solid solution contained some short-range order. The heats of formation of the disordered and ordered alloys from the elements were measured as -1124 ± 55 and -1682 ± 30 cal per gram-atom, respectively. The difference between the latter two quantities (−558 cal per gram-atom) provides an internal check on the directly determined energy change for the ordering of the disordered solution. The measured value of the energy of ordering is in reasonable agreement with some values predicted from theory and an experimental value determined by a different method.

The degree of long-range order was determined by X-ray diffraction. The electrical resistivities of the ordered and disordered alloys were measured and agreed with published values. The hardness increased from about 60 to about 84 Knoop numbers; this finding is not in agreement with a previous investigation.

Acknowledgments

This work was performed under Contract No. AT(30-1)-1002 with the United States Atomic Energy Commission. The authors wish to express their great indebtedness to Professor Carl Wagner for helpful advice and discussions. Thanks are also due to Norman Hansen and Benjamin Howell for their aid in the performance of the calorimetric experiments.

Discussion of this paper, if any, will appear in JOURNAL OF METALS, November 1955, and in AIME Metals Branch *Transactions*, Vol. **203**, 1955.

References

[1] W. L. Bragg and E. J. Williams: *Proceedings* Royal Society, London (1934) **145A**, p. 699.

[2] R. Peierls: *Proceedings* Royal Society, London (1936) **154A**, p. 207.

[3] H. A. Bethe: *Proceedings* Royal Society, London (1935) **150A**, p. 552.

[4] J. M. Cowley: *Physical Review* (1950) **77**, p. 669.

[5] T. Eguchi: *Memoirs* Faculty of Science, Kyusyu University, Japan (1951) **1B**, p. 25; *Chemical Abstracts* (1952) **46**, p. 3933c.

[6] C. Sykes and F. W. Jones: *Proceedings* Royal Society, London (1936) **157A**, p. 213.

[7] F. Weibke and von Quadt: *Ztsch. für Elektrochemie* (1939) **45**, p. 715.

[8] M. Hirabayashi, S. Nagasaki, and H. Maniwa: *Nippon Kinzoku Gakkai-si* (1950) **14B**, No. 3, p. 1; *Chemical Abstracts* (1952) **46**, p. 7390h.

[9] R. A. Oriani: *Acta Metallurgica* (1954) **2**, p. 608.

[10] L. B. Ticknor and M. B. Bever: *Trans.* AIME (1952) **194**, p. 941; JOURNAL OF METALS (September 1952).

[11] J. S. Smart, Jr., A. A. Smith, Jr., and A. J. Phillips: *Trans.* AIME (1941) **143**, p. 272.

[12] C. Sykes and H. Evans: *Journal* Institute of Metals (1936) **58**, p. 255.

[13] W. Shockley: *Journal of Chemical Physics* (1938) **6**, p. 130.

[14] G. Sachs and J. Weerts: *Ztsch. für Physik* (1931) **67**, p. 507.

[15] C. S. Barrett: *Structure of Metals*. (1952) 2nd Ed., p. 291. New York. McGraw-Hill Book Co. Inc.

Technical Note

Metallographic Techniques for Cu-Au Alloys

by Robert Bakish and William D. Robertson

IN the course of a study of stress corrosion cracking of $AuCu_3$, it was necessary to develop new electropolishing and metallographic etching methods. The techniques are generally useful for Cu-Au alloys, including the AuCu composition in which transformation markings are well delineated.

For electropolishing, the only satisfactory electrolyte and procedure that has been found[1] has the composition given in Table I. The solution must be vigorously stirred while polishing and the temperature maintained in the range of 55° to 62°C. The electrolyte is very unstable and can be used only for 10 to 15 min after which its color changes and a dark-brown precipitate forms. The polishing time is between 1 and 4 min depending on the initial surface preparation. The use of a hood is recommended to avoid the danger of cyanide gas which may form at one of the electrodes even though the solution is alkaline. The optimum current and voltage conditions for vertical anode and platinum cathode are on the plateau shown in Fig. 1, in which voltage is measured across the cell terminals. At voltages below the plateau, etching of grain boundaries occurs and under some conditions, which have not been clearly defined, octahedral etch figures are observed.

For general purpose grain-size determination in polycrystalline alloys, a 3 pct solution of iodine in methyl alcohol is used with excellent results. However, when it is necessary to reveal small orientation differences or concentration gradients in an alloy, the iodine etch is not satisfactory. For this purpose, a highly satisfactory etching procedure was developed during this investigation. It involves the use of the vapor given off by freshly prepared aqua regia. The solution employed is 3HCl to $1HNO_3$ which decomposes in accordance with the reaction $HNO_3 + 3HCl = NOCl + 2H_2O + Cl_2$.

The polished specimen surface is held about 1 to 2 cm above an aqua regia solution for 2 to 10 sec depending on the intensity of the contrast required and the surface is not subsequently washed. The results obtained with a coarse grained cast structure are shown in Fig. 2.

Subgrain boundaries in a single crystal and concentration gradients within the boundaries are developed by the same treatment with the results shown in Fig. 3. Obviously, any conclusions regarding structure-dependent properties will be modified by the pronounced heterogeneity, which is not clearly evident when more conventional methods are used.

Interesting structural details are also revealed by treatment for 4 hr at 850°C in unpurified tank argon. Fig. 4 shows a pattern characteristic of orientation-dependent oxidation.

R. BAKISH, Student Associate AIME, and W. D. ROBERTSON, Member AIME, Associate Professor of Metallurgy, are associated with Hammond Metallurgical Laboratory, Yale University, New Haven, Conn.

TN 261E. Manuscript, Oct. 26, 1954.

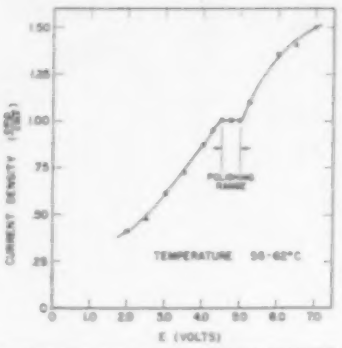

Fig. 1—Current voltage characteristics are shown for electropolishing of $AuCu_3$. Voltage was measured across the cell terminals.

Table I. Composition of Electrolyte

Compound	Quantity*
Potassium cyanide	67.5 g
Potassium-sodium-tartrate	15.0 g
Potassium-ferro-cyanide	15.0 g
Phosphoric acid, 85 pct	18.5 ml
Ammonium hydroxide (Sp.G. 0.9)	2.5 ml

* Based on one liter of solution.

[1] *Metal Finishing* (August 1950) 50, p. 84.

Fig. 2—Specimen etched with aqua regia vapor shows dendrites in a coarse grained cast structure. X50. Area reduced approximately 15 pct for reproduction.

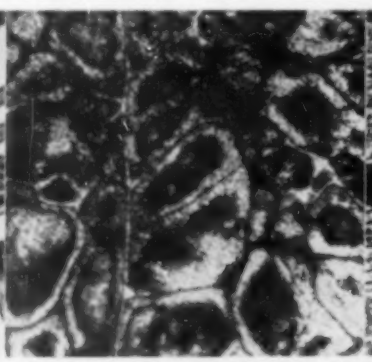

Fig. 3—Cell structure of a single crystal etched with aqua regia vapor is shown after heating 24 hr at 850°C. X200. Area reduced approximately 15 pct for reproduction.

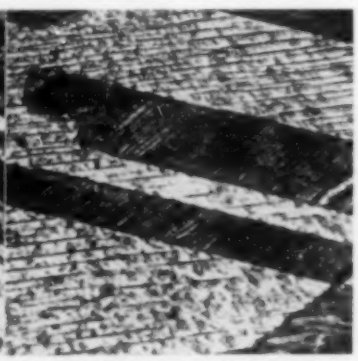

Fig. 4—After 4 hr at 850°C in unpurified argon, specimen shows oxidation figures. X800. Area reduced approximately 15 pct for reproduction.

Appreciation is gratefully acknowledged to the following organizations whose support has helped to make possible AIME's extensive publications program of metallurgical research:

Allis-Chalmers Mfg. Co.
Aluminum Co. of America
American Iron & Steel Institute
American Metal Co. Ltd.
American Smelting & Refining Co.
American Zinc, Lead & Smelting Co.
Anaconda Copper Mining Co.
Bridgeport Brass Co.
Bunker Hill & Sullivan Mining & Concentrating Co.
Calumet & Hecla, Inc.
Cerro de Pasco Corp.
Climax Molybdenum Co.
Consolidated Coppermines Corp.
Consolidated Mining & Smelting Co. of Canada Ltd.
Copper Range Co.
Crane Co.
Cyprus Mines Corp.
Dow Chemical Co.
Electro Metallurgical Co., div. of Union Carbide & Carbon Corp.
Engineering Foundation
Freeport Sulphur Co.
General Electric Co.
Howe Sound Co.
Hudson Bay Mining & Smelting Co. Ltd.
International Nickel Co., Inc.
Kennecott Copper Corp.
Magma Copper Co.
Mallory-Sharon Titanium Corp.
Miami Copper Co.
Molybdenum Corp. of America
National Lead Co.
New Jersey Zinc Co.
Newmont Mining Corp.
Noranda Mines, Ltd.
Phelps Dodge Corp.
Raytheon Mfg. Co.
Rem-Cru Titanium Inc.
St. Joseph Lead Co.
Texas Gulf Sulphur Co.
Titanium Metals Corp. of America
U. S. Smelting, Refining & Mining Co.
Vanadium Corp. of America